Publication of Theses

Please complete in block capitals

NAME: PHILLIP ANGUS TEASDALE

DEPARTMENT: GEOGRAPHY & EARTH SCIENCES

TITLE OF THESIS: THE LATE HOLOCENE EVOLUTION OF COASTAL WETLANDS IN ARGYLL, WESTERN SCOTLAND

PLEASE COMPLETE EITHER PART A OR PART B

A. I agree that the abstract of my theses may be published by the university without further reference to me.

In accordance with the University's handbook of procedures, the Head of Library Services may allow my thesis to be copied in whole or in part without further reference to me. Such Authority shall apply only to single copies made for study conditions and shall be subject to normal conditions of acknowledgement. **(see notes at the bottom of this page)**

Signature: Phillip A Teasdale Date: 15th NOVEMBER 2005

If you have completed Part A please return this form directly to the Library with evidence of your award.

B. I request that my thesis be held under confidential cover in the Library for a period of ____years for the following reasons:_____

_____

Once the period of confidentiality has expired, I agree that the conditions set down in Part A will apply without further reference to me.

Signature:_____ Date:_____

Please pass this form to your supervisor who should sign below indicating his/her agreement to the retention of the thesis under confidential cover.

Signature of Supervisor:_____

Additional comments:_____

Date:_____

Signature:_____ (Deputy Head of Registry)

If you have completed Part B, please return this form to Secretary to the Deputy Head of Registry

For the attention of candidates who have completed Part A

i) Attention is drawn to the fact the copyright of a thesis rests with its author.

ii) A copy of a candidate's thesis is supplied to the Library on condition that anyone who consults it is understood to recognise that its copyright rests with its author and that no quotation from the thesis and no information derived from it may be published without the prior written consent of the author or the university, as appropriate.

Requests for such permission should be addressed in the first instance to the Head of Library Services.

THE LATE HOLOCENE EVOLUTION OF COASTAL WETLANDS IN ARGYLL, WESTERN SCOTLAND

A thesis submitted for the degree

of

Doctor of Philosophy

Phillip Angus Teasdale

BSc (Hons)

Department of Geography and Earth Sciences

Brunel University

2005

ABSTRACT

The Late Holocene Evolution of Coastal Wetlands in Argyll, Western Scotland

by

Phillip Angus Teasdale

A detailed geochronological and geochemical study has been undertaken on selected sediment cores from four lowland coastal marsh environments in Argyll, Western Scotland. This region of northern Britain has experienced differential crustal uplift and relative sea-level changes throughout the Holocene in response to glacio-isostatic adjustment. The complex interplay between land movements and relative sea-level continues to influence the morphological development of the Scottish coast. The study of lowland inter-tidal sedimentary environments from this region provides an opportunity to investigate the linkages between current estimated crustal movements, regional relative sea-level rise and the evolution of contemporary coastal saltmarshes derived from the record of historical sedimentation. The four sites are located across a ca.70 km transect extending from the head of Loch Scridain (western Isle of Mull), across the Firth of Lorne to the head of Loch Etive, (mainland Argyll).

Vertical activity distributions of the natural radionuclide ^{210}Pb and anthropogenic isotopes (^{137}Cs and ^{241}Am) have been measured and are used to assess the depositional history of marsh sediment accumulation recorded in the four marsh cores. Down-core activity profiles of radionuclides are only reliable as a means of modelling recent marsh evolution provided no early-diagenetic (redox) reactions have compromised the historical depositional record within the marsh sediments. Solid-phase major and trace element down-core geochemical distributions provide a means of assessing the extent to which post-depositional (redox) reactions may have influenced the reliability of the radiometric dating methods. Marsh sediment geochemistry also serves as a useful proxy for identifying compositional variability over the period of marsh development investigated.

Dating of the Argyll saltmarsh cores indicates that over the period corresponding to mature marsh conditions rates of sedimentation vary significantly across the study area. At Loch Scridain an average rate of 1.1 mm yr^{-1} corresponding to an historical period of ca. 130 years is recorded. Comparison with estimated rates of regional sea-level rise suggest an established asymptotic relationship between marsh accretion and coastal forcing, implying historical crustal stability at this site.

At sites within the Firth of Lorne (Loch Don and Loch Creran) average rates of 2.5 and 3.3 mm yr-^{1} are recorded for the ca. 70 year period to 1995 with a figure of 2.2 mm yr^{-1} recorded in the marsh core from the head of Loch Etive. These values are well in excess of estimated relative sea-level rise during the twentieth century suggesting that these marshes may not yet have reached full equilibrium with sea-level. Microfossil analysis of the Loch Etive core helps to identify a more complex depositional history with an underlying trend of marine transgression for the ca. 110 year period of marsh development recorded in these sediments.

Over the most recent period of marsh development (ca. 5 years) a significant increase in the rate of marsh sedimentation at all sites is recorded. This signifies the response of these marshes to a very recent increase in the rate of relative sea-level rise across the region. Comparison with available storm frequency data indicates that the evolution of these marsh environments have not been subject to the influence of significant storm activity over the last in the late Twetieth century. The findings suggest that the more clastic sedimentary composition of the Argyll marshes results in these inter-tidal areas being extremely sensitive to changes in coastal forcing (sea-level rise). The implications of recent relative sea-level rise, current vertical crustal movements and future coastal management are discussed.

Keywords: saltmarsh; radiometric dating; sea-level rise; western Scotland; ^{210}Pb; ^{137}Cs; ^{241}Am; marsh geochemistry; diatoms.

This thesis is dedicated to the memory of my father

Henry (Harry) Joseph Teasdale M.B.E.

who gave me inspiration as a child, taught me more than I can ever remember and instilled in me a lasting interest in the natural world.

CONTENTS

ACKNOWLEGEMENTS

The completion of this research would not have been possible without the help, assistance and encouragement of quite a large a number of people.

Firstly, I would like to thank the Department of Geography and Earth Sciences at Brunel University for providing the bursary to undertake the research in Western Scotland.

Most importantly, I would like to extend huge thanks to my supervisers, Phil Collins and Steve Kershaw, for continued enthusiasm and encouragement in getting the work to this stage during a particularly difficult period of impending change and the future of Geography at Brunel.

Thanks and appreciation are also extended to Andy Cundy and Callum Firth (my initial project supervisers) who have been happy to provide continued interest in the work from further afield during recent years. I would also like to thank all the staff at the Geosciences Advisory Unit, Southampton Oceanography Centre for advice and training in the preparation and measurement of samples for the various geochemical analyses undertaken in this work. In particular I would like to thank Phill Warwick and Fran Dyer for useful discussions along the way over the data during a hectic period of lab work.

Finally, thanks to all my close friends for their support and encouragement over a difficult period of personal bereavement which has coincided with the latter part of this research.

In particular, I would like to extend a very special thanks to my dear friend Alex for love and support through hard times and heartfelt motivation throughout. Here's to your future success and happiness in all you do.

CONTENTS

LIST OF FIGURES

CHAPTER FOUR

CHAPTER FIVE

CHAPTER EIGHT

LIST OF TABLES

Chapter One

INTRODUCTION
AND
AIMS OF THE PRESENT STUDY

1.1: Introduction:

Salt marshes are the characteristic halophytic vegetated landforms which commonly develop within the upper inter-tidal environments of temperate lowland estuaries and other low-energy coastal settings. The morphological evolution of these landforms is determined by a complex interaction of processes including:

- movement of relative sea-level
- environmental setting and localized topography
- sediment supply and availability (minerogenic and organogenic material)
- in-situ production of organic material
- human exploitation of lowland coastal environments

The movement of relative sea-level over various time-scales is considered to be the ultimate driving force influencing the survival or destruction of marsh sedimentary sequences (Gehrels and Leatherman, 1989; Reed, 1990). This further controls the supply of sediment to the marsh surface over the diurnal tidal cycle. Sediment accretion can be viewed as the geomorphological response of the marsh environment to rising sea-levels (Pethick, 1992) which under gradual 'steady-state' rising conditions and sediment availability ensures marsh survival (Reed, 1990).

The recognition of this geomorphological response mechanism results from work by Pethick (1981) and other workers (e.g. Allen, 1989, 1990; Allen and Pye, 1992; French, 1993; Allen, 1997; Reed, 1995 Allen, 1997), undertaken in the North Norfolk marshes U.K. He established the discrete asymptotic relationship that exists between sediment accretion upon a mature marsh which illustrates how the marsh surface adjusts in response to relative sea-level (RSL) rise.

Marsh sediment accretion has been examined by numerous other authors from a large variety of locations within the northern hemisphere where temperate marshes are numerous in low energy coastal settings (e.g. Letzsch and Frey, 1980a; DeLaune, 1983; Hatton *et al.*, 1983; Stumpf, 1983; Oenema and DeLaune, 1988; Reed, 1990; Craft *et al.*, 1993; French, 1993; Jennings *et al.*, 1993; Kearney *et al.*, 1994; Cahoon *et al.*, 1995; Pye, 1995; Reed, 1995; Cahoon *et al.*, 1996; Cundy and Croudace, 1996; French, 1996; Allen, 1997; Orson *et al.*, 1998; Reed, 1998; Allen, 2000; van Wijnen *et al.*, 2001; Temmerman *et al.*, 2003).

The responses of these systems to increases in RSL rise, which can lead to marsh drowning and in many cases landward migration of the inter-tidal prism, have been reviewed by Reed (1995) and have been the subject of evolutionary based one dimensional models developed by Allen (1990) and French (1993), (see Chapter Two).

Most of these studies have concentrated on coastal wetland settings where relative sea-level rise affecting a particular coastal region is also accompanied by land subsidence due to residual glacio-isostatic adjustment (GIA) of landmasses. This process continues to influence the coastlines of countries outside the extent of maximum ice-cover following melting of the Late Quaternary (Devesian) ice-sheets (Mörner, 1971; Mörner, 1980; Devoy, 1987; Peltier and Andrews, 1976; Emery and Aubrey, 1985; Shennan, 1989; Lambeck *et al.*, 1990; Lambeck, 1991; Carter, 1992; Jelgersma and Tooley, 1995).

Formerly glaciated coastal regions of the northern hemisphere are areas where crustal uplift contributes to the present-day neotectonic setting (Peltier and Andrews, 1976; Mörner, 1980 a; Shennan, 1989, Firth and Stewart, 2000). In such regions intense research over a sustained period during the latter half of the last century has been focussed to promote greater understanding of the coastal evolution around these regions (e.g. Fennoscandia, Northern Canada, Greenland). Such studies have been aimed at elucidating the evolution of Late Quaternary coastal environments where land/ocean interactions driven by changing eustatic sea-level and regional crustal emergence have resulted in a complex history of coastal development. (Kaye and Barghoorn, 1964; Redfield, 1967; Morner, 1971; Peltier and Andrews, 1968; Kjemperud, 1986; Scott *et al.*, 1987; England, 1991; Eronen and Ristaniemi, 1992; Peltier, 1996b; Long *et al.*, 1999; Rostami *et al.*, 2000; Peltier, 1999; Peltier, 2002a).

Scotland is no exception to such interest and has been the focus of palaeo-sea-level and vertical land movement investigations for well over a century (Smith, 1997). The extent and estimated thickness of former ice cover over much of Scotland is considered to have been less extensive than other for other northern hemisphere regions (e.g. Fennoscandia). This has resulted in a more subtle GIA process following unloading of the Devensian ice (Sissons, 1974; Dawson, 1984; Smith *et al.*, 1992; Firth *et al.*, 1993; Smith, 1997 and references therein; Smith *et al.*, 2000). An extensive literature now exists which documents relative sea-level changes and crustal movements from around the Scottish mainland (e.g. Jardine, 1966; Gray, 1972; Sissons, 1972; Gray, 1974; Dawson, 1982; Dawson, 1984; Gray, 1985; Ritchie, 1985; Smith and Cullingford, 1985; Smith *et al.*, 1992; Firth, 1993; Shennan *et al.*, 1993; Shennan *et al.*, 1994; Shennan *et al.*, 1995b; Shennan *et al.*, 1996; Dawson and Smith., 1997; Smith, 1997; Dawson *et al.*, 1998; Firth and Stewart, 2000; Selby *et al.*, 2000; Dawson, 2001).

These studies, employing measurement of geomorphological raised marine features or bio-stratigraphical dating of raised sediment cores have facilitated the development of a large database of sea-level index points. From these data reconstruction of relative sea-level changes around much of the Scottish coast during the Late Quaternary period has been possible. The geomorphological investigations identify two main coastal landforms associated with land/ocean interactions over the last ~ 12000 years. These are the Main Late-glacial shoreline estimated to have formed in late Devensian times, and the Main Post-glacial shoreline corresponding to a circa mid-Holocene RSL high-stand between 6300-6800 ^{14}C years BP (e.g. Dawson, 1980b, 1982, 1984; Gray, 1972, 1974, 1975, 1978, 1983; Jardine, 1966; McCann, 1968; Sissons *et al.*, 1965, Sissons, 1972, 1974b,1982,1983).

The area of Argyll around the Firth of Lorne represents a coastal region in the western highlands where land uplift has been greatest relative to that for the Scottish landmass as a whole. The geomorphological work in this area by Gray (1972; 1974) helped to develop and prove the hypothesis of the dome-shaped uplift over a west-east transect across central Scotland in response to ice unloading (Figure 1.1). This research suggests maximum Holocene uplift centered over the Rannoch Moor area.

The interpretations of these raised marine features is in general supported by the various relative sea-level curves from many sites around the Scottish coast (e.g. Smith *et al.*, 1992; Shennan *et al.*, 1993; Robinson, 1993; Shennan *et al.*, 1994a, 1994b, 1995; Dawson *et al.*, 1998; Smith *et al.*, 1999; Selby *et al.*, 2000). The recent sea-level curve derived from the work of Dawson *et al.*, (1998) from Islay, western Scotland is shown in Figure 1.2. Little work of this nature has been done within the Firth of Lorne to corroborate the raised shoreline studies of Gray (1974).

Very little published data exists from western Scotland which considers land/ocean interaction over historical time-periods. Of the few papers that do exist, the ecologically based study of Adam (1978) suggests that isostatic uplift may play a significant part in driving the ecological succession. Although his studies did not include marshes from the Firth of Lorne study area (Figure 1.1) Adam also highlights other observational factors that may have influenced the development of coastal wetlands in the Argyll region:

- Generally the areal extent of marsh development is small supporting few communities (but occasionally many species).
- Unbroken transition across the marshes into non-tidal vegetation with the halophytic communities dominated by species of *Puccinella*.
- The quantity of tide-borne sediment delivered to the marsh surface is low.
- Marsh sediments would appear to be characterized by a fairly high organic content.

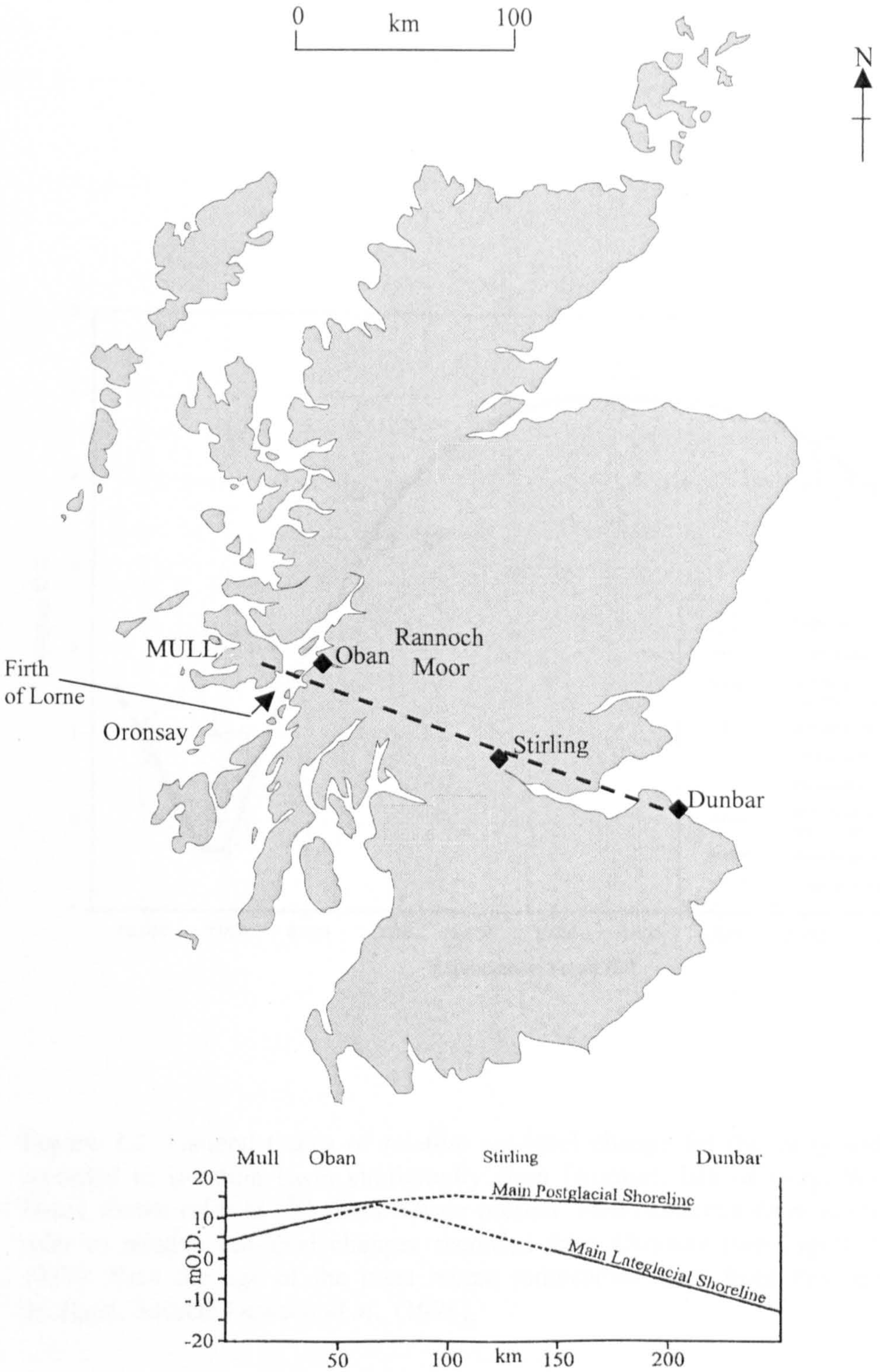

Figure 1.1: The predicted centre of the Scottish uplift dome identified from geomorphological studies of shoreline data relating to the Main Lateglacial and Main Postglacial shorelines aligned from Dunbar to Mull. Note the implied shift in the centre of the dome between Late Devensian and Mid Holocene times, as yet unproven.

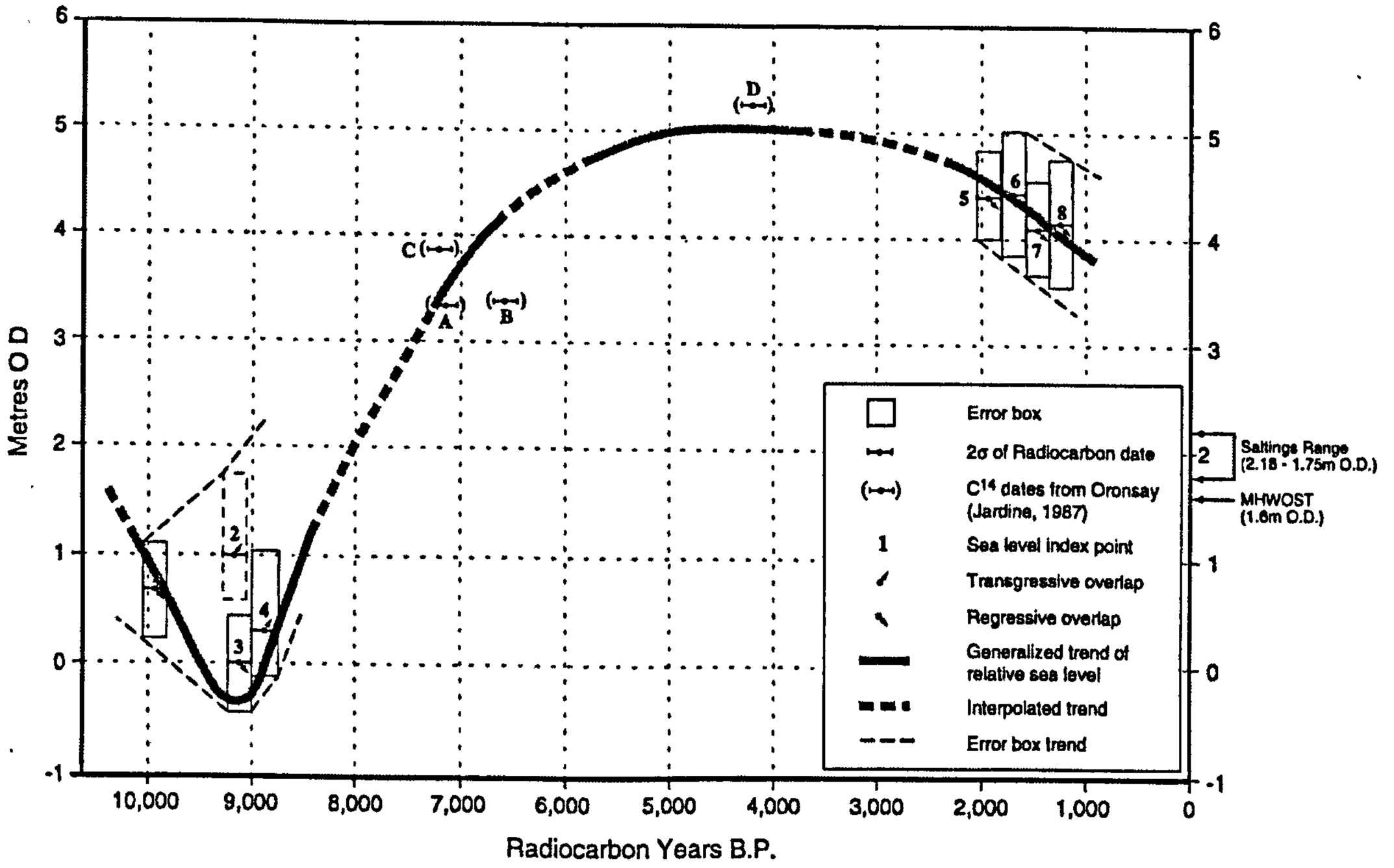

Figure 1.2: General trends of relative sea-level change for the early and late Holocene recorded in isolation basin stratigraphy from Gruinart, Isle of Islay, Western Scotland. Dates shown refer to ^{14}C years before present. Mid-Holocene dates shown on the graph refer to relative sea-level changes recorded from Oronsay (see Figure 1; after Jardine, 1987). Note the age of the most recent radiocarbon date from this region of western Scotland. Source: Dawson *et al.*, (1998).

However, at the time of publication this work further states that very little is known about the development of these coastal wetlands. This still appears to be the case, with no published work relating to the morphodynamic evolution of contemporary inter-tidal marshes from the west coast of Scotland.

1.2: Twentieth century and present-day RSL movements in Scotland

Estimates of present-day relative sea-level movements and rates of crustal uplift around the Scottish coast are currently determined from two distinct methods.

The first of these is through the development of geophysical modeling techniques which have been used primarily to simulate Late Devensian and Holocene land/ocean interaction. Such models combine earth rheological criteria and incorporate the empirically derived sea-level index points to produce calculated estimations of crustal response to former ice loading and relative sea-level altitudes relative to present day Ordnance Datum (e.g. Lambeck, 1991; Lambeck, 1993a; Lambeck, 1993b; Johnston *et al.*, 1998; Lambeck, 1995; Lambeck *et al.*, 1998; Peltier *et al.*, 2000; Shennan *et al.*, 2000a; Shennan *et al.*, 2003).

Periodic refinement of these models as more data become available results in a general improved fit to the empirical data although discrepencies between modeled estimations and observed data still exist for some areas (e.g. the Morvern and Ardnamuchan regions to the north of Mull, Smith, 2000).

Holocene crustal uplift patterns are varied with estimations of between 0.5 – 1.6 mm ^{14}C yr^{-1} (Shennan, 1989; Shennan and Horton, 2002) ranging across the peripheral areas of the Scottish landmass to those where ice cover was considered to be thickest. Lower values of between 0.2 – 1.0 ± 0.1 mm ^{14}C yr^{-1} have also been proposed (e.g. Smith *et al.*, 1993; 1995; Firth *et al.*, 1997). The most up to date refinement of these estimations is shown Figure 1.3 (Firth and Stewart, 2000).

An important point with regard to these estimations is that the data derived from ^{14}C dating of raised sediment sequences are extrapolated to the present day. As such current estimations of RSL change and crustal movements provide only first estimations of current relative sea-level movements and land uplift. The second and more routine method is by direct measurement obtained from tidal gauge stations at locations around the coastline. To achieve reliable estimates of current trends in mean sea-level key criteria are needed for improved accuracy. These include records from long established tide-gauges with historical and verifiable data extending back as far as possible. Ideally, this should be for a period of

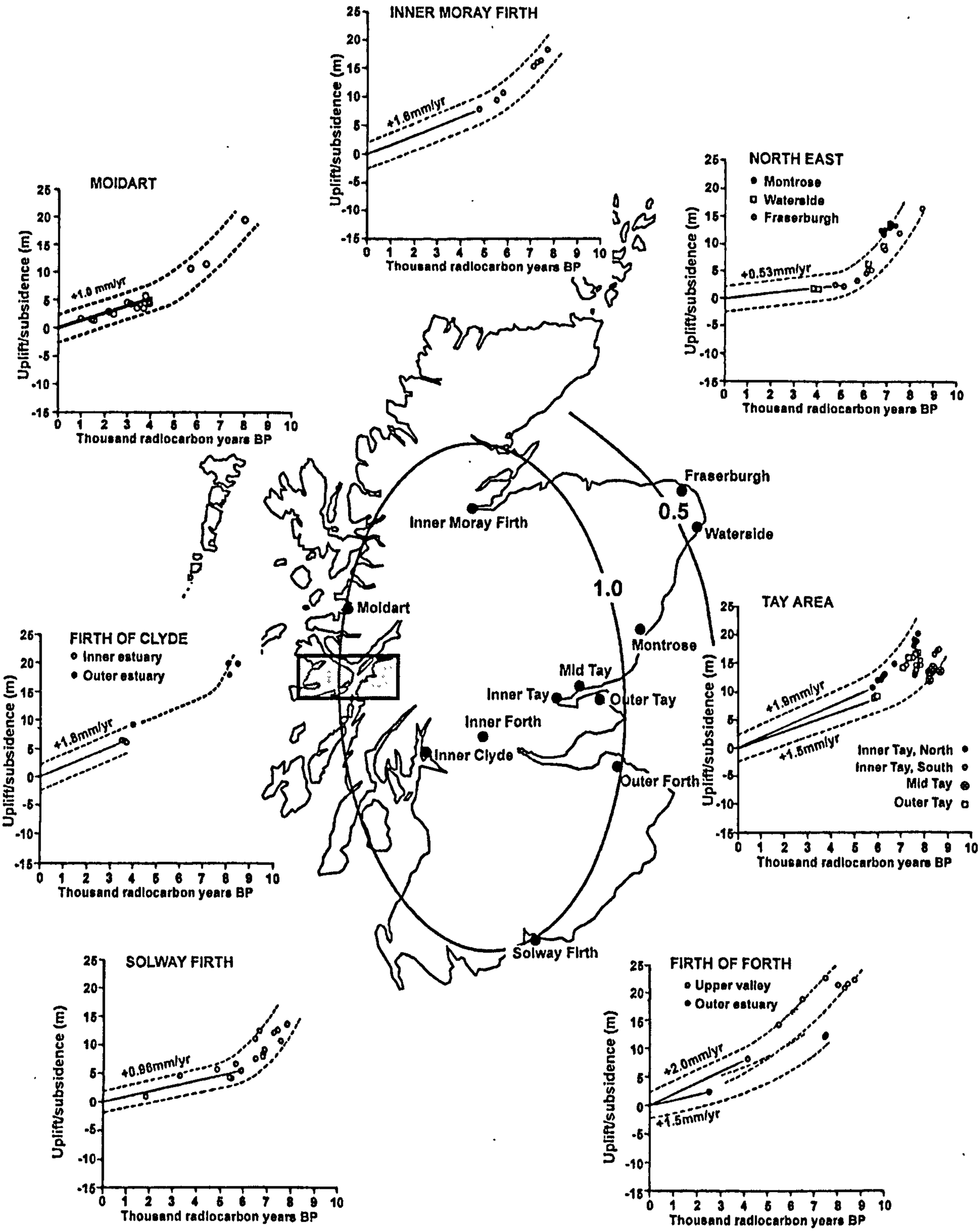

Figure 1.3: Distribution patterns of net crustal uplift, showing general trends (dashed lines) and estimates of current uplift rates (solid lines) in mm/^{14}C year. Shown on the inset map are current estimates of uplift modified from Shennan, (1989). Source: Firth and Stewart (2000). The infilled rectangle marks the location of the current study area around the Firth of Lorne

more than 40 years (Douglas, 1991). Best estimations for twentieth century sea-level rise around northern Britain derived from this approach yield a value of 1.0 ± 0.15 mm yr^{-1} (Shennan and Woodworth, 1992). This estimation has recently been revised by Nakada and Inoue (in press) who calculate an average value of 1.5 mm yr^{-1} from six northern hemisphere tide gauges with long duration records.

1.3: Future predictions of RSL change for western Scotland

Future predictions of RSL rise for the west coast of Scotland are highly problematic to say the least. This is primarily a function of the distinct lack of long-term tide-gauges records from western Scotland. Of all the estimations for future predictions one publication stands out.

In a recent paper Pethick (1999) has examined the Holocene relative sea-level curves derived from two differing areas of the Scottish coast, namely the north-west from palaeo RSL data provided by Shennan *et al.*, (1995) and the inner Forth estuary using data derived from Robinson (1993).At both these sites relative sea-level has fallen over the period 6000 years BP – 1000 years BP and 6000 years BP – 2000 years BP respectively. Following statistical analysis of these relative sea-level curves, which for north-west Scotland show a fall in relative sea-level from *circa*.6.0 m ODN to 1.0 m ODN over this time period, the author suggests that the rate of sea-level fall may have reduced over the recent past and that existing rates of residual crustal uplift may now be less than 1.0 mm per annum. Similar analysis of the inner Forth estuary data reveals that the rate of uplift may be as little as 0.5 mm in this region of the eastern coast.

Pethick (1999) extends this analysis by combining the extrapolated palaeo sea-level curve for the Holocene with the Inter-governmental Panel on Climate Change (IPCC) predicted sea-level curves for the 50 year period 1998-2048 (Figure 1.1).

This analysis of the data reveals that an imminent reversal in relative sea-level movement is to be expected around north-west Scotland with a mean sea-level rise of 4 mm yr^{-1} estimated for this region over the forthcoming 50 years. For the inner Forth estuary a similar trend is forecast with a predicted relative sea-level rise of 3.4 mm yr^{-1} for the fifty-year period to 2048 (Pethick, 1999).

The analysis of this data and the predictions arising from this work are supported by further consideration of the UK tidal station data collected by Graff (1981), cited in Pethick (1999), for the period 1960- 1980. Interestingly, although quite variable, some records for locations such as Rosyth and Grangemouth in the inner Firth of Forth and Methil and

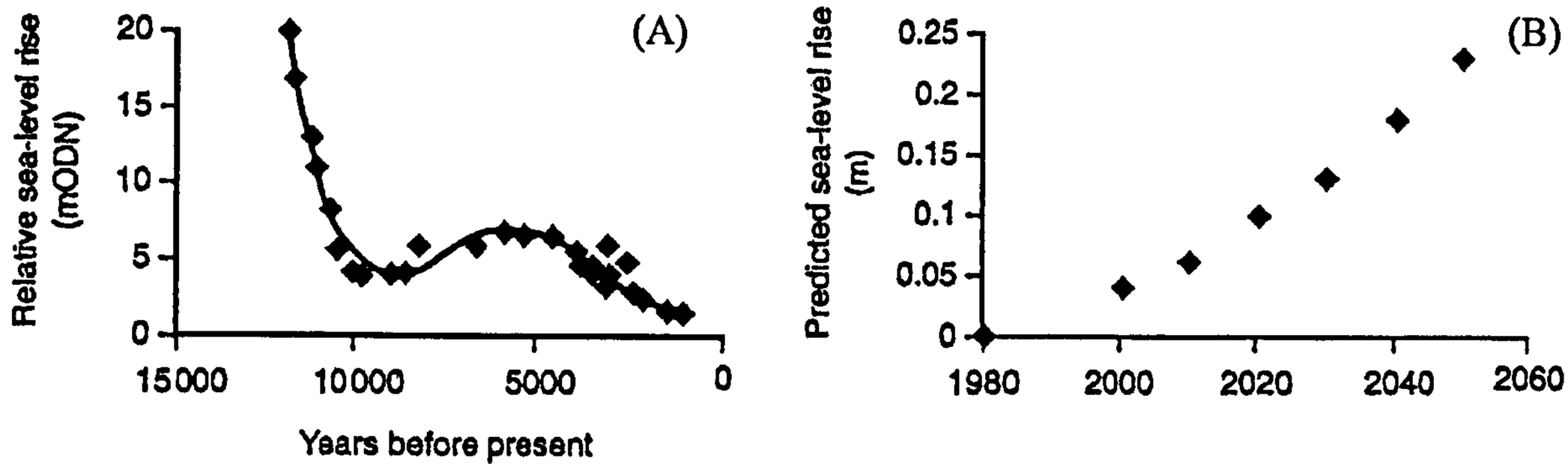

Figure 1.4: Analysis of past relative sea-level changes with IPCC projected increases for the region of western Scotland. Graphical plots are as follows: A) Best-fit regression of Holocene RSL change for north-west Scotland (Shennan *et al.*, 1995). B) IPCC predicted sea-level rise to 2050 AD (Warrick, 1993). C) Best-fit regression to the data in (A) for the period 2000 BC to 1000 AD extrapolated to 2050 AD. D) Addition of curves from (B) and (C) to give predicted change in RSL to 2048 AD (Source: Pethick, 1999).

Kirkcaldy in the outer Forth estuary reveal a strong relationship to the predicted 50-year curves of Pethick (1999).

Pethick (1999) concludes that the earlier tidal data of Graff (1981) would seem to suggest that certain locations within Scotland situated in fairly close proximity to the centre of glacial rebound were already exhibiting an indication of the reversal in sea-level tendency as predicted by this authors later analysis. Some further credence to the suggested reversal in relative sea-level trend is also provided by Flather *et al.*, (2001) who estimate an average 4 mm yr^{-1} rise for coastlines around north-west Britain over the next 66 years to AD2075.

Current estimates of crustal uplift reflect the time-transgressive nature of glacio-isostatic recovery that has taken place within Scotland. If these estimates are reliable a comparison with recently published predicted estimates of sea-level rise for northern Britain (Pethick, 1999; Flather *et al.*, 2001) suggest the onset of a similar time-trangressive reversal in relative sea-level tendency which may already be taking place.

1.4: Rationale for the present study

Previous studies of sediment accretion on coastal marsh surfaces have suggested that longer-term sediment accumulation on the mature marsh is driven primarily by coastal focing mechanisms linked to sea-level or hydrological change (Churma *et al.*, 2001; Haslett *et al.*, 2003). Hence, sediment accretion in these environments may act as a surrogate with which to assess relative sea-level rise, provided certain morphological/response relationships are maintained (Allen, 1990; Cundy and Coudace, 1996).

This asymptotic relationship between sediment accretion on a marsh surface and relative sea-level rise was identified by Pethick (1981) in the North Norfolk marshes of the UK. This morphological response mechanism has been shown to exist in other marsh settings (e.g. Reed, 1990; French, 1993, Cundy and Coudace, 1996; Reed, 1995; Allen 2000). The relationship has also been examined in marshes where tide gauge data of suitable duration provides a direct comparison between sediment accretion and recent trends in sea-level rise (e.g. Cundy and Croudace, 1996).

Radiometric dating methods applied to recent coastal sediments provide the basis for reconstructing the depositional history of substantial depths of inter-tidal salt marsh deposits. Such methods present the opportunity to assess the developmental history of marsh sediment sequences over an extended time-frame in comparison to shorter-term marker horizon experiments. These tend to be limited to periods of less than a decade (e.g. Richard, 1978; Stumpf, 1983; DeLaune, 1983; Roman *et al.*, 1997).

This study therefore aims to investigate the historical evolution of previously unstudied coastal wetlands from the Argyll region of western Scotland. In this region of northern Britain crustal uplift throughout the twentieth century is considered to have contributed to ongoing present–day relative sea-level fall. In so doing the work introduces established radiometric dating techniques using natural and artificial radionuclides (^{210}Pb, ^{137}Cs & ^{241}Am) and other geochemical analyses to develop geochronological models and estimations of marsh sedimentation over the past 120-150 years.

Measurement of historical recent rates of sedimentation at suitable sites across the region may, therefore, provide a test of twentieth century RSL rise estimations extrapolated to the western Scottish coast in the absence of longer-term tide gauge records from the region. Additionally, such data may also provide a means of assessing current geophysical derived estimations of crustal uplift, considered by Adam (1978) to have influenced the development of coastal wetlands within western Scotland.

1.5: Overview of project aims

The use of radiometric dating, utilizing the naturally occurring radionuclide ^{210}Pb, provides a suitable method for assessing longer-term (120- 150 years) historical coastal marsh development. In radiometric dating studies using the ^{210}Pb method the use of alternative/additional methods employing artificial radio-isotopes (e.g. ^{137}Cs and/or ^{241}Am) is recommended (Allen *et al.*, 1997; Smith, 2000). These techniques can be used to corroborate ^{210}Pb geochronologies providing an independent test of the reliability of this widely used method (e.g. Cundy and Croudace 1995; French, 1996; Thompson *et al.*, 2001; Dyer, 2002).

Radiometric dating techniques have been shown to be reliable provided no significant post-depositional re-mobilization has occurred during the historical development of the marsh sequence. Remobilization may occur as a result of early-diagenetic post-depositional geochemical reactions and can result in significant modification of the down-core distributions of radionuclides used for dating purposes. An assessment of the geochemistry of sedimentary sequences under investigation is therefore of key importance when implementing radiometric dating techniques. This can be achieved by analyzing the major and trace element solid-phase geochemical composition of the sediments and evaluating the redox zonation resulting from the early-diagenetic behaviour of redox-sensitive elements. Such data can also be used to assess the status of marsh sediments in terms of trace metal concentrations and levels of contamination over historical time-periods (e.g. Cundy *et al.*, 2003).

Other techniques can also be employed to reveal information concerning marsh evolution. Micropalaeontology has been widely applied to the study of contemporary marsh environments in efforts to assess the effectiveness of biological indicators of salinity variations recorded within inter-tidal sediment. Of the various microfossil techniques available, changes in the species assemblages of diatoms within inter-tidal sediments can provide highly sensitive indicators of the record of sea-level change (Robinson 1993; Nelson and Kashima, 1993: Shennan *et al.*, 1995; Zong and Horton, 1998; Dawson *et al.*, 1998; Gehrels *et al.*, 2001; Selby *et al.*, 2001).

This project aims to combine radiometric dating techniques coupled with geochemistry and diatom analysis to investigate Late Holocene (historical) coastal wetland evolution within low energy inter-tidal environments in the Argyll region of western Scotland.

1.6: Summary of research aims

- Implementation of radiometric dating methods to selected coastal sites in Argyll western Scotland to assess the historical record of sediment accumulation and marsh evolution within coastal environments characterized by recent/ongoing crustal uplift.

- Assessment of the reliability of the radiometric dating methods via analysis of the early-diagenetic/redox zonation and controls on the down-core element distributions within the marsh sequences obtained from determination of major and trace element geochemistry

- Comparison of the records of sediment accumulation with estimated rates of RSL rise and crustal uplift for northern Britain during the twentieth century.

- Further assessment of marsh evolution derived from geochemical fluxes of elements and the use of microfossil evidence from one site for assessing historical environmental coastal change recorded in the marsh sediments.

- Use of the multi-proxy methods to further understanding of marsh sedimentary processes and the recent coastal evolution of marsh systems in western Scotland and responses to coastal forcing.

1.7: Format and structure of the thesis

The format of the thesis is structured as follows:

Chapter Two: provides detailed background concerning coastal marsh sedimentary processes and the mechanisms responsible for the initiation and development of coastal marsh systems in relation to sea-level movements and coastal forcing. This is followed by an overview of some of the empirical methods employed to investigate saltmarsh evolution and the development of conceptual and numerical models used to describe the nature of marsh coastal dynamics.

The latter part of this chapter provides an overview of some of the more important geochemical processes (e.g. early diagenetic post-depositional reactions) that take place within developing marsh systems and the documented behaviour of major and trace element components and why these are worthy of study in the context of this research.

Chapter Three: provides an account of the various methods used for the determination of natural and artificial radioactivity (^{210}Pb, ^{137}Cs & ^{241}Am) in the marsh sediments. This is followed with an account of the laboratory procedures required for determination of major and trace element geochemistry. Manipulation of obtained raw data is discussed and full calculation spreadsheets for all aspects of the data are presented in the Appendices.

An overview of the use of diatoms in coastal studies and method of slide preparation and examination is also presented, with short accounts relating to other field-based work including instrumental levelling. As a whole this chapter provides detailed overview of the multi-proxy methodology applied to the Argyll marsh cores.

Chapter Four: constitutes the first of four sections of the thesis which examine distinct aspects of the results obtained from the various analyses. This chapter focuses upon the nature of the site locations and sedimentary log descriptions of the marsh sequences. Focus is also centered on the use of both major and trace element geochemistry as a proxy tool for assessing sedimentary components and the dynamics of marsh development within the four sites. At the Loch Etive diatom analysis is used to further understand the development of the more complex depositional history of this core. Core photographs are included in Appendix Two with aerial photographs used in the study shown in Appendix Three. Major and trace element geochemical data is presented in Appendix Four.

Chapter Five: provides the backbone to the study with detailed geochronologies of the four marsh cores. These are derived from the use of ^{210}Pb dating and artificial radionuclides (^{137}Cs & ^{241}Am) which are present in the marsh cores as a result of known periods of discharge. Rates of sediment accumulation over different periods of marsh development are presented via the different ^{210}Pb models providing inter-comparison of this method. These are then compared with sedimentation rates derived from the artificial marker horizons. Details of all calculations are presented in Appendix Five.

Chapter Six: provides a concise overview of marsh redox-conditions in the four cores through presentation and assessment of the down-core distributions of solid-phase redox-sensitive major and trace elements. This facilitates an understanding of the degree to which remobilization of key elements has occurred and provides the basis for thorough scrutiny of any possible influence on the depositional record of radionuclides used for dating.

Chapter Seven: investigates various aspects of trace metal and halide (I & Br) geochemistry in the marsh sediments and identifies other key geochemical processes that also serve to influence the down core depositional history within the four cores. Element fluxes to the marsh surface over time are considered and these data provide additional information regarding distinct periods of marsh development. Finally, this chapter then explores the influence of various marsh developmental process (physical and chemical) via the use of statistical analyses (PCA) in these highly mineralogenic sediments.

Chapter Eight: summarizes the data from the results sections to provide a composite overview of the geochronology, geochemical and detrital evolution of the marsh sequences.

The reliability of the radiometric dating methods is given due attention and here the influence of redox-controlled remobilization of elements is examined with respect to the depositional record of these radio-isotopes. The chapter is then extended through comparison of the calculated rates of sediment accumulation with estimated relative sea-level rise during the twentieth century. In conjunction with geochemical fluxes to marsh surfaces these are further compared with the record of storm frequency from north-west Britain to ascertain the possible influence of periods of known storm activity on marsh evolution in Argyll.

More recent sedimentation rates are then compared to predictions of relative sea-level movement for the forthcoming century and the implications of recent findings are stressed with respect to future coastal forcing and resulting management options.

Chapter Nine: highlights the key findings of the research and relates these to previously published predictions of anticipated coastal environmental change in western Scotland

Chapter Two

SALTMARSH EVOLUTION
PHYSICAL
AND
GEOCHEMICAL PROCESSES

2.1. Introduction: the definition of a saltmarsh

Coastal wetlands or saltmarshes are ecosystems occupying many highly variable low energy coastal inter-tidal environments. They can be found within estuaries, lagoons, tidal inlets and back barrier settings. Indeed, it can be argued that the existing coastal topography is frequently the controlling factor governing the position within which coastal wetlands develop (Reed, 1990). The influence of topographical setting and types of salt marsh development have been extensively reviewed and characterised by Dijkema (1984, 1987) who proposed a five tier classification scheme for European saltmarshes with seven sub-categories based upon the geological, geomorphological and ecological character of these coastal wetlands. Work undertaken by Pye and French (1993a) reduced this overall classification to seven distinct types commonly found on Atlantic and southern North Sea coasts. The differing environmental settings used by these authors for classification purposes are illustrated in figure 2.1 and consist of the following principal types:

a). open coast (eg: Dengie peninsula, Essex, UK).

b). open coast back barrier settings (eg: Stifflkey marsh, North Norfolk, UK).

c). open embayment (eg: selected areas within the Severn estuary, UK).

d). resricted-entranced embayment settings (eg: Langstone Harbour, Hampshire, UK; Poole Harbour, Dorset, UK; Loch Don, Isle of Mull, Argyll, UK).

e). estuarine fringing coastal wetlands (eg: Solent estuary, Hampshire, UK; West--erschelde estuary, SW Netherlands).

f). estuarine back-barrier locations (eg: Pagham Harbour, West Sussex, UK; Porlock Bay, Somerset, UK).

g). drowned ria/loch-head environments (eg: Fal estuary Cornwall UK; Loch Fynne, Argyll, Scotland).

Coastal wetlands exist at the land-sea interface in locations generally sheltered from high-energy wave action where sediment accumulation takes place. They act as sinks for fine-grained sediment derived from both marine input and that supplied by hydrological run-off from adjacent upland areas, (Davidson-Arnott *et al.*, 2002).

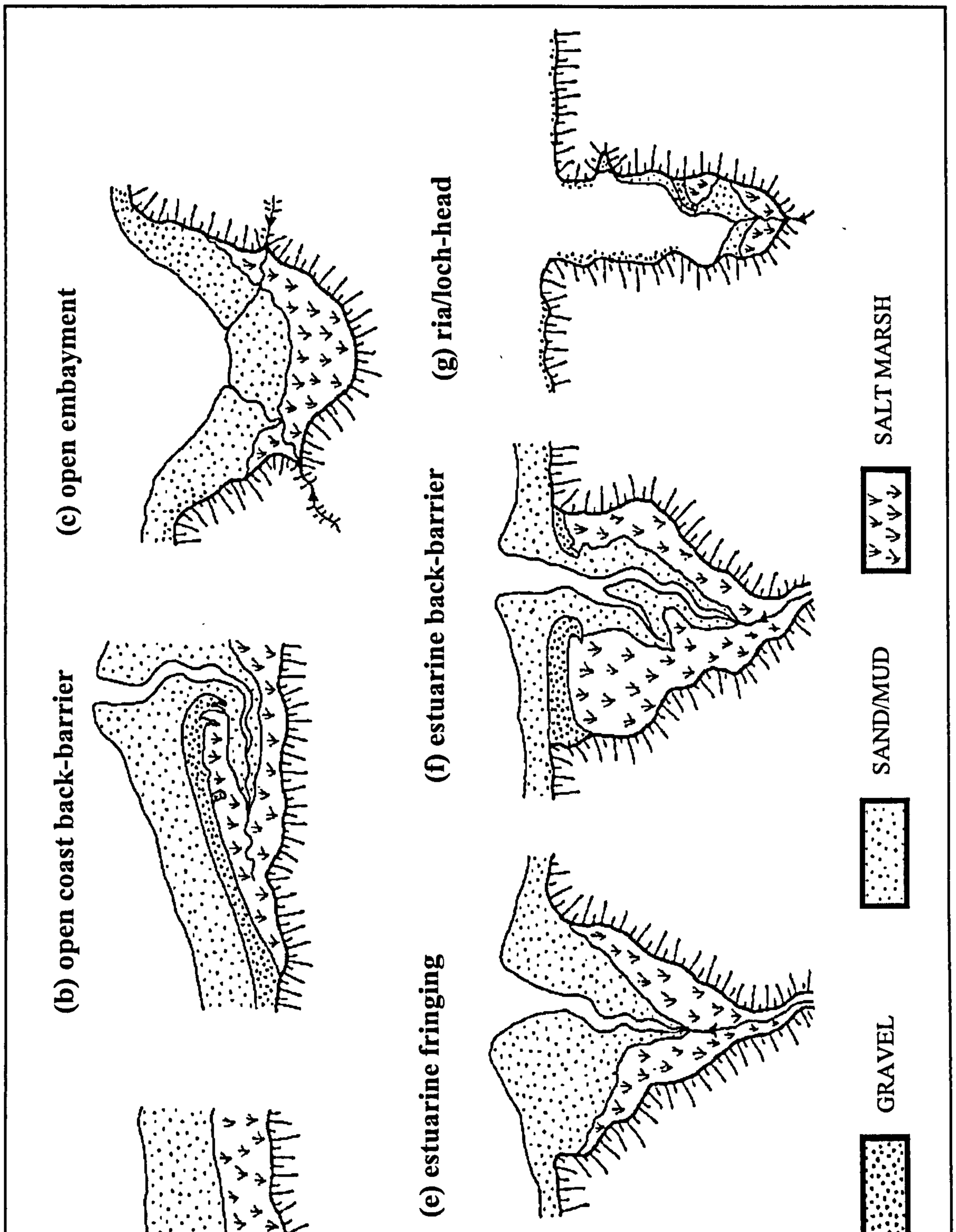

Figure 2.1: Geomorpohlogical classification of saltmarshes to illustrate the influence of variable coastal topography on marsh development. (Adapted from Pye and French 1993b)

2.2.The importance of coastal wetlands

The value ascribed to coastal wetlands is inherently dependent upon the perspective from which they are considered (Doody, 1992). The various interests in coastal wetland utilization range from industrial/urban development and agricultural practices through to ecologically based interests such as conservation and ecological importance.

The former concern the practice of reclamation of coastal wetland environments for food production and building. The latter are inherently interested in preservation issues and the study of scientifically important ecological systems. To the geomorphologist salt-marshes offer the opportunity to understand the functioning and response of a unique coastal morphological system and the relationship/dependence upon other integrated physical and biogeochemical processes that operate within coastal environments. Relatively recently the engineering significance of salt-marshes as a natural coastal defence system, which by their very nature dissipate incident wave energy and tidal current velocities, in the face of envisaged sea-level rise has been recognised (Green, 1984; Owen, 1984; Hydraulics Research Ltd, 1987; Doody, 1991).

Coastal wetlands consist of both organic and inorganic predominately fine sediments often rich in clay particles derived from reworked marine material. These fractions of coastal wetland sediments may be derived from both autochothonous and allochothonous processes occurring within the inter-tidal environment. Additional allochthonous material is delivered to estuaries via riverine input. Owing to the fine nature of saltmarsh and mudflat sediments these low energy environments can potentially become sedimentary sinks for particle reactive trace metals derived from marine sources and those entering the upper estuary delivered by riverine input. Understanding the geochemical behaviour of sub-tidal and inter-tidal estuarine sediments has become an important objective for environmental scientists/geochemists and coastal managers along with conservationists interested in the preservation of estuarine environments.

2.3: Sedimentary processes in the intertidal zone: implications for the morphological development of coastal marshes

Saltmarshes occupy a position high within the inter-tidal profile (figure 2.2) and although generally situated within low-energy locations in parallel with other morpho-dynamic features within the coastal zone they will evolve as a direct response to applied energy (Pethick 2001).

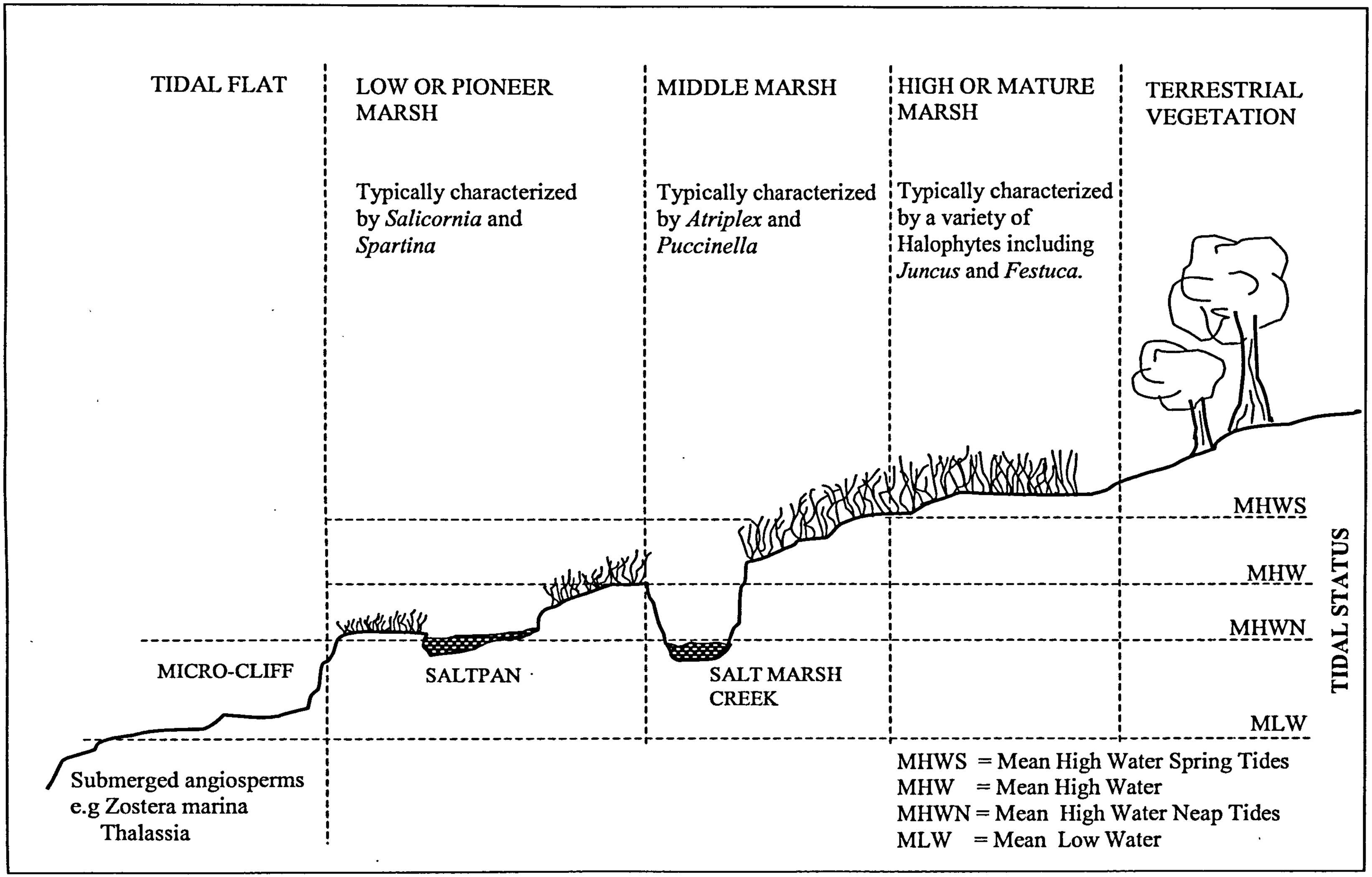

Figure 2.2: Diagramatic across a tidal flat grading into saltmarsh to illustrate principal physiographical features and zonation related to tidal status and flooding periodicity, (re-drawn from Williams *et al.*, 1994).

Generally speaking the composition of saltmarsh deposits consist of two principal sediment sources. The inorganic fraction may contain a variety of sands, silts and clays with occasional inclusion of fine/medium gravels as a result of higher energy events influencing the depositional/erosional pattern of sedimentation. The organic fraction may contain a variety of different sized material derived from external sources delivered to the marsh surface by tidal currents and wave action. Additionally, organic material will be present from the in-situ production derived from the halophytic vegetation growing on the marsh substrate.

Coastal marsh areas exhibit characteristic geomorphological features (tidal creeks and salt-pans) unified by low gradients the morphology of which will be directly related to the prevailing incident energy regime apparent at a specific locality. Such features are intrinsically linked to the antecedent morphology derived from the fronting mudflat. Indeed, the mudflat environment which occupies a lower altitude within the tidal prism has been described as being genetically linked to that of the overlying younger coastal wetland deposits (Allen, 2000).

From the inception of marsh development, characteristic morphological features evolve as an equilibrium function between the pre-existent topography, tidal/wave energy regime, available sediment supply, deposition/erosion threshold and biological productivity, (Pethick, 1992). The more prominent of such features are the creek and gully networks that dissect the marsh substrate (figure 2.2). The principal function of these creeks and gullies is to distribute tidal water and suspended sediment (Allen, 2000) and in common with the fronting mudflat to dissipate tidal/wave energy incident at the marsh edge (Pethick, 1992). The engineering significance of energy dissipation across the mudflat/saltmarsh substrate has recently been recognised as a potential natural defence mechanism in the face of rising sea-levels affecting many coastal lowlands, (Brampton 1992).

The temporal nature of external forcing mechanisms which influence the development of salt marshes are two-fold. These are processes which occur over longer time-scales (hundreds to thousands of years) and those which determine coastal wetland morphology over shorter–term duration (hourly to decadal) periods (Allen, 2000).

2.3.1: The role of longer-term physical processes

The dominant process that controls coastal marsh evolution over longer-term time-scales is the movement of relative sea-level (Reed, 1990). Relative sea-level may be transgressive or

regressive and result in morphological adjustment of the inter-tidal area realative to the movement of the tidal prism when change occurs. Such changes are intrinsically linked to fluctuations in global climate in particular the Devensian (last glacial/interglacial cycle). This has resulted in large-scale global sea-level variability with low stands at (circa. –120m-140m) correlated with the last glacial maxima (~ 18000-22000 years BP). High stands during the mid-Holocene occurred as a result of climate amelioration and deterioration of the vast ice-sheets that covered large areas of the northern and southern hemisphere.

Super-imposed on the general pattern of relative sea-level changes throughout the Late Pleistocene/Holocene has been the vertical movement of continental land masses which were formerly depressed as a result of significant ice thickness during the last glacial maximum. Glacio-isostatic recovery of these landmasses coupled with glacio-hydroisostatic processes has significantly influenced the overall pattern of relative sea-level change recorded from sites that were formerly glaciated and from sites beyond the limit of former ice cover (see Chapter 1). These longer-term fluctuations in relative sea-level initiate a morphological/ecological response in order for continued coastal wetland survival.

Under a scenario of regressive relative sea-level change the morphological response of the marsh will be a seaward movement of the inter-tidal area and possible colonization of the upper-marsh by less halophytic tolerant plant species. As such the overall position of the inter-tidal area relative to the tidal frame is maintained.

Conversely under a transgressive scenario the reverse takes place and the marsh will tend to move landward as relative alteration of the position occupied by the tidal frame proceeds in this direction. Morphological adjustment will take the form of increased vertical accretion on the marsh surface and horizontal erosion at the outer edges (Pethick, 1993). Under such conditions the ecological zonation will also be shifted landward resulting in upper-marsh halophytic plants colonizing marginal areas of coastal habitats formerly dominated by less saline tolerant species.

The influence of glacio-isostatic vertical land movements along paraglacial coastlines and the interplay with climatic induced relative sea-level changes will therefore have been the dominant processes determining the temporal and spatial evolution of coastal wetlands within such settings. Also of importance over longer time periods and in particular throughout the Holocene will have been the influence coastal neotectonic movements resulting from earthquake activity. Within seismically active parts of the world sudden and severe events resulting in uplift or downthrow of the coastal plain can result in 'drying out' or 'drowning' of marsh sediments if they are moved vertically above the limit of the tidal prism or submerged. The latter scenario may be as a result of tsunami waves with large-scale

erosion of sections of the marsh accompanied by deposition of coarse-grained material derived from further off-shore and terrestrial material derived from the action of wave backwash. (Dawson, 1994). Other neotectonic influences upon coastal evolution in para-glacial settings have been suggested by many authors (Davenport and Ringrose, 1985; Davenport *et al.*, 1989; Ringrose, 1991; Fenton, 1992; Ota *et al.*, 1992 Morner, 1996; Troften, 1999; Firth and Stewart, 2000) as a result of re-activation of pre-existent fault structures following the retreat of ice from former glacially covered regions.

2.3.2: The role of shorter–term physical processes: marsh initiation, intertidal sedimentation and erosion

The role of processes acting on shorter timescales than glacial/interglacial cycles and long-term neo-tectonic land movements arguably plays a more significant role in the morphological development of coastal wetlands.

Saltmarsh systems generally experience relatively lower energies in comparison to that experienced on open coasts where the existent coastal physiography affords less protection from incident waves. The energy influencing coastal wetland development is principally derived from the action of tidal currents and generally lower-energy incident waves that reach the marsh surface.

Within estuaries, the initial development of intertidal deposits is intrinsically linked to the chemical gradients experienced within the water column during the tidal cycle, the interaction with freshwater delivery and sediment supply to the upper estuary where the turbidity maximum fluctuates with the trangressive and regressive phases of the tidal cycle (Postma, 1972). The fluctuating movement of the salt-wedge and subsequent interaction with overlying freshwater results in alteration to the chemical charge associated with fine suspended sedimentary particles (predominately clay material). This results in flocculation of clay particles which promotes the settling out of larger agglutinated material (flocs), from the water column.

Deposition of flocculated fine sediment results in the formation of mudflat environments, characteristic of many mid-latitude Northern-European estuaries (eg: The Wash, Eastern UK; Severn Estuary, Western UK). Sediment deposition occurs upon the developing mudflat/marsh surface owing to settling of the suspended material in the water column during the period of slack water between the flood and the ebb tide (Stumpf, 1983).

Over time the level of sediment built up on mudflats raises the surface elevation within the tidal frame (above mean low water; Orson et al., 1985) such that the periodicity of flooding and reduction in tidal current velocity permits the colonization of the surface by halophytic (salt-tolerant) vegetation. Once established the vegetation further acts to reduce tidal current velocities and enhances sediment deposition owing to current attenuation within plant canopies, (Lopez and Garcia, 1998). Sediment deposition can also take place upon the plant leaves and stems. Such material can be incorporated onto the surface of the marsh via washing down from subsequent tidal inundation or rainfall (Boorman, 1988). Stumpf, (1983) estimated that approximately 50% of suspended material was deposited upon plants during a spring tide.

Other vegetative mechanisms which influence sediment deposition include the nature of plant architecture (Ward, 1976; Van Eerdt 1985b; Allen, 2000) and the role of microscopic algae and bacteria which produce biofilms that are capable of sediment entrapment/binding and hence increased resistance to erosion, (Paterson, 1997: Austen et al., 1999). These in turn provide the necessary inorganic substrate for continued vegetative colonisation and sediment accretion (Stumpf, 1983; Pethick, 1992; Allen, 2000).

At this stage of development the key to steady state survival of the marsh is the continued supply of detrital sediment to the marsh surface and the maintenance of a low energy environment capable of permitting continued vegetative production and enhancement of sediment deposition. The continued interaction between tidal imports, vegetation development and sediment deposition result in changes over time to the elevation of the marsh surface relative to the tidal frame (Pethick, 1982; Allen, 2000; Reed, 2002).

At a certain point in time the marsh achieves an elevation relative to the tidal prism which results in a gradual reduction in the periodicity of flooding and subsequent sediment supply to the marsh surface. Postma, (1961) introduced the concept of a 'settling lag-time' to explain the reduced sedimentation rate witnessed on higher marsh settings in comparison to marsh areas experiencing more frequent tidal inundation.

This further results in vegetative changes owing to the extended period of time when the marsh surface is exposed. As such, a distinct vegetative zone can often be identified within plants that are less dependent upon halophytic conditions colonising the sedimentary surface. Hence, it is often possible to distinguish between low-marsh (immature) surfaces and the high-marsh (mature) sections of coastal wetlands (Frey and Basan 1978).

2.3.3: Sediment accretion, erosion and sea-level rise

In section 2.3.2 the influence of fluctuating sea-levels upon marsh development were briefly introduced. Although the movement of relative sea-level is indeed the dominant process controlling coastal wetland development other physical factors exert an influence upon sediment accumulation within the intertidal zone. The horizontal extent of intertidal sedimentation will be largely controlled by the extent of the existing tidal range and prevailing wind/wave climate. Sea-level rise upon a particular coastline will ultimately influence the tidal range which may be expected to vary over time as a result of the interplay between topography and sea-level change.

The vertical extent of marsh growth is ultimately controlled by the interplay between these processes and sediment availability. Under normal tidal conditions sediment accumulation resulting in vertical growth and elevational change relative to the tidal prism will proceed. However, the annual sediment accumulation upon a marsh surface will also be dependent upon factors such as storm frequency and sediment availability as well as any short-term sea-level rise.

Storm frequency and intensity have been highlighted by Roman et al., (1997) as being major factors controlling the short-term depositional history of saltmarsh environments both spatially and temporally. Strictly speaking storms can be viewed as recurring short-term physical events the cause and effect of which are to initiate an ephemeral relative sea-level rise often resulting in extended periods of morphological change in comparison to the forcing agent. Rates of sediment accumulation can be greatly enhanced during storm periods in comparison to those that occur during storm-free periods (Roman et al., 1997).

During storm events enhanced sediment accumulation is likely to occur as a result of increased suspended sediment concentration within estuarine waters which leads directly to an increase in the suspended load transported to the marsh surface. Stevenson (1998) suggests that most of the sediment transported within coastal systems is achieved during storm periods. If conditions prevail whereby canopy overflow takes place then this can result in an increase of material transported to the back (higher portion) of the marsh (Stumpf,1983).

Under storm conditions erosion of the lower marsh/marsh cliff environment has been highlighted by some authors (eg: Allen and Pye, 1992; Pethick,1992; Janssen-Stelder, 2000). Erosion of inter-tidal sedimentary facies can be varied and result in significant modification to mudflat/marsh morphology. Such modification may involve both the export and import of

material from the marsh. General features indicative of recent/ongoing erosion are as follows:

- Removal of material from the marsh edge resulting in the formation of cliffed edges and development of spur and groove topography extending into the marsh, (particularly evident within estuaries with large tidal range eg: Severn Estuary UK)

- Enlargement of the seaward sections of saltmarsh creeks, as a response to increased or existent higher energy conditions and widening and/or deepening of salt pans.

- Overall deterioration and (in some cases) removal of marsh vegetation leading to scouring and general lowering of surface elevation.

Pethick (1992) observed both a vertical reduction in marsh height and horizontal land-ward retreat of up to 5 m during a storm event which affected the marshes at the Dengie Peninsula, Essex during the period 1987-1989. During the same period the mudflat surface exhibited net accretion of approximately 0.5 m (figure 2.3). The interchange of material resulted in an overall flattening of the inter-tidal profile. This lead Pethick (1992) to concur that coastal wetlands act as a safety valve within the inter-tidal zone and that modification resulting from erosion of the marsh surface and fronting cliff edge is the natural geomorphological response to increased energy derived from the storm. From further work relating to a study of elevational change on the Blackwater marsh also in Essex the same author postulated that following morphological adjustment owing to storm influence the marsh surface elevation would take some 5 years to recover to the pre-storm level (figure 2.4). This model raises the question that storm return periods of less than 5 years may seriously influence the ability of this marsh to recover any vertical height reduction lost during such periods.

It should be stated however that the particular morphological alteration to the marsh environment under storm conditions will be dependent upon the type of sediment (ie; lithology and texture) from which the marsh is composed (Allen, 1989) and the location in which the marsh has developed. Widdows (2000) has observed reduced levels of storm induced sediment accretion upon mature/upper marsh surfaces owing to bio-stabilisation of

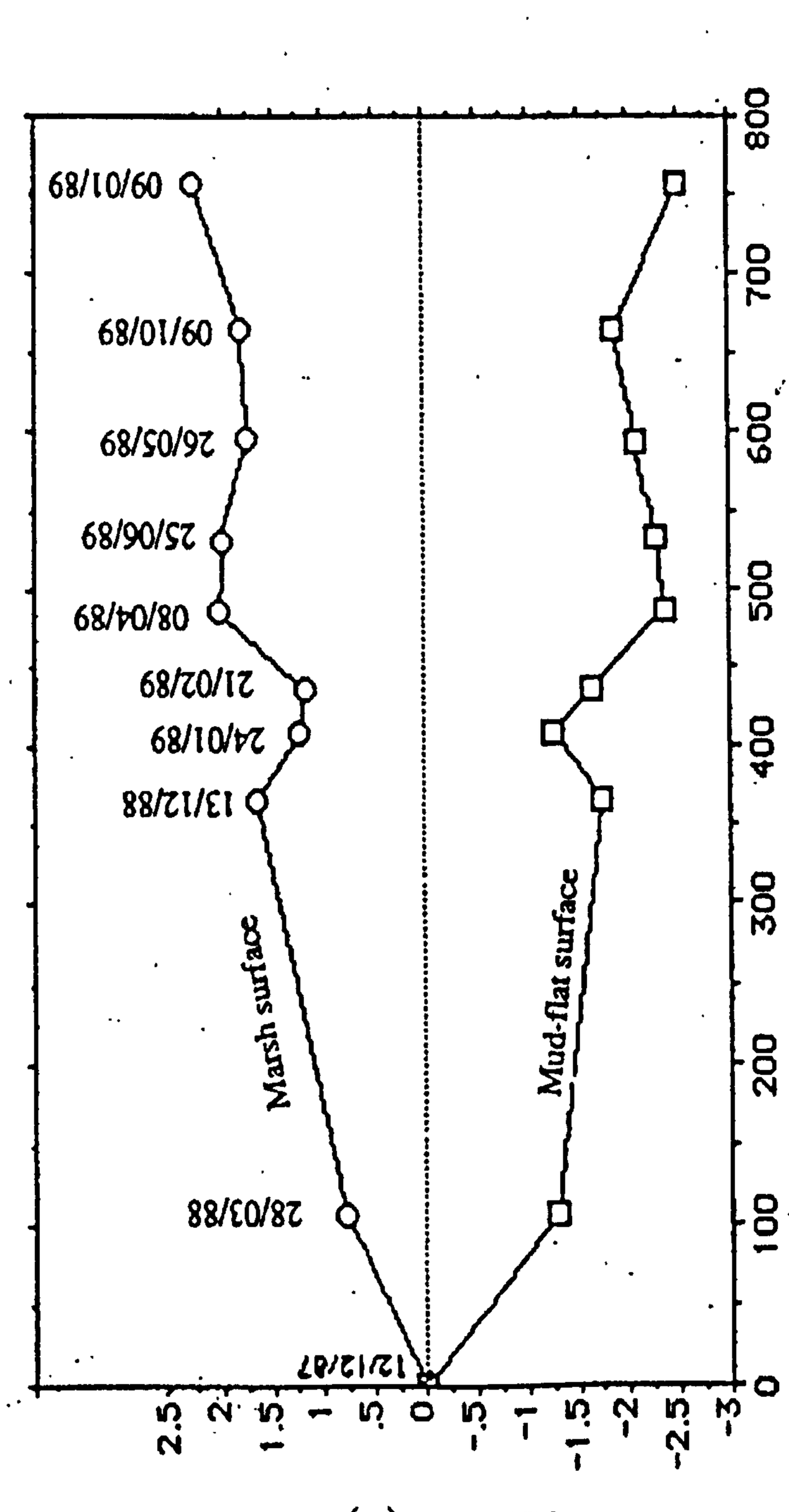

Figure 2.3: Variation in mudflat and salt marsh elevations during and following a single storm event which affected the Dengie Peninsula, Essex, UK in December 1987 (After Pethick, 1992)

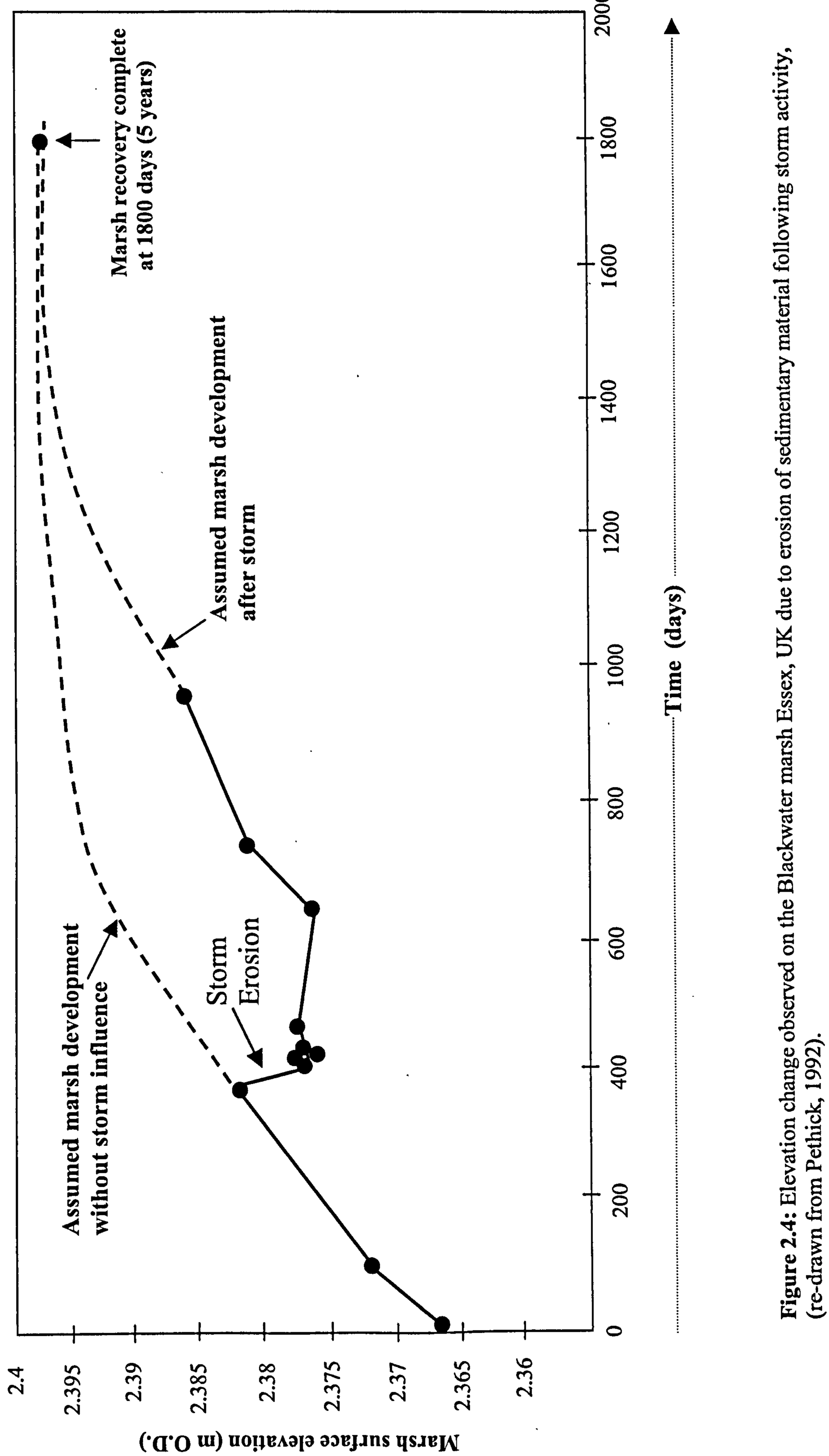

Figure 2.4: Elevation change observed on the Blackwater marsh Essex, UK due to erosion of sedimentary material following storm activity, (re-drawn from Pethick, 1992).

the fronting mudflat surface resulting in lower suspended sediment concentrations during higher energy conditions.

Overall the processes that lead to sediment import to the marsh surface (ie; tidal current energy and that derived from wind/wave energy) are the same processes that also export material from the marsh environment. Understanding the interaction between these physical processes and the direction of net sediment movement between the marsh and mudflat environment are still key questions for the coastal scientific community.

It has been highlighted within this overview that relative sea-level rise is likely to exert a significant morphological response within saltmarsh environments owing to the complex interplay between several physical parameters.

Estimated rates of global sea-level rise over the past 100 years vary within the range of 0.5 to 3.0 mm a^{-1} (Warrick and Oerlemans, 1990). Such estimations are derived from tide gauges with adjustment performed to remove the effect of neotectonic movements and atmospheric/oceanographic forcing factors.

The long-term general response of coastal wetlands to relative changes in sea-level were introduced in section 2.2. Under a scenario of rising sea-level however the shorter-term response may be quite varied depending upon the interaction of physical processes and sediment supply previously highlighted. A common assumption derived from some published data is that inter-tidal marshes are able to maintain their vertical elevation relative to the tidal framework (Pethick, 1981; section 2.5 below) and that sea-level rise enhances sediment accumulation upon the marsh surface (Phillips, 1986). Some interesting developments in our understanding of coastal wetland responses to sea-level rise have emerged over the past few decades or so. Generally speaking rapid rates of sea-level rise tend to be detrimental to continued marsh development whereas slower rates would seem to encourage continued marsh development. Orson (1985) has identified three major responses in an extensive review of existing literature and recent research.

- Drowning of the marsh surface if rates of submergence exceed sediment accumulation. This may occur as a result of inadequate sediment supply as DeLaune *et al.*, (1983) report for a marsh in Louisianna, USA. This study revealed that the rates of accretion (0.8 cm yr^{-1}) were being outpaced by sea-level rise of 1.2 cm yr^{-1}. The predicted consequences for the marsh assuming continuation of existing processes and rates of change would be deterioration of the marsh environment and conversion of the saltmarsh environment to open embayment within a period of 40 years or so.

- Saltmarshes may remain stable or continue to accrete under steady-state and/or slowly rising sea-level. This scenario is dependent upon supply of sediment being equal to or even slightly greater than the rate of submergence. Additionally this response will also be dependent upon the production of in situ organic matter derived from the growth of marsh vegetation.

- Alternatively if sediment supply and marsh vegetative production are sufficient to outpace the rate of rising sea-level the marsh may be able to expand. This may be possible even under conditions of rapid sea-level rise (Orson, 1985). Letzsch and Frey (1980) identify that an increase in tidal range can lead to increased sediment deposition as the tidal prism moves land-ward with relative increase in water depth enhanced by subsidence (sediment compaction and/or land movement) and rising sea-level. Additionally tidal range is considered by Reed (1990) to be an important indicator of sediment transport potential. The same author draws attention to the fact that within areas with high tidal ranges the marshes present may be less vulnerable to relative sea-level change.

Any increase in flooding frequency as a consequence of relative sea-level change will also influence the vegetative zonation which is primarily controlled by salinity gradients across the marsh surface. Some evidence has been presented suggesting that the survival of salt marshes will also be dependent upon the reaction of varying halophytic plant species to any increases in sediment shear stresses initiated by increased tidal range (Jansen-Stelder, 2000). As such the ecological stability of coastal wetlands will also be sensitive to the relationship between marsh surface elevation and sea-level rise (Christiansen, 2000).

2.3.4: Recent sediment accretion and modelling saltmarsh development

Interest in coastal wetland environments and geomorphological development dates back to the latter part of the nineteenth century. One of the earliest accounts of peat formation relating to saltmarsh accretion was put forward by Mudge (1862) from work examining a section of the Romney marsh, near Lynn, Massachusetts. In this account the author clearly identifies the concept of higher-marsh environments being able to maintain their position during a gradual change in relative sea-level. However, the underpinning mechanism he invoked as a physical process controlling marsh development (ie;

undercutting of the peat by water currents acting on the diluvium beneath the marine clay) somewhat curtailed any further application of these ideas (Mudge, 1862, cited in: McCaffrey and Thompson, 1980).

Shaler (1885) articulated a contrasting hypothesis derived primarily from field observations of Eastern USA coastal wetlands in which he suggested that marsh formation occurred during advance of halophytic grass species over mudflats that had become silted-up. This implies an early recognition of the concept of marsh sediment accretion. Shaler (1885) also realised that sediment accumulation was intrinsically linked to the trapping of sediment by the marsh vegetation. Davis (1910) was the first researcher to identify that the driving mechanism controlling saltmarsh formation was in fact rising sea-levels since post-glacial time. Some years later the key concepts of marsh formation postulated by Mudge (1862) and Shaler (1885) were reconciled by Johnson (1925, republished in 1967).

At around the same time period early work by Yapp *et al.*, (1916; 1917) and Yapp (1922) undertaken in the Dyfi estuary, Wales UK developed a conceptual model (*the Yapp-Johns Model*) which in parallel with the work previously described was descriptive in character. Such studies permitted the interest in marsh morphological development to proceed. The *Yapp-Johns Model* along with those developed by Mudge (1862) and Davis (1910) identified a number of key concepts inherent in coastal wetland evolution. Further studies of both the Eastern USA marshes, (Bloom, 1961, 1967; Redfield and Rubin, 1962; Bloom and Stuvier, 1963; Johnson, 1967; Redfield, 1972; McCaffrey and Thompson, 1980) and the Dyfi estuary marshes, Wales, UK (Haynes and Dobson, 1969; Shi, 1993, Shi *et al.*, 1995) bear testament to the earlier studies and indicate that many of the postulated process/morphological response concepts inherent in coastal wetland evolution are relevant to our present day understanding of marsh development.

Further descriptive-based conceptual models characterising the geomorphological and ecological development of coastal wetlands became more prevalent over the past sixty years or so (Chapman, 1942; Chapman, 1960; Bouma, 1963; Pestrong, 1965; Beeftink, 1966; Pethick, 1969; Frey and Basan, 1978, 1985; Beeftink and Rozema, 1988; Pethick, 1992).

The development of numerical simulation models applied to saltmarsh development processes is a more recent addition to the literature. Many of these studies have sought to quantify sediment accumulation rates on marsh surfaces over varying time-scales in an attempt to resolve the interaction between actual sedimentation, factors that result in submergence (i.e. sediment compaction and sea-level rise) and longer-term geological processes (i.e. crustal movements). Several methods have been employed in attempts aimed at quantifying sediment accumulation rates.

On time-scales of a few years the use of marker horizons has been a popular method to evaluate recent sediment accumulation. This method is fairly easy to implement and involves the spreading of a discernable marker horizon over an area of the marsh surface, normally to a depth of a few millimetres or so. Sediment is then allowed to accrete over the marker horizon. Measurement of estimated sediment accumulation is achieved by removal of short, small diameter cores from the marsh surface at discrete time intervals during the period of study. Various materials have been successfully used for this purpose and include brick dust (Richard, 1978), aluminium glitter (Stumpf, 1983) and kaolin (DeLaune, 1983; Roman et al., 1997). Marker horizons of this nature are however susceptible to bioturbation (Letzsch and Frey, 1980) and may be completely removed by storm induced wave activity over the marsh surface.

In some studies bamboo canes have been employed to estimate sedimentation rates on coastal wetland surfaces. These give a broader-based estimation of sediment accumulation (Cundy and Croudace, 1996) owing to the influence of the cane on actual sedimentation processes. In a study by Eckman and Nowell (1984) attention was drawn to the effect of plant stems and animal tubes in influencing sediment erosion owing to the transfer of fluid momentum to the marsh surface and subsequent entrainment of previously deposited material. This transfer of momentum has the potential to remove sediment around the base of the cane in contact with the marsh surface. As such misleading results may therefore be recorded.

In other experiments sedimentation plates of differing material have been used in preference to marker horizon substrates, for example perforated aluminium metal plates and plastic "Feno" blocks (Boorman, 1998) and "wet burst" filter papers (Brown, 1998). All of these methods are designed to allow sediment to be deposited on the marker plate which is discretely placed upon the marsh surface. In the study by Cahoon *et al.*, (2000) the use of the sediment elevation table (SET) permits the actual change in marsh elevation to be evaluated more precisely following experimental use and collation of data derived from the marker plates. SET's were originally developed in the Netherlands for the monitoring of tidal flat environments (van Erdt 1985) and adapted for use within saltmarshes by workers at Louisianna Stae University (see Bormans and Day 1993). The essential features of the SET and method of deployment are illustrated in figure 2.5. The use of SET's also provides a method of incorporating sediment compaction into developmental models which is not the case for the studies conducted by Boorman (1998) and Brown (1998).

2.3.5: Historical sediment accretion and marsh development

All the methods discussed thus far for determining sediment accretion only take into account current or recent sedimentation. An important area of coastal wetland research over recent decades has been the development of methods to more fully evaluate the historical rates of sediment accretion. These are particularly useful for investigating the response of marshes to historical changes in sea-level derived from longer-term trends or the reaction to sudden events such as coastal subsidence following earthquake events. Such methods include assessment of geomorphological changes derived from old maps and air photogrammetry, investigation of historical geochemical marker horizons, bio-stratigraphic techniques and radiometric dating using both natural and artificial radionuclides (e.g. Pethick 1981; Allen and Rae, 1987; Long and Shennan, 1994; Cundy *et al.*, 2000).

The use of bio-stratigraphical analysis techniques are derived from well established longer-term studies of Late Quaternary sea-level change (eg: Tooley *et al.*, 1983; Shennan, 1982; Gehrels *et al.*, 1996;). These methods are now being applied with some rigour to contemporary coastal wetland sediment sequences (Scott and Medioli, 1978; Zong and Horton, 1998, 1999; Horton *et al.*, 2000; Gehrels *et al.*, 2001) and hinge upon the identification of key microfossils including species of Diatoms and Foraminifera. Statistical determination of the vertical distribution of these species relative to the tidal frame permits good estimation of palaeo-tidal levels derived from modern sediment sequences. These are then applied to Holocene palaeo sea-level reconstructions.

All of the modelling techniques and methods described above provide information permitting a distinct aspect of marsh development to be more comprehensively understood. However, these techniques are limited to either the longer-term evolution of coastal wetlands constrained by radiocarbon (^{14}C) dating techniques and associated errors (Stuvier and Reimer, 1993) or measurement of recent/current sediment accretion rates.

In many estuarine locations the development of contemporary saltmarsh sediments can be witnessed that broadly correspond to the major period of industrialization and in some cases historical land reclamation. The measurement of historical sediment accretion rates can provide useful data regarding the marsh response to historical sea-level changes induced by either climatic fluctuations, geological phenomena (eg: earthquakes Cundy *et al.*, 2000) or anthropogenic activities such as estuarine channel dredging.

Useful methods for the measurement of historical accretion rates can be via geochemical determination of defined reference horizons (Allen *et al.*, 1990; Cundy and Croudace, 1995, 1996; Callaway *et al.*, 1998; Turner, 1999). However the geochemical

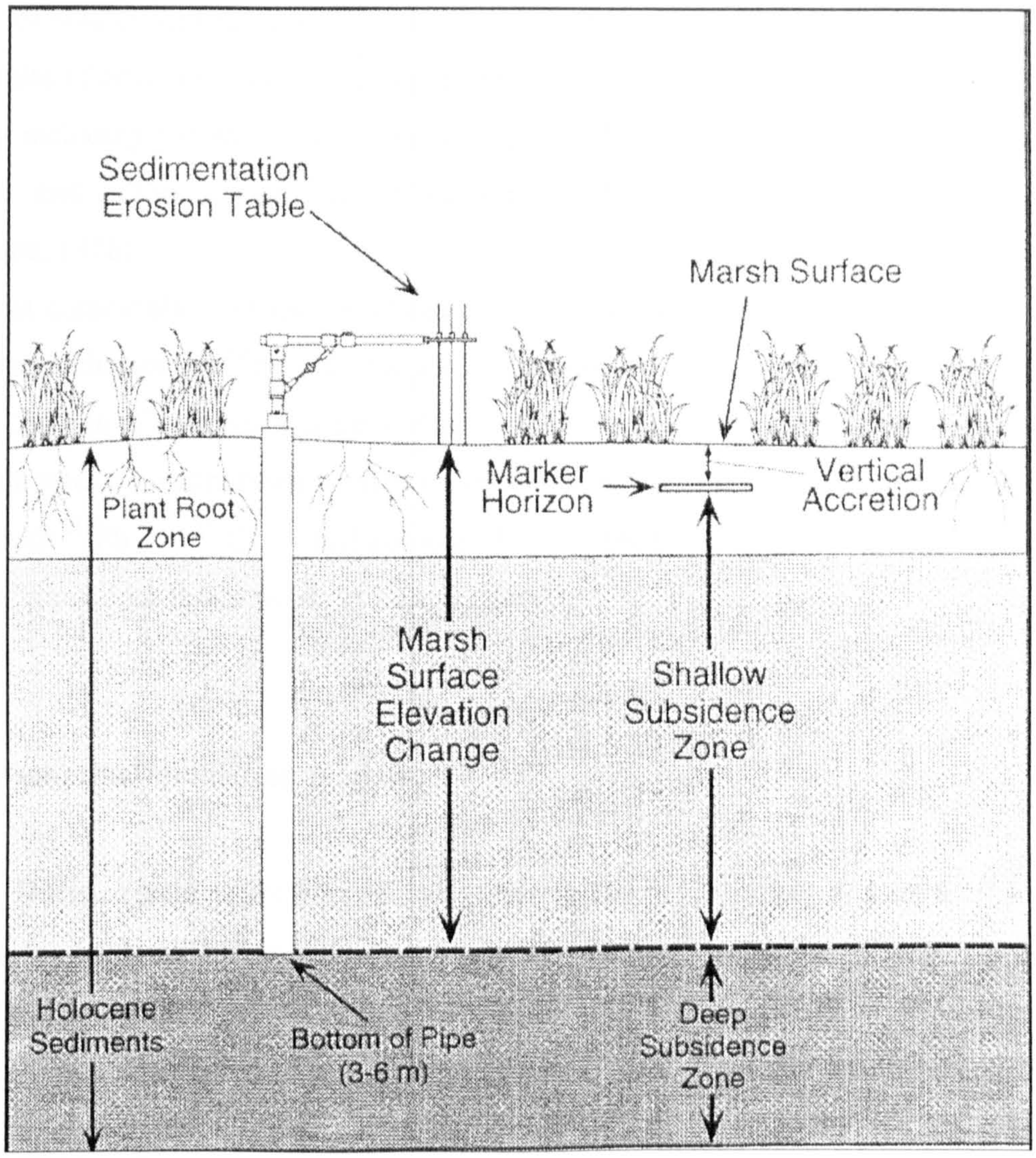

Figure 2.5: Conceptual illustration to show the key components of the Sediment Elevation Table used in both tidal flat and saltmarsh environments for assessing actual marsh elevation change. Also shown is a diagramatic representation of the use of a metal marker plate utlised in studies of recent sediment accretion on contemporary salt marsh surfaces.
(For a full explanation of the deployment process and method see Cahoon *et al.*, 1995)
(Source: Cahoon *et al.*, 2000).

approach still requires a robust geochronological control with which such horizons can be dated.

Radiometric dating using determination of both natural and artificial radioisotope activity levels throughout a contemporary sedimentary sequence has been demonstrated to be a useful and valid approach to such studies. Specific radionuclides have been used in a variety of studies and include the natural radioisotope ^{210}Pb (Appleby and Oldfield, 1978), and a suite of artificial radioisotopes present in the environment as a consequence of human activity including the short-lived ^{7}Be (Clifton *et al.*, 1995), the Plutonium isotopes (^{238}Pu, ^{239,240}Pu and ^{241}Pu) (Cundy and Croudace ,1996), ^{241}Am (Appleby, 1991) and ^{137}Cs (DeLaune, 1978).

The most commonly used radionuclides used for saltmarsh geochronology are the naturally occurring radioisotope ^{210}Pb and the artificial isotope ^{137}Cs.

As one of it's principal aims, this investigation attempts to define historical sediment accretion rates on saltmarshes located in the Western Highlands of Scotland and employs the use of both ^{210}Pb and ^{137}Cs. A full account of the methodology and geochemical behaviour of these radionuclides is discussed in Chapter Three.

2.3.6: Numerical simulation models

During recent years interest has grown in the development of numerical simulation models of saltmarsh morphodynamics and application of these models to improving understanding of marsh responses to intrinsically unsteady forcing mechanisms such as climate related changes in mean relative sea-level, tidal range and sediment supply (Allen, 1997).

Development of numerical models has hinged on the acquisition of empirical field based observations (derived from the field experiments previously described) and determination/comparison with available tide-gauge data, suspended sediment regime over or within vegetation canopies and importantly assessments of sediment autocompaction (Lenoard and Luther, 1995; Cahoon *et al.*, 1995; Cundy and Croudace,1996).

Initially such data facilitated the establishment of zero-dimensional time-stepping models (Allen, 1997) and were developed for predominately mineralogenic marshes in meso-macrotidal settings (Figure 2.6). These models are based essentially on a mass-balance type approach and describe in essence the change in altitude be this positive or negative derived from the measurement of parameters over a defined time period.

In the basic simulation model (Allen, 1997), these parameters include elevation change over a time period relative to the moving tidal frame (ΔE), change in thickness of both the mineral and organic matter fraction added to the marsh surface (ΔS_{min} and ΔS_{org} respectively) and the change in regional relative sea-level determined from tide gauge data (ΔM, can be positive or negative value). Essentially the mass balance equation is generally written as:

$$\Delta E = \Delta S_{min} + \Delta S_{org} - \Delta M$$

(ΔM is positive if sea-level movement is upward)

Simulation models based upon this mass-balance equation approach are fairly simplistic and take no account of processes likely to affect actual elevation change such as sediment compaction. However they do provide a mechanism for discerning the accretionary status of any particular marsh under investigation. This sedimentary related status (either negative or positive) has been further developed by French (1994), (Figure 2.7). Although the relationship between accretionary balance and tidal range is considered to be highly complex owing to differential sedimentation over the surface of a marsh (Wood *et al.*, 1989; French, 1994), the view articulated by Stevenson *et al.*, (1986) and Craft *et al.*, (1993) suggesting a more positive accretionary status with increased tidal range is informative.

Allen (1997) draws attention to the benefit of specifying the various parameters within the equation and further states that integration over time provides a mechanism with which to consider the development of either youthful marshes or longer-established coastal wetland sequences. This approach has also been used in verifying the earlier empirical work of Pethick, (1980, 1981) which suggested that total sediment deposition rate declines steeply as a function of increased marsh elevation (Allen, 1990a; French, 1991, 1993).

Numerical modelling over shorter-time periods (e.g. 1 year) requires an alternative strategy of developing a one- or two-dimensional approach (Allen, 1994, Woolnough *et al.*, 1995). This requirement stems from the significant variation in spatial rates of sedimentation over the marsh surface which is influenced by factors such as proximity to marsh creeks and type and density of vegetative growth (French and Spencer, 1993; French et al., 1995; Leonard, 1997). However for longer-term/historical time periods the various zero-dimensional models (e.g. Krone, 1987; Allen, 1990 and French, 1993) do seem to provide an acceptable approach to the simulation of marsh evolution despite the fact that at the time of their inception these models were rather generalised and exploratory in nature. Additionally

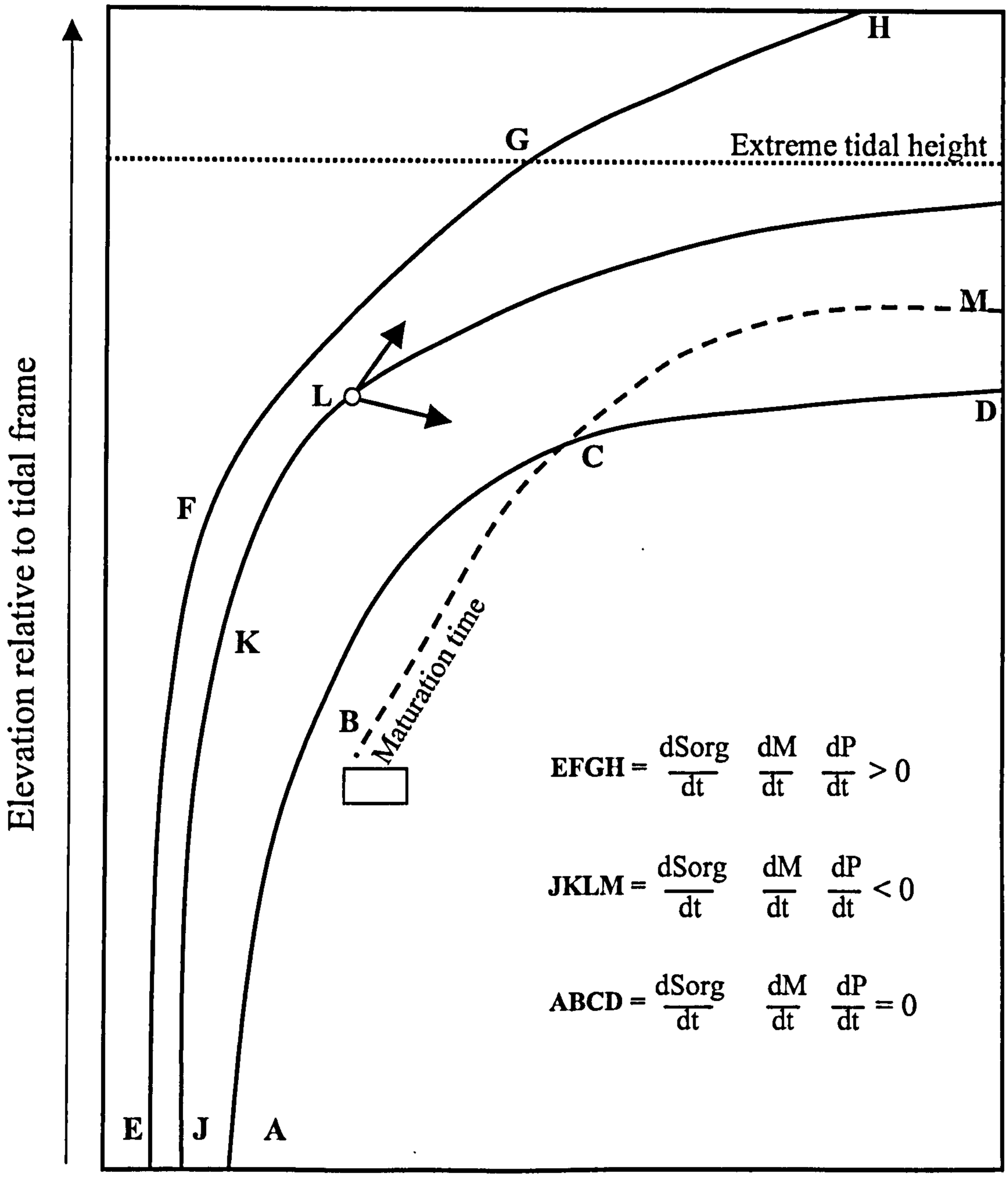

Figure 2.6: Various zero-dimensional models to show pathways of salt marsh growth, after Allen (1990b). The curve ABCD represents the negative feedback loop between marsh surface elevation and tidal inundation frequency and corresponds to the asymptotic relationship identified for the North Norfolk marshes by Pethick, (1982). The curves JKLM and EFGH represent marsh systems dominated by organic peat growth and represent marsh platforms which may attain the upper limits of tidal inundation or even grow above this limit. Adapted from Viles and Spencer (1995).

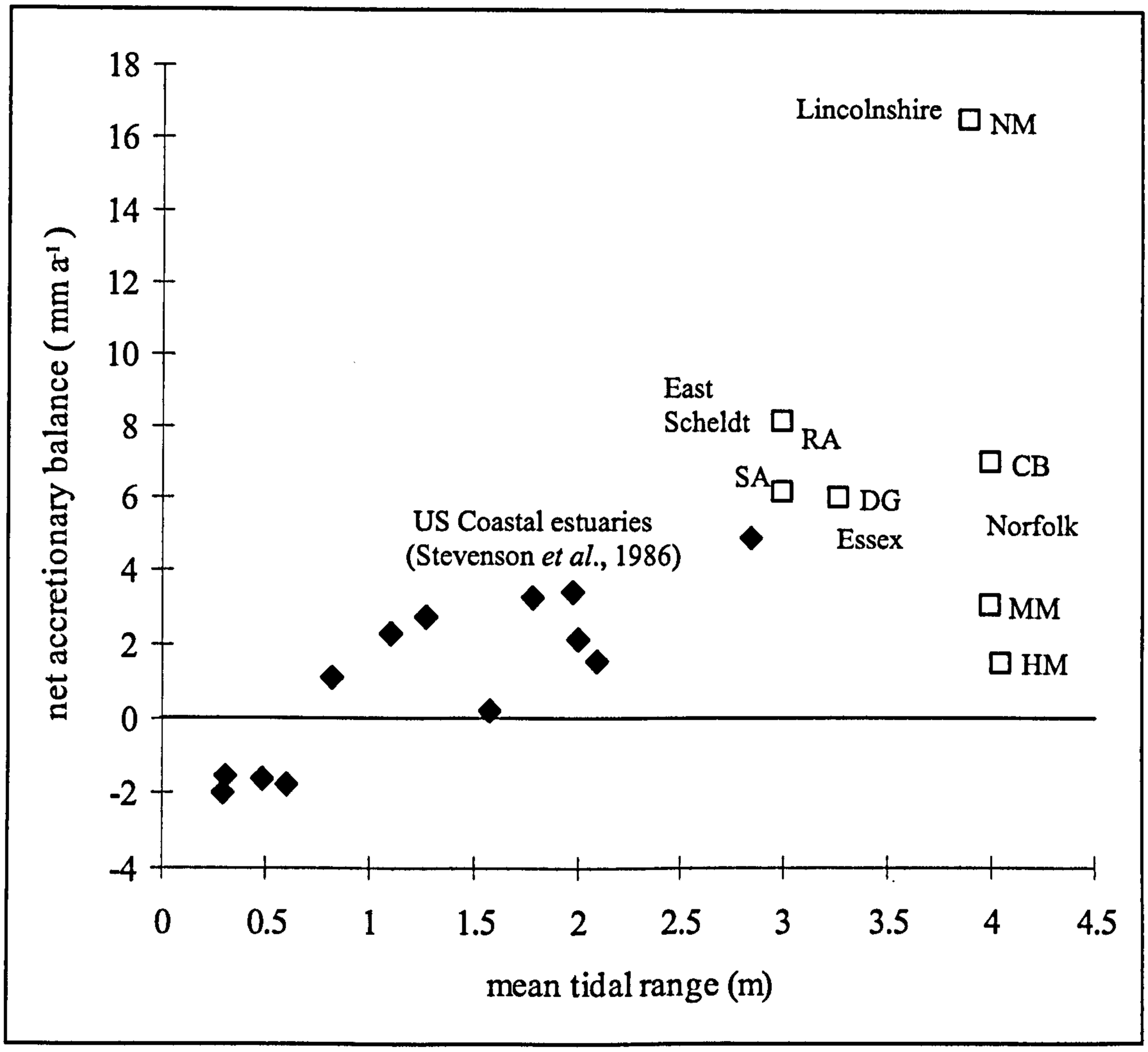

Figure 2.7: Plot of accretionary balance (mean annual accretion-local sea-level rise) versus mean tidal range. (After French, 1994, Source: Viles and Spencer, 1995).

CB = Cockle Bight, Scolt Head Island. MM = Missel Marsh, Scolt Head Island

HM = Hut Marsh, Scolt Head Island. DG = Dengie Marsh, Essex

NM = New Marsh, Gilbratar Point. RA = Rattekaai, East Sheldt, The Netherlands

SA = St. Annaland, East Sheldt, The Netherlands

the mass-balance equations put forward in the models are all based upon the same basic principal of a negative feedback between marsh surface elevation and the frequency of tidal inundation (Temmerman, 2003). This has resulted owing to the continued poor understanding of the complex physical processes occurring over a marsh surface such as flow structure over the marsh platform, the interaction of tidal current velocities with differential vegetative canopies and the influence of variable sediment supply and settling velocities over a tidal cycle. Despite some intermittent studies in recent years (eg: Stevenson *et al.*, 1988; French and Spencer, 1993; Cahoon and Reed, 1995; Boorman *et al.*, 1998; Moller *et al.*, 1999; Christiansen *et al.*, 2000), the recent work of Temmerman (2003) gives some insight into possible methods which may facilitate improvement of the existing models.

2.4: Summary of marsh physical and sedimentary processes

An extensive literature now exists which addresses contemporary coastal wetland evolutionary processes. Many of the more recent studies undertaken have focussed upon the need to quantify the response of these ecosystems to the threat of rising sea-levels in terms of predicting marsh sustainability (Penland and Ramsey, 1990; Gooselink and Sasser, 1995; Titus and Narayanan, 1995; Roman *et al.*, 1987; Reed, 1990, 1995, 2000; Allen and Pye; 1992; Viles and Spencer, 1995).

Vertical marsh accretion is the process by which saltmarshes maintain their position within the inter-tidal profile relative to the normal tidal prism thus preventing deterioration of marsh morphology (DeLaune *et al.*, 1978; Pethick, 1982, 1992). Measurement of accretion and incorporation of such data into existing models provides a framework for understanding the response of these coastal environments to the real threat of rising sea-levels. Additional refinement of modelling parameters will be a distinct requirement to more fully evaluate relationships between sea-level rise, marsh response and physical sedimentary processes occurring on marsh platforms over varying tidal conditions.

Within paraglacial coastal settings which have been experiencing vertical crustal uplift during the Holocene since deglaciation, the application of sediment accumulation measurements and application of modelling techniques will serve as a useful tool for assessing future coastal wetland development in such regions.

2.5: Saltmarsh geochemistry and geochemical processes

As coastal wetlands develop a complex sedimentary sequence consisting of inorganic and organic fractions displaying predominately fine-grained silts and clay particles builds up ultimately forming a marsh platform. The physical processes controlling this sedimentary evolution have been highlighted in the previous sections and include discussion on the linkages to external forcing mechanisms in particular relative sea-level change. Indeed the hydraulic evolution of the marsh platform and depositional setting are primary controlling factors on the geochemistry of marsh sediments (Turner, 1999).

Estuaries represent bodies of water within which significant fine-grained sediment accumulation takes place within the sub-tidal and inter-tidal zones. Owing to the large property gradients exhibited within estuarine waters estuaries can be viewed as sinks for both particulate and dissolved marine inorganic/organic material and that delivered via catchment derived transportation.

Within pristine environments not directly influenced by anthropogenic activities the levels of major elements and trace metals in conjunction with other geochemical and sedimentary characteristics (eg: grain size; mineralogy & organic content) will reflect the natural processes of transport, deposition, adsorption an occlusion taking place within any particular estuarine system. Rates of weathering and erosion taking place within a catchment area coupled with hydrologically driven mixing, sediment deposition and burial within the upper estuarine waters will also influence salt marsh geochemical composition. Tidal inundation of saltmarsh environments will increase the potential for sediment re-suspension and encourages the development of anoxic conditions at depth in the sediment profile.

The natural background geochemistry of a marsh soil will primarily be dependent upon sediment provenance and sediment dynamics of the depositional environment and will be characterised by the diffusion and flux of interstitial pore-water ions that react with the soilid phases within the sediments (Lord and Church, 1983).

Around many estuaries of the world large scale industrial and urban development has resulted in alteration to the natural background geochemical signal recorded within historical marsh sequences. Such alteration is largely due to increased levels of contaminants such as heavy metals, radionuclides and persistent organic compounds derived from either direct release into aquatic systems or from atmospheric deposition (Santschi et al., 1990; Fox et al., 1999). Such contaminants then tend to be incorporated within the fine fraction of estuarine sediments (Cundy et al., 2003). The fine-grained fraction (< 2μm) especially clay

minerals and organic matter have been shown to be preferential to the adsorption and retention of these contaminants supplied to the inter-tidal zone (Allen et al., 1990; Zwolsman *et al.*, 1993; Cundy and Croudace, 1995; Cacador *et al.*, 1996; Cochran *et al.*, 1998). The large adsorption capacity of these sediments can therefore result in marsh sediments becoming significant repositories for both naturally weathered and anthropogenic contaminants.

2.5.1: Why study marsh geochemistry and geochemical processes?

The geochemical study of marsh sediment sequences provides a valuable method with which to study the historically-integrated fluxes of elements to the marsh surface be they natural background concentrations or those influenced by industrial contamination (Vallette-Silver, 1993; Gallagher *et al.*, 1996 Cochran *et al.*, 1998; Dyer, 2001). Additionally, geochemical investigations can offer considerable insight into the historical nature of the sedimentary record within inter-tidal areas and compliment studies of sediment accretion and saltmarsh evolution.

Where marsh environments have become exposed to increased levels of contaminants the possibility of detrimental effects to marsh vegetation are worthy of consideration. 'Die-back' of marsh plants may lead to loss of sediment substrate through erosion which may be significantly enhanced under projected levels of relative sea-level rise (O'Reilly Wiese *et al.*, 1995). This may additionally remobilize pollutants and as such re-introduce contaminants into the water column and hence the food chain. This in turn presents potential problems in terms of health risks to human beings and detrimental effects to estuarine fauna and flora. Remobilization of geochemical constituents may result from physical forcing factors (e.g. erosion of marsh substrate) but may also occur as a result of early diagenetic processes following burial Allen *et al.*, (1990).

Where marsh sediments being studied exhibit elevated levels of contaminants and within areas exhibiting low levels related to background conditions early diagenetic and redox mediated effects on the geochemical signature are important to assess and are of interest.

Additionally, where geochronology is implemented in such studies the effect of early diagenetic processes (eg: redox potential, fluctuating salinity conditions, organic content, pH and microbial activity) on the radionuclides utilised requires rigorous assessment to account for any remobilization of elements that may render the derived geochronology invalid.

2.5.2: Early diagenesis and geochemical processes in coastal sediments

Early diagenetic changes are those that result in the formation of new mineral phases or those that chemically alter existent elemental profiles following sedimentary deposition and burial. Additionally, alteration to the interstitial pore waters and the water column itself can occur through the release of metabolites during organic matter decomposition (Chester, 2003).

Berner, (1980) describes sediment diagenesis as 'the sum total of processes that bring about changes in a sediment or sedimentary rock subsequent to it's deposition in water'.

Most of these changes are redox-mediated i.e. they depend upon the redox conditions within the sediment-interstitial water-estuarine water system (Chester, 2003).

Salt marsh sediments undergo alternating periods of flooding and exposure to air over successive tidal cycles which results in fluctuating redox conditions within marsh soils. Redox conditions are themselves largely controlled by the remineralization of organic matter under oxic conditions. In the majority of marine systems the main method of supply to the sediment surface is via debris deposition. Within salt marsh environments the major input of organic carbon occurs beneath the sediment surface through the development of extensive rhizome root mats. As a consequence the upper sections of marsh soils are rich in organic matter derived from *in situ* production. Underground root production is considered to play an important role in the fluxes of greenhouse gases emanating from the marsh surface and comprises a major proportion of the carbon sequestered in salt marsh sediments (Connor and Chmura, 2000).

Organic carbon remineralization normally occurs through the action of aerobic bacteria which act as a kind of biological catalyst and result in the overall reduction in oxygen concentration progressively down through the sediment column and within the interstitial pore waters at depth. Additional loss of oxygen also takes place when reduced inorganic species such as NH_3, Mn^{2+}, Fe^{2+} and H_2S are oxidised. These reactions are also biologically mediated and will result in oxygen depletion with increased depth in the sediment column (Santschi *et al.*, 1990). The oxidation of organic material leads to the formation of zones within the sediment column which exhibit successively more reduced conditions with depth. This arises as a result of the consumption of available electron acceptors (oxidants) by bacteria in order of thermodynamic advantage (Froelich *et al.*, 1979). Through extensive investigations of organic matter diagenesis Frolich *et al.*, (1979) and Berner (1980) a sequence of diagenetic reactions has been identified commencing with

aerobic metabolism during which oxic diagenesis continues until sufficient oxygen has been consumed to drive the redox potential low enough to favour the next most efficient oxidant (Lewis, 1997; Chester, 2003).

As a consequence continued decomposition of organic material will occur as sub-oxic diagenesis although within salt marsh sediment facies the decomposition of organic matter will be more pronounced in the oxic zone owing to exposure of the upper sediment sections to the atmosphere between tidal inundations (Boulegue *et al.*, 1982). Anaerobic metabolism will continue the process of organic matter breakdown once the dissolved oxygen content falls to extremely low levels or is entirely exhausted and will utilise secondary oxidants including nitrate, manganese oxides, iron oxides and sulphate.

The general sequence of organic matter diagenesis can therefore be written as:

$O_2 \geq$ Mn Oxides ~ Nitrate $\geq$ Fe Oxides > Sulphate > Methanogenesis

Froelich *et al.*, (1979) point out that the fate of nitrogen may influence the sequence described above and suggest that if all the nitrogen in the oxic stage is transformed to N_2 then the use of nitrate as a secondary oxidant will overlap with the use of MnO_2. Additionally if the nitrogen is released as ammonia and not oxidized to N_2 then MnO_2 will be reduced before nitrate and result in subtle changes to the early part of the diagenetic sequence (Froelich *et al.*, 1979; cited in Chester, 2003). It is pertinent to note that the diagenetic processes do not always occur sequentially and that within highly reduced sediments the reduction of sulphate is followed by methanogenesis and these processes can occur simutaneously (Oremland and Taylor, 1978). The sequence of diagenetic zonation has largely been determined from studies of deeper-sea sediments. However it still can be applied to salt marsh environments provided due consideration is given to the extended depth of the oxic upper layer which will, as previously stated, be in the order of decimetres to centimetres rather than a few millimetres (Zwolsman *et al.*, 1993). The general sequence of early diagenetic zonation is illustrated in table 2.1.

Other key diagenetic reactions also take place within salt marsh soils. These include the precipitation of Mn^{2+} and Fe^{2+} as oxyhydroxides within the oxic zone and the reduction of Fe and Mn oxides and hydroxides in the post oxic zone. Additionally the formation of sulphides will proceed if the anoxic zone is rich in Fe (modified from Allen, 1990; cited in Dyer, 2001).

Diagenetic Zone	**Principal Electron Acceptors**
Oxic	O_2
Non-Sulphidic post-oxic (Sub-oxic)	MnO_2 NO_3^- Fe^{III}
Sulphidic	SO_4^{2-}
Non-Sulphidic methanic	CO_2

Table 2.1: Early diagenetic zonation resulting from the oxidation of organic matter (after Berner, 1980 and 1981).

The development of a distinct diagenetic profile can be indicative of mature marsh soils and the behaviour of redox-sensitive elements within this framework provides an indication of the stability of the redoxcline and as such the reliability of any chemical record of deposition (McCaffrey and Thompson, 1980). However, the presence of a dynamic water table commonplace within salt marsh environments may result in significant fluctuations of the redox boundary (Casey and Lasaga, 1987). If this is the case then formation of definitive diagenetic peaks of Fe and Mn are likely to be precluded, (Zwolsman *et al.*, 1993; Cundy and Croudace, 1996). Williams *et al.*, (1994) suggest that the position of the redox boundary can be determined when compared to the frequency of tidal inundation.

Some discussion of the behaviour of redox sensitive elements in an idealised marsh soil now follows.

2.5.3: *The role of Iron* (Fe)

Fe is present in salt marsh sediments as a result of deposition of Fe-bearing particles on the sediment surface and their subsequent geochemical recycling following burial. The proportion of the Fe that reacts with marine sediments is the oxidised fraction and typically this is known to react most readily with sulphides (Kostka and Luther, 1994). This 'reactive'

Fe may only represent a small proportion of the total ferric iron present (Froelich *et al.*, 1979).

Fe oxyhydoxides are significantly more stable under reducing conditions than Mn and the oxidation kinetics of Fe^{2+} are also generally faster than those of Mn^{2+}. As a result diagenetic enrichment of Fe within the sediment column will occur at greater depths than the diagenetic enrichment of Mn (Zwolsman *et al.*, 1993). Brumsack and Gieskes (1983) have used thermodynamic calculations to predict the reduction of Mn^{4+} before the reduction of Fe^{3+}. These authors show that the zone of Mn^{4+} reduction is generally situated between the zone in which reduction of nitrate occurs, i.e. within the oxic zone and that in which sulphate reduction takes place i.e. under anoxic conditions.

In the schematic diagram of Froelich *et al.*, (1979), (figure 2.9), dissolved Fe^{2+} is produced within zone 7 as a consequence of ferric oxide reduction and the oxidation of organic carbon. The dissolved Fe then tends to diffuse upward through the interstitial pore water where it is consumed at the top of zone 7. Only a small proportion of the total Fe in sediments is mobile which may be due to ferric oxyhydroxide coatings on the surface of the mineral lattices. Reactive Fe in the solid phase has a pronounced effect upon salt marsh soil geochemistry and that within deeper ocean sediments and determines the formation of pyrite, release of phosphates and the sequestering of trace metal concentrations (Kostka and Luther, 1994).

The rate of diagenetic reactions involving Fe and Mn solubility are much faster than processes such as diffusion and mixing resulting from bioturbation and are also responsible for changes in redox potential (Eh), (Brumsack and Gieskes, 1993).

2.5.4: *Manganese* (Mn)

Both manganese and iron are dominant participants in the bacterially driven aquatic redox processes (Dyer, 2001). Manganese oxyhydroxides are deposited on the marsh surface as mineral coatings and are then buried as sediment accumulation takes place (assuming +ve accretionary status, section 2.3.5). In figure 2.8. a schematic representation of Mn and Fe remineralisation is shown. At the point at which the deposited sediment passes through zone 4 MnO_2 is reduced to Mn^{2+}. The Mn^{2+} then diffuses upward through the sediment column where it becomes oxidised and re-precipitated. The zone at which reduction takes place i.e. zone 4, will migrate upward through the sediment sequence at the same rate at which sediment accumulation is occurring. As new sediment is deposited any new MnO_2 passing

into zone 4 will be remobilized in the same manner. This results in a type of sedimentary trap within steady-state systems in which Mn becomes sequestered within the sediment column and subsequently concentrated into a layer highly enriched in Mn situated in narrow zone at the redox boundary (Lynn and Bonatti, 1965; Froelich *et al.*, 1979; cited in Chester, 2003).

McCaffrey and Thompson, (1980) suggest that a strong diagenetic processes is responsible for the occurrence of a maximum peak in dissolved Mn occurring below a solid phase peak in Mn involving reductive dissolution of Mn^{4+} and re-oxidation of Mn^{2+}. The resulting pore water and solid phase profile is shown in figure 2.9.

2.5.5: *Sulphur* (S)

Sulphate ions found within offshore marine sediment interstitial pore-waters are largely derived from the overlying water column. The supply of sulphate ions to salt marsh pore waters occurs during periods of tidal inundation. Sulphur atoms have the capacity to undergo many oxidation state changes (over an eight electron shift) and to form a large variety of chemical compounds. This results in sulphur being intimately involved in a large number of biogeochemical reactions (Lewis, 1997). Within marsh soils the key chemical reaction sequence of interest is the role sulphur plays in catabolic enzymatic processes. Baterially-catalysed reduction of sulphate ions under anoxic conditions releases energy utilised in metabolic processes and results in the production of hydrogen sulphide (H_2S). Sulphate reduction normally occurs beneath the zone of Fe reduction in anoxic sediments and the production of H_2S is usually accompanied by production of associated metal sulphides (e.g. FeS). The measurement of sulphate ion reduction rates have demonstrated that pore water distribution of sulphate ions within marsh sediment sequences are only a reflection of the net outcome of diagenetic reactions (Thamdrup *et al.*, 1994). Additionally the variable predominance of different sulphur species in marsh pore waters also dictates the distribution of authegenic mineral phases. Of these phases the formation of pyrite represents the only thermodynamically stable iron and sulphur compound present in marine sediments (Berner 1967). Pyrite formation also ultimately controls the sedimentary burial of these minerals in salt marsh sediments (Cutter and Velinsky 1988; Lewis, 1997).

A number of studies have been conducted to explore the mechanisms responsible for pyrite formation within salt marsh sediments (Nedwell and Abraham 1978; Howarth, 1979; Howarth and Teal 1979; McCaffrey and Thompson 1980; Luther *et al.*, 1982; Lord and Church, 1983; Giblin and Howarth, 1984; Luther and Church, 1988). Some of these studies

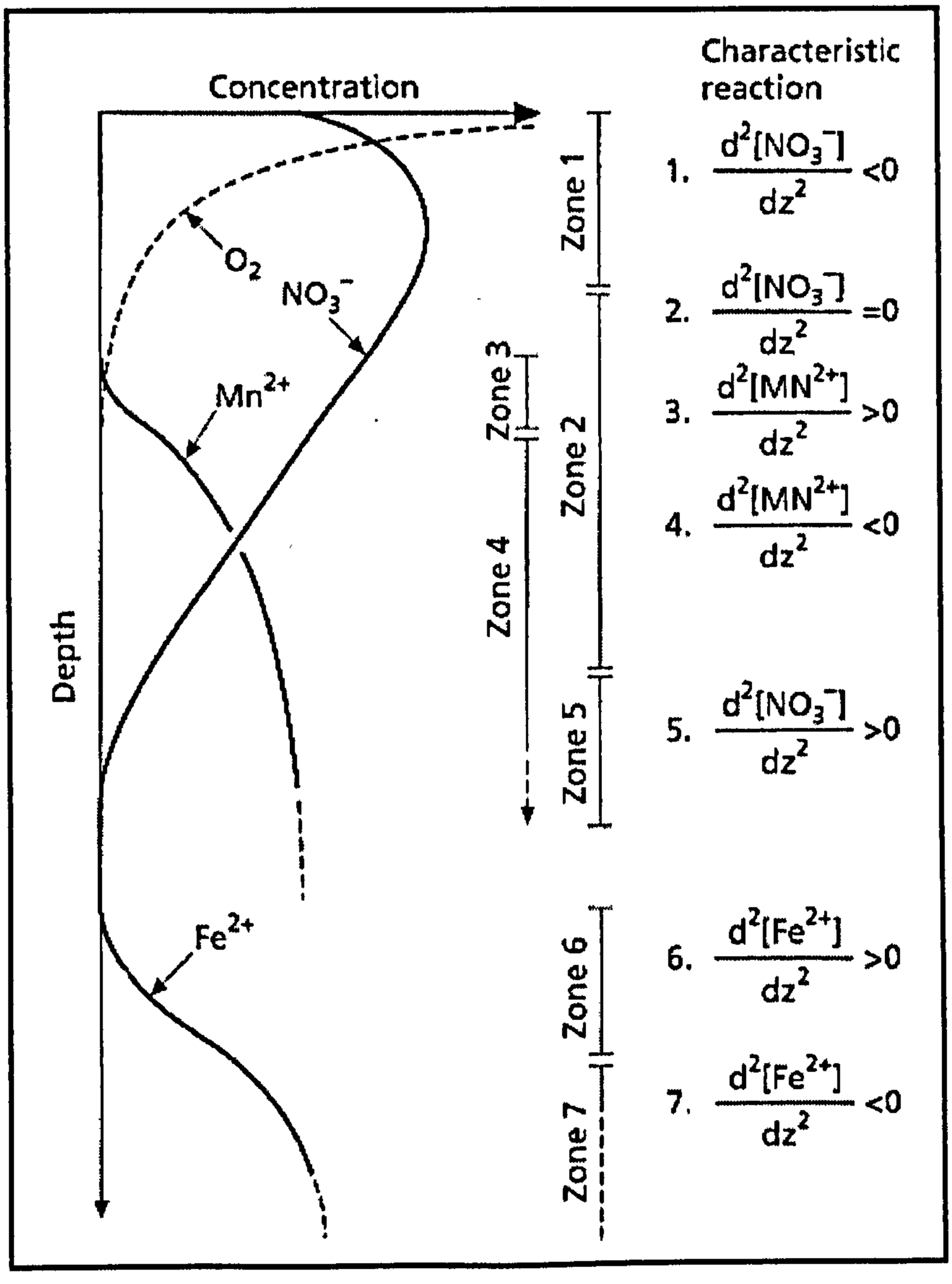

Figure 2.8: Schematic representation of Oxygen, Nitrate, Manganese and Iron trends in pore water profiles and diagenetic zonation (After Froelich *et al.*, 1979)

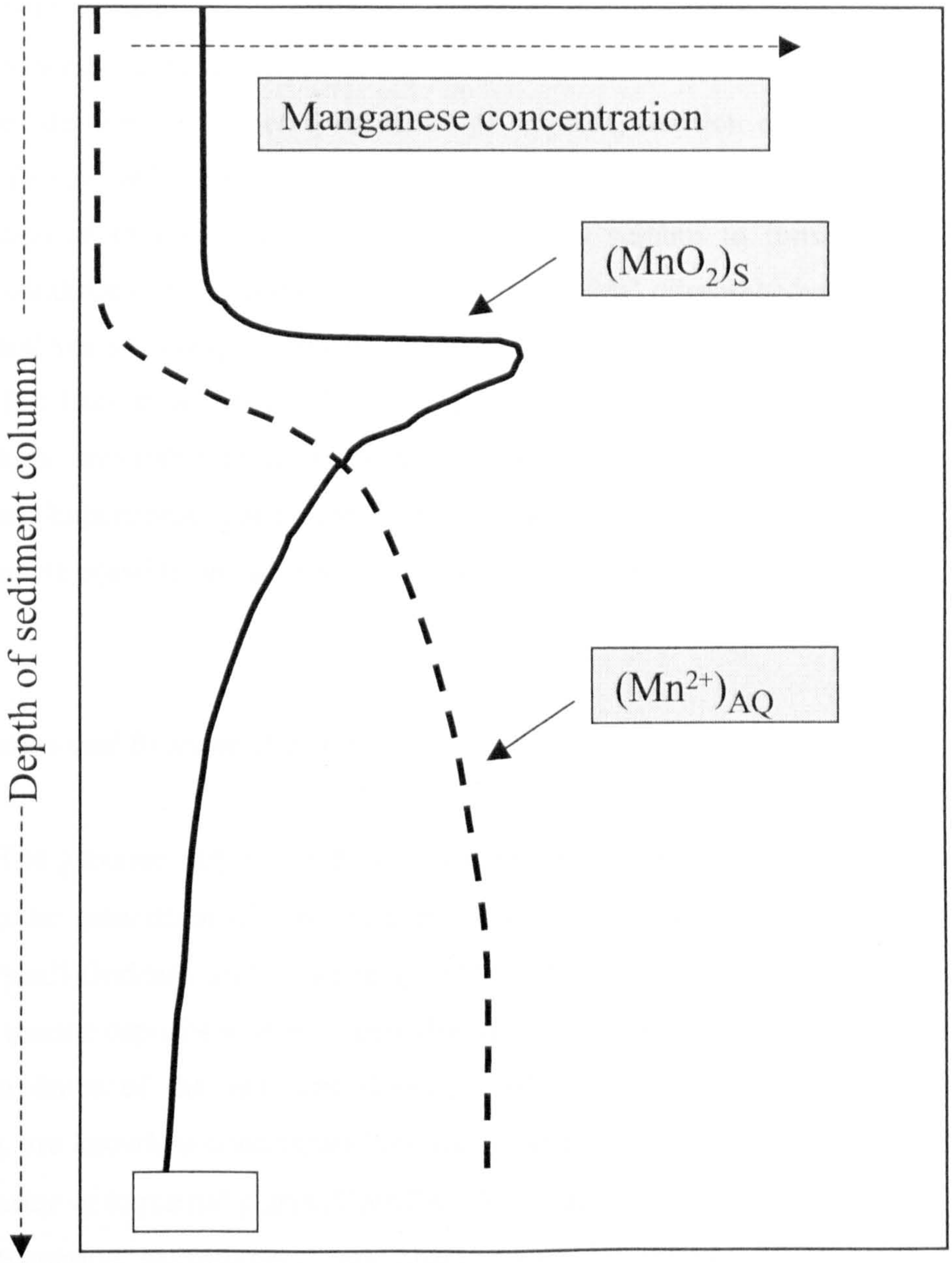

Figure 2.9: Diagramatic representation of Mn solid and aqueous phase remobilization within deep ocean sediments under steady state conditions. (After: Froelich *et al.*, 1979).

have concluded that two forms of pyrite are generally present within the inter-tidal sedimentary environment. These are single crystalline Rickard (1975) and framboidal pyrite which have also been empirically investigated by Berner (1970) and Goldhaber and Kaplan (1974). In the earlier study of Berner (1970) the mechanism for marine pyrite formation involves the reaction of iron monosulphides (FeS) with elemental sulphur and/or polysulphides present in the sediment matrix or the interstitial pore water. The general reaction scheme can be described as a sequence intrinsic to that of organic matter synthesis. This takes the form of bacterial reduction of sulphate, reaction of H_2S with Fe_3 minerals forming Fe monosulphides such as mackinawite ($FeS_{0.94}$) and greigite (Fe_3S_4), followed by the reaction of iron monosulphides with elemental sulphur to form pyrite. Under such reaction conditions crystallisation of pyrite as framboidal microspheres takes place and may take several years to complete despite abundant concentrations of sulphate ions.

The later study by Goldhaber and Kaplan (1974) suggest that there may be two mechanisms favourable to pyrite formation which operate under differing geochemical conditions. Experiments conducted by these authors concluded that direct precipitation of pyrite may be possible through the reaction of Fe_2 minerals with polysulphides.

2.5.6: *Iodine and Bromine* (I & Br)

The geochemistry of the halogens within marine sediments is of particular interest owing to the association of these elements with marine organic matter (Price and Calvert, 1977; Upstill-Goddard and Elderfield, 1988). The particular ratio of either halogen in surficial marine deposits will be largely dependent upon the nature of organic matter and the oxidation status of the sediment (Lewis, 1997). Many marine organisms, in particular plankton, are known to concentrate both iodine and bromine to markedly higher levels than either marine or terrestrial plants (Upstill-Goddard and Elderfield, 1988).

Estuarine environments are characterised by mixing of terrigenous catchment derived organic material and that derived from marine sources. As such estuarine sediments may often display halogen/organic carbon ratios that are much lower than those from sites further off shore. Previous studies have indicated large variations in Br/C_{org} ratios from different geographical locations however, the ratio at any particular sample site tends to be quite constant. ten-Haven *et al.*, (1988) point out that this is not the case for all estuaries. Some examples of typical I/C_{org} and Br/C_{org} values for various nearshore and estuarine surficial sediments are presented in table 2.2.

Both iodate (IO_3^-) and iodide (I^-) species of iodine are associated with the redox geochemistry of this element. Within the oxic and anoxic zones of marine sediments IO_3^- and I^- will exhibit distinct and prominent enrichment in either of these geochemical environments resulting from remobilization within the sediment column (Thompson *et al.*, 1995). Conversion of iodate within sediment pore waters to iodide takes place at pH ~ 8.1 and pE of 10.5. This is slightly below the pE value for the reduction of nitrate in the oxic (upper zone). Iodine is therefore used as both an electron acceptor and donor during stages of organic carbon remineralization (Shimmield and Pederson, 1990). The oxidation status of the sediment exerts a strong influence upon the relationship between iodine concentrations and levels of organic carbon (Price and Calvert, 1977).

Geographical Location	**I / C_{org}**	**Br / C_{org}**	**Study Reference**
Barents Sea	380	120	Price et al., (1970)
Namibian Self	20-250	40-130	Price and Calvert (1977)
Panama Basin	50-395	146	Pederson and Price (1980)
Various Continental Margins	265	131	Shimmield and Pederson (1990)
Loch Etive, Scotland	160	180	Malcolm and Price (1984)
Tamar Estuary, UK	20-65	5-35	Upstill-Goddard and Elderfield (1988)

Table 2.2: Reported values for I/Corg and Br/Corg ratios in surficial marine sediments from various geographical locations. (Units are ppm halogen / wt. % organic carbon; modified from Lewis 1997).

The redox geochemistry of bromine is far less complicated owing to the fact that bromine only exists with an oxidation status of $^-1$. This results in bromine being largely unsusceptible to redox-mediated speciation changes and commonly bromine profiles within marine sediments tend more closely resemble the pattern of organic carbon distribution (Lewis, 1997).

The physical and chemical mechanisms governing the binding of both iodine and bromine to organic material are still poorly understood and very few published works exist

that explore these processes. Of notable exception with regard to bromine is the study undertaken by Harvey (1980) who used a series of chemical extractions to ascertain that bromine exists in a variety of water-soluble and organic-soluble states within marine sediments. Francois (1987) showed that humic substances can reduce iodate to electropositive species including HOI and I_2. These are then able to substitute onto the organic molecules. Work by Price and Calvert (1977) indicated that iodide-bearing solutions were not taken up in significant quantities by organic-rich material from experiments conducted using reduced sediment conditions.

However in the same study these workers postulate that hypoiodous acid and I_2 can be produced from I^- during oxidation by iodine oxidase which is an enzyme present in the early degradation products of marine plankton (Price and Calvert, 1977). This enzymatic reaction requires the presence of free oxygen and is thought to be absent in reducing conditions within marine sediments (Shimmield and Pederson, 1990). These authors further concluded that the predominance of either IO_3^- or I^- within the marine sediments studied is dependent upon the oxidation status of the interstitial pore waters. As such any enrichment of iodine within the organic fraction will be entirely due to redox-controlled sorption processes (Shimmield and Pedersen, 1990).

From studies conducted thus far observed exponential decline of I/C_{org} with depth is fairly commonplace (e.g. Pedersen and Price, 1980) and is indicative of the preferential release of iodine under microbial decomposition. Redox-zonation within marine sediments can influence the relationship between I to Br and sorption of these elements onto C_{org} (Thompson *et al.*, 1995). A less dramatic decline and in some cases an increase in the Br/C_{org} ratio with depth appears to be typical of continental margin sediments as reported by Price and Calvert (1977). This would seem to indicate that bromine is more strongly bound to the organic carbon components of these sediments than iodine. Further enrichment of bromine at depth may be as a result of degradation and loss of organic carbon relative to bromine causing a residual enrichment effect (Mayer *et al.*, 1981).

2.5.7: The influence of coastal wetland vegetation on marsh geochemical processes

Salt marsh vegetation typically ranges across the marsh surface in response to salinity gradients largely determined by marsh platform altitude relative to the tidal frame, seasonally mediated rainfall, rates of evapo-transpiration and solute exchange within the sediment. Rainfall has been suggested as being as important as tidal flooding in controlling the surface water composition for much of the year in some locations (Casey and Lasaga,

1987). The vigour of marsh plants will also be controlled as a function of seasonality resulting in variation in growth and decay rates. Decay of organic material is also enhanced by direct exposure of the marsh surface to atmospheric oxygen over the tidal cycle.

In many salt marsh environments the bulk quantity of organic matter is produced below the surface as a consequence of root/rhyzome growth. This variability in organic matter production and decay is accompanied by variation in the oxidative capacity of sediment pore waters which surround the plant roots owing to seasonally regulated photosynthetic activity of the halophytic plant communities. As a consequence of these processes rates of sulphate reduction tend to vary significantly over depth and time (Lord and Church 1983; Howarth and Teal 1979).

The presence of salt marsh vegetation within the sediment sequence provides a mechanism which enables atmospheric O_2 to enter the marsh soil. An additional source of O_2 is also derived from the root-mass of the vegetation whereby oxygen is directly injected into the soil structure. These biologically mediated processes result in distinct influences to the geochemical signature recorded within salt marsh sediments.

A notable consequence is an increase in the depth to which the upper oxic layer extends. This can be several orders of magnitude greater than that recorded within other (deeper) marine sediments. Zwolsman *et al.*, (1993) identified an increased depth of the oxic boundary in marsh sediments of the Westerschelde estuary, Netherlands in the order of cm – dm compared to deeper ocean sediments which are typically in the order of only a few millimetres.

In more sandy coarser-grained sediments this depth can extend to 40 cm (Williams *et al.*, 1994). The increased depth to which the oxic zone has been shown to extend within salt marsh soils has implications for the diagenetic signals of Fe and Mn. These key indicators of the redoxcline can have peaks that are also separated by several centimeters indicative of the differing redox conditions between salt marsh environments and other marine sediments.

The depth of the oxic boundary can also be influenced by seasonally controlled organic matter production with increased oxygen levels penetrating the marsh soil during warmer periods when photosynthetic processes are elevated (Williams *et al.*, 1994).

The injection of O_2 into the marsh soil structure can also result in the formation of oxidising microenvironments (Dyer 2001) which encourage both Fe and Mn oxides to precipitate from the pore waters surrounding the root-mass. As a consequence of this distinct rhizo-concretions can be seen in many coastal wetland sediment sequences with examples being described in the study by Sunby *et al.*, (1998). These authors describe an iron rich

plaque evident on the outer layer of the roots of *Spartina* species derived from the precipitation of Fe2+ present in the pore waters surrounding the roots. Furthermore they postulate that the localised redox boundary extends radially outward from the root structure as Fe is precipitated thus extending the zone of direct precipitation further into the soil structure.

2.5.8: The influence of early diagenetic and geochemical processes on the behaviour of contaminants and pollutants within coastal wetlands.

The silty and clay rich nature of many estuarine inter-tidal sediments has lead to the generalised view that salt marsh environments and associated mudflats tend to act as sinks for suspended particulate matter, nutrients and trace metals. The natural (or background) levels of trace metals are a reflection of the combination of inputs to estuaries derived from local catchments and marine sources, Rae (1997). Natural levels of trace metals in estuarine sediments are now only found in so-called pristine areas where the influence of industrial development has been non-existent or extremely low and has not increased levels to above background values (Van Alsenoy *et al.*, 1993)

Many north-european marshes have witnessed a large increase in levels of industry situated in close proximity to the coast. As a result of such activities marsh sediment sequences from many sites previously studied reveal an historical record of elevated levels of trace metals derived from industrial processes, (McCaffrey and Thompson, 1980; Allen and Rae, 1986; Rae and Allen, 1993; Cundy and Croudace, 1995; Croudace and Cundy, 1995; O'Reilly Wiese *et al.*, 1995; Cundy *et al.*, 1997; Cearreta *et al.*, 2000; Lloyd, 2001).

The diverse interest in estuarine environments has lead to concerns relating to the bio-availability of trace metal contaminants and relationship to environmental health Rae (1997).

Within natural aquatic environments such as estuaries the speciation and chemical reactivity of trace metals play an additional role in parallel with element concentrations that determine the bio-availability and degree of toxicity to both fauna and flora (Morse, 1994; O'Reilly Wiese *et al.*, 1995).

Many of the physio-chemical processes governing the accumulation, mobility and bio-availability of metals in salt marshes are still poorly understood (Allen and Pye, 1992). In recent years however these inadequacies have become less problematic with several publications relating to in-depth investigations of some of the problems encountered in assessing trace metal contamination within the inter-tidal zone . Notable among these

studies is the extensive review by Williams *et al.*, (1994) and Rae (1997). These authors provide a detailed explanation of many of the key processes controlling the behaviour and bio-geochemical status of contaminated marsh areas.

Some of the key points to emerge from these works relate to the difficulty arising from treating salt marsh environments as a simple system. A number of inter-linked physio-chemical processes are responsible for trace metal mobility and bio-availability. These include estuarine circulation, periodicity of tidal inundation and sediment supply which in turn control a variety of physical and chemical parameters including:

- salinity gradients over the marsh surface,
- vegetation zonation and organic matter content
- temperature
- redox potential (Eh) and pH.
- sediment type and particle size distribution
- levels of biotubation within the sediment column

Additionally, these processes are significantly affected to variable degrees by differences in the type and quantity of trace metals delivered to the marsh surface via the variable mechanisms responsible for input (Williams *et al.*, 1994).

Trace metal profiles can be significantly altered by early diagenetic processes which influence the dissolved and the solid phase distribution of metals in sedimentary sequences (Panutrakul and Baeyens, 1991). During the early diagenetic breakdown of organic matter trace metals associated with this fraction of the sediment profile can be remobilised as can those more associated with the reactive mineral phases such as Fe and Mn oxides owing to chemical dissolution owing to reduced Eh and pH conditions (Morse, 1994).

Trace metals that become remobilised from Fe and Mn oxy-hydroxides during early diagenetic reactions can also become co-precipitated with and adsorbed onto authigenic sulphide minerals within the anoxic zone of marsh sediments (Morse, 1994). Cu, Pb, Zn and As are good examples of such metals (Dyer, 2001). As a consequence of this process the potential exists for iron sulphides to become secondary type sources of contamination during oxidation of reduced sediments. This mechanism is likely to be prevalent in salt marsh environments owing to the fluctuating nature of the redoxcline resulting from variable periods of tidal inundation. Huerta-Diaz and Morse (1990) identify three mechanisms by which trace metal concentrations are controlled in the presence of sulphides. These are namely, formation of solid solutions from Fe and other metal sulphides: precipitation of pure

metal sulphides and adsorption of trace metals on pre-existent Fe sulphides present within the sediment sequence.

2.6: Summary of marsh geochemical processes and their importance in coastal wetland development

A detailed overview of marsh geochemical processes has been presented in the preceeding sections and this attempts to draw attention to some of the key influences likely to affect the historical record of sediment deposition within marsh environments.

Importantly, consideration is focused on the diagenetic (post burial) reactions which mediate this signature. These include bacterially driven remineralisation of sulphur compounds and the redox driven diagenetic behaviour of elements that are sensitive to fluctuating oxidation and reduction conditions characteristic of inter-tidal sedimentary environments.

In any intended study of saltmarsh development that incorporates geochronological constraint of marsh sediment accretion via geochemical/radiometric techniques a comprehensive assessment of the diagenetic signature and behaviour of the key redox-controlled elements is required to ensure the robustness of any derived interpretation relating to depositional history.

Geochemical investigations of historical sediment accumulation within salt marsh environments have typically relied upon the use of techniques such as ^{210}Pb dating of discrete sediment horizons from acquired cores. Often such studies require the use of additional chemically differing radionuclides (e.g. ^{137}Cs; ^{241}Am) to compensate for any post-depositional remobilization. Geochemical assessment of the redox status and post-depositional diagenetic signature within such sediments serves as a robust method with which to further assess whether any post-depositional re-mobilization of key elements has affected the integrity of the dating methods.

Details of the analytical techniques employed in this study are now presented in the following chapter.

Chapter Three

Analytical Methods

3.1: Introduction

Analysis of recent salt marsh sediments have been used extensively to gain insight into geo-morphodynamic processes occurring within low-lying coastal settings (Letzsch and Frey, 1980a; Pethick, 1981; Allen. 1988; Carter *et al.*, 1989; Patrick and DeLaune, 1990; French, 1991; Pethick, 1992; French and Stoddart, 1992; French, 1993; French and Spencer, 1993; French *et al.*, 1994; Pye, 1995; Callaway *et al.*, 1996; Reed, 1998).

The application of other multi-proxy methods including micro-palaeontology and geochemistry to such studies (e.g. McCaffrey and Thompson, 1980; Gehrels, 1994; Cundy *et al.*, 1996; Cundy *et al.*, 1998; Horton *et al.*, 1999a; Cearreta *et al.*, 2000), provides the basis for further assessment of recent environmental change and anthropogenic impacts upon present-day salt marshes.

This study seeks to investigate morphological changes with respect to sediment accretion and changing marsh elevation using a multi-proxy methodology. The study employs both geochemical and microfossil analytical techniques and focuses upon radiometric dating methods and the distribution of natural and artificial radionuclides (specifically, ^{210}Pb, ^{137}Cs and ^{241}Am) within marsh sediment sequences as tool for geochronological control of marsh development and modelling of accumulation processes. Other specific techniques include the determination of major and trace element distribution within the cores to provide detail of marsh composition, post-depositional geochemistry and assessment of any anthropogenic impacts to the coastal lowlands. Microfossil analysis, in particular diatoms are used to provide ecological detail of environmental change within the one of the cores.

This chapter gives a detailed overview of these various techniques used and an account of the analytical work undertaken now follows.

3.2: Radiometric dating techniques

3.2.1: Geochronology using ^{210}Pb

The measurement of radioactive decay provides the principle basis for a wide range of dating techniques within the geological sciences. Carbon-14 (^{14}C) has been used extensively for the dating of older coastal sediments (e.g. Shennan *et al.*, 1995) however sedimentary depositional processes occurring within the coastal zone also take place over considerably shorter time-scales and, hence, are not capable of being dated using the conventional ^{14}C method.

In the latter part of the last century there has been a substantial increase in the volume and range of studies focussed upon recent sedimentation and sedimentary processes (Appleby and Oldfield, 1992). In order to obtain a reliable chronology for the more recent historical development of many sedimentary environments the use of radioisotopes with shorter half-lives than that of ^{14}C and more applicable to the time-scale of the processes being studied are required.

The naturally occurring radioisotope ^{210}Pb, part of the ^{238}U decay series, has a radioactive half-life of 22.26 years (Appleby and Oldfield, 1992). This makes this isotope a highly appropriate dating tool with which to study recent sedimentary processes and historical development. Following the seminal paper of Goldberg (1963) in which the author measured accumulation rates upon a Greenland glacier using ^{210}Pb other authors soon extended this work (e.g. Crozaz *et al.*, 1964; Crozaz and Langway, 1966).

The application of ^{210}Pb to sedimentary environments occurred early within the following decade with the study of lake sediments undertaken by Krishnaswami *et al.* (1971). Koide *et al.* (1972) applied the technique to marine sediments and later studies by Armentano and Woodwell (1975), Benninger *et al.* (1975) and Nittrouer *et al.* (1979) to name but a few, established the applicability of the method to a wide range of environmental settings.

^{210}Pb has now been used extensively in a large variety of environmental investigations ranging from studies of atmospheric behaviour (Kim *et al.*, 2000), floodplain sediment deposition (He and Walling, 1996), oceanic sedimentary processes (Norton-Smith *et al.*, 1987; Crusius and Anderson 1991), lake sediment studies (Pennington *et al.*, 1976; Binford 1990; Gale *et al.*, 1995; Alvisi and Frignani, 1996) and a large number of coastal/estuarine studies (e.g. Chanton *et al.*, 1983; French *et al.*, 1994; Cundy and Croudace, 1996; Cundy *et al.*, 1998; Goff *et al.*, 1998; Kirchner and Elhers, 1998; Turner, 1999).

The development of the ^{210}Pb dating technique and its applicability as a geochronological tool for use with recent sediments has been extensively reviewed by Appleby and Oldfield (1992). A summary of the important points that need to be fully understood by potential researchers now follows.

3.2.2: The geochemistry and formation of ^{210}Pb

^{210}Pb is a naturally occurring radionuclide and is one of many radio-isotopes that constitute part of the ^{238}U decay series. A simplified graphical illustration of this decay series is shown in Figure 3.1. Decay of the parent isotope ^{226}Ra (half-life ($t_{1/2}$) = 1600 years) present in the solid bedrock via series of relatively short-lived daughter isotopes results in the formation of ^{210}Pb secular equilibrium with ^{226}Ra. Within this closed system ^{210}Pb present is referred to as being the supported component ($^{210}Pb_{supported}$).

Disequilibrium between ^{210}Pb and ^{226}Ra occurs in open systems as a result of the loss and subsequent decay of the intermediate inert gaseous isotope ^{222}Rn ($t^{1/2}$ = 3.8 days) from the solid matrix. This occurs either via diffusion through the interstices of soils and crustal rocks or due to recoil on ejection of an alpha particle (Appleby and Oldfield, 1992). Following diffusion of ^{222}Rn into the atmosphere ^{210}Pb is formed via a series of short-lived decay reactions that take place whereupon ^{210}Pb is rapidly adsorbed onto atmospheric aerosols.

3.2.3: Pathways of ^{210}Pb to surface sediments: Atmospheric Deposition

The formation of $^{210}Pb_{excess}$ in the atmosphere results in rapid adsorption onto aerosols whereby removal is facilitated by wet and dry depositional processes. Residence time for atmospheric $^{210}Pb_{excess}$ and hence flux to the earth's surface will largely be determined by geographical position and climatic conditions (Turner, 1999). Appleby and Oldfield (1992) identify that global patterns of $^{210}Pb_{excess}$ fallout are strongly influenced by the movement of air masses over continental areas where diffusion of ^{222}Rn occurs and over oceanic regions where depletion of $^{210}Pb_{excess}$ takes place.

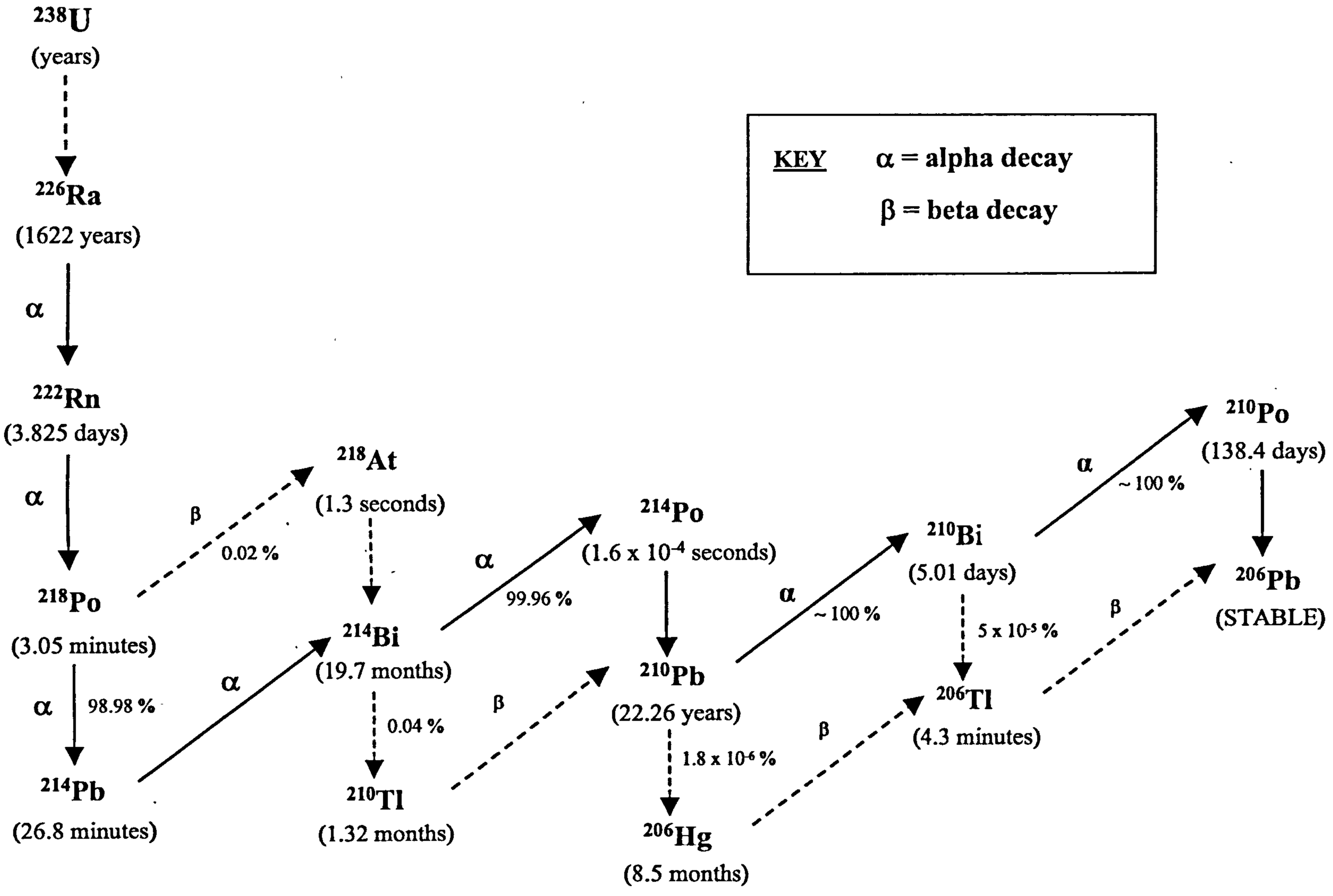

Figure 3.1: Schematic representation of the 238-Uranium decay series and the genertion of ^{210}Pb (Source: Wise, 1980)

Additionally, seasonal variation between wet and dry depositional process within a defined geographical region will also influence annual atmospheric $^{210}Pb_{excess}$ flux (Turekian *et al.*, 1977). Periods of low rainfall will also enhance the contribution of dry fallout which constitutes a proportion of the total flux to the surface over a given time period.

Average residence times for atmospherically derived ^{210}Pb within the northern hemisphere range from between 5-10 days (Wise, 1980) and various studies have highlighted the inverse correlation between ^{210}Pb concentration and average rainfall for sites within the UK (Peirson *et al.*, 1966; Lewis, 1997; Smith *et al.*, 1998). These range from 41 ± 4 Bq m^{-1} yr^{-1} to 147 Bq m-1 yr^{-1} with a mean annual flux of 62 ± 8 Bq m^{-1} yr^{-1} reported for the Solent. Lewis (1997) has estimated that the dry fallout represents approximately 40% of the total ^{210}Pb flux based upon calculations of measured data and derived via the method of Turekian (1977). This is in good agreement with the dry fallout estimations over the Netherlands reported by Zuo (1992).

Estimations of historical fluxes of ^{210}Pb may be a matter for some conjecture when consideration is given as to how representative these are with respect to the true average for a given studied area. Peirson *et al.* (1966) have noted that short term variability in the flux of ^{210}Pb derived from wet depositional processes may not be compensated for by calculation of averages taken over a short time period of say only a few years. Additionally, Turekian *et al.* (1977) draw attention to the potential influence of various meteorological processes on ^{210}Pb fluxes at any given location and highlight that assessment of several years worth of data may in fact fix the calculated average flux to no better than between 10-50%.

Independent estimation of the historical deposition rate at a give location may be possible by obtaining long-term average annual rainfall from the Meteorological Office and the mean UK relationship between rainfall and ^{210}Pb flux calculated by Smith *et al.* (1998). The theoretical value of 58 ± 11 Bq m^{-2} yr^{-1} have been shown by Lewis (1997) to be in good agreement with values obtained for the Solent region of southern England indicating that this approach may be a more representative method with which to assess true historical flux. A schematic diagram to illustrate the modes of supply to coastal marsh environments is depicted in Figure 3.2.

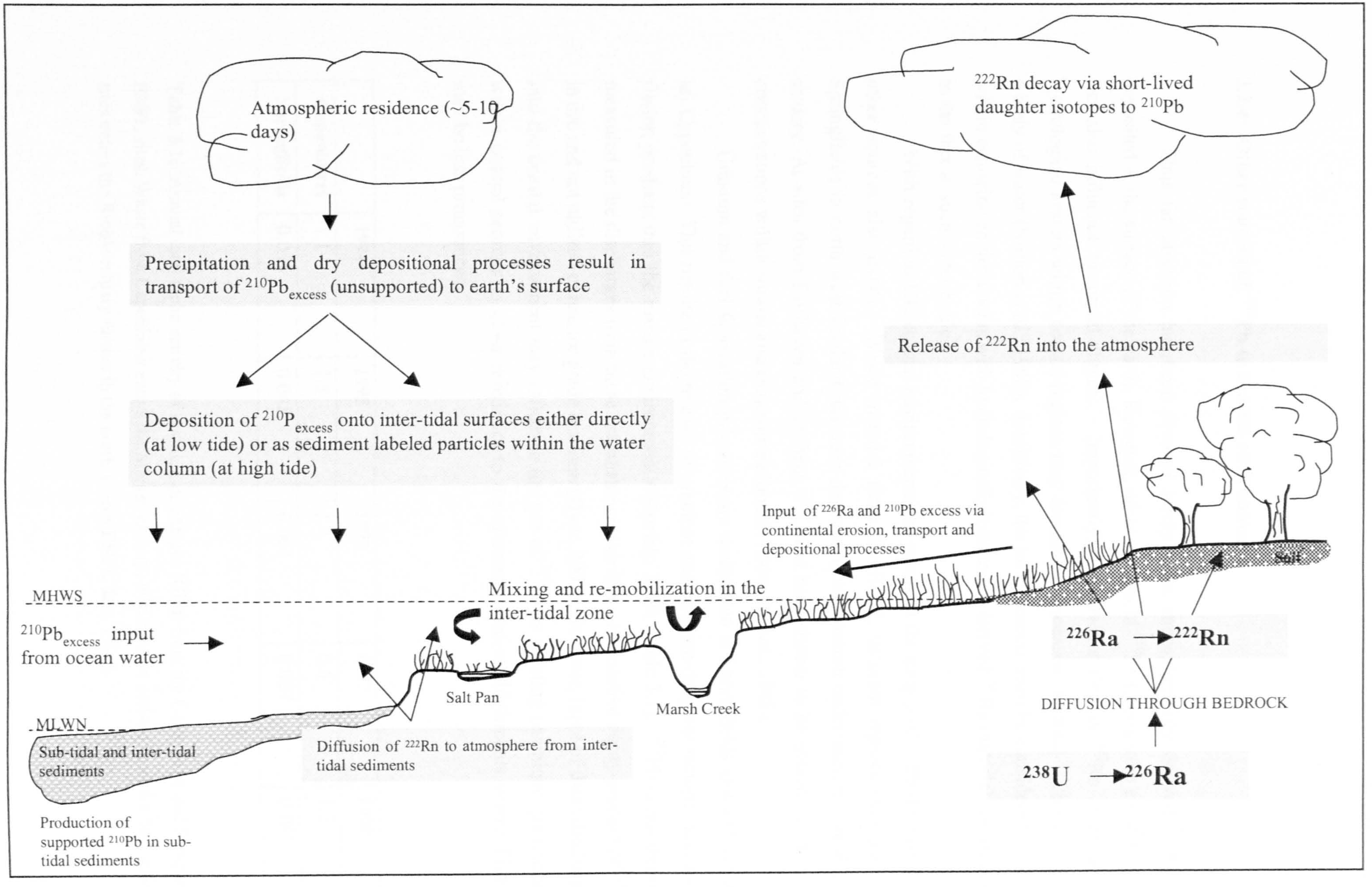

Figure 3.2: Schematic diagram to show the formation of ^{210}Pb, transport pathways and mode of supply to the saltmarsh environment (adapted from Wise (1980).

3.2.4: Other sources of ^{210}Pb to coastal environments

Thus far attention has been focused solely upon atmospherically derived $^{210}Pb_{excess}$ deposited at the surface of the earth. However, other sources of ^{210}Pb to estuarine environments can also influence historical fluxes. Importantly, groundwater rich in ^{222}Rn entering the hydrological system within coastal regions may dramatically increase the total ^{210}Pb supplied to a body of water (Norton *et al.*, 1995). Intuitively, the same process must be considered to occur within estuarine environments with hydrologically/catchment derived ^{226}Ra material contributing to the flux to such water bodies.

With regard to UK coastal environments the potential for supply of ^{210}Pb derived from other sources also exists. Waste material from the BNFL uranium reprocessing plant at Springfields in north west England has been detected from research undertaken on the Ribble estuary. At sites from Fairhaven and Lytham, ^{238}U has been shown to be present in elevated concentrations within coastal and estuarine sediments (Bonnet *et al.*, 1988).

Uranium and fuel fabrication processes are undertaken at Springfields and additionally at Capenhurst. This results in the release of uranium and uranium-daughter isotopes and some fission products into the marine environment (Warrick, 1999; Table 3.1). ^{210}Pb is not directly measured in the discharges from these establishments as it is a radioactive decay product of ^{238}U in ore and not utilized in reactor grade uranium (Dyer, 2001). However, input of these discharges into the coastal environment may influence the use of ^{210}Pb as a dating technique, particularly within coastal settings in close proximity to the aformentioned establishments where dilution may be less pronounced.

	1994	1995	1996	1997	1998
Capenhurst	1.1	1.8	1.4	0.6	1.3
Springfields	0.055	0.048	0.061	0.057	0.047

Table 3.1: Annual total alpha activity of uranium discharges (GBq) from the Capenhurst and Sringfields BNFL sites. Waste from Capenhurst enters the Mersey estuary, whilst waste derived from the Springfields sites enters the Ribble estuary further to the north. (From BNFL data, 1998).

A further source of ^{210}Pb to UK coastal waters results from the activities of the phosphoric acid plant run by Albright and Wilson at Whitehaven in Cumbria. Material used in the production process such as phosphorite contains uranium in the form of an impurity. Waste from the plant discharged into the marine environment of the Cumbrian coast contains all of the original uranium present and as such the daughter isotopes related to the ^{238}U decay series. Certainly, the potential for enhanced levels of ^{210}Pb and modification of coastal sediment ^{210}Pb profiles may exist owing to such inputs and those derived from eroded terrestrial soils.

3.2.5: The behaviour of ^{210}Pb in sedimentary environments.

The levels of supported ^{210}Pb incorporated into a sedimentary prism will largely be determined by factors such as the bulk mineralogy of the sequence, sediment grain-size and importantly in the case of salt-marshes environments, the geochemistry. Factors that directly influence the levels of unsupported ^{210}Pb within the sediment matrix include the rate of mass accumulation, sediment mixing and diffusion rates and sediment porosity which is also a function of grain-size and mineralogenic content. Under steady-state atmospheric flux and sediment deposition the down-core activity will exhibit an exponential decline with increased depth in accordance with the radioactive decay law ($A_x = A_o\, e^{-\lambda t}$, depicted in figure 3.3) and discussed further in section 3.1.6.

Total flux of ^{210}Pb received on a sedimentary surface such as that of a coastal marsh will additionally be influenced by the spatial and temporal nature of various physical and bio-geochemical processes operating within estuarine sedimentary environments.

Santschi *et al.*, (1983) have suggested that the mobility of ^{210}Pb and other radionuclides is largely controlled by the affinity of the element for inorganic and organic particles and the subsequent transport mechanisms that influence the distribution of such material. Such inputs may derive from marsh or mudflat erosion seaward of the site of deposition and may be due to a number of factors such as storm activity, increases in tidal current velocities or may result from hydrological input from catchment derived material.

Differences in calculated fluxes of $^{210}Pb_{excess}$ across coastal marsh surfaces have been recorded by Cundy and Croudace, (1995). These authors suggest that higher fluxes recorded towards the seaward edge of the marsh are representative of higher quantities of tidal

mineralogenic input derived as a consequence of increased tidal current velocities experienced over this section of the marsh. In the same study, investigation of cores abstracted from the mudflat environment revealed low $^{210}Pb_{excess}$ inventories (0.001-0.003 Bq cm^{-2} yr^{-1}) with apparent low annual fluxes resulting from erosion of material derived from the marsh seaward edge and/or high sedimentation rates.

Within salt-marsh environments the establishment of halophytic vegetation that initiates the formation of coastal peat from mudflat will create preferential areas of sediment deposition, (French and Stoddart, 1992; Craft *et al.*, 1993; French and Spencer, 1993; Callaway, 1998). These areas are not only responsible for enhanced geomorphological modification, they are also sites within the marsh where spatial and temporal variation in $^{210}Pb_{excess}$ activity and hence flux may be evidenced. Importantly, the presence of vegetation creates a suitable environment for organo-chemical reactions to occur resulting in $^{210}Pb_{excess}$ adsorption onto the surface of halophytic plant material (Church *et al.*, 1981). This may also enhance the spatial variation in marsh surface and near-surface $^{210}Pb_{excess}$ activities.

Further to consideration regarding depositional processes and how these may influence the behaviour of $^{210}Pb_{excess}$ arriving at the marsh surface, attention must also be given to post-depositional processes that are also capable of altering the $^{210}Pb_{excess}$ activity profile. These may be classified as those resulting from actual physical disturbance and hence post-depositional mixing of the sediment column, those resulting from post-depositional diagenetic/redox controlled bio-geochemical remobilization and those occurring as a result of bioturbation processes (Figure 3.4). Post-depositional physical disturbance may result from high-energy storm events or anthropogenic disturbance to the sediment sequence and are likely to be evidenced by disturbance directly proportional to the energy impacted from the process and the resistance of the sediment to erosion (Turner, 1999).

The effect of diagenetic/redox controlled biogeochemical interactions will be witnessed in more subtle post-depositional remobilization (Hardaway *et al.*, 1998). Such redistribution has also been correlated with fluctuating Eh and pH conditions within the sediment column.

Studies concerning the post-depositional mobility of ^{210}Pb, (Urban *et al.*, 1990) have revealed significant remobilization of Pb and ^{210}Pb in peat-land sediments. ^{210}Pb has also been shown to be significantly associated with solid phases including oxides and oxyhydroxides which have become solubilized within the reducing environment of lake sediments (Benoit and Hemond, 1991). This study also presented evidence to suggest that ^{226}Ra can become

concentrated within oxic/post-oxic/anoxic boundaries where increased levels of manganese oxides are detected. Coupled with the distinct possibility that diffusion driven migration of ^{222}Rn can still occur within such sediments the authors concluded that these processes could certainly influence ^{210}Pb profiles.

3.2.6: Measurement of ^{210}Pb activity: Alpha spectrometry

Determination of alpha (^{210}Pb) activity is commonly achieved via electrodeposition of a purified acid leachate onto polished stainless steel or platinum discs following a double acid leach of the oven-dried sediment from discrete depth intervals throughout the down-core profile. The geochemical preparation follows the method outlined in Flynn (1966) and a full account of the methodology is given in Appendix 2.

Electro-deposition is a well established and reliable technique providing high quality alpha spectrometry sources derived from mildy acidic to alkaline aqueous solutions. Most alpha spectrometry measurements are carried out using an internal yield monitor and the activity of the radionuclide under investigation is calculated by comparing the peak integral or region of interest (ROI) of the plated leachate with that of the known activity of the yield monitor added. As a consequence absolute determination of the counting efficiency is not an essential requirement although this can be useful in providing estimates of the chemical yield.

The quantitative measurement of alpha emitting radionuclides is achieved using silicon surface barrier detectors or in some cases non-implanted silicon detectors. Both of these provide high-energy resolution with excellent stability over time and very low background levels (typically in the order of 0.001 to 0.003 count per minute (cpm)). Efficiency in the order of 20 to 30% is almost constant at energy levels ranging from 2.5 – 8 MeV. For alpha emitters below this range (such as ^{210}Pb and other daughter isotopes) the efficiency is maintained provided that suitable count times are implemented and adhered to and possible interferences and background levels are accounted for (Longworth, 1998).

Certain spectral interferences can result from the presence of radionuclides on the counting source which emit alpha particles of similar energy to the analyte which leads to degradation of the alpha spectrum. A *priori* assessment of radionuclides likely to disrupt the spectrum can provide useful information and aid in the resolution of any detected interferences (Longworth 1998).

Other interferences can arise from high background activities which are usually the result of the build-up of unacceptable levels of alpha particles produced by recoil nuclei in alpha decay across the gap between the source and the detector. To remove any recognized build-up modern detectors can be cleaned periodically to remove the presence of unwanted recoil nuclei. Alternatively reduction of the implantation of recoil nuclei can be achieved by applying a suitable back-bias voltage between the source and the detector and either/or increasing the distance between the source and the detector (P.E. Warwick personal communication 2001).

In this study ^{210}Pb activity was determined through the measurement of its granddaughter isotope ^{210}Po as a proxy method and assumes secular equilibrium between ^{210}Pb and ^{210}Po (Flynn, 1966). A double acid leaching of the sediment was undertaken followed by auto-deposition of the Polonium isotope in the leachate onto silver disks. A known mass of ^{209}Po spike was added to approximately 2 grams of oven-dried sediment to act as the isotopic yield tracer in order to determine sample activities (Cundy and Croudace, 1995; Appendix 5).

3.2.7: Determination of ^{210}Pb total activity

The activity of each individual depth increment measured is calculated by determination of the integral of the area under the measured total peaks for ^{210}Po (assumed to be in secular equilibrium with ^{210}Pb) and the added isotopic tracer ^{209}Po. The actual activity is obtained from the equation:

$$^{210}\text{Pb total activity} = \frac{\left(\text{Total } ^{210}\text{Po peak} \;/\; \text{Sample dry mass}\right)}{\left(\text{Total } ^{209}\text{Po peak} \;/\; \text{Mass } ^{209}\text{Po spike}\right)} \times \left(4.28 / 60\right)$$

where: ^{210}Po and ^{209}Po represent the integral of the measured region of interest for each radionuclide obtained from alpha spectrometry.

Sample masses of dry sample sediment and ^{209}Po spike are measured in grams, and 4.28 is the radioactive decay constant of ^{209}Po (Bq minute^{-1})

3.2.8: ^{210}Pb dating models for sediment geochronology

Dating of sedimentary materials utilizing ^{210}Pb hinges upon a number of different assumptions surrounding the mechanisms by which the flux of the radionuclide becomes incorporated into the sedimentary prism. Hence, the behaviour of ^{210}Pb within aquatic, terrestrial and atmospheric systems may influence the validity of certain assumptions routinely incorporated into the various mathematical models with which dating is facilitated (section 3.1.5). The relationship between depositional processes , $^{210}Pb_{excess}$ assimilation and ^{210}Pb activity profiles can be used effectively in the choice of model used for gechronological control.

One of the principal assumptions is that $^{210}Pb_{excess}$ supply to the marsh soil surface and sediment supply has been constant over time. As outlined in the previous section this may not always be valid when consideration is given to fluctuating wet and dry atmospheric deposition and labeled sediment transport processes. Turner (1999) points out that during the evolution from mudflat environment to mature marsh within dynamic hydrological systems such as estuaries, wetland surfaces are likely to have experienced temporal fluctuations in atmospheric deposition. Human activity at the coast which results in physical disturbance and sediment mixing will cause significant deviation from this ideal situation and artificial sources of ^{210}Pb may influence the total annual flux occurring on an estuarine depositional surface (section 3.1.4).

It is apparent then that the idealized exponential decline in $^{210}Pb_{excess}$ activity with depth (Figure 3.3) may not always be evidenced in marsh soil profiles owing to some or all of these processes. Nevertheless this basic assumption does constitute the basis for the ^{210}Pb dating models that are frequently employed in sedimentary studies.

3.2.9: The Constant Flux : Constant Sedimentation (CF : CS) or "Simple" Model

Measurement of mean sediment accumulation over time forms the principal basis of the constant flux : constant sedimentation model. This is calculated from a logarithmic plot of the exponential radioactive decay curve for $^{210}Pb_{excess}$ derived from a constant supply of $^{210}Pb_{excess}$ to a steadily accreting soil profile (Appelby and Oldfield, 1992). Average sediment

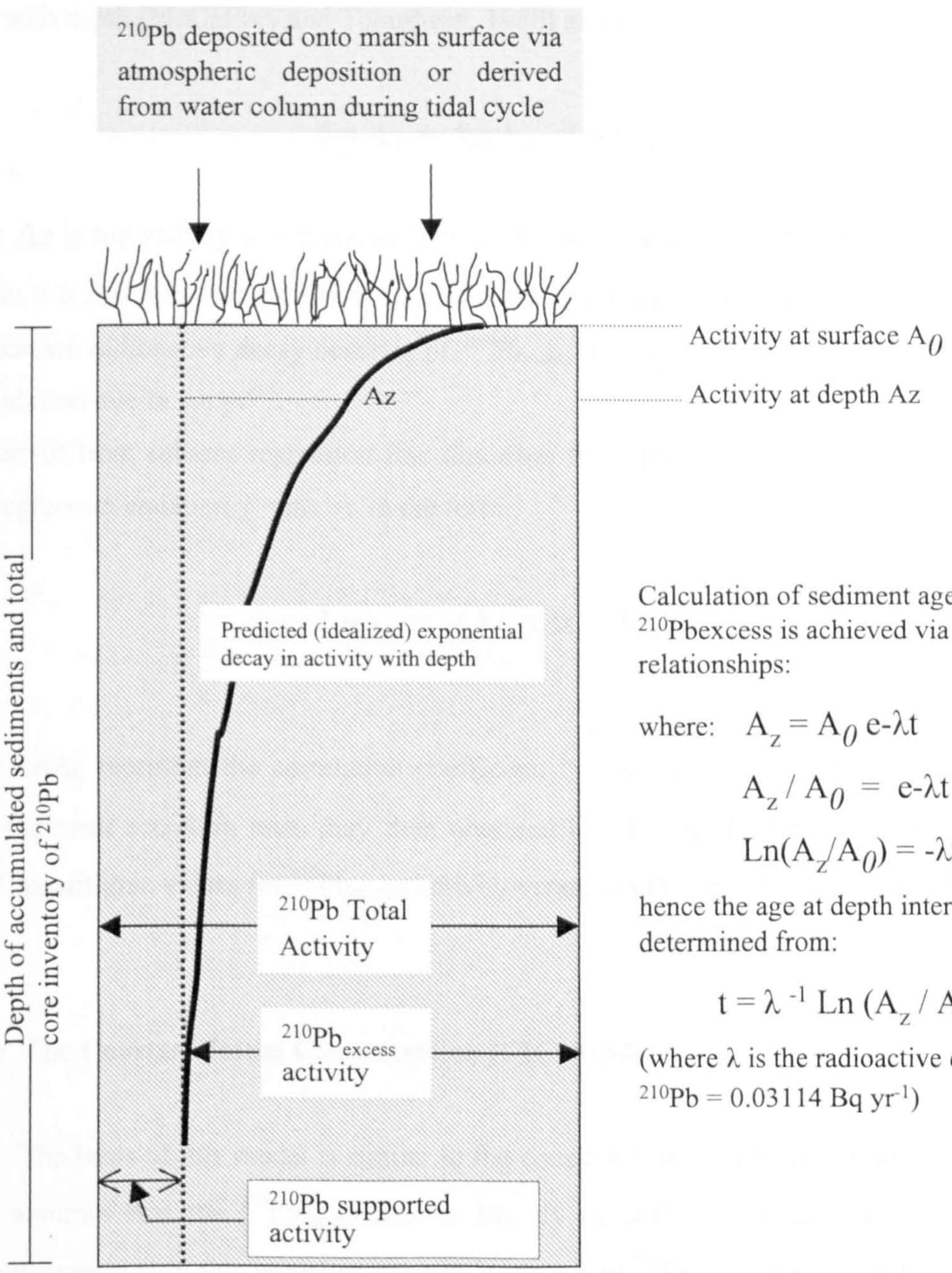

Calculation of sediment age at depth z using ^{210}Pbexcess is achieved via the following relationships:

where: $A_z = A_0 \, e^{-\lambda t}$

$$A_z / A_0 = e^{-\lambda t}$$

$$\mathrm{Ln}(A_z/A_0) = -\lambda t$$

hence the age at depth interval z is determined from:

$$t = \lambda^{-1} \, \mathrm{Ln} \, (A_z / A_0)$$

(where λ is the radioactive decay constant of ^{210}Pb = 0.03114 Bq yr^{-1})

Figure 3.3: Components of ^{210}Pb in accreted sediments and relationships to show age-depth determination. (Modified from Turner, 1999; see text for full discussion of method and critical assumptions)

accumulation is estimated via the best-fit straight-line equation which describes this radioactive decay with depth (McCaffrey and Thompson, 1980) and takes the form of:

$$\mathbf{Ln\ A_z = LnA_o - (\lambda / S_r)z}$$

where: Az is the activity at a certain depth z, A_o is the initial activity (if ^{210}Pb flux has been constant it is assumed that each layer of new material has the same sediment surface activity), λ is the known radioactive decay constant of $^{210}Pb_{excess}$ (0.03114 Bq yr^{-1}) and S_r is the sediment accumulation rate in cm yr^{-1}.

The best-fit least squares regression line describes the gradient of the line that equates to the basic regression equation y = mx +c in the form:

$$\mathbf{LnA_z = -(\lambda / S_r)z + LnA_0}$$

where: LnA_0 represent the correlation coefficient "c" and the gradient "m" is given by λ/S_r. Mean sediment accretion rates may then obtained by plotting the least squares regression of normal logarithmic values for $^{210}Pb_{excess}$ activity versus depth (Appleby and Oldfield, 1992).

3.2.10: The Constant Initial Concentration (CIC) Model

The basis of this model is similar to the constant flux : constant sedimentation model in that it assumes that the $^{210}Pb_{excess}$ flux is directly proportional to the mass of accumulated sediment. Importantly this model assumes that the initial $^{210}Pb_{excess}$ activity will have remained constant regardless of changes to the overall accumulation rate. The CIC model unlike the constant flux : constant sedimentation model can still be utilized effectively if there have been moderate changes in the sediment accumulation rate over time. This is not the case with the CF:CS model although it has been suggested that the CIC model may be used in conjunction with the CF:CS model (Appleby and Oldfield, 1992; Dyer, 2001).

3.2.11: The Constant Rate of Supply (CRS) Model

In many depositional environmental settings of which estuarine salt-marshes are no exception, the rate of sediment accumulation over time is unlikely to have been uniform throughout the entire development of a sedimentary sequence. The constant rate of supply (CRS) model can be applied to take account for this phenomenon. Implicit in the CRS model is the constant rate of supply of unsupported ^{210}Pb to the sediment surface over time. This results in the initial unsupported ^{210}Pb activity varying inversely with the sediment mass accumulation rate as a consequence of $^{210}Pb_{excess}$ dilution by increased sedimentation. Calculation of sediment age within sections of the sediment prism that have experienced fluctuating sediment accumulation rates over time is thus facilitated.

The calculation of sediment age at a given depth utilizing the CRS model compares the ratio of $^{210}Pb_{excess}$ (the unsupported component) below a certain depth interval to the $^{210}Pb_{supported}$ (background activity) throughout the sedimentary prism. This latter measurement is referred to as the ^{210}Pb core inventory.

The equation employed takes the form of:

$$t_z = \lambda^{-1} \, \mathrm{Ln} \, (A_z / A_{total})$$

where t_z = sediment age at depth z, λ = the ^{210}Pb radioactive decay constant (0.03114 Bq yr-1), A_z = $^{210}Pb_{excess}$ activity below a defined depth z (or unsupported component) and A_{total} = the total ^{210}Pb core inventory (Appleby and Oldfield, 1992).

Calculated sediment ages at discrete depths throughout the down-core profile provide the mechanism for the construction of age/depth curves. Periods of variable sediment accumulation can be identified by inflections on these curves and are represented by alteration to the curve gradient.

The CRS model has been widely employed in many environmental settings where variable sedimentation rates have been recorded (Chanton *et al.*, 1983; Binford, 1990; Allen *et al.*, 1993; Cundy and Croudace, 1995; Gale *et al.*, 1995; Alvisi and Frignani, 1996; He and Walling, 1996; Goff *et al.*, 1998; Thorndycraft *et al.*, 1998; Carroll *et al*, 2001; Dyer *et al.*,

2002). It is however prudent to consider that without actual site-specific measurements of for example, sediment depositional variability, rainfall and $^{210}Pb_{excess}$ supply over time to a depositional surface, any derived sediment age/depth curves will only represent an approximation of the time dependent development of a sedimentary sequence. Any dating undertaken using the various models available to the researcher will need to rigorously consider the possible influence of processes likely to affect the integrity of the activity profiles obtained. These are by nature of the critical assumptions implicit in the various models quite numerous as previously discussed.

In order to rectify these potential problems in terms of improving the overall rigor of the methodology, comparison with other time-compatible radiometric dating methods can be used. Such methods provide a suitable means of comparing and assessing the ^{210}Pb models and hence an independent test of the ^{210}Pb dating method. The use of artificial radionuclides where present in sediment sequences is one such method and details of this methodology are presented in the following section .

3.3: Geochronology using artificial radionuclides

3.3.1: The application of ^{137}Cs dating to coastal wetland sediments

In recent years much attention has focused upon the use of ^{137}Cs as a dating tool for sediment geochronology (Ritchie and McHenry, 1990). The method has been applied to a wide range of sedimentary environments including lakes (Krishnaswamy *et al.,* 1971; Robbins and Edington, 1975), coastal sedimentary basins (Chanton *et al.,* 1983; Zuo, 1992;) and salt marshes (DeLaune *et al.,* 1978; Milan, 1995; Cundy and Croudace, 1996; Callaway, 1996; Lewis, 1997; Dyer, 2001).

Where detectable, artificial radionuclides from known periods and sources of discharge provide an independent method with which to assess ^{210}Pb derived geochronologies (Cundy and Croudace, 1995). However, there are reported studies where unreliable core chronologies have resulted owing to failure of the method (Davis *et al.*, 1984; Longmore *et al.*, 1986). As a consequence of these studies it is essential that the assumptions underlying the technique are

critically evaluated and fully understood prior to any attempt to utilize the method for sedimentary core dating purposes.

3.3.2: The origin of ^{137}Cs

Caesium-137 (^{137}Cs) is an artificial radio-isotope produced solely from anthropogenic activities as a result of nuclear fission and weapons generation processes. Release via the detonation of thermonuclear weapons testing and authorized discharges from civil power generating installations are the principal methods by which ^{137}Cs has entered the environment. Other inputs of ^{137}Cs have been derived from accidents at nuclear power generation facilities and discharges from military sites for which few data are available. Radioactive decay of ^{137}Cs occurs through beta emission with an associated gamma energy of 662 keV. With a radioactive half-life of 30.2 years assessment of ^{137}Cs activities within soils and sediments provides a useful method of dating recent (~ 40 years) sediment accretion rates.

3.3.3: The supply of ^{137}Cs to surface environments: Atmospheric input

The first introduction of ^{137}Cs to the environment occurred in the early 1950's as global atmospheric input following the detonation of the first of a series of above-ground, high-yield thermonuclear weapons tests conducted by various nations over the period AD1945-1963. Significant levels of atmospheric fallout occurred in AD1954 (DeLaune *et al.*, 1978; Wise 1980), with marked maxima occurring between AD1958-1959 and AD1963-1964 (Figure 3.5). These marked peaks in the depositional record reflect the frequency and magnitude of the detonations which have not been constant over time and have resulted in temporal variability of the supply of ^{137}Cs to the environment derived from this source. Fallout from this source was greatest within the northern hemisphere (Ritchie and McHenry, 1990).

Following the signing of the international above ground Nuclear Weapons Test Ban Treaty between the US, UK and USSR in October of 1963 significant reduction of atmospherically derived ^{137}Cs into the environment has taken place (Ritchie and McHenry, 1990). Further atmospherically derived ^{137}Cs to the environment and in particular the northern hemisphere occurred in 1986 as a result of the Chernobyl nuclear power reactor accident on the 26th of April of that year. This released a considerable quantity of radioactive material into the

atmosphere but unlike the radioactivity resulting from the earlier weapons testing programs did not penetrate the stratosphere. As a consequence much of the radioactivity derived from this source was returned to the Earth's surface via wet deposition in the days following the accident. This resulted in the deposition of ^{137}Cs and other radioisotopes throughout many European countries (Anspaugh *et al.*, 1998) including the British Isles (Playford *et al.*, 1992; Callaway, 1996).

Contaminated air and radioactive particles reached the UK on the 2nd of May and the subsequent deposition has been the subject of much scrutiny. Importantly, distribution of ^{137}Cs was patchy across most of the region owing to the nature of rainfall that occurred in the days following the accident. However Cambray *et al.* (1987) estimate that this accident increased the world-wide inventory of ^{137}Cs by as much as 5% and in the UK by a larger amount estimated to be nearly 40% owing to the dose received which was proportionally higher. The distribution of Chernobyl derived radioactivity over Northern Europe following the reactor accident is shown in Figure 3.4)

3.3.4: Marine input of ^{137}Cs

In terms of the present study, atmospherically-derived radio-caesium is not the only source of ^{137}Cs that may affect the western Scottish coast. Over the last half-century historical authorized discharges from the BNFL Sellafield fuel reprocessing plant in Cumbria north-west England have introduced significant quantities of ^{137}Cs and other artificial radionuclides into the eastern Irish Sea (Figure 3.5). Such discharges have also been the subject of much scientific investigation. ^{137}Cs has been used effectively as a tracer to study marine transport pathways and ocean circulation in the Scottish and Norwegian coasts (Livingstone *et al.*, 1982a; 1982b) and through the Hebridean Sea (McKinley *et al.*, 1981). Collectively a transport lag period of approximately one year has been suggested in terms of travel-time for ^{137}Cs derived from Sellafield discharges and that entering the western Scottish marine environment. Importantly the behaviour of ^{137}Cs in the marine environment will influence the overall transport lag period as well as the incorporation of such material into sedimentary sequences in estuarine settings. Some of the more pertinent points regarding the behaviour of ^{137}Cs in environmental settings now follows.

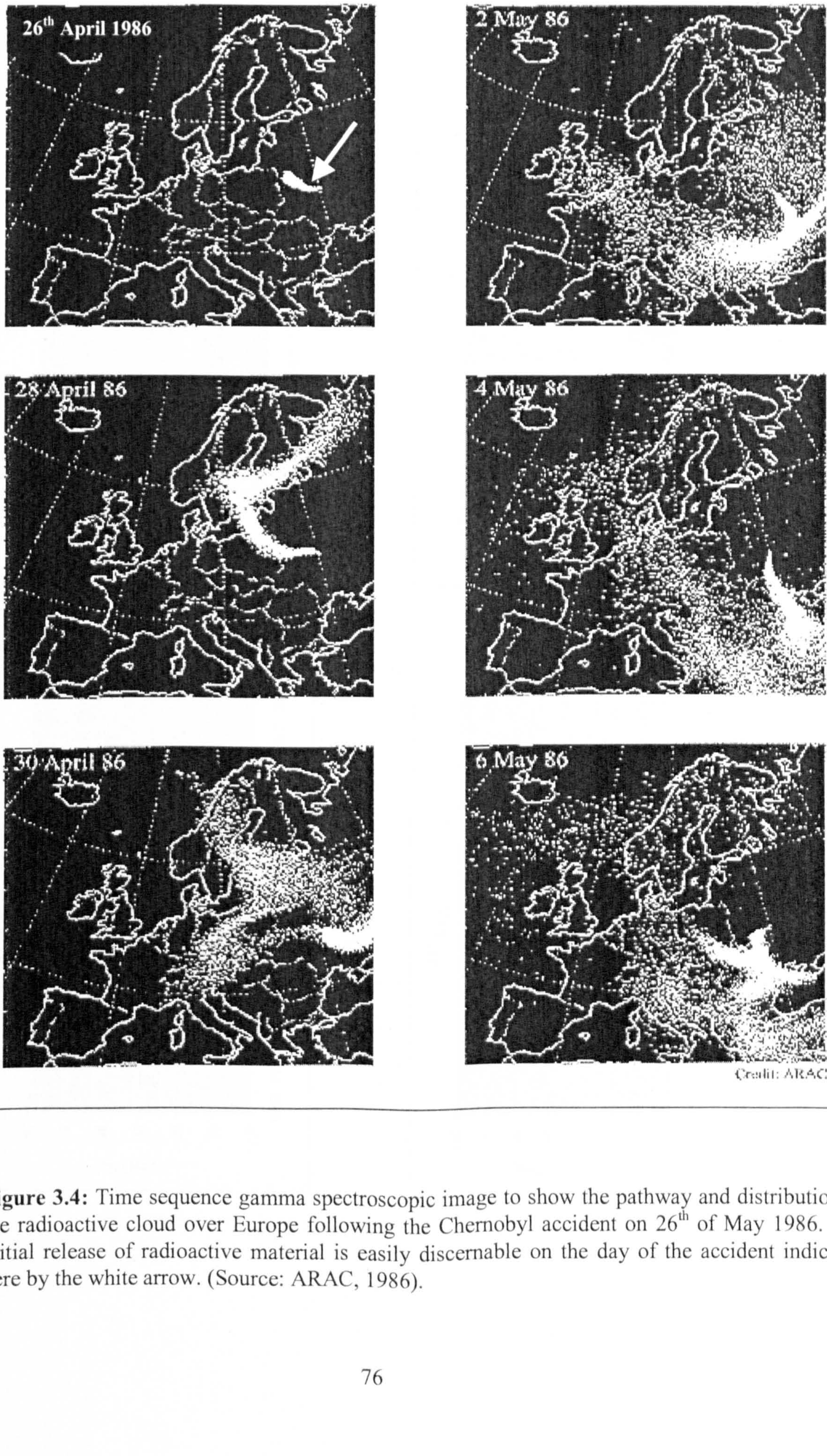

Figure 3.4: Time sequence gamma spectroscopic image to show the pathway and distribution of the radioactive cloud over Europe following the Chernobyl accident on 26th of May 1986. The initial release of radioactive material is easily discernable on the day of the accident indicated here by the white arrow. (Source: ARAC, 1986).

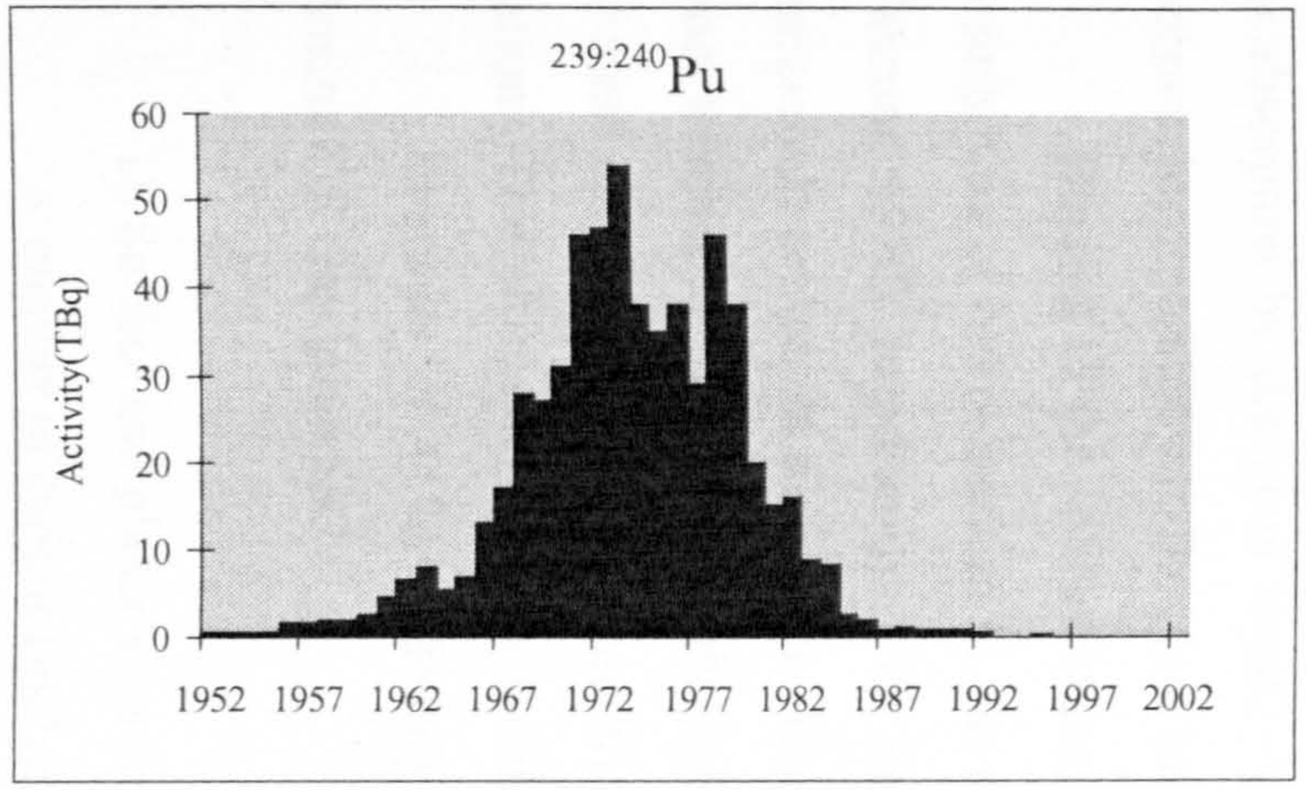

(a)

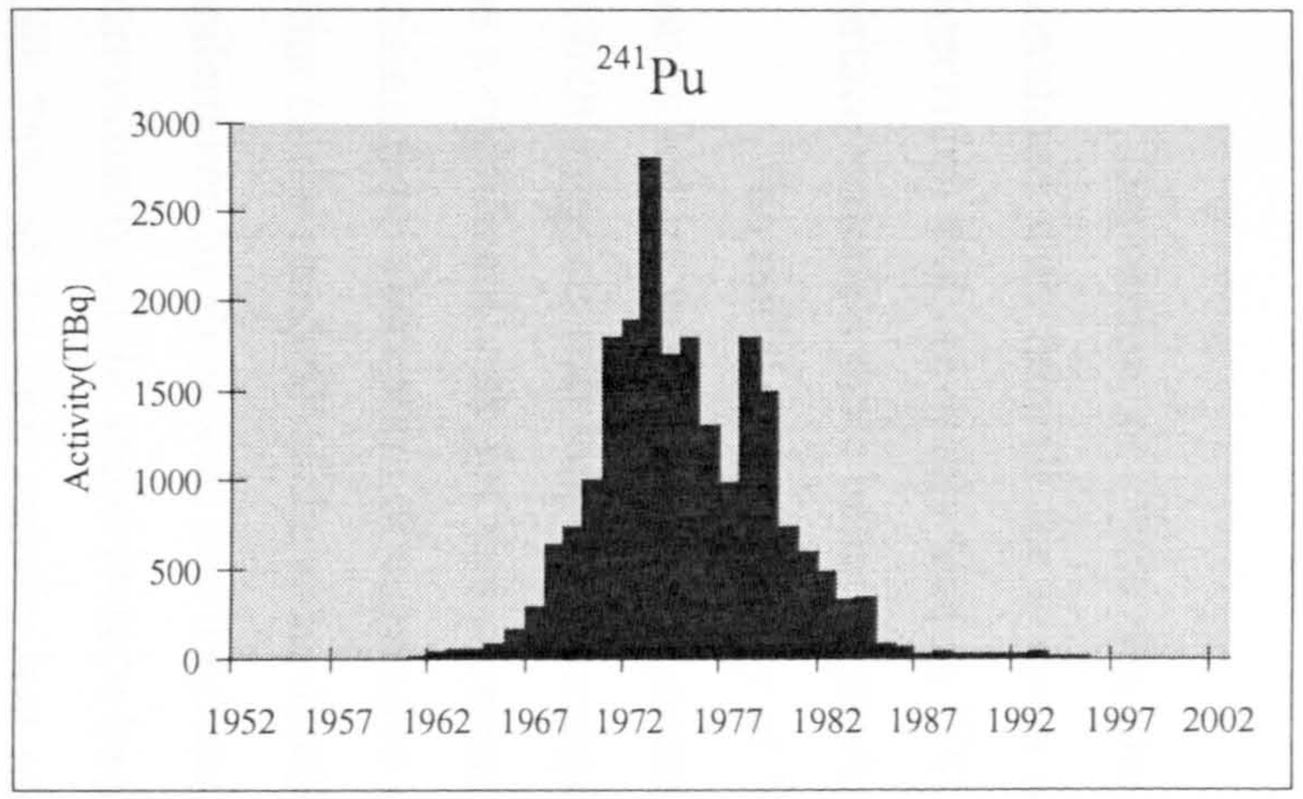

(b)

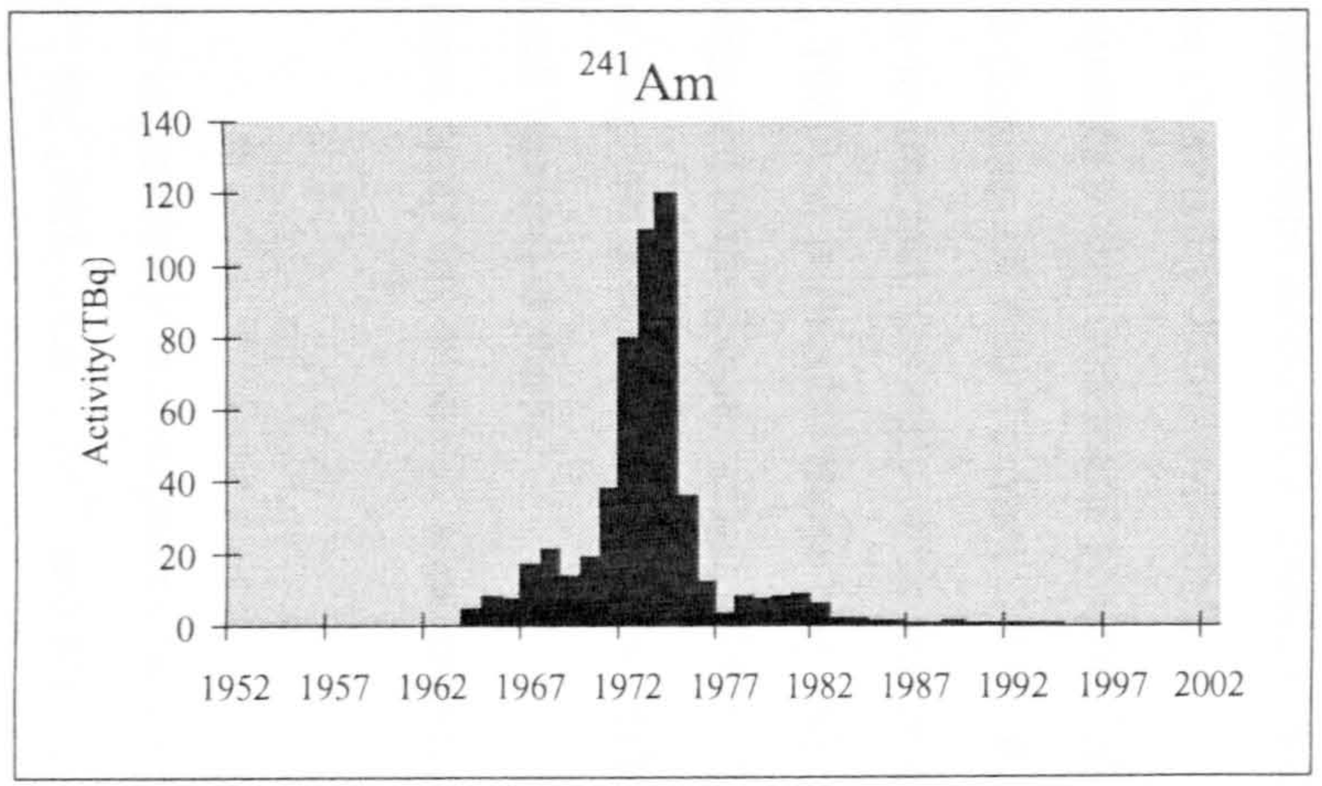

(c)

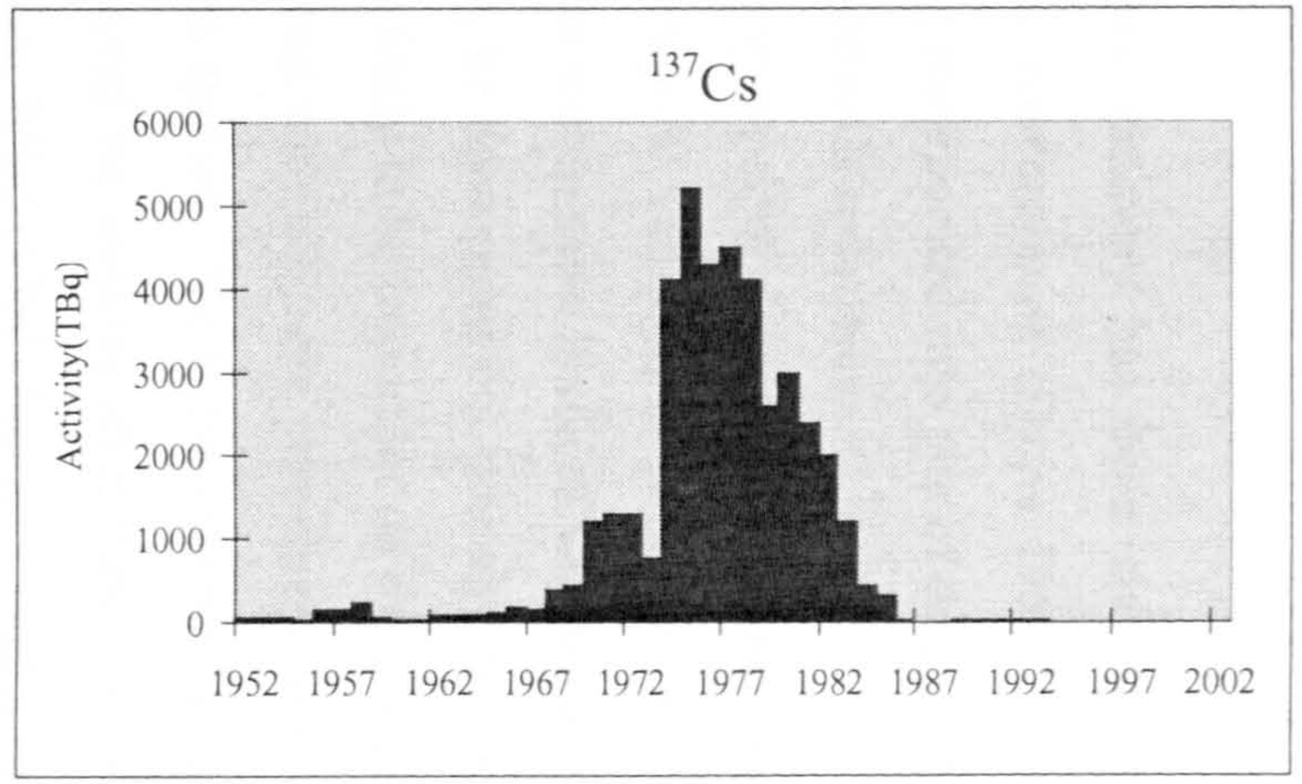

(d)

Figure 3.5: Discharges of selected artificial radionuclides into the Irish Sea from the BNFL Sellafield fuel reprocessing plant in Cumbria UK. (a) $^{239:240}$Pu, (b) ^{241}Pu, (c) ^{241}Am, (d) ^{137}Cs. ^{137}Cs and ^{241}Am are utilized in the present study. The total ^{241}Am activity in the Irish Sea is likely to have been greater than the discharge record owing to isotopic in-growth from ^{241}Pu elevating levels of ^{241}Am activity. (Source: Kershaw *et al.*, 1996)

3.3.5: The behaviour of ^{137}Cs: Environmental pathways and chemical mobility

Deposition of ^{137}Cs via the atmospheric pathway has been shown to be linearly correlated with rainfall for a given atmospheric concentration (Davis 1963). Subsequent wet deposition will inevitably lead to ^{137}Cs becoming incorporated into one of three distinct types of surface materials these being vegetation, water and soils/sediments.

The initial rate of supply of ^{137}Cs to many types of vegetation will therefore largely be controlled by wet depositional processes and temporal variation in atmospheric activity. Wise (1980) suggests that long-term storage of caesium within most kinds of vegetation is unlikely to be a significant sink for this element. However, he does point out that any potential reservoir arising from absorption to vegetative surfaces is likely to be important on time-scales of months prior to the removal of the radio-isotope and arrival within a more permanent sink. Experiments undertaken by Rogowski and Tamura (1970) who applied ^{137}Cs to the leaves of grasses revealed that virtually all the radio-isotope had been removed via washing after period of twelve months with 75% of the total activity lost after 153 days. Wise (1980) has also suggested that radio-caesium is more likely to be adsorbed onto soil particles sitting on the foliage surface as opposed to absorption by the plant itself. Whichever mechanism dominates caesium will inevitably become incorporated into the plant litter and hence eventually to the soil surface.

Binding to the soil/sediment substrate represents the dominant process influencing the distribution of radio-caesium in the environment (Lomenick and Tamura, 1965; Rogowski and Tamura, 1970). Importantly ^{137}Cs has be shown to interact strongly with the micaceous clay component present in many soils (Comans *et al.*, 1989) in particular those clay minerals derived from weathering of clay minerals such as muscovite and illite (Evans *et al.*, 1983). The structure of these clay minerals is important in terms of the sorption potential and exchangeability of ^{137}Cs cations. This ultimately controls the degree to which binding occurs.

Evans *et al.* (1983) identify three distinct types of binding sites present within the structure of clay minerals.

1). Surface and planar sites from which Cs is generally exchangeable in the presence of a number of cations (including Cs^+, H^+, Na^+, NH_4^+, Ca^{2+}, Fe^{2+} and Mn^{2+}).

2). Wedge sites where exchange of Cs is limited through sterical geochemical processes

involving cations of similar size and charge (e.g. NH_4^+, Cs+, K^+, and possibly H_3O^+).

3). Interlayer sites from which caesium is not readily exchangeable.

Weathered clay minerals also possess what are termed "frayed edges" and these are also sites where selective sorption of Cs^+ and K^+ can take place. These occur as consequence of the low hydration energies of such cations which when sorbed cause dehydration of the illite layers in the clay mineral structure generating collapse of the inter-layered configuration. Comans and Hockley (1992) consider this inter-layer collapse mechanism to be the essentially irreversible method by which caesium is adsorbed to clay minerals such as illite.

Interaction of ^{137}Cs with illite is characterized by an initial rapid uptake which slows significantly over the following weeks and months. A fraction of the caesium has been shown to diffuse slowly to the selective inter-layer sites described above from where it is not readily mobilized and this can occur over time-scales of years (Lomenick and Tamura, 1965; Davis, 1963). Investigations by Comans *et al.* (1991) have indicated that even where desorption processes result in the release of a fraction of the caesium from the more accessible sites within the clay mineral structure slow uptake still proceeds resulting in a quasi-equilibrium state. This process constitutes part of the model describing the kinetic control of caesium sorption onto illite proposed by Comans *et al.* (1991) and further developed by Comans and Hockley (1992).

Despite the fact that caesium adsorption in the inter-layer sites is considered to be an irreversible process by these authors some evidence to the contrary has been put forward following the investigations by Sawhney (1972). This author shows that caesium cations can indeed be replaced by K^+ and NH_4^+ ions within the edge-inter-layer sites and that this takes place in preference to replacement by Ca^+ and Mg^+ ions (Sawhney, 1972). Evidence supporting this hypothesis has also been presented by Evans *et al.* (1983) who attribute the re-mobilization of ^{137}Cs within anaerobic lake sediments to ion exchange replacement by HH_4^+, Mn^{2+} and Fe^{2+}.

3.3.6: ^{137}Cs dating of estuarine sediments

Introduction of ^{137}Cs to coastal environments may also be via atmospheric deposition or that derived from marine input in either the soluble (conservative) form or that formerly adsorbed to particulate matter (i.e. non-conservative) transported to the marsh surface

(Thompson *et al.* 2001). Hence the behaviour of radio-caesium in estuarine aquatic environments is largely controlled by adsorption onto the solid particulate phase such as the clay minerals outlined above. Additionally, the distribution of dissolved caesium has been shown to be roughly proportional to salinity (Simpson *et al.*, 1976). The elevated values recorded in more saline estuarine waters have been attributed to cationic competition with dissolved K^+ becoming adsorbed resulting in a decrease in the removal of ^{137}Cs derived from the atmospheric source sorbed onto sediment particles. The presence of the pre-AD1963 peak in ^{137}Cs activity and that identified in sedimentary prisms from northern hemisphere sites resulting from the AD1986 Chernobyl accident provide two distinct peaks that can be considered as time horizon markers with which to consider the depositional history of recent sedimentary environments.

As with the use of ^{210}Pb as a radiometric dating tool assumptions relating to the lack of any post-depositional mobility are also valid for the use of ^{137}Cs. DeLaune *et al.* (1978) assumed little or no mobility would affect the depositional record of fallout owing to the expected adsorption of the radio-isotope onto the clay fraction of soils and sediments. In some environments post depositional remobilization of ^{137}Cs has been attributed to the lack of weathered micaceous clay minerals present and hence the lack of abundant inter-layer sites where possible irreversible adsorption can occur (e.g. Evans *et al.*, 1983; Davis *et al.*, 1984).

Within salt marsh sediments that are accumulating in response to external forcing mechanisms the use of ^{137}Cs dating has been shown to be a good method for estimating relative accumulation rates (DeLaune *et al.*, 1978; Miller and Heit, 1986; Callaway *et al.*, 1996; Cundy and Croudace, 1996; Dyer, 2001). However, Milan (1995) highlights the fact that based upon one definable activity horizon, related to AD1963 ^{137}Cs dating may not always be accurate enough to assess actual marsh sediment accretion rates owing to the fact that the inferences deduced from this activity horizon represent only one defined peak with which estimations can be conducted.Furthermore, Milan (1995) highlights three major assumptions which should be taken into account when assessing the reliability of dating sediments using the ^{137}Cs method.

These are:

1. The salt marsh is undergoing a period of accretion with no interferences to the natural sedimentary depositional regime over the historical time during which the marsh is being investigated

2. There is no contribution or removal of ^{137}Cs to or from the marsh surface other than that derived from atmospheric fallout.

3. Any ^{137}Cs present in the marsh substrate is fixed to the minerogenic or organic fraction and has not been affected by significant vertical migration resulting from re-mobilization.

Further to the concerns of Milan (1995) it is worthy to note that re-mobilization of radio-caesium may occur within higher saline estuarine waters (Aston and Duursma, 1973; Patel *et al.*, 1978; Longmore *et al.*, 1986) or if the sediment or sedimentary pore waters are anoxic whereby Cs ions may be re-placed by K^+ , Fe^{2+}, Mn^{2+} or NH_4^+ cations (Evans *et al.*, 1983; Smith and Comans, 1996). Further re-mobilization may take place following the decay of organic matter and the subsequent release of ^{137}Cs bound to the organic fraction as suggested by Davis *et al.*, (1983) in a study of clay-deficient lake sediments.

Of particular relevance to this study is the second of the points put forward by Milan (1995). Discharges from the BNFL fuel reprocessing facility at Sellafield are highly likely to represent a potential source of input of artificial radionuclides to western Scottish coastal environments as demonstrated by the studies undertaken by McKinley *et al.*, (1981) and Livingstone *et al.* (1992a; 1992b). Cundy and Croudace (1996) also draw attention to the potential for error resulting from input to the marine environment from a non-atmospheric source resulting from the lag time between the peak discharge and incorporation into accumulating coastal sediments. The present study will also demonstrate that radionuclides derived from a non atmospheric source entering a coastal salt-marsh environment may nevertheless be useful to the study of coastal sediment sequences provided the discharge records of the relevant nuclear installations are known.

The complex interaction of time with depth in any sedimentary sequence can be better discerned where both the pre AD1963 weapons fallout peak and the AD1986 Chernobyl peak are identified. If this is achieved then a distinct segment of the sedimentary prism can be assessed in terms of its depositional history. However, it is necessary to be aware of the limitations still imposed by the method in that the two peak activity horizons are only two

distinct input impulses within the section of the sediment prism, which may represent a substantial period of marsh development.

3.2.7: Measurement of ^{137}Cs activity: Gamma spectrometry

Preparation of sources for gamma spectrometry do not generally require extensive sample preparation apart from homogenisation of depth interval sub-samples. Importantly sub-samples should be of uniform consistency and symmetrical to ensure accurate calibration.
Radiation spectrometry is highly dependent upon the mode of interaction that takes place between the radiation emitted and the material from which the detector is manufactured.
The three major types of gamma ray interaction that take place are as follows:

(a). Photoelectric absorption (an interaction in which the incident gamma- ray photon disappears producing a photoelectron that replaces the gamma photon);

(b). Compton scattering (an interaction involving the scattering of the gamma ray photon following collision between the γ-ray photon and an electron forming a recoil electron. In such cases the resulting energy division is ultimately dependent upon the scattering angle);

(c). Pair production (the process by which a gamma photon is converted into an electron positron pair in the field of an electron or nucleus).

The dominant type detected will be dependent upon the energy of the incoming radiation emanating from the radiation source and the atomic number of this source matter. For low energy gamma emitters (up to several hundred keV) photoelectric absorption predominates. Compton scattering is the predominant interaction mechanism for medium range gamma emissions (up to 5MeV) and for high energy gammas above this figure (up to ~10 MeV) pair production is the most likely interaction mechanism to be encountered (Knoll 1989).

Gamma ray photons are essentially uncharged and as such do not create excitation of material through which they may pass. Therefore, in order to detect gamma rays it is critically important to initiate an interaction which transfers all or part of the photon energy to an electron

in the absorbing material of the detector (Knoll, 1989; Gilmore and Hemmingway, 1995; Longworth, 1998).

High purity germanium is commonly used for construction of gamma ray detectors being derived from industrial use in the manufacture of semi-conductors (Knoll, 1989). The high-purity Ge detectors used in this study are essentially semi-conductor diodes which take the form of electron-hole pairs that are formed as the physically altered charged particle passes through the detector. Consequently these electron-hole pairs act as the principal charge carriers by migrating along the pathway taken by the γ-ray photons towards the opposing pole created by the application of an electric bias (several kilovolts). The resultant charge is recorded and measured by a sensitive charge preamplifier which converts the energy to a voltage pulse. This converted voltage pulse has an amplitude which is proportional to the original gamma ray photon (Knoll, 1989; Gilmore and Hemmingway, 1995).

Gamma radiation is capable of travelling quite large distances between interactions which can result in detector counting efficiencies often being less than 100%, a problem commonly encountered with planar-type detectors. This study uses high-purity germanium (HPGe) coaxial well-type detectors designed specifically for the measurement of small radioisotope sources in which the γ-ray source is nearly completely surrounded by germanium resulting in unusually high detection efficiency. The efficiency of an individual detector is a function of the physical properties and thickness of the material used in manufacture, the counting geometry (which controls the distance from the source to the detector) and the specific activity of the radiation energy emitted from the source. Self-absorption in the source can also influence the overall efficiency albeit to a lesser extent (P.E. Warrick, Southampton Oceanography Centre, personal communication 2001).

In simple terms the activity of a gamma ray source is derived by dividing a measured gamma ray count-rate by the gamma ray emission probability and the counting efficiency (Longworth 1998). Importantly, as with other radiation spectrometry methods a correction is usually made to account for background count rates. Gamma detectors are therefore surrounded by lead castle-type shielding sometimes also containing an inner copper-cadmium lining to protect the detector and source from external interference (Gilmore and Hemingway, 1995).

Measurements undertaken in this study have used two Canberra 45% N-Type HPGe well detectors courtesy of the Geosciences Advisory Unit at the Southampton Oceanography Centre and these are both of the coaxial type and open at one end. An illustration of the general

configuration of these detectors is shown in Figure 3.6. The active volumes are 168 ml and 239 ml with a well depth of 45 mm. The resolution of these detectors at 122 keV and 1332 keV is 1.59keV and better than 2.25 keV respectively.

In order to assess and calibrate the counting efficiency on a regular basis known radionuclide standards with the same physical and geometrical characteristics as the sample under investigation were routinely counted. Over the time period of this study counting efficiency was determined at regular intervals using a mixed gamma source standard (the Amersham reference solution QCY4A) containing accurately documented activities of various gamma emitting radio-isotopes including ^{241}Am, ^{137} Cs, ^{60}Co and ^{54}Mn (Figure 3.7). Detector accuracy was also verified on a weekly basis using the International Atomic Energy Authority standard reference material IAEA135 Irish Sea sediment. Additionally, background counts were determined on both detectors at regular intervals (at least once per week) to provide continuous assessment for activity determination during the study and throughout other commercial operations.

Sub-samples of approximately 20g were oven-dried for 48 hours and then homogenised using an Agate pestal and mortar and then weighed into polythene scintillation vials and the mass recorded. Count times were typically of the order of 25000 seconds. Most count times were considerably longer with samples being left to count overnight (generally in the order of 55000 seconds). On occasions the requirement for commercial sample counting led to count times being somewhat reduced. Where this was the case, a general rule of counting near-surface samples was implemented based upon the intuitive consideration that activity levels may be expected to be higher and, hence, more efficiently detected.

All gamma spectra were processed using the commercially available Fitzpeaks software package (J.F. Computing Services, Stanford in the Vale, Oxfordshire). This software compares identified peaks in the spectrum and the areas of these peaks to library archived peaks from a wide a range of gamma emitters. The package also takes into account the recorded background

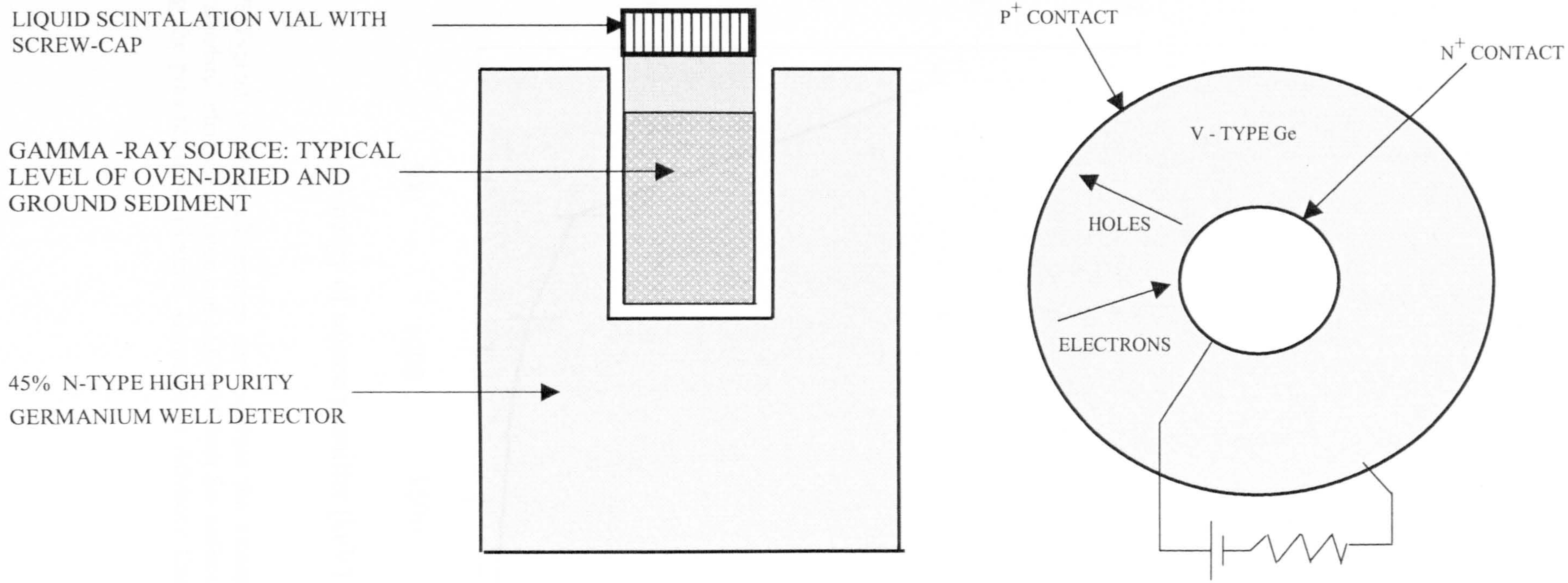

Figure 3.6: Schematic representation of the Canberra High-Purity Germanium Coaxial well-type detector (N-Type coaxial) used in this study for determination of gamma emitting radio-nuclides (e.g.^{137}Cs and ^{241}Am).

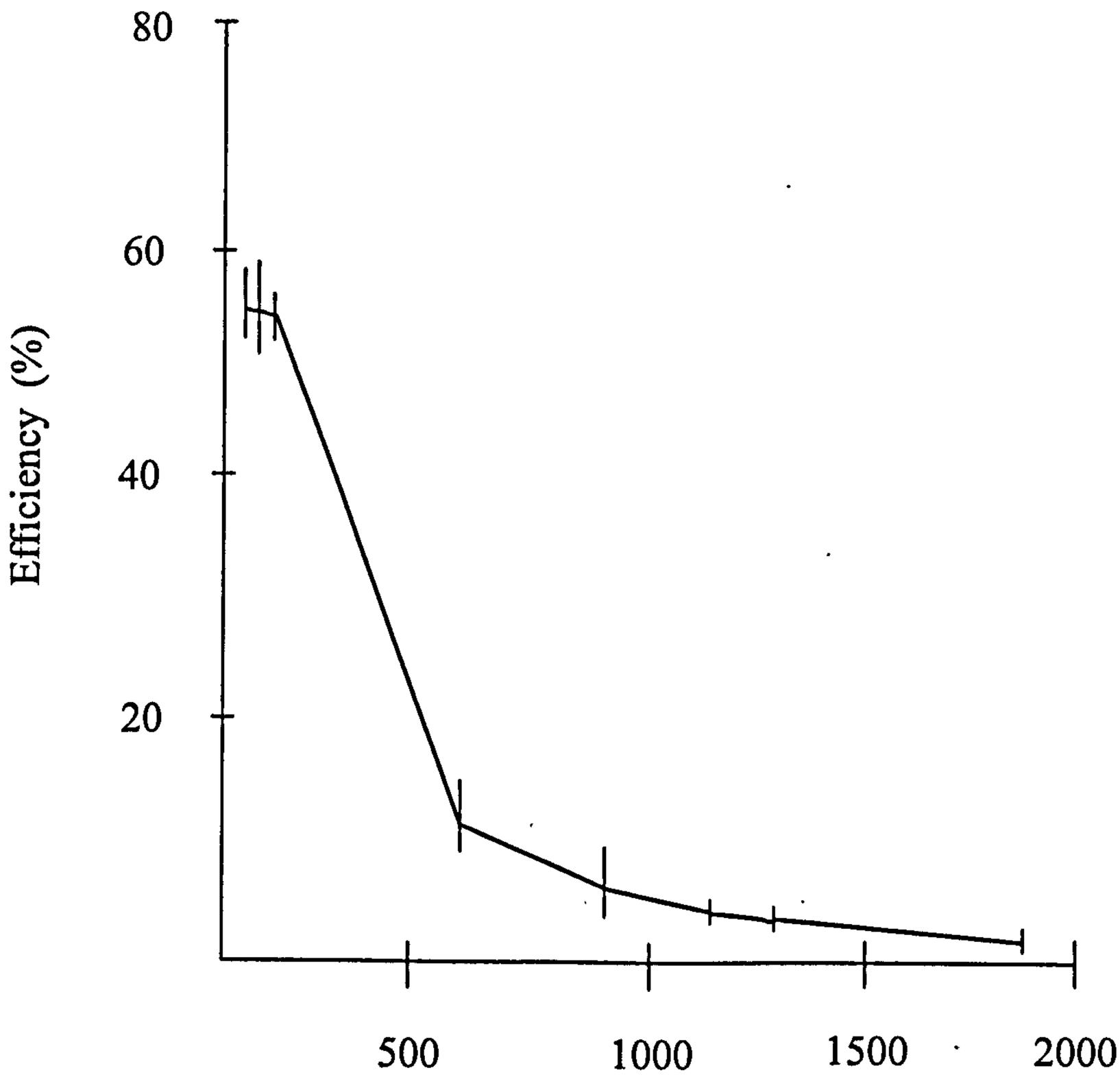

Figure 3.7: Typical counting efficiencies derived from the measurement of the QCY4A Amersham standard reference solution and IAEA135 Irish Sea sediment for the well detectors used during the present study. (Source: Geosciences Advisory Unit courtesy of Dr P. E. Warwick).

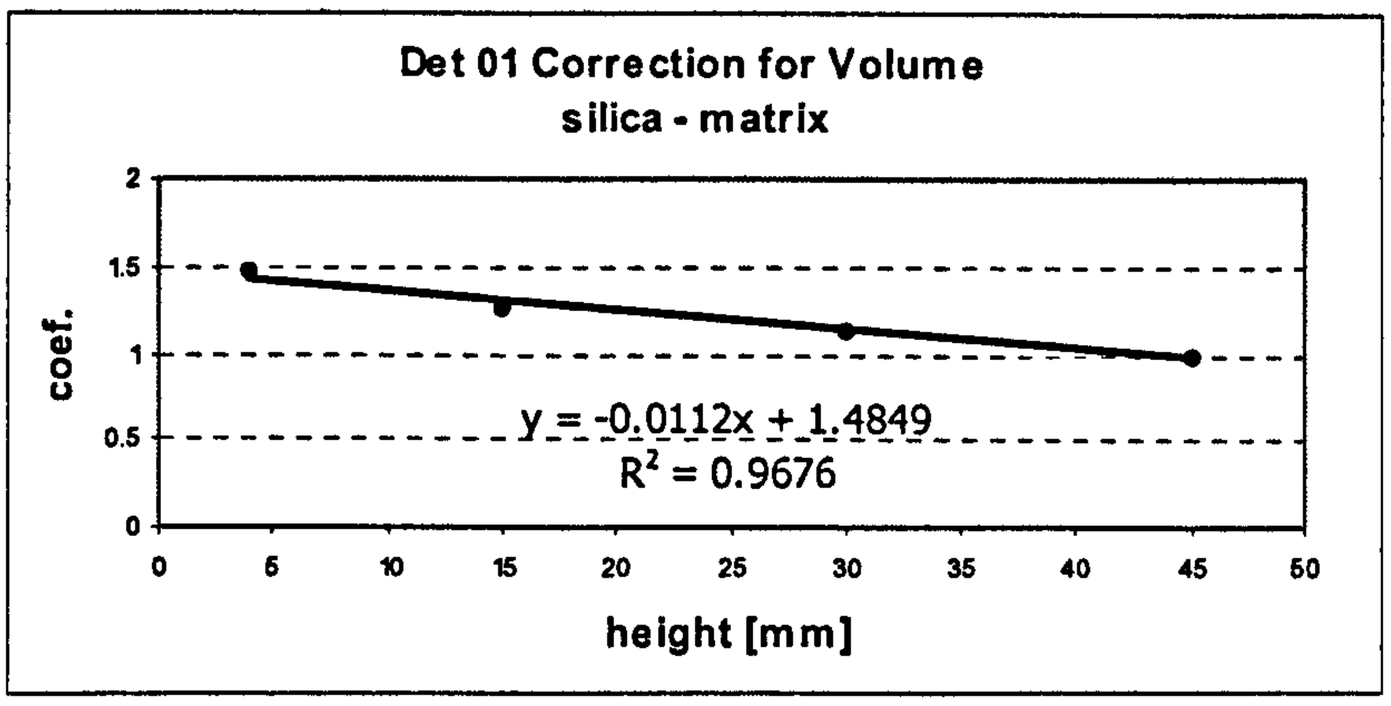

(a)

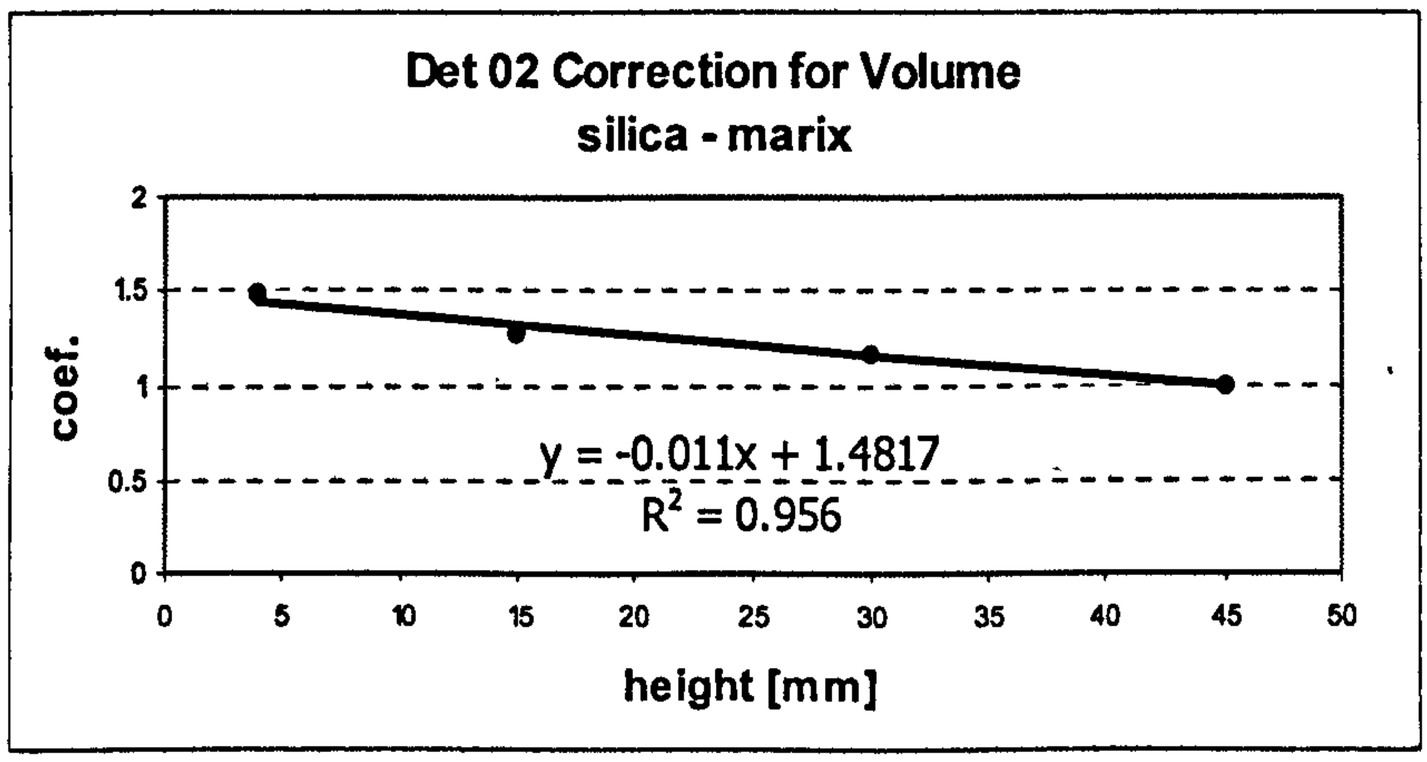

(b)

Figure 3.8: Derived height coefficient correction from variable height measurement of internal mixed gamma source for the two well-type detectors used in the present study (Source: Geosciences Advisory Unit, Southampton Oceanography Centre).

activities derived from the regular background measurements which are updated after each measurement.

One problem encountered by researchers within the Geosciences Advisory Unit has been the lack of sufficient sediment substrate obtainable from the surface layers of marsh cores to adequately fill the polythene vials. A similar situation was encountered during gamma spectrometry analysis of samples for this study and the concern here centered around the potential lack of sediment within the surface layers and the implications for the efficiency of γ-ray detection.

Interestingly the well-type detectors used in this investigation described above have a characteristic that does indeed influence detector efficiency. One consequence of the well-type 4 π geometry (Figure 3.6) is a reduced counting efficiency with vials that are near to full capacity with sample material. This can result in the non-detection of gamma particles that are able to escape detection as a consequence of the near 180° horizontal plane created by filling the vial to the full capacity bringing the level of the sample close to the height of the detector at the open end. Researchers requiring gamma spectrometry analysis conducted measurements of another prepared mixed gamma source with similar physical characteristics at varying heights within the polythene vials. Details of the measurements obtained for the solid silica based standards are shown in Appendix 3 for both the well-type detectors used in this study. These activity/height measurements were then used to create a height correction coefficient which has been applied to the calculated activity derived from the spectral analysis. The derived regression curves for both the well detectors are shown in Figure 3.8.

The depth-dependent correlation coefficient has also been applied to all samples from the four marsh cores analysed in the present study following accurate determination of the height of homogenised substrate present in the vial for each sample. Details of these measurements are shown in Appendix 5.

3.4: Sediment geochemistry: Determination of marsh core geochemistry using X-Ray Fluorescence Spectrometry

X-ray fluorescence spectrometry is one of the most widely used geochemical analytical techniques utilised within the earth sciences and provides a rapid non-destructive method of determining sample elemental concentration whilst not requiring extensive training on the part of the analyst (Gill, 1997). Early systems employed energy dispersive technology however this technology is not considered adequate for the precise quantitative analyses generally required by researchers at present. Modern day systems now employ wavelength dispersive spectrometry which provides the highly accurate capability for quantitative elemental measurements (La Tour, 1989). Additionally the X-ray spectra of most elements are generally less complex than other optical spectra (Fabbi, 1978).

XRF spectrometers use a primary source of radiation from an X-ray tube to excite secondary emission from the sample being analysed. The composition of the wavelength generated is highly dependent upon the material from which the anode is manufactured. For most applications (e.g. environmental studies), the optimal choice is a rhodium anode although other materials such as molybdenum and chromium are also used.

When an atom associated with a particular element within the sample is excited in this manner an electron is ejected from the inner electron orbital. This secondary X-ray radiation (or fluorescence) contains the characteristic peaks of the major and trace elements present in the sample. This excited atom can return to its original ground state by transfer of an electron from an outer atomic shell thus filling the vacancy present in the inner atomic shell. If this transfer proceeds an X-ray photon is emitted which has an energy equal to the energy difference between the initial and final states of the transferred electron.

These X-ray photons can be easily designated as those of the K, L or M shell depending upon the source of the electron filling the shell vacancy (Jenkins 1988). Further sub-division can also be achieved (Kα 1, Kα2, Kβ1 etc.) denoting the electron sub-shell position.

The relationship between the characteristic X-ray photon and the atomic number of certain elements is written as:

$$1/\lambda = K (Z - \sigma)^2$$

where: K is a constant which has a different value for each electron sub-shell.

σ is the shielding constant having a value of just less than 1

The energy E of the X-ray photon is inversely proportional to the wavelength and, therefore, also proportional to the atomic number of the element being irradiated (Jenkins 1988).

This methodology is thus used in X-ray fluorescence spectrometry to generate both the primary and the secondary (fluorescence) X-rays. Figure 3.9 shows a schematic representation of the Philips PW1400 XRF wavelength dispersive spectrometer used in the present study.

Primary X-rays were generated using a 3 kW side window Rh anode X-ray generating tube fitted with a beryllium window which delivers characteristic intense and continuous radiation that interacts with the sample producing the secondary flourescent X-rays. These secondary X-rays are then passed through a primary collimator onto an analysing crystal (Figure 3.9) which diffracts the X-ray continuum into differing wavelength groups. This forms the principle basis of the wavelength dispersive system. The analysing crystal is usually made of pure material such as germanium and will have lattice planes running parallel to the surface. These lattice planes are separated by a definitive distance thereby initiating the separation of various wavelengths via diffraction. Radiation striking the crystal at an angle θ will only be diffracted when the distance traveled by the X-ray photons between successive planes differs by a complete number (n) of wavelengths. Multi-element analysis is made possible by rotating the crystal thus initiating diffraction of different wavelengths by alteration to the angle θ (Philips Analytical Services XRF Information Sheet, 2000).

After passing through the analysing crystal which is mounted on a goniometer the diffracted X-rays pass through a second collimator and are further diffracted prior to arrival at the detector mechanism. The X-ray fluorescence spectrometer used in this study (the Phillips PW1400 model) has two detector mechanisms which enable detection of the X-ray spectrum from low to high energy. Low to medium range X-ray energy (long wavelengths produced by light elements) is detected using a gas flow proportional detector, whilst the medium to high range energy (short wavelengths produced by heavy elements) is detected by the presence of a sodium-lithium scintillation detector. Both of these detector mechanisms convert the photon

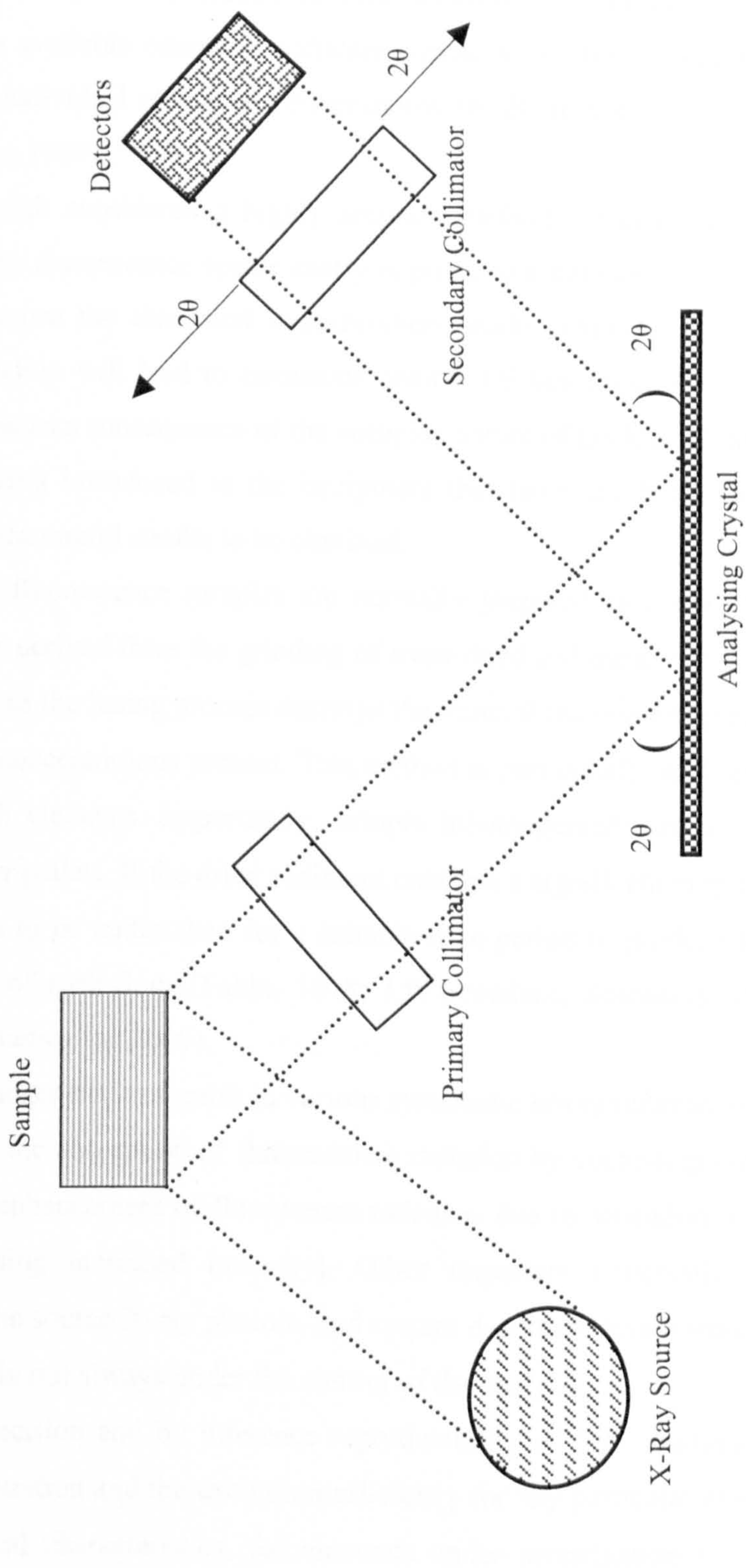

Figure 3.9: Schematic representation of the Philips PW1400 wave dispersion x-ray fluorescence spectrometer used in this study

energy into measurable voltage pulses and because the relationship between emission wavelength and atomic number is known, isolation of individual elemental characteristic concentrations can be estimated from the characteristic line intensities. Quantitative analysis is facilitated by commercially available computer software which is capable of delivering highly accurate and reproducible individual elemental concentration results in the range of 1ppm to 100% (Jenkins, 1988; La Tour, 1989).

Although considered a highly accurate method for quantitative analysis of geological materials X-ray fluorescence spectrometry is prone to a number of random and systematic errors that can influence the elemental concentration results obtained. Contamination of the sample during preparation will lead to erroneous results. Of key importance is sample inhomogeneity which can arise as a consequence of the complex nature of geological samples and also as a result of samples being introduced to the equipment that have not been homogenised to the degree required for meaningful results to be obtained.

X-ray fluorescence samples are normally prepared as fused glass beads or as pressed powder pellets derived from the grinding of oven-dried sediment. The former method poses little or no problem as the fusing process destroys the mineral fraction and permits full identification of the elemental concentrations present. This method is particularly applicable for the determination of major earth elements. Importantly, sample inhomogeneity can arise in the preparation of pressed powder pellets. If the dried sediment contains a significant proportion of coarser material, grinding needs to be undertaken for a suitable time period to produce the required consistency, generally that of rock-flour (Fabbi, 1978; I.W.Croudace, Southampton Oceanography Centre, personal communication 2000).

Inhomogeneity can result in various systematic errors referred to as matrix effects. These can arise from the absorption of fluorescence radiation by coexisting elements (causing reduced intensity) and enhancement of fluoresence radiation due to secondary radiation from coexisting elements (causing increased intensity). Other important systematic errors include primary absorption of the source X-ray photons and system dead-time losses which can be significant and are unfortunately not always under the control of the analyst.

The precision and by inference reproducibility of XRF analysis is dependent upon the element concentration and the excitation efficiency for any particular element. As a consequence of these physical characteristics, for elements under investigation those yielding results well

above their limit of detection will generally have a precision of less than ± 1%. For other trace elements that are near to detection limits precision can be enhanced by extending the analysis time period typically yielding a precision of ± 5%.

Equipment accuracy is normally assessed by the regular use of certified standard reference materials and calibration is achieved by measuring the intensities of these standards to establish response curves (Croudace and William-Thorpe, 1988). Matrix effects are also commonly taken into account and correction for such anomalies is normally reliably rectified by computer algorithms that compensate for such interferences. These are generally provided by the manufacturer and included in any purchased package of equipment (Philips Analytical Services XRF Information Sheet, 2000). The preparation proceedure for XRF analysis undertaken in this study is described in Appendix 1 and follows the method outlined in Croudace and Williams-Thorpe (1988).

The precision of the analyses were routinely monitored by comparing a range of standard reference materials (typically USGS; MAG-1 marine shale) run prior to and following the range of samples. Precision for major elements was less than 2% with occasional samples showing error in the order of < 4%. For trace element data precision was generally of the order of 5%.

During the preparation of some sediment sub-samples, most notably those from the basal sections of cores, the distinct coarse fraction required extra attention with regard to obtaining the desired rock flour consistency . Due care was, therefore, taken to adequately grind these samples to minimize potential error and damage to equipment . In some cases intact samples that had been run and appeared upon closer inspection to be insufficiently homogenous were reground and run for a second time and the results compared. In most cases differences of generally less than 3% total concentration of certain elements were noted (data not shown) and are considered to be reflective of the extra grinding time expended on these samples. The data from the second analysis derived for such samples has been included in the tables of geochemical results for all cores and these data can be found in Apendix 4.

3.5: Geochemical data manipulation: Normalization

The procedure of normalizing geochemical data arises from the requirement to take account of mineralogical variations within sediment samples that result from grain-size effects.

Sediment grain size is possibly the single most important physical factor that controls the distribution of trace elements and contaminants within estuarine and coastal sediments (Loring, 1992). In order to make direct comparisons between sediments and sub-samples thereof, it is necessary to assess whether or not differences in bulk concentration are due to variation in the abundance of the detrital mineral phase. This leads to the phenomena of the 'constant sum problem' in sedimentary geochemistry further discussed by Rollinson (1992).

A variety of normalizing techniques have been developed ranging from trace metal analysis of a specific grain size fraction of the sediment (e.g. Ackermann *et al.*, 1983; O'Reilly Wiese *et al.*, 1995), use of regression curves based upon grain size, surface area or conservative elements (e.g. Salomons and Mook, 1977; Ackermann, 1980; Loring, 1990) and calculation of ratios of trace elements relative to conservative elements (e.g. Din, 1992, Thompson *et al.*, 1995, 2001; Cundy *et al.*, 1997). A review of these methods can be found in Rae (1997).

This latter method has received much attention particularly in studies undertaken in marine and coastal environments. Within such settings Al and other conservative metals such as Rb and Li have proven to be effective in the quantification of anthropogenic inputs of heavy metals (Loring, 1990; Grant and Middleton, 1993 Croudace and Cundy, 1995; Cundy and Croudace, 1995).

In some studies caution has been advised in the use of a normalizing method (particularly conservative metals such as Al) within heavily industrialized locations (e.g. Cearreta *et al.*, 2000). Similarly, the use of Al has been questioned in studies undertaken within coastal settings in proximity to formerly glaciated igneous terrains (Loring, 1991). In the latter case the concern regarding the use of Al surrounds the fact that natural trace metal concentrations may not always vary with changes in grain size and mineralogy in such sediments owing to the presence of significant quantities of feldspars containing alumino-silicate minerals (Loring, 1991). However, the study by Gallagher *et al.* (1996) investigating the trace metal content of Northern Irish coastal marshes, does implement a normalizing method based upon the technique outlined in Ackermann *et al.* (1983). From the published literature it would seem that there is no universally applicable technique for normalizing trace element data (Rae, 1997). As a consequence individual studies must be considered on their own merit with regard to the environmental setting and background geology, the degree to which anthropogenic input may have influenced the locality and equipment availability and overall cost of the analysis. A simple method of assessing elevated concentrations

of heavy metals is through direct comparison with the background geology (e.g. Cearreta *et al.*, 2000) or where available geochemical survey data of the surrounding or regional geology.

In the present study geochemical data has been determined from X-ray fluorescence spectrometry (XRF). This technique has provided a wealth of accurate data pertaining to trace element concentrations within the four sediment cores analysed. Contained within the data are values for Al and Rb, two metals which are routinely employed as normalizing elements. X-r-f analysis does not provide the capability for determination of Li suggested by Loring (1991) as being superior to Al within formerly glaciated areas for normalizing purposes.

The geology of the four study sites are distinctly diverse from one another (see relevant sections in Chapter Four) and as a consequence the normalizing procedure will be discussed in detail with reference to the use of Al and Rb at individual sites. Addtionally, comparison with background levels of trace elements will also be undertaken at each site from published data for the Argyll region (British Geological Survey, Regional Geochemical Atlas, Argyll, 1990) providing a method with which to assess trace element concentrations in the coastal wetlands of this part of western Scotland.

3.6: Determination of organic carbon content: Loss on ignition analysis (LOI)

In many environmental investigations the routine determination of carbon content within sediments has been undertaken (e.g. Hatton *et al.*, 1983; Grimshaw, 1989; Bierman *et al.*, 1997; Brezonik and Engstrom, 1998). Carbon can be divided into two distinct fractions the first of these being organic carbon (i.e. the remains of plant and animal tissue incorporated into the sediment matrix. The second of these two fractions is the inorganic fraction which largely comprises the amount of calcium carbonate present within the sediment matrix (Dean, 1981). Both of these fractions can be determined via the measurement of weight loss following ignition (Dean, 1974) of a sub-sample of sediment from for example the depth increment of a sediment core under investigation.

This method is fairly straightforward to implement however it is important to understand that the accuracy of the LOI technique is dependent upon both the concentration of organic matter present and the composition of the sediment (Boyle, 2001). Problems arise as a consequence of

the percentage of structural water that can be contained within the mineralogical fraction of sediments (mainly clay minerals). Boyle (2001) draws attention to the fact that some clay minerals can contain as much as ten weight percent structural water. When samples such as these are heated during the ignition process this water is progressively released from the mineral lattice. As a consequence any sediment recording an LOI value of around 10 weight percent need not necessarily be indicative of the presence of organic carbon. This problem has been previously discussed by Mackereth (1966) who highlights a significant discrepancy between the actual carbon measured by instrumental carbon analyser and the values obtained via the LOI method.

Ball (1964) suggests that a lowering of the ignition temperature (maximum = 375 °C) offers a suitable means of minimizing this problem. However, Boyle (2001) highlights the fact that at this temperature not all the organic carbon will necessarily be combusted.

Salt-marshes develop at the land-sea interface in inter-tidal lowland settings. As such organic carbon will be present as both autochthonous material (e.g. Hatton *et al.*, 1983; Cundy and Croudace, 1995), derived from the in situ growth of haolphytic plant species and an allochthonous component (e.g. Craft *et al.*, 1991; Bierman *et al.*, 1997), derived from both freshwater and marine aquatic transport processes and subsequent incorporation into accreting sediments. Diagenetic (post-burial) processes will also act to affect the below ground organic and inorganic carbon concentration (Rae and Allen, 1993; Reddy and D'Angelo, 1995).

In the case of estuarine and salt-marsh sediments near-linear relationships have been established between organic carbon and measurement via LOI determination (Cundy, 1994; Lewis; 1997; Turner, 1999). Comparison with total carbon elemental analyser techniques further support the use of the loss on ignition technique as a proxy method for organic and inorganic carbon determination. Boyle (2001) recommends that LOI investigations should be viewed from the standpoint of compromise in relation to the focus of the investigation and that further more expensive analysis may only be required where extremely low LOI-derived organic carbon results are obtained and only if this is a definitive requirement of the investigation.

In the present study organic and inorganic carbon determination has been undertaken via the LOI method and full details of the technique relevant to this study are outlined in Appendix 1.

3.7: Microfossil investigation of saltmarsh sediments: Diatom analysis

Diatoms amongst other distinct microfossils (*Foraminifera*, Ostracods and *Testate Amoeba*) have provided the ecologically based methodology with which assessment of Late Quaternary changes in coastal salinity has been developed (van de Plassche 1982).

Many diatom taxa are recognised as being tolerant or otherwise of variable saline conditions experienced within coastal settings. Within the confines of taxonomic and reliable habitat data many diatom species are now classified according to their sensitivity to varying salt water conditions (Hustedt, 1957; Simonsen, 1962, 1969; Hendy, 1964; van de Plassche, 1982; Shennan *et al.*, 1983; Vos and de Wolf, 1988a, 1993a; Denys and de Wolf, 2000).
The classification of salinity follows the scheme developed by some of these authors and can generally be described as:

1) *Polyhalobian* (generally consisting of marine species which can tolerate salinity at and above 30 parts per thousand ($^{o}/_{oo}$)).

2) *Mesohalobian* (those species that can tolerate brackish waters ranging from 2–30 $^{o}/_{oo}$)

3) *Oligohalobian* (consisting entirely of freshwater species with tolerance of salt at levels less than 2 $^{o}/_{oo}$ and further divided into halophillic and indifferent classes)

4) *Halophobous* (consisting of true fresh water species that are totally intolerant of any salt), (adapted from van de Plassche, 1982).

This generally accepted classification has been the subject of alteration in the past, for example the reclassification undertaken by Patrick and Reimer (1966) who simplified the groups by including halophillic, indifferent and halophobic classes into the *Oligohalobian* group. Further methodological development has been the subject of reviews by Shennan *et al.*, 1983, Palmer and Abbott (1986) and Vos and de Wolf (1988a; 1993a).

The application of diatoms using this classification scheme to investigations of coastal palaeo-environmental change has received very wide coverage by a multitude of authors from sites around the world (e.g. Simonsen, 1969; Denys,1982; Stabel, 1982; Tooley, 1982; van de Plassche, 1982; Eronen *et al.*, 1987; Palmer and Clague, 1991; Long, 1992; Plater and Shennan,

1992; Hemphill-Haley, 1995a; Vos and de Wolf, 1993b; Denys and Bateman, 1995; Zong and Tooley, 1996, to name but a few). Studies of coastal evolution in Scotland have been no exception with diatom-based investigations contributing significantly to the abundance of published data that has utilised bio-stratigraphical techniques (e.g. Robinson, 1982, 1993; Haggart, 1986, 1987; Smith *et al.*, 1992; Shennan *et al.*, 1994a, 1995; Dawson, 1998; Smith *et al.*, 1999; Selby *et al.*, 2000). These studies have attempted to constrain the movement of relative sea-level by identifying distinct taxonomic variation with depth indicative of salinity changes resulting from either trangressive or regressive sea-level tendency.

As with other microfossil-based investigations, the use of diatoms can be prone to mis-interpretation if suitable consideration is not given to key thanatocoenose in fossil/sub-recent tidal environments (Brockman, 1940 cited in: Vos and de Wolf, 1988). Hence, the influence of autochthonous versus allochthonous species identified in sedimentary sequences is vitally important to the interpretation of the localised palaeo-enviromental conditions (Beyens and Denys, 1982). Autochthonous species will be indicative of coastal environmental change that has taken place in a particular locality. Such species are likely to be predominately benthic taxa occuring in sufficiently high density to be considered typical of a well-defined environment (Simonsen, 1969). Allochthonous species on the other hand, will be more indicative of environmental conditions within the surrounding area (König, 1983) and may be derived from the influence of fluvial input or transportation of benthic and planktonic taxa from neighbouring coastal environments.

Other physical and chemical environmental factors can also exert a significant influence upon the ratio of autochthonous and allochthonous taxa present in coastal palaeo-sediments (Simonsen 1969). Diatom frustules are constructed from silica which is precipitated from the water column during the life cycle of the organism. Generally, within low energy sedimentary environments the frustules of diatom taxa are found well preserved owing to the rigidity of the valve structure and resistance to chemical dissolution following burial. Where breakage and dissolution are considered to have influenced the assemblage record (Andrews, 1972, Beyens and Denys, 1982), care is needed in the counting procedure and measures must be uniformly implemented in attempts to accurately document species assemblages (Beyens and Denys, 1982; Batterbee, 1986; Flower *et al.*, 1993). Predation is also a factor considered by Romeyn and

Bouman (1983) to exert an influence on recorded assemblages from coastal estuarine environments.

As a method for recording sea-level changes, diatom analysis has proven to be a powerful and valuable biostratigraphic tool providing information regarding salinity fluctuations in conjunction with appropriate dating methods applied to coastal sediments (usually ^{14}C). More modern-day studies are now focusing on contemporary coastal wetland sediments and in conjunction with powerful computer-aided statistical methods identification of discrete species zonations in terms of water depth and marsh hydroperiod are facilitating improved interpretations of palaeo-water depths in older Holocene coastal sediments (Zong and Horton, 1998; Gehrels *et al.*, 2001).

Diatom analysis is a reasonably straightforward analytical process involving sub-sample pre-treatment processes to remove unwanted organic material. The sample is then centrifuged and a small volume of the clear aliquot is carefully pipetted onto a cover slip. This is allowed to dry and is then mounted onto a microscope slide using Naphrax solution (Battarbee, 1986). Prepared slides are then examined under a light microscope at x1000 magnification or greater. The diatom species assemblage can then be assessed and for sea-level research this entails counting a representative coverage of the slide (typically 200 – 500 species per slide) or the entire slide if valves are not seen in abundance. Species assemblages are then expressed as a percentage of the total counted from each individual slide (Tooley, 1982; Dawson, 1998). A full account of the preparation and analytical procedure is summarized in Appendix 1. Various computer software packages are available for the plotting of microfossil data and in this study the package derived from pollen studies referred to as TILIA Version 2 incorporating the CONISS total sum of squares cluster analysis has been employed to aid in data presentation.

In this study diatom analysis has been applied to the core extracted from the head of Loch Etive, one of two loch-head sites situated within mainland Argyll. The stratigraphy of this core revealed the presence of a 12 cm thick organic-rich, black, coarse sandy unit and as such it was felt that diatom analysis would provide detailed information regarding the provenance of this sub-unit and hence aid in the interpretation of the depositional history of this marsh core .

The diatom stratigraphy of this core is presented in Chapter 4.

3.8: Aerial Photography

To compliment the analytical techniques air photographs covering the locations of the four study sites have been purchased from the offices of the Royal Commission on the Ancient and Historical Monuments of Scotland (RCHAMS). These cover three distinct time periods over the past sixty years or so. The earliest set are derived from former Lufftwaffe fly-overs taken towards the end of the second world war in 1945-46. Although not of high quality sufficient geomorphological features can be identified to make these of use. The second set of images derive from Royal Air Force reconnaissance flights during the1960's and images for each site have been obtained over the period 1966-1967. These are generally of good quality with shadow interference at the head of Loch Etive being the most significant detrimental effect. The most recent images are also derived from RAF and RCHAMS activities and were all taken during 1988. These are also of good quality especially those covering sites on the Isle of Mull with mountain shadow at the head of Loch Etive again being the only major detrimental problem.

These images have proven useful in aiding site description and indicating both the topographical setting of the individual study sites whilst also helping to indicate key goeomorphological features of the site locations and the contemporary marsh morphology.

3.9: Instrumental Levelling

At all the study sites the accurate determination of the individual core altitudes was undertaken to help provide data relating to the height of the sediment cores relative to Ordnance Datum Newlyn (ODN) and to provide a means of assessing the altitude of any particular core relative to the tidal range derived from the nearest tidal gauge stations (see Chapter 4). Measurement was achieved using a Leica 700 TPS EDM total station set up at each site to measure the altitude of all sedimentary sequences abstracted from the four sites.

Accurate determination was further facilitated following purchase of 1:10000 scale Ordnance Survey maps from which bench mark data could be obtained. Some of these sites are quite remote and have not been surveyed since the 1955 Ordnance Survey of Great Britain. As a consequence some bench marks proved very difficult to locate and resulted in leveling of temporary benchmarks in order to obtain the required data which constitutes the first of four

sections highlighting the results obtained from the analysis of the Argyll marsh cores. Core altitudes relative to ODN are included in the following chapter

3.10: Determination of Study Sites

Initial reconnaissance for potential contemporary marsh sites within the Western Highlands followed examination of the 1:25000 scale Ordnance Survey maps, reference to recently reviewed isobase maps (Smith *et al.*, 2000) and consultation of MAFF. Report No. ES23 (Pye and French, 1993). Potential field site locations across the Firth of Lorne region (shown in Figure 4.1) were investigated to establish the presence or otherwise of significant contemporary coastal marsh development at a number of locations. This area of Argyll has been previously investigated from a geomorphological standpoint by Gray, (1972 and 1974a) over 30 years ago. The work of this author was one of the earliest published research papers to demonstrate the presence of the uplift dome and hence, differential crustal uplift across the Scottish mainland based upon the analysis of raised shoreline features within the area (see Figure 1.1).

Considerable coastal wetland development was observed at a number of different locations. These included coastal marshes of variable extent at the head of some of the large fjords on mainland Argyll. Sites on the Isle of Mull were also visited to assess the potential for inclusion in the project. Two sites were identified situated on the south-east side of the Isle of Mull at Loch Don and on the western side of the island at the Head of Loch Scridain where extensive marsh development had been previously reported (Prof. M.J. Tooley, personal communication).

Study sites were eventually selected on the basis of overall marsh development with preference being awarded to those sites with adequate areas of 'high – marsh' (mature) sediments. Sediment sequences of this nature are critical in terms of evaluating the relationship between coastal marsh morphodynamics and the response of salt marsh environments to relative sea-level movements (Pethick, 1981; Allen 1990).

The final selection of suitable study sites facilitated the construction of a transect extending across several isobase contours (Smith *et al.*, 2000; Figure 3.10) in a coastal region characterised by maximum uplift for the Main Postglacial shoreline. This decision was based upon the rationale that it might be possible to identify the signature of recent differential relative sea-level changes across the study area from ongoing crustal movements derived from the

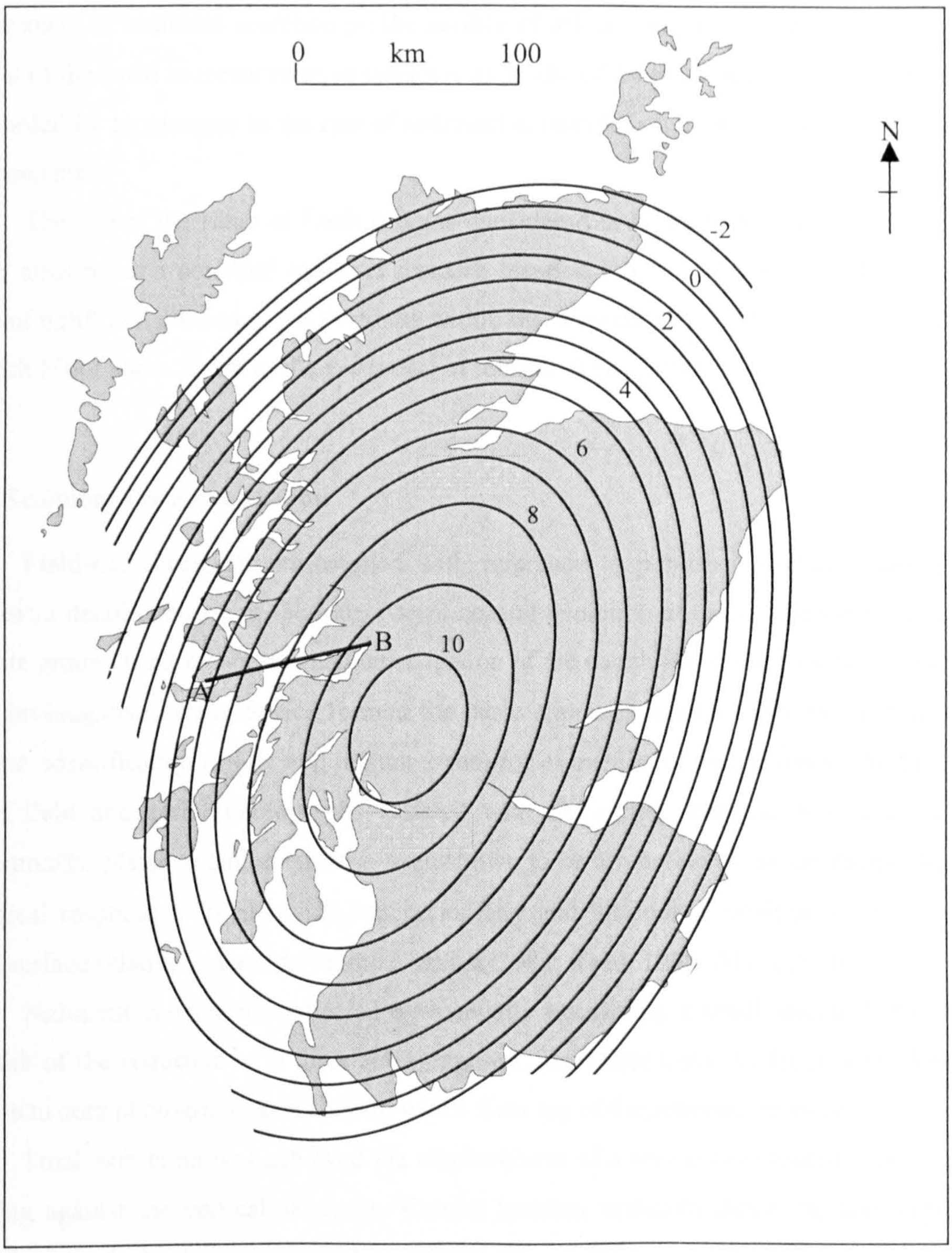

Figure 3.10: Isobases for the Main Postglacial shoreline in Scotland based upon quadratic trend surface analysis (after Smith *et al.*, 2000). The line A-B represents the transect across these isobases from selected contemporary marsh sites across the Firth of Lorne investigated in the present study.

measurement of sediment accretion on the surface of mature marsh environments. The proposed reversal of the trend in recent relative sea-level as predicted by the model of Pethick (1999) might be recorded by an increase in the rate of sediment accumulation upon the surface of these marsh environments.

The site at the Head of Loch Etive is considered to be an important site in terms of the project aims being a potential sea-level research location in close proximity to the hypothesised centre of uplift and maximum ice thickness within the Western Highlands, formerly centered over Rannoch Moor some 20 km to the north-east of this site (Gray, 1974).

3.11: Sediment Core Acquisition

Field-site investigations coupled with reference to published literature have provided some extra detail concerning the longer-term coastal evolution at the selected study locations.At each site ground truthing and manual investigation of the marsh sub-surface using an extendable 1 metre investigative coring device formed the basic approach used to identify suitable sampling sites (i.e. identification of low and mature areas) for extraction of marsh cores. Additionally the use of field and aerial photographs assisted with delimiting inter-site low and high marsh environments. Marsh zonation has also been shown to be a function of the geomorphological and ecological response to tidal inundation periodicity and altidudinal position of location on the marsh surface relative to the tidal frame (Pethick, 1982; Reed, 1995; Allen, 2000).

Sediment cores were collected by manually excavating a small area to leave an in-situ monolith of the sequence with three sides exposed. The unprotected surfaces were then cleaned and in-situ core photographs taken along with a field log of the sediment monolith.

Final extraction was achieved via emplacement of a previously cleaned section of plastic guttering against the vertical sequence. Careful incision vertically down the core depth on the remaining attached side accompanied by gradual tilting of the monolith sequence proved to be an effective method with which to separate the monolith from the surrounding sediments. Following successful extraction the cores were then carefully sealed with 'cling-film' wrapping and labeled in preparation for transport back to the laboratory. In order to provide for some insurance against transit or other possible damage to the integrity of the extracted cores a minimum of two monoliths were taken from various suitable sampling locations across the salt-marshes at each site

Once back at the laboratory individual cores were logged in detail and digitally photographed prior to the commencement of sample preparation.

Logged cores where then sliced at 1cm intervals and the entire one cm slice obtained was oven-dried for a minimum of 48 hours at 45^{O}C. Representative sub-samples from each slice were then taken for the various analytical methods. Approximately 2 grams was used for ^{210}Pb with a further 20 grams used for gamma spectrometry. A minimum of 3 grams of dried sediment was used for LOI determination and this material was retained for major element geochemistry. Trace element geochemistry required at least 10 grams of ground oven-dried sediment. In many cases this constituted material derived from post-gamma spectrometry. Microfossil slide preparation required a 1gram representative sub-sample. Any remaining oven-dried sediment was retained and archived.

The results derived from the physical field site surveys, core extraction and the various analytical methods outlined earlier in this chapter are now presented in the following four results chapters which focus on the specific aspects of the study highlighted in Chapter One.

Chapter Four

THE SALTMARSHES OF ARGYLL

FIELD STUDY SITE DESCRIPTIONS

AND

CORE CHARACTERISTICS

4.1: Introduction

Chapter Four constitutes the first of four sections of the thesis which present in detail the various different facets of the research undertaken in the interpretation of contemporary coastal wetlands situated in Western Scotland.

In this chapter a concise overview of the four study sites and their environmental context is given and this is followed by a comprehensive presentation of the sediment logs with description of the core material.

Major element geochemistry data (element oxides) are presented for each sediment core and used as a proxy for ascertaining the compositional variability and detrital sediment dynamics within the four marshes studied. The trace element compositional data is also introduced here to give a complete perspective regarding the overall sediment composition.

Cluster analysis of the geochemistry raw data (using the TILLIA software program, Grimm, 1991) provides a means of assessing geochemical zonation in relation to the compositional variability described in the sedimentary logs.

Inclusion of a detailed microfossil (diatom) analysis for the core from the head of Loch Etive is presented and used here to facilitate a more comprehensive insight into the depositional history of this in light of the more complex stratigraphy recorded in the sediments of this marsh.

4.2: Geographical location of the study sites

The four research sites are located on the western and south-eastern coasts of the Isle of Mull and across the Firth Of Lorne situated on mainland Argyll. These are shown in Figure 4.1 and the grid reference based upon Ordnance Survey of Great Britain 1:25000 scale maps is presented below.

			OS Reference (1:25000 Scale)
Isle of Mull:	*West:*	Head of Loch Scridain	NM 542286
	East:	Upper Loch Don	NM 724323
Mainland Argyll:		Head of Loch Creran	NM 208451
		Head of Loch Etive	NM 114453

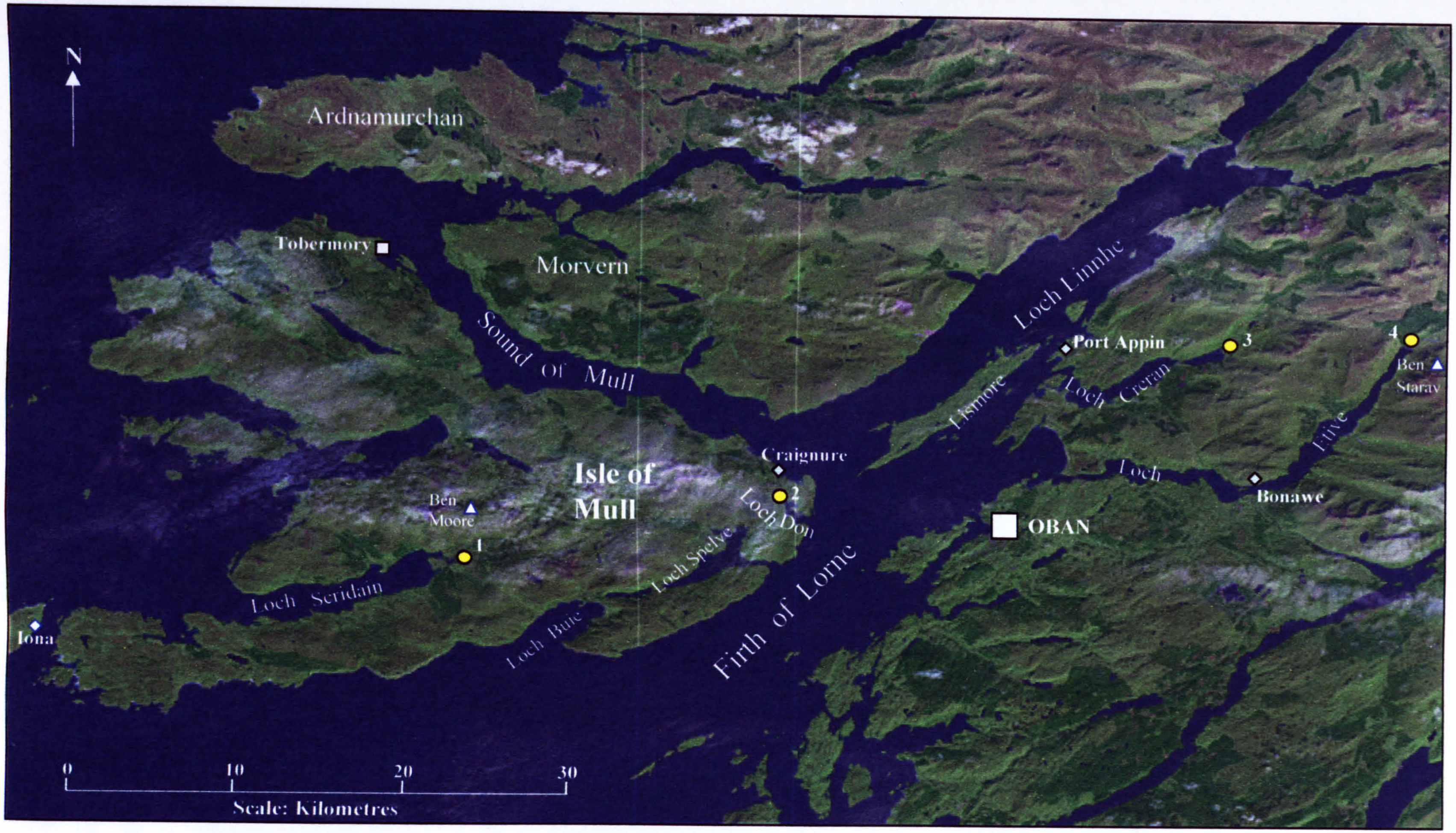

Figure 4.1: Landsat TM image of the Argyll region around the Firth of Lorne. Selected study sites are indicated by the yellow circles at the Heads of the Lochs investigated: 1) Loch Scridain, 2) Loch Don, 3) Loch Creran and 4) Loch Etive. Recently implemented tide gauge stations for the region are indicate by white diamonds.

4.3: Tidal data for the study region

Longer–term tide-gauge data for Western Scotland is relatively sparse when compared to other coastal regions of Northern Europe. The Firth of Lorne region is no exception to this general trend. However, the implementation of some very recent tide-gauges has occurred at several locations within the study region (Figure 4.1) and these provide some indication of the tidal range in close proximity to the selected study sites (Table 4.1).

Tide Gauge Site	MHWS	MHWN	MLWN	MLWS	Tidal Range
Iona (Western Isle of Mull)	4.0	3.0	1.50	0.50	3.50
Craignure (Eastern Isle of Mull)	4.0	3.0	1.70	0.60	3.40
Oban (mainland Argyll)	4.0	2.90	1.80	0.70	3.30
Port Appin (mainland Argyll)	4.20	3.10	1.90	0.80	3.40
Bonawe (central Loch Etive)	2.20	1.20	0.50	0.20	2.00

Table 4.1: Tidal ranges for selected tide-gauge stations from Western Isle of Mull across the Firth of Lorne to mainland Argyll. All heights and ranges given are in metres OD. (Data from Belfield Tideplotter version 3.1, 2000).

Mean tidal range at Loch Scridain, Loch Don and Loch Creran range from 3.4 m OD to 3.50 m OD. However the mean tidal range at Bonawe central Loch Etive is ~ 2 m OD. The discrepancy in tidal range between the gauge inside Loch Etive compared to that from outside Loch Etive within the Firth of Lorne e.g. at Oban results from the effect on tidal range caused by the presence of the Falls of Lora at Connell Bridge and the submerged rock platform associated with the restricted entrance to Loch Etive.

The tidal range data further aided the selection of coring sites from mature marsh settings at the four locations. Final selection of individual core sampling sites followed field visits timed to coincide with spring tides. This facilitated an assessment of the extent of tidal

incursion over the Highest Water Ordinary Spring Tides (H.W.O.S.T) period across the marsh surface. Additionally, actual sampling sites were visually observed during such conditions using surveying ranging poles and the flooding characteristics of each sampling point in relation to marsh inundation could also then be assessed.

4.4: Marsh core elevations from the four sites

All core sites were leveled to Ordnance Datum Newlyn using a Leica research surveying level relating all measurements to a standard bench-mark height. These were determined from the 1 :10000 scale Ordnance Survey maps of the four site locations. Reduced level altitudes of all cores from the four sites are shown in Table 4.2 below.

Study Site Location	Core ID	Surface Altitude (m O.D)
Loch Scridain	Core 1	1.716
	Core 2	1.927
	Core 3	1.787
Loch Don	Core 1	1.962
	Core 3	1.744
	Core 4	1.886
Loch Creran	Core 1	1.869
	Core 2	1.659
Loch Etive	Core 1	1.141
	Core 2	1.318

Table 4.2: Altitudes in m O.D. Newlyn of all cores abstracted from the study sites in Argyll. The grey-shaded core numbers and measured altitudes indicate the sequences used for further analysis in this study.

4.5: Major element geochemistry and core detrital composition

The inorganic component of sedimentary material supplied to a marsh surface will ultimately be derived from a combination of both physically weathered substrate delivered via fluvial transportation and that derived from marine sources (allocthonous sediment). As such the

variability of the inorganic sedimentary composition can be revealed used to make inferences concerning the core composition and sediment provenance based upon the relative abundance of individual elements, their down-core distribution and association with other inorganic components and organic content. Major element abundances are recorded as oxides (according to XRF convention) and include silica (SiO_2), titanium (TiO_2), aluminium (Al_2O_3), iron (FeO_2), manganese (MnO), magnesium (MgO), calcium (CaO), sodium (Na_2O), potassium (K_2O) phospherous P_2O_5 and sulpher (SO_3). These major constituents marsh core have been determined for the four marsh core profiles examined. Elements such as Al and K serve as useful proxies for fine sediment whereas Si and Ti are more closely associated with the coarse material. Fe, Mn and S will also be associated with the detrital phase but the distribution of these elements is also mediated by early diagenetic reactions (see Chapter Six). Mg and Ca may represent biogenic material incorporated into the sediment matrix whereas Na and P are likely to associated with the above and below ground organic accumulation.

Trace elements form an important component of all estuarine sediments and inter-tidal saltmarshes are no exception to this. The distribution of these components can also be influenced by a variety of different physical and chemical processes that occur within estuarine environments (e.g. detrital inputs, association with marsh organic material and post-depositional inorganic/organic chemical reactions). Some of these may act alone and therefore solely control trace element distributions. However, owing to the complex chemistry of estuarine waters this is very seldom the case and usually the behaviour of trace elements is controlled by a number of processes which are in turn influenced by the environmental gradients particular to any one estuary. These are discussed further in Chapter Seven.

The down-core profiles of major element constituents from the four cores are now discussed in the following sections. At the end of each core sub-section trace element profiles are presented. Statistical analysis of the distribution of both major and trace elements enables a general comparison of the down-core compositional variability derived from the measurement of inorganic and organic components of marsh core sediments. Inferences regarding sediment provenance and inputs to the marsh are examined by means of regression correlation undertaken on the major element and LOI data.

4.6: The Isle of Mull: Geology and Environmental Setting

The Isle of Mull contains the most complex assemblage of volcanic and sub-volcanic rocks in the British Tertiary Volcanic Province (Figure 4.2). Older rocks outcrop at certain localities. The oldest of these are the Lewisian Gneisses which underlie Mull and outcrop on the island of Iona to the west. In the north-east and to the east of Fionnphort, Moine metasediments that were intruded by the late Caledonian Strontian granite are evident. In the south east of the island rocks of Dalradian age including black limestone and grey phyllites can be seen within the upper regions of Loch Don where Devonian Lavas are also present. Narrow strips of Tertiary, Jurassic and Cretaceous sediments are evident on the south and east coast of Mull around Loch Buie and within the Duart Bay and upper Loch Don area.

Undoubtedly the geology of Mull is dominated by the extensive series of plateau lavas. Richey *et al.* (1961) describe these as being "the most complete sequence of plateau lavas within the Inner Hebrides". They consist largely of basalt and in several locations several steps representative of individual lava flows emminating from the early intrusive and pyroclastic centre of Glen More may be seen. These are especially well developed on the Ardmeanach peninsula (Gray 1973). The centre of Mull is also dominated by the series of igneous intrusive rocks that derive from the former caldera. This later centre of volcanicity shifted on two separate occasions moving first to the north-west around Beinn Chaisgidle followed by a second shift to the Loch Ba area where a significant ring dyke of felsite has been intruded forming a complete ring fault that surrounds the former final caldera position.

4.7: Loch Scridain (south western Isle of Mull)

4.7.1: Site Description and environmental setting

Loch Scridain is situated on the western side of the Isle of Mull and represents a fjord with open access to the Atlantic Ocean some 26 km in length and 3 km wide at the seaward extremity (Figure 4.1). At the head of the fjord the rock outcrop "Aird of Kinloch," consisting predominately of extrusive basalt with N-S trending dykes of mugearite, benmorite, dolerite and early basic olivine rich dolerite and craignurite, forms a topographic constriction at which point the upper part of Loch Scridain leads into Loch Beg (Figure 4.3). At low tide the easternmost section of this outcrop is exposed. Landward of "Aird of Kinloch" the sheltered area of "An

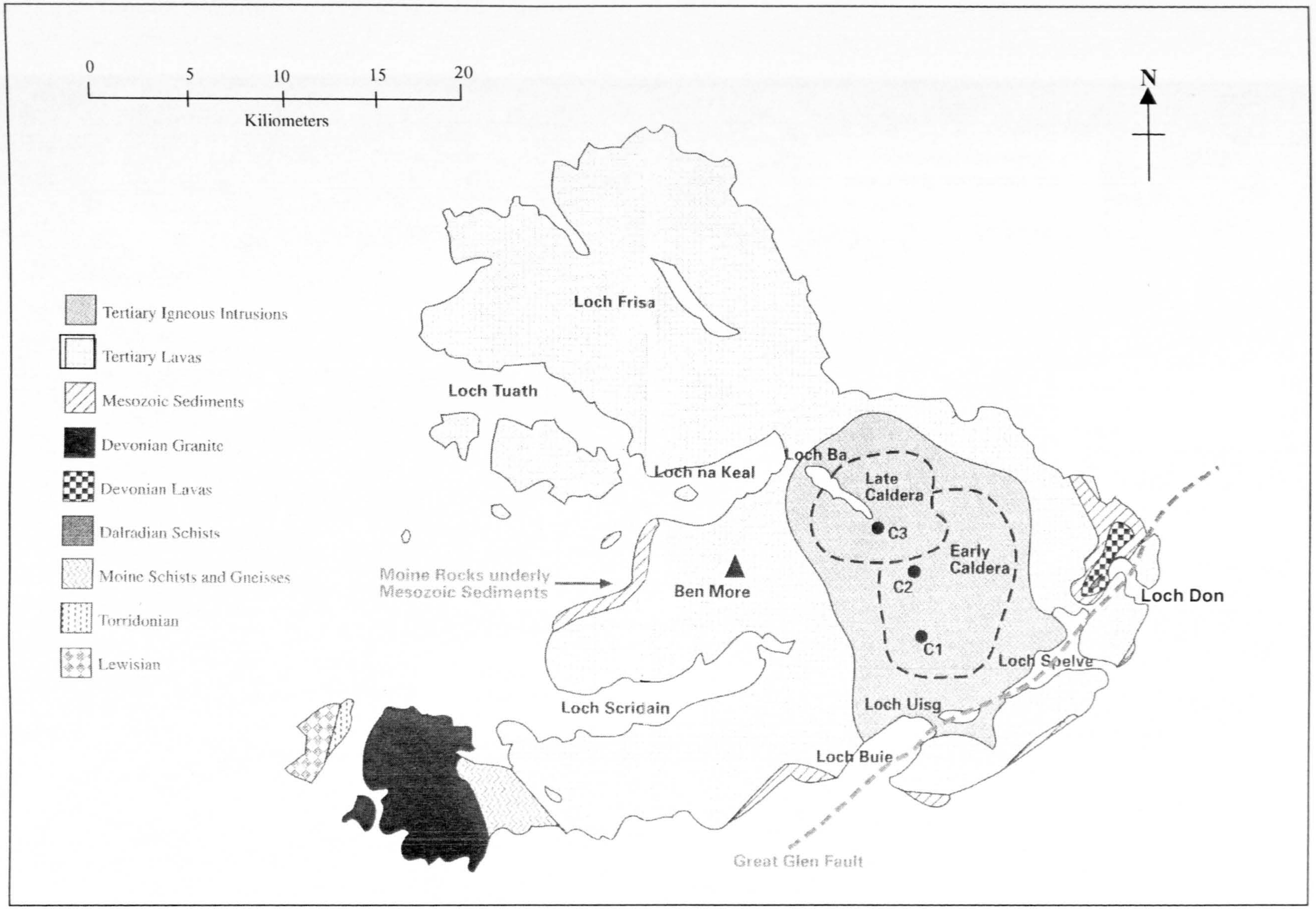

Figure 4.2: Simplified geological map of the Isle of Mull showing the distribution of the three major Tertiary igneous centres in geo-chronological order of formation and the extent of basaltic flood lavas derived from these centres over the period 65Ma – 52Ma ago. Also shown are the older Lewisian rocks and Moine ssociated schists and gneisses to the west. Note the presence of the Dalradian schists around the Loch Don syncline and the position of the major tectonic feature of the Glen Fault trending North East – South-West through the south-eastern area of the island (source: Jones, 1997).

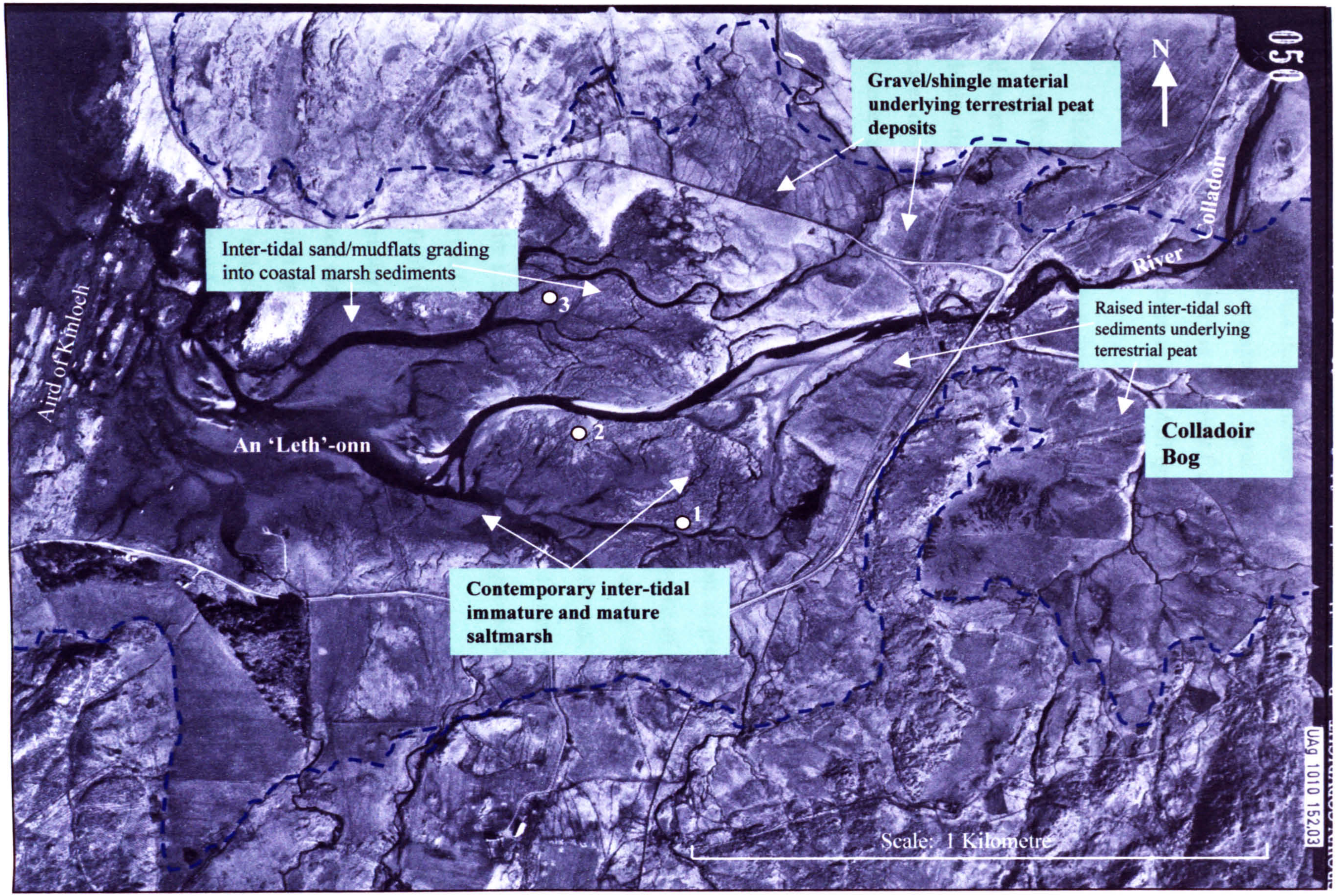

Figure 4.3: Annotated aerial photographic image (1988) to illustrate the general geomorphological features at the Head of Loch Scridain. The fossil cliffline is indicated by the dashed blue line and the core sites indicated by the white numbered circles (Source: Royal Commision for Historical and Archaeological Monuments of Scotland, (RCHAMS), Edingburgh).

Leth-onn" consists of tidal flats that grade into extensive sands/muds and Late Holocene coastal peat sediments (Figure 4.3). Freshwater input to the Head of Loch Scridain is derived directly from the Ben More catchment via the river Colladoir, the source of which is located some 7-8 km inland in towards the centre of the Mull igneous province at the head of Glen More (Figure 4.3).

Field site investigations around the upper marsh area landwards of the tidal strand-line resulting from highest water ordinary spring tides (H.W.S.T) were undertaken using a 1 metre hand corer to try to ascertain the nature of the up-shore substrate. At nearly all locations, in particular the area immediately above the coastal road and below the 10 m contour line at altitudes of < 8 m, coring revealed a stratigraphy consisting of an upper unit of dark organic-rich peat underlain by sands and gravels. This basal substrate was generally more rounded than material present in both the Coladoir river bed and the contemporary inter-tidal sand/mudflat areas (Figure 4.3). This suggests that the up-shore area skirting the present-day marsh at the site may have been a former beach consisting largely of coarse sand and shingle during the Mid to Late Holocene when relative sea-levels were higher than at present. Certainly the outcrop of 'Aird of Kinloch' would not have afforded the same degree of protection from incident wave energy during such periods. The covering of peat negates the identification of any discernable beach morphology related to this deposit. Conversely, to the east of the bridge crossing the river Coladoir and set in an area of low-lying topography (< 10m) somewhat delineated from the contemporary marsh by a north-trending outcrop of Mugearite lava is a present-day freshwater wetland referred to as the Colladoir Bog.

Although difficult to access some investigative coring was undertaken in Colladoir Bog and revealed a stratigraphy in marked contrast to that found in the more exposed area above the present-day high water mark. All the cores have an upper unit of very organic-rich peat of variable thickness which grades into an underlying unit of more clay rich silt with less organic content. Beneath this exists a basal unit of coarse sands and gravel. The general stratigraphy is very similar to that recorded in the present-day salt-marsh and may represent a former pocket-marsh characteristic of contemporary sea loch-head environments within Western Scotland. It is possible that this small relict marsh was formed at the same time as the buried beach deposits when higher relative sea-level would have permitted sea water to enter the area and deposit re-worked material into the embayment although radiocarbon (^{14}C) dating would be required to provided more conclusive evidence.

The present-day estuarine morphology at the head of Loch Scridain exhibits two distinct lower tidal channels which develop into meandering channels within the marsh interior where the major extent of coastal wetland sediments have developed (Figure 4.3). The characteristic geomorphology of the marsh at this site indicates the dominance of tidal current energy and interaction with fluvial processes. These both influence sediment deposition and erosion.

Investigative coring of the present inter-tidal sediments identified a variable thickness of coastal peat (maximum 76 cm depth) overlying coarse sand and gravels. These clastic deposits may be largely fluvial in origin linked to the formation of channel bars and small deltaic features which show evidence of tidally-induced re-working (Figure 4.3).

The intertidal area of the present-day marsh is dominated by the halophytic species *Plantago maritima* with swards of *Glaux maritima* and *Juncus geradi* more prevalent towards the seaward edge of the vegetated surface. *Armeria maritima, Agrostis stolonifera* and *Triglochin maritimum* form the bulk of the early colonizing vegetation more prevalent upon the sand/mudflat environment. A fairly distinct zonation between lower (immature marsh) and higher (mature marsh) is discernable based upon air photographic evidence where the high marsh appears as a lighter grey surrounding the upper marsh areas (Figure 4.3).

4.7.2: Core sedimentology

Three cores in total were extracted from the marsh at the head of Loch Scridain and the position of these is indicated in Figure 4.3 and Figure 4.4. Also shown in Figure 4.4 is an inset image demonstrating the method used for extraction of the core monolith. A laboratory digital photographic image of the core from this site is shown in Appendix 3.1. A detailed sedimentary log with description of the core composition is presented in Figure 4.5.

The core consists of an upper unit of dark-brown peat with abundant rootlets, some fine to medium sand present throughout and some small clasts of very angular pebbles at discrete depths. This unit extends to a depth of 57 cm and within the lower 18 cm the sediment consists of a more clay-rich material which was noticeably less water-logged and compact. Contact with the underlying unit is quite diffuse and is indicated more adequately by the increased content of fine to medium gravel present in the basal unit. This becomes coarser where at the very base of the core the gravel is quite large and angular (maximum measured long-axis = 27 cm; Figure 4.5).

(A)

(B)

Figure 4.4: (A). Overview of the southern section of the marsh site at the Head of Loch Scridain looking East across the south shore of inner Loch Beg towards Glen Moore. Sample sites for cores 1 & 2 extracted are shown numbered and the profile shown in (B) is that collected from site 1. Note the raised shoreline feature to the right of the road in the foreground, relating to older periods of higher relative sea-level and the fossil cliff line marked by dashed white line. Colladoir Bog lies immediately behind the volcanic dyke into which the palaeo-shoreline has been formed.

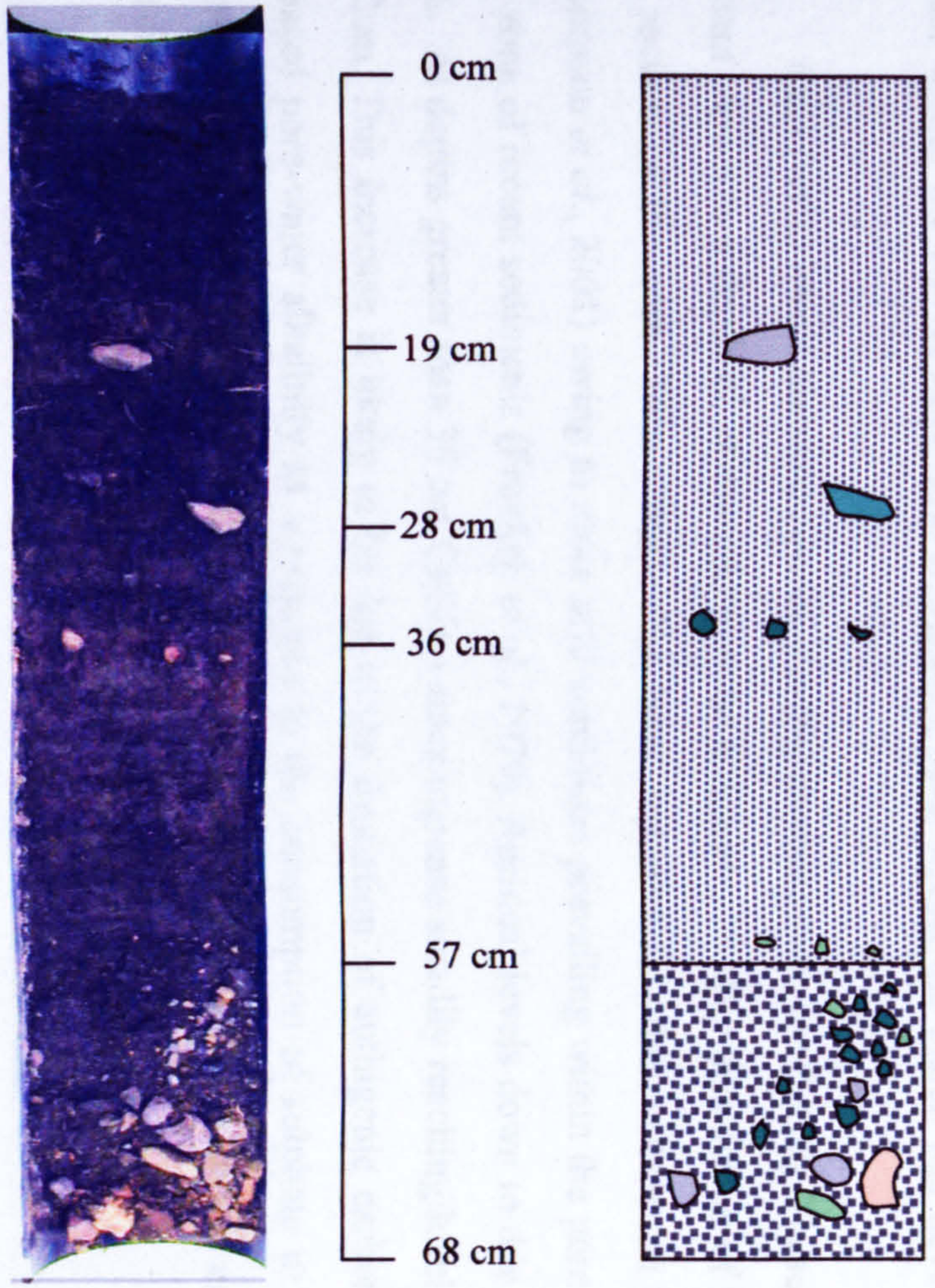

Sediment Description

Upper unit of dark brown peat which is very silt rich with occassional clasts of small to medium very angular pebbles.

Some fine to medium sand also present within the silt matrix which increases slightly down through the upper section.

Abundant rootlets and organic material throughout.

Towards the base of this unit and the very diffuse contact with the underlying unit the peat becomes less waterlogged and is more stiff and compact.

Some small angular pebbles present at the base of this section.

Basal unit of dark gray/dark brown course sand supporting medium to course gravels and pebble-sized material which is quite angular. Sand at the base is very reddish/dark orange in colour

Figure 4.5: Digital photograhic image and sedimentary log of the marsh sequence from the Head of Loch Scridain, Western Isle of Mull, Argyll.

4.7.3: Major element geochemistry

The major element geochemistry raw data for the Loch Scridain core is shown in Appendix 4.1 and the down-core depth/elemental abundance profiles for these oxides indicating the general core composition are shown in Figure 4.6. A strong degree of homogeneity is illustrated by the profiles of the major elements Si, Ti and K which are shown normalized to Al to take account for differences in clay mineral content and variation in sediment composition (i.e. the constant sum problem highlighted by Rollinson, 1992; Figure 4.7).

These profiles show relative constancy with depth down to 60cm below the marsh surface with a more pronounced increase in the K/Al ratio occurring at 36cm and are indicative of a consistent record of deposition with little fluctuation in composition of accumulated inorganic material over time. The grain size of this material is also interpreted to have remained consistent over the period of marsh development. If this was not the case, then the profiles of Si, Ti and Zr (data not shown) relative to Al would be seen to increase indicating a coarsening of the sediment composition owing to a greater contribution of resistant or heavy minerals such as quartz, rutile and zircon relative to clays (Spears and Kanaris-Sotiriou, 1976; Salomans and Mook, 1977). This effect is indicated at the very base of the core where the material becomes coarser within the fluvial sandy/gravel deposits upon which the marsh has developed (Figure 4.7).

CaO (wt%) levels are used here as a proxy measurement for $CaCO_3$. These remain fairly constant down to a depth of 38 cm and may be indicative of little dissolution of $CaCO_3$ within this section of the core. This process has been reported in other salt-marsh environments (Thompson *et al.*, 2001) owing to more acid conditions prevailing within the pore waters of the oxic zone of recent sediments (Froelich *et al.*, 1979). Residual levels down to this depth are < 6 wt %. At depths greater than 38 cm $CaCO_3$ values increase steadily reaching levels of < 9 wt % at 60cm. This increase is likely to be due to the formation of authigenic carbonate owing to increased pore-water alkalinity as a response to the consumption of sulphate in the post-oxic zones and formation of metal sulphides (Gaillard *et al.*, 1989). Conversely, this may also result from dissolution in the upper part of the core.

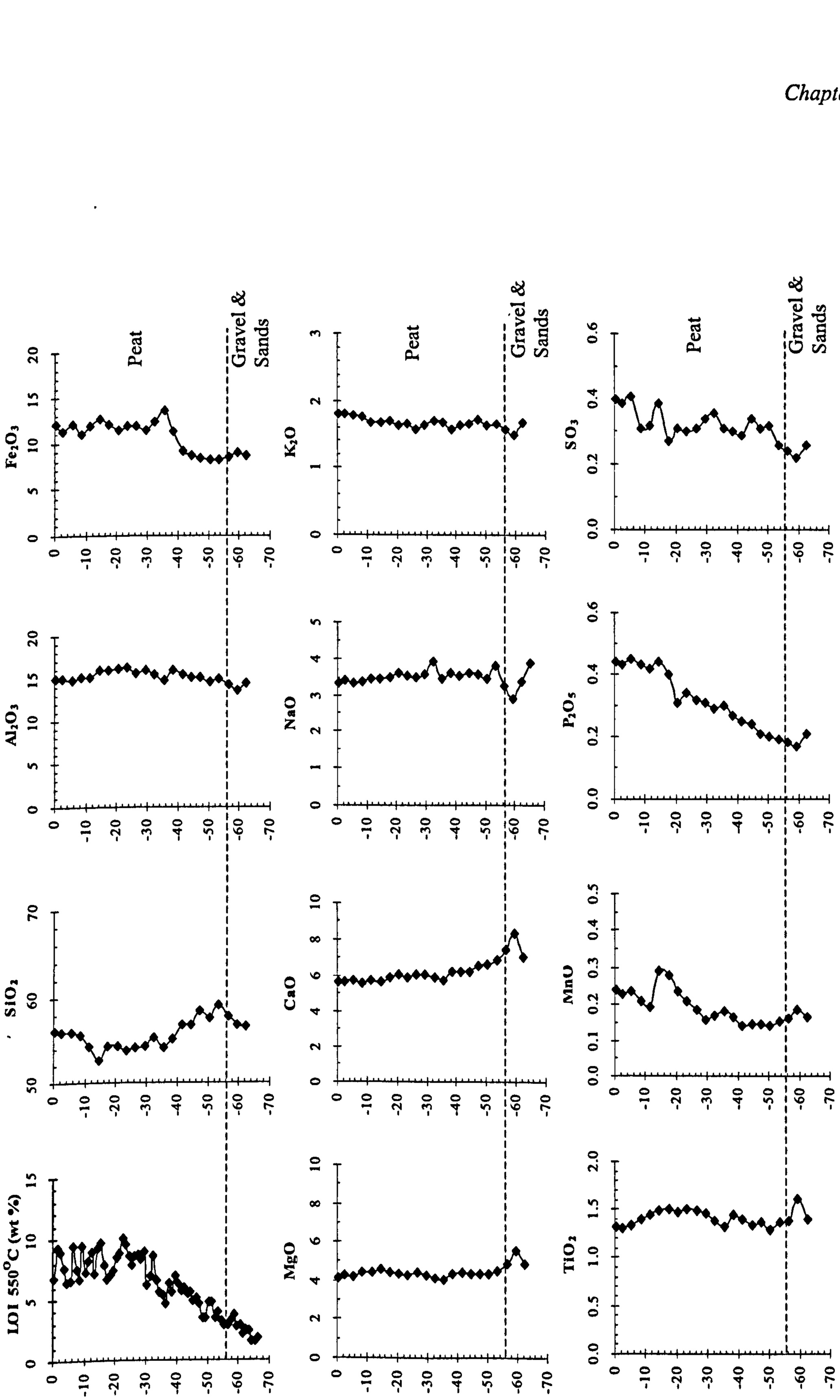

Figure 4.6: Loss on ignition (% dry mass, 550°C) and major element geochemistry profiles for the core from Loch Scridain, Western Isle of Mull. Elements are reported as oxides (wt %) according to XRF convention.

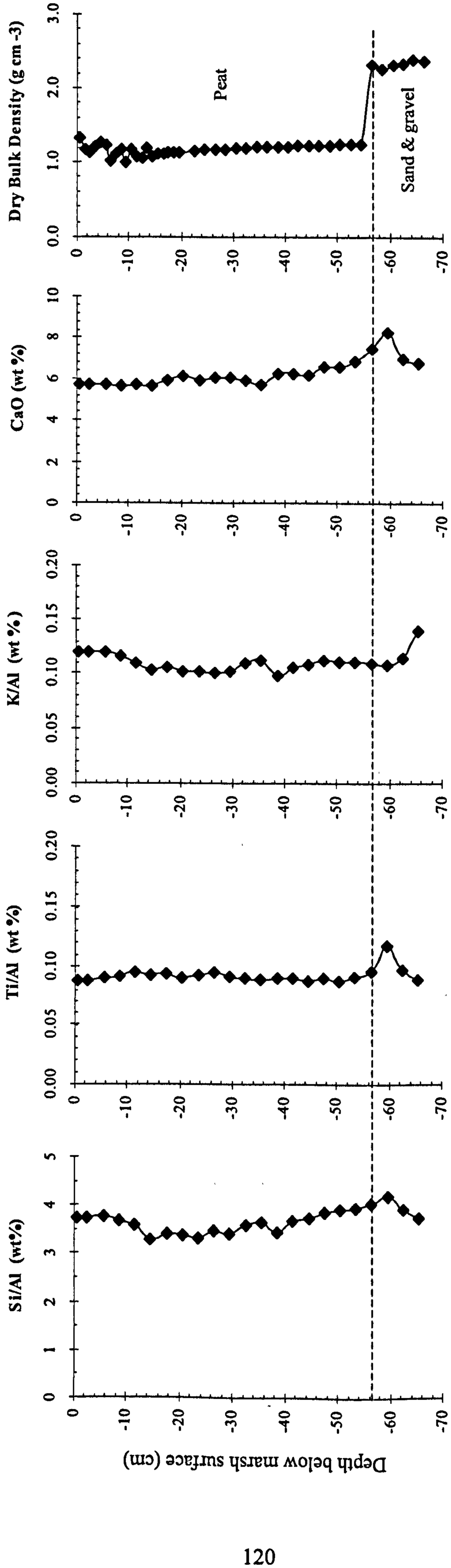

Figure 4.7: Al-normalized weight ratio plots for Si, Ti, and K, with the depth-profiles of Ca (wt %) and dry bulk density (g cm-3) for the Loch Scridain marsh core, western Isle of Mull.

4.7.4: Organic matter, core composition and chemical zonation

Two main stratigraphic chemozones were identified using total sum of squares in the cluster analysis program CONISS (Grimm, 1991). The plots of major element abundance in relation to chemozone stratigraphy are shown in Figure 4.8. The two main zones extend from the base of the core at 66 cm to a depth of 41 cm (LSrid A) and from 41 cm to the marsh surface (Lsrid B). Additional sub-zones were also identified and are presented within the same figure.

Detailed analysis of these sub-zones reveals that in the basal section of the core corresponding to zone LSrid A1, organic matter (via LOI 550°C proxy) Fe, Ti, Mn, Mg and Kare all enriched relative to Si, Al and Na. LScrid A2 is characterized by unvarying values of Si,, Ti, Fe, Mg, Mn, Na and K which show a gradual increase towards the lower boundary of zone LSrid B. Over the same depth/zone P and S show a quite marked increase in element abundance. Al shows a less pronounced increase in element abundance. This is not mirrored by the profiles of LOI and Ca which indicate a reduction over the same the section of the core.

Within zone LSrid B1 Ti, Fe, Mn, P, S and Na profiles increase in element abundance with distinct peaks evident in profiles of Fe, Mn, S and P. This is accompanied by a corresponding decrease in the values of LOI, Si, Al, Ca, Mg and K. These remain more uniform and do not show similar evidence of comparative fluctuations.

In chemozone LSrid B1 Fe abundance is maintained at levels above those in LSrid A. Mn, S and Na attain maximum values below the boundary with LSrid B2. C_{org} values fluctuate significantly within this zone where the lowest core values is recorded at ~ 6.5 wt %. This value then returns to an element abundance value comparable with that recorded in the lower section of LSrid B1. All other major elements are relatively unvariable throughout this sub-zone.

The upper section of zones LSrid B1 is characterized by unchanged levels of Si, Al, Mg, Ca and Na. A slight increase in the abundance of K is mirrored by a similar decrease in Ti. In zone LSrid B2 Fe and Mn profiles indicate slight enrichment compared to the basal chemozones with P and S also enriched within the near-surface layers (Figure 4.8).

This corresponds to fluctuating values for organic carbon content within the upper decimetre of the core (Figure 4.7).

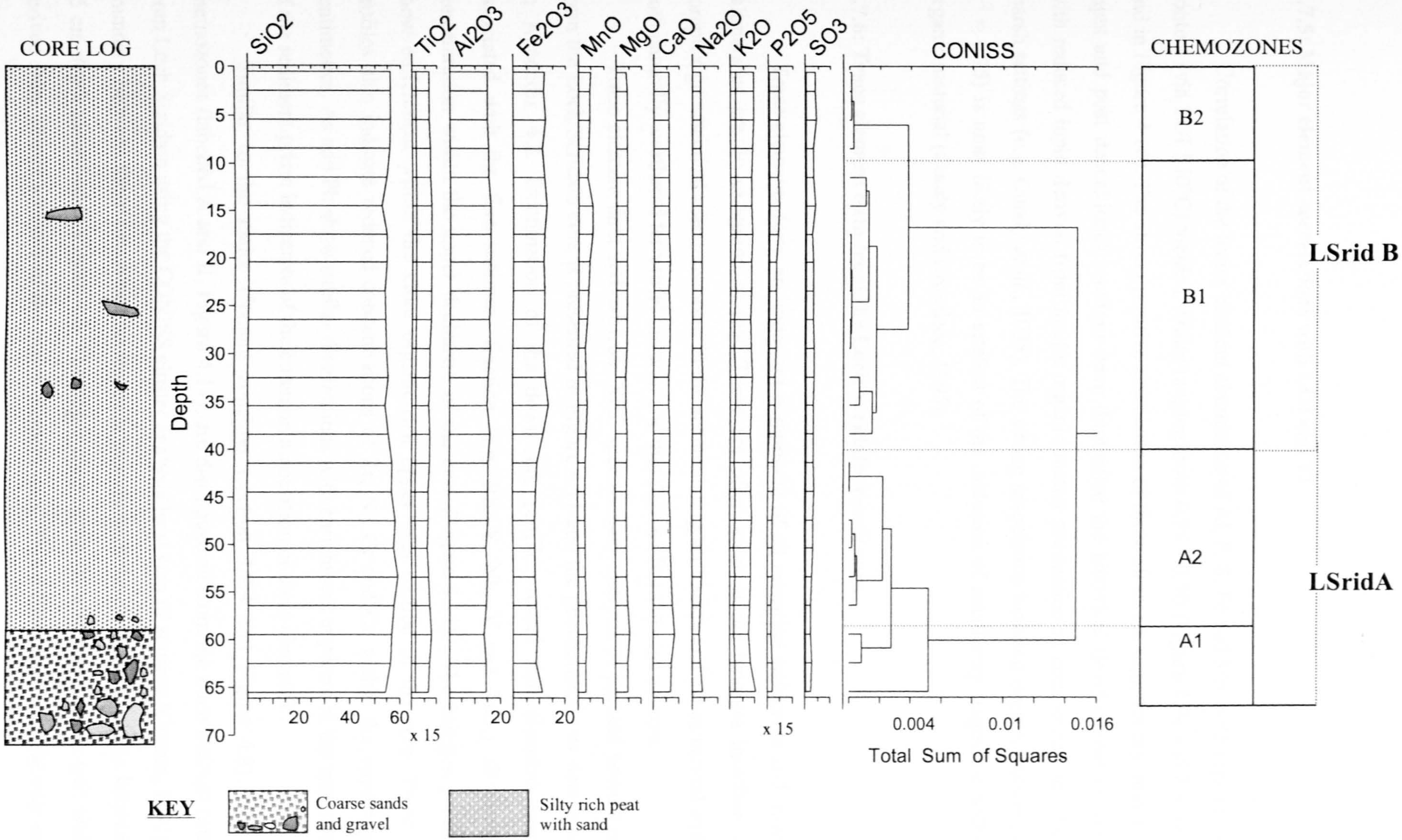

Figure 4.8: Major element chemostratigraphy of the Loch Scridain marsh core, element abundance (% ashed mass) and CONISS zonation. TiO_2, ,K_2O P_2O_5 and SO_3 shown on exaggerated scales (x 15).

4.7.5: Major element correlations with LOI and Ti

Correlation of the major element abundance of Al, P, S, Fe and Mn with organic carbon content (via LOI 550°C) yields r values ranging from 0.75 - 0.50 (Figure 4.9a and Figure 4.9b, and in Figure 4.10). The strong positive association of these elements suggests that minerogenic input and post depositional reactions have dominated the historical development of this core with reduced input derived from *in-situ* organic matter production in comparison to other UK marsh settings (e.g. Cundy *et al.*, 1995). The strong association between organic carbon and Al ($r^2 = 0.75$) is most likely to be an artefact of the inclusion of small clay fragments within the organic material (Cundy and Croudace, 1995).

4.7.6: Trace element data from the Loch Scridain marsh core

Trace elements form an important component of all estuarine sediments and inter-tidal saltmarshes are no exception to this. These are often areas at the land-sea interface where complex geochemical reactions occur in the accumulating sediments and act as natural sinks for both naturally weathered terrestrial material and that derived from marine sources.

Trace element data derived from XRF spectrometry analysis of pressed powder pellets from the Loch Scridain core is presented in Figure 4.11 and the geochemical raw data is shown in Appendix 4.2. Examination of the down-core profiles reveal that elements normally associated with the fine sediment fraction (e.g. Rb, Y, Nb, V and TiO_2) all decline in concentration within the upper decimetre of the core (Figure 4.11). The halogen profiles all show enrichment within the more organic-rich upper peat section of the core. Trace metal profiles also indicate reduced concentrations of Zr, Ni, Cr and Ce within the uppermost ten centimetres. As and Pb show similar distributions with enrichment apparent in the upper section of the sediment prism indicative of the common association of these elements.

Similar to the major element zonation (section 4.7.4 and Figure 4.8), two main chemozones (labelled A and B, Figure 4.11), are distinguished from the trace element raw data from Loch Scridain using the CONISS cluster analysis least sum of squares (Grimm, 1991). The boundary between these two zones corresponds exactly with the chemical zonation between 40-45 cm depth identified in Figure 4.8. The upper chemozone B2 also corresponds well with that derived from cluster analysis of the major element data. This differentiation in the near-surface

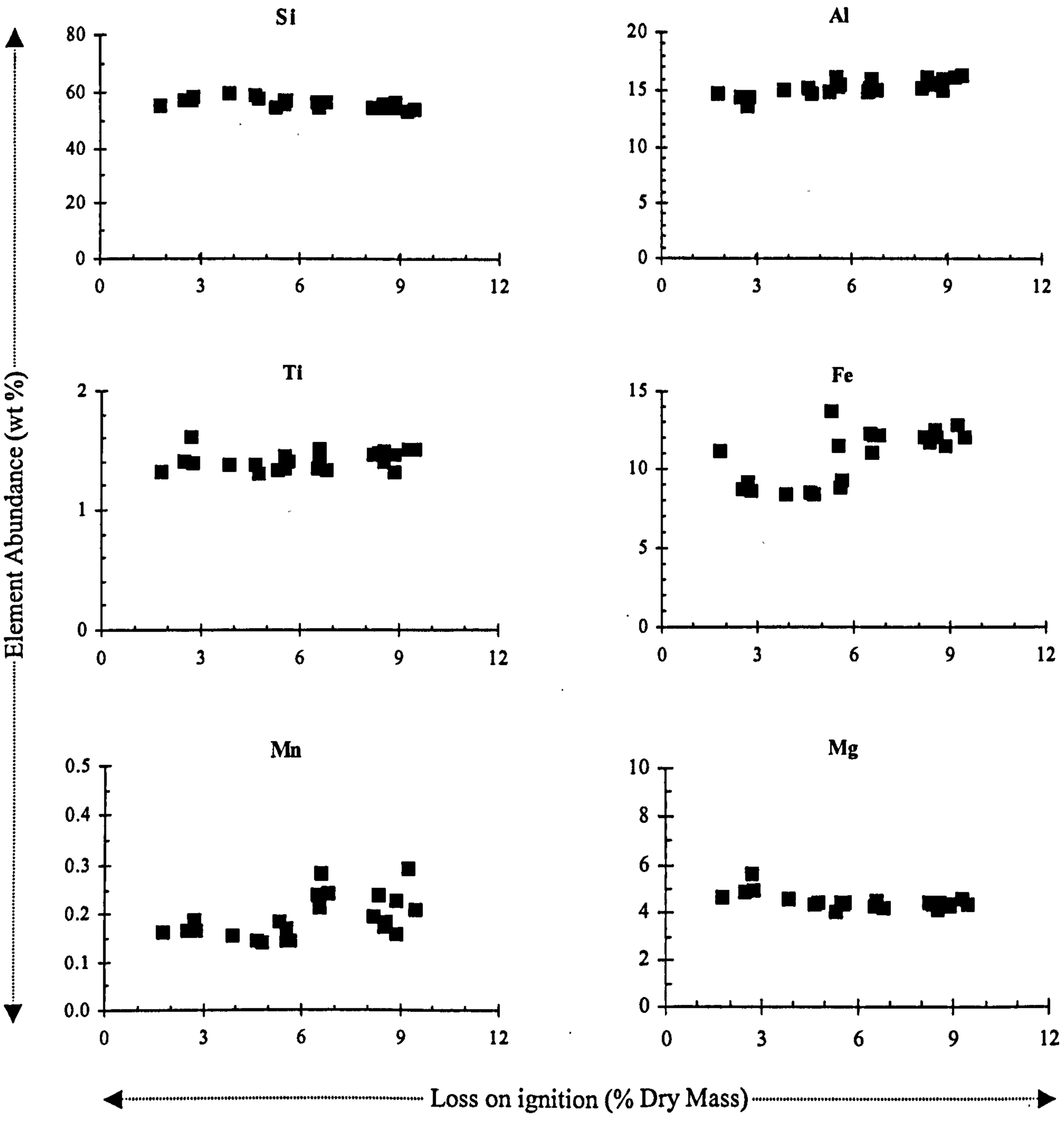

Figure 4.9a: Major element abundance and Fe/Mn ration vs. organic content (LOI 550^{o}C) from Loch Scridain, core 1.

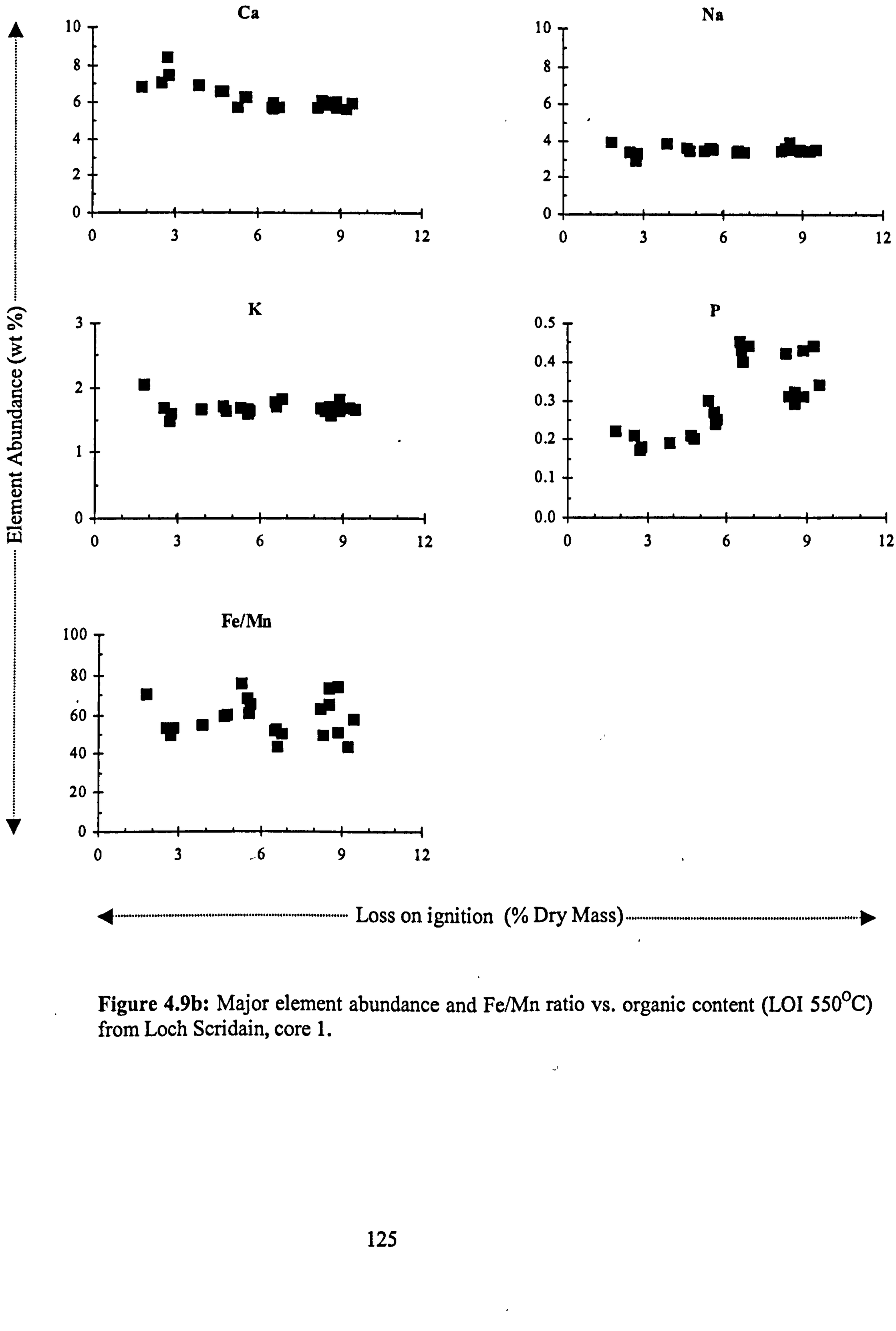

Figure 4.9b: Major element abundance and Fe/Mn ratio vs. organic content (LOI 550^{o}C) from Loch Scridain, core 1.

(a)

Element	Core Average	(r) LOI
LOI	6.20	
Al2O3	15.22	0.75
P2O5	0.31	0.72
SO3	0.31	0.70
Fe2O3	10.82	0.66
MnO	0.19	0.50
TiO2	1.41	0.26
Na2O	3.50	0.13
K2O	1.68	-0.07
MgO	4.45	-0.57
SiO2	55.72	-0.62
CaO	6.27	-0.78

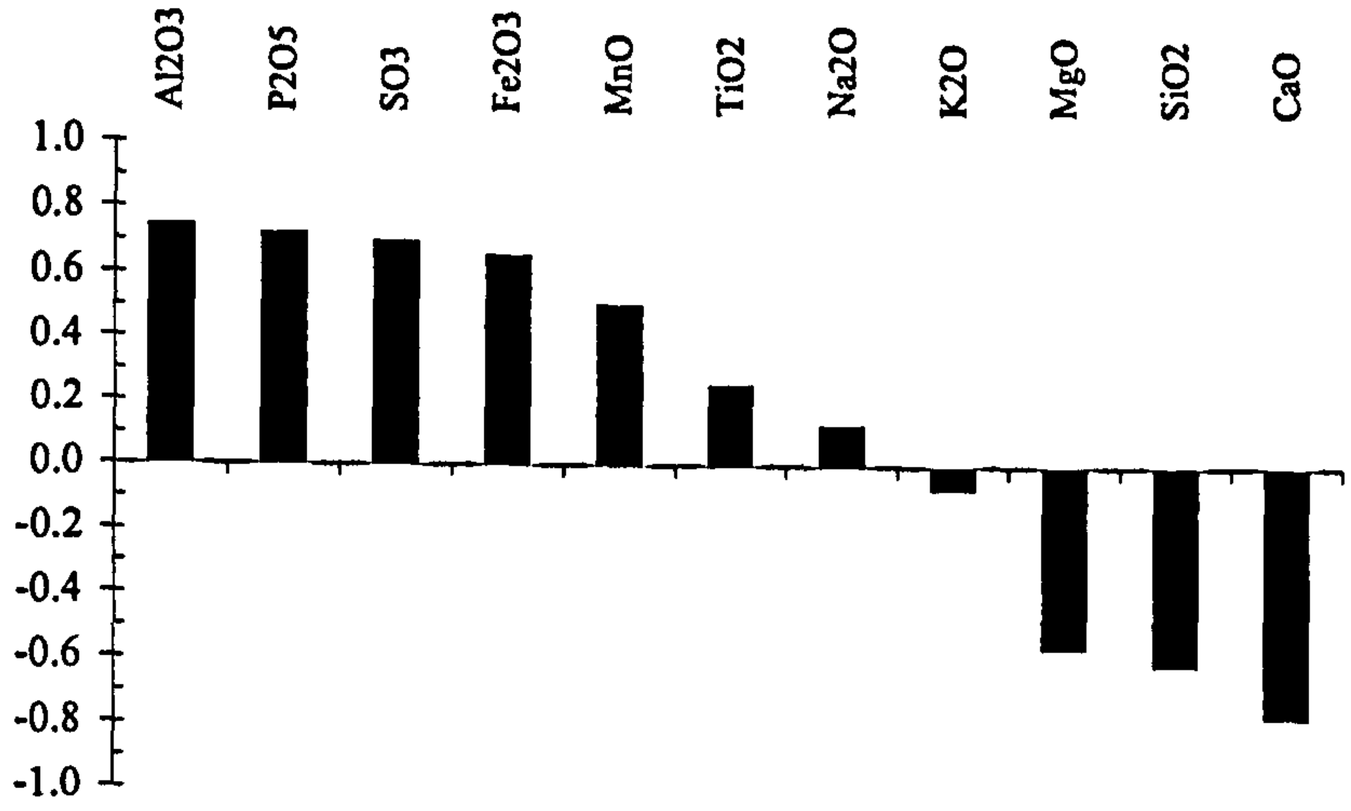

(b)

Element	Core Average	(r) TiO_2
TiO2	1.4067	
MgO	0.1905	0.49
MnO	0.1905	0.31
Al2O3	15.2235	0.28
LOI	6.2000	0.26
CaO	6.2680	0.22
Fe2O3	10.8193	0.15
P2O5	0.3052	0.04
SO3	0.3122	-0.28
Na2O	3.4954	-0.36
SiO2	55.7154	-0.40
K2O	1.6831	-0.61

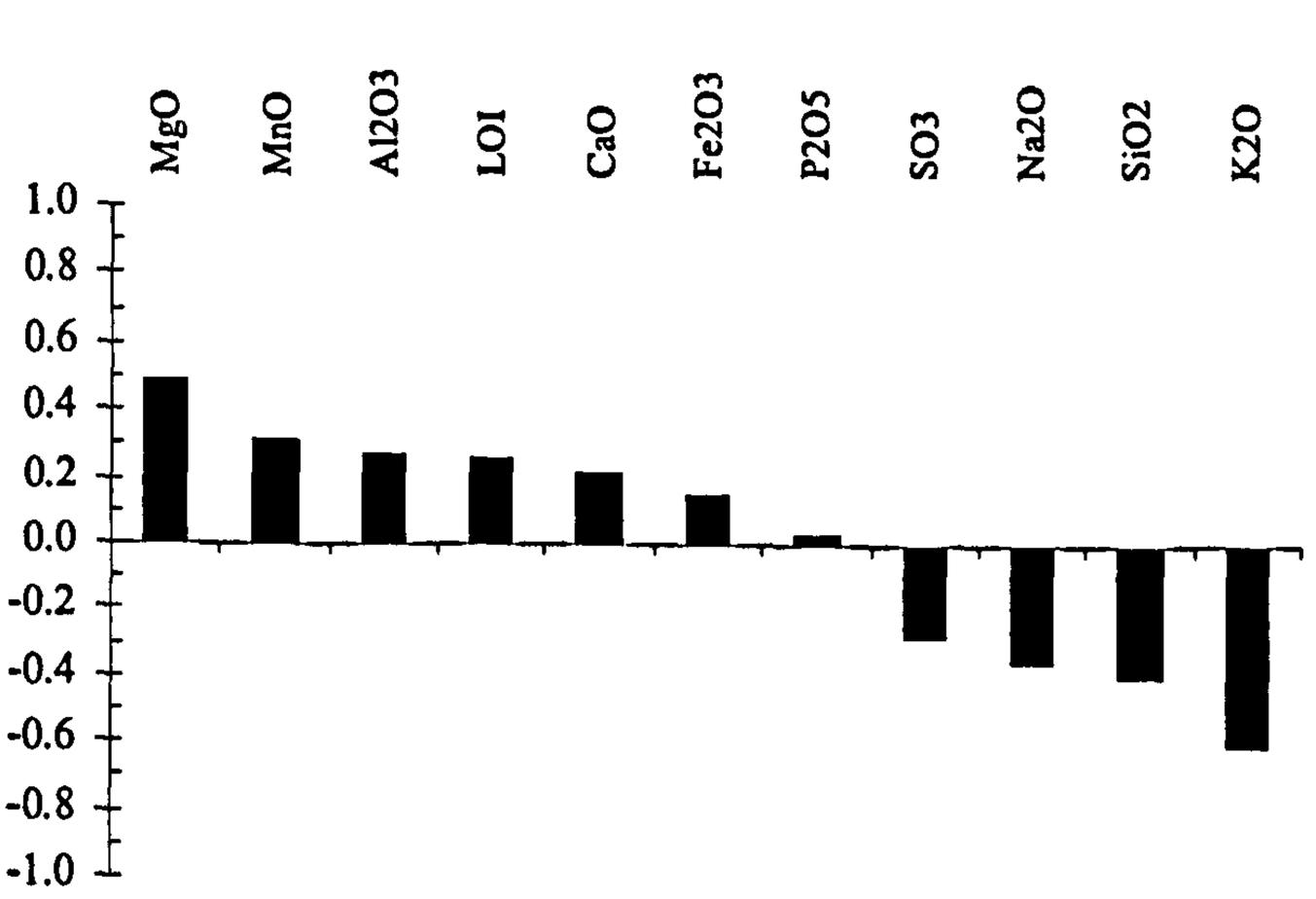

Figure 4.10: Core average major elemental abundances and correlation with (a) LOI (550°C) and (b) TiO_2 (wt %) as a proxy for detrital input for the Loch Scridain marsh core.

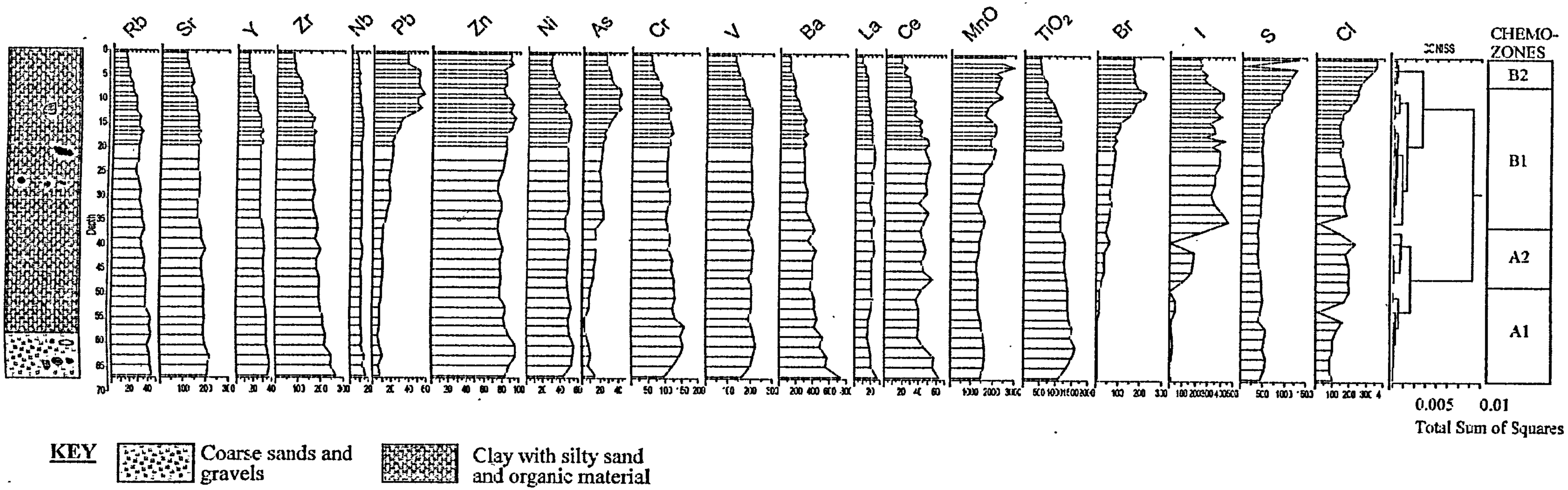

Figure 4.11: Trace element concentrations (ppm) for the Loch Scridain marsh core (oven-dried pressed pellets) and CONISS zonation

sediments is due mainly to enrichment of key trace elements including Cl, S, Mn, Zn, Pb, As and Br. More detailed analysis of trace element data is presented later in Chapter Seven of this thesis.

4.8: Loch Don (south easterm Isle of Mull)

4.8.1: Site description and environmental setting

The Loch Don estuary represents a lowland semi-enclosed estuarine setting situated on the south- eastern side of the Isle of Mull (Figure 4.1). From the mouth at Grass Point the main tidal channel extends NNW for approximately 1.5 km where, just south of the shoreline at Loch Don village, at the island of "Eilean Ban" the tidal channel takes a distinct U-turn to trend SSW passing under a bridge (Figure 4.12). This serves as the crossing point from the village to Auchnacraig and the Grass Point peninsula. This upper section of the loch up-shore from the bridge is called "Leth-fhonn" and represents an area of extensive salt-marsh development which grades into grazed peat pasture below the Caledonian igneous outcrop of "Torr, a Bhradain" (Figure 4.12).

This section of the Loch represents part of a marked syncline extending through the south-eastern corner of the Isle of Mull and contains the deeply ice- scoured sea-lochs of Loch Buie and Loch Spelve. These are situated to the SW and NE respectively of Loch Uisg which contains freshwater. The syncline extends to the north of Loch Don to Duart Bay. It has been suggested by Lee *et al.* (1925), to represent the course of the Great Glen fault on which major displacements occurred prior to the formation of Mesozoic and Tertiary igneous rocks (Figure 4.13). Micro-seismicity continues to be recorded along the course of the Great Glen Fault within the area. In September of 1986 a larger magnitude event registering 4.1 ML occurred with the epicentre immediately offshore south-east of Craignure Bay within the Sound of Mull. An event of similar position and magnitude occurred in early 1998 which registered 4.2 ML indicating that this is still an active section of the fault.

The geology of the area around Loch Don is markedly different to that found in the south-west of the island. Here the estuary is situated within bedrock consisting of Dalradian schists, black limestones and grey phyllites surrounded by Devonian lavas and younger Mesozoic sediments which outcrop to the north of Loch Don and around Craignure (Figure

Figure 4.12: 1988 aerial photograph of the Loch Don estuary annotated to show the general geomorphology around the estuary. Fragments of the Main Postglacial shoreline identified by Gray (1974) are shown as dashed yellow lines. The palaeo-sediment core locations referred to in Appendix 7.1 are labelled A and B respectively and the sites from which contemporary marsh cores were abstracted are labelled 1- 4 accordingly (source: The Royal Commission for Historical and Archaeological Monuments of Scotland, (RCHAMS) Edingburgh).

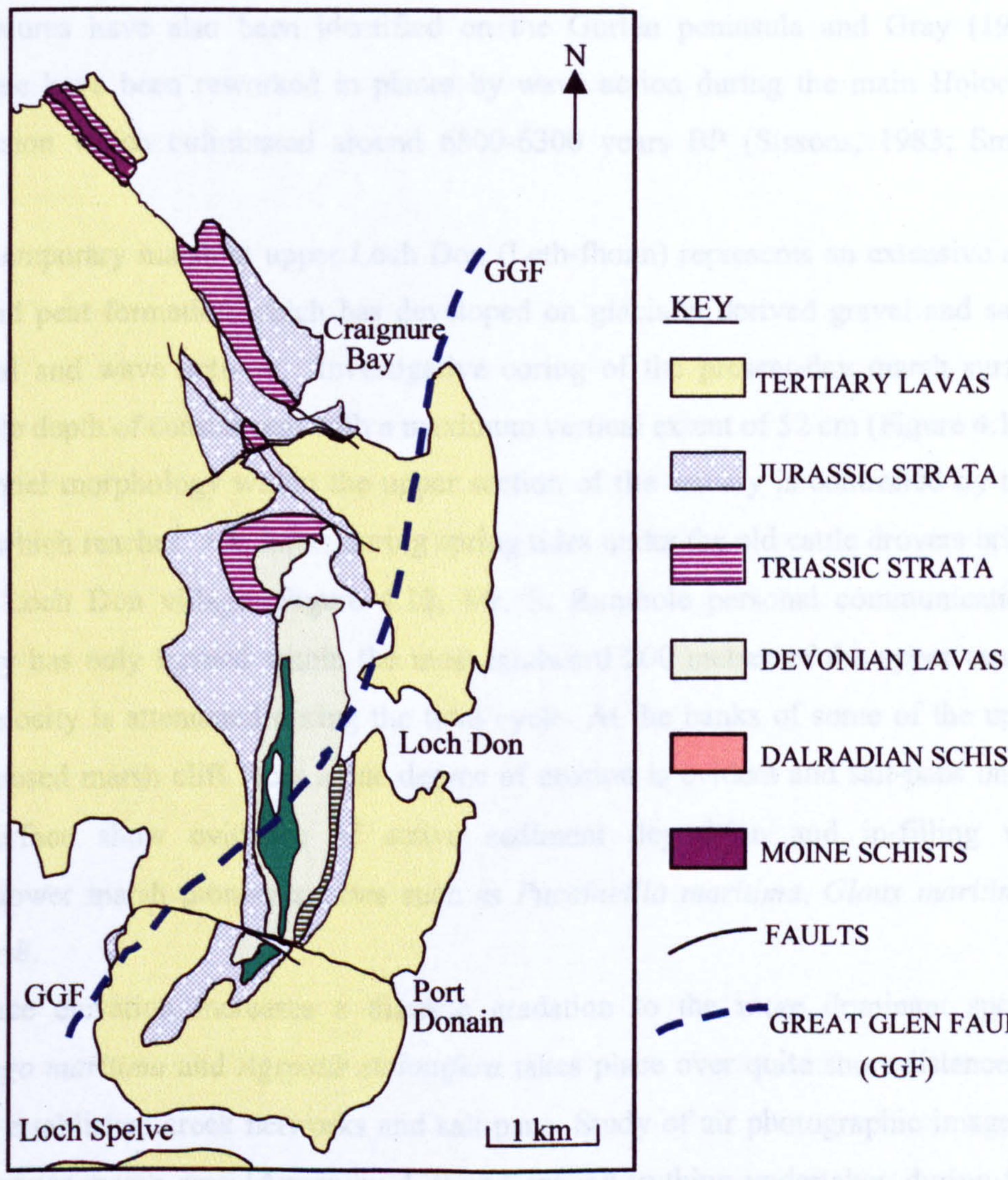

Figure 4.13: Geology of the area around Loch Don south-east Isle of Mull, (adapted from Jones, (1997) and BGS Sheet Nos. 44 (W) and part of 44 (E)).

4.13). The outer estuary consists of headlands principally constructed of flood basalt lavas of Tertiary age.

The coastal geomorphology of the Loch Don area has been extensively mapped (Gray 1974), with the most prominent features being the Late Glacial beach situated on the Gorten peninsula between Gorten Farm and Duart Castle and the extensive development of the Main Post-Glacial Shoreline around the entire outer and inner estuary (Figure 4.12). Moraine and kame terrace features have also been identified on the Gorten peninsula and Gray (1974) suggests that these have been reworked in places by wave action during the main Holocene marine transgression which culminated around 6800-6300 years BP (Sissons, 1983; Smith, 1997).

The contemporary marsh at upper Loch Don (Leth-fhonn) represents an extensive area of coastal wetland peat formation which has developed on glacially derived gravel and sands reworked by tidal and wave activity. Investigative coring of the present-day marsh surface revealed a variable depth of coastal peat with a maximum vertical extent of 52 cm (Figure 4.14).

The channel morphology within the upper section of the estuary is controlled by tidal current velocity which reaches > 6 knots during spring tides under the old cattle drovers bridge to the south of Loch Don village (Figure 4.12, Mr. S. Rumbole personal communication). Channel sinuosity has only formed within the most landward 200 metres of the upper estuary where current velocity is attenuated during the tidal cycle. At the banks of some of the upper channels and exposed marsh cliff faces some degree of erosion is evident and salt-pans on the upper marsh surface show evidence of active sediment deposition and in-filling with colonization by lower marsh pioneer species such as *Puccinellia maritima*, *Glaux maritimum* and *Juncus gerardi*.

As surface elevation increases a discrete gradation to the more dominant species including *Plantago maritima* and *Agrostis stolonifera* takes place over quite short distances (< 10 metres) from established creek networks and salt-pans. Study of air photographic images of the present-day upper marsh area (Appendix 4.2) and ground-truthing undertaken during field site work enables some degree of delineation between the lower and upper more mature marsh areas.

4.8.2: Core sedimentology

Several cores were initially extracted from various locations around the Loch Don estuary (Figure 4.12 and Table 4.2). The position of the sampling sites within the upper estuary is shown in more detail in Figure 4.14. This also shows an insert photograph of the core monolith prior to extraction. Core 4 was eventually chosen for detailed analysis owing to the high inter-tidal location and the level of coastal protection evident in the upper estuary area. Incident wave energy affecting this section of the marsh is extremely limited and this suggested stable marsh conditions and hence, the likelihood of little physical disturbance to the accumulated sediments.

A laboratory digital photographic image of the core is shown in Appendix 3.2. A detailed sedimentary log with core description is presented in Figure 4.15. The core consists of an upper unit of brown/light-brown silty clay containing lenses of fine sand extending down to 11 cm depth. Abundant rootlets are visible in this upper section. These are still present in the underlying sub-unit in which the fine sand content increases down to a depth of 27 cm. A further underlying sub-unit of more clay-rich material with sandy lenses extends from 27 cm to a depth of 35 cm. This unit is darker in colour and grades to a dark-brown/dark grey at the boundary with the basal coarse sand and gravel where some angular clasts of pebble-sized material is also evident (Figure 4.15).

4.8.3: Major element geochemistry

The major element geochemistry raw data is presented in Appendix 4.3 and the plots of the major element down-core profiles are presented in Figure 4.16. Normalized element profiles of Si, Ti, and K to Al reveal less homogeneity than seen in the Loch Scridain core (Figure 4.17).

The Si /Al ratio persists at levels of between 4 and < 5 wt % down to 39 cm beyond which the level rises slightly to 5.7 wt % within the lower sandy/gravel unit present at the base of the core. Similarly, the Ti/Al profile shows near constant levels fluctuating around the 0.08 wt % figure down to a depth of 39 cm whereupon an increase to 0.1 wt % is recorded in the coarser sediments at the base of the monolith. The gradual decrease in the ratios of these elements with increased height indicates a gradual fining with increased marsh elevation over time. This is supported by the K/Al down-core depth profile, which reveals a general increase in the amount

(A)

(B)

Figure 4.14: (A) Overview of the upper estuary area of Loch Don, South-Eastern Isle of Mull looking South West. Sampling stations for cores 3 and 4 are shown as numbered and the *in situ* sediment sequence from site 4 is shown in (B) prior to abstraction.

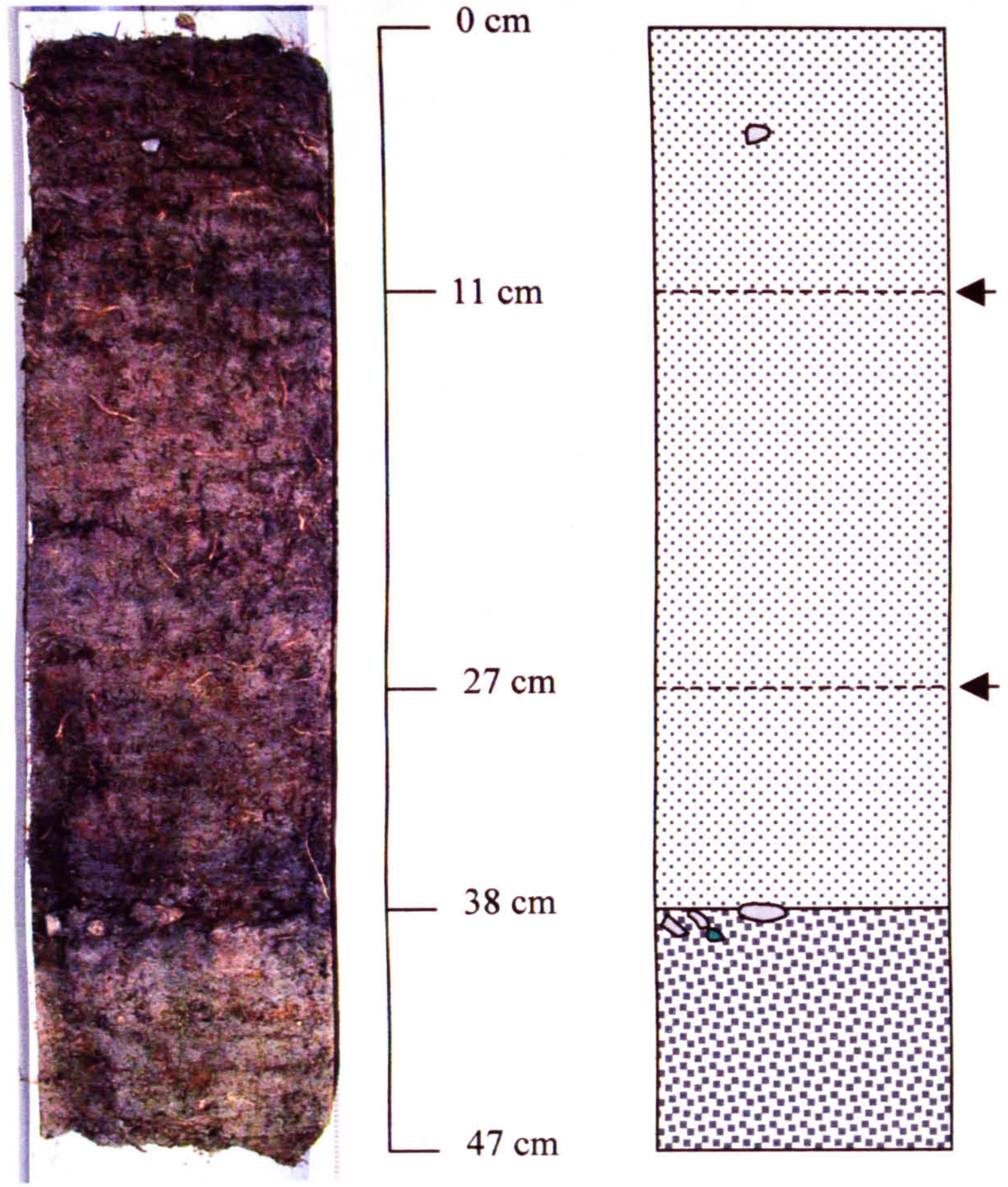

Sediment Description

Upper unit of brown/light brown silty clay containing lenses of fine to medium sand throughout. Very poor stratification no really discernable laminated structure. Occassional clasts of angular/sub-angular gravel. Unit becomes more sandy with increasing depth.

Abundant vegetation at surface (Figure 4.14) with rootlets and buried organic material present throughout

At base contact with underlying unit is quite diffuse and grades to darker brown than that evident in uppermost section.

Underlying unit of light-brown silty clay with some sandy lenses which grade to more anoxic brown/dark brown at base.

Roottets and organic material still present but less abundant than in upper unit.

Lower basal unit of light brown medium to coarse sand and gravel with angular to sub-angular clasts present at contact with overlying unit. Few rootlets and little organic material present.

Figure 4.15: Digital photograph and sedimentary log of the marsh sequence from the upper region of Loch Don, South-East Isle of Mull, Argyll. Small black arrows indicate a gradational boundary within the more organic-rich upper 35 cm of the core.

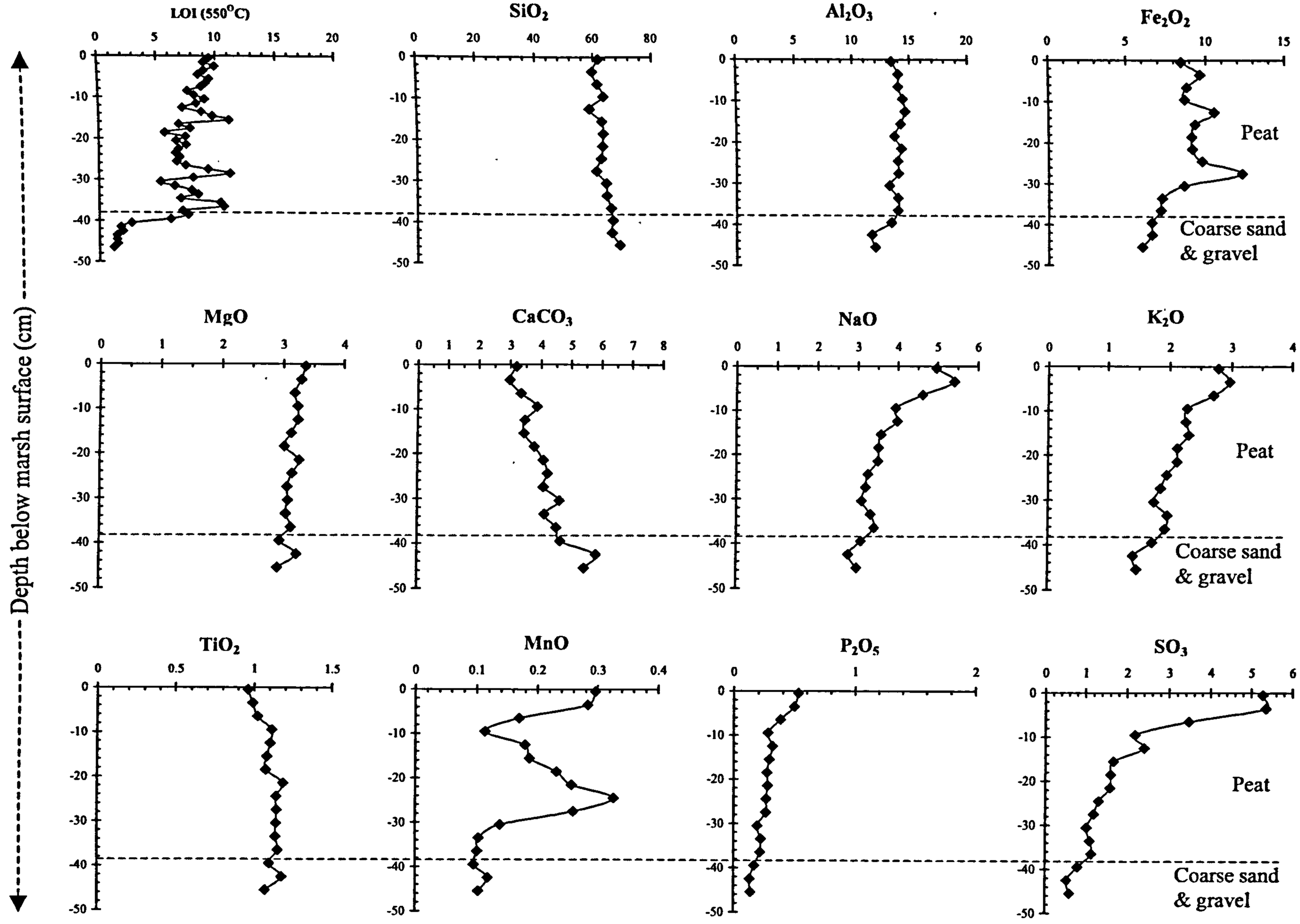

Figure 4.16: Loss on ignition (% dry mass @550°C) and major element profiles (wt %) for core 4, upper Loch Don estuary, Isle of Mull, Argyll. Element abundances are reported as oxides (wt %) in accordance with XRF convention.

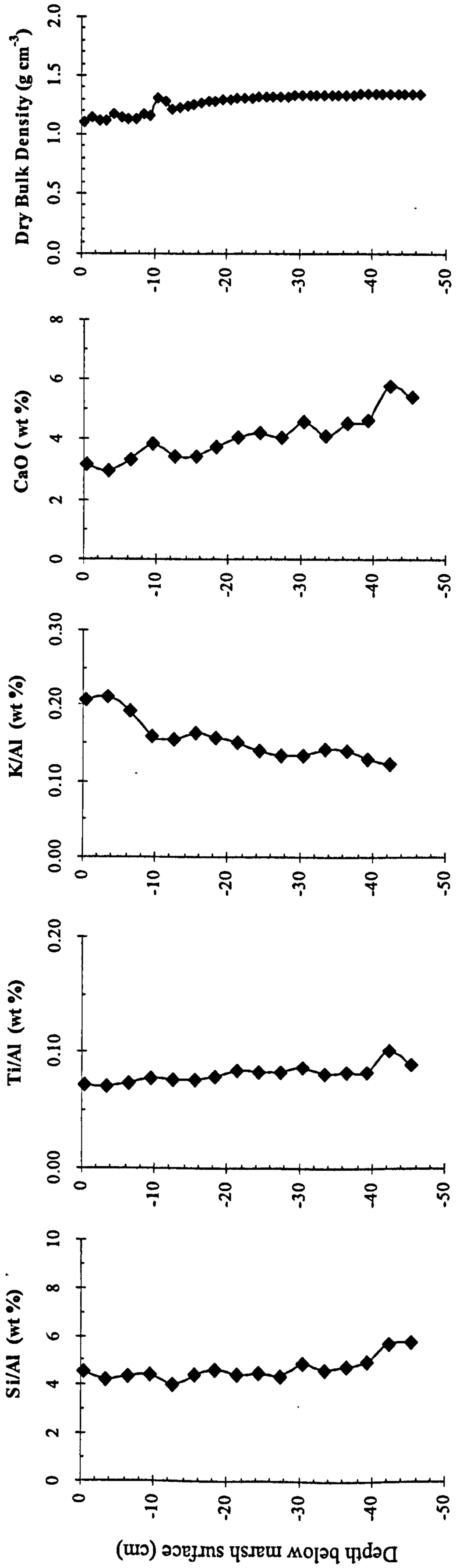

Figure 4.17: Al-normalised weight ratio plots for Si, Ti, and K, with the depth-profiles of Ca (wt %) and dry bulk density (g cm^{-3}) for the Loch Don marsh core, south-east Isle of Mull.

of K relative to Al at depths of 16 cm and 39 cm respectively and is indicative of more K-rich clay material being deposited on the marsh surface over time. The dry bulk density down-core profile indicates very little variation in the nature of inorganic material being deposited on the marsh surface over time with a small increase evident at 10-11 cm depth. This corresponds to a minor increase in CaO and K_2O (Figure 4.17). However, the LOI profile does show fluctuating values for the organic component of this core within the upper 39 cm.

CaO wt % as a proxy for $CaCO_3$ shows a general increase down through the sediment sequence from > 3 wt % at the surface to < 6 wt % at depths below 40 cm. This is likely to be attributable to increased pore-water acidity within the upper oxic zone leading to increased dissolution of $CaCO_3$. This trend continues into the underlying anoxic zone where $CaCO_3$ levels increase owing to the more alkaline conditions present at depth which favour the formation of authegenic carbonate (Figure 4.17).

4.8.4: Detrital composition and geochemical zonation

The CONISS cluster program (Grimm, 1991) has been used to identify two distinct chemozones within the Loch Don core and these correspond well with the visual stratigraphy. Within each of these zones further sub-zones were additionally identified (Figure 4.18).

In LDon A1 LOI content is very low at values of 1-2 wt %. Similarly, P, S and Mn are all recorded at the lowest levels. Ca is significantly enriched in this zone (see above). In zone LDon A2 organic carbon (via LOI 550°C), Fe, Mn, Na, K, P and S all increase and a significant peak in Fe and Mn is apparent at a depth of 27-28 cm corresponding to the boundary with zone LDon B. Zone LDon B1 is characterized by reducing abundance of Fe and Mn and Ca. LOI values are seen to fluctuate between maximum values, which nevertheless maintain a general enrichment throughout the zone (Figure 4.17). Si, Al, Mg, and Ti all maintain near-constant values as is the case throughout the core profile for these elements. Na, K, P and S all indicate continued enrichment to the boundary with the near surface zones.

The upper chemozones LDon B2 and LDon B3 show increasing values for organic carbon, Na, K, P, S. Increased Fe is apparent with the presence of two smaller peaks relative to that in LDon A2 and this is accompanied by a significant enrichment of Mn in the upper surface layers of the sequence. Ti and Ca show a further slight reduction. The abundance of Si, Al and Mg maintain their approximately constant values to the marsh surface (Figure 4.18).

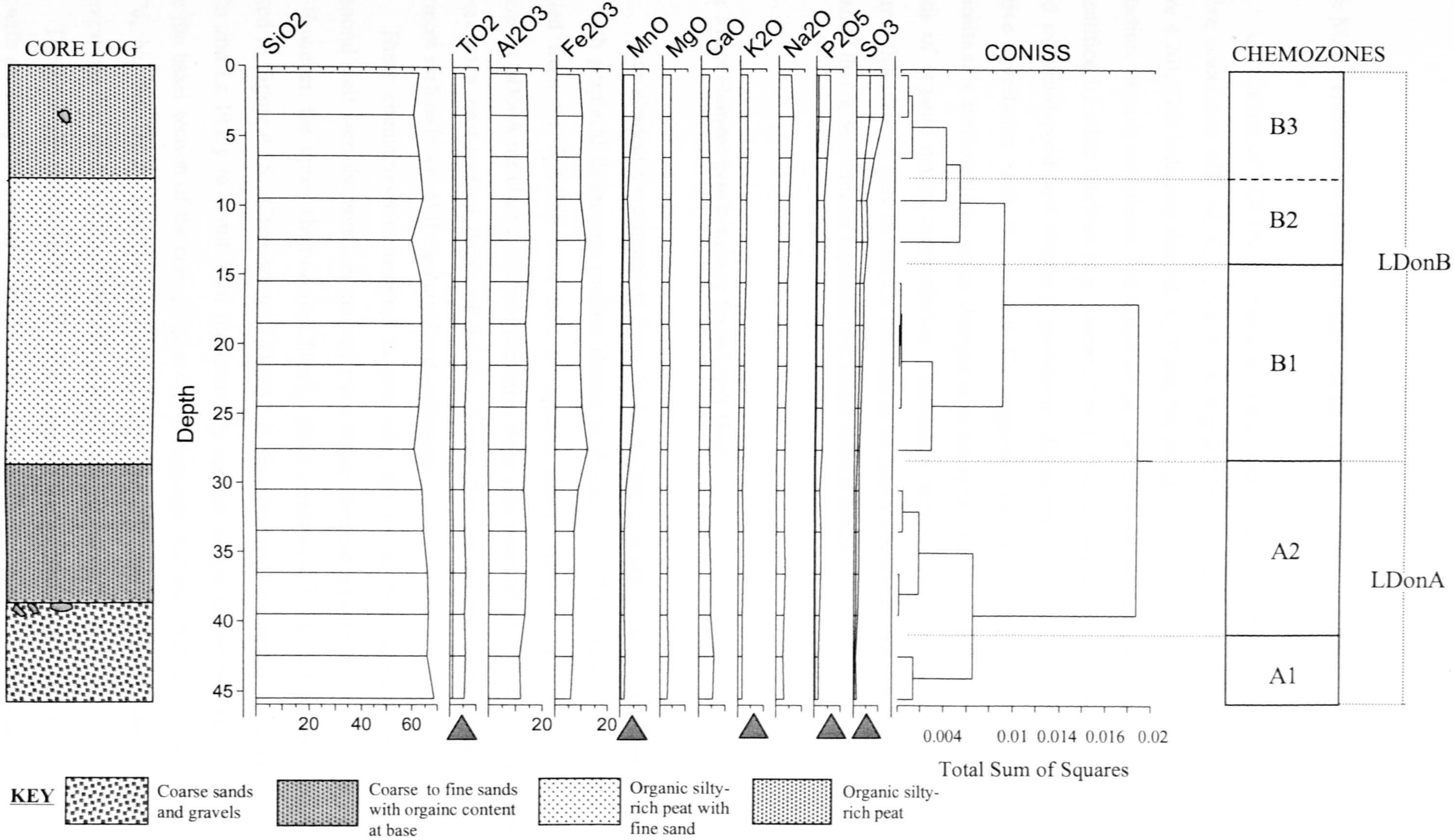

Figure 4.18: Major element chemostratigraphy of the Loch Don marsh core, element abundance (% ashed mass) and CONISS zonation. TiO_2, MnO, MgO, P_2O_5 and SO_3 shown with exaggerated scale (x 15) for clarity , marked with the symbol ▲

4.8.5: Major element correlations with LOI and Ti

Correlation of LOI (% dry mass) with the major element distributions reveals a strong positive association with Al, K, P, Na, Fe, S, Mg and Mn (Figure 4.19a and Figure 4.19b, and Figure 4.20). This indicates that Al, K, P and Na are all associated with vegetative litter, plant production, organic complexes and saline evapo-transpiration processes in this marsh sequence as identified by other workers (e.g. Turner, 1999). Organic matter, Fe and Mn association are linked to post-depositional chemical processes (discussed fully in Chapter Six). The strong negative correlation with Si, Ti and Ca suggests that down-core variation in sediment composition is attributable to minor changes in minerogenic sediment delivery and not linked to periods of organic matter accumulation. Correlation with Ti (as a proxy for detrital input) confirms this view as only Si and Ca are seen to be positively associated with Ti (Figure 4.20) indicating that these elements represent the major detrital inputs.

4.8.6: Trace element geochemistry from Loch Don

Trace element concentrations from the Loch Don core are presented in Appendix 4.4 a & b, with graphical down-core profiles shown in Figure 4.21. Two distinct chemozones are revealed from the CONISS least sum of squares cluster analysis (Grimm, 1991). Within chemozone LDonA the cluster analysis identifies three sub-zones which extend from the base of the core to a near-surface depth of 5-6cm. Above this chemozone LDonB represents the uppermost surface layers of the accumulated sediments.

These chemozones correspond in part with the visual base stratigraphy but do not correspond well with the zonation derived from major element geochemistry shown in Figure 4.18. However, the upper chemozone LDonB1 does correspond to the uppermost 5cm depth depicted in Figure 4.18. Chemozones LDonA1 is characterized by slightly enriched levels of Ce, Co and La likely to result from the generally coarser nature of the sedimentary material within the basal section of the core (Figure 4.21). Elements that are relatively depleted include As, Cu, Ni, Pb, U, Zn and the halides Br, I, S and Cl. The remaining elements exhibit concentrations that tend to fluctuate less throughout the entire core.

The principle characteristics of zone LDonA2 are a small enrichment of Ce at 36 cm depth with generally increasing concentrations of most other elements in particular Br, I, S and

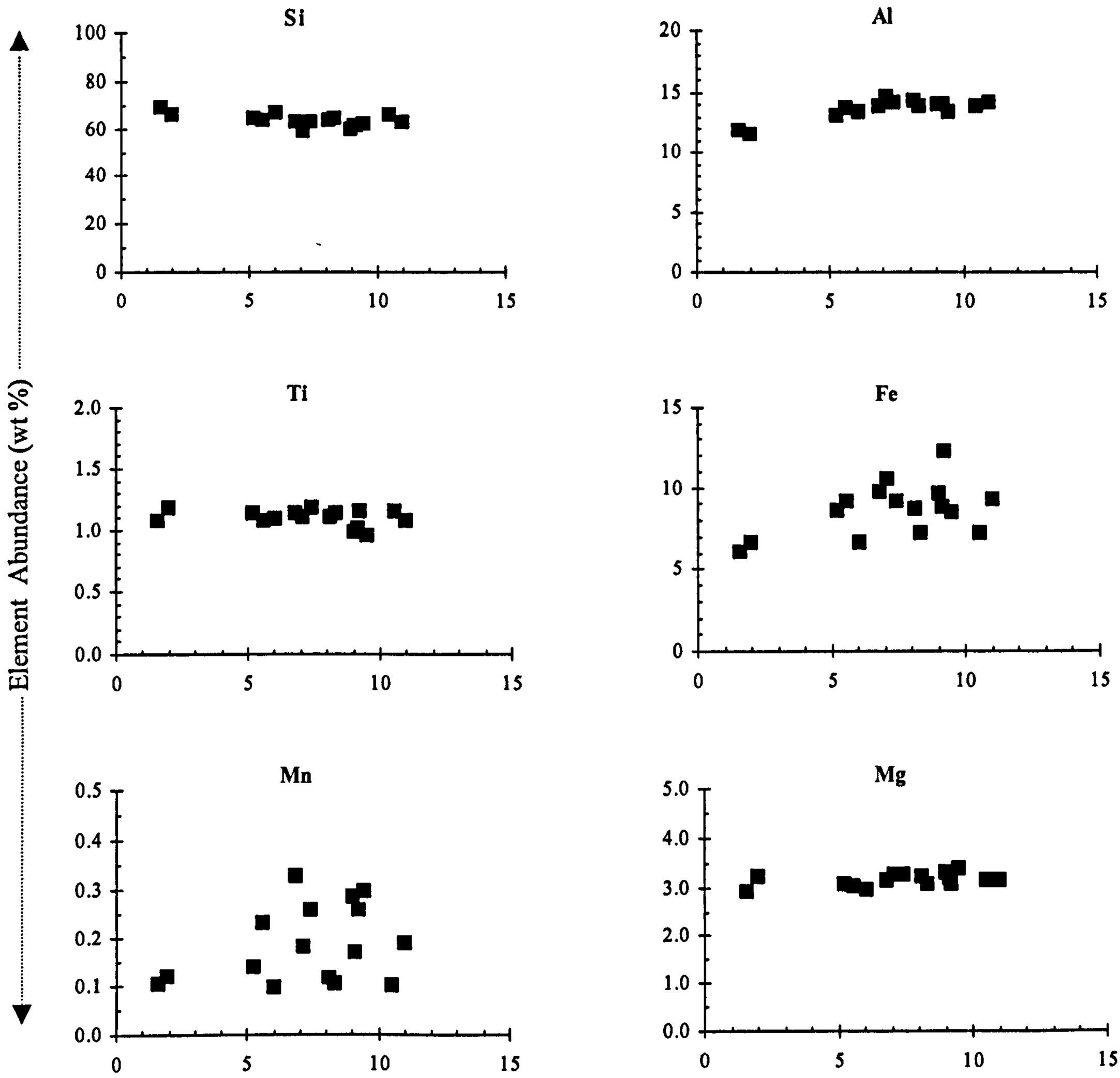

Figure 4.19a: Major element abundance and Fe/Mn ratio vs. organic content (LOI 550^{o}C) from Loch Don core 1.

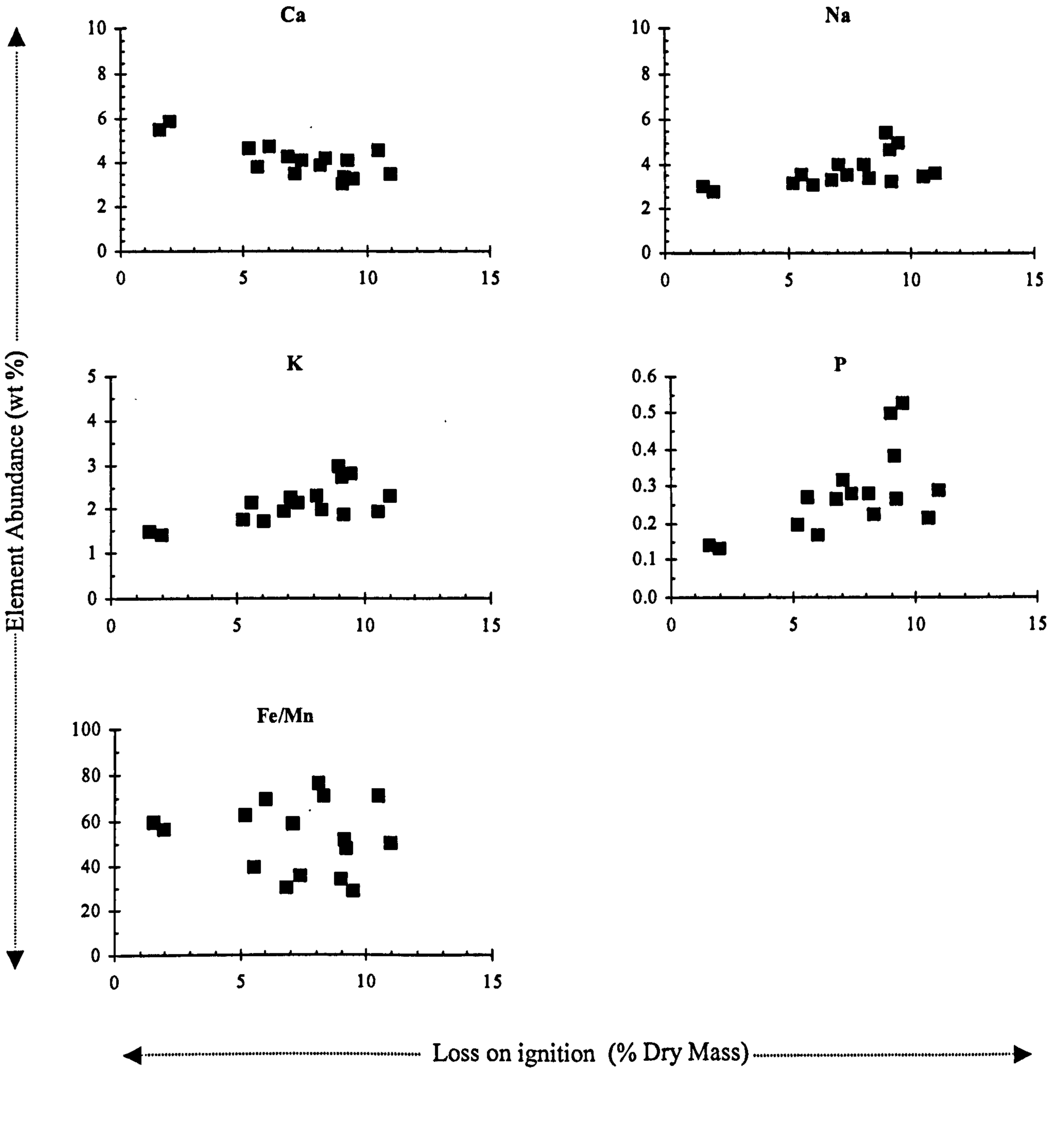

Figure 4.19b: Major element abundance and Fe/Mn ratio vs. organic content (LOI 550^{o}C) from Loch Don, core 4

(a) Element	Core Average	(r) LOI
LOI	7.30	
Al_2O_3	13.63	0.81
K_2O	2.10	0.68
P_2O_5	0.28	0.60
Na_2O	3.67	0.54
Fe_2O_3	8.63	0.48
SO_3	1.96	0.48
MgO	3.14	0.39
MnO	0.19	0.31
TiO_2	1.10	-0.27
SiO_2	63.30	-0.57
CaO	4.10	-0.77

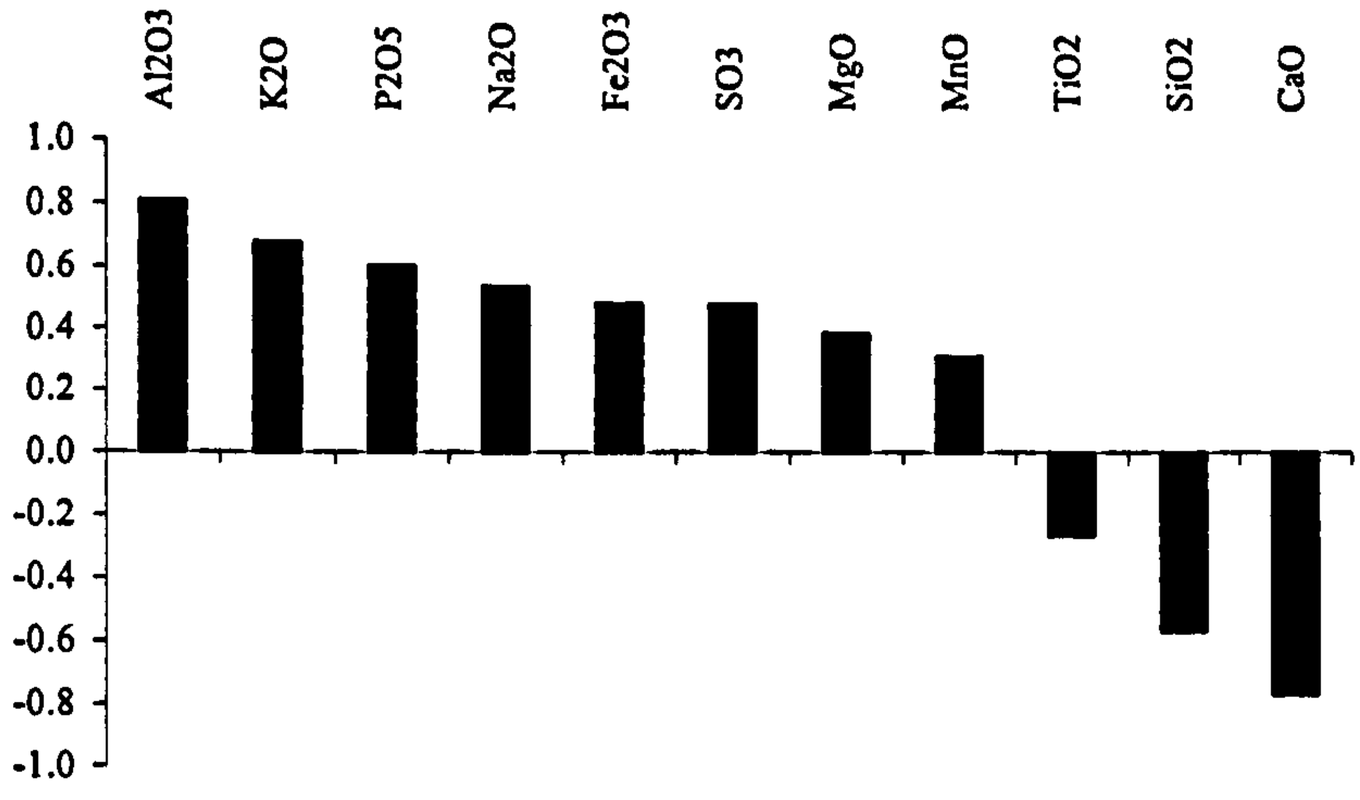

(b) Element	Core Average	(r) TiO_2
TiO2	1.10	
CaO	4.10	0.61
SiO2	63.30	0.33
Fe2O3	8.63	-0.04
Al2O3	13.63	-0.08
MgO	8.63	-0.26
LOI	7.30	-0.27
MnO	0.19	-0.31
K2O	2.10	-0.74
P2O5	0.28	-0.77
Na2O	3.67	-0.81
SO3	1.96	-0.83

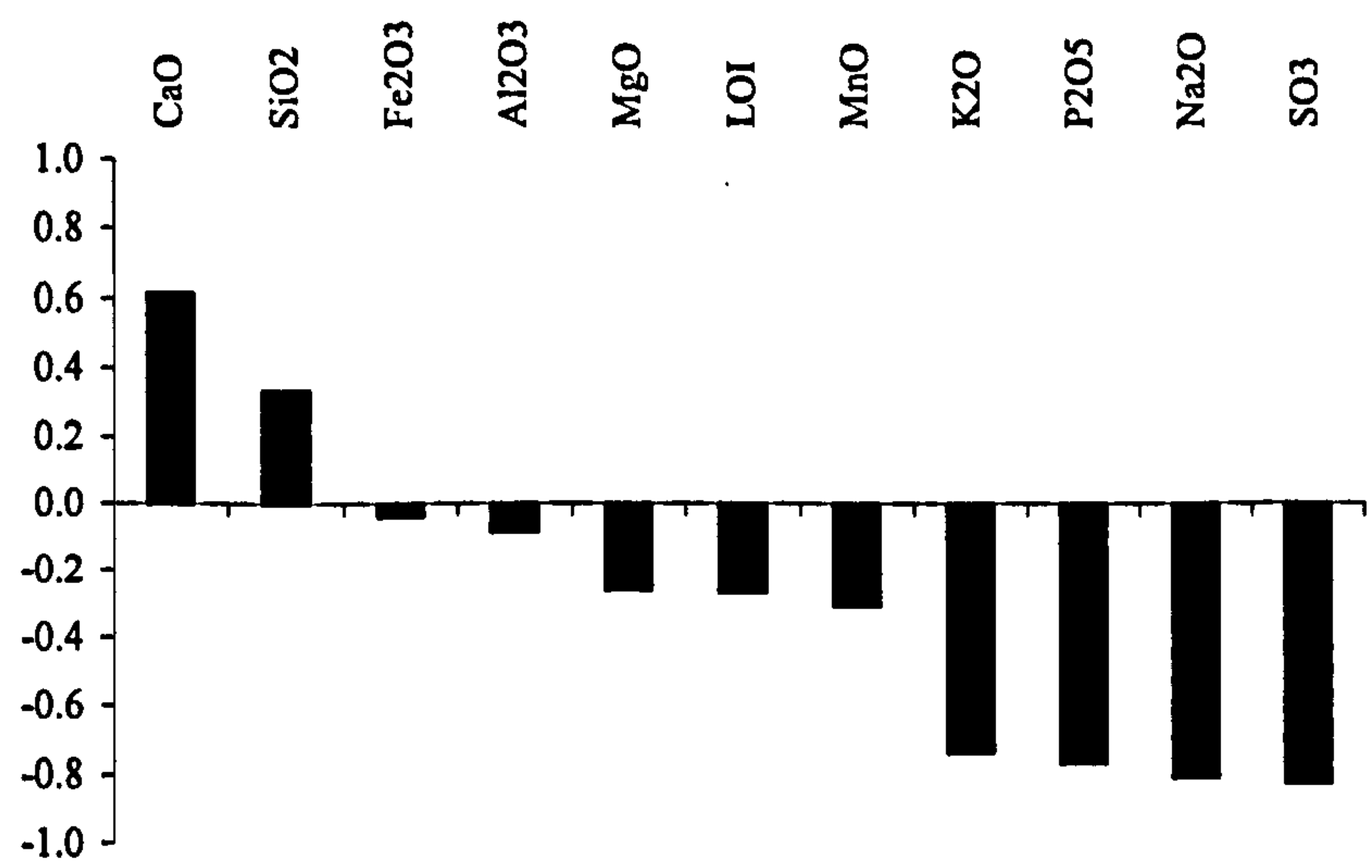

Figure 4.20: Core average major elemental abundances and correlation with; (a) LOI (550°C) and (b) TiO_2 (wt %) for the Loch Don marsh core. Elements are ordered by correlation with LOI and TiO_2

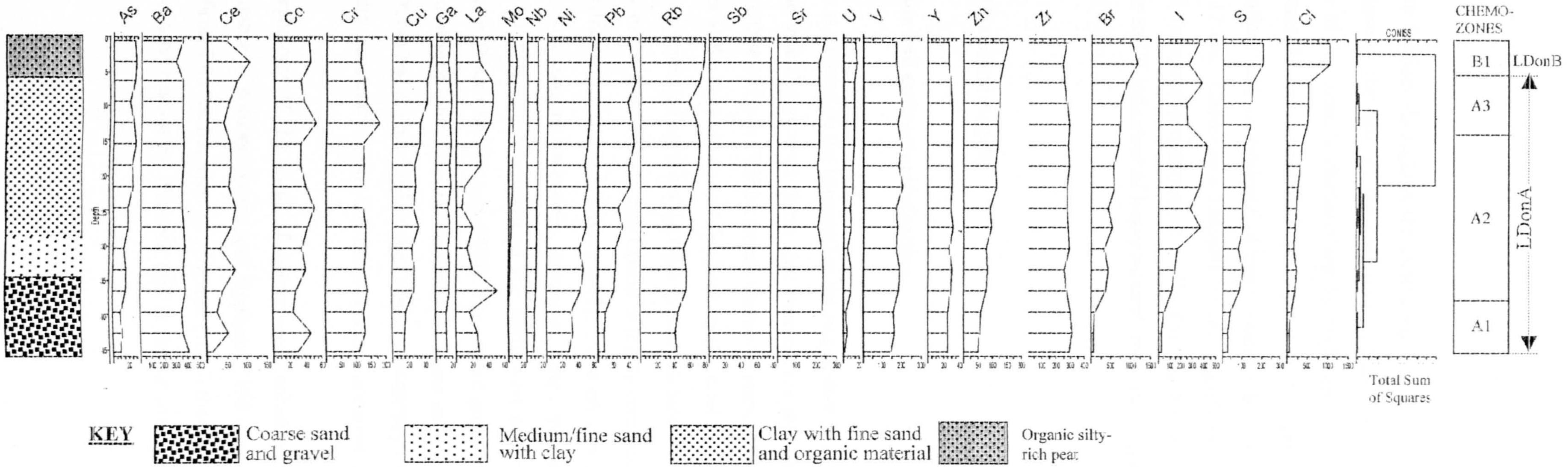

Figure 4.21: Trace element concentrations (ppm) for the Loch Don marsh core (oven-dried pressed pellets) and CONISS zonation

Cl. La concentration declines throughout the central section of this zone returning to values comparable with those at the base of the core near in LDon A3 below the boundary with LDonB1. The base of this zone is characterized by slight enrichment of Co and Cr with a corresponding decrease in the concentration of I. Most of the other elements show steadily increasing concentrations with no evidence of major changes in input over this depth interval extending from 5- 17 cm. Chemozone LDonB1 reveals significant enrichment of the halide elements along with increased concentrations of Ce, Co, Cu, Ni, Rb, and Zn, and to a lesser relative extent Zr, Sr and U indicative of heavy mineral, trace metal and fine particulate surface enrichement (Figure 4.21).

4.9: Loch Creran (mainland Argyll)

4.9.1: Site description and environmental setting

Loch Creran is situated on the mainland of the Argyll district some 15 km north of Oban and is typical of the glacially scoured fjords that characterize the western coast of Scotland (Figure 4.1). The coastline of Loch Creran extends eastwards some 13km inland from the island of Eriska, which lies at the seaward end of the Loch to the head of the fjord where the River Creran discharges freshwater derived from the Glen Creran catchment into the estuary.

The geology of the area around Loch Creran is highly complex but principally consists of rocks from the Dalradian super group (Figure 4.22). These are sub-divided into two distinct groups the first of which contains limestones, dolomites, slates, quartzites and green phyllites which outcrop around Port Appin situated to the north-west and now referred to as the Ballachulish Succession (Harris and Pitcher, 1975). The second group consists of an underlying highly laminated unit of grey quartzites and black shales. These extend over a much larger area to the east of Glen Creran and are bounded by the Cruachan Boundary Fault which delineates the Dalradian sedimentary succession from the Etive igneous intrusion to the east (Litherland, 1980).

The geomorphology of the Firth of Lorne area including Loch Creran has been investigated by a number of authors (Synge and Stephens, 1966:Gray, 1972; Peacock, 1971). Peacock (1971) confirmed the earlier view of McCann (1966) that Loch Creran lies within the limits of the Loch Lomond readvance. Peacock (1971) further concludes that the area of outer

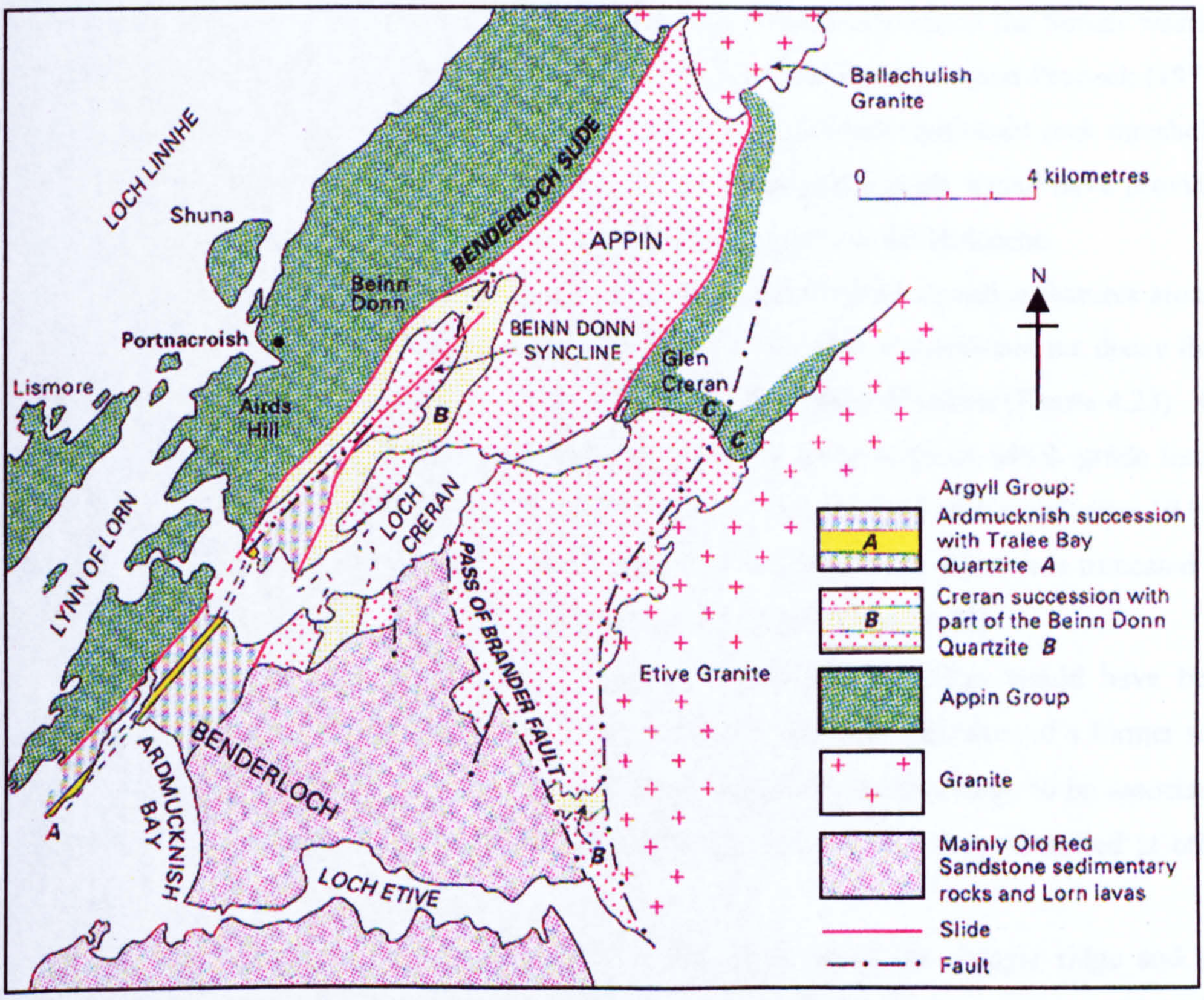

Figure 4.22: The geology of the area around Loch Creran showing the distribution of the Ardmucknish and Creran Dalradian metasedimentary succession of the Argyll group. Note the position of the major tectonic structures within the region that include the Pass of Brander fault and the Cruachan Boundary Fault delineating the Etive igneous intrusive complex from the Dalradian succession to the west. (Source: British Geological Survey, simplified from Litherland, 1980).

Loch Creran is one of four sites within the Western Highlands that does not exhibit an end moraine complex typical of other readvance glacier locations within the region.

Within the outer area of the Loch significant out-wash material consisting of sands and gravels lies in close proximity to the terminal moraine feature mapped by McCann (1966). It has been suggested that this is likely to have been deposited proglacially across the former wasting of the terminal moraine following the retreat of ice from its maximum position Peacock (1971). Further inland from the outer area of the fjord, Loch Creran exhibits significant rock thresholds associated with valley narrowing. As ice retreated the sands and gravels would have provided the principal source of sediment for coastal readjustment throughout the Holocene.

Detailed geomorphological mapping of the glacial and raised shoreline features around upper Loch Creran was undertaken by Gray (1972), who describes a significant ice decay limit in the form of a dead-ice hollow now occupied by Loch Baile Mhic Chailein (Figure 4.23). On the north-west side of the Glen this feature is bounded by kame terraces which grade into a substantial outwash plain. This extends down the valley from an initial altitude of circa 19.9 m OD at an ice contact slope situated between Invercreran and Glassdrum where it is truncated by a later shingle ridge which has a maximum altitude of 14 m OD (Figure 4.23).

Gray (1974a) has suggested that formation of the shingle ridge would have been consistent with the deposition of an outwash terrace in this area and indicative of a former sea-level at least as high as 13–14 m OD. Consequently, he attributed this ridge to be associated with a relative sea-level comparable with the Main Post-Glacial Shoreline identified at other locations.

Further seaward from this point between the position of the shingle ridge and the contemporary salt marsh, Gray also identifies a post-glacial shoreline feature at an altitude of approximately 3.0 – 4.0 m OD (Figure 4.24). No specific age has been proposed for this shoreline but it is likely to be an artifact of relative sea-level fall during the mid to late Holocene.

Field site investigations using the 1 m coring device at this site were undertaken at various locations above the present-day tidal limits. At the site of the shingle ridge close to Glassdrum identified by Gray (1974; Figure 4.23) sedimentary sub-strata consisting of rounded pebble sized material and gravel rests beneath a thin layer (12-16 cm maximum) of peat soil which is used for agricultural grazing. These sedimentary deposits are consistent with the formation of the Main Postglacial beach proposed by Gray (1974). Other investigative coring was undertaken above the present-day high water mark over an area to the south east of the River Creran at greater altitude than the present day shoreline. This feature was also identified

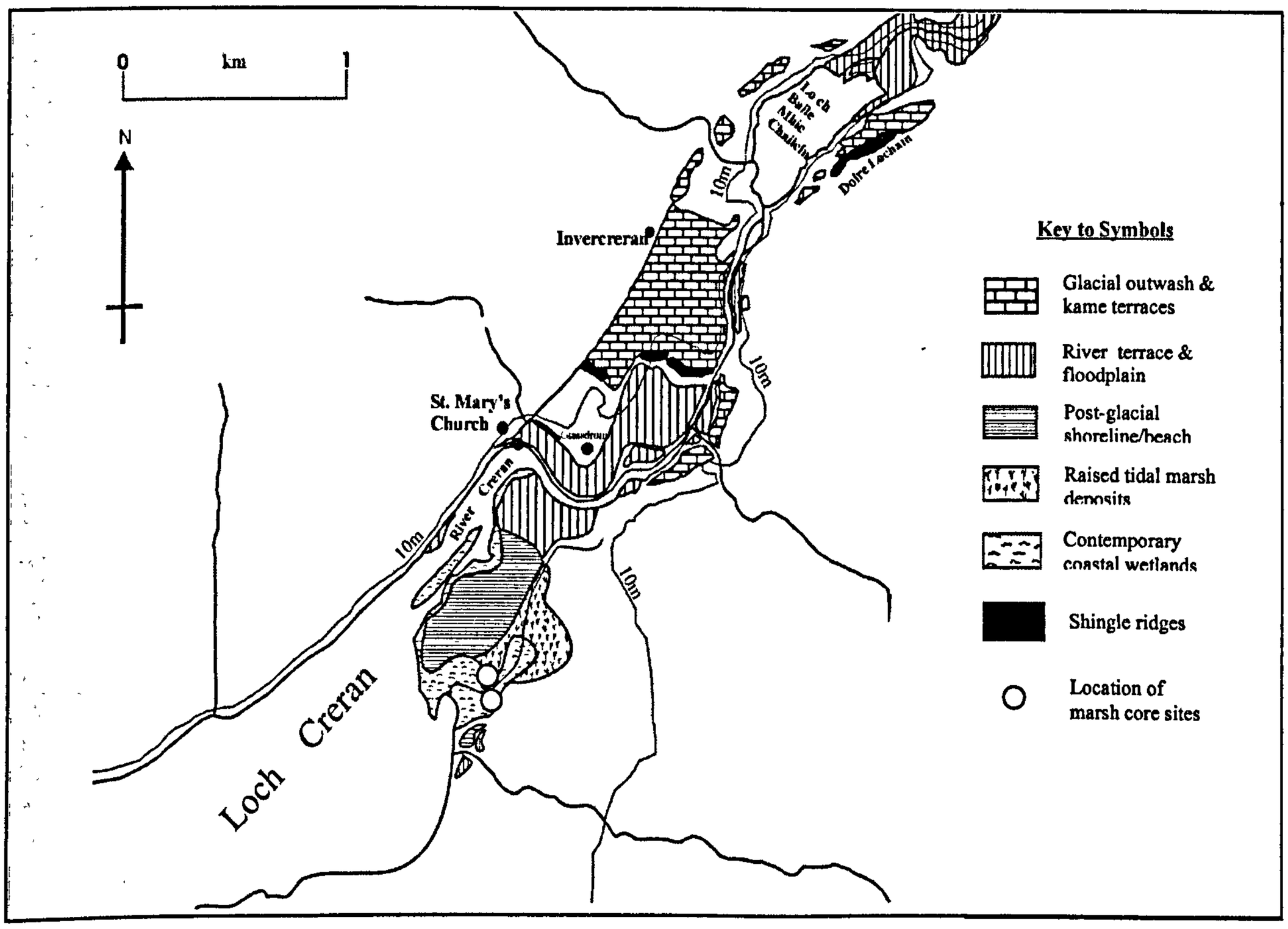

Figure 4.23: Geomorphological features within Glen Creran and at the Head of Loch Creran (adapted from Gray 1974). Also shown are the sampling locations on the contemporary marsh at this site.

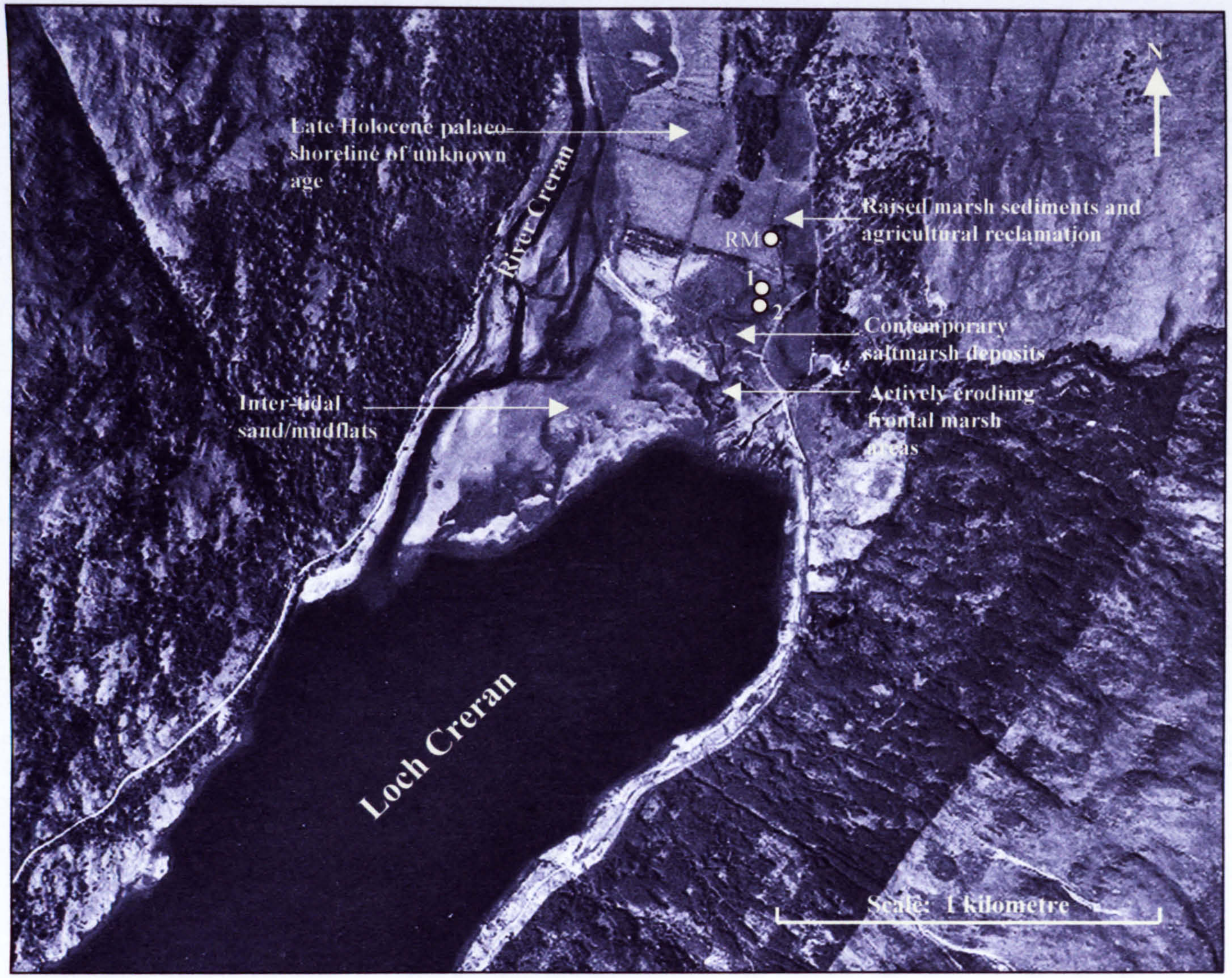

Figure 4.24: Aerial photograph (1967) of the inter-tidal area at the Head of Loch Creran showing general geomorphological features. The core sites on the marsh surface are indicated by the yellow circles marked 1 and 2 respectively. The position of the raised marsh sequence of likely Late Holocene age is marked RM. (Source: Royal Commission for Historical and Archaeological Monuments of Scotland, (RCHAMS), Edinburgh.

by Gray (1974). The coring revealed a sedimentary sequence of upper soil overlying clastic sediments with clay in turn overlying a stiff grey/blue clay and may represent a raised coastal wetland sequence of as yet undefined age. Levelling across this surface gave a maximum altitude for the surface of this feature of 5.12 m OD (Figure 4.24).

Seaward of this feature there is a large expanse of contemporary saltmarsh development although not as extensive as that witnessed on both the Isle of Mull sites. Situated in close proximity to the A828 public highway and Druimavuic House, the marsh has developed in a pocket of the estuary head not directly influenced by the River Creran (Figure 4.24 and Figure 4.25).

The marsh here is dominated by *Plantago maritima* and *Glaux maritima* with *Juncus gerardi* also prominant. Some zonation between the high marsh environment and that of the lower marsh is discernable from inspection of air photographs and oblique field photographs obtained by the present author (Figure 4.25). Noticeable in the photograph is the recent colonisation of marsh vegetation within the lower section of the Druimavuic House garden immediately south of the A828 road.

Coring of the preset-day expanse of marsh revealed a variable depth of coastal peat which has developed upon the underlying gravel and sands, ranging from 36 cm to 69 cm across the high-marsh environment. The variability in marsh sediment thickness results from the differential morphology of the underlying gravel and sand substrate which consists of fluvial gravel and pebble bars. The material within these features is also likely to have been reworked by wave and tidal currents as the present marsh environment became established. Coring site locations are shown in Figure 4.24 and Figure 4.25.

4.9.2: Core sedimentology

Two cores were abstracted from the marsh at the head of Loch Creran. Core 1 was selected for analysis and a digital photographic image of core taken in laboratory conditions is shown in Appendix 3.3. An upper unit of dark-brown/black silty peat soil with clay is visible extending down the core to a depth of 36-37 cm. This is shown in greater clarity in the detailed sedimentary log presented in Figure 4.26. Rootlets are quite abundant within this upper unit and some small angular pebble-sized clasts are visible at 14-15 cm. Beneath this unit the lithology grades over a short depth interval of no more than 2-3 cm into an underlying unit of coarse sand

(A)

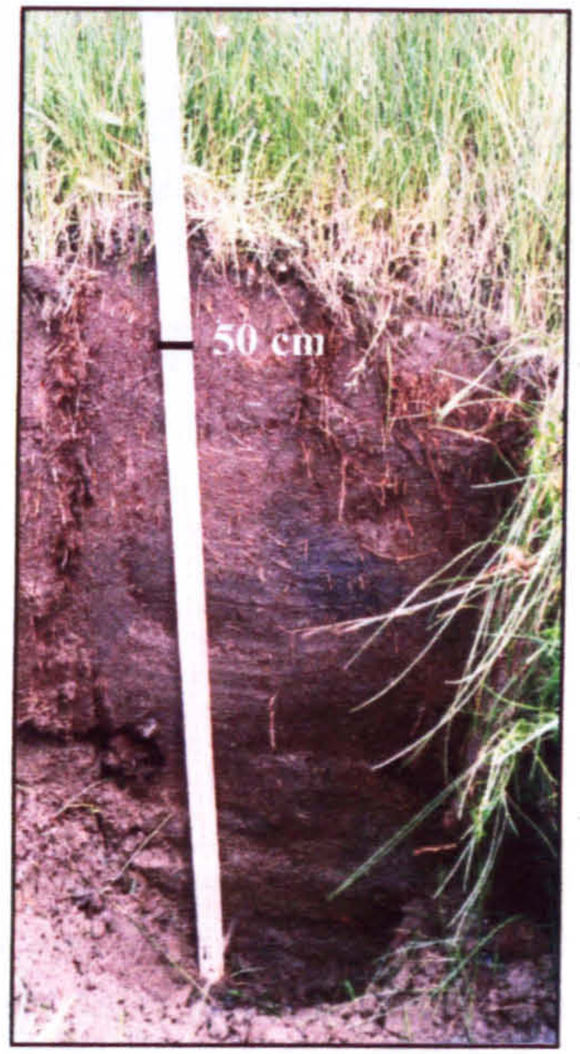

(B)

Figure 4.25: Overview of the pocket-type marsh at the Head of Loch Creran looking towards the South-East. (A) showing the sampling sites for the sediment cores abstracted from this location as numbered. (B) The core from site number one prior to abstraction. The area of possible Late Holocene shoreline is delineated by the blue dashed line with the position of the raised marsh sequence labeled RM. The extent of contemporary salt marsh is marked by the black dashed line. Note the area of marsh which is now forming within the lower part of the Druimavuic House gardens across the main roadway.

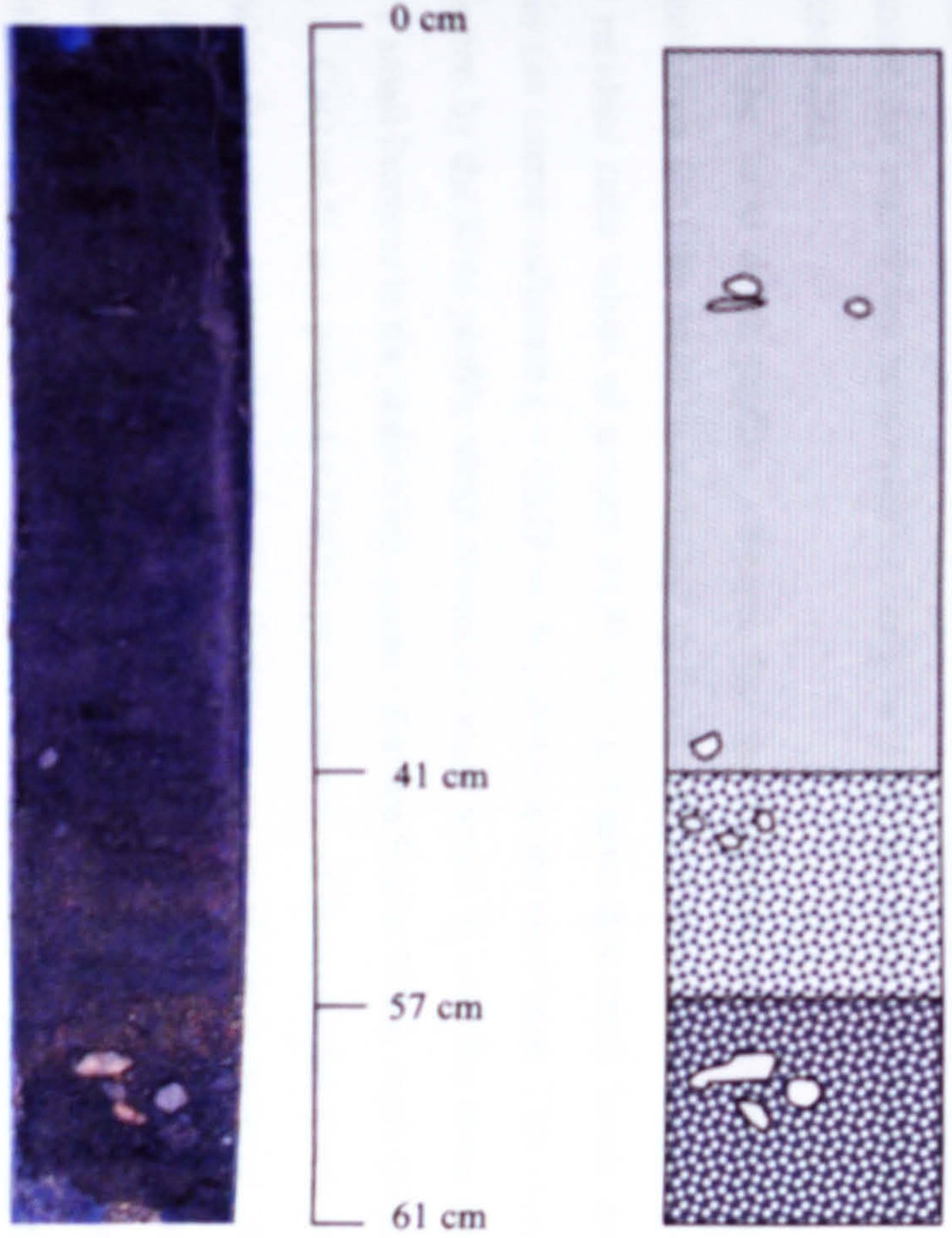

Sediment Description

Dark brown/black upper silt rich peat unit with some clay material. Fine to medium sand particles also present with very occasional clasts of fine to medium sized gravel and small pebbles.

This unit is very organic rich with vegetation at the surface and abundant rootlets throughout.

No laminated structure visible.

Lower unit of fine to medium sandy material with organic rich silt also present. Distinct lenses of dark brown silt rich material present which is fairly well mixed with the coarser sand substrate throughout and the unit grades to gradually becoming more gravel rich at the base with sub-angular clasts.

Few organic rootlets are visible in this lower section of the core. Angular pebbles comprise the bulk of the basal material.

Figure 4.26: Digital photograph image and sedimentary log of the marsh core sequence from the Head of Loch Creran, mainland Argyll.

and fine gravel material extending from 37 cm to a depth of 55 cm. Rootlets are virtually absent from this section of the core which overlies a basal unit of gravel-rich material consisting of coarse angular and sub-angular small to medium pebbles (Figure 4.26).

4.9.3: Major element geochemistry

Major element geochemistry raw data is presented in Appendix 4 and the graphical plots of the down-core profiles of major element abundance from this sequence are presented in Figure 4.27. Normalized major element plots of Si, Ti and K (Figure 4.28), indicate a more subtle decrease of coarse silt/sand material being deposited on the surface of the marsh within the upper 20 cm of core as indicated by the Si/Al plot. This depth interval also corresponds to a slight increase in CaO. The dry bulk density depth profile corresponds quite well with the visual stratigraphy and the organic matter profile determined by LOI and indicates a little variation in the supply of detrital material to the marsh from a depth of 40 cm. Si/Al ratios fluctuate within the upper section of the core down to a depth of 40 cm between values < 4 wt % to > 5 wt % recorded at a depth of 21cm. Levels decrease slightly down to 34 cm and below this depth show an increase where the core stratigraphy indicates a change in lithology from silty/peat with organic material to sandy/gravel substrate at 40 cm depth. This basal sediment is likely to represent the underlying sand/mudflat composed of reworked predominately fluvial material (Figure 4.28).

The Ti/Al depth profile indicates that the sediment composition has remained quite constant over the time period represented by the 0 – 40 cm depth interval down through the core with residual ratio values of around 0.055 wt %. Below this depth levels decrease markedly within the coarser substrate (~ 0.039 wt %) down to the core base. This interpretation is also supported by the K/Al profile which shows constant levels K over the same depth interval with only a small increase in the underlying coarse substrate below 40 cm depth (Figure 4.28).

CaO wt % as a proxy for $CaCO_3$ shows increased but constant levels of around 0.25 wt % within the upper peat unit which then decline in the basal coarse material. The interpretation here is that slightly higher levels of $CaCO_3$ dissolution are occurring in the upper peat layer and that alkalinity does not markedly increase within the underlying sandy/gravel material. As such significant authegenic carbonate formation at this depth does not appear to be taking place at the base of this core as has been recorded from the sediment sequences acquired from the Isle of Mull (Figure 4.28).

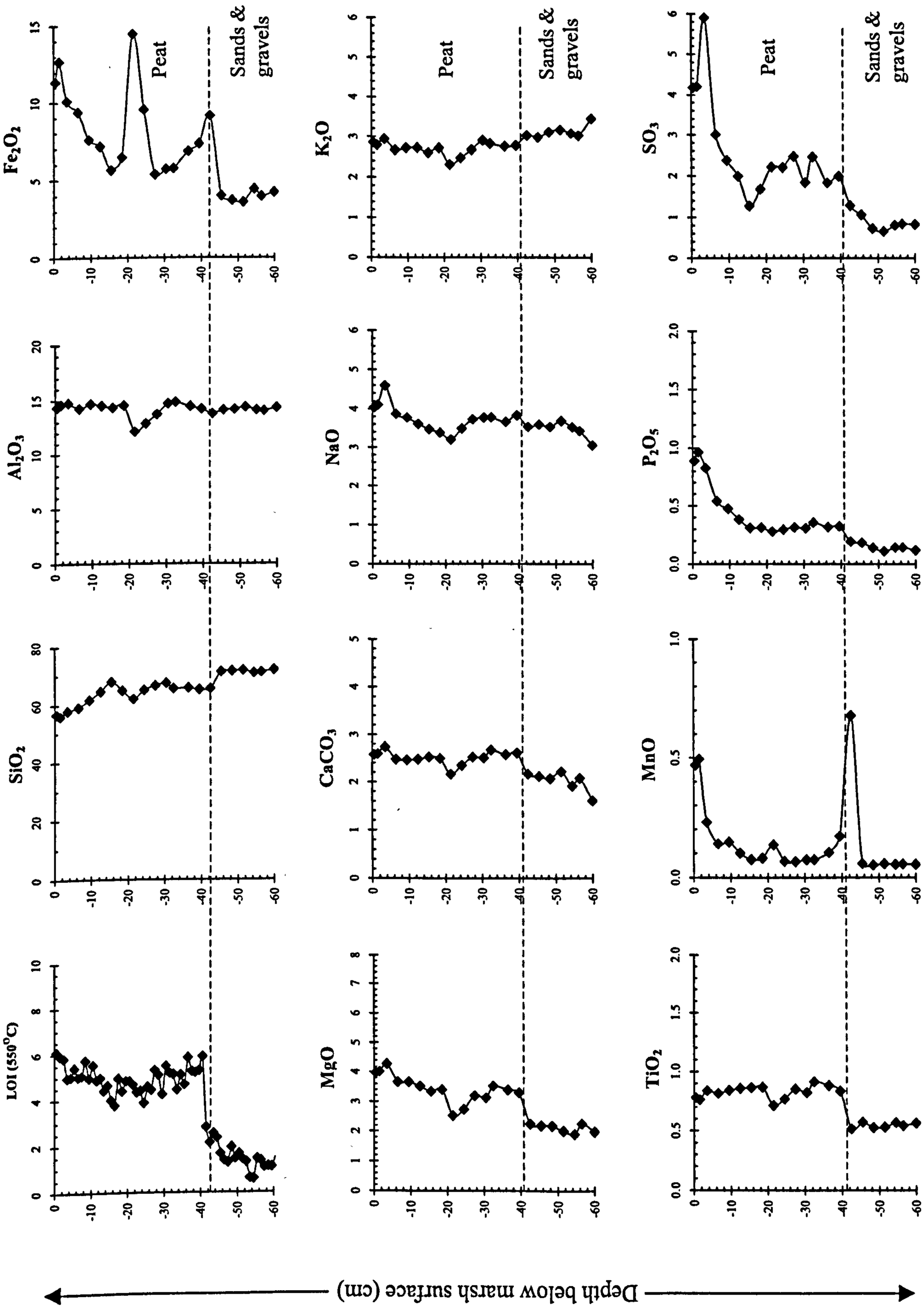

Figure 4.27: Loss on ignition (550°C) and major element profiles (wt %) for core 1, Loch Creran mainland Argyll. Element abundances are reported as oxides (wt %) in accordance with XRF convention.

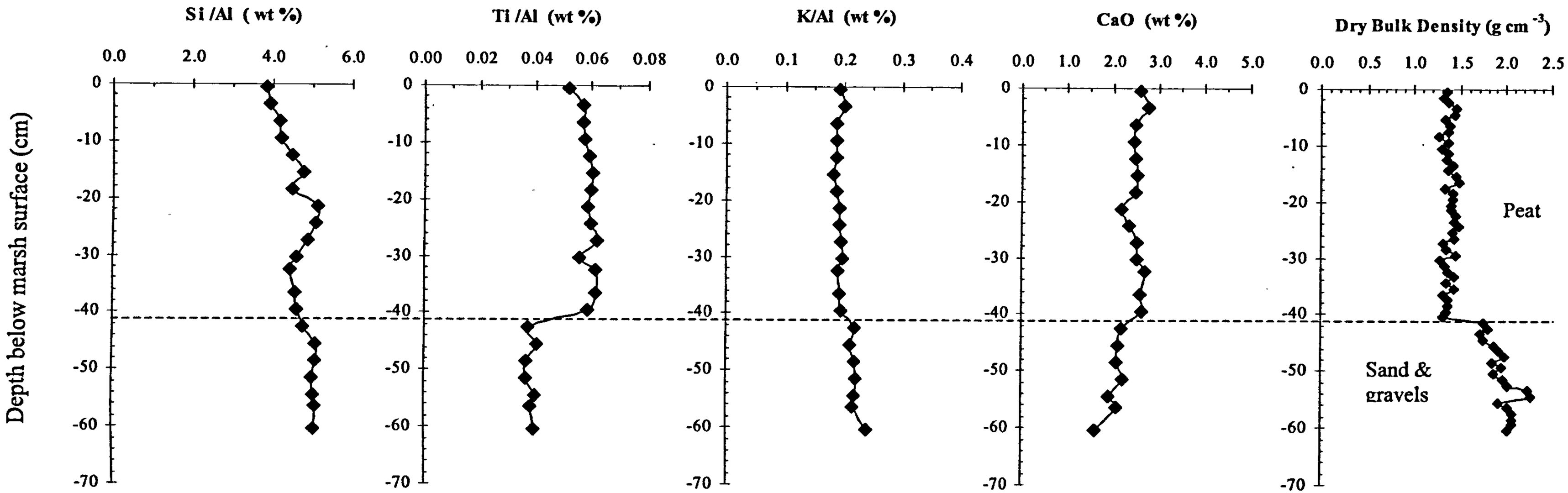

Figure 4.28: Al-normalised weight ratio plots for Si, Ti, and K, with the depth-profiles of Ca (wt %) and dry bulk density (g cm^{-3}) for the Loch Creran marsh core, mainland Argyll.

4.9.4: Detrital composition and geochemical zonation

Detailed examination of the major element abundance using the CONISS cluster analysis reveals two distinct chemozones. Within these further sub-zones are also identified (Figure 4.29). Chemozone LCre A extends from the base of the core up to the near surface where the boundary with Lcre B is situated at a depth of 6-7cm. This then extends to the marsh surface. LCre A1 is characterized by the lowest dry mass abundance of organic material (via LOI proxy method), Fe, Mg, Ca (see below), Na, Ti, Mn, P and SO_3. This probably reflects the proportion of these elements present in the coarse sand and gravels at the base of the core. In this basal zone Si is recorded at its highest value. Al and K values are representative of the average throughout the core sequence, with highest values for K being recorded at the very base of the core. LCre A2 is characterized by significant peaks in element abundances of organic material, Fe and Mn. Fe and Mn values then decrease rapidly with increased elevation through this zone. C_{org} values are however maintained and fluctuate around an average value of ~5 wt %. Mg, Ca, Na, Ti, P and S all show an increase in abundance within this zone (Figure 4.29).

Si, and K profiles indicate a slight reduction whilst Al remains unvariable. Chemozone LCre A3 shows a marked reduction in Si, Al, Mg, Ca, Na, K and Ti close to the boundary with the lower zone LCre A2. Fe values show a significant increase at the same depth and a smaller peak in Mn abundance indicates enrichment at the same depth. Just above this depth increment organic carbon values are also seen to be slightly reduced with a larger relative decrease in SAll elements quickly recover to values similar to those evident in LCre A2 towards the boundary with LCre B1 apart from Fe, Mn P and S which are enriched within the top of this zone. In the upper section of the core chemozone LCre B1 reveals the highest abundance of organics with Fe, Mn, P and S all significantly enriched within the near-surface. Mg, Ca, Na, and K profiles also show evidence of enrichment near the marsh surface. Si and Ti on the other hand show a reduction in abundance whilst Al values are relatively unchanged (Figure 4.29).

4.9.5: Major element correlation with LOI and Ti

Correlation of the major element abundance reveals a strong association between LOI and Mg, Ti, Ca, P, S, Fe and Na (Figures 4.30a & 4.30b, and Figure 4.31). Na and P are associated with marsh plant litter, organic complexes and saline evapo-transpiration processes particularly in the near surface environment of salt marshes. The strong positive correlation

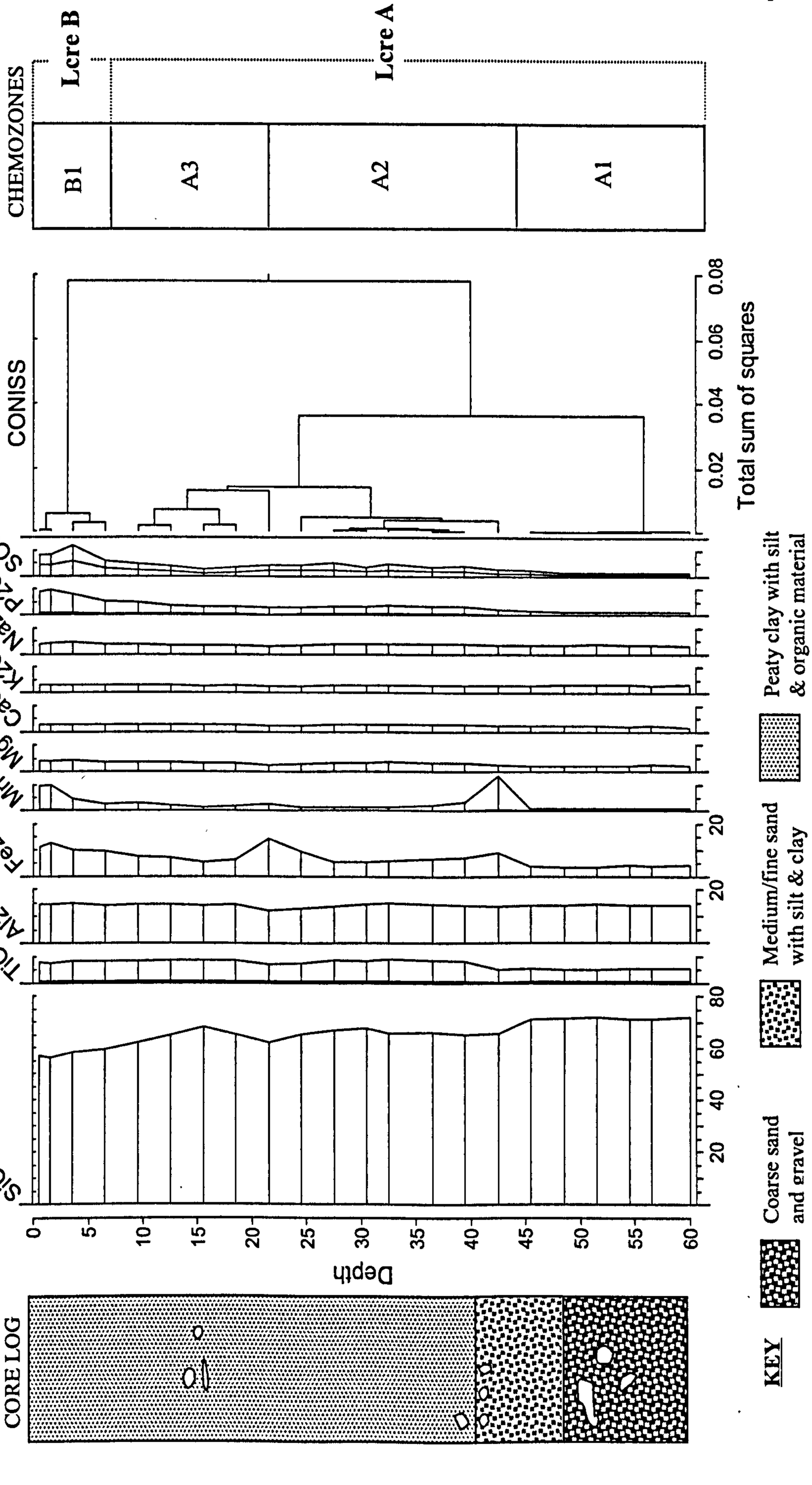

Figure 4.29: Major element chemostratigraphy of the Loch Creran marsh core, element abundance (% ashed mass) and CONISS zonation with P_2O_5 and SO_3 shown on exaggerated scale (x 10).

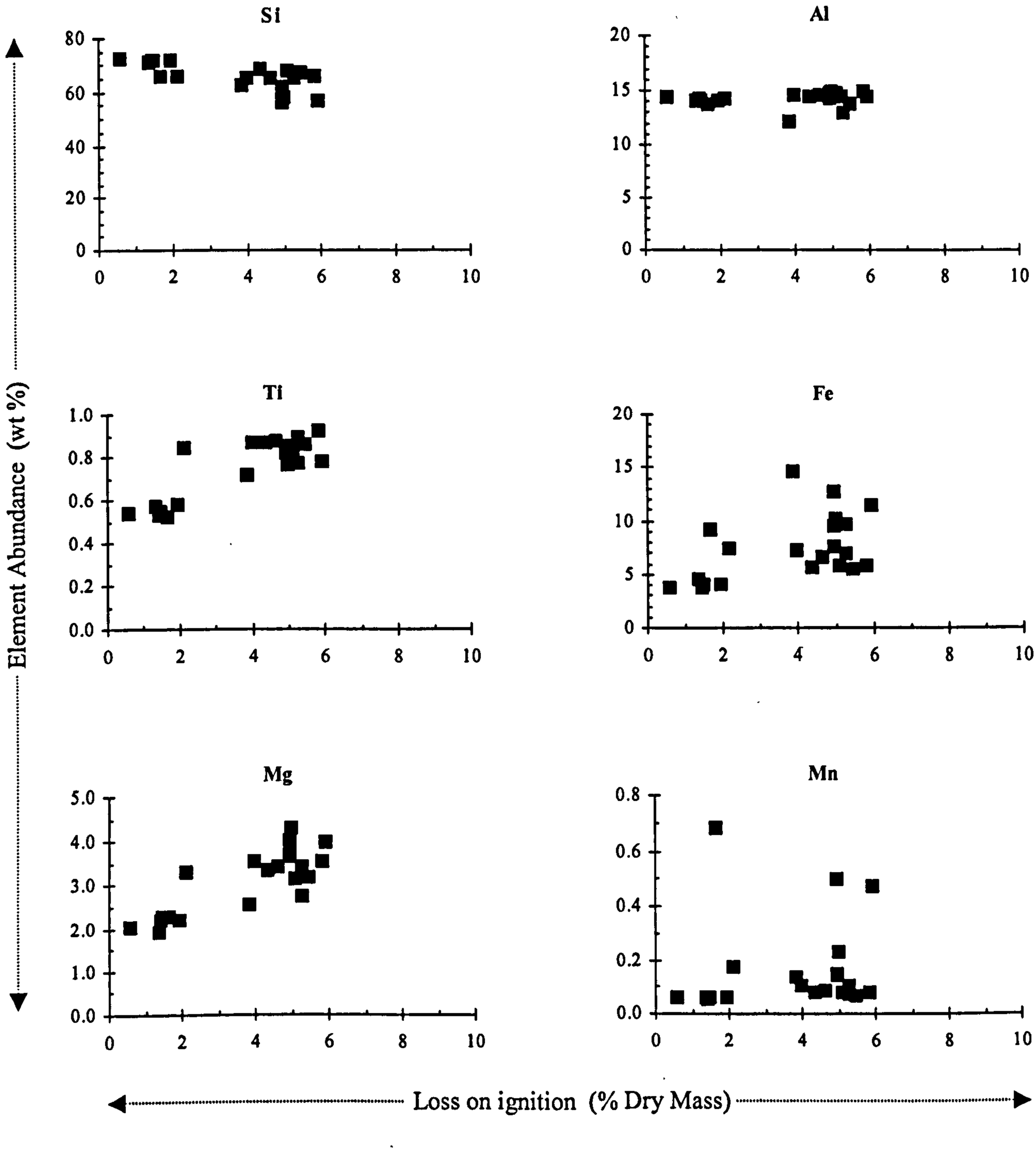

Figure 4.30a: Major element abundance and Fe/Mn ratio vs. organic content (LOI 550^{o}C) from Loch Creran, core 1.

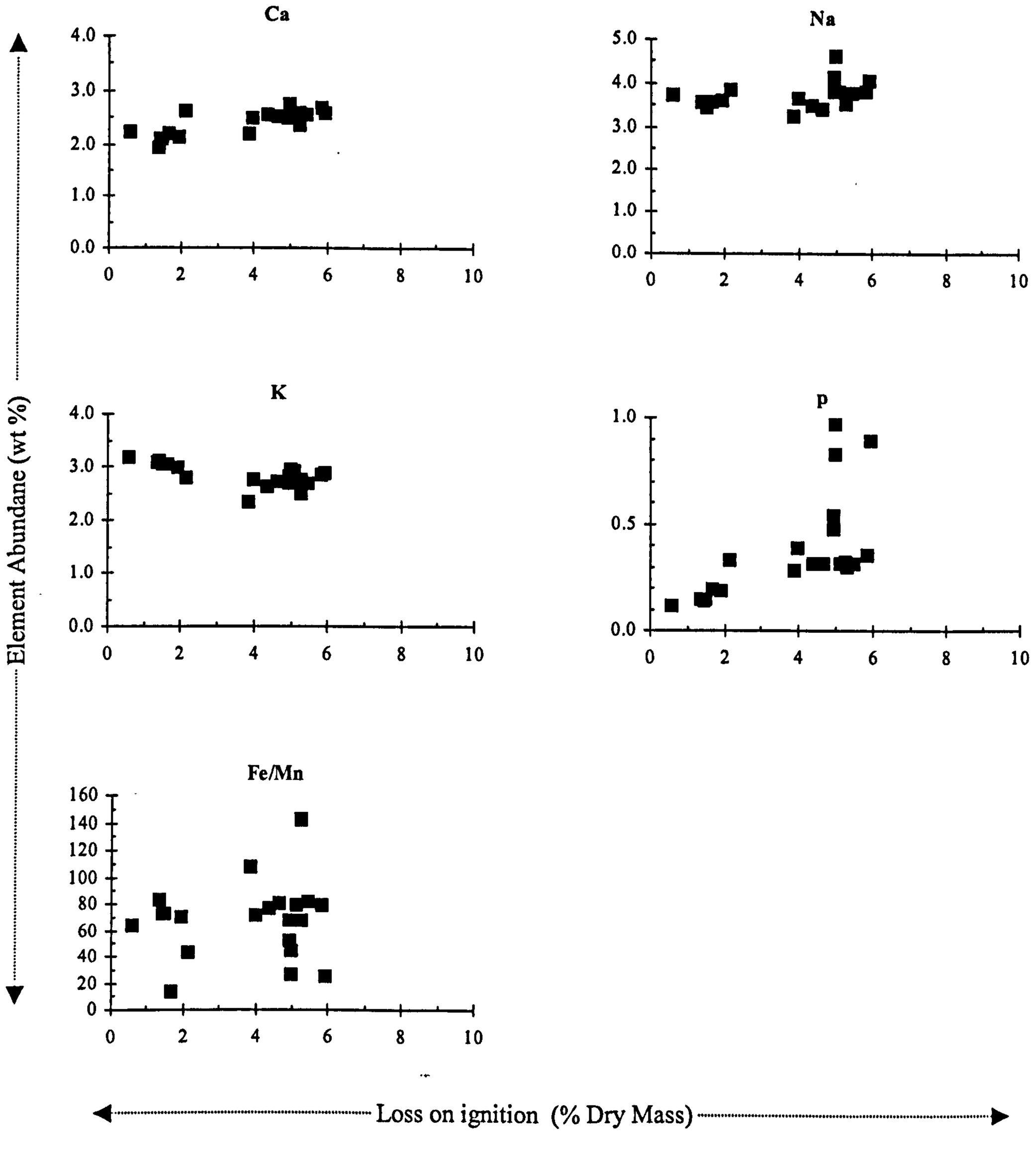

Figure 4.30b Major element abundance and Fe/Mn ratio vs. organic content (LOI 550^{o}C) from Loch Creran, core 1.

(a) Element	Core Average	(r) LOI
LOI	3.94	
MgO	3.02	0.89
TiO_2	0.74	0.88
CaO	2.36	0.85
P_2O_5	0.36	0.70
SO_3	2.08	0.70
Fe_2O_3	7.23	0.59
Na_2O	3.67	0.52
MnO	0.16	0.23
Al_2O_3	14.17	0.16
K_2O	2.84	-0.64
SiO_2	65.69	-0.77

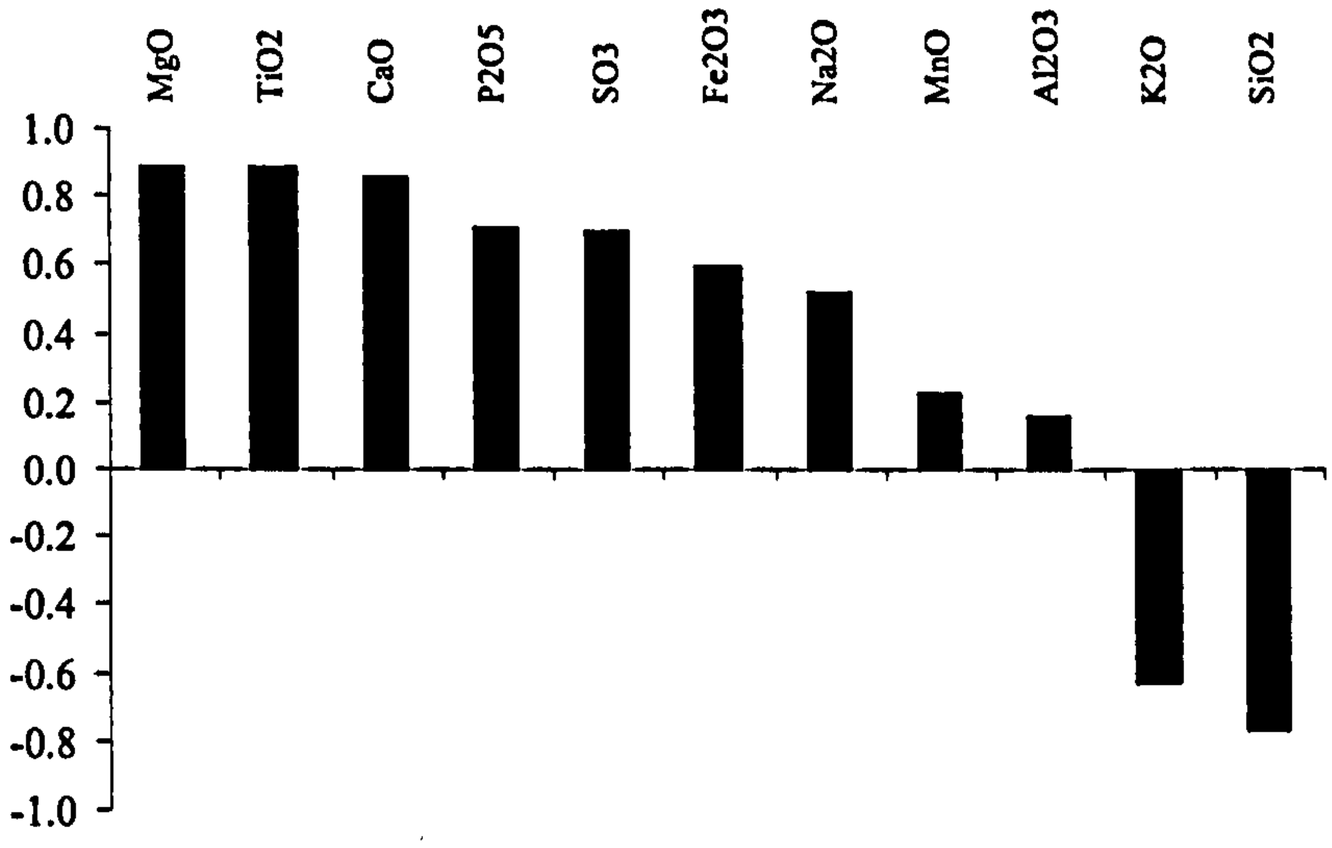

(b) Element	Core Average	(r) TiO_2
TiO_2	0.74	
LOI	3.94	0.88
MgO	3.02	0.85
CaO	2.36	0.84
SO_3	2.08	0.54
P_2O_5	0.36	0.50
Na_2O	3.67	0.39
Fe_2O_3	7.23	0.32
Al_2O_3	14.17	0.26
MnO	0.16	-0.09
SiO_2	65.69	-0.57
K2O	2.84	-0.65

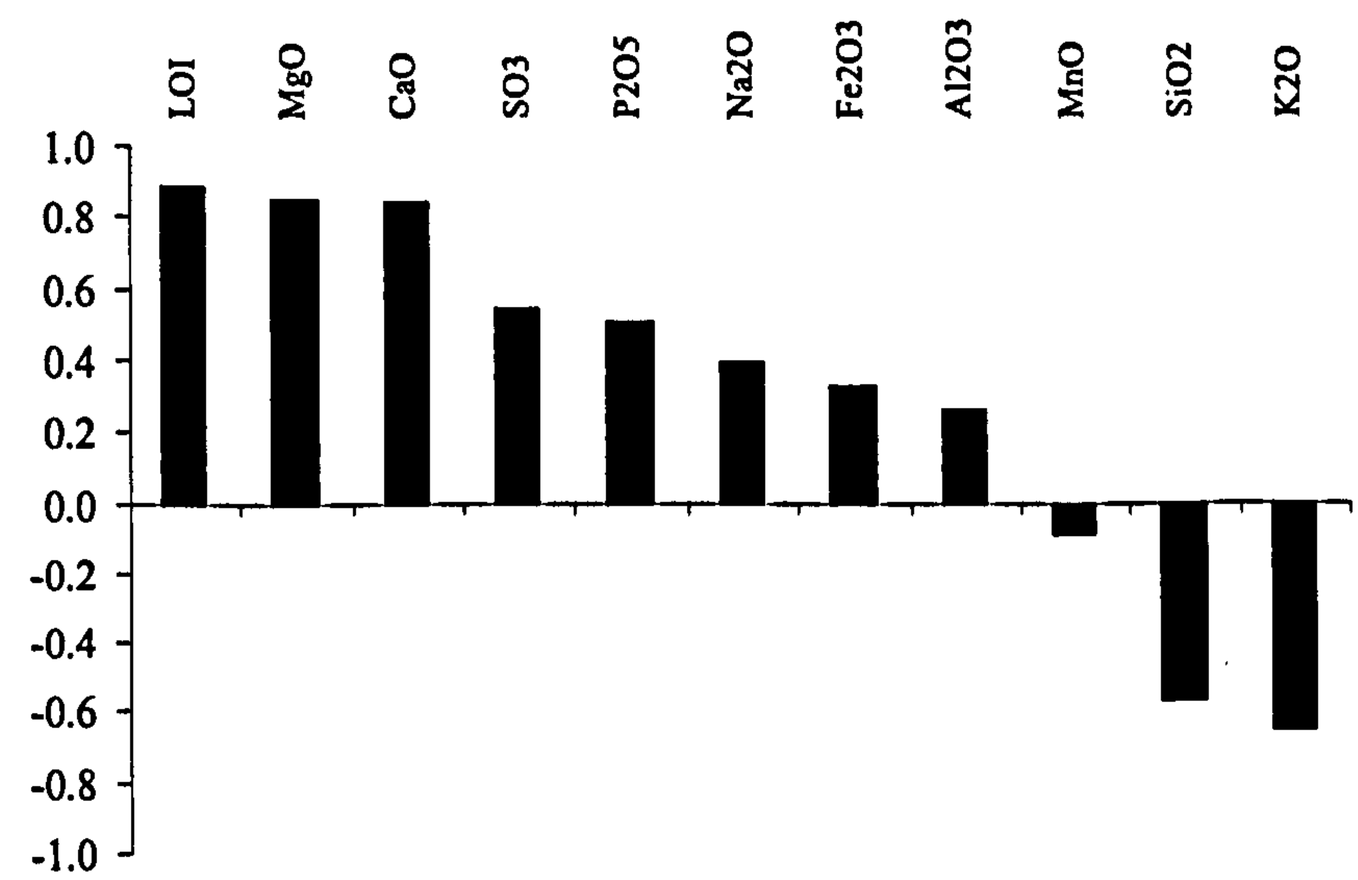

Figure 4.31: Core average major elemental abundances and correlation with; (a) LOI (550°C) and (b) TiO_2 (wt %) for the Loch Creran marsh core. Elements are ordered by correlation with LOI and TiO_2

between LOI, Mg, Ti and Ca suggests an association with marine detrital minerals. The weaker correlation with Fe, Mn and S is likely to be a product of the association of these elements in redox-mediated post-depositional reactions (see Chapter Six). LOI is also weakly correlated with Al in comparison to the marshes on Mull.

Further correlation with Ti (as a proxy for detrital input, Figure 4.31) reveals a strong negative association with Si and K. However, Ti is strongly correlated with Ca and Mg suggesting marine influence.

4.9.6: Trace element geochemistry

The trace element concentration down-core raw data for the marsh core from Loch Creran are presented in Appendix 4.6 a & b with graphical down-core profiles shown in Figure 4.32. Also shown in this figure is the dendogram derived from the CONISS cluster anaylsis performed using the Tilia plotting program (Grimm, 1991). Two distinct chemozones are identified with the basal zone LCre A1 corresponding well with the lower zone identified in the major element cluster diagram (Figure 4.29). Within this basal section of the core many trace elements are relatively depleted in comparison to the overlying sediments (e.g. As, Ce, Cu, Mo, Ni, Pb, U, V, Zn and the halides Br, I and Cl). Zone LCre B comprises three sub-zones and in the central section of the core between 5-45 cm zones LCre B1 and LCre B2 are similar to the major element zonation ascribed to LCre A in Figure 4.29. Within the lower section of zone Lcre B1 As, Ce, Co, Mo, Pb V and I concentrations all exhibit distinct peaks representing significant enrichment of theses elements between 42-47 cm depth. Above this depth interval element concentrations for these elements are more uniform at reduced levels (Figure 4.32). Above the boundary with LCre B1, the overlying zone LCre B2 shows minor increases in the concentration of Cr, Cu, La, U, Y, Zn and I. This corresponds with a decrease in the concentration of Co, Zr. Chemozone LCre B3 also corresponds well with the upper zonation identified in Figure 4.30. Cluster analysis suggests that this upper section of the core differs quite significantly from the underlying sections. Many trace element profiles show significant enrichment in the near-surface layers (e.g. As, Co, Cu, Ni, Pb, U, V, Zn). The halides (Br, I, S and Cl) also show significant enrichment in this upper near surface zone (Figure 4.32).

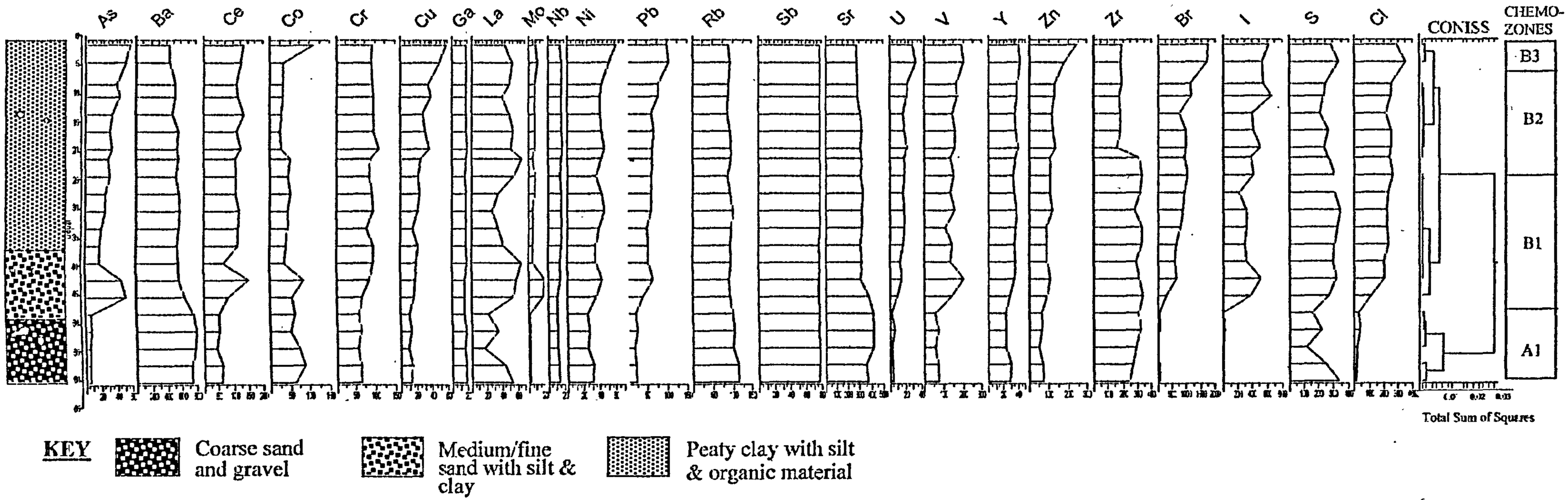

Figure 4.32: Trace element concentrations(ppm) for the Loch Creran marsh core (oven-dried pressed pellets) and CONISS zonation

4.10: Loch Etive (mainland Argyll)

4.10.1: Site description and environmental setting

Loch Etive is situated some 5 km north of Oban and represents one of the most extensive fjords within western Scotland extending inland some 29 km from the seaward entrance to the head of the estuary located beneath the northern slopes of Ben Starav (Figure 4.1 & Figure 4.33). The Loch is characteristic of other fjord environments containing multiple over-deepened anoxic basins (Edwards and Sharples, 1985) resulting from the action of glacial ice scouring. For convenience the Loch can be divided into two main basins (Overnell *et al.*, 2002) and the upper of these is strongly influenced by fresh water derived from the river Etive catchment. A detailed account of the physical oceanography of Loch Etive can be found in Ridgeway and Price (1987) and Overnell *et al.* (2002).

The geology around the upper Loch Etive area (Figure 4.33) is dominated by the suite of Caledonian igneous intrusive rocks which have formed an elliptical composite pluton exhibiting three distinct phases of development (Anderson and Batchelor 1987, cited in BGS, 1995).

Within the lower region of Glen Etive the rocks consist largely of monzogranite of the Cruachan phase which becomes gradually more silica rich and finer in texture northwards where it grades into igneous material associated with the Glen Coe cauldron subsidence (Anderson, 1937). At the head of Loch, the geology is composed of rocks formed by the emplacement of the Starav granite intrusion and is considered to be the latest phase of plutonic intrusive activity associated with the suite of igneous emplacement in this area. The Starav Granite exhibits three distinct petrochemical zones which become more acidic towards the area occupied by the Central Starav Granite and typically contain medium-grained leucocratic monozgranite (Figure 4.33).

The geomorphology of the head of Loch Etive has been studied by Gray (1974a) who documents some of the key features which include the Falls of Lora at the entrance to Loch Etive situated at Connell (Figure 4.1). These reflect the presence of a shallow rock outcrop at the constricted entrance to the Loch which causes the flow of tidal rapids both in and out of the Loch during the flood and ebb tides.

Other morphological features include several raised shoreline fragments which are dispersed throughout the lower and middle Loch (as defined by Gray, 1974a) such as those at Inveresragan and Bonawe on the north shore and at Taynuilt on the south shore (Figure 4.33). At

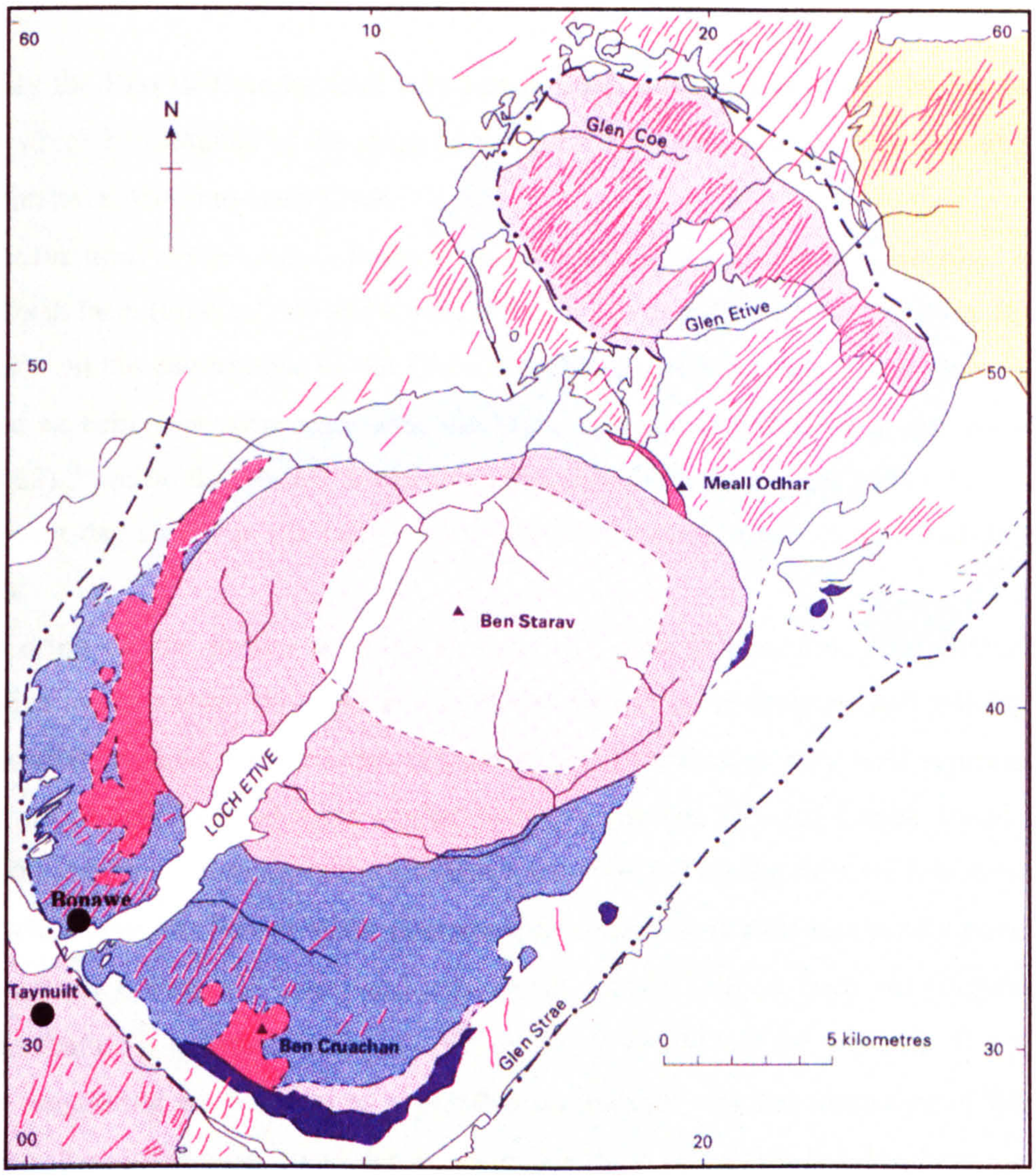

Figure 4.33: Simplified geology of the area around the Head of Loch Etive and Glen Coe showing the distribution of the Caledonian igneous magmatic intrusions. (Source: British Geological Survey; (After: Anderson, 1937 and Batchelor, 1987).

this locality the Pass of Brander fault cuts across Loch Etive and may well be the controlling influence which has resulted in the sharp northward trend of the fjord and the draining of Loch Awe via the river Awe into Loch Etive.

At the head of the Loch in lower Glen Etive a post glacial beach is described below the Druimachoish farm (Figure 4.34) and coring of this area supports this interpretation. Seaward of this location on the eastern side of the Glen, a visible strandline exists which Gray (1972) has interpreted as being commensurate with the Main Postglacial Shoreline at around 14 m OD (Figure 4.35). Beneath this feature and occupying a significant area of the valley floor land-ward of the present-day shoreline the same author describes a series river terraces and an historical floodplain.

Coring of this feature revealed an extensive area of peat formation extending from Kinlochetive to the present shoreline and in places distinct relict channels and salt-pan features now somewhat in-filled were evident (Figure 4.35). This feature may well represent a Late Holocene depositional environment similar to that witnessed at Loch Creran based upon the nature of the sediments corresponding to relative sea-level fall during the Late Holocene.

Delineating this feature at the contemporary shoreline is a distinct sandy/gravel bar that traverses around the central Loch-head into which a small cliff as been cut (Figures 4.34 & 4.35). This feature is approximately 0.4 – 0.5 metres in height and the presence of a significant strandline suggesting wave action as a possible mechanism for the formation of this feature. Draped over the cliffed terrace and deposited on the small beach that has developed seaward of the cliff, there are at least three distinct strandlines related to tidal heights associated with Highest Astronomical Tide and where erosion of the sand/gravel bar appears to be concentrated.

The contemporary salt-marsh development at the head of Loch Etive has taken place in two distinct areas to the west and the east of the point at which the River Etive reaches the estuary (Figure 4.34). The vegetation of these areas is dominated by *Puccinellia maritima* and *Armeria maritima* occupying the lower marsh and *Plantago maritima*, *Juncus gerard,* interspersed with *Argrostis stolonifera* within the higher marsh. Landward of the contemporary salt-marsh the vegetation grades into species typical of shallow, wet peaty soils including *Juncus acutiflorus*, *Sphagnun spp. Calluna vulgaris* and *Erica tetralix* (Figure 4.35)

Owing to the restricted overall size of these pocket–type marshes the gradation from lower to high marsh takes place over a short distance, in this case less than 8 m. Oblique field photographs acquired during field visits illustrate this zonation (Figure 4.35). Although air photographs of the head of Loch Etive have been acquired (Figure 4.34) these are unfortunately

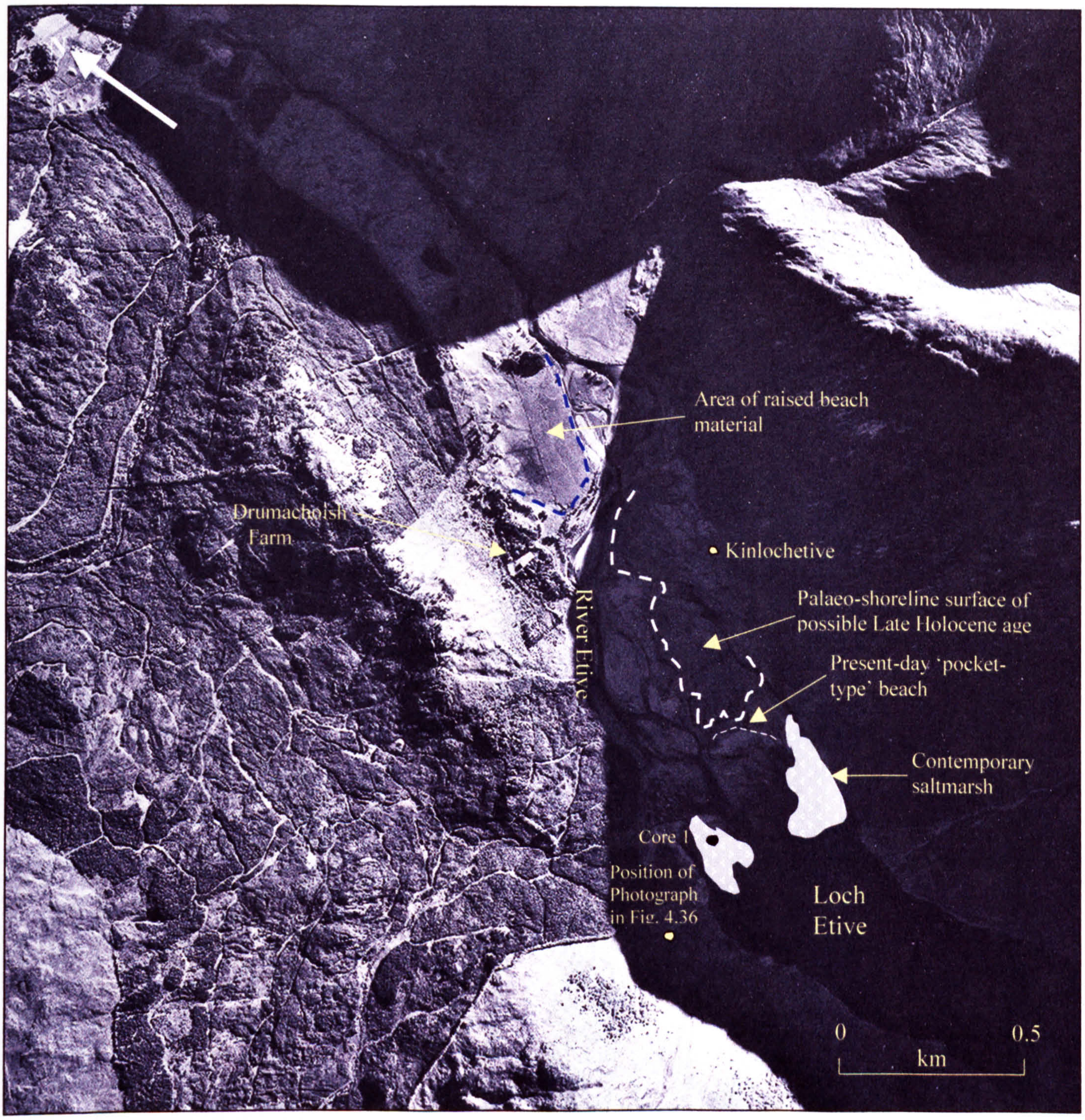

Figure 4.34: 1988 aerial photographic image of Head of Loch Etive and lower Glen Etive. The geomorphology of the inter-tidal area is shrouded in mountain shadow although the course of the River Etive is discernable and other locations within the Glen referred to in the text can be seen. The raised beach identified by Gray (1974) and the Late Holocene shoreline are bounded by the dashed blue and white lines respectively. Marsh morphology is shown in Figure 4.35 overleaf (Source: Royal Commission for Historical and Archaeological Monuments of Scotland, (RCHAMS), Edinburgh.

(A)

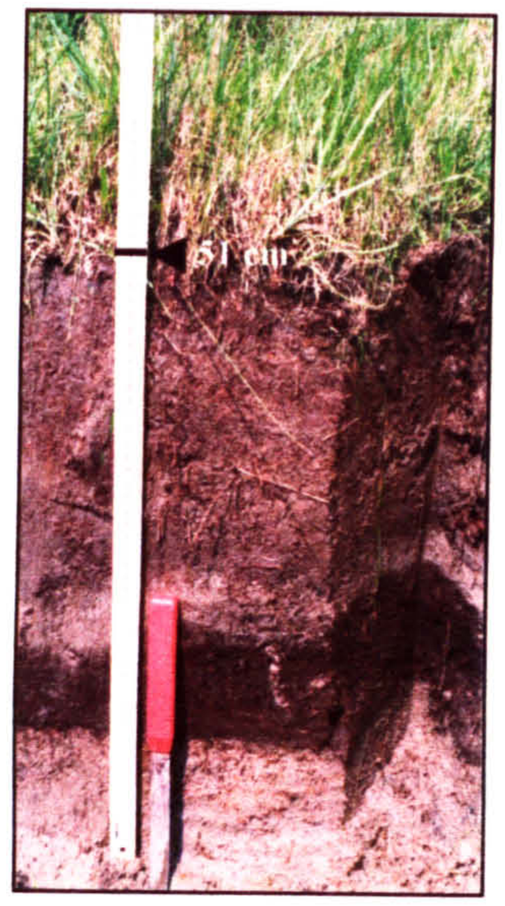

(B)

Figure 4.35: Overview of the pocket-type marsh at the Head of Loch Etive (looking due East) showing the general morphology of the upper estuary setting and core sampling locations in (A) and (B) the core profile extracted from site 1. Note the older Holocene surface occupying the central valley floor (line a – b) and the Main Late Glacial shoreline (depicted by the line c – d) after Gray (1972). The small beach and cliffed terrace is delineated by the blue dashed line.

shrouded in shadow resulting from the close proximity of large mountains such as Ben Starav immediately to the east. As a result these do not permit easy recognition of the geomorphology and plant zonation of the marshes. However, the field site photographs do provide some useful indications of marsh zonation (Figure 4.35) and field observations are shown annotated in Figure 4.34.

4.10.2: Core sedimentology

Two cores were extracted from the marsh situated on the northern side of Glen Etive and the locations of these sites are shown in Figure 4.35. A digital photograph of the core lithology taken under laboratory conditions is shown in Appendix 3.3. A detailed core log and sediment description of the Loch Etive core is presented in Figure 4.36.

The core consists of an upper lithological unit of brown-dark/brown silty clay peat with lenses of fine, medium and some coarse sand. Rootlets are present throughout this upper unit however the concentration visible decreases with depth down to 24cm. Some laminated structure has also developed in the lower section of this peat unit. Underlying this is a shallow sub-unit of light-brown/tan coloured fine to medium sand with occassional clasts of fine gravel material extending down-core from 24 cm to 29 cm. Lenses of organic-rich material are evident at the base of this sub-unit close to the quite sharp boundary with the underlying unit (Figure 4.36).

This represents a significant change in lithology and consists of a 12 cm depth interval of very dark-brown/black silty soil with fine to medium clasts of angular granite-type gravel. Preserved and fragmented rootlets are recorded in this sub-unit of the core but are not as prevalent as in the upper peat soil. The basal unit of the core consists of light-brown medium to coarse sand which has been deposited upon an underlying substrate of semi-rounded large cobble-sized material. This is comparable to the material currently seen in the fluvial deltaic deposits in the bed of the River Etive immediately beyond the area of marsh develoment (Figure 4.36).

4.10.3: Major element geochemistry

The major element geochemistry raw data is shown in Appendix 4.7 and the down-core profiles of major element abundance from this sequence are shown in Figure 4.37. These reveal

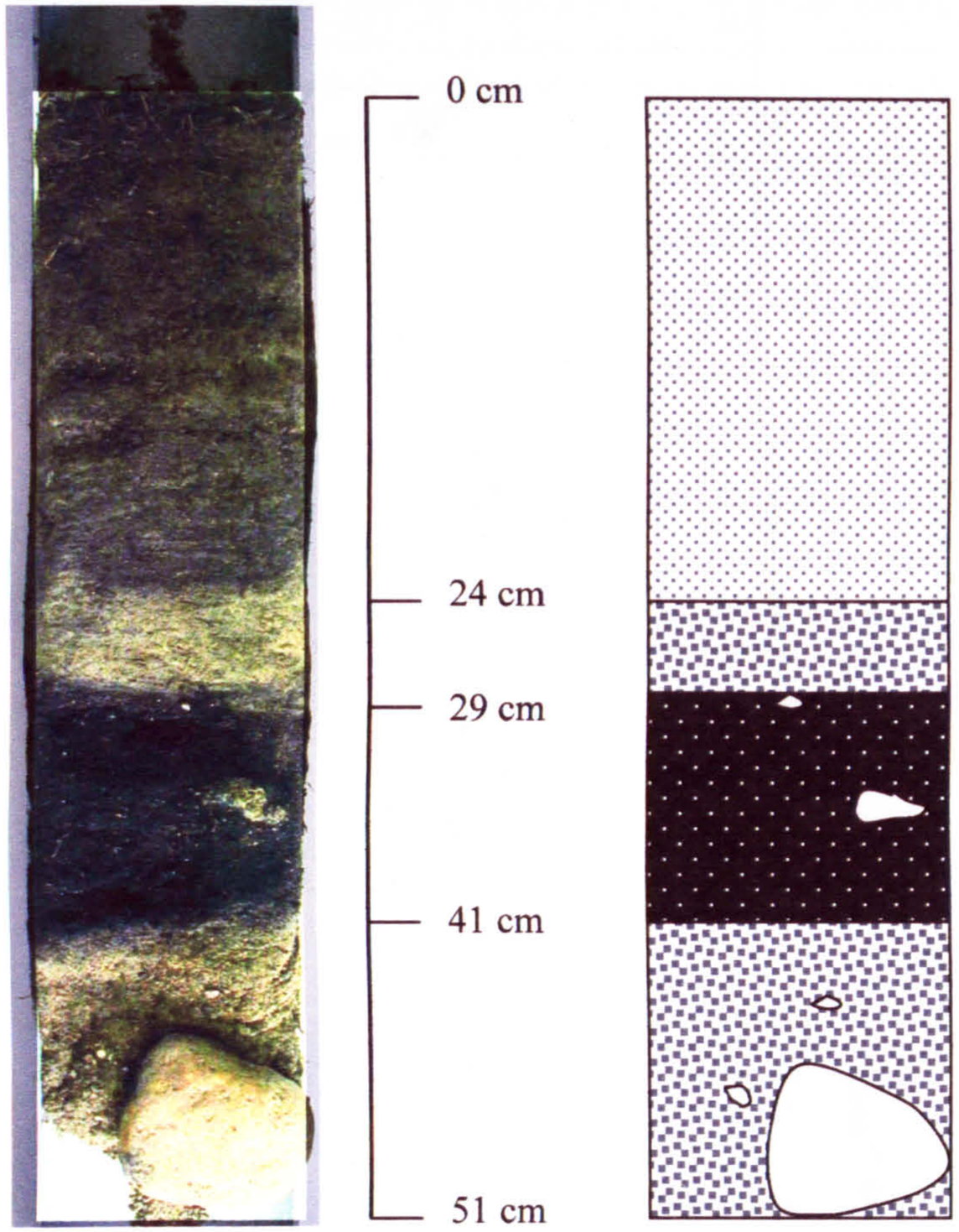

Sediment Description

Upper unit of brown to dark brown silty clay with lenses of fine to coarse sand which are more prevalent towards the base.

Organic-rich at the surface with the presence of rootlets (rhyzomes) evident, particularly within the upper 10-12 cm. The lower section of this upper unit also exhibits some weak laminated structure between 16-24 cm depth

Light brown/tan coloured underlying unit composed of predominately fine sand with occasional clasts of fine gravel. Fewer rootlets present with lenses of organic material evident at the base.

Very dark-brown/black undifferentiated silty sand containing coarse sand and fine to medium angular to sub-angular clasts of granite. Peaty material in the form of rootlets more evident than in the overlying sandy layer.

Lower light brown/tan coloured basal unit consisting of course sands and medium to course gravel. Large sub-angular to rounded cobble sized clasts at the base.

Figure 4.36: Sedimentary log and description of the marsh sequence from the Head of Loch Etive, mainland Argyll

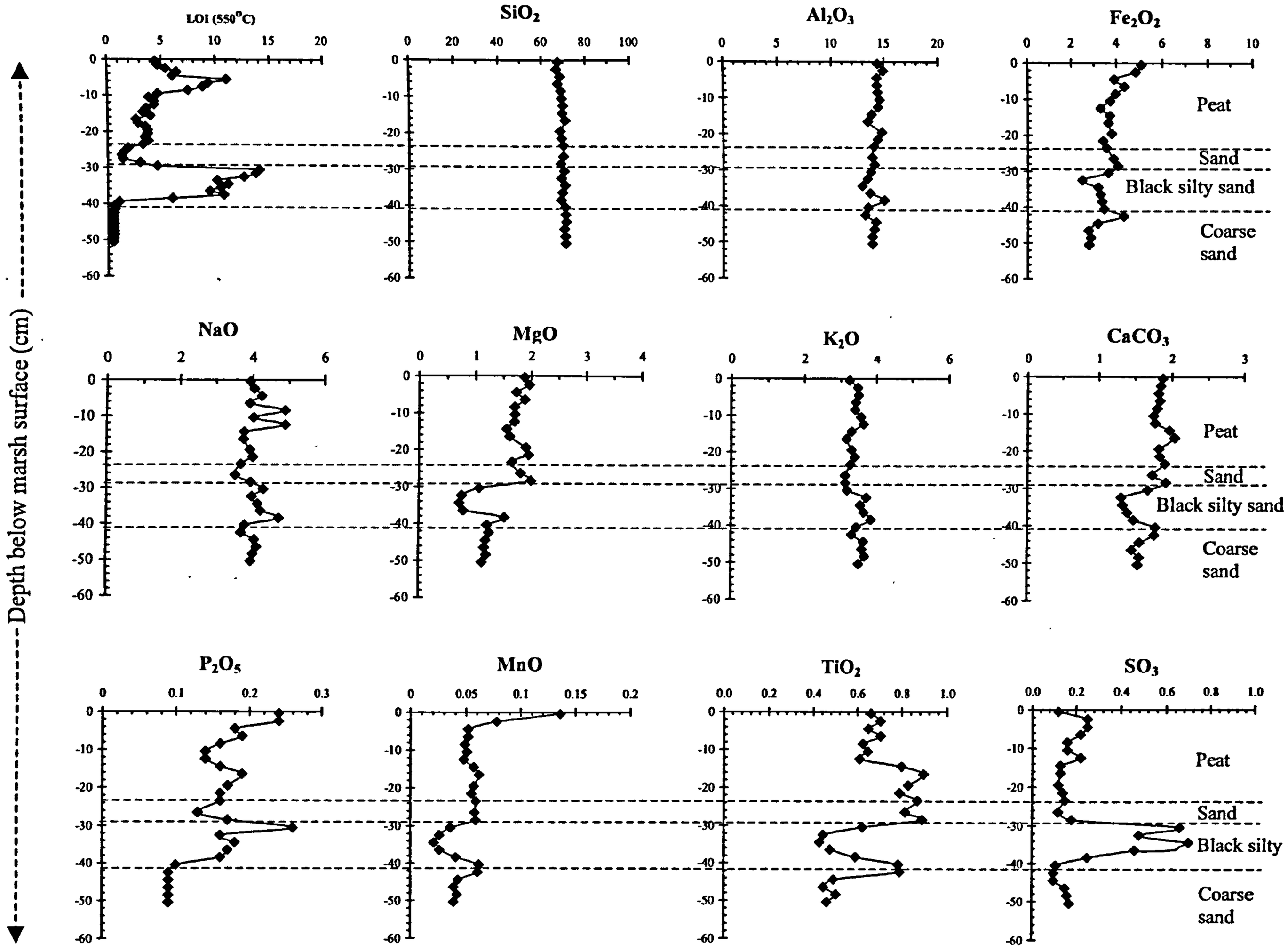

Figure 4.37: Loss on ignition (550°C) and major element geochemistry profiles for the core from the Head of Loch Etive, mainland Argyll. Element abundances are reported as oxides (wt %) in accordance with XRF convention.

a compositional variabilty in which major element changes in abundance correspond well with the distinct visual lithological changes evident in the core log.

Selected element abundance ratio plots normalized to Al are shown in Figure 4.38. The Si/Al ratio indicates a fairly constant level throughout fluctuating around 5 wt % with the exception of minor peaks at 13 cm and 34 cm which represent slight coarsening of material at these depths. The lowest value of 4.59 wt % occurs at a depth of 38 cm being recorded in the basal section of the more organic-rich sub-unit (Figure 4.36). The Ti/Al profile shows distinct variation throughout with levels of ~0.055 wt % down to a depth of 12 cm (Figure 4.38). Below this depth horizon a marked increase occurs extending down the profile to 29 cm with a maximum value of 0.066 wt % recorded at 16 cm. This variation in the Ti/Al ratio within the upper section of the core (down to 29 cm) is interpreted as being indicative of a coarser lower section which grades to a finer inorganic sediment within the uppermost 12 cm.

Below the 29 cm depth point, the Ti/Al ratio declines to a minimum value of 0.033 wt % within the dark organic rich sub-unit (29-40 cm) and is seen to increase to 0.060 wt % within the underlying sandy/fine gravel at the base of the core. Only slight variation recorded as a very small increase below 29 cm depth in the K/Al profile is apparent (0.28 wt%). Otherwise this profile indicates fairly constant supply of K relative to Al throughout the profile. The dry bulk density depth profile corresponds to heavier material within the coarse basal sediments. This decreases significantly within the dark-brown silty soil and increases once more throughout the overlying sand and the basal section of the uppermost peat soil. At a depth of 10-11 cm the dry bulk density reduces to values comparable to the buried silty soil horizon. Values increase once more in the near-surface to surface sediment layers and are comparable to the intermediate underlying fine/medium sand (Figure 4.38).

CaO as a proxy for $CaCO_3$ shows a gradual decline in levels down the core profile with a distinct reduction immediately below the 29 cm depth point (Figure 4.38). Significant production of authigenic carbonate would appear to not be taking place at depth within the core. This may be due initially to the lower levels recorded at this site which is located at the head of one of the longest and narrowest sea-lochs within Western Scotland with restricted access of coastal more saline/carbonate-rich water to the loch head. Additionally the lower sandy basal sediments present immediately above and below the organic-rich unit may not develop the alkalinity levels at which authegenic carbonate formation is favoured owing to maintenance of more acid pore waters throughout the core profile. As such the development of a distinct anoxic zone in this core is questionable. This is discussed in greater detail in Chapter Six of this thesis.

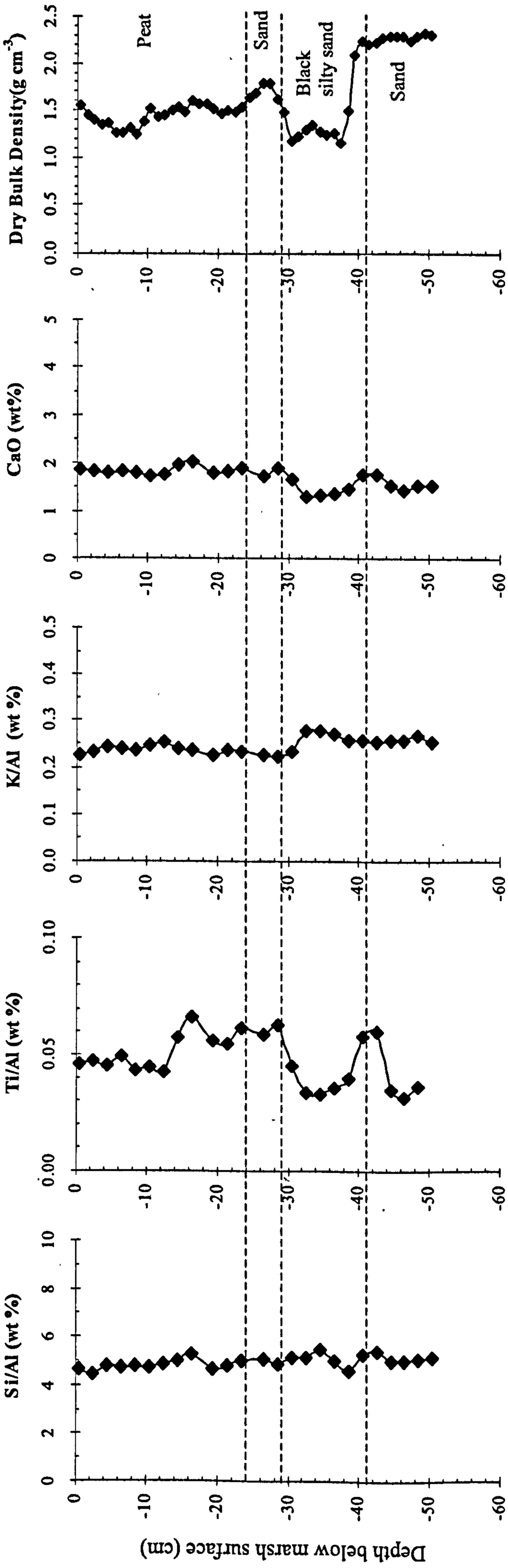

Figure 4.38: Al-normalised weight ratio plots for Si, Ti, and K, with the depth-profiles of Ca (wt %) and dry bulk density (g cm^{-3}) for the Loch Etive marsh core, mainland Argyll.

4.10.4: Detrital components and geochemical zonation

Detailed analysis of the major element abundance in the Loch Etive core was undertaken using the CONISS program. This revealed three distinct chemozones (Figure 4.39) and further sub-zones were also identified. LEt A1 corresponds to the coarse sand and gravel unit at the base of the core and is characterized by very low values for LOI and P. Fe, Mn, Ti and Ca all increase in an upward direction and small peaks in the abundance of these elements are evident in this zone close to the boundary with LEt B1. Highest values for Si are recorded in this zone. LEt B1 is a very distinct chemozone and corresponds well with the visual stratigraphy (Figure 4.39). This zone is characterized by a significant increase in LOI values. Similarly, P and S also show distinct enrichment with the profiles of Na, K and Al revealing less significant increases. Conversely, the profiles of Fe, Mg, Ca, Mn and Ti indicate depletion of these elements within LEt B1. Values for Si remain unvaried throughout these lowermost zones. Chemozone LEt C1 shows an initial reduction in LOI which then increases steadily towards the base of LEt C2. Similar profiles are evident for Fe, Mn, Ca and P with small peaks indicating enrichment of Fe, Mg, P and Mn and present in the base of chemozones LEt C1. Ti and Ca enrichment is apparent throughout zone LEt C. Chemozone LEt C2 shows a peak in LOI which declines towards the marsh surface. Al, Fe, Mg, Ca, P, Mn and S all show enrichment in the near surface or surface layers. Ti abundance is reduced and Si and K both show very slight decline in values over this depth increment (Figure 4.39).

4.10.5: Major element correlation with LOI and Ti

Correlation of the major element abundance with the distribution of LOI (Figure 4.40a, Figure 4.40b, and Figure 4.41) reveal both strong and weaker positive association between organic matter content and the elements SO_3, Na, P and K. This suggests these elements are associated with vegetal litter, various organic complexes and saline evapo-transpiration processes (Turner, 1999). A negative and quite uniform correlation exists between the detrital elements and LOI within this core which further suggests that organic accumulation has not been associated with variations in detrital input. Correlation with Ti (as proxy for detrital input) would seem to confirm this (Figure 4.41). Overall, the moderate negative correlation between Si, Ca,

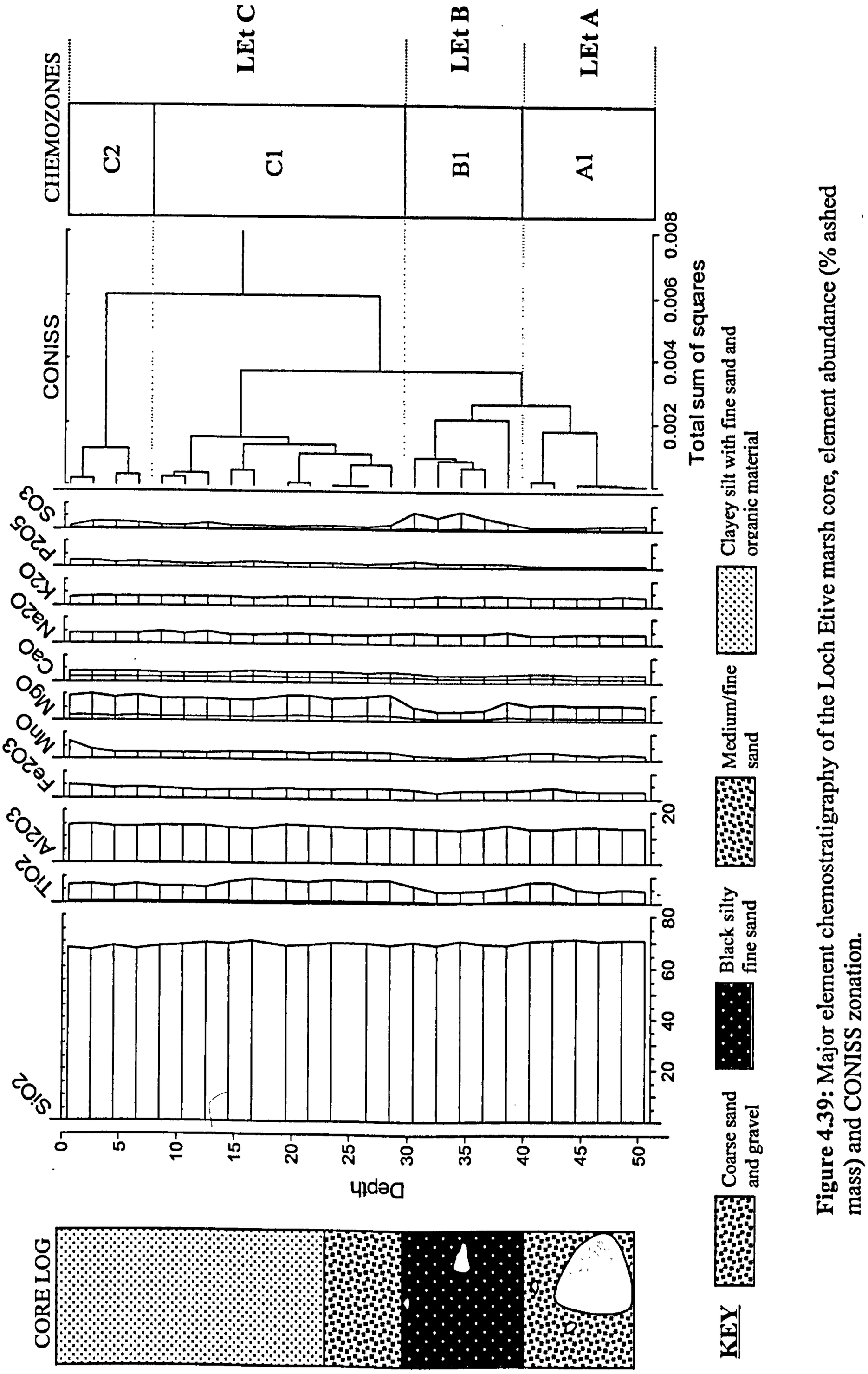

Figure 4.39: Major element chemostratigraphy of the Loch Etive marsh core, element abundance (% ash mass) and CONISS zonation.

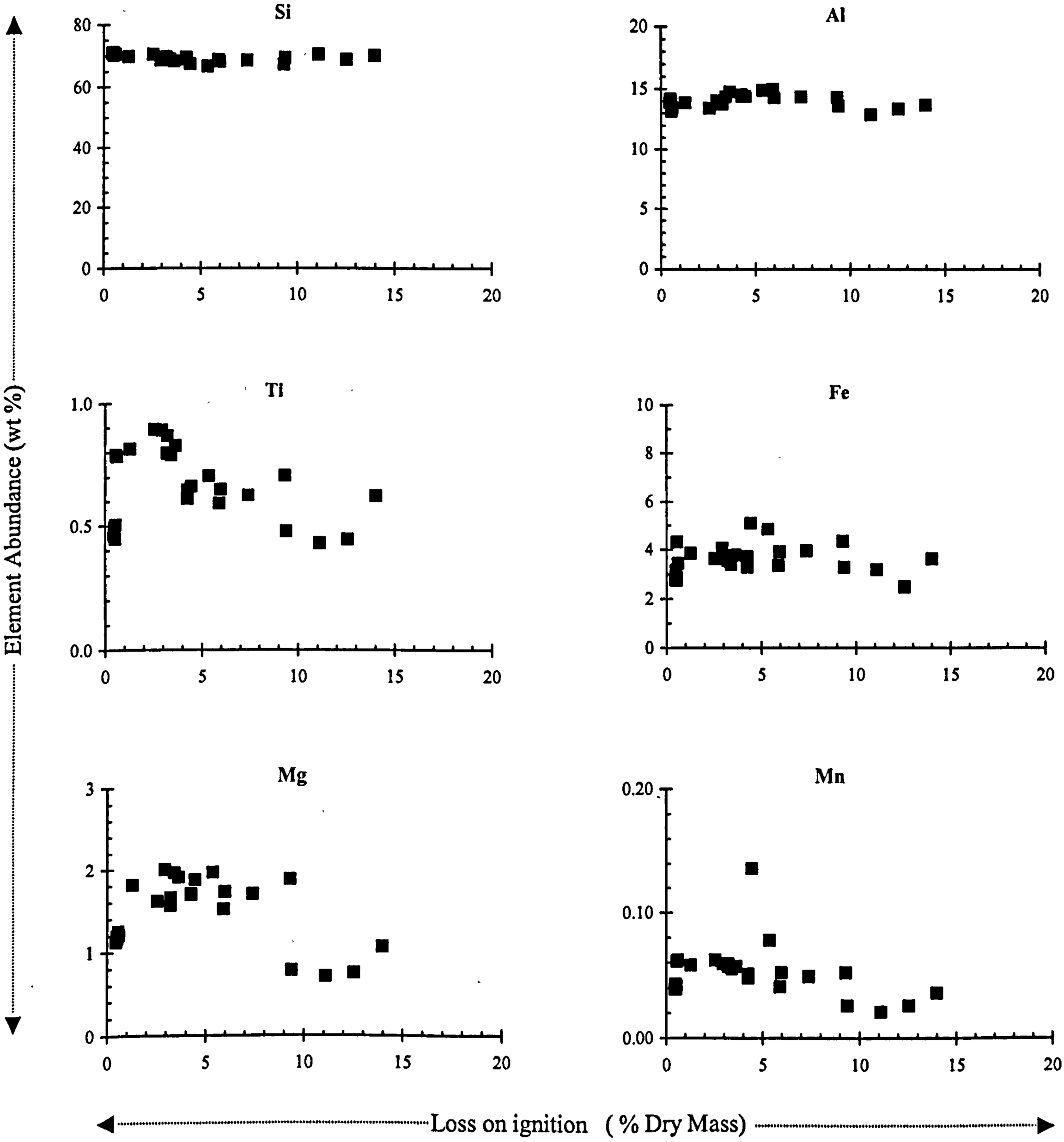

Figure 4.40a Major element abundance and Fe/Mn ratio vs. organic content (LOI 550^{o}C) from core 1, Loch Etive

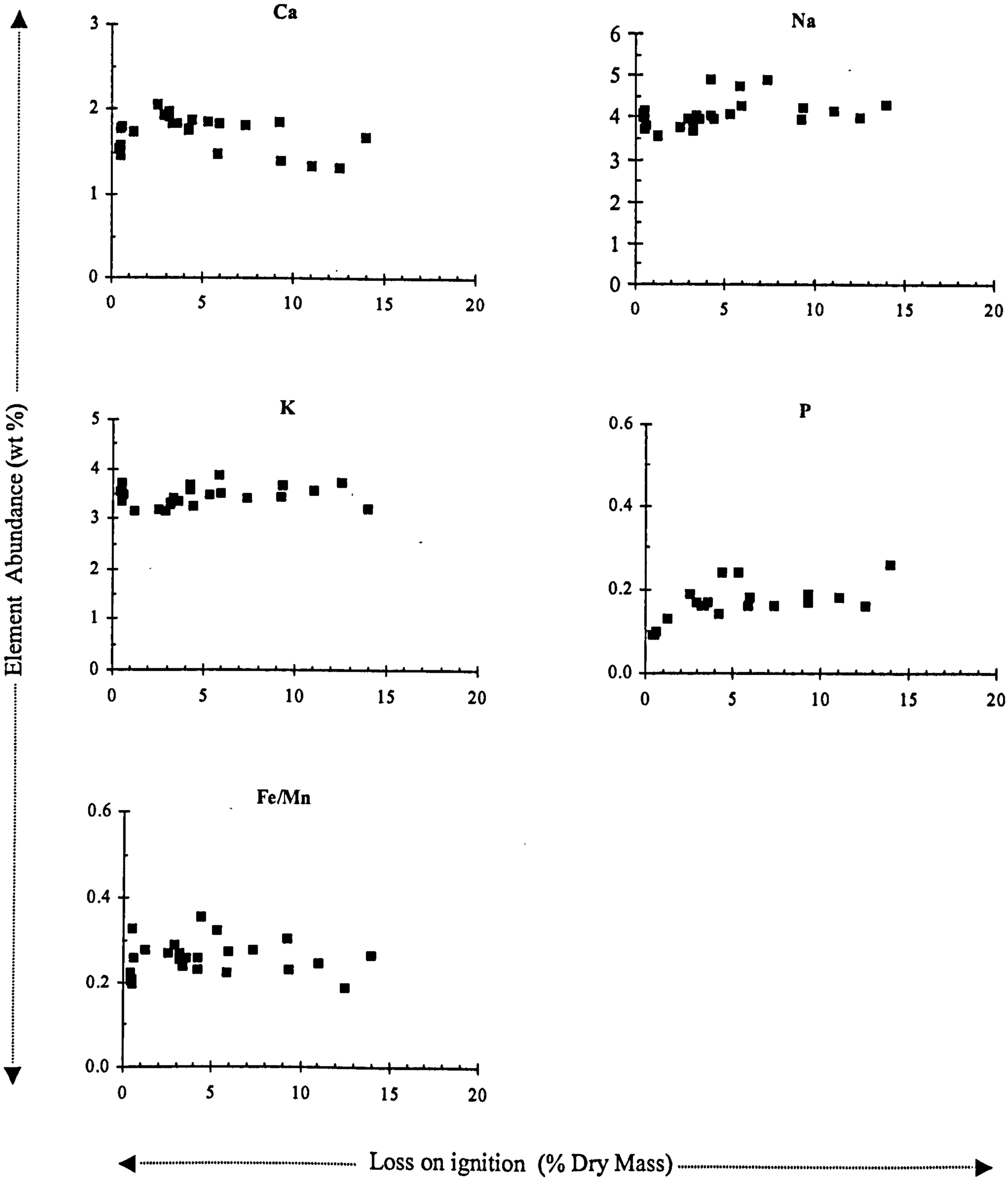

Figure 4.40b Major element abundance and Fe/Mn ratio vs. organic content (LOI 550^{o}C) from core 1, Loch Etive.

(a) Element	Core Average	(r) LOI
LOI	5.29	
SO_3	0.23	0.86
P_2O_5	0.16	0.67
Na_2O	4.06	0.36
K_2O	3.45	0.12
Al_2O_3	14.04	-0.11
MgO	1.48	-0.30
TiO_2	0.66	-0.32
MnO	0.05	-0.32
CaO	1.71	-0.32
SiO_2	69.42	-0.35

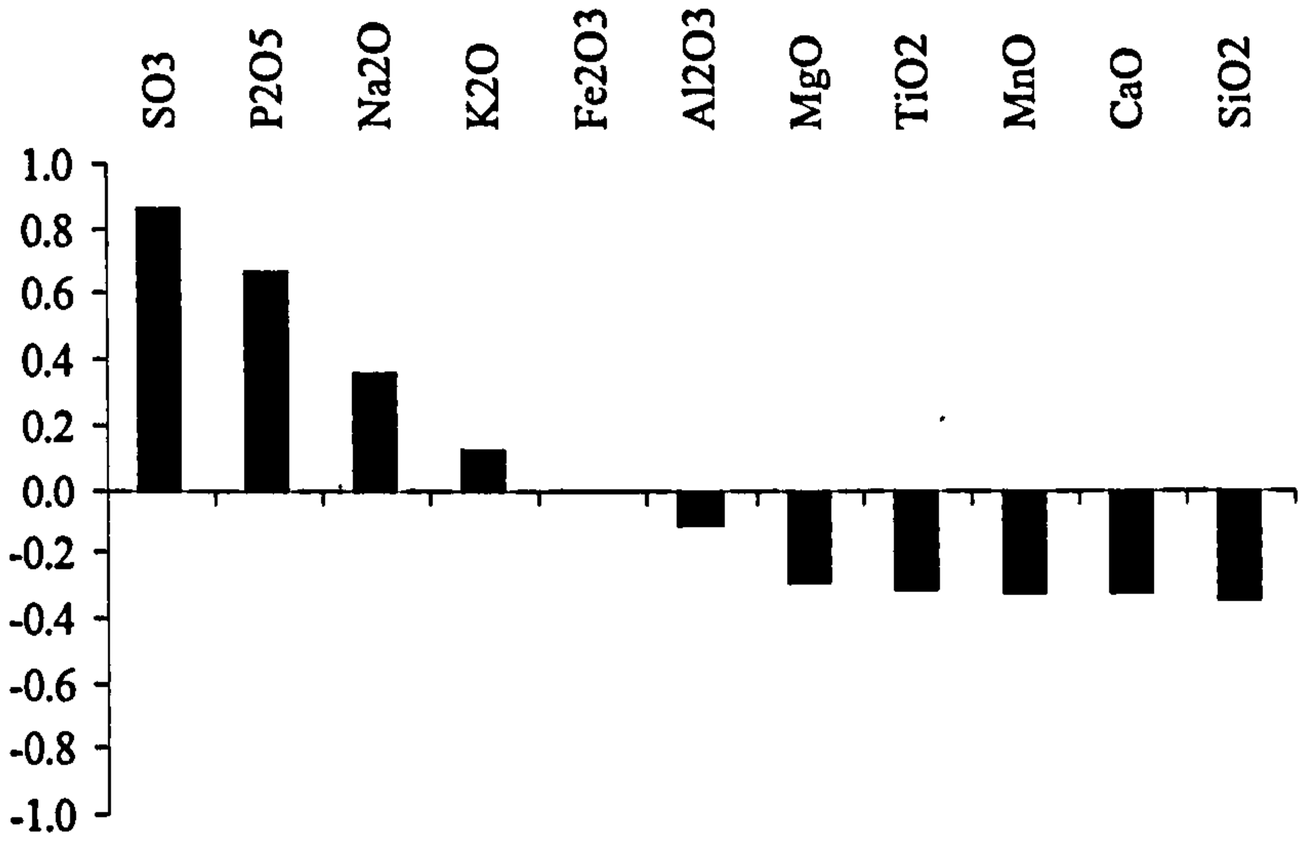

(b) Element	Core Average	(r) TiO_2
TiO_2	0.66	
CaO	1.71	0.88
MgO	1.48	0.71
Fe_2O_3	3.62	0.56
MnO	0.05	0.50
P_2O_5	0.16	0.21
Al_2O_3	14.04	0.12
SiO_2	69.42	-0.22
LOI	5.29	-0.32
Na_2O	4.06	-0.45
SO_3	0.23	-0.49
K_2O	3.45	-0.77

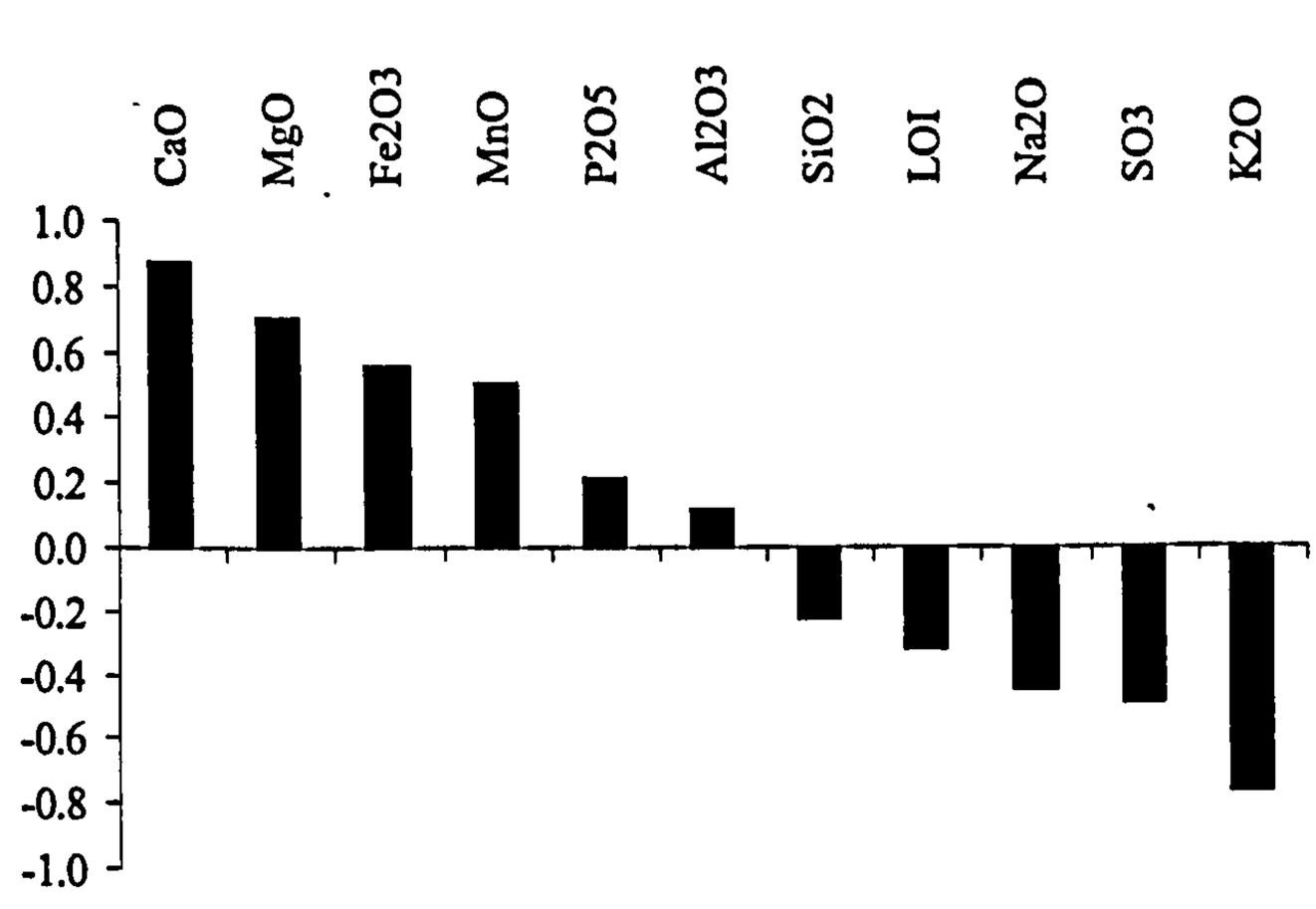

Figure 4.41: Core average major elemental abundances and correlation with; (a) LOI (550°C) and (b) TiO_2 (wt %) for the Loch Etive marsh core. Elements are ordered by correlation with LOI and TiO_2

Mn, Ti and Mg indicates that down-core variations appear to be largely due to fluctuations in sediment provenance rather than post-depositional associations of elements.

4.10.6: Trace element geochemistry

Trace element data from the Loch Etive marsh core is presented in Appendix 4.8 and the graphical down-core distributions are shown in Figure 4.42. Cluster anaylsis using the CONISS least squares regression component from TILIA (Grimm, 1991) reveals two distinct chemozones in close similarity with the dendogram derived for major elements (Figure 4.39). The first of these LEt A1 corresponds to the basal coarse sands and gravels and is characterized by low concentrations of the halides (e.g. Br, I, Cl and S). Other elements with low concentrations in this zone are As and Ni. Towards the top of this zone at a depth of 41 cm Y, Zr, Cr, V, Ce, Mn and Ti all show a pronounced peak indicative of enrichment elements associated with heavy mineral and coarse-grained material (Figure 4.42).

Chemozone LEt B1 corresponds to the dark-brown/black silty sand unit and is characterized by an obvious depletion of all trace elements apart from As, Br and S. Chemozone LEt C1 comprises two sub-zones and extends over the uppermost 30 cm of the core from the onset of the medium/fine sand to the top of the clayey silt with organic unit and the marsh surface. Zone LEt C1 reveals the recovery of all element concentrations to levels similar to those within the basal unit with generally increasing concentrations to the boundary with LEt C2. The exceptions to this trend are the concentration profiles for As, Br, and S which are depleted at the base of LEt C1. These elements follow A general pattern of enrichment within LEt C1.

The uppermost chemozone LEt C2 is characterized by enrichment of Pb, As, V, Mn, and the halides Br, I and Cl are relatively enriched throughout the upper 25 cm of the core with significant enrichment in the near-surface layers corresponding to chemozone LEt C2. Concentrations of S are relatively reduced within zone LEt C (Figure 4.42).

4.10.7: Isocon graphical plots for the Loch Etive sediments

The detrital minerals deposited in the marshes at the head of Loch Etive are derived from fluvial transport of weathered material from the Glen Etive catchment and subsequent re-working and re-distribution by wave and tidal energy. The visual log of this core coupled with a

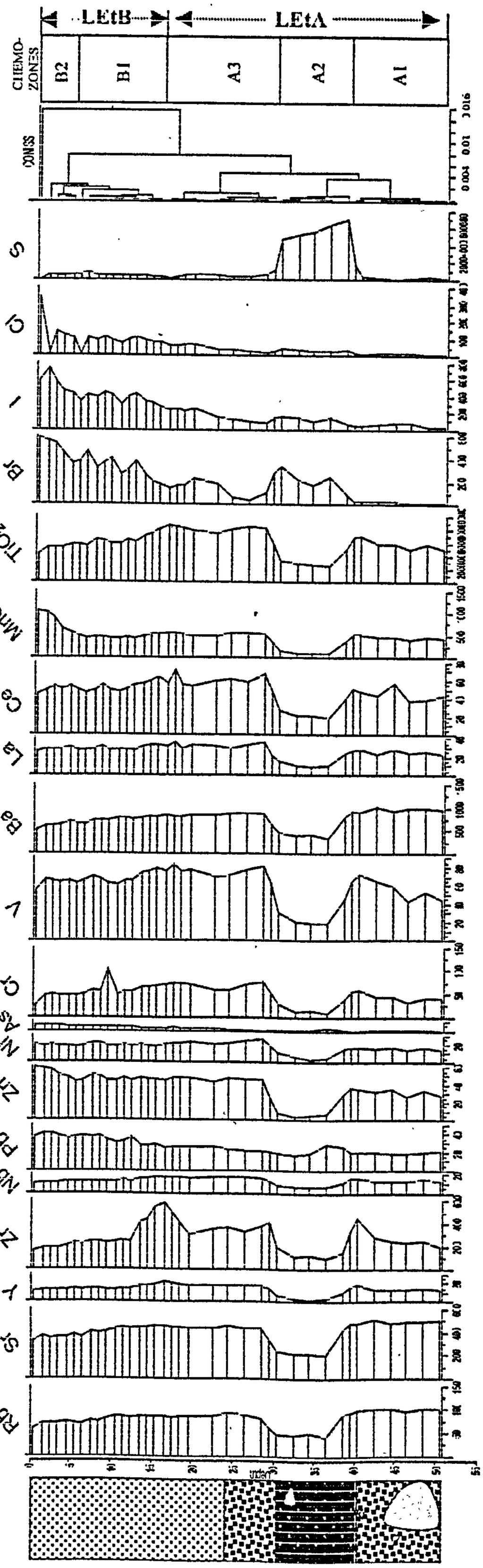

Figure 4.42: Trace element concentrations (ppm) for the Loch Etive marsh core (oven-dried pressed pellets)and CONISS zonation

preliminary inspection of the major and trace element geochemistry suggests a differing provenance and geochemical composition for dark-brown/black silty sand unit situated at 29-41 cm depth.

Variation in sedimentary element concentration between the different lithological units may be examined using the method of isocon plots (Grant, 1986; Cundy *et al.*, 1997). Geochemical data for the concentration in each lithological unit are averaged and then transformed using an arbitrary multiplication factor that allows each element from any two separate stratigraphic horizons to be plotted on the same pair of axes. Visual inspection of the graphs facilitates comparison of the average elemental composition between any two units. Elements that plot close to or on the line of equal concentration indicate the general similarity between sub-units being examined. Elements that plot above or below the line of equal concentration are indicative of element enrichment in the specific sub-stratigraphic units.

Comparison plots for the average elemental concentration of the various lithological units within the Loch Etive core are shown in Figure 4.43a and Figure 4.43b. Graph (a) in Figure 4.44a shows the comparison between the basal coarse sand/gravel unit and the overlying dark silty/sand. Most of the major elements plot on or near to the isocon line (SiO_2, Na_2O and P_2O_5 shown) indicating a general similarity in composition. However, the overlying dark silty/soil unit is clearly enriched with S (also as SO_3), I and Rb with elevated levels of As, Br, Cl, and Rb. Conversely the basal sand unit shows enrichment of several heavy metals including Ba, Ce, Cr, Mn, Ti, V and Zn.

Similarly, in plot b of the same figure the upper fine/medium sand unit is compared with the same underlying dark silty/sand. This also reveals some similarity between the major elements with SiO_2, Na_2O, K_2O and P_2O_5 all on or close to the isocon line. Dissimilarity is revealed with the lower silty/sand unit showing enrichment of S (also as SO_3), and to a lesser extent Br. The upper fine/medium sand unit is enriched in many other elements including CaO, Fe_2O_3, and MnO. Various other elements including the heavy metals Ba, Ce, Cr, Ni, Rb, Ti, V, Zn and Zr are also enriched within the upper sand indicating a distinct lithological difference between the two sub-units.

In Figure 4.43b, graph (a) illustrates the broad similarity between the basal sand and the upper sand unit of the core. Most elements plot on or close to the line with the exception of Iwhich shows significant enrichment relative to the lower basal sand unit. Some metals are also seen to be at elevated levels and these include Ce, Cr, Rb, Ti, V and Zn.

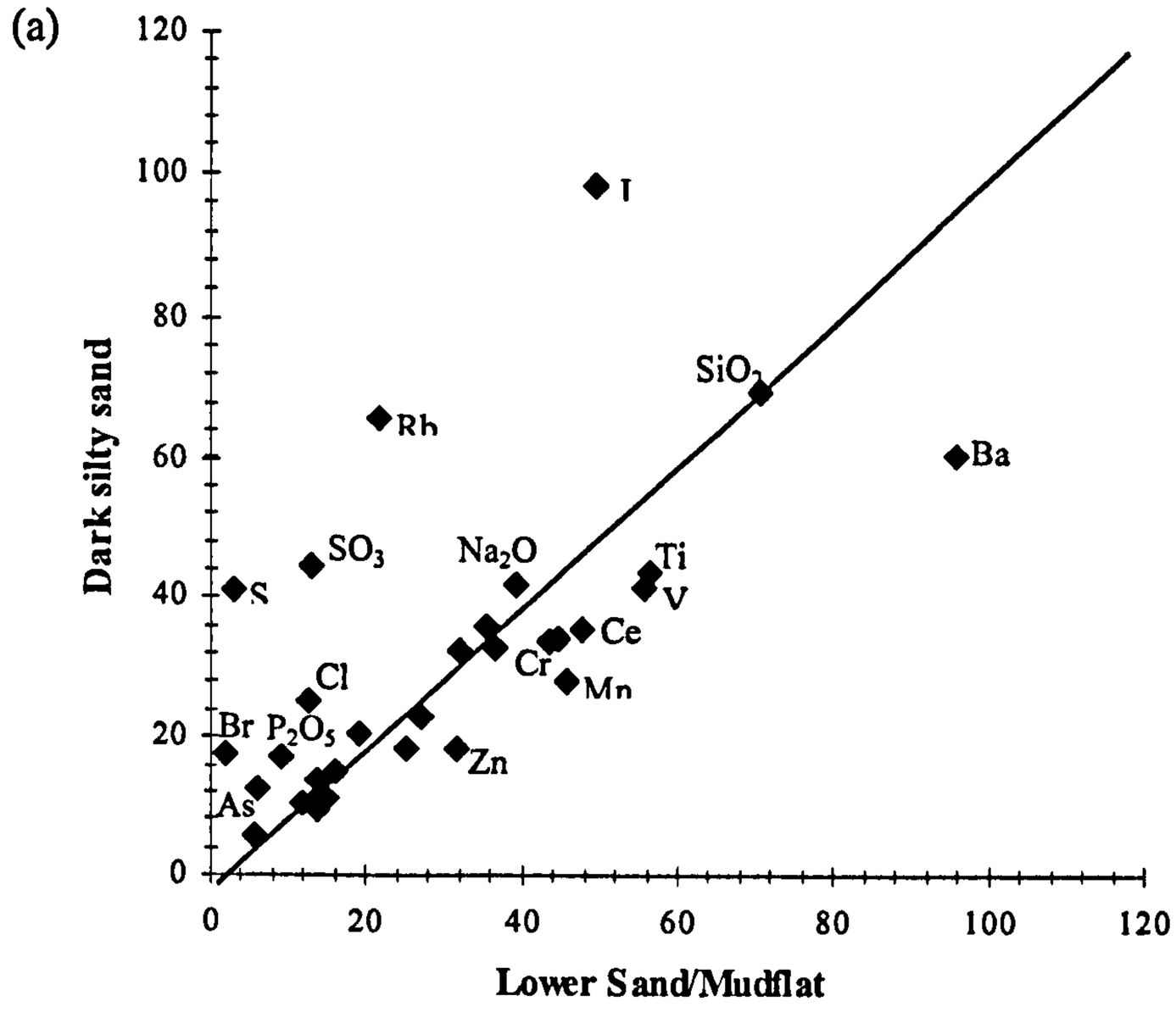

Upper Sand Unit

Figure 4.43 (a): Isocon diagrams for stratigraphical units within the Loch Etive marsh core after (Grant, 1986) and modified after (Cundy *et al.*, 1997). Individual points represent average element concentrations for the defined sedimentary units. These values are calculated by applying the following multiplication factor to ensure all element concentration values plot on the same scale. Major elements (wt %): SiO_2, 1; TiO_2, 10; Al_2O_3, 1; Fe_2O_3, 10; MnO, 100; MgO, 10; CaO, 10; Na_2O, 10; K_2O, 10; P_2O_5, 10; SO_3, 100. Trace elements (ppm): As, 10, Ba, 0.1; Br, 0.01; Ce, 1; Cl, 0.01; Cr, 1; Pb, 1; Ni, 1; S, 0.01; V, 1; Zn, 1. For legibility only elements indicating enrichment in any stratigraphical unit are shown.

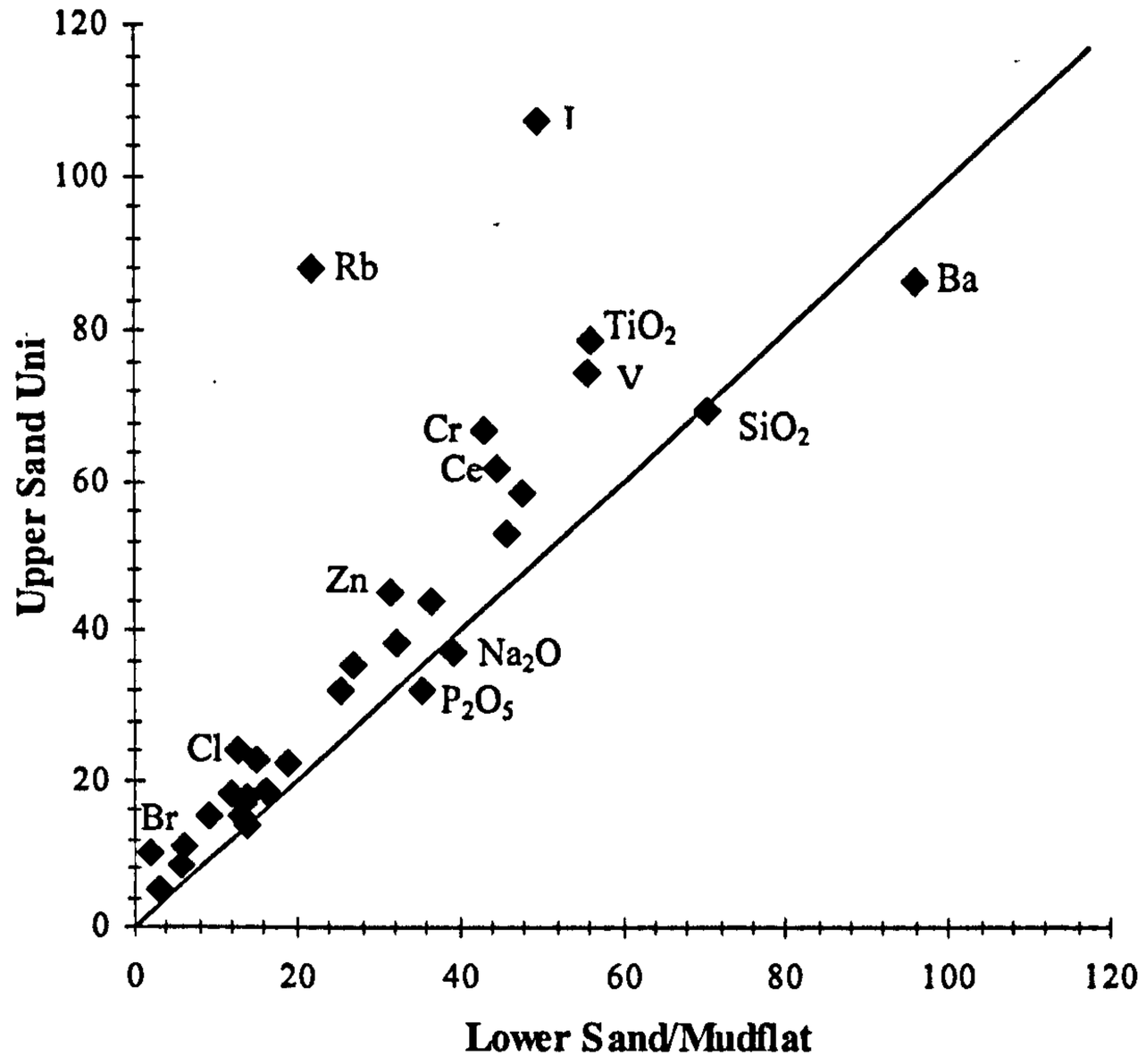

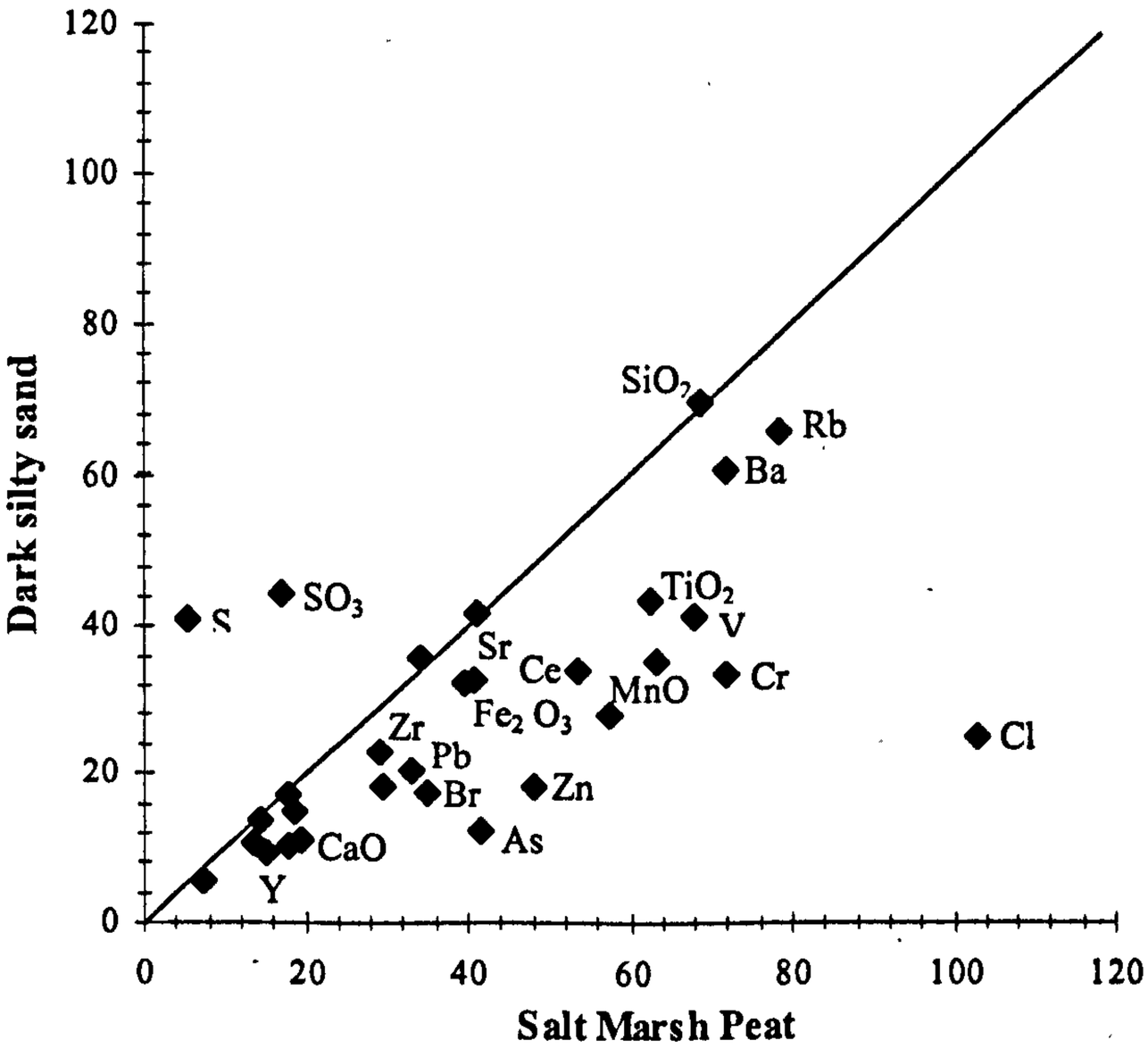

Figure 4.43(b): Isocon diagrams for stratigraphical units within the Loch Etive marsh core after (Grant, 1986) and modified after (Cundy *et al.*, 1997). Individual points represent average element concentrations for the defined sedimentary units. These values are calculated by applying the following multiplication factor to ensure all element concentration values plot on the same scale. Major elements (wt %): SiO_2, 1; TiO_2, 10; Al_2O_3, 1; Fe_2O_3, 10; MnO, 100; MgO, 10; CaO, 10; Na_2O, 10; K_2O, 10; P_2O_5, 10; SO_3, 100. Trace elements (ppm): As, 10, Ba, 0.1; Br, 0.01; Ce, 1; Cl, 0.01; Cr, 1; Pb, 1; Ni, 1; S, 0.01; V, 1; Zn, 1. For legibility only elements indicating enrichment in any stratigraphical unit are shown.

In the final plot graph (b) of the same figure the overlying organic clayey silt unit is compared to the dark silty/sand. Despite some elements plotting on or very close to the line of equal concentration (e.g. SiO_2), an obvious dissimilarity exists in terms of geochemical composition between the two sub-units with the silty black sand unit only showing enrichment of S (and SO_3). All other elements including trace metals and the halides (I and Br and Cl) are significantly enriched within the uppermost organic silty clay sediments (Figures 4.43a and 4.43b).

4.10.8: Microfossil Analysis of the Loch Etive core: Diatoms

The Loch Etive core represents a marsh sequence with distinct stratigraphical and compositional differences to the other three marsh cores investigated in this study. Major and trace element geochemistry suggests a different provenance for the silty dark brown/black sub-unit situated between 29-41 cm below the marsh surface (Figure 4.37 & Figure 4.39). The nature of this sub-unit is of interest in terms of the depositional history of this core. As a result, bio-stratigraphic (diatom) analysis was considered to offer potential in terms of gaining further information insight regarding the historical development of the sequence from the Head of Loch Etive and in particular the provenance of the distinctive organic-rich sub-unit.

Sample preparation followed the general overview presented in Chapter three and a full description of the microscope slide preparation can be found in Appendix 1, based upon well established techniques to produce high quality microscope slides for the counting procedure (Battarbee, 1986).

The diatom assemblage data in relation to core lithology is presented in Figure 4.44. The selected taxa shown are expressed as percentage total diatom valves with counts of ~ 300 valves for each depth increment analysed. Where species have been counted which amount to low percentage total values these have been amalgamated to provide an 'others' column for the various halobian groups identified in the classification of Vos and DeWolf (1993).

Diatom taxa within the entire core are totally dominated by pennate forms with only one centric individual marine planktonic species (*Paralia Sulcata*) identified at a depth of 20-21 cm. No other centric species have been recorded in this analysis.

The lowermost unit of coarse sand and gravels (diatom zone LEt A1D) contains taxa derived from polyhalobian, mesohalobian and oligohalobian ecological groups. Polyhalobous

taxa include the cosmopolitan marine species *Navicula directa* and *Cocconeis scutellum.* Mesohalobian taxa include the benthic epipsammic species *Acnanthes delicatula*, *Diploneis incurvata, Diploneis interrupta, Diploneis smithii, Fragillaria puchella* var. *pulchella, Mastogolia pulmilla, Navicula bipustulata, Navicula menisculus, Navicula peregrina, Opephora minuta, Pinularia baltica* var. *lundii,* and *Planothidium delicatulum.* Oligohalobous taxa within this zone include *Caloneis alpesti*, *Cymbella helvetica*, *Pinnularia microstauron, Eunotia fallax, Frustulia rhomboides, Navicula radiosa* and a significant percentage (~20 % total) of the freshwater taxa *Tabellaria flocculosa.* The presence of representative taxa from the three major ecological groups is summarized in the summation columns to the right-hand side of the diagram (Figure 4.44).

The diatom zone LEt A2D immediately above the basal unit corresponds well with the visual stratigraphy and represents the sub-unit of dark-brown/black silty sand at a depth of 29-41 cm. (Figure 4.44) This zone contrasts markedly with the basal zone being dominated by oligohalobous taxa. These include the continued presence of *Cymbella helvetica, Eunotia fallax, Navicula radiosa, Pinnularia microstauron* and *Tabellaria flocculosa.* Other oligohalobous taxa identified within this zone are those of *Eunotia arcus*, *Eunotia pectinalis* var. *minor* and the large freshwater pennate species *Pinnualria lata. Fragillaria contruens*, *Mastogolia smithii*, *Navicula opugnata* and *Suriella bifrons* are also recorded in the upper section of this diatom zone. *Pinnularia lundii* var. *baltica* and *Acnanthes delicatula* are the principal mesohalobous species recorded in this zone albeit at low percentage total diatom valves. The latter species declines quite rapidly in an up-core direction and is not recorded in the mid to upper section of LEt A2D. A similar low percentage is also evident for the two species of polyhalobous taxa *Cocconeis scutellum* and *Navicula directa* which are also seen to decline rapidly with increased elevation within this distinct stratigraphical sub-unit.

An important point of necessary inclusion here is the significant amount of breakage and fragmentation of large pennate forms in particular, species of *Nitszchia*, *Pinnularia* and *Synedra.* This resulted in very low total counts of diatom valves within the depth increment between 33-34 cm and other depth increments within this sub-unit relative to the over and underlying lithology.

The transition between diatom zone LEt A2D and LEt A3D corresponds well with the visual stratigraphy (Figure 4.37), which shows the change in core lithology from the dark-brown/black silty sand to a unit of light-brown fine to medium sand with some evident inclusion of organic-rich lenses. In diatom zone LEt A3D a rapid decline in all oligohalobous taxa is

evident with a concomitant rise in the percentage total of mesohalobous species. This is also accompanied by a very slight percentage increase in polyhalobous taxa. The principal mesohalobous taxa present within this zone include an increasing total percentage of *Caloneis aemula, Fragilaria vaucheriae, Navicula digitoradiata, Navicula perigrina, Navicula phylleptosoma, Nitszchia sigma, Pinnularia lundii* var. *baltica, Suriella patella* and *Taballaria investians*. The polyhalobian species *Navicula radiostriata* is recorded within this unit and is noticeable by its absence in the underlying basal coarse sand and in the overlying organic-rich silty clay which extends to the marsh surface (Figure 4.44).

Diatom zone LEt A3D also corresponds well with the stratigraphy of the Loch Etive core and represents the transition from fine/medium sand into the more organic-rich silty clay in the upper 24 cm of the core This zone is characterized by the continuing decline of oligohalobian species and increase of mesohalobous taxa in particular *Caloneis aemula, Fragillaria pulchella* var. *pulchella, Mastogolia lanceolata, Navicula gregaria* and *Nitzschia sigma.* Polyhalobous taxa here include *Cocconeis scutellum* var. *parva*, low percentages of the species *Navicula marina* and *Opephora marina*.

Zone LEt A3D continues to be characterized by low percentage totals of all oligohalobous taxa with *Eunotia fallax, Mastogolia smithii, Navicula radiosa* and *Tabellaria floculosa* providing a continuing and slightly variable background concentration of freshwater species. Mesohalobous taxa include elevated counts of *Acnanthes delicatula*, with the continued presence of *Caloneis aemula*, *Diploneis smithii*, *Fragillaria pulchella* var. *pulchella*, reducing percentages of *Navucula diditoradiata, Navicula gregaria, Nitzschia sigma* and *Pinnularia lundii* var. *baltica*. Other mesohalobians are recorded at this elevation and increase within this zone including *Pinnularia quadraterea* var. *cuneata, Pinnularia aestuarii* and *Rhopaloidia rupestri*. Polyhalobian species are also recorded in low percentage values but include the continued presence of *Cocconeis scutellum* and the replacement of *Navicula radiostriata* with low counts of *Navicula vara* (Figure 4.44).

At this elevation corresponding to a depth of aproximately 14-15 cm below the marsh surface the CONISS cluster analysis identifies the onset of the diatom zone LEt BD. Within this zone two sub-zones are identified between this depth and the marsh surface (Figure 4.44). The first of these LEt BD1 is characterized by low total percentages of polyhalobous and oligohalobous taxa. Mesohalobous taxa dominate this zone and still include *Caloneis aemula, Diploneis smithii* and *Mastogolia lanceolata.* A reduction and increase in the percentage totals of the species *Pinnularia quadraterea var. cuneata*, *Pinnularia aestuarii* and *Rhopaloidia rupestri*

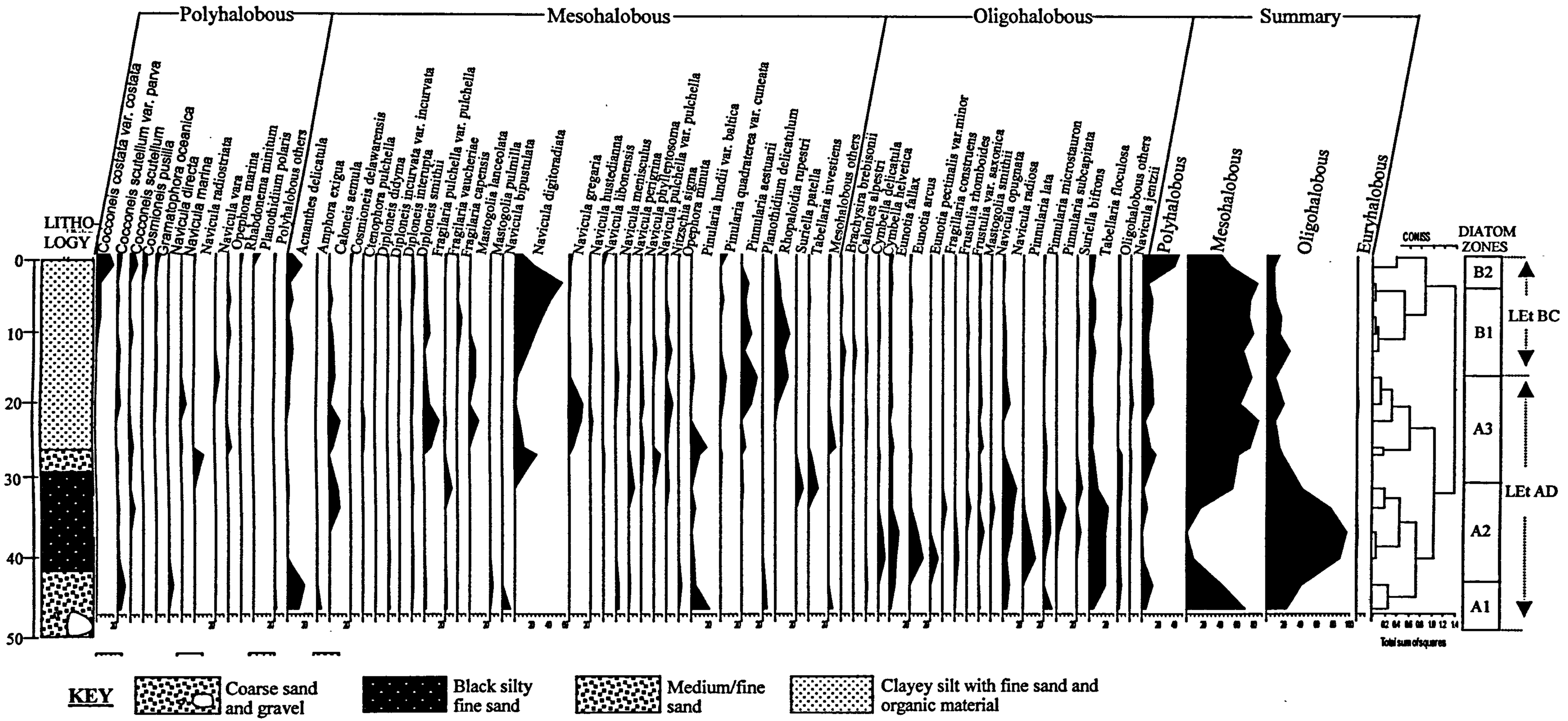

Figure 4.44: Diatom assemblages from the Loch Etive marsh core. Selected taxa are shown as percentage total diatoms counted and those taxa with low percentage values have been grouped to form an additional summary for the specific ecological groups.

is accompanied by a significant increase in the counts of *Navicula digitoradiata.* The base of this zone sees the first introduction of the polyhalobian species *Cocconeis costata var.costata. Cocconeis scutellum* var. *parva* is still evident at this elevation with low total counts of *Opephora marina* (Figure 4.44).

The upper section of zone LEt B1D continues to be dominated by mesohalobous taxa. In particular a significant increase in the total percentage of the species *Navicula digitoradiata* (to > 50% total diatom valves) represents a striking feature of the diatom distribution within the near-surface sediments. *Acnanthes delicatula*, *Pinnularia aestuarii* and *Rhopaloidia rupestri* also contribute to the total percentage of mesohalobous species present. *Navicula digitoradiata* is commonly found inhabiting tidal sandflats being a predominately epipsammic species. The sandy nature of the coastal peat in this core therefore provides a suitable substrate for this species to exist higher within the inter-tidal prism.

In the near-surface layers diatom zone LEt B2D indicates a fall in the total percentage of mesohalobous taxa. This is accompanied by a concomitant increase in polyhalobian species within the near-surface sediments which is mirrored by the trace element profiles for I and Br (Figure 4.42) indicating the greater influence of sea-water and hence increased salinity. Increased counts of *Cocconeis costata* var. *costata*, *Cocconeis scutellum, Cocconeis scutellum* var. *parva* and *Gramatophora oceanica* are accompanied by the presence of other polyalobian species including *Cosmioneis pusilla, Planothidium polaris* and *Rhabdonema minitum.* The mesohalobous taxa show a decline in total percentages of *Acnanthes delicatula* and the previously prevalent *Navicula digitoradiata. Diploneis smithii, Pinnularia aestuarii* and *Rhopaloidia rupestri* also decline and are replaced by the presence of *Cosmioneis delawarensis, Navicula libonensis, Navicula peregrina, Nitzschia sigma* and *Pinnularia quadraterea* var. *cuneata.* Small increases in the percentage totals of the species *Eunotia fallax* and *Tabellaria floculosa* contribute to the slight increase in oligohalobous taxa within this upper section of the marsh. However, these are still at percentages representing a background input of freshwater species (Figure 4.44).

A full discussion of the microfossil data presented here is integrated with further results and is fully discussed in Chapter Eight of this thesis.

4.11: Summary of Chapter Four

A detailed overview of the site selection and subsequent core acquisition process has been presented. Major element geochemistry has been determined from XRF spectrometry analysis of fused glass beads with trace element data being obtained from pressed powder pellets. These data, in conjunction with LOI, are utilized to assess the compositional variability and chemical associations of the major components of the marsh sequences from the Argyll region.

The core from the head of Loch Etive displays quite obvious stratigraphic differences in comparison to the other three cores investigated in this study. Loss on ignition, dry bulk density and major element geochemical data suggest a varied provenance and interaction with coastal processes for the overall development of this sedimentary sequence. This is confirmed by the use of microfossil (diatom) analysis of the core, which reveals both distinct and more subtle environmental changes which have occurred during the historical and recent development of the sediment prism from this site. The addition of diatom analysis as part of a multi proxy approach undertaken at this site supports the geochemical investigations undertaken on the other three marsh cores.

A full analysis and discussion of the data presented here is undertaken in Chapter Eight.

The following chapter now focuses upon the geochronological development of the marsh cores from Argyll modeled through the application of the various radiometric dating techniques outlined in Chapter Three.

Chapter Five

THE GEOCHRONOLOGY OF THE ARGYLL SALTMARSHES

5.1 Introduction:

The ^{210}Pb dating method has received much attention over recent decades and has been widly used to successfully date salt marsh sediments from a variety of locations (Armentano and Woodwell, 1975; Goldberg *et al.*, 1963; McCaffrey and Thompson 1980; Church *et al.*, 1981; Chanton *et al.*, 1983; Beninger and Chanton, 1985; Kirchner and Ehlers, 1998; Cundy *et al.*, 1998; 2002; 2003). In many of these studies the use of ^{137}Cs has been effective in fulfilling the requirement for an independent dating technique to assess the reliability of the ^{210}Pb method as proposed by Anderson *et al.*, (1987) and Allen *et al.*, (1993).

Accurate determination of the natural (^{210}Pb) and artificial (^{137}Cs and ^{241}Am) radionuclide activities provide a chronological framework for the reconstruction and estimation of the recent (120-150 years maximum.) depositional history of the Argyll marsh cores investigated in the present study. Activity depth profiles for the above isotopes were determined via the alpha and gamma spectrometry techniques outlined in detail in Chapter Three.

5.2: ^{210}Pb dating: use of the CF:CS or 'Simple Model'.

Constant atmospheric deposition provides the basic assumption employed in the calculation of sediment age using the ^{210}Pb method. This hinges upon the known decay constant of the ^{210}Pb radioisotope. Sediment age is calculated from the equation:

$$t = \lambda^{-1} \, \mathrm{Ln} \, (Az / A_0)$$

where: t = age at depth z;

A_0 = the ^{210}Pb activity at the marsh surface

Az = the activity of ^{210}Pb at depth z

and λ = the radioactive decay constant of ^{210}Pb (0.03114 Bq yr^{-1})

Age determination using this equation constitutes the 'simple model' outlined in Appleby and Oldfield (1992) and Appleby (2001), and provides an estimate of average sediment accumulation rates for the entire marsh core sequence. This is obtained from the least squares regression of the plot of the natural logarithm of $^{210}Pb_{excess}$ versus depth.

Calculated activity values from the raw data for the four cores analysed are shown in the spreadsheets contained in Appendix 5. Determination of the background or unsupported ^{210}Pb used in further calculations follows the procedure outlined in Chapter three and is indicated in the appropriate total activty/depth profiles presented in this chapter .

5.3: Other ^{210}Pb dating models

As contemporary depositional systems develop they typically contain depth horizons which represent periods of fluctuating sediment accumulation through time. Variable sedimentation rates identified within sediment sequences will compromise the validity of the Constant Flux: Constant Sedimentation (CF:CS) or 'Simple model' (A.B.Cundy, personal communication; Sratton-Noller, 2000; see Chapter Three). As a consequence of this the (CF:CS) model is now rarely used to assess sedimentation rates within modern estuarine systems. The similarity of the Constant Initial Concentration (CIC) model with the CF:CS model (chapter three) results in the use of this model being restricted to sedimentary environments where there is negligible change through time with respect to sediment accumulation rates. Implicit in the CIC model is the assumption that ^{210}Pb is derived predominately on labelled particles deposited on the marsh surface. For the CIC model the calculation of sediment age uses the equation:

$$\textbf{Age at depth (z)} = \textbf{(1 / } \lambda \textbf{) x Ln (}^{210}\textbf{Pb activity at depth / }^{210}\textbf{Pb}_{\textbf{excess}}\textbf{ surface activity)}$$

Where: λ = the radioactive decay constant of ^{210}Pb (0.03114 Bq yr^{-1})

Ln = the natural logarithm.

More common-place within estuarine settings is the application of the Constant Rate of Supply (CRS) or Constant Flux model. The key assumption with this model is that the ^{210}Pb arriving on the marsh surface is dominated by atmospheric inputs. For mature marsh environments this assumption has been shown to provide a robust and effective method for the accurate determination of sediment chronologies where conditions of varying sediment accretion have occurred (e.g. Appleby and Oldfield, 1978; McCaffrey and Thompson, 1980; Wise, 1980; Cundy and Croudace, 1994; Cundy and Croudace, 1996).

The CRS model seeks to determine the age of any given depth increment within the down-core sediment sequence via the determination of the inventory of ^{210}Pb within the

sediment column (Appleby and Oldfield, 1992; Oldfield, 2001). The CRS equation takes the form of:

$$\textbf{Age at depth (z)} = (1/\lambda) \times \frac{\textbf{Ln (}^{210}\textbf{Pb unsupported inventory below depth z)}}{\textbf{(}^{210}\textbf{Pb unsupported inventory of entire core)}}$$

Where: λ and Ln are the same as for CIC model equation.

Sediment chronologies have been determined from both the CIC and CRS models and the results from these calculations are presented in later sections of this chapter in tandem with the use of the artificial radionuclide methods which are now discussed. All calculation spreadsheets are shown in Appendix 5.

5.4: ^{137}Cs and ^{241}Am

Calculation of sediment accretion and mass accumulation rates have been determined from detectable peaks in sub-surface activity related to known specific periods of peak input to depositional systems. These can then be used as distinct marker horizons and provide and independent test of the ^{210}Pb method. In the case of ^{137}Cs these relate specifically to the 1963 weapons test fallout maximum and the 1986 Chernobyl accident.

A key consideration when attempting to qualify sub-surface activity peaks with known periods of peak atmospheric fallout is the time-lag between actual weapons testing periods, subsequent stratospheric transport and deposition on the marsh surface. For pre-1963 weapons test fallout this lag-time has been estimated to be in the order of 6–13 months (Playford *et al.*, 1992). For the Chernobyl accident in 1986 maximum fallout across the UK occurred some 4-7 days after the reactor explosion. As such consideration of a lag-time period is unnecessary unless continued supply of ^{137}Cs derived from catchment supply can be seen to have influenced any detectable activity maxima. Importantly, any peaks detected must represent the actual age/depth horizon to which they are attributed. As such it is important to ascertain that no post-depositional mobility of the radionuclide has occurred within the sediment column owing to physical reworking, bioturbation or chemical/diagenetic processes that may alter the true position of the peak maxima (Cundy and Croudace, 1996). This more fully discussed in chapter six of this thesis.

Although the direct input of ^{241}Am to Scottish coastal environments derived from weapons test fallout was low (Krey *et al.*, 1976; Appleby *et al.*, 1991) input of ^{241}Pu did occur following the documented periods of above ground detonation of high yield thermonuclear devices. This has lead to increased ^{241}Am activity levels associated with these events due to the in-growth of ^{241}Am from radioactive decay of ^{241}Pu which was a significant component of weapons test fallout. Detectable activity horizons within recent sediment sequences are therefore likely to play a more prominent role in dating contemporary sedimentary materials as ^{241}Am in-growth increases with time (Appleby *et al.*, 1991). Little or no ^{241}Pu or ^{241}Am was discharged into the atmosphere as a result of the Chernobyl accident. As such ^{241}Am is not expected to provide a suitable dating horizon if found in sediments at depths corresponding to Chernobyl derived deposition and therefore another source or re-mobilization must be considered.

Other non-atmospheric inputs of artificial radionuclides to the Argyll inter-tidal zone are those derived from the BNFL Sellafield facility via authorized discharges into the Irish Sea. These include ^{137}Cs, ^{241}Pu and ^{241}Am. Authorized discharges of ^{137}Cs commenced in 1952 and peaked in 1975. ^{241}Pu and ^{241}Am discharges commenced in 1954 and 1964 culminating in maximum effluent releases of these two radionuclides in 1973/1978 and 1974 respectively. A summary of the artificial radionuclide deposition resulting from atmospheric and non-atmospheric sources is presented in Figure 5.1. and more fully documented in Chapter three. Sellafield derived ^{241}Am is present within in the Scottish coastal zone owing to the decay of the more soluble (10% of total discharged and 5+ oxidation state) fraction of ^{241}Pu transported from the Irish Sea. As a consequence of in-growth during and following transport northwards from the Irish Sea and in-situ radioactive decay post deposition, the distribution of ^{241}Am has been more widespread than expected (Williams *et al.*, 1988). Measured activity related to specific point discharges can also be used to assess the depositional history of sediments into which these radioisotopes have become incorporated. This is only possible providing that the discharge history is fully documented and the lag-time between the known period of discharge and transit time to the point of deposition is fully understood for each radionuclide detected. Of key importance is the environmental/geochemical behaviour of individual radionuclides used which directly affects the time period between the point source of discharge and deposition at any location.

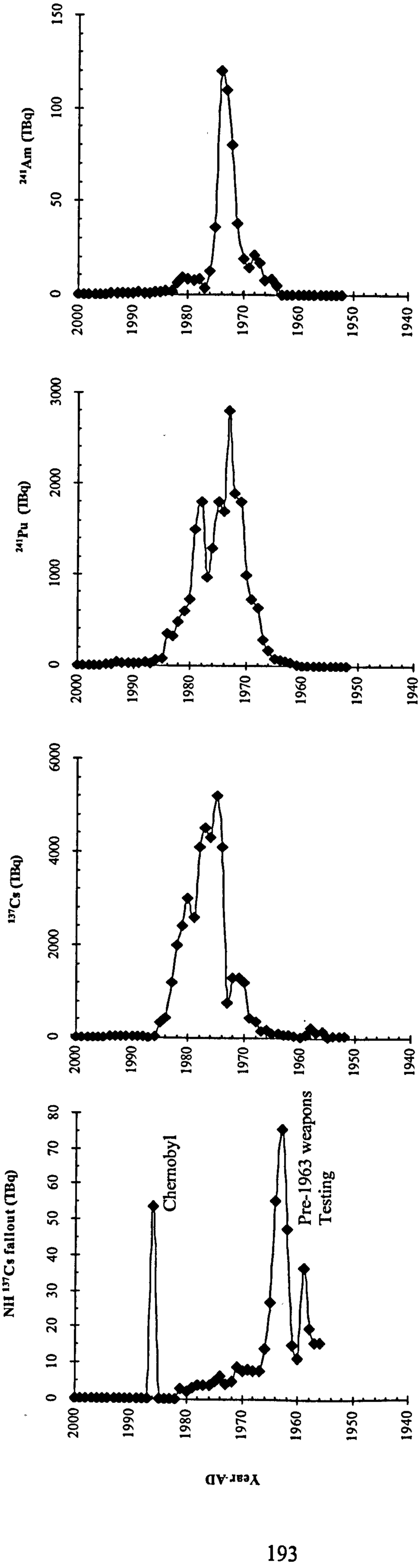

Figure 5.1: Data used from atmospheric fallout and discharge history of selected radionuclides from the BNFL Sellafield fuel reprocessing facility for reconstructing sediment accretion in the Argyll marshes Western Scotland: (a).Northern Hemisphere ^{137}Cs fallout and (b). ^{137}Cs (c). ^{241}Pu and (d) ^{241}Am Sellafield discharge. Source: British Nuclear Fuels, (1998).

5.5: Structure of radiometric results

The results of the various radionuclide dating techniques are now presented in specific site sections as a composite site by site account. These include the calculated sediment accretion rates and mass accumulation rates derived from the combination of natural and artificial dating models.

Results derived from the alpha and gamma spectrometry analysis are presented as actual depth vs. activity profiles and cumulative dry mass vs. activity profiles from which sediment accretion rates (mm yr^{-1}) and mass accumulation rates (g cm^{-2} yr^{-1}) are calculated. The latter plots are additionally important as the reporting of actual accumulated mass removes any effects resulting from sediment auto-compaction.

5.6: Loch Scridain

5.6.1: ^{210}Pb data

The ^{210}Pb total activity/depth profile within the core sequence from the head of Loch Scridain shows a near-exponential decline with depth down to 15 cm (Figure 5.2). This curve is in good agreement with the theoretical profile described in Chapter three (Figure 3.3) and displays no noticeable peaks or troughs associated with fluctuations in activity levels down the core depth profile. Comparison with the loss on ignition (550°C) down core profile (as a proxy for organic content) reveals no significant association of ^{210}Pb total activity with the organic fraction of the sediment matrix (Figure 5.2; r^2 value of 0.018). At depths below 16 cm ^{210}Pb total activity is dominated by the supported (or background) component derived from the *in-situ* decay of ^{226}Ra (Figure 5.3). The ^{210}Pb excess activity versus depth profile and ^{210}Pb excess plotted against cumulative dry mass indicates that background (unsupported) activity levels resulting from the decay of ^{226}Ra are reached at a depth of ~ 16-17cm and cumulative mass of 19.5 g cm^2 (Figure 5.3).

The natural log of ^{210}Pb excess (unsupported) activity plotted against depth for the Loch Scridain core records an r^2 value of 0.64 for the entire depth sampled for dating (Figure 5.4). This value is largely attributable to the two sections of the ln $^{210}Pb_{xs}$ profile which exhibit distinct gradient changes as the activity levels become dominated by unsupported levels. These differing sections extend from the marsh surface down to ~16-17 cm depth and then from this depth down through the core to the lowest sampled increment at 50 cm, where the

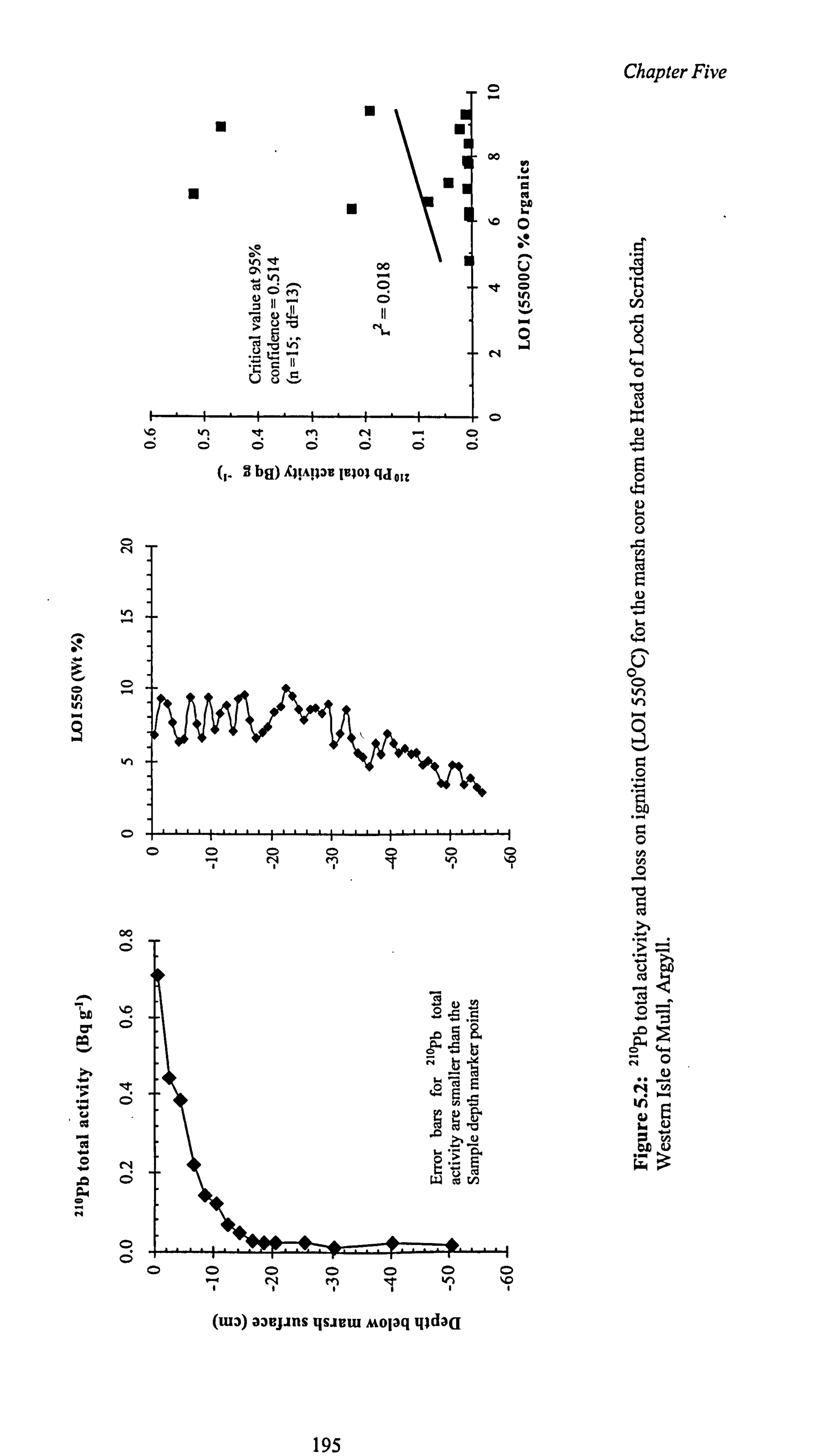

Figure 5.2: ^{210}Pb total activity and loss on ignition (LOI 550°C) for the marsh core from the Head of Loch Scridain, Western Isle of Mull, Argyll.

Error bars for ^{210}Pb total activity are smaller than the Sample depth marker points

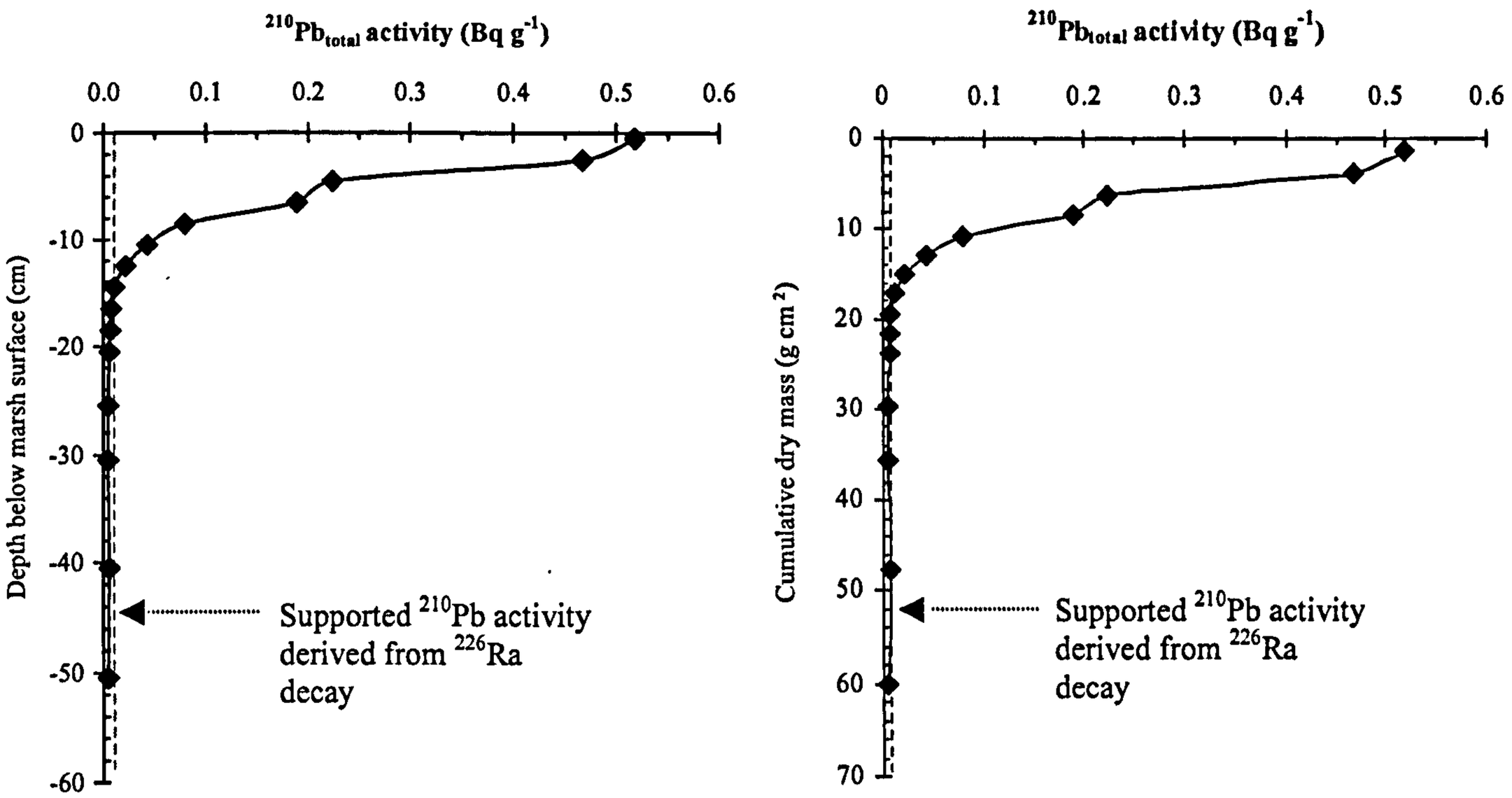

Figure 5.3: ^{210}Pb total activity plotted against sediment depth (cm) and cumulative dry mass (g cm^{-2}) for the marsh core from Loch Scridain

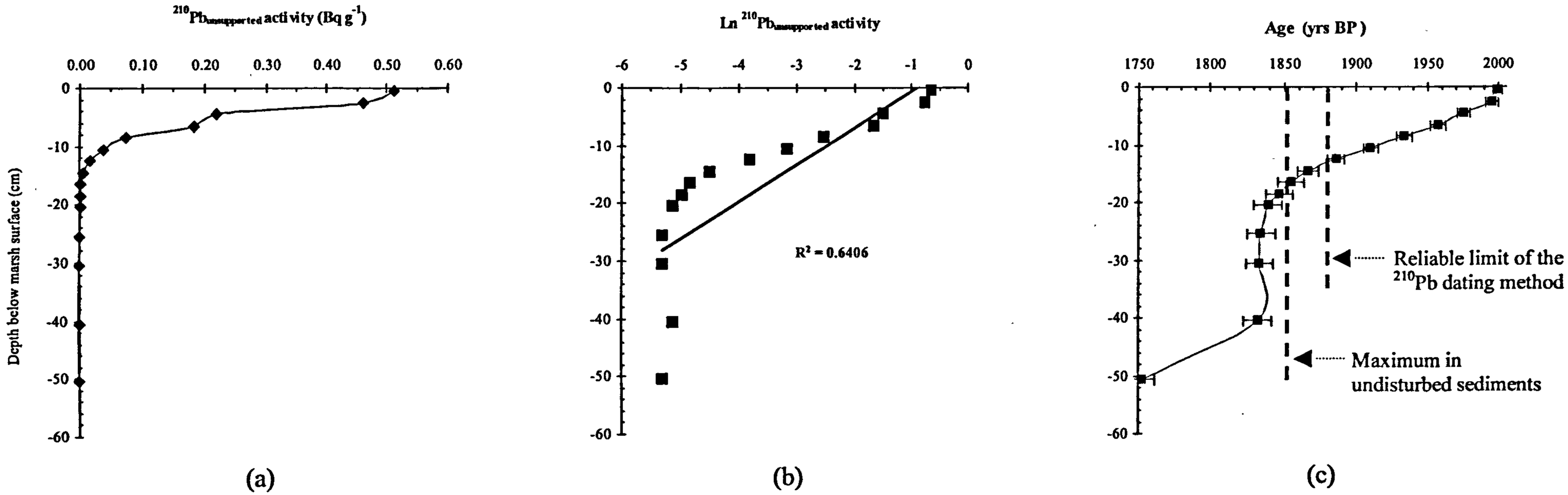

Figure 5.4: (a) ^{210}Pb unsupported activity, (b) Natural Log of unsupported ^{210}Pb activity versus depth and (c) ^{210}Pb constant flux (CRS) model derived age/depth profile for the marsh core from the head of Loch Scridain, Western Isle of Mull, Argyll. Error bars on the age/depth curve relate to the % error resulting from alpha spectrometry measurement of ^{210}Pb total activity and are a product of the random nature of radioactive decay. The actual age error bars are the calculated % error of determined age.

supported component takes over. The calculated age/depth curve indicates lower ages that must be considered as unreliable in terms of providing a chronology for the deeper section of this core and indicate ages beyond the 120 years maximum 'safe' limit . The limit of reliable calculated ages is shown in Figure 5.4.

The mean estimated sediment accretion rate for the core derived from the least squares regression of the plot in Figure 5.4b is calculated from the constant flux: constant sedimentation (simple model). From the limit of reliable ages this gives a value of 1.1 mm yr^{-1} with the 2 σ range (at the 0.05 level of significance) being between 0.9 – 1.3 mm year $^{-1}$. The average rate of sediment accretion determined from the Constant Initial Concentration (CIC) model reveals a value of 1.0 mm yr^{-1}, in good agreement with the figure derived from the simple model. The rate of sediment accretion calculated from the CRS (constant flux) model also yields a value of 1.1 mm yr^{-1} acquired from use of the reliable limit of the ^{210}Pb calculated ages at depths extending down to14-15 cm and CRS model age of 1886 AD (± 7 years).

Cumulative dry mass versus CIC and CRS model ages for the marsh core from Loch Scridain are shown in Figure 5.5. The two dating models are in very good agreement with one another and record sediment mass accumulation over time of 0.14 and 0.10 g cm yr^{-1} respectively for the marsh sediment from cumulative dry mass of 3.6 to 15 g cm^{-2}. Within the upper section of the core from the surface to 3.6 g cm^{-2} a distinct increase in mass accumulation is recorded with the CIC model yielding a value of 1.2 g cm yr^{-1}, in good agreement with the value of 0.90 g cm yr^{-1} calculated from the CRS model.

The CRS model is used to investigate variable sediment accretion over time in the Loch Scridain core. Detailed inspection of the marsh soil sediment accretion rates derived from the incremental CRS model are shown in Table 5.1. These highlight the more discrete changes in sedimentation rate plotted against depth (cm) and age (years AD) during the more recent period of marsh development within the reliable capability of the ^{210}Pb method . As the sedimentary sequence has developed a small decline in rates of accretion with increased elevation has taken place from the CRS dated horizon at 16-17 cm depth (age 1867 AD ± 10 years; and slightly beyond the absolute safe limit indicated in Figure 5.4c), to the depth increment at 10-11 cm (CRS model age 1910 AD ± 4 years). Above this age/depth horizon sedimentation rates are maintained at values between 0.8 – 1.1 mm yr^{-1} for a period of ~ 85 years. At 2.5 cm depth (age 1995 AD ± 0.20 years) recent sediment accretion has increased from 1995 to 1999 (time of core sampling) to a rate of 6.2 mm yr^{-1} over the most recent period of marsh development. The implications of this finding are discussed in Chapter Eight.

Depth (cm)	Age (years BP)	Age (years AD)	Sediment Accretion Rate (mm a^{-1})
0.5	0 (+/- 0.15)	1999	3.7 (3.6 – 3.8)
2.5	4 (+/- 0.17)	1995	1.0 (0.9 – 1.1)
4.5	24 (22.68 – 24.72)	1975 (1974 – 1976)	1.1 (1.0 – 1.2)
6.5	42 (39.75 – 44.23)	1957 (1955 – 1959)	0.8 (0.7 – 0.9)
8.5	66 (62.08 – 69.04)	1933 (1930 – 1936)	0.9 (0.8 – 1.0)
10.5	87 (84.18 – 93.11)	1910 (1906 – 1914)	0.8 (0.7 – 0.8)
12.5	113 (105.81 – 119.86)	1886 (1879 – 1893)	1.1 (1.0 – 1.2)
14.5	132 (122.27 – 142.48)	1867 (1857 – 1877)	1.7 (1.6 – 1.8)
16.5	144 (131.23 – 156.71)	1855 (1843 – 1867)	2.5 (2.3 – 2.7)
18.5	152 (139.00 – 165.85)	1847 (1834 – 1860)	2.5 (2.3 – 2.7)
20.5	160 (144.85 – 174.83)	1839 (1824 – 1854)	10.0 (9.1– 10.9)
25.5	165 (149.38 – 179.79)	1834 (1819 – 1849)	50.0 (45.4 – 54.6)
30.5	166 (150.47 – 181.12)	1833 (1818– 1848)	100.0 (90.8 – 109.2)
40.5	167 (151.60 – 182.54)	1832 (1817 – 1847)	1.3 (1.2 – 1.4)
50.5	240 (223.43 – 269.21)	1753 (1730 – 1776)	

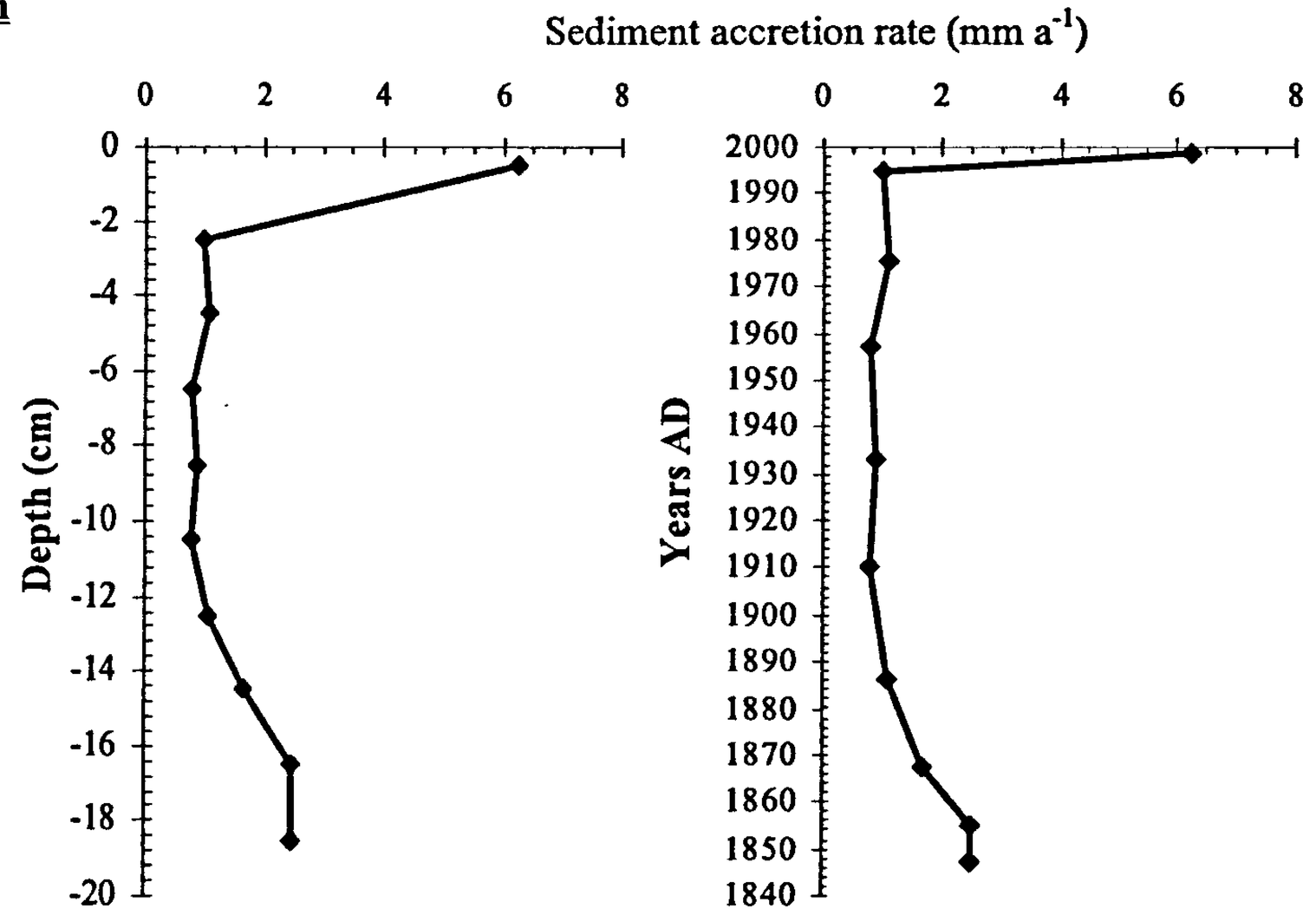

Table 5.1: ^{210}Pb CRS model derived dates and sedimentation rates for Loch Scridain (core 1) western Isle of Mull, Argyll. Sedimentation rates calculated for incremental depth interval between actual sample and one previous and are plotted against core depth and time (Years AD). Figures representing age and sedimentation ranges (shown in brackets) are derived from calculated maximum and minimum measured ^{210}Pb unsupported activity and relate to the random nature of radioactive decay. The maximum limit of reliable dates for the reconstruction of the depositional history of this core are shown as the gray dashed line.

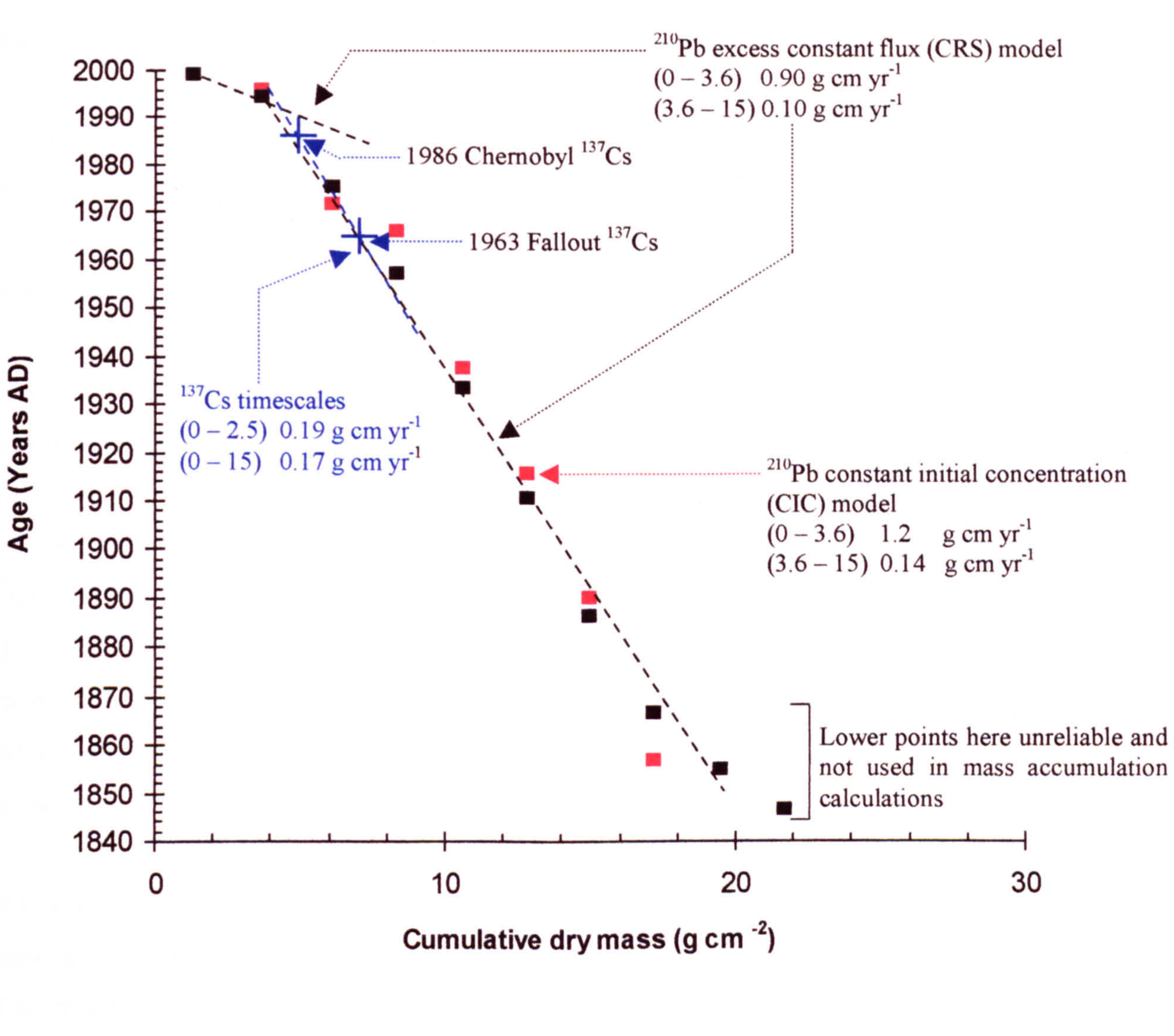

Figure 5.5: Year versus cumulative dry mass plot for the Loch Scridain marsh core with estimates from the ^{137}Cs 1963 fallout and 1986 Chernobyl accident marker horizons (the 'atter being uncertain; blue crosses and dashed blue lines). Also shown are the ^{210}Pb constant x (CRS) model estimates (black squares and black dashed lines) and the ^{210}Pb constant l concentration (CIC) model estimates (red squares, line not shown for clarity).

5.6.2: ^{137}Cs and ^{241}Am profiles

Activity depth profiles for the artificial radionuclides ^{137}Cs and ^{241}Am are shown in Figure 5.6. These are also presented as plots against cumulative dry mass to assess the position of subsurface maxima more comprehensively. The ^{137}Cs profile exhibits a distinct peak at 4.5 cm depth and cumulative dry mass of 6.1 g cm^{-2}. Above this peak a more pronounced broader increase in activity is evident which extends from the marsh surface to a depth of 2-3 cm and cumulative mass of between 0 and 3.6 g cm^{-2}.

The ^{241}Am profile reveals lower levels of activity throughout. Nonetheless two distinct peaks are evident at depths of 6-7 cm (cumulative mass of 8.3g cm^{-2}) and at 4-5 cm depth (cumulative mass of 6.1 g cm^{-2}).

The lower ^{137}Cs peak may at first glance be taken to represent the signature derived from above-ground weapons testing corresponding to 1963 AD. However, comparison with the ^{210}Pb derived ages from the CIC and CRS model calculations indicates that this does not correspond to a date co-incident with the 1963 peak in activity placing this peak at an age of between 1972 – 1975. The comparable peak in ^{241}Am activity would seem to indicate that this is also too young to be associated with 1963 weapons test fallout. It seems likely therefore that the true position 1963 AD peak related to weapons testing is situated at 6-7 cm depth and the ^{137}Cs peak in this core has been somewhat masked by marine input from Sellafield discharges which are inferred to be responsible for the activity peak of both radionuclides situated at 4-5 cm depth (Figure 5.6). The uppermost broad activity peak in ^{137}Cs is consistent with the activity vs. depth profiles from Loch Don (discussed below), which displays a distinct signature resulting from Chernobyl.

Sediment accretion rates calculated from the artificial radionuclide activity peaks give estimated values of 1.8 mm yr^{-1} for ^{137}Cs for the lower peak which if actually assigned to the weapons test signature is somewhat elevated in comparison to the 'simple model' estimations of accretion derived from ^{210}Pb dating (Table 5.1). Accretion rate based upon the lower ^{241}Am peak also provide a value of 1.8 mm yr^{-1}.

Mass accumulation rates calculated from the ^{137}Cs age marker horizons vs. cumulative dry mass give values of 0.19 g cm yr^{-1} and 0.17 g cm yr^{-1} for upper and lower peak respectively. From the lower ^{241}Am peak at 6-7 cm depth a value of 0.23 g cm yr^{-1} is calculated (^{241}Am data not shown in the diagram for clarity). The slight increase in mass accumulation is in fact significant and supports the ^{210}Pb derived increase in most recent sedimentation rates occurring on the marsh surface (see Chapter Eight for detailed discussion).

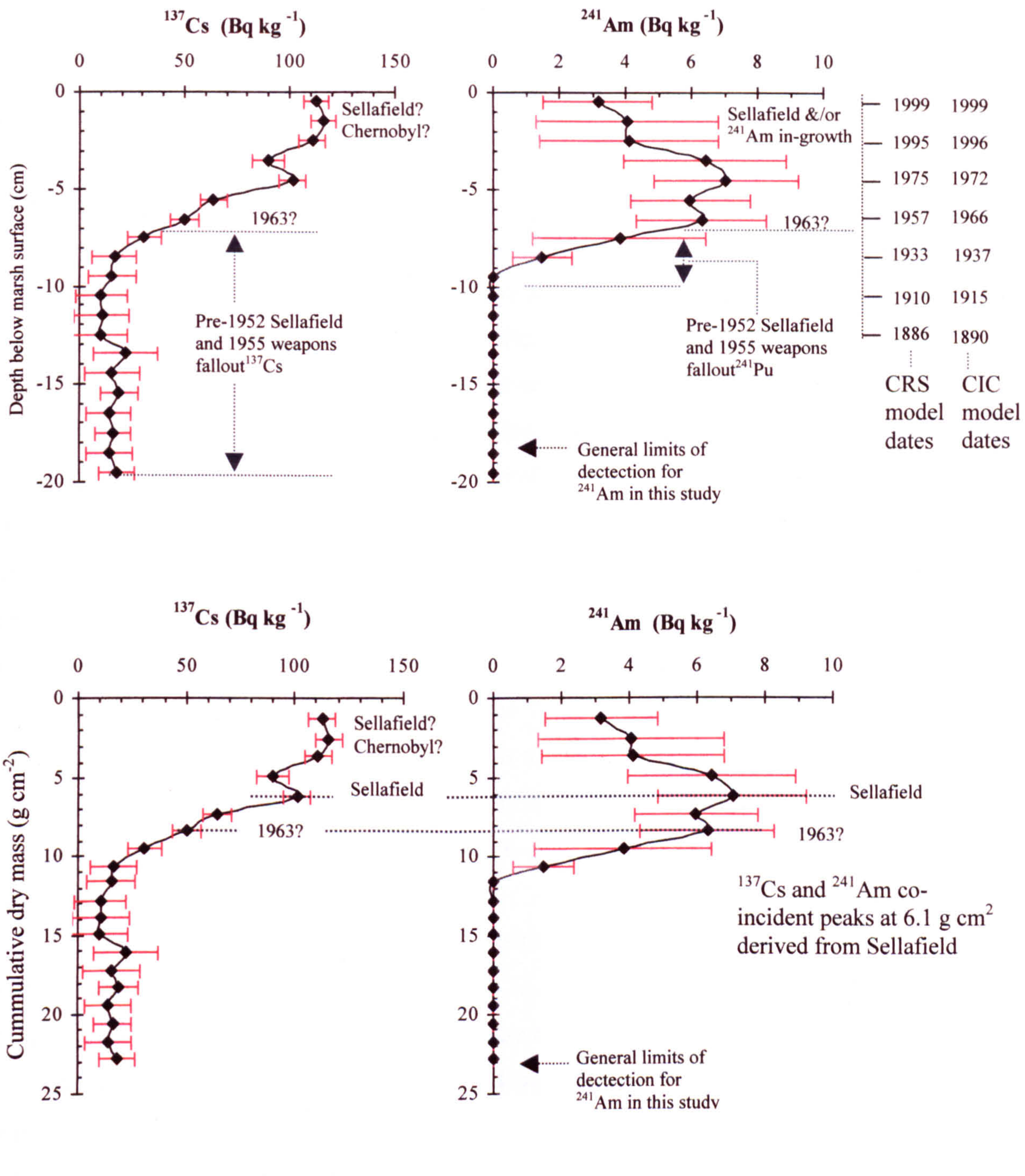

Figure 5.6: ^{137}Cs and ^{241}Am activity/depth profiles for the marsh core from Loch Scridain. CRS and CIC model dates are shown for comparison. Also shown are the activity profiles for ^{137}Cs and ^{241}Am plotted against cumulative dry mass to remove the effects of sediment auto–compaction and changes in mineral vs. organic content. Note the presence of ^{137}Cs and ^{241}Am at age/depth increments prior to the onset of 1952 Sellafield derived ^{137}Cs, ^{241}Pu and 1955 weapons test fallout and 1964 ^{241}Am discharges. Also note the position of the co-incident peak in ^{137}Cs & ^{241}Am related to maximum discharges from Sellafield. Error bars relate to % estimated error in activity measurement.

Importantly, the ^{137}Cs profiles indicate the presence of caesium at depths and ^{210}Pb model dates that correspond to periods prior to any atmospheric and Sellafield derived known periods discharge. Despite this activity levels within the upper section of this core still indicate quite distinctive peaks and these are fully discussed in chapter seven of this thesis.

5.7: Loch Don

5.7.1 ^{210}Pb data

Measured ^{210}Pb total activity within this core sequence declines gradually down to a depth of 10 cm in an exponential type decay profile (Figure 5.7). Immediately below this depth a small decrease in total activity is evident between 10 and 11cm. This isolated section of the activity profile may represent an influx of older unsupported ^{210}Pb with lower activity. Below the 11 cm depth increment the down-core profile of ^{210}Pb total activity continues to decline in an exponential profile. At 30-31 cm depth ^{210}Pb total activity levels correspond to background activity associated with the in situ decay of ^{226}Ra. Supported activity levels then extend down-core to the lower points of measured total activity at 40 and 47cm. These are shown in the ^{210}Pb total activity vs. depth and cumulative dry mass plots in Figure 5.8 where supported levels of activity occur at 38.6 g cm^2. The ^{210}Pb total activity profile shows a very week correlation with the loss on ignition 550°C (as a proxy for organic content, r^2 value of 0.319, Figure 5.7). The critical value at the 95% confidence level and degrees of freedom (13 = n-2) yields a value of 0.514 indicating that there is little association of organic matter with ^{210}Pb activity.

The down–core profile of the natural logarithm (Ln) of ^{210}Pb excess (unsupported) activity vs. depth from the Loch Don site reveals an r^2 value of 0.94 (at the 0.05 level of significance) for the entire core depth sampled down to 50 cm (Figure 5.9). The average sediment accumulation rate for the entire core calculated from the constant flux : constant sedimentation (or 'simple' model) yields a figure of 3.4 mm yr^{-1} (at the 0.05 level of significance, 2 σ range 3.0 – 4.0 mm yr^{-1}). Average sediment accretion for the entire core derived from the CIC model calculations gives a value of 3.5 mm yr^{-1} from a depth of 30-31 cm, in good agreement with the simple model derived estimate. Similar to the Loch Scridain core a distinct gradient change corresponding to the point at which supported levels of activity are reached is apparent in the age/depth profile (Figure 5.9) at a depth of 20-21 cm and a CRS model derived age of 1928 AD (± 2.17 yrs). Calculation of the rate of sediment accumulation

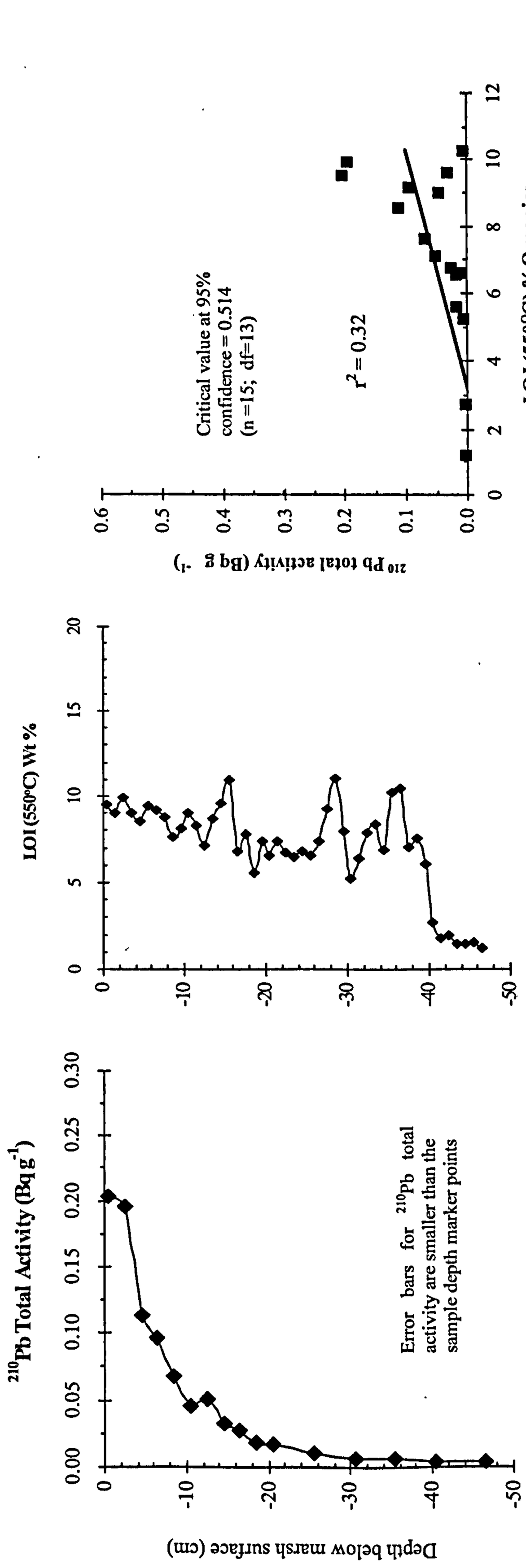

Figure 5.7: ^{210}Pb total activity and loss on ignition (LOI 550°C) for the marsh (core 3) from upper Loch Don, South Eastern Isle of Mull, Argyll.

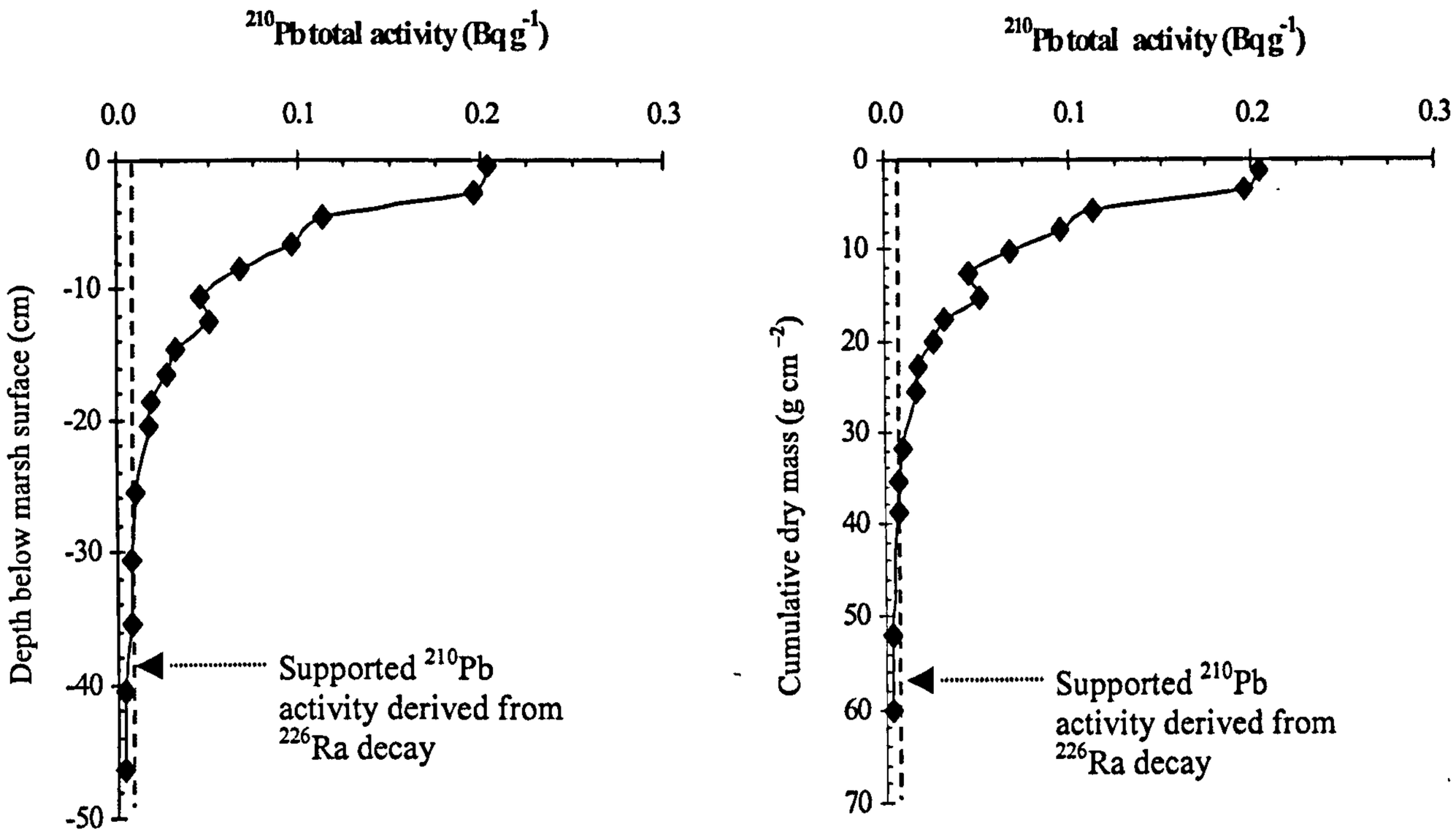

Figure 5.8: ^{210}Pb total activity plotted against sediment depth (cm) and cumulative dry mass (g cm^{-2}) for the marsh core from Loch Don

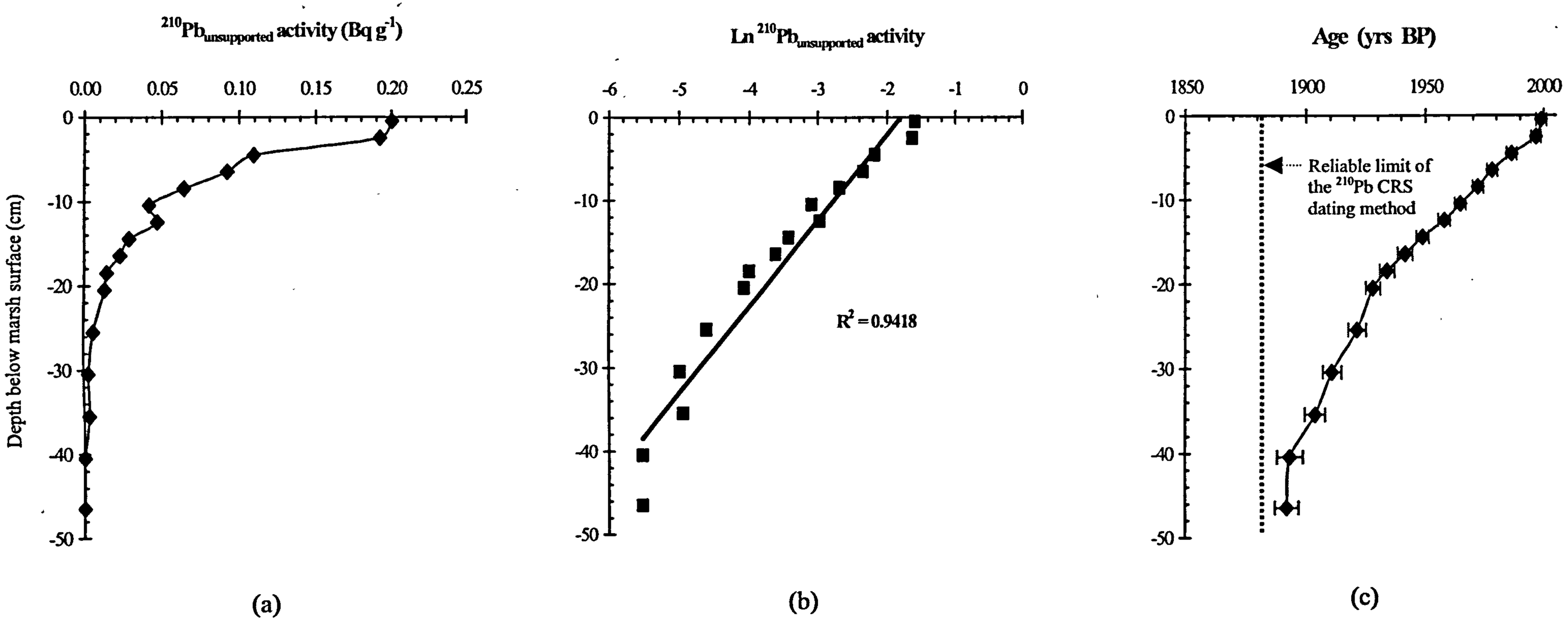

Figure 5.9: (a) ^{210}Pb unsupported activity, (b) natural Log of unsupported ^{210}Pb activity and (c) CRS derived age/depth profile for the marsh core from Loch Don, South -Eastern Isle of Mull, Argyll.

from the inflection point on the age/depth profile at 21 cm depth to the marsh surface (Figure 5.9) yields a figure of 2.4 mm yr^{-1} (2 σ range 2.2 – 2.7 mm yr^{-1}). This corresponds markedly with average sediment accretiontion rate for the lower sections of the profile characterized by the steeper gradient for the periods 1892 AD - 1893 AD and 1893 AD – 1928 AD (CRS model derived age and error range 1887 AD – 1930 AD).

The lowest section of the core between 47 cm – 41cm depth (CRS derived age of 1892 AD ± 5.2 yrs – 1893 AD ± 5.6 yrs) indicates a period of very rapid sediment accumulation of ~ 6.0 cm prior to a significant increase in the organic content of sediment above 41cm, (inferred from the LOI 550°C vs. depth profile; Figure 5.7). Above the 41cm depth increment to the inflection point at 20-21cm, (CRS model ages 1893 AD – 1928 AD) marsh accretion has taken place at an average rate of 5.7 mm yr^{-1} .

Closer inspection of the CRS age/depth model permits calculation of the incremental accretion rates giving a more comprehensive overview of the development of the marsh over the last century. The more detailed sedimentary history for the Loch Don marsh core is shown in Table 5.2. This highlights well the more rapid rates of accretion that have taken place throughout the lower section of the core beneath the inflection point at 20-21cm depth. Two distinct periods are recognized where rates of accumulation exceed 7 mm yr^{-1}. In the upper section of the core the more detailed sedimentary history provided by the incremental nature of the CRS model clearly shows the relatively reduced rates of accretion with increasing marsh elevation up to 3.0 cm depth (Table 5.2). Of interest here, is the most recent phase of marsh development indicated by the CRS model. From a depth of 3.0 cm (age 1997 AD ± 2.2 yrs) a relatively rapid increase in sedimentation rate is suggested with a possible maximum of 10 mm a^{-1} over the last few years.

CIC model and CRS model ages plotted against cumulative dry mass are presented in figure 5.10. For the CIC model derived age calculations mass accumulation rates of 0.30 g cm yr^{-1} are recorded for the increment between 5.7 – 32 g cm^2. Above this depth between 3.4 – 5.7 g cm^2 the rate of accumulation reduces to 0.13 g cm yr^{-1}. In the uppermost near-surface section from 0-1 g cm^2 the accumulation rate increases significantly to an estimated value of 1.1g cm yr^{-1}. CRS model derived rates of accumulation are in very good agreement for the same depth intervals (Figure 5.10). Calculated rates are 0.33, 0.23 and 1.1 g cm yr^{-1}. The lower section of the core from 25-60 g cm^2 indicates a rate of accumulation similar to that in the uppermost section of 0.96 g cm yr^{-1}.

Depth (cm)	Age (years BP)		Age (years AD)	Sediment Accretion Rate (mm a^{-1})
0.5	0	(+/-0.047)	2000	3.7 (3.6 - 3.8)
2.5	2	(2.12 – 2.21)	1997	2.0 (1.9 - 2.1)
4.5	12	(12.21 – 12.74)	1987	2.2 (2.1 - 2.3)
6.5	21	(20.23 – 21.17)	1978	2.2 (2.1 – 2.3)
8.5	27	(26.15 – 27.39)	1972	3.3 (3.2 – 3.4)
10.5	34	(33.45 – 35.05)	1965	2.9 (2.8 – 3.0)
12.5	41	(40.03 – 42.01)	1958 (1957 – 1959)	2.9 (2.8 – 3.0)
14.5	50	(48.82 – 51.40)	1949 (1948 – 1950)	2.2 (2.1 – 2.2)
16.5	57	(55.67 – 59.17)	1942 (1940 – 1944)	2.9 (2.8 – 3.0)
18.5	65	(62.94 – 66.99)	1934 (1932 – 1936)	2.5 (2.4 – 2.6)
20.5	71	(68.74 – 73.08)	1928 (1926 – 1930)	3.3 (3.2 – 3.4)
25.5	78	(74.78 – 80.44)	1921 (1918 – 1924)	7.1 (6.8 – 7.4)
30.5	88	(84.73 – 91.61)	1911 (1908 – 1914)	5.0 (4.8 – 5.2)
35.5	95	(91.32 – 99.28)	1904 (1900 – 1908)	7.1 (6.8 – 7.4)
40.5	106	(100.01 – 111.16)	1893 (1888 – 1898)	4.5 (4.3 – 4.7)
46.5	106.99	(101.80 – 112.17)	1892 (1887 – 1897)	

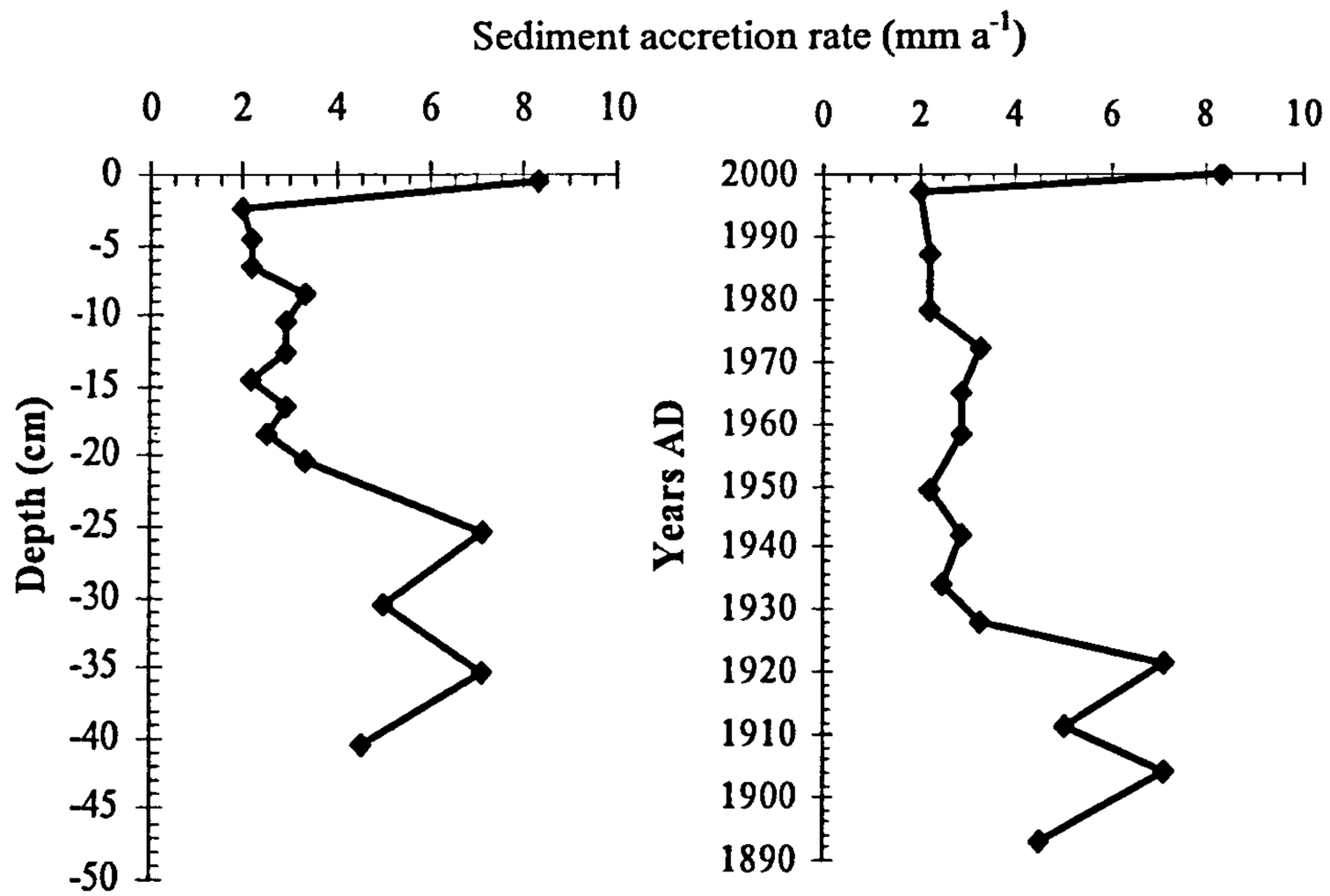

Table 5.2: ^{210}Pb CRS model derived dates and sedimentation rates for Loch Don (core 4) south eastern Isle of Mull, Argyll. Sedimentation rates calculated for incremental depth interval between actual sample and one previous and plotted against core depth and time (Years AD). Figures representing age and sedimentation ranges (shown in brackets) are derived from calculated maximum and minimum measured ^{210}Pb unsupported activity and relate to the random nature of radioactive decay. In this core sequence the reliable dates extend throughout the entire

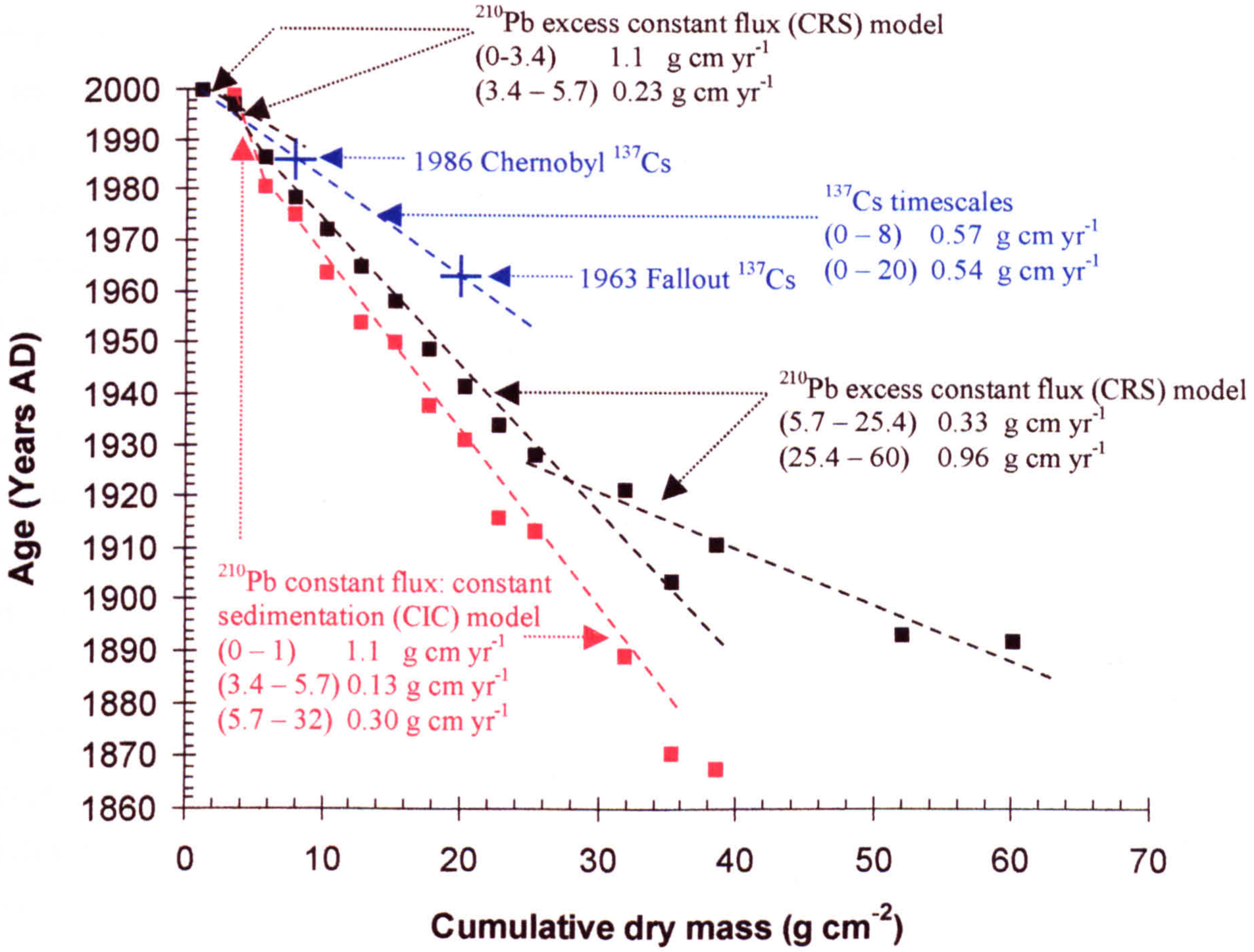

Figure 5.10: Year versus cumulative dry mass plot for the Loch Don marsh core with estimates from the ^{137}Cs 1963 fallout and 1986 Chernobyl accident marker horizons (blue crosses and dashed blue lines). Also shown are the ^{210}Pb constant flux (CRS) model estimates (black squares and black dashed lines) and the ^{210}Pb constant flux:constant sedimentation (CIC) model estimates (red squares and red dashed lines).

5.7.2: ^{137}Cs and ^{241}Am profiles

^{137}Cs and ^{241}Am activity/depth and activity vs. cumulative dry mass profiles are shown in Figure 5.11. Two distinct peaks are evident within the ^{137}Cs down-core profile at depths of 8-9 cm and 3-4 cm with cumulative dry mass values of 10.3 and 4.5 g cm^{-2} respectively. The lower of these two peaks is likely to be the activity maximum resulting from 1963 weapons-test fallout. Comparison with the ^{210}Pb CIC model derived age for this peak reveals an estimated age of 1964 for the maximum activity at the 8-9 cm depth increment. The CRS model ages are also indicative of this peak being co-incident with 1963 atmospheric deposition with an estimated age of 1965 (± 2.3 yrs) for the base of this activity peak at 10-11 cm depth. Notable in this core is the presence of ^{137}Cs at depths below 14-15 cm depth and corresponding to ages which pre-date the onset of Sellafield discharges and 1954 above-ground weapons testing.

The upper ^{137}Cs peak at 3-4 cm depth represents the relatively higher activity maximum resulting from depostion following the Chernobyl accident. ^{210}Pb model ages give estimated dates of 1987 (CRS derived date ± 0.3 yrs) for the depth increment immediately below this peak. However, the CIC model estimation is less conclusive with an estimated age of 1981 AD. This activity maximum within the core is superimposed upon generally increasing activity levels and ^{210}Pb estimated ages that pre-date the Chernobyl accident and are present owing to the influence of discharges from Sellafield. The upper section of the graph shows a quite rapid reduction in activity levels likely to be the result of declining runoff following the Chernobyl accident and the lack of significant catchment derived input of ^{137}Cs to the upper Loch Don marsh site.

Average sediment accretion rates calculated from the use of these two peaks gives values of 2.3 mm yr^{-1} for the 1963 peak and 2.5 mm yr^{-1} for Chernobyl input in 1986. These values are in good general agreement with the ^{210}Pb model estimations for the upper section of the core.

^{137}Cs plotted against cumulative dry mass for the two ages of principal deposition are shown in Figure 5.10 in conjunction with the ^{210}Pb model estimates. This indicates some discrepancy between the ^{137}Cs and the two ^{210}Pb model derived sediment accumulation rates with estimates of 0.57 and 0.54 g cm yr^{-1} for the Chernobyl and 1963 activity peaks respectively compared to the estimations given in the previous section for the ^{210}Pb models. ^{137}Cs is likely to give higher estimations of sediment accretion/accumulation if downward mixing has occurred following deposition (Cundy *et al.*, 1998). Other variation between the methods may result from variation in sediment source and/or composition thereby influencing

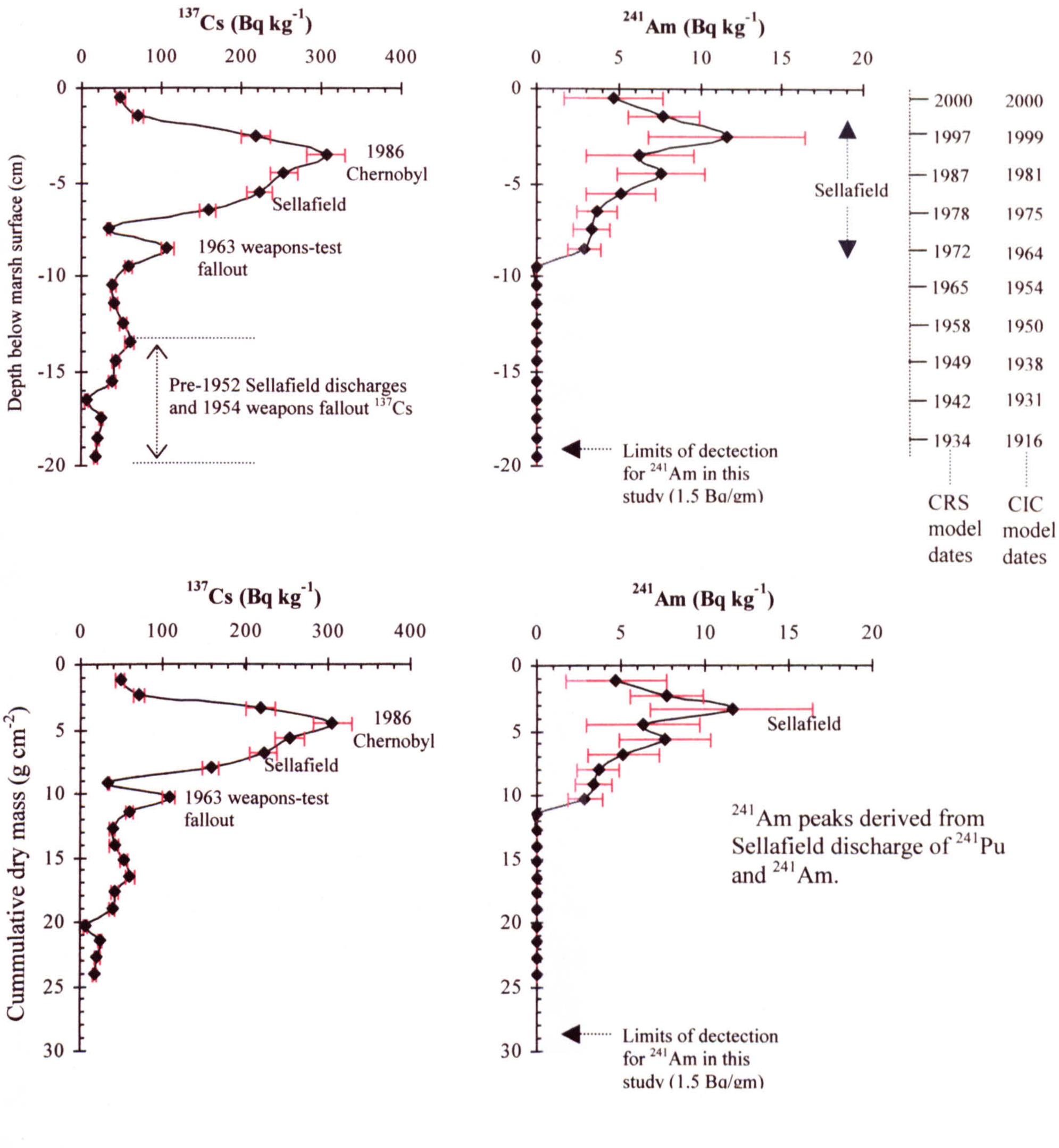

Figure 5.11: ^{137}Cs and ^{241}Am activity vs. depth and activity vs. cumulative dry mass profiles for the Loch Don core. ^{210}Pb CRS and CIC model dates are shown for comparison. Note the absence of any discernable ^{241}Am peak at age/depth and cumulative mass co-incident with the 1963 weapons-test fallout signature.

the ^{210}Pb excess flux to the surface of the marsh and also affecting the values if supported ^{210}Pb (Cundy *et al.*, 1998). The calculated flux of ^{210}Pb excess to the Loch Don marsh is 0.037 Bq cm^2 yr^{-1} which is higher than the estimates for typical atmospheric input of ^{210}Pb for northern hemisphere landmasses (0.014 Bq cm^2 yr^{-1}, Appleby and Oldfield 1992). This indicates that a fraction of the ^{210}Pb excess supplied annually to the Loch Don marsh surface is derived from labelled sediment particles. This may account for the discrepancy between the ^{210}Pb CIC and CRS models and ^{137}Cs estimates of sediment accretion (Figure 5.10).

^{241}Am is first recorded in the Loch Don core at a depth of 8-9 cm and CRS model age of 1972 (± 0.6 years, Figure 5.11). The CIC model estimates this age to be older at 1981 AD. Distinct peaks in ^{241}Am activity are evident at depths of 4-5 cm and 2-3 cm corresponding to cumulative dry mass values of 5.7 and 3.4 g cm^2). Estimated ages for these peaks are 1987 (± 0.3 yrs) and 1997 via the CRS model. These activity peaks do not correspond with any ^{137}Cs peaks and there appears to be no discernable peak in ^{241}Am which can be associated with the 1963 weapons-test fallout signature in this core sequence. As such the detectable levels of ^{241}Am are likely to be result of Sellafield derived discharges and the subsequent in-growth of ^{241}Am from ^{241}Pu. Without detailed knowledge of the ^{241}Pu transit time and subsequent ^{241}Am in-growth period it is not possible to utilize measured ^{241}Am activity for dating purposes within this core. Importantly, the presence of ^{241}Am within the near-surface and surface depths of the marsh does indicate a continuing supply of marine delivered ^{241}Am to the marsh at Loch Don.

5.8: Loch Creran

5.8.1: ^{210}Pb

The ^{210}Pb total activity down core profile for the core taken from the head of Loch Creran shows an approximately linear decrease in activity within the upper section down to 10-11 cm depth (Figure 5.12). Immediately below this depth increment ^{210}Pb total activity declines slightly down a depth of 16-17cm at which point the exponential-type decay curve is resumed reaching supported levels at depths below 30-31cm. Supported levels of ^{210}Pb are shown in Figure 5.13 with ^{210}Pb total activity also plotted against cumulative dry mass. Comparison with the organic content of the core (Figure 5.12) derived from loss on ignition analysis (LOI 550^{O}C) does not indicate any significant correlation (r^2 value of 0.215) and association of ^{210}Pb activity with the organic fraction.

The plot of the natural logarithm of ^{210}Pb unsupported activity vs. depth (Figure 5.14) yields an r^2 value of 0.86 (at the 0.05 level of significance) with a calculated average accretion

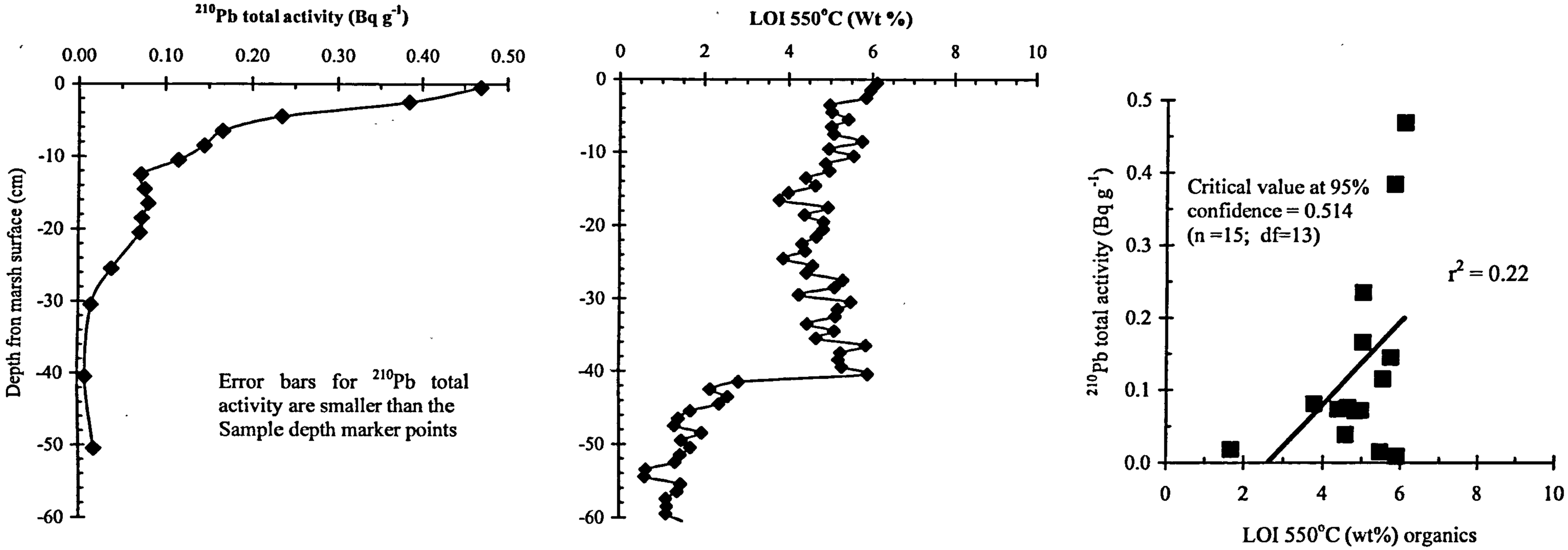

Figure 5.12: ^{210}Pb total activity and loss on ignition (LOI) at 550°C for Loch Creran upper marsh site (core1) mainland Argyll.

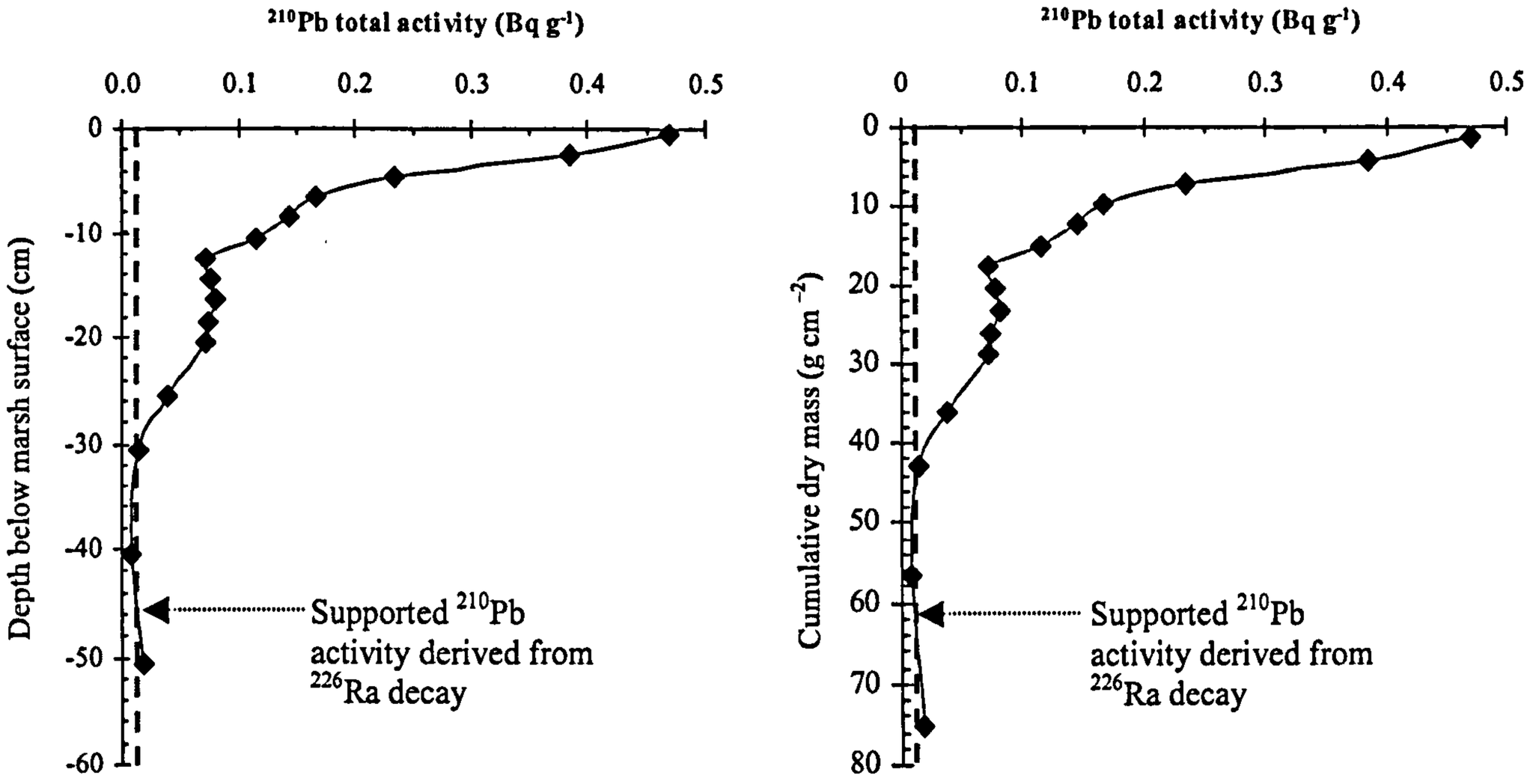

Figure 5.13: ^{210}Pb total activity plotted against sediment depth (cm) and cumulative dry mass (g cm^{-2}) for the marsh core from Loch Creran. The supported (background) value for ^{210}Pb is indicated by the red dashed line at 0.0087 Bq g^{-1}.

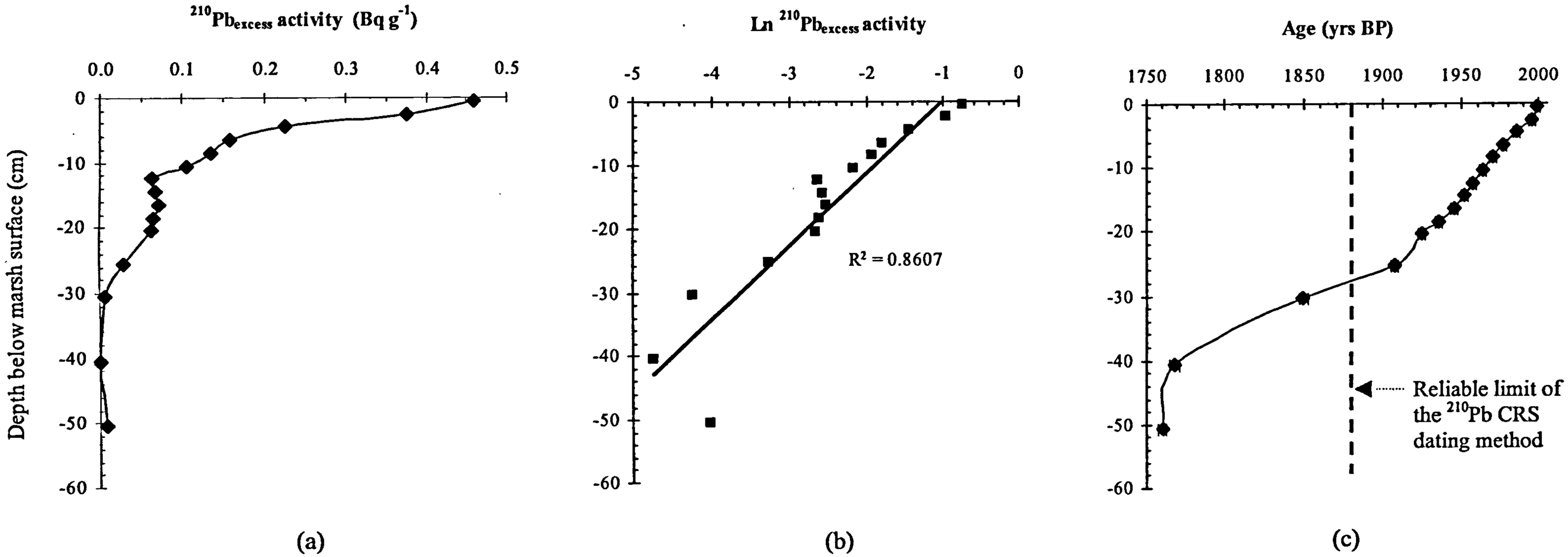

Figure 5.14: (a) ^{210} unsupported activity, (b) natural Log of unsupported ^{210}Pb activity and (c) CRS derived age/depth profile for the marsh core from the head of Loch Creran, mainland Argyll.

rate of 3.7 mm a^{-1} (2 σ range 3.2 – 4.5 mm yr^{-1}) derived from the constant flux : constant sedimentation ('simple model') for the entire core profile. The reliable limit of the ^{210}Pb technique within this core occurs at the depth increment of 25-26 cm and CIC model age of 1909 AD gives a figure of 2.9 mm yr^{-1}. The CRS model derived sediment accretion rate for the same depth interval and age of 1907 AD (± 2.4 yrs) and gives an average rate of accretion of 3.3 mm yr^{-1} (2 σ range 2.7 – 4.3 mm yr^{-1}). This indicates good general agreement of the two models within this core.

The CRS method has been used to calculate ages for the sub-sample increments which reveal two prominent periods of varying sediment accumulation shown in the age/depth plot in Figure 5.14c). The lower of these at a depth increment of between 31–26 cm corresponds to a CRS model calculated age range of c.1849 AD (± 4 yrs) to 1907 AD (± 2.2 yrs). The upper 26 cm depth to the core surface is dated with the CRS model at age range of c.1907 AD (± 2.2 yrs) to 1999 AD. Average sediment accumulation rate has been calculated for these two distinct gradients of the age/depth model and yield rates of accretion of 1.2 mm a^{-1} over the period 1849 AD – 1907 AD. However, the likelihood of the lower date being unreliable must be considered here.

Interestingly at this site the rates of historical sedimentation within this core differ from the other cores studied in that an older period of relatively reduced sediment accretion is followed by a period of more rapid accretion throughout the last century. For the period 1907 AD to 1999 AD (26 cm depth to the marsh surface) the ln ^{210}Pb unsupported activity vs. depth profile reveals an improved r^2 value of 0.90 (at the 0.05 level of significance, Figure 5.12). The mean sediment accretion rate for this upper section of the core calculated from the least squares regression of this plot gives a figure of 2.4 mm a^{-1} (2 σ range 0.22 – 0.27 cm a^{-1}).

The depth incremental nature of the CRS model provides the mechanism by which the more detailed sedimentary history of the core can be investigated. The breakdown of the historical sedimentary development of the Loch Creran core is shown in Table 5.3 and indicates the generally lower rates of accretion that occurred in the marsh up to *circa.*1945 AD in comparison to the upper core section (Table 5.3). An exception to this trend occurred between *circa.* 1849 AD (± 4 yrs) and 1907 AD (± 2.2 yrs) when the average rate of sedimentation reached 2.9 mm yr^{-1} (CRS derived error range of 2.8 – 3.0 mm yr^{-1}). Although the lower date here lies outside the 120 year maximum usually limiting the ^{210}Pb method this may be more reliable owing to the lack of physical disturbance evident in the core sequence. Above the 17 cm depth horizon accretion rates fluctuate around an average of 3.2 mm yr^{-1} to the 7 cm depth interval (age of c. 1977 ± 0.45 years). From this age/depth interval to the 3 cm depth point (age of c. 1995 ± 0.1 yrs) rates decrease slightly to a minimum of 2.0 mm yr^{-1}.

Depth (cm)	Age (years BP)		Age (years AD)	Sediment Accretion Rate (mm a^{-1})
0.5	0	(+/- 0.8)	1999	3.7 (3.6 – 3.8)
2.5	4	(3.68 – 3.82)	1995	2.0 (1.9 – 2.1)
4.5	14	(13.26 – 13.79)	1985	2.5 (2.4 – 2.6)
6.5	22	(21.22 – 22.12)	1977	2.9 (2.8 – 3.0)
8.5	29	(28.03 – 29.21)	1970	3.3 (3.2 – 3.4)
10.5	35	(34.77 – 36.11)	1964	2.9 (2.8 – 3.0)
12.5	42	(41.26 – 43.07)	1957 (1956 –1958)	4.0 (3.9 – 4.1)
14.5	47	(46.21 – 48.15)	1952 (1951 –1953)	2.9 (2.8 – 3.0)
16.5	54	(52.26 – 55.13)	1945 (1943 – 1947)	1.8 (1.7 – 1.9)
18.5	63	(61.96 – 64.69)	1936 (1934 – 1938)	1.6 (1.5 – 1.7)
20.5	75	(73.13 – 76.36)	1924 (1922 – 1926)	2.9 (2.8 – 3.0)
25.5	92	(89.44 – 93.89)	1907 (1905 – 1909)	0.9 (0.8 – 1.0)
30.5	150	(145.69 – 154.06)	1849 (1845 – 1854)	1.2 (1.1 – 1.3)
40.5	231	(223.09 – 238.74)	1768 (1760 – 1776)	14.3 (13.8 – 14.8)
50.5	238	(232.13 – 244.61)	1761 (1755 – 1767)	

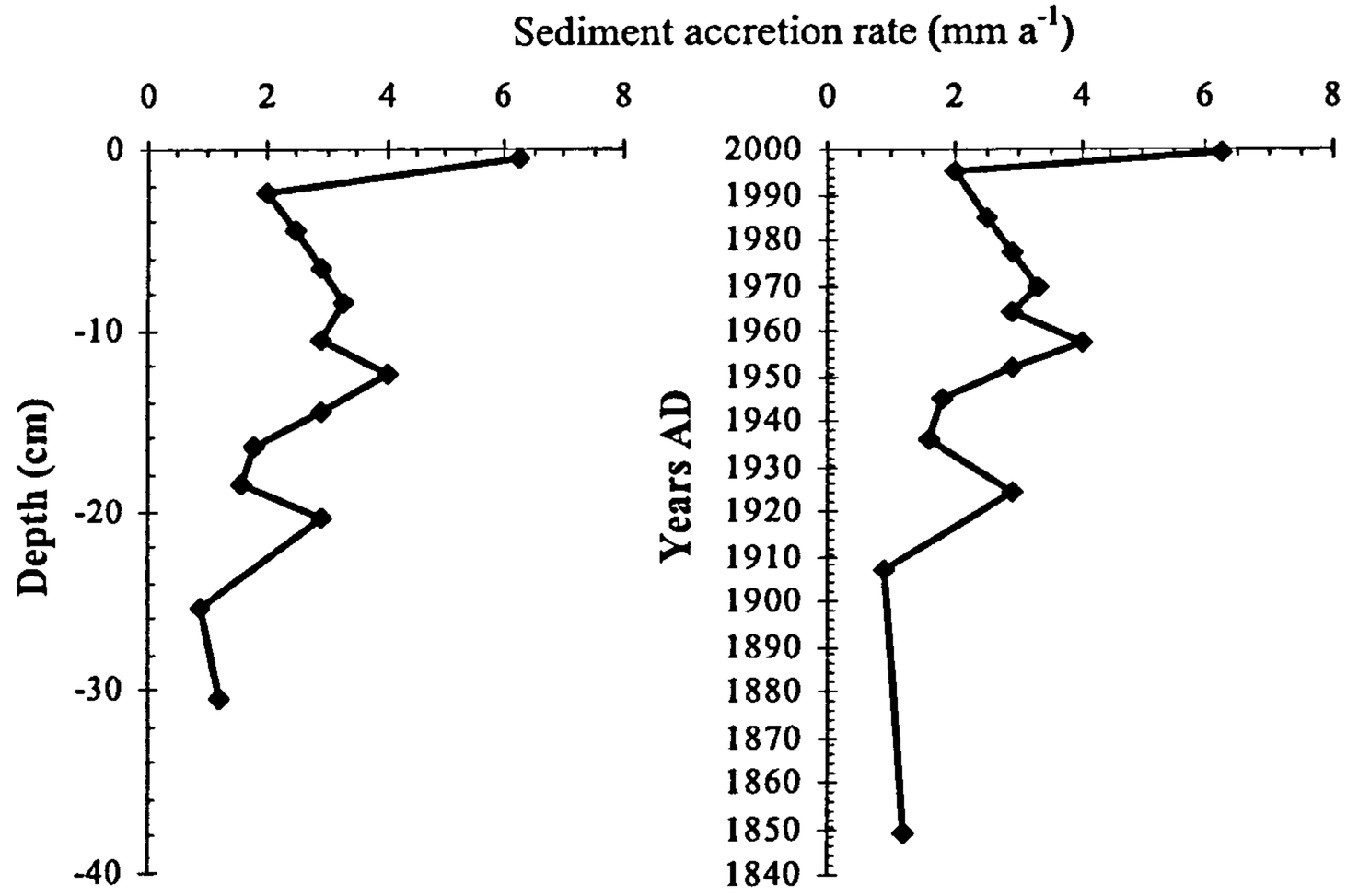

Table 5.3: ^{210}Pb CRS model derived dates and sedimentation rates for Loch Creran (core 1) mainland Argyll. Sedimentation rates calculated for incremental depth interval between actual sample and one previous and plotted against core depth and time (Years AD). Figures representing age and sedimentation ranges (shown in brackets) are derived from calculated maximum and minimum measured ^{210}Pb unsupported activity and relate to the random nature of radioactive decay. Reliable dated ages are indicated by the gray dashed line

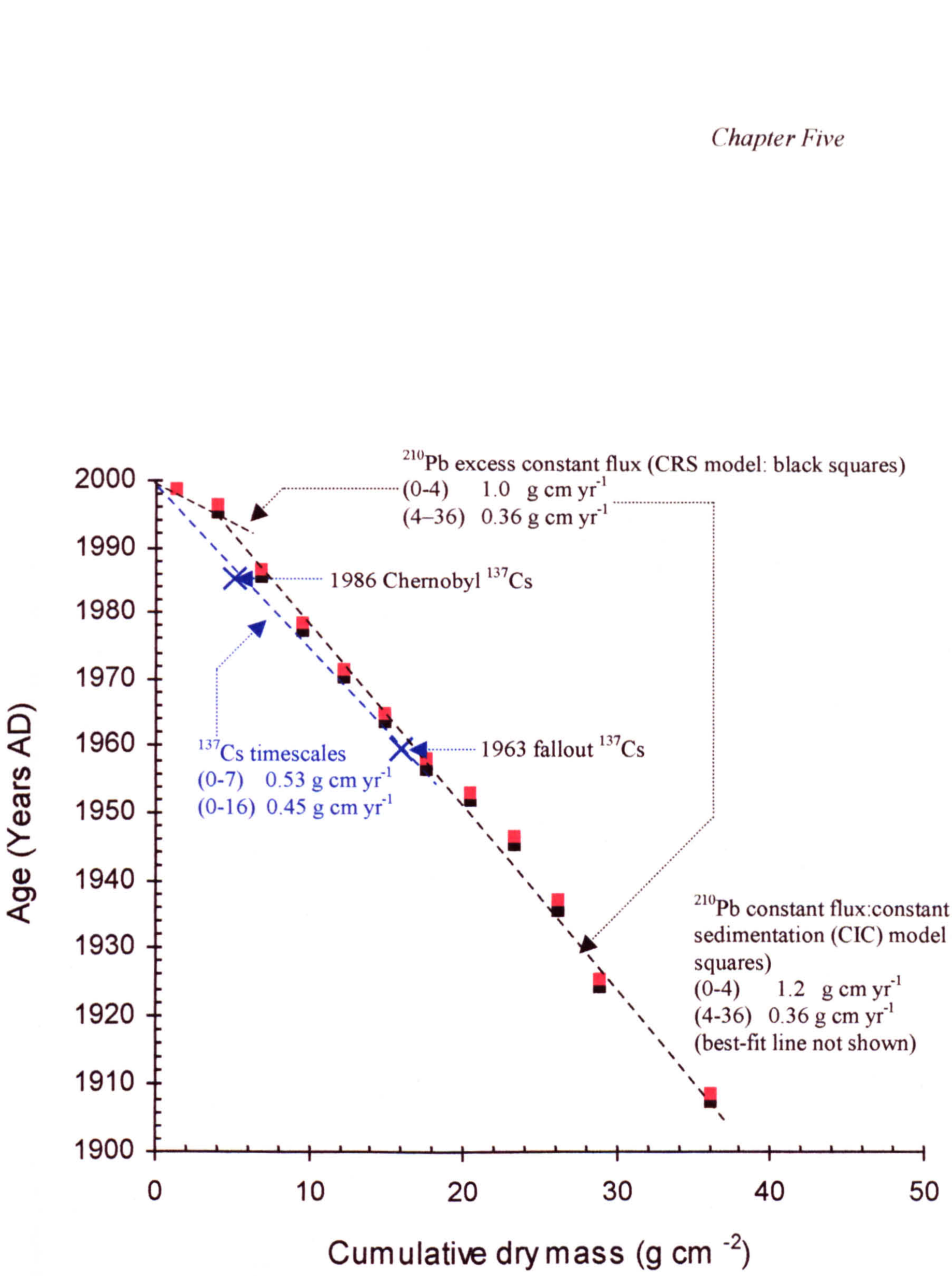

Figure 5.15: Year versus cumulative dry mass plot for the Loch Creran marsh core with estimates from the ^{137}Cs 1963 fallout and 1986 Chernobyl accident marker horizons (blue crosses and dashed blue line) and the constant flux ^{210}Pb (CRS) method (dashed black line and black squares). The best fit line for the constant flux/constant sedimentation (CIC) method is not shown owing to the close approximation of the two models (red squares).

Figure 5.16: ^{137}Cs and ^{241}Am activity/depth and activity vs. cumulative dry mass profiles for the Loch Creran core. ^{210}Pb CRS and CIC model dates are shown for comparison. Note the co-incident peaks in ^{137}Cs and ^{241}Am which correspond to 1963 weapons fallout signature recorded in this core sequence and the low values for ^{241}Am which fall within limits of detection.

Importantly, the calculated rate of very recent sediment accretion within this core sequence has increased significantly over the period 1995- 1999 to a rate comparable with that identified within the core sequences from the Isle of Mull calculated at 6.2 mm yr^{-1} (Table 5.3). This is highlighted further in the summary section at the end of this chapter and discussed fully in chapter seven.

The cumulative dry mass vs. age plots for the ^{210}Pb CIC and CRS models are shown in Figure 5.15. This indicates the close agreement of the two models for dating the core from Loch Creran and the line of best fit to describe the rate of sediment accumulation is shown for the CRS model only for improved clarity. The CIC and CRS calculated rates of sediment accumulation are 0.36g cm yr^{-1} for both models for the increment corresponding to 4 – 36 g cm^2. For the uppermost section of the profiles the models are also in good agreement recording accumulation rates of 1.2 and 1.0 g m yr^{-1} for the increment corresponding to 0 – 4 gm cm^2.

5.8.2: ^{137}Cs and ^{241}Am profiles

The ^{137}Cs and ^{241}Am activity/depth and activity vs. cumulative dry mass profiles are shown in Figure 5.16. The ^{137}Cs activity down-core profile reveals two distinct peaks at 9-10 cm depth and an increased activity peak at 4-5 cm depth. These depths correspond to a cumulative dry mass of 13.6 and 6.9 g cm^{-2} for the lower and upper activity peaks respectively. For the lower of these two peaks the ^{210}Pb CIC and CRS model calculated ages gives an estimated age of 1965 and 1964 respectively for the depth increment at 10-11 cm immediately below 9-10 cm depth increment. In light of these ages it is possible to therefore assign this activity peak to the 1963 weapons fallout signature with a high degree of confidence. Similarly the upper activity peak is dated via the two models at 1987 and 1985 (± 0.26 yrs) respectively. This therefore represents the activity peak associated with 1986 Chernobyl derived atmospheric deposition. Sediment accretion rates calculated from the two peaks in ^{137}Cs activity yield values of 2.7 mm yr^{-1} for the 1963 weapons signature and 3.5 mm yr^{-1} for the peak associated with Chernobyl derived ceasium. Similarly, the cumulative dry mass accumulation rate for the two activity peaks are 0.45 and 0.53 g cm yr^{-1} (Figure 5.15).

Both of these peaks are superimposed upon generally increasing levels of activity associated with the onset of Sellafield derived discharges in 1952 and the discharge maximum which occurred in 1975 and to a slightly lesser extent in 1980. Importantly, measured levels

of ^{137}Cs activity occur at age/depths prior to both the onset of Sellafield discharges and pre-1963 above-ground weapons testing.

The ^{241}Am profile reveals a series of peaks which are accompanied by extremely low levels of activity. ^{241}Am is first recorded in the marsh core from Loch Creran at a depth of 15-16 cm (cumulative dry mass 15 g cm^2) and age corresponding to the mid 1940s. This indicates the presence of ^{241}Am at depth increments that also pre-date the onset of ^{241}Pu and ^{241}Am derived from Sellafield discharges and 1963 weapons test fallout. The lowest activity peak in this core occurs at a depth of 13-14 cm and corresponds to a ^{210}Pb CRS model age of between 1952 and 1957. This may well represent the time period during which initial deposition of Sellafield derived ^{241}Pu occurred on the marsh surface at Loch Creran. The next peak in ^{241}Am activity does correspond exactly with the 1963 peak in ^{137}Cs attributed to weapons test fallout and this therefore represents the signature of this artificial radionuclide derived from ^{241}Pu in-growth associated with above-ground nuclear testing.As such, the sediment accretion and dry mass accumulation rates are the same as those calculated for ^{137}Cs down-core activity.

Above this depth/age increment the two activity peaks occurring between 5 and 8 cm and 4-5 cm are likely to be the result of continued in-growth of ^{241}Am derived from Sellafield as no ^{241}Pu or ^{241}Am was associated with the Chernobyl accident in 1986. Importantly the presence of detectable levels of ^{241}Am activity within the near-surface of this core sequence does indicate the influence of marine derived input of this radionuclide to the upper marsh at Loch Creran.

5.9: Loch Etive

5.9.1: ^{210}Pb data

Within the down-core profile of the marsh sequence from the head of Loch Etive ^{210}Pb total activity declines steadily with depth in a near-exponential curve (Figure 5.17) reaching background (supported) levels of activity at depths below 30 cm (Figure 5.18). Comparison of the ^{210}Pb total activity with the organic content (using LOI 550°C as a proxy measurement) reveals no significant association of ^{210}Pb with the organic fraction in the sediment (r^2 value of 0.023, Figure 5.17). This is confirmed by the critical value for the significance at 95% confidence levels (n=15; df=13) of 0.514.

The ln ^{210}Pb unsupported activity versus depth profile yields an r^2 value of 0.70 (0.05 level of significance) for the entire core depth sampled. The mean sediment accretion rate

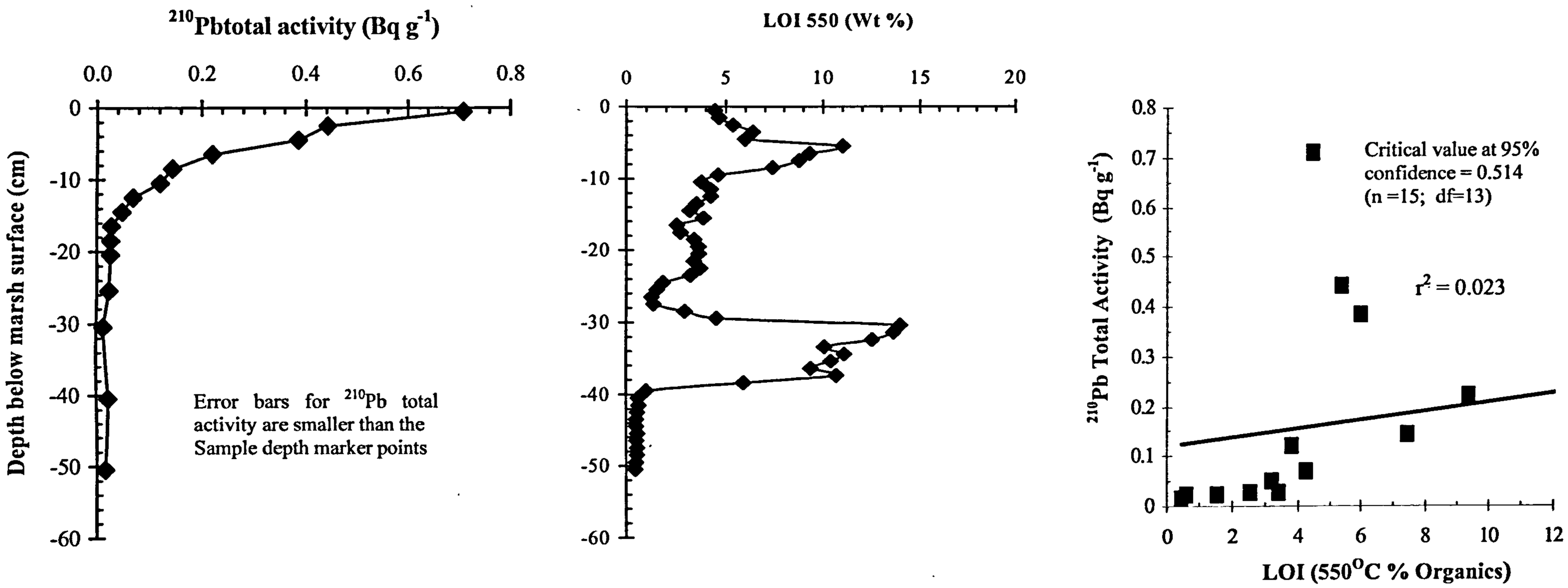

Figure 5.17: ^{210}Pb total activity and loss on ignition (LOI 550^{O}C) profiles and correlation plot of ^{210}Pb activity vs. LOI for the marsh core from the head of Loch Etive, mainland Argyll, Western Scotland.

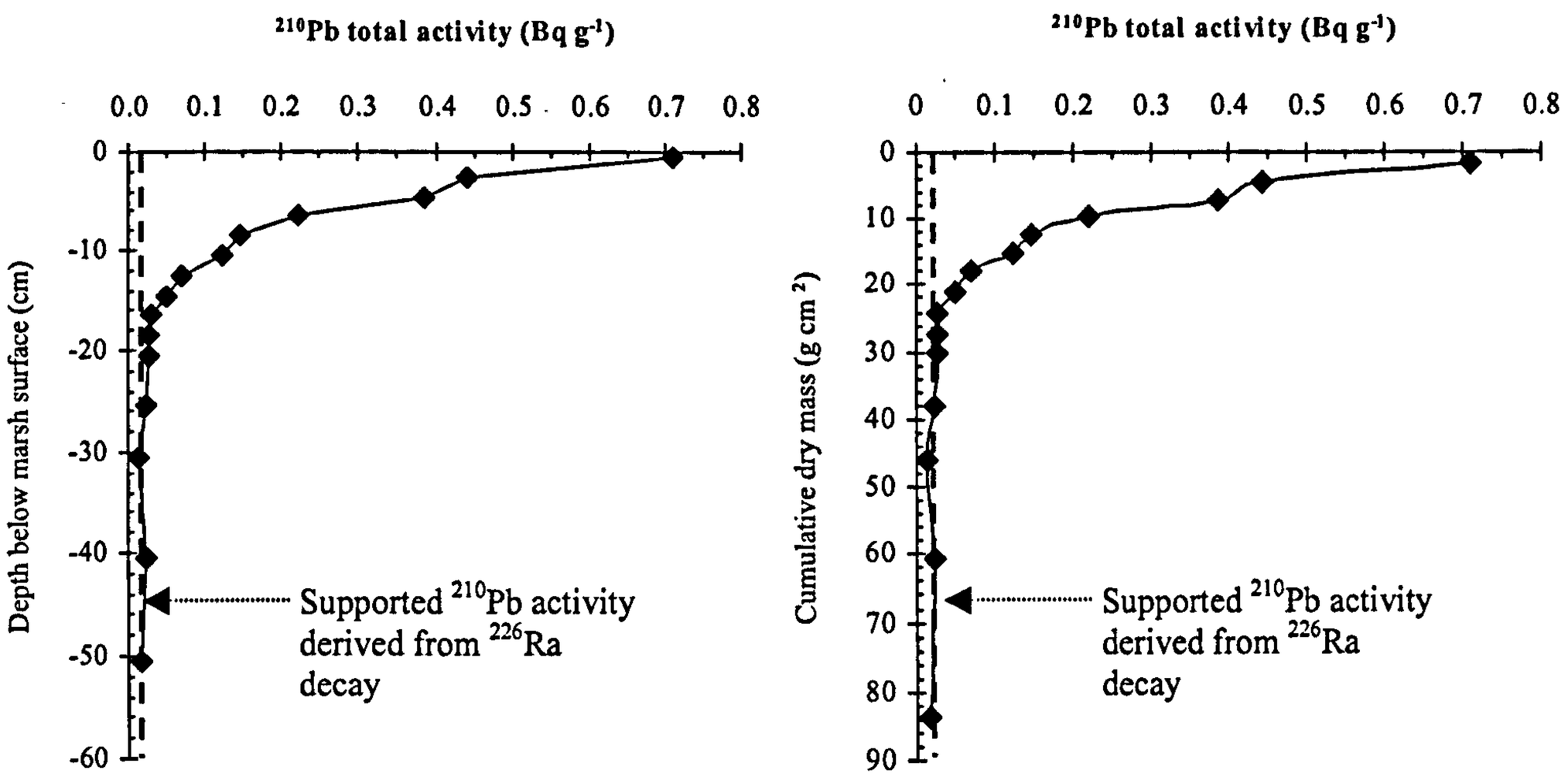

Figure 5.18: ^{210}Pb total activity plotted against sediment depth (cm) and cumulative dry mass (g cm^{-2}) for the marsh core from Loch Etive.

calculated from the constant flux:constant sedimentation or ('simple model') gives a figure of 4.0 mm yr^{-1} (2 σ range 2.9 – 6.6 m a^{-1}, Figure 5.19). The CIC model reveals an accretion rate of 1.9 mm yr^{-1} down to a depth of 26 cm below which calculated dates become highly spurious as they indicate ages below the reliable limit of the ^{210}Pb method. The CRS model calculated accretion rates for the same age/depth interval yield a value of 2.2 mm yr^{-1} indicating the good overall agreement between the two model derived accretion rates for this defined depth. Below this point the CRS dates are more reliable and give improved estimates of sediment accretion within the lower section of this core with an average figure of 4.9 mm yr^{-1} for the age increment between 1872 AD (± 4.9 yrs) to 1923 AD (± 4.4 yrs) and depth 25 – 51 cm. The cumulative dry mass vs. age plot (Figure 5.20) also highlights the similarity in the sediment accumulation rates derived from the two models. CIC model derived values of 0.21 g cm yr^{-1} and CRS derived values of 0.28 g cm a^{-1} are calculated for the accumulated dry mass between 4.4 and 21 g cm^2.

The CRS model is further utilized to calculate incremental ages and sediment accretion rates for the entire core profile and this is shown in Table 5.4. This reveals distinct periods where variable rates of sediment accretion have occurred during the development of this core sequence. Notable in the core is the very rapid (possibly instantaneous) deposition revealed by the upper and lower dates at depths corresponding to the lower and upper contact of the dark black silty sand unit shown in detail in chapter four. The calculated CRS model derived dates for these two contacts are 84.2 and 85.7 years giving an age of 1914 AD (± 4.8 years). Rates of accretion then decline at distinct incremental periods to a depth (up-core) of 10-11 cm and age of 1954 (± 2 yrs) from which point accretion rates average between 1.5 – 2.0 mm yr^{-1} until 1995 (± 0.1 yrs).

In the near surface the CRS model reveals an increased rate in sedimentation over the most recent period of the last five years with a calculated average figure of 3.7 mm yr^{-1}. This increase is also apparent in the cumulative dry mass vs. age plot which indicates sediment mass accumulation of 1.1 g cm a^{-1} over the period corresponding to 0 - 4.4 g cm^2 (Figure 5.20).

5.9.2: ^{137}Cs profiles

The down-core profile of ^{137}Cs activity for the Loch Etive marsh core is shown in Figure 5.21. Two distinct activity peaks are immediately obvious situated at 8-9 cm depth (cumulative dry mass of 12.2 g cm^2) and 3 – 4 cm depth (cumulative dry mass of 5.8 g cm^2).

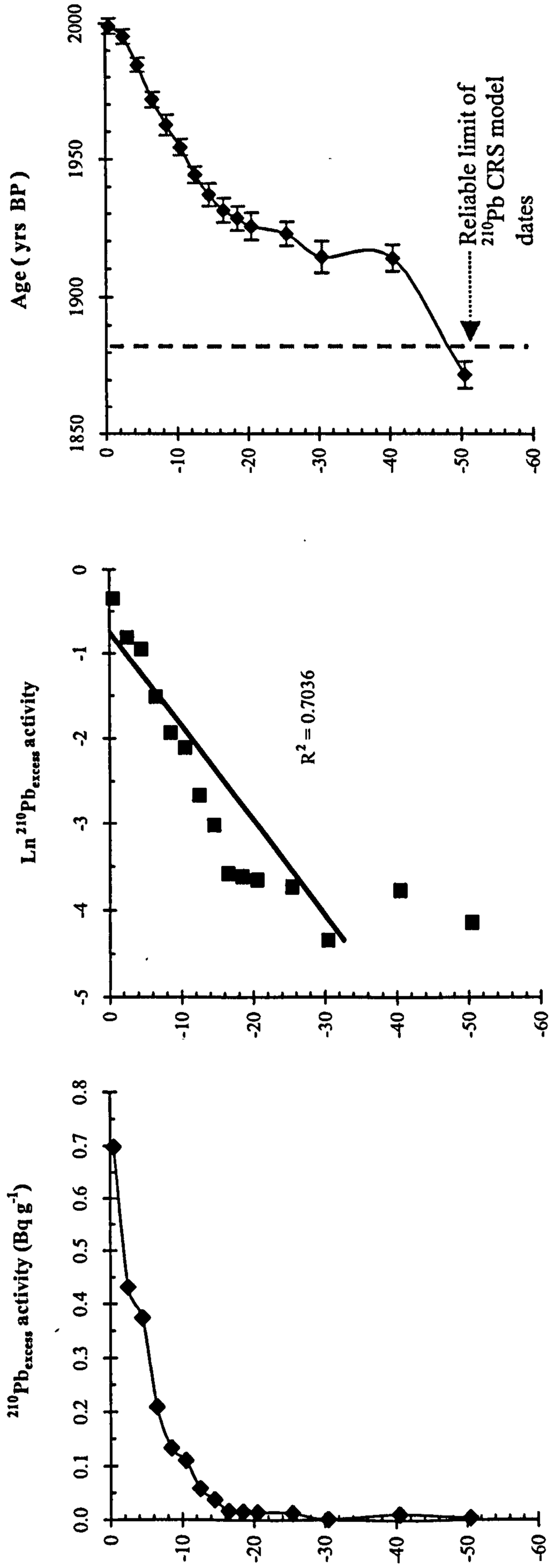

Figure 5.19: (a) ^{210}Pb unsupported activity (b) Natural Log of unsupported ^{210}Pb activity versus depth and (c) ^{210}Pb constant flux (CRS) model derived age/depth profile for the marsh core from the head of Loch Etive mainland Argyll.

Depth (cm)	Age (years BP)		Age (years AD)	Sediment Accretion Rate (mm a^{-1})
0.5	0	(+/- 0.1)	1999	3.7 (3.6 – 3.8)
2.5	4	(3.73 – 3.94)	1995	2.0 (1.9 – 2.1)
4.5	14	(14.07 – 14.82)	1985	1.5 (1.4 – 1.6)
6.5	27	(26.57 – 28.08)	1972	2.2 (2.1 – 2.2)
8.5	37	(35.10 – 37.81)	1963 (1961 – 1965)	2.2 (2.1 – 2.2)
10.5	45	(43.32 – 45.98)	1954 (1952 – 1956)	2.0 (1.9 – 2.1)
12.5	55	(52.88 – 56.20)	1944 (1942 – 1946)	2.9 (2.8 – 3.0)
14.5	61	(59.44 – 64.56)	1937 (1934 – 1940)	3.3 (3.2 – 3.4)
16.5	68	(64.68 – 70.75)	1931 (1928 – 1934)	6.6 (6.3 – 6.9)
18.5	71	(67.50 – 73.81)	1928 (1925 – 1931)	6.6 (6.3 – 6.9)
20.5	74	(69.89 – 77.32)	1925 (1921 – 1929)	25.0 (23.7 – 26.3)
25.5	76	(73.03 – 79.82)	1923 (1920 – 1926)	5.5 (5.3 – 5.7)
30.5	85	(79.97 – 89.46)	1914 (1910 – 1919)	110.0 (103.8 – 116.2)
40.5	85	(81.20 – 89.33)	1914 (1909 – 1918)	2.5 (2.4 – 2.6)
50.5	127	(120.80 – 133.19)	1872 (1866 – 1878)	

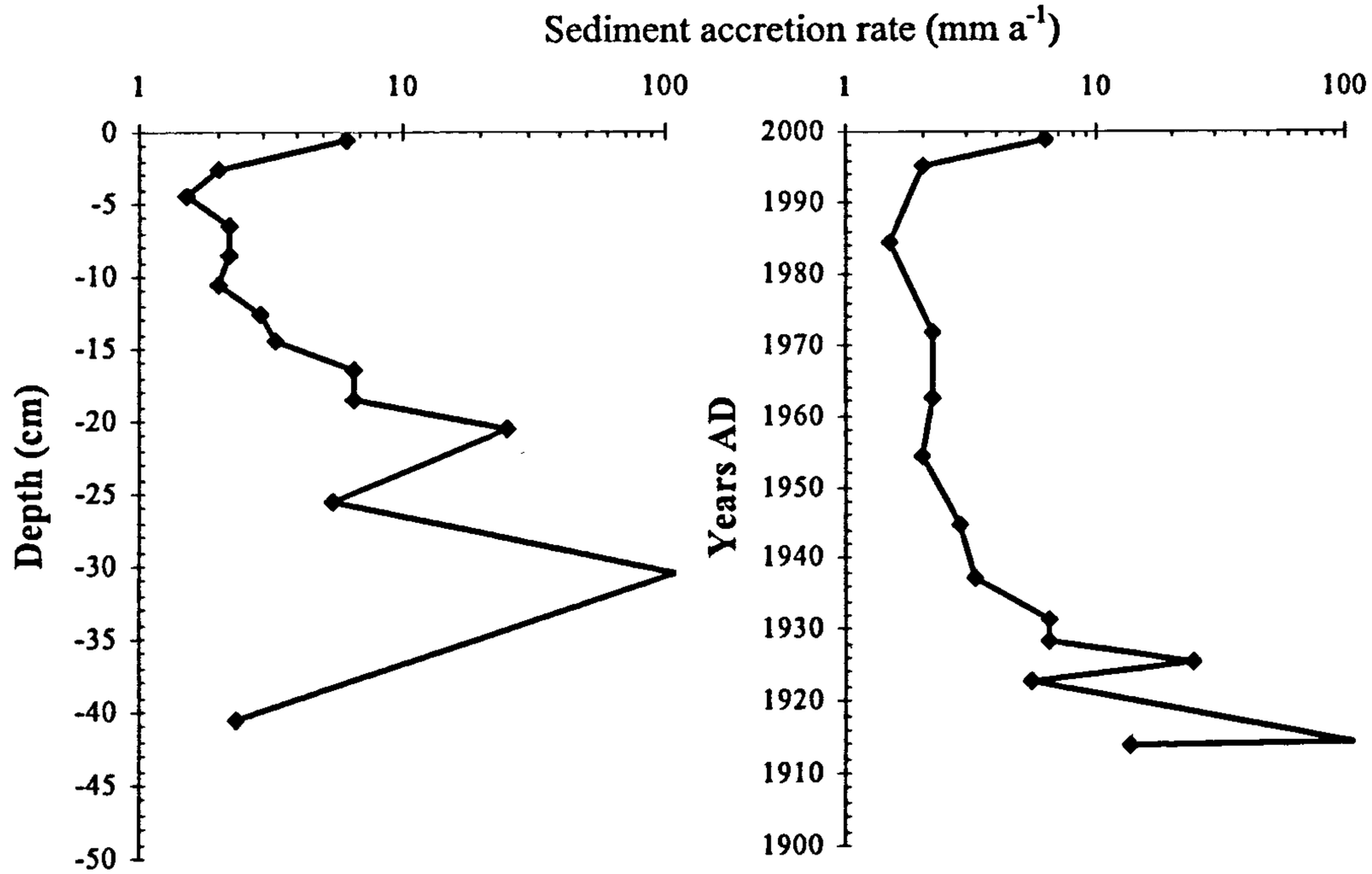

Table 5.4: ^{210}Pb CRS model derived dates and sedimentation rates for the marsh core from the head of Loch Etive (core 1) mainland Argyll. Sedimentation rates are calculated for incremental depth intervals between actual sample and the one previous and plotted against core depth (cm) and time (Years AD), note the logarithmic scale of the two plots. Figures representing age and sedimentation ranges (shown in brackets) are derived from calculated maximum and minimum measured ^{210}Pb unsupported activity and relate to the random nature of radioactive decay. Reliable limits of the CRS model dates are indicated by the gray dashed line and arrows.

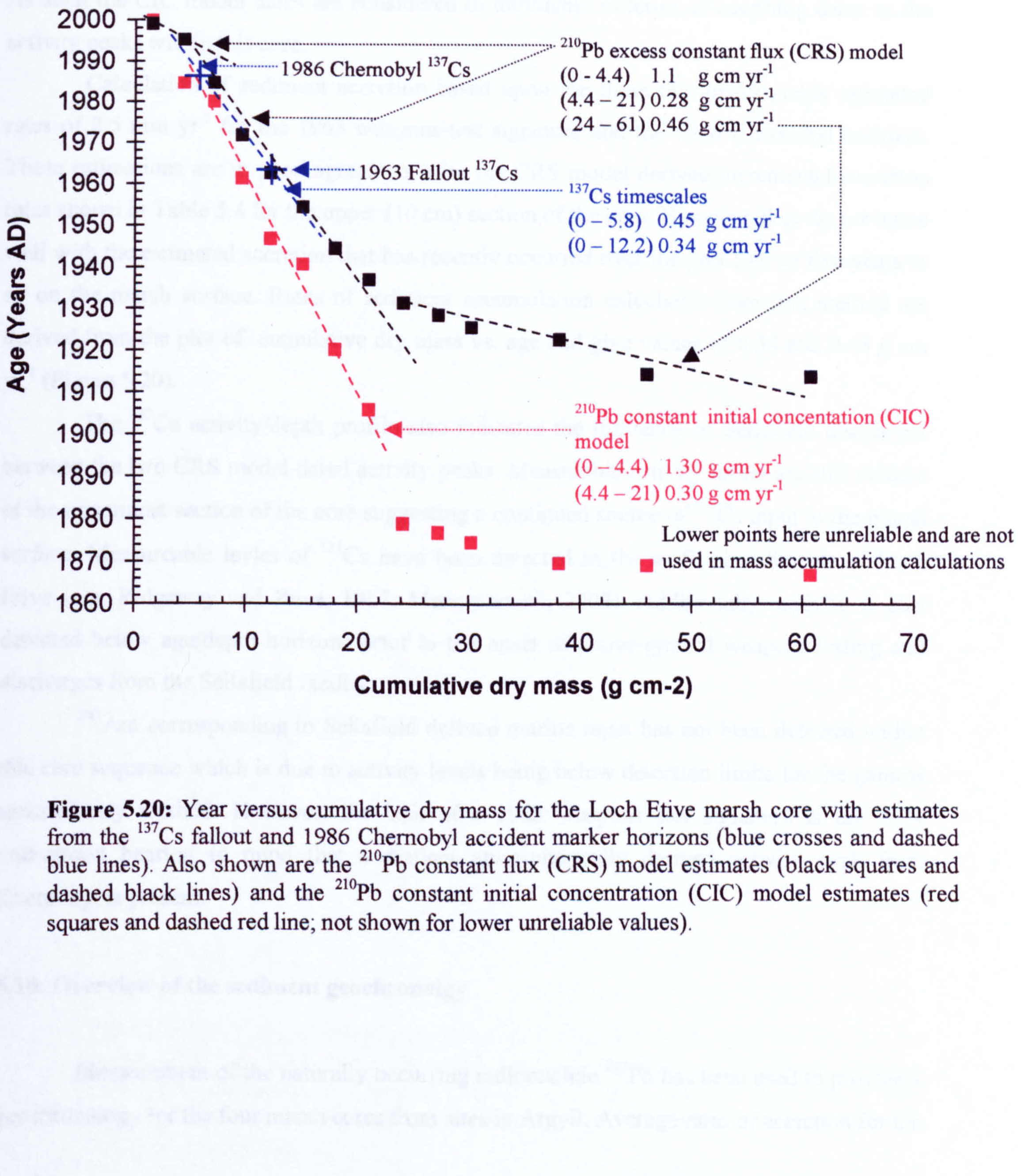

Figure 5.20: Year versus cumulative dry mass for the Loch Etive marsh core with estimates from the ^{137}Cs fallout and 1986 Chernobyl accident marker horizons (blue crosses and dashed blue lines). Also shown are the ^{210}Pb constant flux (CRS) model estimates (black squares and dashed black lines) and the ^{210}Pb constant initial concentration (CIC) model estimates (red squares and dashed red line; not shown for lower unreliable values).

These two peaks correspond extremely well with the 1963 weapons fallout signature and the 1986 Chernobyl accident based upon ^{210}Pb CRS model dates giving ages of 1963 AD (± 3.7 yrs) and 1985 AD (± 2.6 yrs) for the depth increment immediately below this peak at 4-5 cm.

The CIC model derived dates are far less precise and give age estimations of 1946 and 1979 for the lower and upper peaks respectively. These are considerably older than the CRS calculated dates and suggest activity at depths which cannot be attributed to either the onset of Sellafield discharges in 1952, pre-1963 weapons-test fallout or the 1986 Chernobyl accident. As such the CIC model dates are considered to unreliable in terms of ascribing dates to the activity peaks within this core.

Calculation of sediment accretion based upon the these two peaks yields estimated rates of 2.5 mm yr^{-1} for the 1963 weapons-test signature and the 1986 Chernobyl accident. These estimations are in good agreement with the CRS model derived incremental accretion rates shown in Table 5.4 for the upper (10 cm) section of the core. However, they do not agree well with the estimated accretion that has recently occurred over the past four to five years or so on the marsh surface. Rates of sediment accumulation calculated from this method are derived from the plot of cumulative dry mass vs. age and give values of 0.34 and 0.45 g cm yr^{-1} (Figure 5.20).

The ^{137}Cs activity/depth profile also indicates the influence of Sellafield discharges between the two CRS model dated activity peaks. Measurable activity levels are still evident in the uppermost section of the core suggesting a continued source of ^{137}Cs input to the marsh surface. Measureable levles of ^{137}Cs have been detected in the surficial sediments of Loch Etive (e.g. Ridgeway and Price, 1987; Murray *et al.*, 2003). Additionally, activity is also detected below age/depth horizons prior to the onset of above-ground weapons-testing and discharges from the Sellafield facility.

^{241}Am corresponding to Sellafield derived marine input has not been detected within this core sequence which is due to activity levels being below detection limits for the gamma spectrometry method. However, the lack of a 1963 weapons test signature is not fully understood bearing in mind that a distinct atmospherically derived activity peak from Chernobyl is present.

5.10: Overview of the sediment geochronolgy

Measurement of the naturally occurring radionuclide ^{210}Pb has been used to provide a geochronology for the four marsh cores from sites in Argyll. Average rates of accretion for the

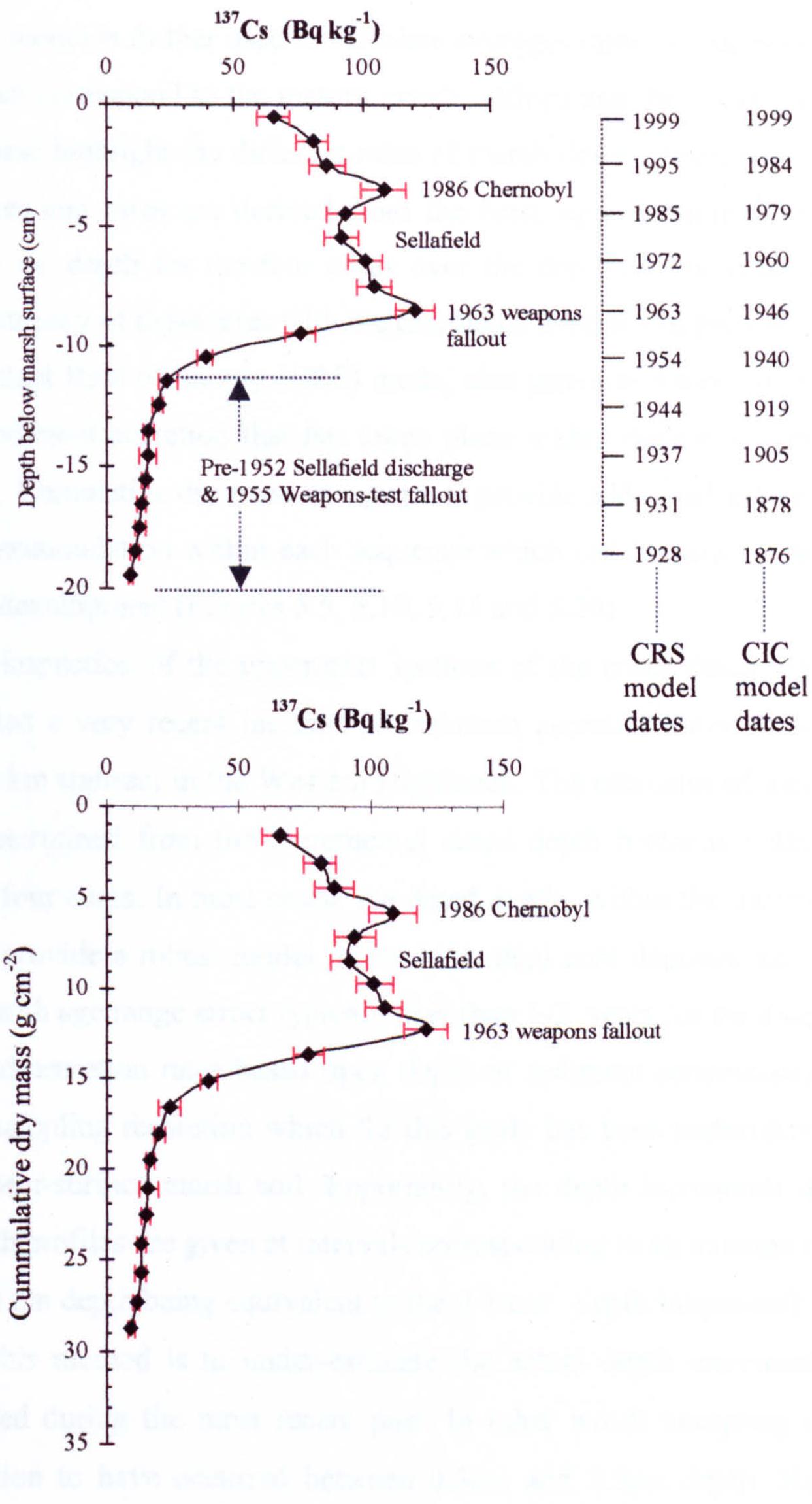

Figure 5.21: ^{137}Cs activity/depth and activity/cumulative dry mass profiles for the marsh core from Loch Etive, mainland Argyll. ^{210}Pb CRS and CIC model ages are shown for comparison. No detectable levels of ^{241}Am via gamma spectrometry were recorded within this sedimentary sequence. Error bars relate to % estimated error in activity measurement.

entire core obtained from the 'Simple model' calculations are an over-estimate of the true rates of sedimentation occurring on the mature marsh surfaces.

Rates of sediment accretion derived from the CIC and CRS models are generally in good overall agreement with slight deviation evident in the cores from Loch Don and Loch Etive.

The CRS model is further used to calculate averages rates of sediment accretion from specific depths that correspond to the mature marsh settings and the reliable capability of the ^{210}Pb method. These highlight the different rates of marsh development over the last century from the four sites and rates are derived from the least squares regression plots of Ln of $^{210}Pb_{excess}$ activity vs. depth for the four cores over the depth and time period indicated in Figure 5.22. A summary of these rates with the calculated estimations presented in Table 5.5 .

The Constant Rate of Supply (CRS) model also provides a more detailed breakdown of the variable sediment accretion that has taken place within the cores from each site (see Tables 5.1 – 5.4). Cumulative dry mass vs. age plots provide additional information regarding the rate of mass accumulation within each sequence which can be seen to vary over distinct periods of marsh development (Figures 5.5, 5.10, 5.15 and 5.20).

Detailed inspection of the uppermost sections of the cores dated via the ^{210}Pb CRS model has revealed a very recent increase in sediment accretion rates recorded in all four cores across a 70 km transect in the Western Highlands. The estimates of increased sediment deposition are determined from the incremental dated depth horizons within the sediment sequences of the four cores. In most cases, the dated depths within the sediment column can be considered to provide a robust model of the individual core depositional history over the last two decades with age range errors typically less than 1-2 years for the dated depth points.

Calculated accretion rates based upon depth of sediment accumulated over time are dependent upon sampling resolution which for this study has been undertaken at intervals of 2cm within the near-surface marsh soil. Importantly, the depth increments described in the modeled age/depth profiles are given at intervals corresponding to an average of the 1cm thick core slice (i.e. 0.5 cm depth being equivalent to the 0-1 cm depth increment). The immediate consequence of this method is to under-estimate the actual depth increment by which the marsh has accreted during the most recent past. In other words accepting the most recent period of deposition to have occurred between 0.5cm and 2.5cm depth. Hence, the actual depth increment must include the uppermost 5mm and also the lower 0.5mm with respect to the depth of sediment represented by the 1 cm thick sampling resolution. This is vitally important as the calculated activity of these 1cm thick core slices contains a proportion of the ^{210}Pb corresponding to both the upper and lower sub-increment and as such both higher and l

Core Site Location	Sediment Accumulation Rate		
	Mean ($mm\ a^{-1}$)	1σ range ($mm\ a^{-1}$)	2 σ range ($mm\ a^{-1}$)
Loch Scridain (core 1)	3.1	2.6 – 3.6	2.2 – 5.6
Loch Don (core 4)	3.4	3.2 – 3.7	3.0 – 4.0
Loch Creran (core1)	3.7	3.5 – 4.0	3.2 – 4.5
Loch Etive (core 1)	4.0	3.4 – 1.9	2.9 – 6.6

Table 5.5: Summary of the ^{210}Pb 'Simple model' derived average sediment accumulation rates for the entire marsh core sequences from Argyll Western Scotland based on the natural logarithm of ^{210}Pb excess activity vs. depth profiles for the Argyll marshes

Core Site Location	Sediment Accumulation Rate		
	Mean ($mm\ a^{-1}$)	1σ range ($mm\ a^{-1}$)	2 σ range ($mm\ a^{-1}$)
Loch Scridain (core 1 upper 19 cm) CRS age = 1847 AD (± 9 yrs) - present	1.1	1.0 – 1.2	0.9 – 1.3
Loch Don (core 4 upper 36 cm) CRS age = 1904 AD (± 4 yrs) - present	2.4	2.3 – 2.5	2.2 – 2.7
Loch Creran (core1 upper 26 cm) CRS age = 1907 AD (± 2yrs) - present	3.3	3.0 – 3.7	2.7 – 4.3
Loch Etive (core 1 upper 30cm) CRS age = 1925 AD (± 5 yrs) -present	2.2	2.1 – 2.5	1.9 – 2.8

Table 5.6: ^{210}Pb 'Simple model' derived average sediment accumulation rates for the upper sections (depth and CRS age with errorr as indicated) for the Argyll salt marsh cores derived from the least squares regression of the natural logarithm vs. depth plots shown in Figure 5.22

lower values of activity. Put more plainly, the activity is only an average of the entire 1cm slice and will contain unsupported ^{210}Pb both older and younger than the 0.5 or 2.5 specific depth interval. If the 0-1 cm depth increment is taken to include the uppermost 5mm and the 2.5cm increment includes the lower 5mm to depth of 3 cm then the total depth sub-sampled is increased from 2 to 3 cm. This has important implications for the recent rates of sediment accretion during the latest period of the last century. These are summarized in Table 5.6 below.

Core Site Location	**Age Period (years AD)**	**Sediment accretion rate (mm a^{-1})**	
		0.5 cm to 2.5 cm	Surface to 3.0 cm
Loch Scridain (core 1)	1995 - 1999	5.0	7.5
Loch Don (core 4)	1997 - 2000	6.6	10.0
Loch Creran (core 1)	1995 - 1999	5.0	7.5
Loch Etive (core 1)	1995 – 1999 1985 – 1999 (0 – 50 mm)	5.0 2.8	7.5 3.6

Table 5.6: Revised sediment accretion rates during the latter part of the last decade for the four marsh cores from re-evaluation of shallow sub-surface depth increments and ^{210}Pb unsupported activity within the specific depth horizons measured in this study.

These data indicate that during the very recent period of marsh evolution a significant increase in the rates of surface sediment accretion at all four sites has occurred. The implications of these findings are fully discussed in chapter seven of this thesis.

Measurement of the artificial radionuclide ^{137}Cs has provided a suitable method with which to estimate of sediment accretion derived from the various ^{210}Pb dating models. Conversely, the ^{210}Pb does permit identification of ^{137}Cs and ^{241}Am at depths that pre-date the onset of anthropogenic discharges. This indicates that both ^{137}Cs and ^{241}Am show evidence for mobility within the Argyll marsh sediments as reported in other studies (e.g. Evans et al., 1983; Davis *et al.*, 1984; Anderson *et al.*, 1987; Comans *et al.*, 1989; Hunt and Kershaw, 1990; Short, 1995).

In all cores an activity peak associated with 1963 weapons-test fallout signature has been determined. Similarly, an activity peak corresponding to the rapid deposition resulting from the Chernobyl accident in 1986 is superimposed upon the generally increasing activity levels associated with Sellafield discharges in all cores except that from Loch Scridain on Western Mull. Here the identification of the near surface activity maximum is more problematic and therefore uncertainty exists as to whether this is actually due to input derived from Sellafield.

Estimations of sediment accretion using the ^{137}Cs activity peaks ascribed to these dates are in good general agreement with the average rates determined via the incremental nature of the CRS model for the marsh development in the latter half of the last century. These are summarized in Table 5.7.

Dating with ^{241}Am activity profiles is more problematic in the Argyll marsh cores. A 1963 activity peak is discernable in the core from Loch Creran and therefore will yield sediment accretion rates comparable to the ^{137}Cs estimations. It is likely that the small peak in the core from Loch Scridain is associated with in-growth of ^{241}Am from ^{241}Pu and thus may represent the 1963 signature within this core. However, in the cores from Loch Don and Loch Creran ^{241}Am is detected at age/depths that correspond to periods that post-date the influence of 1963 weapons testing fallout. Detectable levels of ^{241}Am are likely to result from Sellafield ^{241}Pu discharge and subsequent in-growth to ^{241}Am. As such this does illustrate the continuing marine influence in the near- surface sediments of the sites from sites situated on the Isle of Mull and at Loch Creran. The lack of measurable ^{241}Am activity in the core from the head of Loch Etive is somewhat unexpected although previous studies have only detected extremely low values (e.g. Williams *et al.*, 1988). This is most likely to be the result of low ^{241}Am activity levels below levels of detection, the limited exchange between the anoxic upper basins of the loch and the inter-tidal environment and the differential relative mobility of ^{137}Cs and ^{241}Am radionuclides.

Importantly, the presence of ^{241}Am detected within the upper sections and surface sediments of the cores from Mull and Loch Creran does illustrate the continuing marine influence within the high (mature) marsh setting of these locations.

5.11: ^{210}Pb fluxes

Fluxes of $^{210}Pb_{excess}$ can be used to assess the reliability of the chosen models by providing a direct comparison to the concentration vs. depth distribution of elemental Pb. Furthermore, calculation of ^{210}Pb inventories and decay-corrected annual $^{210}Pb_{excess}$ fluxes can

Core Location	**Rate of Sediment accretion / accumulation**			
	1963 Weapons-test fallout		1986 Chernobyl accident	
	(mm a^{-1})	(g cm a^{-1})	(mm a^{-1})	(g cm a^{-1})
Loch Scridain (core 1)	1.8	0.17	Uncertain?	0.19
Loch Don (core 4)	2.3	0.54	2.5	0.57
Loch Creran (core 1)	2.7	0.45	3.5	0.53
Loch Etive (core 1)	2.5	0.34	2.5	0.45

Table 5.7: ^{137}Cs derived sediment accretion (mm yr^{-1}) and mass accumulation (g cm yr^{-1}) rates for the four marsh cores based upon activity peaks within the cores assigned to 1963 weapons test fallout and the deposition resulting from the 1986 Chernobyl accident.

be used to assess the affects of early diagenetic post-depositional remobilization of ^{210}Pb (Allen *et al.*, 1993; Cundy, 1994). In closed stable marsh systems the annual flux should be fairly constant if little or no remobilzation has occurred. Inventories of ^{210}Pb are also useful for inter-site comparisons where dating has been undertaken.

Fluxes are calculated by multiplying the activity at depth (z) by the dry bulk density (ρ) and sediment accretion rate using ^{137}Cs derived values. Decay-correction of ^{210}Pb activity uses the equation:

$$A = A_0 e^{-\lambda t}$$

where: A = the decay corrected activity

A0 = activity at depth (z)

λ = the radioactive decay constant of ^{210}Pb (0.03114 Bq/ yr)

t = sediment age determined from 137Cs accumulation rate divided by depth

These values are then used in the determination of decay-corrected flux calculations.

Calculated fluxes of Pb and $^{210}Pb_{excess}$ are shown in Figures 5.23-5.26. Flux of Pb to the marsh surface has been determined using the CRS model derived variable accretion rates from all cores. The apparent flux of $^{210}Pb_{excess}$ activity has been determined using the ^{137}Cs derived rates of accretion from the 1963 AD activity peak. Also shown are the decay-corrected flux vs. profiles of $^{210}Pb_{excess}$ activity.

The profiles of ^{210}Pb apparent and decay-corrected flux reveal that little correlation with Pb is evident in all cores indicating little association with elemental Pb.

Flux calculations show that the annual flux is fairly constant at each site but an underlying trend of general increase is evident in the upper sediment layers of all cores. In particular the near-surface layers do show significant flux increases in response to most recent increases in marsh sedimentation. This may provide some evidence suggesting an earlier increase in fine particulate material not immediately obvious from the sediment accumulation models. Annual fluxes and inventories of ^{210}Pb are summarized in Table 5.8 along with detail from published works for comparative purposes. These data reveal that the Argyll marshes have experienced comparable fluxes of $^{210}Pb_{excess}$ activity to other sites in particular the more macro-tidal environments of the eastern U.S.A. Additionally, ^{210}Pb inventories are in good general agreement with marsh sites investigated in the Solent region (Cundy and Croudace, 1995). Increased flux recorded in the near-surface sediments of all cores reflects the recent increase in detrital sedimentation as opposed to any early diagenetic influence.

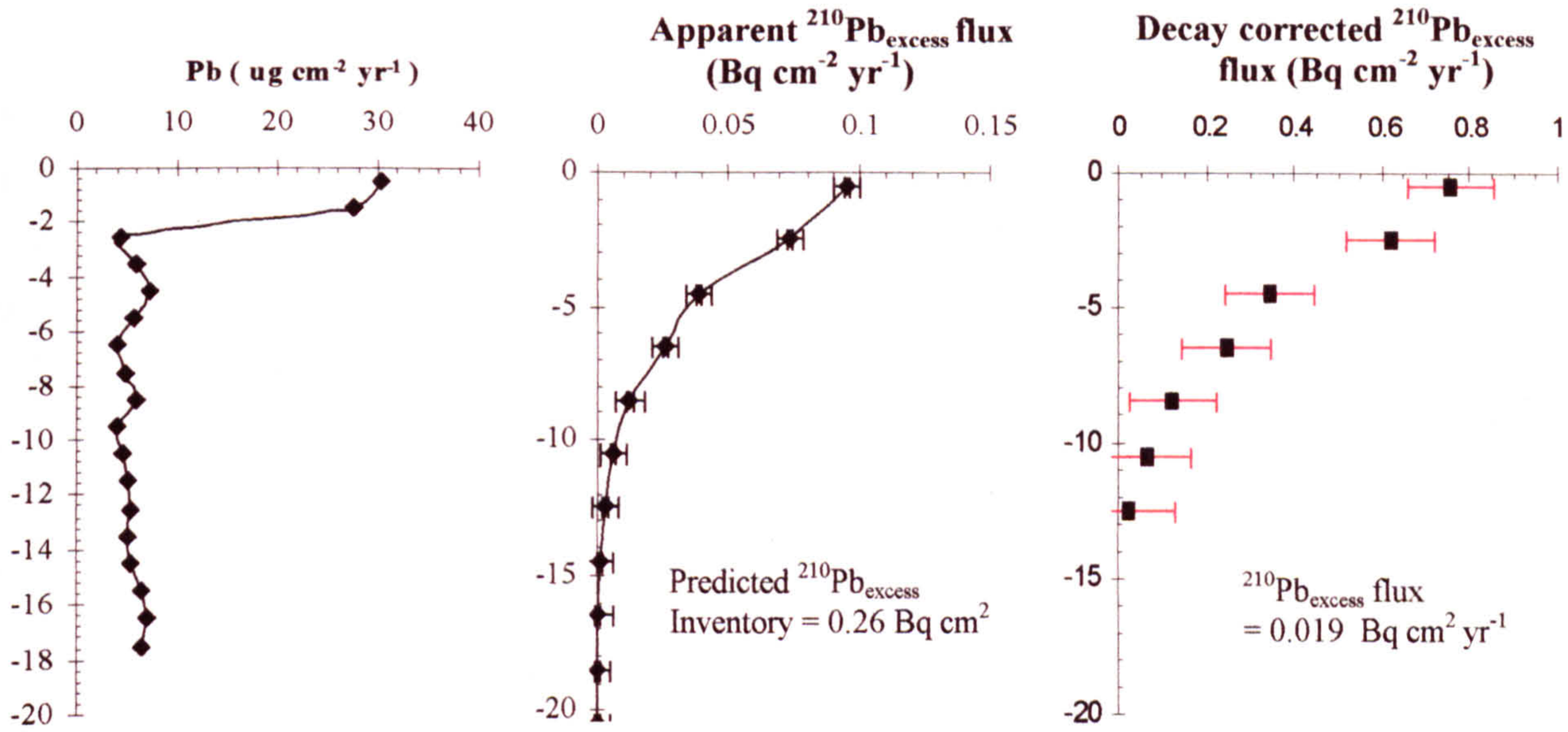

Figure 5.23: Apparent annual flux of Pb and $^{210}Pb_{excess}$ to the marsh core from Loch Scridain. Flux calculations in (a) are derived from the CRS model calculated sediment accretion rates. Calculated flux in (b) uses the ^{137}Cs derived sediment accretion rate based on the 1963 AD peak in the core. Flux in (c) uses ^{137}Cs derived sediment accretion rates which has been decay corrected to the time of sampling. Error bars in (b) and (c) assume a 1.5 Bq/kg error and are based upon uncertainty regarding the actual supported ^{210}Pb value.

$^{210}Pb_{excess}$ Flux = sample density (ρ) x concentration x sediment accretion rate.

$^{210}Pb_{excess}$ Inventory = Σ^{1}_{0} $^{210}Pb_{excess}$ activity x sediment density (ρ) x sample thickness

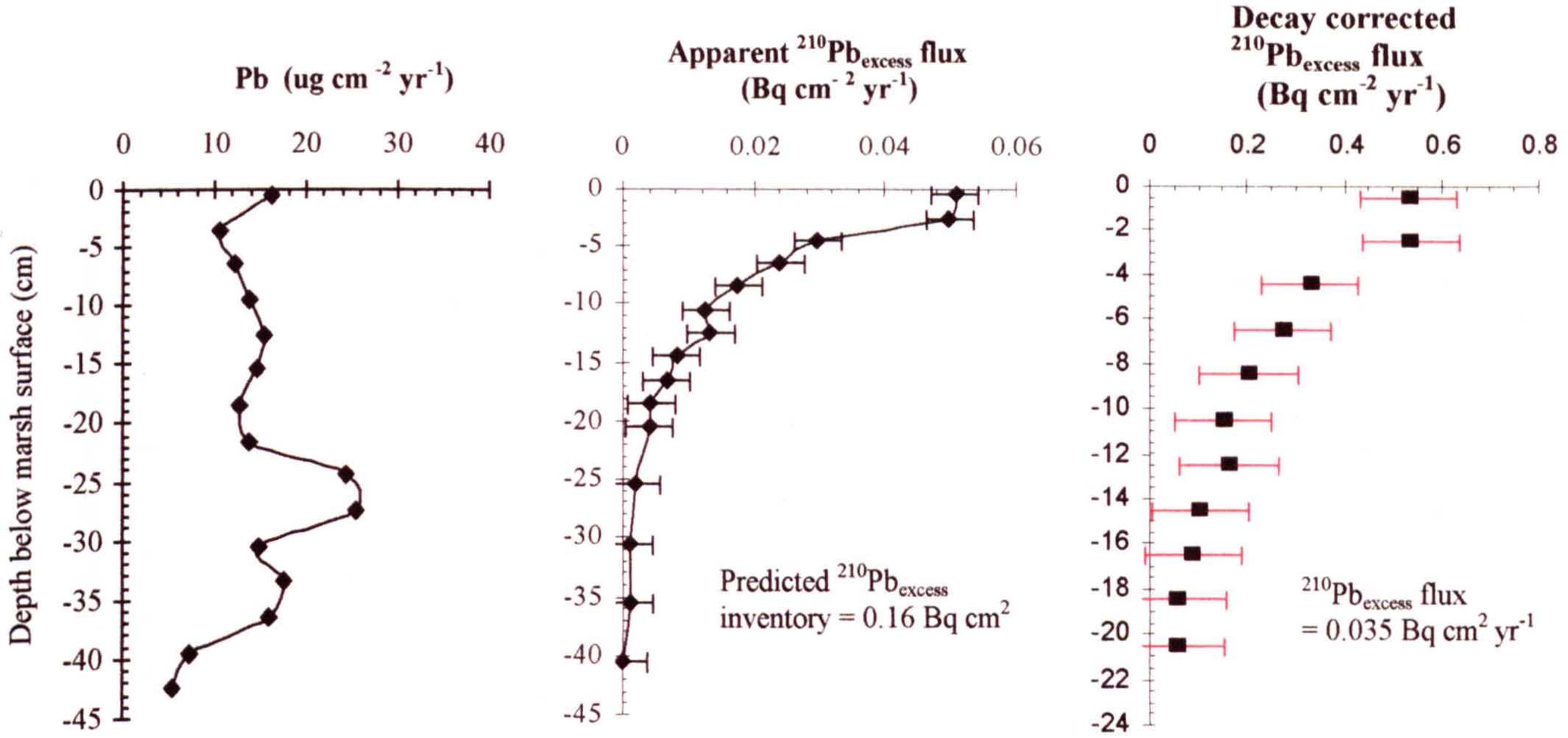

Figure 5.24: Apparent annual flux of Pb and $^{210}Pb_{excess}$ to the marsh core from Loch Don. Flux calculations in (a) are derived from the CRS model calculated sediment accretion rates. Calculated flux in (b) uses the ^{137}Cs derived sediment accretion rate based on the 1963 AD peak in the core. Flux in (c) uses ^{137}Cs derived sediment accretion rates which has been decay corrected to the time of sampling. Error bars in (b) and (c) assume a 1.5 Bq/kg error and are based upon uncertainty regarding the actual supported ^{210}Pb value.

$^{210}Pb_{excess}$ Flux = sample density (ρ) x concentration x sediment accretion rate.

$^{210}Pb_{excess}$ Inventory = Σ^{1}_{0} $^{210}Pb_{excess}$ activity x sediment density (ρ) x sample thickness

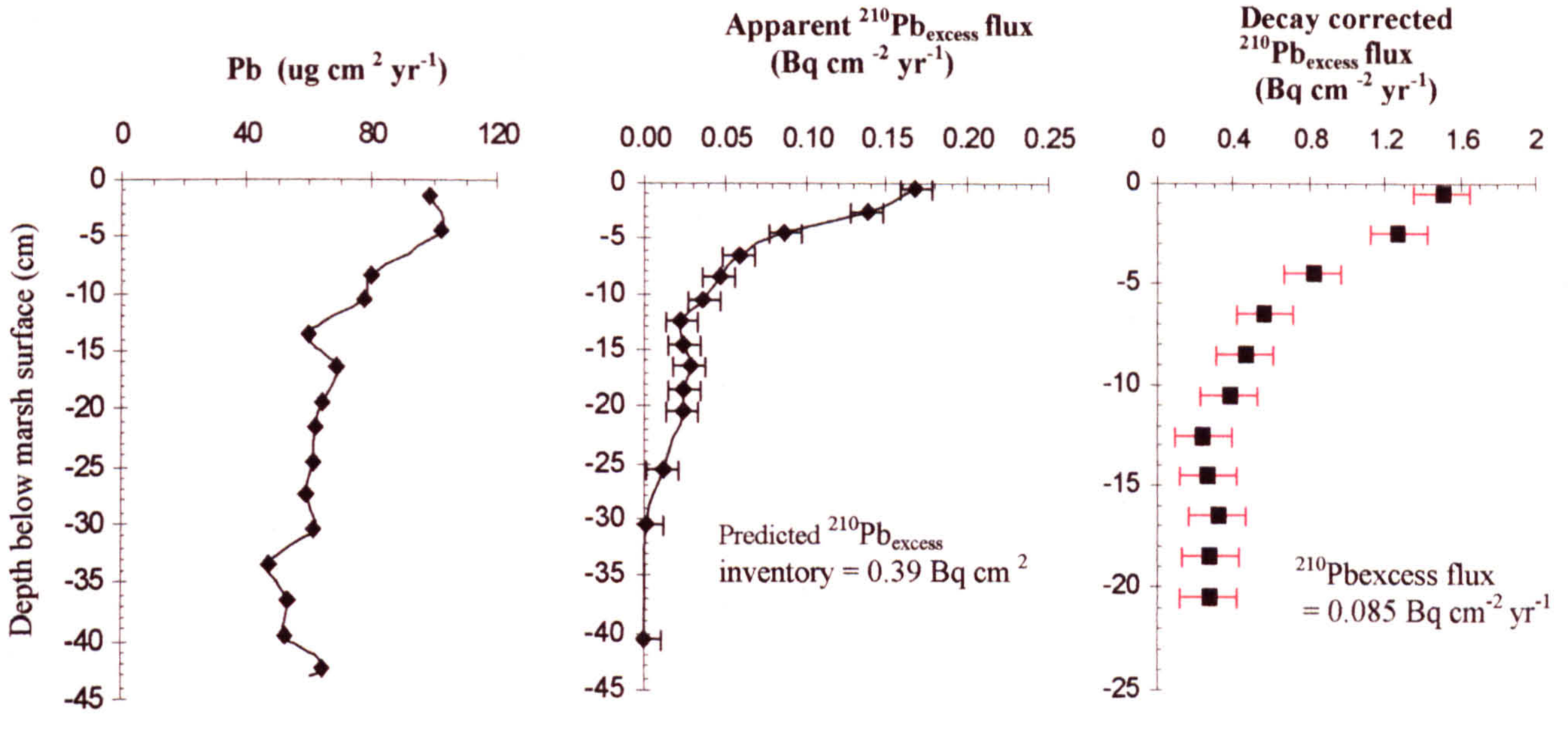

(a) (b) (c)

Figure 5.25: Apparent annual flux of Pb and $^{210}Pb_{excess}$ to the marsh core from Loch Creran. Flux calculations in (a) are derived from the CRS model calculated sediment accretion rates. Calculated flux in (b) uses the ^{137}Cs derived sediment accretion rate based on the 1963 AD peak in the core. Flux in (c) uses ^{137}Cs derived sediment accretion rates which has been decay corrected to the time of sampling. Error bars in (b) and (c) assume a 1.5 Bq/kg error and are based upon uncertainty regarding the actual supported ^{210}Pb value.

$^{210}Pb_{excess}$ Flux = sample density (ρ) x concentration x sediment accretion rate.

$^{210}Pb_{excess}$ Inventory = Σ^{1}_{0} $^{210}Pb_{excess}$ activity x sediment density (ρ) x sample thickness

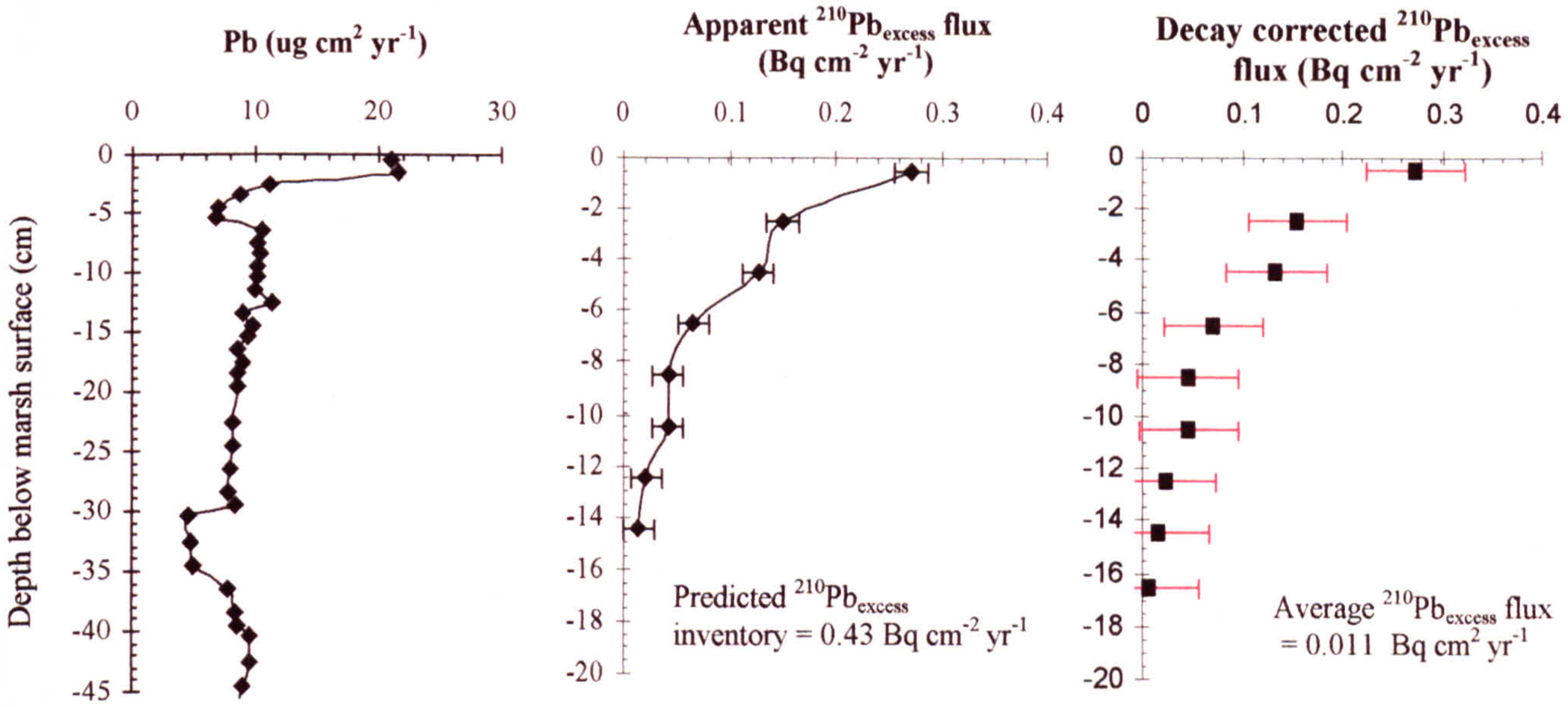

(a) (b) (c)

Figure 5.26: Apparent annual flux of Pb and $^{210}Pb_{excess}$ to the marsh core from Loch Etive. Flux calculations in (a) are derived from the CRS model calculated sediment accretion rates. Calculated flux in (b) uses the ^{137}Cs derived sediment accretion rate based on the 1963 AD peak in the core. Flux in (c) uses ^{137}Cs sedimentation rates and decay corrected ^{210}Pb activity to the time of sampling. Error bars in (b) & (c) assume a 1.5 Bq/kg error equivalent to ~10% of the calculated flux values in (a) and are based upon uncertainty regarding the actual supported ^{210}Pb activity at depth at depth.

$^{210}Pb_{excess}$ Flux = sample density (ρ) x concentration x sediment accretion rate.

$^{210}Pb_{excess}$ Inventory = Σ^{1}_{0} $^{210}Pb_{excess}$ activity x sediment density (ρ) x sample thickness.

Core Site	$^{210}Pb_{excess}$ flux ($Bq/cm^2/yr$)	$^{210}Pb_{excess}$ inventory (Bq/cm^2)	Reference
Argyll Marshes			
Loch Scridain (western Isle of Mull)	0.011	0.43	This study
Loch Don (south-eastern Isle of Mull)	0.035	0.16	" "
Loch Creran (mainland Argyll)	0.085	0.39	" "
Loch Etive (mainland Argyll)	0.019	0.26	" "
Hamble Salt Marshes			
Core (HB2)	0.007	0.22	Cundy (1994)
Core 1	0.007	0.21	Cundy & Croudace (1995)
Core 2	0.012	0.41	" "
Core 3	0.014	0.45	" "
Core 4	< 0.001	0.03	" "
Core 5	0.011	0.32	" "
Core 6	0.003	0.10	" "
Core 7	0.011	0.35	" "
^{210}Pb in rainfall (western Europe)	0.010	-	Appleby & Oldfield (1992)
UK Soils and salt marshes	0.020	0.50	Appleby & Oldfield (1992)
Lowland England lake sediments	0.010	0.30	Appleby & Oldfield (1992)
Upper Chesapeake Bay, USA	0.030	1.10	Helz *et al.* (1985)
Potomac Estuary, USA	0.160	Up to 5.5	Oldfield *et al*, (1989).

Table 5.8: Calculated $^{210}Pb_{excess}$ fluxes and inventories for the Argyll salt marshes with values from other sites included for comparison.

5.12: ^{137}Cs Inventories

Inventories of radionuclide activity beneath a unit surface area can calculated via the integrated sum of activity, sample density and sample thickness (Table 5.9). Calculated inventories therefore provide a means of estimating the total activity in a given core depth.
In marsh sediments this activity (inventory) will be a product of the differential mechanisms controlling the supply and removal of ^{137}Cs from the inter-tidal environment. A number of processes therefore influence the activity at any given time present within the sediment sequence. These include:

- Direct atmospheric deposition (e.g. weapons testing & the Chernobyl accident).
- Deposition of labelled particles from marine and fluvial sources.
- Loss of radioactivity through radioactive decay of the Cs isotope.
- Removal of eroded particulate matter with which ^{137}Cs has become associated.
- Molecular diffusion out of the sediment prism into sediment pore waters and the surrounding water column over the tidal period.

The marshes in western Scotland preserve a record of atmospheric deposition resulting from known periods of atmospheric fallout (weapons testing & Chernobyl). This record of deposition will have been enhanced by marine inputs derived from Sellafield throughout the period of marsh development at these sites. Direct comparison with estimated inventories of cumulative atmospheric deposition (e.g. Playford *et al.*, 1992) are, therefore, highly problematic and unrealistic given the complex depositional history resulting from the combination of the different sources of ^{137}Cs contained in the Argyll marshes.

The detection of Cs at depths pre-dating known periods of atmospheric and marine inputs indicates that some remobilization of the Cs isotope has taken place. This coupled with radioactive decay represents a potential loss from the inventory (depth) for which calculations have been obtained. Continued supply of ^{137}Cs from labelled particles derived from marine re-working of the marsh systems and fluvial input of radioactivity derived from Chernobyl are likely to continue to influence the overall inventories at each site. The recent increases in rates of sediment accumulation recorded at each site suggest that remobilization of eroded and labelled marine particles may represent a significant influence on ^{137}Cs recycling in these marshes. As such, in dynamic coastal systems influenced by coastal forcing mechanisms inventories only provide at point in time estimation of core ^{137}Cs activity.

PAGE
MISSING
IN
ORIGINAL

Chapter Six

EARLY DIAGENESIS AND REDOX ZONATION IN THE ARGYLL MARSHES

6.1: Introduction

Major element geochemistry determined from x-r-f analysis of post 950°C LOI samples fused glass beads is now used to describe the largely mineralogenic composition and variability therein of the marsh cores from Argyll. The elements used for this assessment are associated with the inert lattice-bound phase of sedimentary minerals and are, therefore, useful indicators of changes in sedimentary material recorded in the down-core element abundance/depth profiles (Shotyk *et al.*, 1990). An overview of the trace element composition is also presented from which further analysis is undertaken regarding the marsh geochemistry.

However, the geochemistry of saltmarsh environments is highly complex and not simply constrained by the minerogenic and organogenic input to marsh soils. Other physio-chemical processes occur as a consequence of the interaction between sediment constituents (e.g. Fe, Mn and S), organic matter and early-diagenetic post-depositional chemical reactions. The extent of these processes are highly influenced by the alternating oxidizing and reducing conditions resulting from the regular watering and de-watering that takes place over the tidal cycle. This increases the height of the water table during tidal inundation creating anoxic conditions (Williams *et al.*, 1994) and promotes a gradual return to more oxic conditions following the ebb phase of the tide (Chapter Two). In mature (high) marsh environments diurnal flooding of the marsh surface is only significant during the spring tide phase of the monthly tidal cycle when the marsh is inundated for a limited period in comparison to the low marsh/mudflat. The period during which mature marsh settings are exposed to the atmosphere is therefore longer and likely to provide the mechanism for a sustained period of more oxic conditions within the upper marsh section of the cores.

The distribution of ^{210}Pb and artificial radionuclides (^{137}Cs and ^{241}Am) within marsh sediments can potentially be altered by early diagenetic post-depositional reactions. Evans *et al* (1983), have suggested that in the case of ^{137}Cs, the strong association with the clay fraction and the fact that this isotope has only one oxidation state results in a reduced likleyhood of this anthropogenic isotope being oxidized or reduced. In this study, progressively irreversible sorption of ^{137}Cs over time has occurred within the clay inter-lattice sites as a result of competition and replacement of caesium cations by NH_4^+ ions at the surface and edge sites of clay minerals. Such behaviour has also been described by Comans and Hockley (1992).

The environmental behaviour of ^{241}Am is largely dominated by the formation of strong complexation with oxygen containing ligands (oxides, hydroxides, phosphates, carbonates and sulphates) and fluoride (Dyer, 2001). ^{241}Am has a low affinity for sulphide and chloride ions and is trivalent under both reducing and oxidising conditions. Some studies have suggested that ^{241}Am is not likely to be significantly remobilized in marsh sediments (e.g. Allard *et al.*, 1984; Morris, 2002). However, significant association between ^{241}Am and Fe and Mn oxyhydroxides has been documented which may provide a mechanism by which remobilization of ^{241}Am can occur as highlighted by the study of Short (1995).

The result of early diagenetic processes can lead to significant post-burial redistribution in marsh settings where a strong redox-cline is identified. If this has occurred then the reliability of the established geochronology may be seriously compromised (Ridgway and Price, 1987; Comans *et al.*, 1989: Benoit and Hemond, 1991; Cundy *et al.*, 1996). As a consequence of this possibility it is of great importance to assess whether such processes have influenced the down-core depositional record of radionuclide distributions used for geochronological control. This can be achieved by identification of the redox driven zonation within the marsh cores and assessment of any significant redistribution of redox-sensitive elements within specific depth horizons that are shown to influence the behaviour of radionuclides.

6.2: Fe, Mn and Sulphur geochemistry.

The bio-geochemical cycling of iron, manganese and sulphur within saltmarsh sediments involves a highly complex series of geochemical post-depositional reactions with both the inorganic and organic fraction of the sediment matrix. Such reactions are dependent upon the differential redox conditions prevalent within the sediment column. These result in the dissolution and precipitation of these elements within the oxidized and reduced sections of a core arising also from the sequential utilization of different chemical species during the decomposition of organic material (reviewed in Chapter Two of this thesis). The distribution of these major elements throughout marsh sediment sequences can be used to provide an initial assessment of the redox zonation based upon an understanding of the geochemical processes that govern their post-depositional behaviour. Solid phase Fe, Mn and S have been determined on fused beads by x-r-f analysis and inspection of the down-core concentrations of these elements can be useful in determining the broader redox-zonation in relation to the core stratigraphy.

Further detail is provided from the distribution of certain redox-sensitive trace elements, which help to further constrain redox zonation in the Argyll marshes.

6.3: Redox zonation and early diagenesis in the Loch Scridain marsh core

6.3.1: Iron distribution

Fe distribution within the core from Loch Scridain (Figure 6.1) shows enrichment in the near-surface layers of the sediment prism at a depth of 2-3 cm and 14-15 cm with values up to 12.8 wt %. This corresponds broadly to an the upper section of the LOI profile where multiple peaks in organic carbon content occur within the section of the sediment prism which contains surface vegetation and visible root structures at shallow depths. These elevated levels of Fe are likely to be the result of the burial of oxidised Fe minerals deposited on the marsh surface andthe formation of authigenic ferric oxyhydroxides caused by upward diffusion leading to subsequent oxidation of Fe^{2+} within the oxic/post oxic sediments. Variation in mineralogy is unlikely to have influenced the formation of these peaks due to a lack of coincident variation in the Al and K profiles over the same depth interval.

The colour of the upper sediment prism is dark/brown black and inspection of the core does not reveal the presence of significant orange Fe-rich concretions which have been observed within other studies of marsh sediments (Boulegue *et al.*, 1982; Luther *et al.*, 1982; Cundy and Croudace, 1995; Lewis, 1997; Dyer *et al.*, 2002). Hence, the precipitation of ferric Fe coatings within the sediment of this core is inferred from the wt % content but cannot be identified visually in tandem with the core log. Within the deeper section of the core Fe content is maintained at fairly constant values down to a depth of 29 cm. Below this depth enrichment of Fe occurs between 29 and 41 cm depth with a value of 13.7 wt % indicated by a distinct peak at 35-36 cm. This peak is mirrored in the Fe/Al depth profile (Figure 6.1). The weak correlation of Fe with Al ($r^2 = 0.25$, Figure 6.2) indicates that early diagenetic processes are a more significant factor contolling the distribution in the Loch Scridain core than changes in sediment composition.

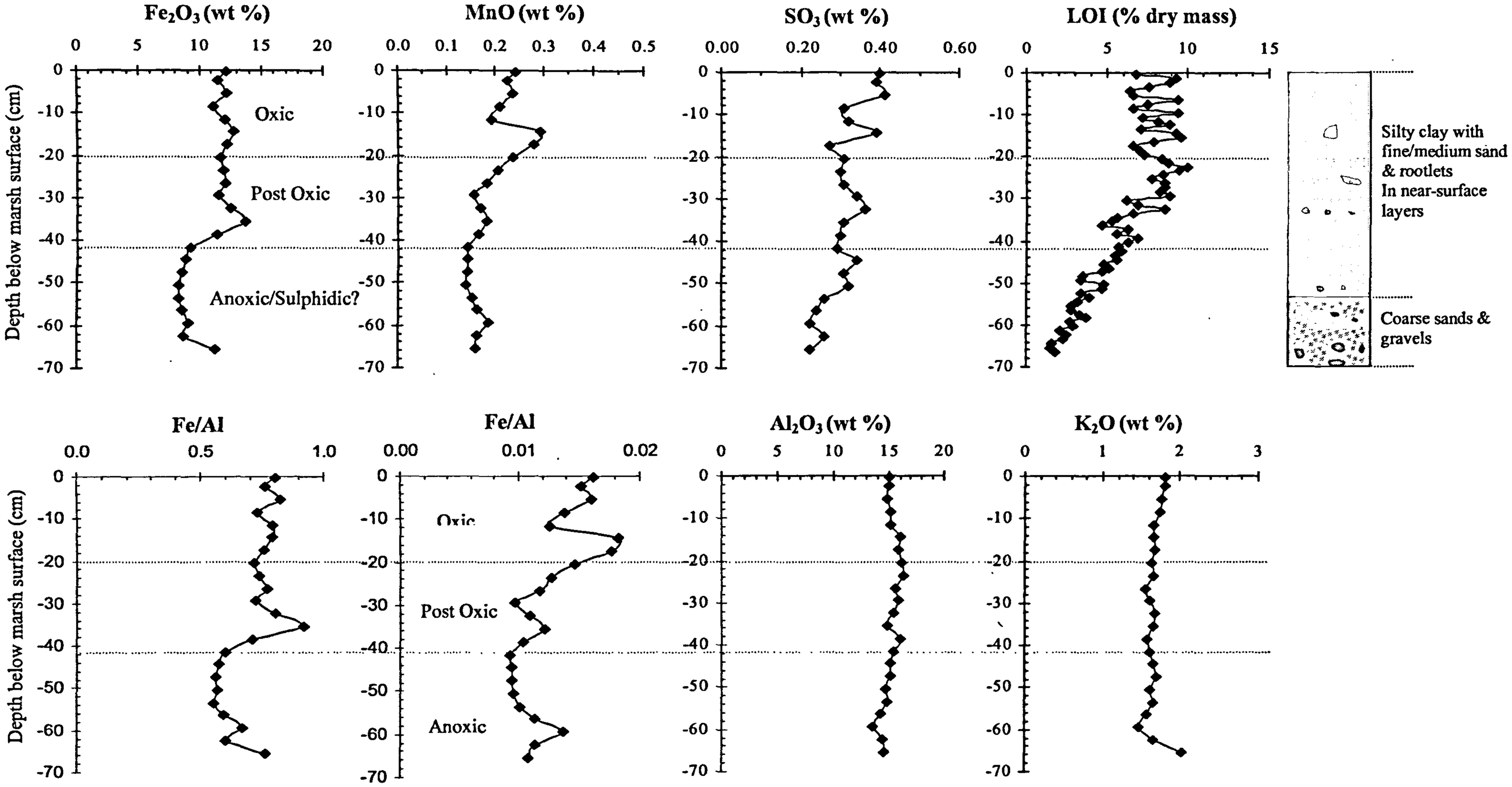

Figure 6.1: Solid-phase depth concentrations of iron, manganese and sulphur from the Loch Scridain marsh in relation to core sedimentology shown by the down-core profiles of aluminium, potassium and organic content (LOI 55O°C) and the core log reproduced from chapter four. Zones of enrichment and reduced element concentration are indicated and are used to determine redox zonation within the sediment prism (see text). Element abundances are reported as wt % according to XRF convention.

6.3.2: Manganese distribution

Mn in the Loch Scridain core shows very slight enrichment in the near-surface layers extending from 10-11 cm depth up-core to the marsh surface with a maximum value in this section of 0.24 wt % (Figure 6.1). These slightly elevated concentrations are maintained in the near-surface layers as a result of the deposition of Mn-bearing particles and the precipitation of authigenic Mn oxyhydroxides. These form from the upward diffusion of Mn^{2+} cations into the prevailing oxic conditions within the surface sedimentary layers of the core. Canfield *et al.*, (1993) have reported the significant adsorption of Mn^{2+} onto sedimentary surfaces containing fully oxidised Mn-oxides which results in reduction of the latter phase (Lewis, 1997). At depths below this surficial section of the core significant enrichment of Mn occurs at the depth increment of 14-16 cm. This is also mirrored in the Mn/Al profile (Figure 6.1). Below this depth depletion of Mn occurs down to 29-30 cm from which point a relatively lower zone of enrichment between 29-41 cm culminates in a small peak in Mn at 35-36 cm (0.18 wt %).

The weak correlation of Mn with Al (r^2 = 0.12; Figure 6.2) also indicates that the distribution of Mn within the core is not primarily related to a grain-size or concentration effect resulting from changes in sediment composition. Below this zone of enrichment Mn values are maintained at relatively low values (Figure 6.1). The small peak indicating enrichment at a depth of 59-60 cm (0.19 wt %) is co-incident with a small peak in Fe (9.1 wt %). This may be due to enrichment of reduced species of Fe and Mn but may in part be an artifact of sediment grinding performed on the coarser material present at this depth and not due to specific diagenetic processes.

6.3.3: Sulphur distribution

Sulphur distribution is fairly uniform throughout the Loch Scridain core ranging from 0.22 – 0.40 wt % over the entire up-core profile (Figure 6.1). S is relatively enriched within the upper decimetre. Similar surface enrichment has been noted in the marshes of the Scheldt estuary (Zwolsman *et al.*, 1993) and the marshes in Southampton water (Lewis, 1997). In these studies surficial enrichment of S was attributed to deposition and subsequent loss via oxidation of sulphide-rich suspended matter from upper estuarine locations or sulphide minerals derived from

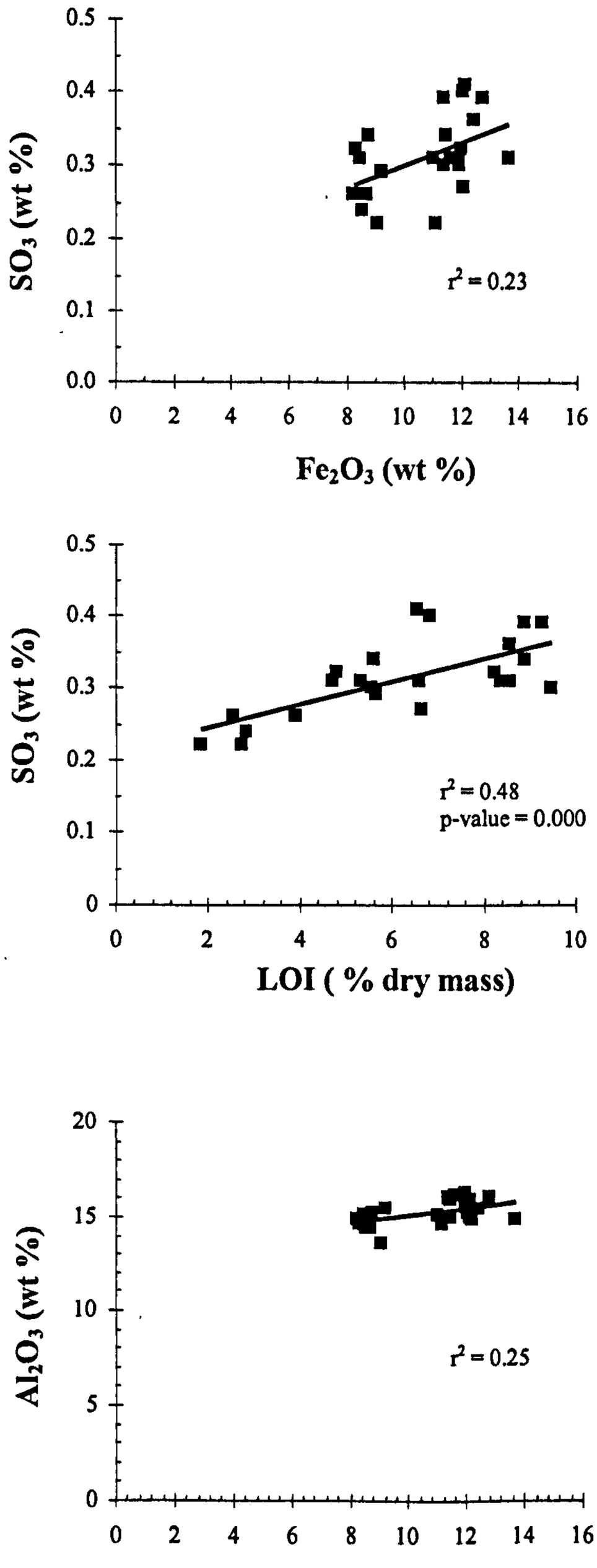

Critical value at 95% confidence level = 0.413 (n=23; df = 21)

Figure 6.2: Correlation plots of Fe vs S, LOI vs. S and Fe vs Al for the marsh core from Loch Scridain.

erosion of anoxic sediments within fronting mudflats or the marsh edge. These two processes are likely to be the mechanisms responsible for the enriched levels of S at this site. Additionally, the marsh at the head of Loch Scridain is exhibiting signs of current active erosion particularly around the seaward edge and the littoral edges of marsh creeks (discussed more fully in Chapter Seven).

Below 10 cm depth a peak in S at 14-15 cm representing enrichment of this element at values close to those within surficial depths coincides with the broader increase in Mn and an increase in LOI (Figure 6.1). Minor increases in S abundance do coincide with small peaks in loss on ignition at 33-34 cm and 42-43cm. Throughout the core profile depths of S enrichment do seem to be accompanied to some degree with iron enrichment in the uppermost 45 cm derived from the Fe and Fe/Al profiles. This may be sufficient evidence to suggest that within the core sequence some degree of iron sulphide mineralization may be responsible for the enriched layers. LOI values are generally below 10 wt % for the surface – 45 cm depth section. Elevated levels of S coincident with peaks in LOI may also result from the presence of organic sulphur compounds particularly within the root-rich layers in the upper half of this core. Dissolved sulphur species are known to react with organic sedimentary material and this can lead to enrichment of S within humic acid complexes present within inter-tidal marine environments (Ferdelman *et al.*, 1984). The correlation of S with LOI ($r^2 = 0.48$; Figure 6.2) may also indicate that organic-sulphide complexation has taken place within the core sequence. S distribution would therefore appear to be largely controlled by the distribution of organic matter. Generally the content of S in the lower sections of the core is less than that apparent in the surficial layers. Comparison with the core log and photograph indicate that the lower section of this core is lighter in colour and therefore is not consistent with intensely reduced/anoxic conditions recorded in some more clay-rich sediments (e.g. Cundy and Croudace, 1995; Thompson *et al.*, 2002).

6.3.4: Trace elemental indicators of redox conditions

The cycling of Fe and Mn oxyhydroxides tends to dominate the dissolution and precipitation post-depositional reactions that occur within salt marsh sediments. However many other elements are also known to be redox-sensitive including many trace metals and members of the halogen group of elements including I, and S. The Fe, Mn and S geochemistry shown in

Figure 6.1 does not adequately highlight the formation of a solid-phase redox-boundary with an oxic-post oxic boundary and a post-oxic-anoxic lower zonation. The S down-core profile is not conclusive as this suggests surface enrichment with no definitive indication of enriched anoxic conditions where sulphide mineralisation is likely to have occurred. The use of other redox-sensitive elements can be useful to fully identify early diagenetic zonation. Members of the halogen group of elements are useful in this respect as the ratio plots of S/Cl and I/Br indicate (Figure 6.3).

Sulphur can be seen to be enriched within the proposed anoxic conditions in the lower section of the core below 40 cm depth when expressed relative to Cl. Precipitation of iodine as iodate has occurred at the base of the post-oxic zone corresponding to the peak resulting from the precipitation of ferric Fe (and to a lesser extent Mn, Figure 6.3) at the depth interval 34-36 cm (Figure 6.1). Arsenic and vanadium are also known to be redox sensitive elements. The small peak in As at the same depth as IO^{3-} precipitation lends further support to the identification of the oxidation/reduction boundary inferred in Figure 6.1 at 41 cm depth. In oxidizing conditions the stable form of vanadium is the cation vanadate (Morford and Emerson, 1999). This is reduced in the absence of O_2 where vanadyl becomes the more prominent thermodynamically stable cation. This differential valancy state would seem to be evident within the Loch Scridain core with enrichment of V as $V(IV)O^{2+}$ in the basal anoxic conditions of the core with smaller multiple peaks of $H_2VO_4^-$ present between 10-16 cm depth indicative of oxic/post-oxic conditions (Figure 6.3).

6.3.5: Ferric Fe association with As and P

Several studies have demonstrated the association between As and P and the sedimentary recycling of Fe across oxic/post oxic boundaries in a variety of environmental settings e.g. continental shelves (Thompson *et al.*, 1995), estuaries (Maher, 1995) and freshwater lakes (Carignan and Fleet, 1981; Farmer and Lovell, 1986; Belzile and Tessier, 1990). Horizontal correlation of Fe with As and P and linear regression plots of these elements indicates that their distribution is only partly controlled by the distribution of ferric iron precipitation inferred from the surface layers down through the core to a depth of 34-37 cm (Figure 6.4). This may well result from only a fraction of the Fe being available to early diagenetic reactions. Some of the Fe will be present as detrital magnetite (A.B.Cundy pers. comm.).

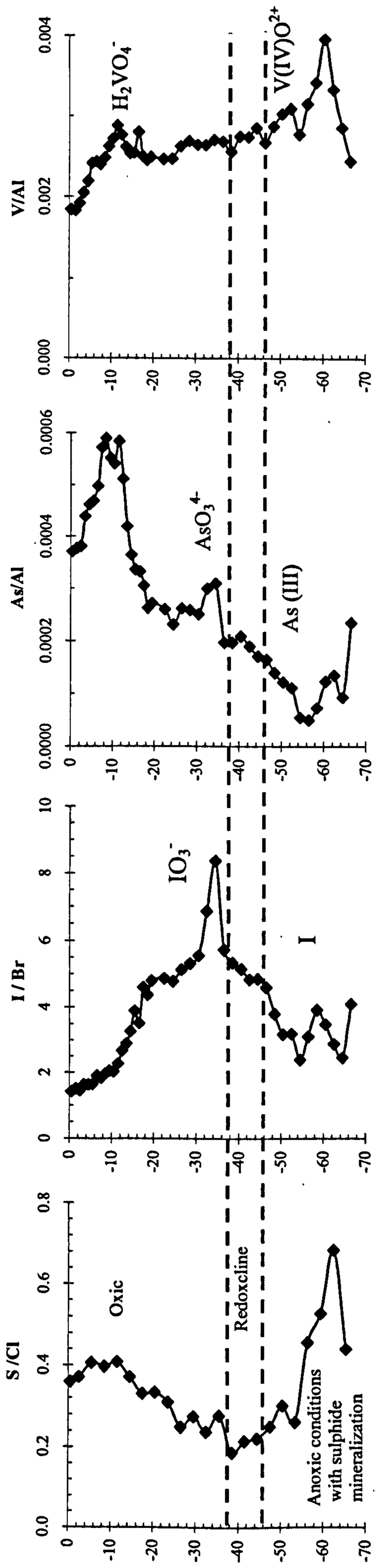

Figure 6.3: Solid-phase profiles from the Loch Scridain core of S normalized to Cl and I normalized to Br to remove the effects of seawater concentrations. Also shown are redox-sensitive trace metal profiles of As and V normalized to Al. The inferred redox boundary is indicated by the grey line (see text). Exact elemental species are inferred from the published literature and empirical studies.

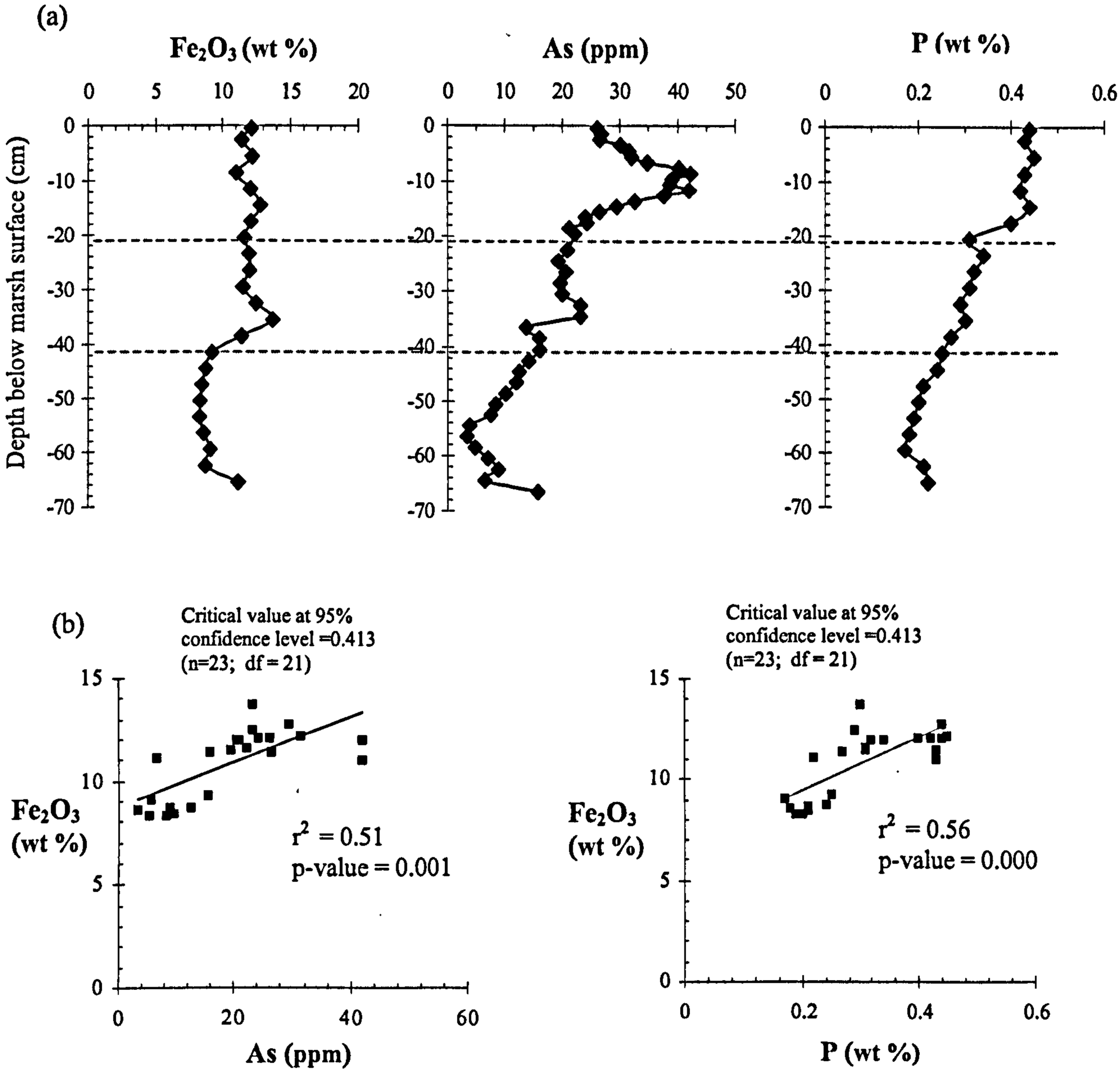

Figure 6.4: (a) Horizontal correlation between Fe, As and P in the Marsh core from Loch Scridain. (b) Correlation between Arsenic and Phosphorous with Iron.

6.4: Redox zonation and early diagenesis in the Loch Don marsh core.

6.4.1: Iron distribution

Fe distribution in the down-core profile from Loch Don indicates slight enrichment at a depth of 3 - 4 cm (9.6 wt %) below surficial layers where Fe content is slightly lower at 8.5 wt % (Figure 6.5). This slightly enriched peak overlies a sub-surface section of the sediment profile where slight reduction in Fe content occurs down to 10 cm depth. Below this depth increment a distinct zone of enrichment between 10-16 cm depth culminates in a peak situated at 12-13 cm depth. Fe content then returns to lower values averaging 9.3 wt % down to a depth of 27-28 cm where a significant peak in Fe (12.3 wt %) is present. This lower peak overlies the basal section of the core below 30 cm depth characterized by the lowest values for Fe recorded at a value of 6.0 wt %.

6.4.2: Mn distribution

The Mn depth profile exhibits enrichment (0.3 wt %) at the surface of the marsh which declines down to a value of 0.1 wt % at 9-10 cm depth (Figure 6.5). Values increase slightly down to a depth of 15-16 cm and below this the profile exhibits a marked increase over the depth increment from 16 to 30 cm with a significant peak evident at a depth of 24-25 cm (0.32wt %). Below this depth values are much reduced to the base of the core averaging 0.11 wt %.

The Fe and Mn profiles of the Loch Don core clearly show early diagenetic remobilization of Fe and Mn ions most likely derived from oxyhydroxide coatings and possibly other mineral phases within the sediment column. Clearly defined peaks are indicative of dissolved Fe and Mn being precipitated in oxidizing conditions. This indicates that the base of the oxic zone is likely to be situated at ~ 31 cm. Below this depth both Fe and Mn levels within mineral coatings have been reduced by dissolution beneath the redox boundary. Fe and Mn show a weak correlation with Al and Rb within this core (Fe vs. Al $r^2 = 0.42$; Figure 6.6), (Mn vs. Al $r^2 = 0.12$; F), (Fe vs Rb $r^2 = 0.39$; Mn vs. Rb $r^2 = 0.44$; data not shown). These values indicate that both Fe and Mn distribution are controlled to a greater extent by redox processes rather than changes in sediment composition.

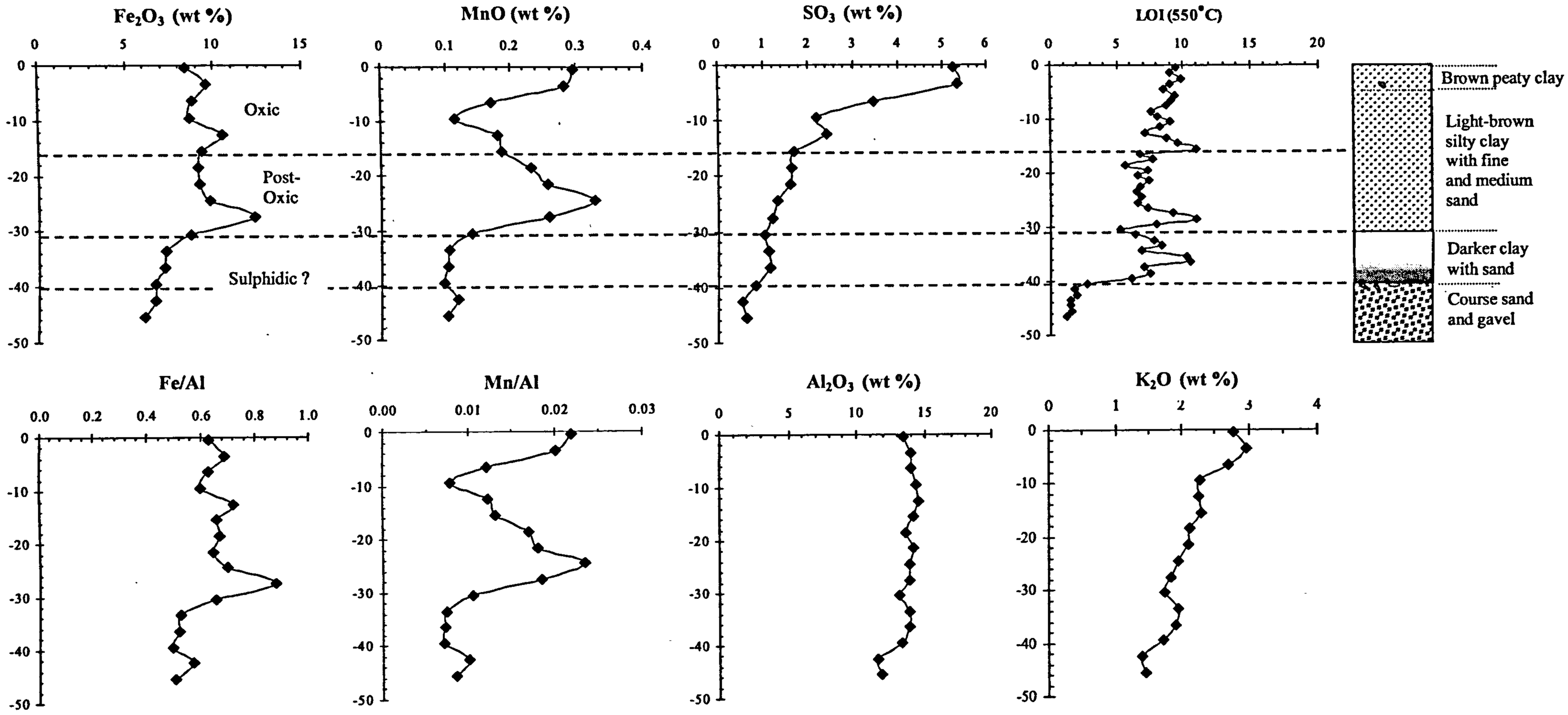

Figure 6.5: Solid-phase depth/concentration profiles from Loch Don marsh core showing down-core distributions of iron, manganese and sulphur in relation to core sedimentology indicated by the profiles of aluminium, potassium and organic content (LOI 550°C) and the core log reproduced from chapter four. Zones of enrichment and reduced concentration are indicated and relate to early diagenetic processes and post-deposition reactions (see text). Elemental abundances are reported as wt % according to XRF convention.

6.4.3: Sulphur

Sulphur distribution within the Loch Don core (Figure 6.5) indicates higher surface values in the upper few centimetres with values of up to 5.25 wt %. This surface enrichment is more pronounced than that within the Loch Scridain core (Figure 6.1). However, similar mechanisms influencing sulphide-rich suspended sediment and the association with organic material following erosion from the seaward marsh edge are likely. Fluvial input to the upper estuary site is limited (Figure 4.11) and will play a less significant role in the transport of weathered material to this area of the marsh. Below 4 cm values decline down-core steadily to reach values less than 0.8 wt % in the lowest depths sampled. A small peak is apparent at 12-13 cm depth which coincides with the upper peak identified within the Fe profile. These two peaks broadly correspond to an increase in organic carbon content visible at 16 cm depth indicating that there may be some formation of organic sulphur compounds and coincidently localised Fe sulphide mineralization in the upper oxic zone (Figure 6.5). However, the correlation between Fe and S ($r^2 = 0.1$; Figure 6.6) indicates a very weak association of these two elements and would suggest that minimal development of Fe-sulphide mineralization has occurred. Similarly, the weak correlation between S and organic carbon ($r^2 = 0.23$) indicates low levels of organic sulphur compounds present despite the increased organic carbon content of the marsh which are elevated in comparison to the core from Loch Scridain.

6.4.4: Trace element indicators of redox conditions

Solid-phase trace element ratios plots provide additional information regarding the position of redox boundaries within the marsh core from Loch Don (Figure 6.7). Sulphur (normalised to Cl to remove the effect of changes in sea-water derived sulphate, Spencer *et al.*, 2003) shows a clear enrichment commencing at 20 cm depth. This increases down to a depth of 28 cm below which values are maintained resulting in significant enrichment of S below 31 cm. The I/Br ratio also shows significant depletion below 31 cm depth with enrichment immediately above this depth increment at 28 cm. This corresponds to precipitation of iodate immediately above the redox-cline. The As/Rb profile shows fluctuating enrichment below 31 cm depth likely to result from the reduction of As and the formation of the more stable arsenite (As (III)) in anoxic conditions. Above the 31 cm depth increment enrichment of As is evident where the

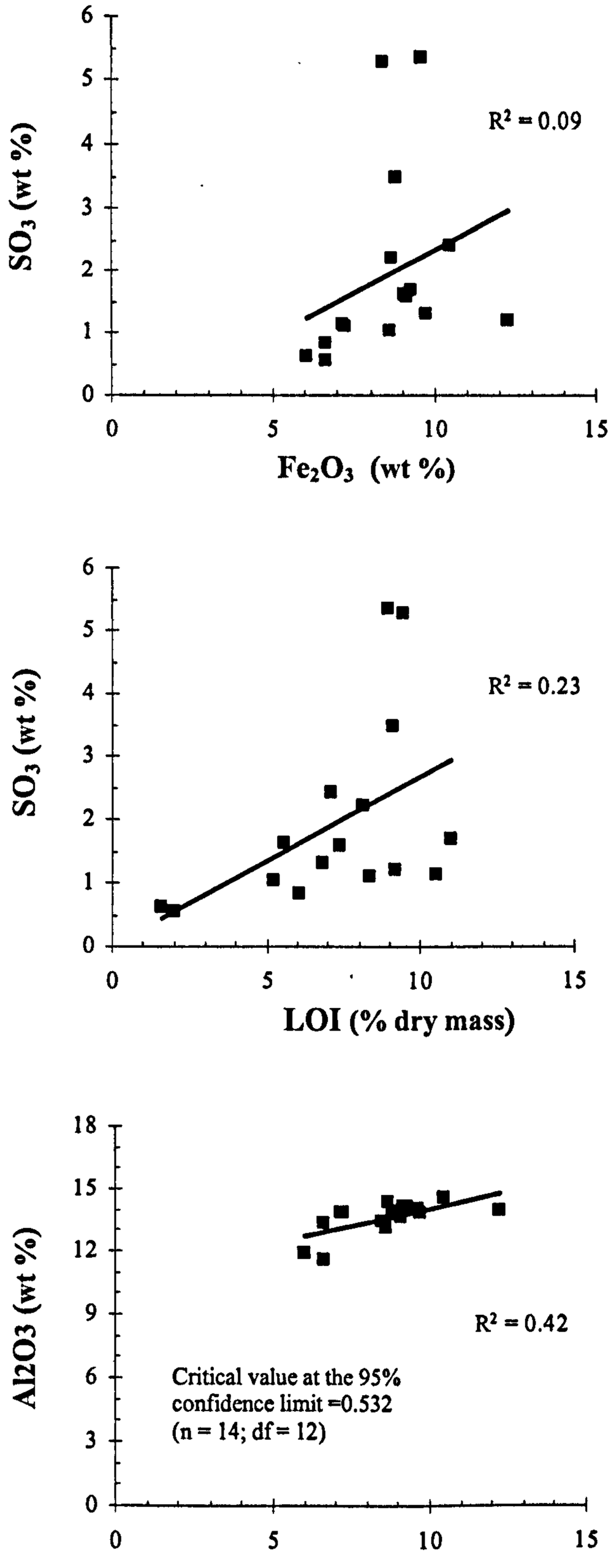

Figure 6.6: Correlation plots of Fe vs. S, LOI vs. S and Fe vs. Al for the marsh core from Loch Don

dominant ion is likely to be arsenate ($AsO^{3}_{4}^{-}$) (Caetano and Vale, 2002). A similar profile can be seen for V normalised to Rb with enrichment of V as vanadyl ($V(IV)O^{2+}$) below 31 cm depth and fluctuating peaks of vanadate (H2VO4-) indicative of V enrichment (Morford and Emerson, 1999). In oxic conditions vanadate is known to adsorb to both Fe and Mn oxyhydroxides (Wehrli and Stumm, 1989). In the Loch Don marsh core the peak in V at 22 cm depth is slightly higher in the core than the main peak in Mn (Figure 6.7) and the V peak between 9-10 cm corresponds to a significant depletion of Mn. A similarly poor horizontal correlation exists for Fe indicating the overall reduced influence of V adsorption onto Fe and Mn oxyhydroxides in the oxic layer of this core.

Data for Mo has been obtained owing to the enhanced capability of the Philips Magix Pro x-r-f system on which these samples were run. Mo below the 31 cm depth increment in the reduced form of Mo(IV) indicates relative depletion despite the corresponding enrichment of S and authIgenic sulphide mineralization within the basal sediments which is known to enhance authIgenic enrichment of Mo (Helz *et al.*, 1996). In the overlying inferred oxic zone significant enrichment of Mo has occurred as MoO^{2-}_{4}. Mo (VI) is known to become concentrated within MnO_2 – rich sediments (Bertine and Turekian, 1973; Crusius *et al.*, 1996). Comparison with the MnO depth profile (Figure 6.5) indicates that significant adsorption to Mn oxyhydroxides is unlikely to account for the enrichment in the post-oxic and oxic surface sediments. No peak occurs over the same depth interval which corresponds to the large peak in Mn between 16 and 30 cm. The inferred position of the redox-cline delineating oxidised and reduced conditions is shown in Figure 6.7.

6.4.5: Trace elements association with oxide phases: ferric Fe, As and P

Horizontal correlation of the depth profiles of Fe with As indicates a weak association between these two elements (Figure 6.8) and this is confirmed by the linear regression which records a weak positive correlation coefficient ($r^2 = 0.38$; Figure 6.8). From this it possible to deduce that arsenic has not become coupled to the sedimentary recycling of Fe across oxic/post-oxic boundaries as identified in some other studies (e.g. Farmer and Lovell, 1986; Belzile and Tessier, 1990; Thompson *et al.*, 1996). The profiles of Fe and P show considerably less correlation supported by the linear regression with an r^2 value of 0.02. Coupling between the recycling of Fe and P occurs as a result of the complexation of dissolved P in saltmarsh

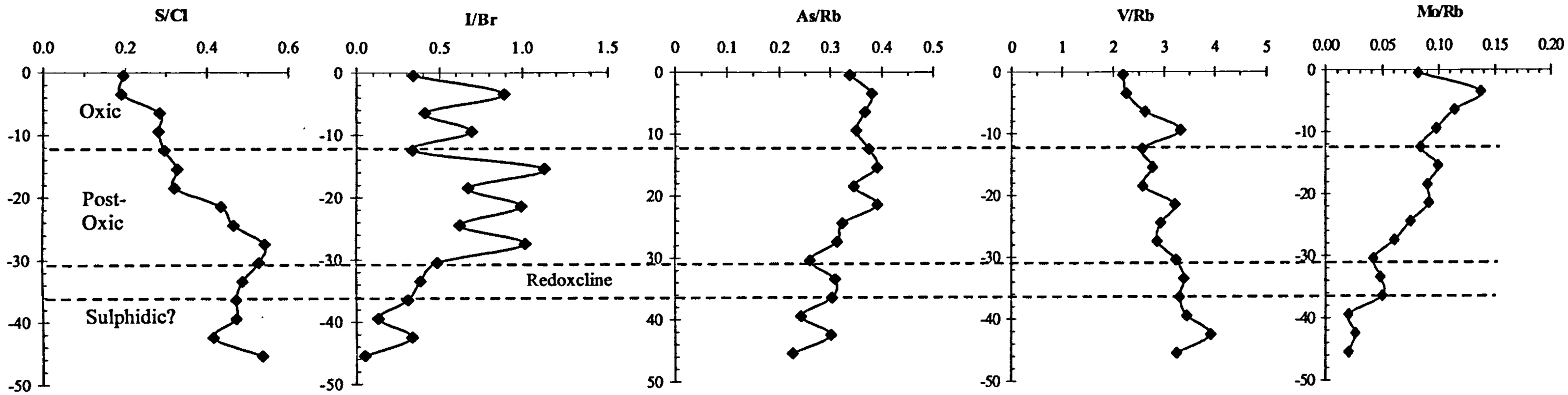

Figure 6.7: Solid-phase profiles from the Loch Don marsh core of S normalized to Cl, I normalized to Br to remove the effects of seawater. Also shown are the depth profiles for the redox-sensitive trace metals As, V and Mo normalized to Rb in line with the predetermined most appropriate normalizing element for this site. The inferred redox-boundary is indicated by the dashed grey line (see text).

(a)

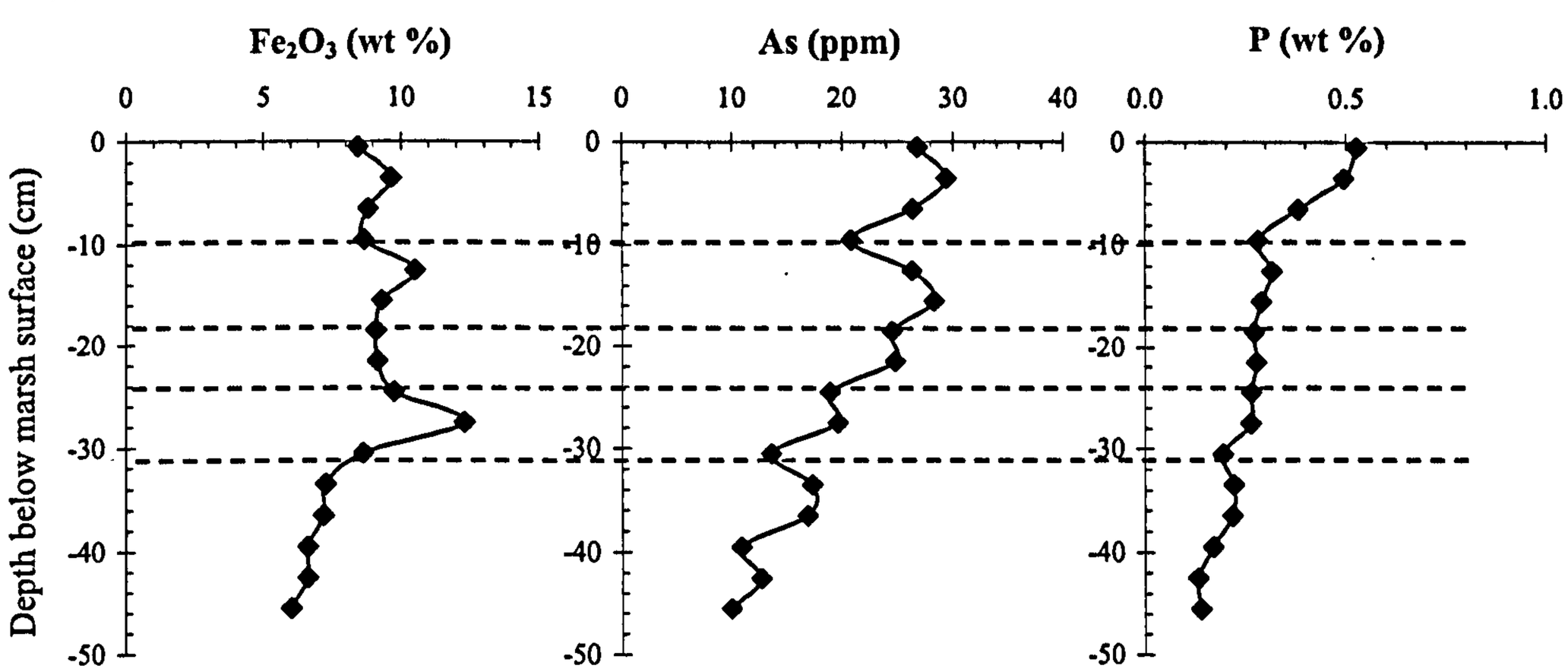

(b)

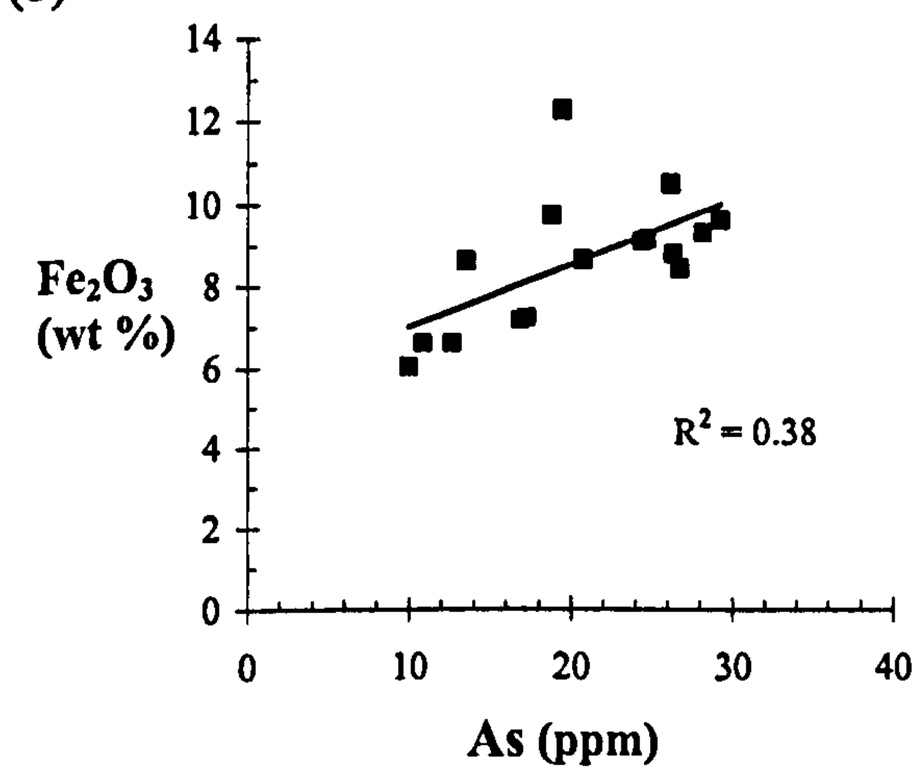

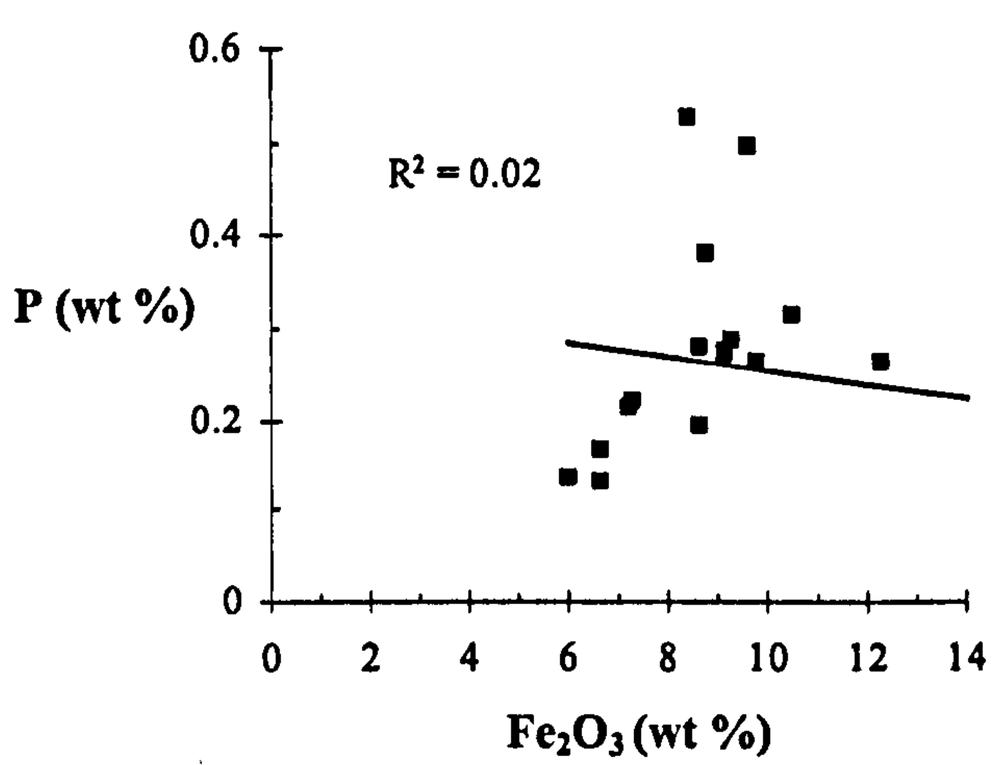

Figure 6.8: (a) Horizontal correlation between Fe, As and P in the marsh core from Loch Don. (b) Correlation plot of Fe with As and Phosphorous.

sediments with the positively charged surfaces of Fe oxyhydroxides. Fe oxyhydroxides precipitating in the oxic zone readsorb dissolved P as they migrate upwards from the post-oxic zone which accounts for the often similar distribution profiles of these elements. This process is therefore inferred to not be actively taking place in the accumulated Loch Don marsh sediments.

6.5: Redoc zonation and early diagenesis in the Loch Creran marsh core.

6.5.1: Iron distribution

Fe distribution in the marsh core depth/profile from Loch Creran shows enrichment in the surficial sediments with a value of 12.7 wt % recorded at the marsh surface (Figure 6.9). Values then decrease to 5.7 wt % at a depth of 16 cm. Beneath this upper section of the core a zone of iron enrichment occurs between 16-28 cm depth with a significant peak situated at 21-22 cm (14.5 wt %). Fe content diminishes rapidly beneath this peak to values of between 5.4 – 5.8 wt % recorded over the depth interval of 32-36 cm. Below this a lower zone of enrichment between 36 – 45 cm culminates in a second peak in iron content at 42-43 cm depth (9.2 wt %). Lowest Fe content is then recorded in the sediments at the base of the core with values averaging 4.0 wt % over the deepest 5 cm (Figure 6.9).

6.5.2: Mn distributuion

Most noticeable in the distribution of Mn in the Loch Creran is the absence of a large peak which corresponds to the peak at 22 cm depth in the profile for Fe. The uppermost section is enriched in Mn with recorded values of 0.5 wt % at the marsh surface (Figure 6.9). Values then diminish down to a depth of 16 cm at which point a slight zone of enrichment is evident with a peak situated at 21-22 cm (0.13 wt %). This small increase in Mn content is coincident with the peak identified in the Fe profile. Below this Mn levels are relatively reduced to a depth of 36 cm at which point a lower zone of Mn enrichment occurs with a distinct peak situated at 41-42 cm depth (0.7 wt %). Fe shows a weak correlation with Al ($r^2 = 0.18$; Figure 6.10) further indicating that its distribution within the Loch Creran core is primarily controlled by redox

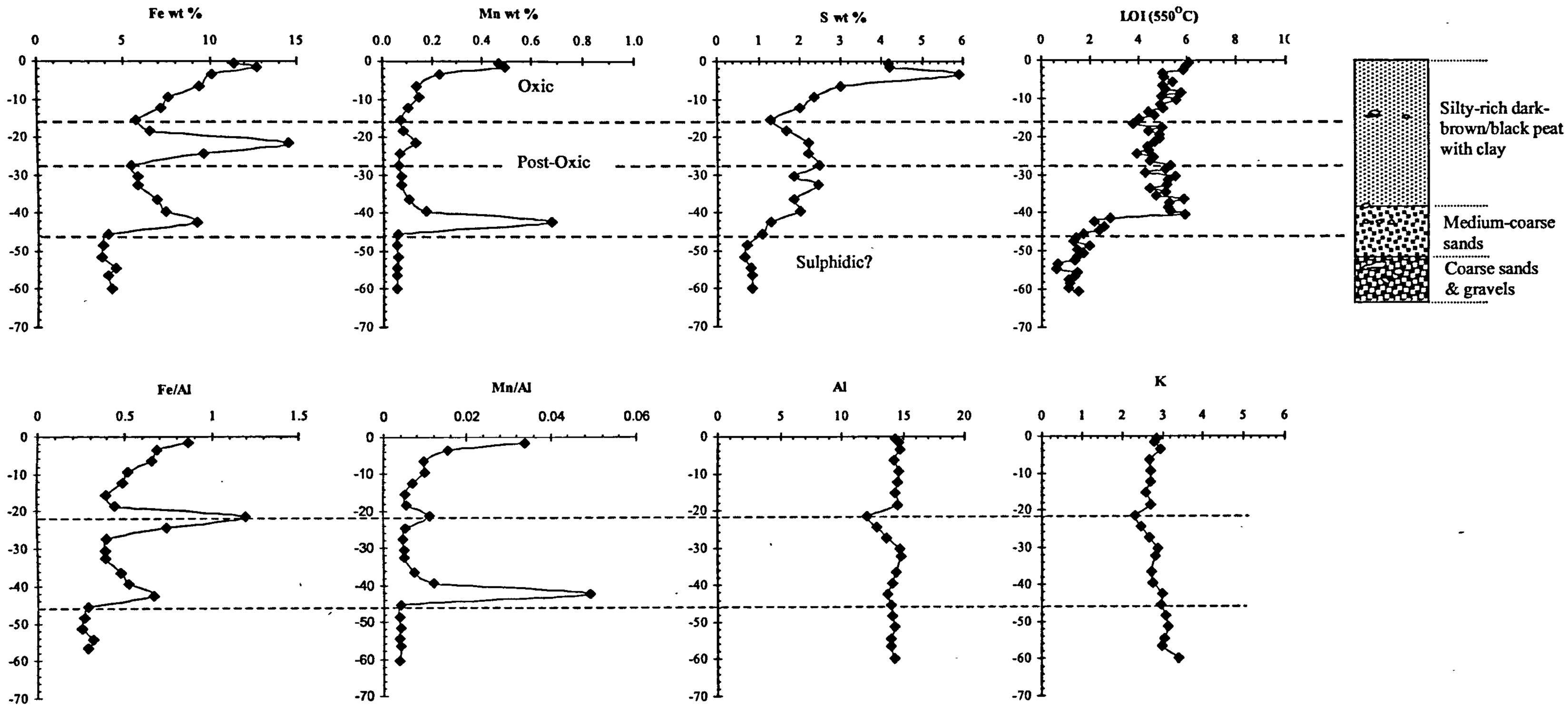

Figure 6.9: Solid-phase depth/concentration profiles for iron, manganese and sulphur for the Loch Creran marsh core in relation to core sedimentology, indicated by the profiles of aluminium, potassium and organic content (LOI 550°C) and the core log reproduced from chapter four. Zones of element enrichment and depletion are also indicated by the dashed lines and are used to interpret the redox conditions and zonation within the core (see text).

processes rather than changes in core sedimentology. The Fe and Mn profiles clearly show evidence for redox controlled diagenetic remobilization with both Fe and Mn being precipitated in the core within oxidizing conditions (Figure 6.9). Below this depth both Fe and Mn levels within mineral coatings have been reduced by dissolution beneath the redox boundary.

6.5.3: Sulphur distribution

Sulphur distribution is similar to that recorded in the Loch Don core with enrichment of this element within the surface sediments (4.2 – 5.9 wt %; Figure 6.9). The recorded surface enrichment is likely to result from the deposition of sulphide-rich minerals deposited upon the marsh surface. This would be consistent with material being derived from the active erosion visible at the seaward edge of the marsh and fronting mud/sandflat environment. The sub-surface decline in S content broadly coincides with a gradual reduction in organic carbon from 6.1 – 3.9 wt % over the depth interval extending from the marsh surface down to 16 cm, although small fluctuations are not mirrored in the S profile (Figure 6.9).

The correlation coefficient between S and LOI over this depth interval ($r^2 = 0.37$) indicates that some formation of organic sulphur compounds is likely to have taken place within this upper section of the core (Figure 6.10). A much stronger correlation ($r^2 = 0.65$) between Fe and S indicates the greater presence of Fe-sulphide mineralization over the same upper depth interval. Below the 16 cm depth increment levels of S are relatively enriched over the section of the sediment prism extending down-core to 46 cm at which point S content is significantly reduced to levels averaging 0.77 wt % over the basal 12 cm. This corresponds quite markedly with the lower LOI profile and the correlation coefficient ($r^2 = 0.57$) indicates the presence of organic sulphide compounds within the deeper section of the marsh soil (Figure 6.10). Over this depth interval the correlation with Fe is much reduced ($r^2 = 0.05$) suggesting much lower levels of Fe-sulphide mineralization at these depths. Therefore, the existence of a definitive sulphidic zone is somewhat questionable.

Comparison with the core stratigraphy (Figure 6.5 and see chapter four Figure 4.32) indicates that the elevated levels of S are contained within the marsh peat that also shows elevated levels of organic carbon. Additionally, the Fe and Mn profiles also indicate that the

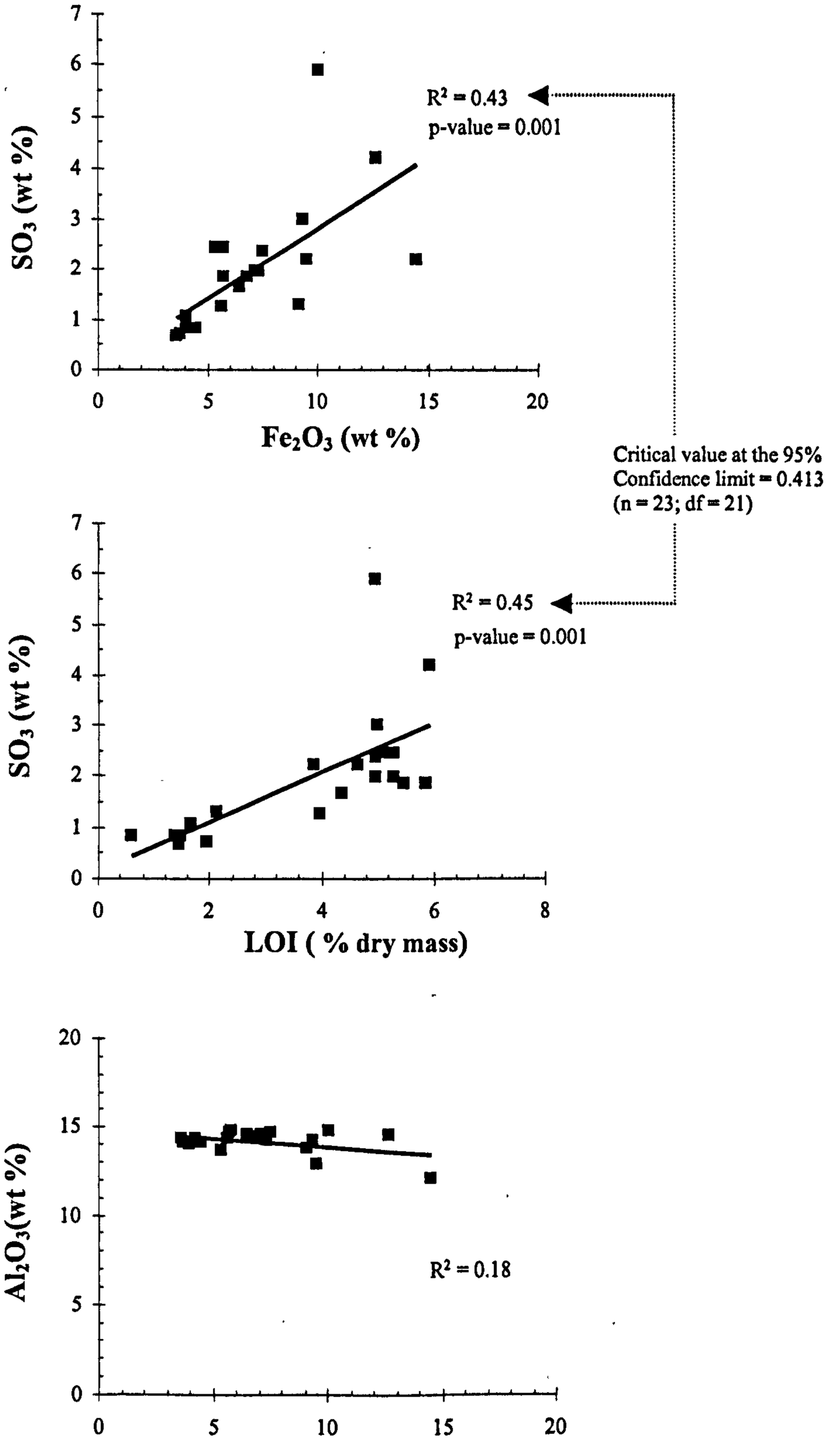

Figure 6.10: Correlation plots of Fe vs. S, LOI vs. S and Fe vs. Al for the marsh core from Loch Creran

oxidation reduction boundary is situated at the base of the peat soil immediately above the transition into more coarse sediments containing relatively more sand and fine to medium gravel.

6.5.5: Trace element indicators of redox conditions

Trace element ratio profiles (Figure 6.11) show an obvious diagenetic signature which re-enforces the inferred position of the redox-cline derived from the position of peaks in Fe and Mn shown in Figure 6.30. Inspection of the S/Cl ratio plot indicates significant enrichment of S below 48 cm depth. This corresponds to distinct peaks in I/Br, As/Al, V/Al and Mo/Al immediately above this depth between 40 and 48 cm. It is therefore possible to accurately identify the true position of the redox-cline within this core (Figure 6.11). Additionally smaller peaks showing enrichment in these various ratio plots between 20 and 24 cm correspond well with similar peaks in Fe and Mn (Figure 6.32). These upper peaks are also due to diagenetic chemical processes and mark the position of the oxic/post-oxic boundary within these sediments (Figure 6.11). It is therefore possible to identify a well-defined redox-zonation in the marsh core from Loch Creran which in tandem with the ^{210}Pb derived sediment ages reflects the maturity of the marsh core from this site.

6.5.6: Association of ferric Fe with As and P

The horizontal correlation between Fe, As and P for the Loch Creran marsh core reveals that the lower peak in Fe at 40-41 cm does correspond to increased concentration of As and the onset of an increase in the concentration of P at the base of the post-oxic zone above 48 cm (Figure 6.12). Declining concentrations of As correlate with declining ferric Fe abundance up through the post-oxic zone. This section of the core corresponds to a depth interval between 29-38 cm over which depth increment concentrations of P are seen to increase. In the upper oxic sediments the large peak in Fe indicative of Fe precipitation above the boundary with the post-oxic zone does not correspond to similar increases in either As or P concentration. The upper oxic zone is characterised by increasing concentrations of all three elements (Figure 6.12) . Linear correlation plots reveal that As (r^2=0.58) and P (r^2=0.45) are coupled to the cycling of Fe to a different extent to that recorded in both the cores from Mull (Figure 6.12).

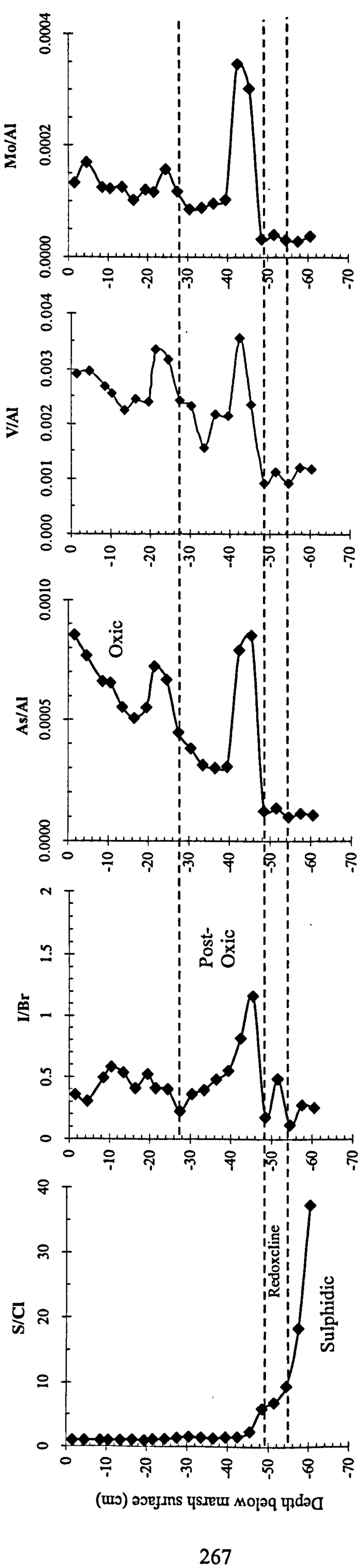

Figure 6.11: Solid-phase depth/profiles for various trace elements and ratio plots showing evidence of early diagenetic redistribution and redox zonation in the marsh core from Loch Creran. The inferred post oxic and sulphidic zones are indicated and discussed in the text.

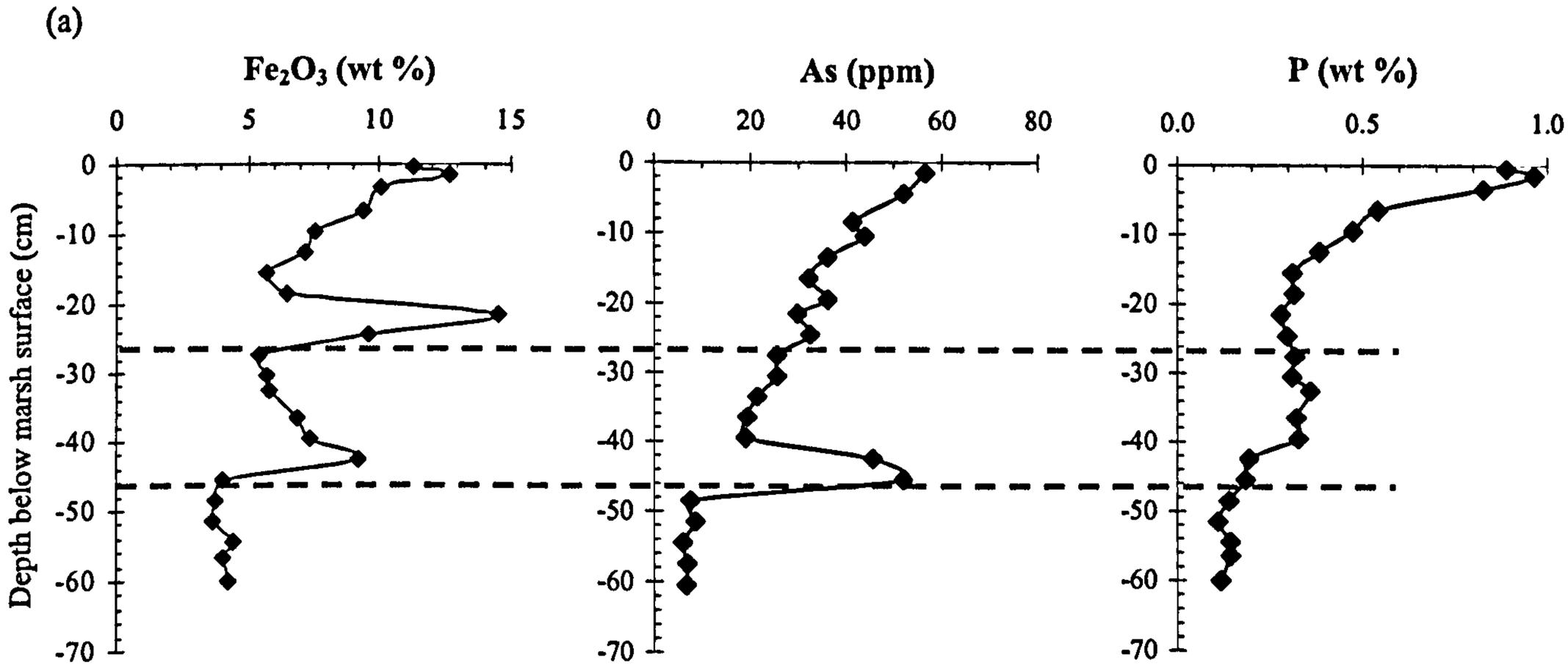

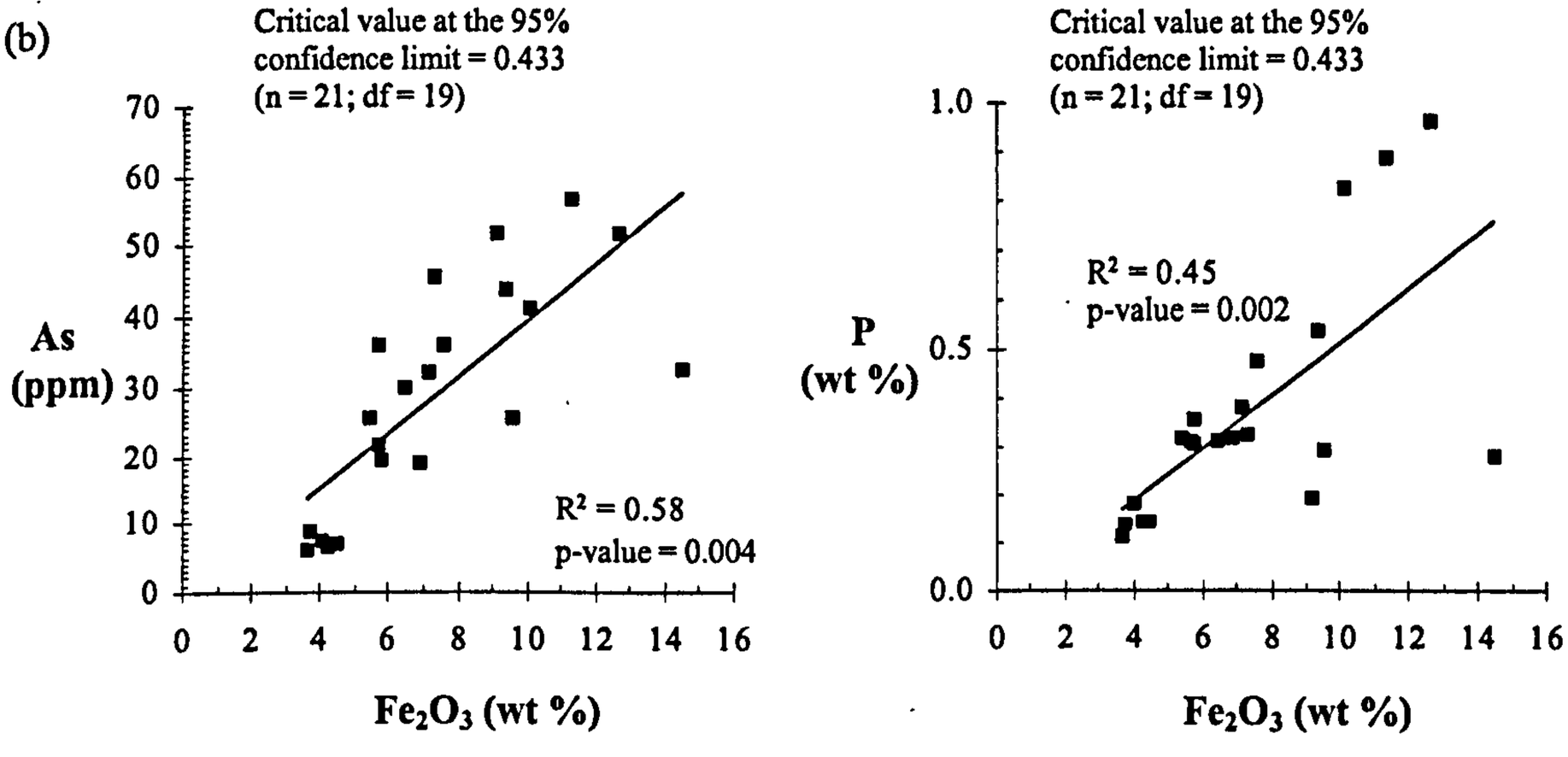

Figure 6.12: (a) Horizontal correlation between Fe, As and P in the marsh core from Loch Creran. (b) Correlation of Fe with As and Phosphorous.

Diagenetically influenced adsorption of As (as Arsenate) by ferric Fe has occurred at a depth within the core which corresponds to the oxidation-reduction boundary situated at 48 cm. Adsorption of both As and P to Fe oxyhydroxides within the upper oxic sediments is likely to account for the enhanced association between these element profiles in the upper 20 cm of the core.

6.6:Redox zonation and early diagenesis in the Loch Etive marsh core.

6.6.1:Iron distribution

Fe is enriched within the upper 13 cm of the Loch Etive core with a recorded value of 5.1 wt % at the marsh surface (Figure 6.13). This value is less than that recorded in the upper layers of the other cores investigated in this study. Areas of frontal marsh at this site are actively eroding (discussed in more detail in Chapter Eight) which suggests that Fe supply to the mature marsh surface is predominately derived from older inter-tidal sediment also of lower iron content. Fe concentrations decline from the surface to values of 3.2 wt % at a depth of 13 cm. These values are maintained averaging 3.7 wt % over the depth interval extending from 13 – 29 cm. Below this depth comparison with the core stratigraphy (Figure 6.13) indicates the presence of the dark/brown-black organic enriched sub-unit extending down-core to 41 cm depth. Within this sub-unit measured Fe levels are reduced with the lowest value of 2.4 wt % recorded at a depth of 32-33 cm. This may be due to the dilution effect resulting from increased organic content apparent at the same depth.

Immediately below this stratigraphic boundary Fe levels return to higher values and a distinct lower peak is evident at a depth of 42-43 cm (4.3 wt %). More subtle fluctuations in the Fe content can be seen in the Fe profile normalized to Al. This enhances lower the peak and also highlights more discrete zones of Fe enrichment situated at depths of 16-17 cm and 28-29 cm (Figure 6.13).

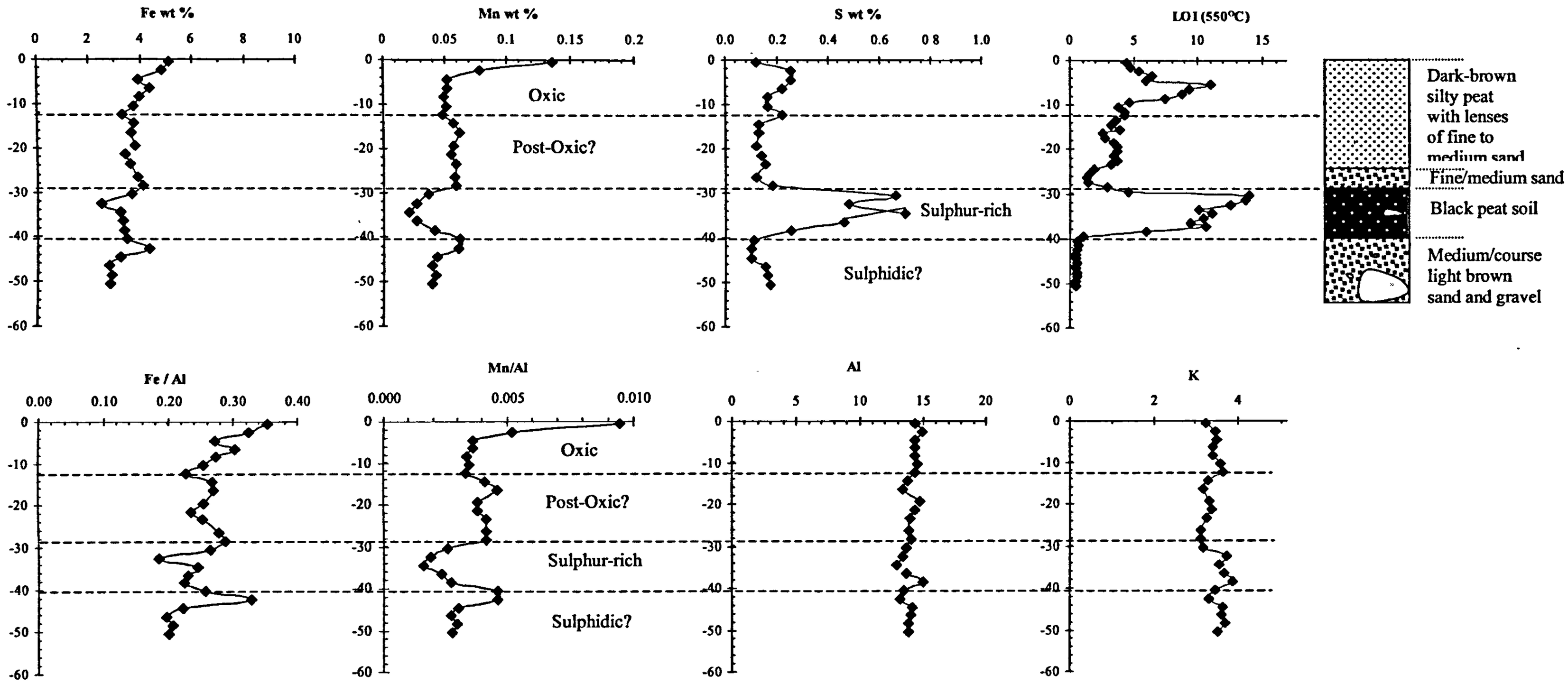

Figure 6.13: Solid-phase depth/concentration profiles for iron, manganese and sulphur for the Loch Etive marsh core in relation to core sedimentology, indicated by the profiles of aluminium, potassium and organic content (LOI 550°C) and the core log reproduced from chapter four. Zones of element enrichment and depletion are also indicated by the dashed lines and are used to describe the redox conditions within this marsh (see text).

6.6.2 Mn distribution

Mn in tandem with Fe in the core from Loch Etive shows surface enrichment with a value of 0.14 wt % (Figure 6.13). This represents the highest Mn level recorded in the entire core and is likely to result from the maintenance of surficial concentrations derived from the deposition of Mn-rich minerals and/or precipitation of Mn^{2+} producing authegenic Mn oxyhydroxides in the upper oxic environment. Below the surface layers Mn levels decline rapidly to values <0.06 wt % which extend to a depth of 29 cm. Between 29 cm and 41 cm depth Mn is also significantly depleted within the organic-rich dark/brown-black peat soil sub-unit of this core (Figure 6.13). The Mn/Al plots highlight the presence of minor peaks in Mn content in other sections of the core which are coincident with increased levels of Fe at 16-17 cm and 42-43 cm (Figure 6.13). The weak correlation of Fe with Al ($r^2 = 0.12$) suggests that Fe distribution is controlled by redox processes as opposed to changes in core sedimentology (Figure 6.14). The Fe and Mn profiles for this core however do not indicate the expected redox zonation described in Chapter Two, section 2.4.3). Certainly, within the deeper sediments below 45 cm depth Fe and Mn levels have been reduced by dissolution of the mineral coatings resulting in depletion of these redox sensitive elements. There does appear to be precipitation of Fe and Mn above this depleted lower section and hence a redox boundary may well exist at this depth. Accurate determination of the redox status of this core is complicated by the existence of the dark/brown-black silty sand unit (Figure 6.13). Above this more discrete peaks in Fe and Mn are evident which may indicate post-oxic/oxic boundaries in the central section of the sediment prism.

6.6.3: Sulphur distribution

The depth profile of S in this core indicates relative depletion of this element within at the marsh surface below which levels are slightly enriched down to a depth of 13 cm (Figure 6.13; sub-surface value of 0.22 – 0.25 wt %). This zone of slight enrichment coincides with the significant increase in organic carbon within the upper decimetre of the core (11.0 wt % at 5-6 cm depth). Below the upper ten centimetres S levels are depleted in tandem with organic carbon content down to 29 cm. The sub-unit of dark/brown-black silty sand described in the preceeding sections is significantly enriched in both S and organic carbon (Figure 6.13). The correlation of these two elements within this depth/section ($r^2 = 0.66$) indicates the strong association and

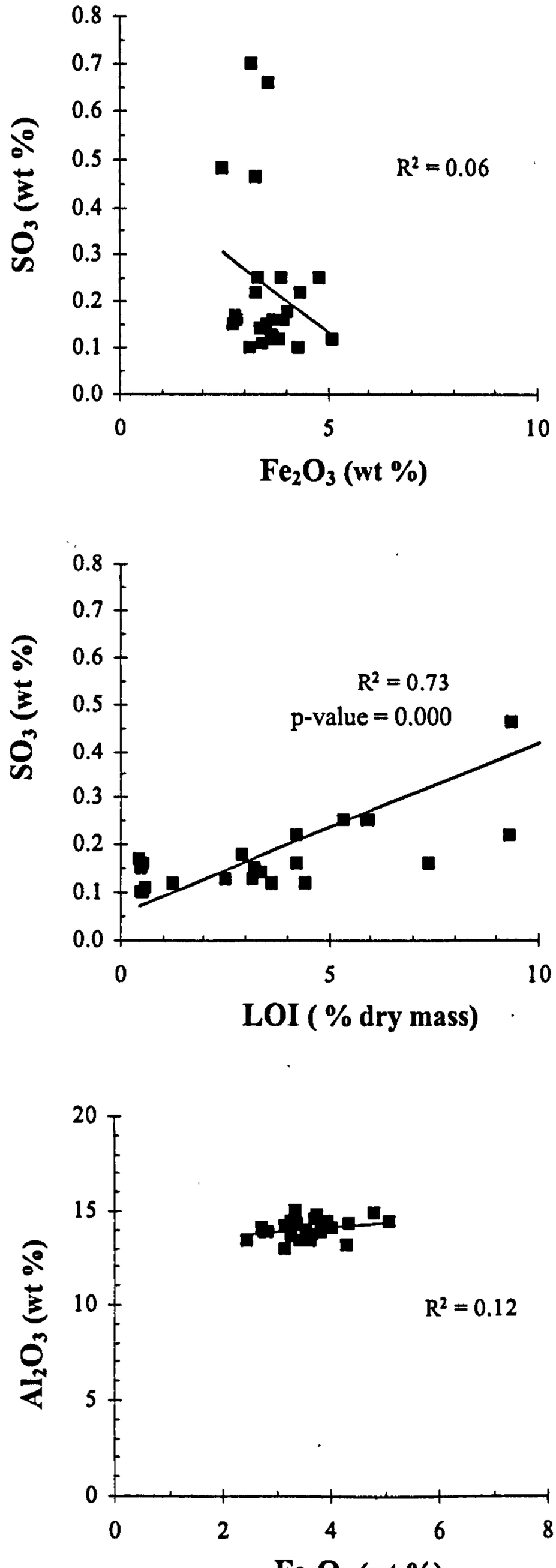

Figure 6.14: Correlation plots for Fe vs. S, LOI vs. S and Fe vs. Al for the marsh core from the head of Loch Etive.

likely presence of significant levels of organic sulphide compounds (Figure 6.14). S shows slight enrichment within the basal sediments but this may be an artifact of sub-sampling within the generally coarser sediments at this depth. Over the entire core depth a strong correlation of S with organic content (via LOI) is evident ($r^2 = 0.74$; Figure 6.14) indicating the greater presence of organic sulphur compounds compared to Fe–sulphide mineralization. This is much reduced within this sediment sequence as indicated by the weak correlation of Fe with S ($r^2 = 0.06$; Figure 6.14).

6.6.4: Trace element indicators of redox conditions

The cycling of Fe, Mn and Sulphur within the Loch Etive core reveals surficial enrichment of these elements in the surface oxic layers with minor peaks occuring in the post oxic layers that correspond to chemozones LEt A3 and LEt B1 (Figure 4.39). Fe and Mn are significantly depleted within the black silty sand unit (LEt A2) whereas S is seen to be significantly enriched over the same depth interval (29-41 cm). Undoubtedly, the more complex stratigraphy within the Loch Etive marsh core has influenced the position of peaks in the major elements used for assessing redox environments. Redox-sensitive trace element ratio plots can also be used to investigate the solid-phase record of element cycling. In the Loch Etive core the development of a distinctive redox profile commonly found in mature marsh settings is not obvious. In Figure 6.15 the ratio plot of S/Cl indicates the dominance of S within the black silty sand unit indicative of reduced conditions in this sub unit. The As/Al profile also shows a lower peak at the base of this unit which may be due to the formation of metal sulphides with As association. The I/Br profile demonstrates that the underlying coarse sand unit is likely to be an oxidizing sub-unit owing to the precipitation of iodate resulting in the significant peak in I/Br ratio recorded between 41-50 cm depth (Figure 6.15). Iodate precipitation is also deemed to be taking place at the top of the medium/fine sand unit overlying the black silty sand with a distinct peak in I/Br ratio evident at 24-25 cm. Additionally, the V/Al profile shows a similar peak to that of I/Br at 41 cm which if due to oxidizing conditions has resulted in the precipitation of Vanadate ($V(IV)O^{2+}$). Vanadate precipitation has also occurred at two separate depth intervals that closely match the precipitation of Iodate with peaks evident in the V/Al profile at 15 and 35 cm depth. Minor peaks in the generally increasing As/Al profile in an up-core direction also

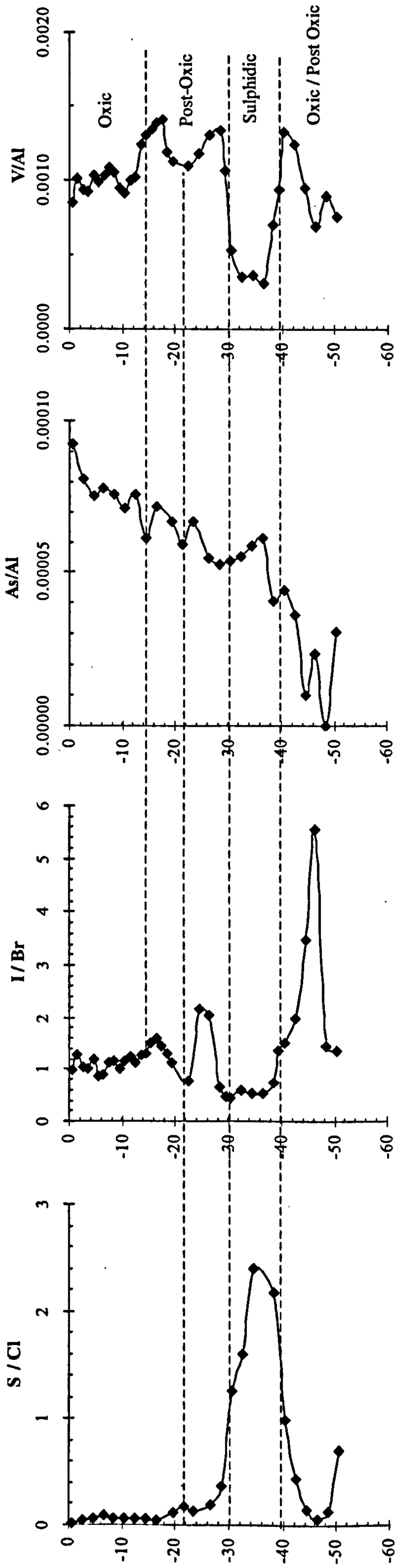

Figure 6.15: Solid-phase depth profiles of S normalized to Cl and I normalised to Br to remove the effects of changes in seawater concentrations for the Loch Etive marsh core. Also shown are redox-sensitive trace metal depth profiles of As and V normalized to Al in line with the previously determined most appropriate normalizing metal for this site. (note that no data for Mo/Al ratio is shown owing to x-r-f determination parameters beyond the control of this author).

correlate horizontally with the I/Br and V/Al profiles (Figure 6.15). These features are likely to represent the base of the upper oxic layer inferred here to be between 16-18 cm with the base of a post-oxic zone situated at a depth of 26-28 cm (Figure 6.15). Clearly the presence of the black silty sand unit between 29-40 cm depth has influenced the oxidation-reduction profile within this core and resulted in a sequence that differs from that of other studied marshes (e.g. Cundy and Croudace, 1997, Dyer, 2002). The implications of this in terms of radiometric dating and remobilization of elements is discussed fully in Chapter Eight.

6.6.5: Association of ferric Fe, with As and P

In the marsh core from Loch Etive lower values are recorded for ferric Fe and P abundance and As concentration (Figure 6.16). The horizontal correlation of the distribution profiles for these elements is less pronounced than in the other three cores from the Argyll region. This is likely to be a result of the magnitude of weathered material transported to the head of the Loch and importantly the presence in this core of the black silty sand layer (discussed above). Both the As and P profiles indicate relative enrichment within this lithological sub-unit in comparison to Fe (Figure 6.16). At the very top of the unit at 30cm depth a pronounced peak in P does not correspond with an associated peak in Fe. Linear correlation over the entire core depth for Fe with As and P yields r^2 values of 0.43 and 0.31 respectively indicative of a poor association and coupling of Fe cycling with As and P throughout the core (Figure 6.16). However, the overlying medium/fine sand which grades into coastal peat is representative of the true extent of saltmarsh development within this core. Linear correlation over the uppermost 28 cm yields r^2 values 0.31 and 0.71 for As and P respectively. This indicates that within the extent of marsh sediments that have developed at the head of Loch Etive, P is indeed being adsorbed by Fe oxyhydroxides within the upper oxic sediments resulting in the distribution of P being intimately coupled to the sedimentary recycling of Fe. The same is not the case for dissolved As which does not appear to be linked to diagenetic Fe distribution (Figure 6.16).

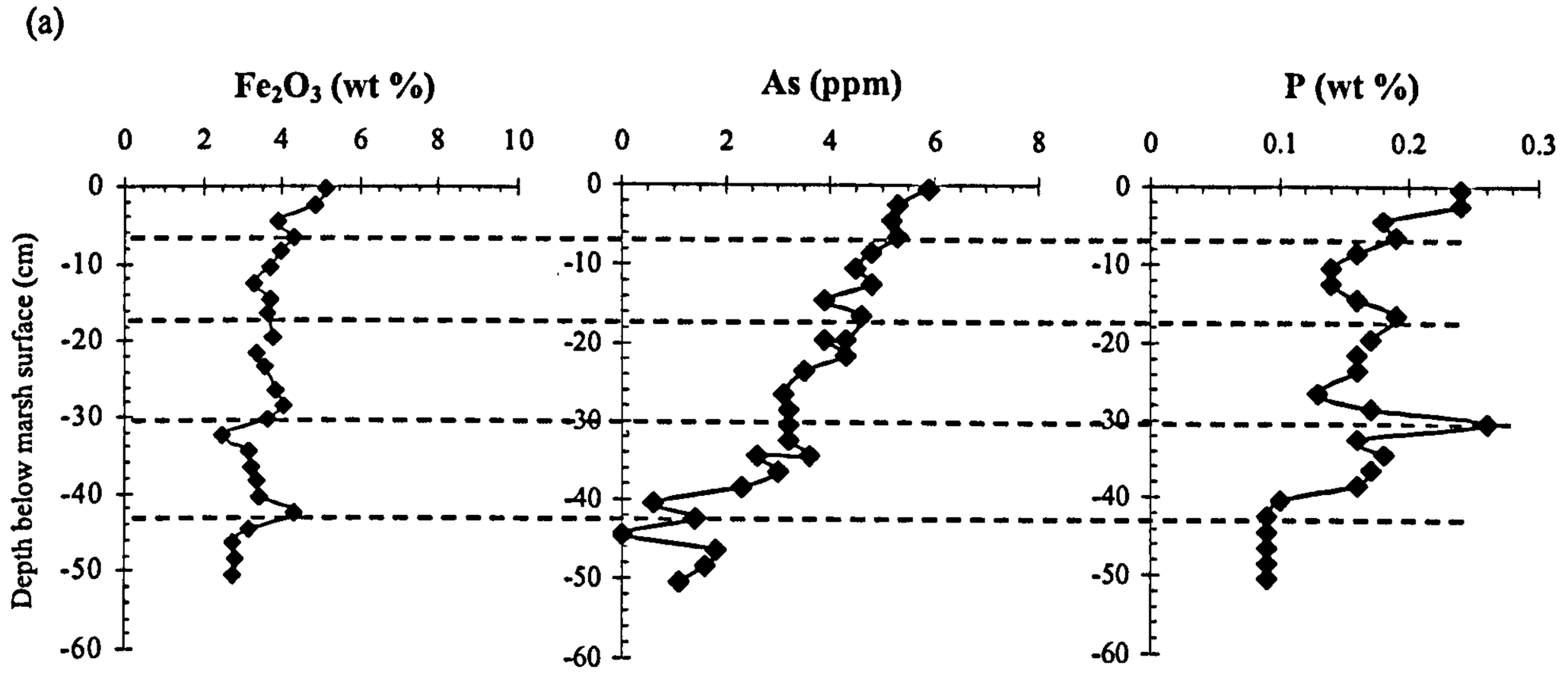

Figure 6.16: (a) Horizontal correlation between Fe, As and P in the marsh core from Loch Etive. (b) Correlation of Fe with As and Phosphorous.

6.8: Summary

In the marsh cores from Mull and Loch Creran a distinct redoxcline has developed at depths that broadly correspond with the visual stratigraphy and the onset of coastal marsh peat conditions inferred from the LOI measurements as proxy for organic content. The visual recognition of anoxic conditions (i.e. dark-grey/black metal sulphide-rich layers) is less obvious in these cores despite the obvious relocation of Fe and Mn oxyhydroxides evident as distinct peaks at the base of the post-oxic zone. Inferences regarding the position of the onset of more anxoic conditions are supported by the profiles of redox-sensitive trace elements, which help to further delineate the geochemical redox profile in these sediments. The development of highly anoxic conditions is therefore uncertain. This is based upon the lack of Fe (II) metal sulphide formation inferred from the correlation with trace metals in these cores. Nevertheless, the development of a redox profile within the sediments of these three cores may be used as additional evidence to infer older more mature marsh conditions. Importantly, the upper depth of sediments containing the measured radioactivity of the key radionuclides used for dating purposes are dominated by oxic conditions. The fact that this is inferred from solid-phase geochemical analysis supports the argument that oxic/post-oxic conditions predominate. This is most likely to result from marsh flooding periodicity and hence the limited time over the diurnal tidal cycle that more reducing conditions occur influencing sediment solid-phase/pore-water reations.

The more complex depositional history recorded in the core from Loch Etive has resulted in a lack of the more commonly found marsh geochemical redox zonation (Williams *et al.*, 1994).

In this core the higher concentration of S within the lower sub-unit of dark-black silty sand is more likely to be due to pre-existent elevated concentrations of S derived from terrestrial sources. In the overlying coastal peat, Fe and Mn do not appear to have developed peaks indicative of major levels of element precipitation.

In cores of this nature, with distinct peat sub-layers an inverted redox zonation is sometimes encountered due to post-depositional reactions being driven by organic matter decomposition (A.B.Cundy pers comm.). This would certainly seem to be true for the core sequence from the Loch Etive site.

In similarity to the cores from Mull and Loch Creran, the true extent of coastal wetland sediments in this core (upper 28 cm) are also predominantly oxic and, therefore, the depositional record of radionuclides is unlikely to have undergone significant post-depositional relocation as a result of diagenetic remobilization. At all sites the altitude of the marsh surfaces relative to the observed tidal prism results in oxic conditions predominating for large periods of the diurnal tidal cycle. This gives an enhanced degree of confidence that the redox signature derived from the solid-phase geochemistry is a reliable indicator of early diagenetic conditions within these marshes.

In the following Chapter more detailed analysis of the behaviour of trace elements is undertaken, with calculation of trace metal fluxes, the geochemistry of U (at two sites) and the application of multivariate statistical techniques which are used to examine the influence of key physical and chemical processes on the evolution of the Argyll marshes.

Chapter Seven

TRACE ELEMENT GEOCHEMISTRY OF THE ARGYLL MARSHES

7.1: Introduction

This chapter provides further detail of geochemical processes/reactions that have influenced the development of the Argyll marshes. Particular focus is concentrated on the geochemistry of trace metals and the processes that govern their overall distribution in the four cores studied. The ^{210}Pb modeled geochronology is further used here to calculate fluxes of trace elements (heavy metals) to the marsh surfaces within the dated period of historical deposition. Such analysis can be a useful method to establish more discrete environmental changes and periods of marsh development that can sometimes be shrouded by the use of radiometric dating methods alone (Cundy *et al.*, 2003). Trace metal distributions are further considered from the standpoint of establishing levels of marsh contamination and/or pollution. This approach provides a mechanism to assess the contamination status of marsh systems in western Scotland used in other studies (e.g. Windom *et al.*, 1989; Zwolsman *et al.*, 1996; Cundy *et al.*, 1998; Cearreta *et al.*, 2000; Spencer *et al.*, 2001; Lee and Cundy, 2001; Cundy *et al.*, 2003; Velde *et al.*, 2003). Similar to coastal wetlands on the west coast of Ireland (e.g. Gallagher *et al.*, 1996) marsh systems in western Scotland have not received significant attention in terms of contamination assessment. This may be due to the common general perception that the western Scottish coastline comprises near- pristine coastal environments.

The behaviour of the halide trace elements (I and Br) is considered. These have received some attention in the published literature and further to their use as redox indicators can also be utilzed to make inferences concerning the influence of marine processes and geochemical reactions with trace metal species.

The geochemistry of uranium is considered at two sites and provides detail of the solid-phase record of U in these more clastic inter-tidal systems. The implications of U enrichment in terms of marsh evolution are also highlighted.

Finally, the chapter considers a range of broad-scale processes involved in the development of saltmarsh sequences via the implementation of Principle Components Analysis of the geochemical data. Inferences concerning documented geochemical associations between individual and groups of elements known to be involved in a suite of marsh processes are made and consideration of the role of such processes in the evolution of the Argyll marshes is undertaken.

7.2: Loch Scridain:

7.2.1: Association of trace metals (As, Pb, Ni, Cr and Zn) with Mn.

The diagenetic cycling of Mn within the oxic and post oxic zones is more pronounced than that of Fe within Loch Scridain marsh core (Figure 7.1). The down-core profile of Fe shows enrichment at deeper depths than Mn which corresponds to the oxidation reduction boundary (Figure 6.1). Horizontal correlation between the Mn profile and those of As and Pb indicates that the distribution of these elements is also controlled to a certain extent by the cycling of Mn (Figure 7.1). Minor peaks at depth in the Mn profile correspond to peaks indicative of As and Pb enrichment above the boundary with the weak anoxic zone in this core.

In the post oxic zone precipitation of Mn is accompanied by enrichment of As and Pb (Figure 7.1). In the oxic upper surficial sediments of the core authigenic production of Mn oxyhydroxides corresponds to a markedly enriched zone of As and Pb. However, the positive correlation of As and Pb with Mn (r^2 values of 0.52 and 0.39 respectively; Figure 7.1) are indicative of only partial As and Pb adsorption onto Mn oxyhydroxides. The profiles of the trace metals Cr, Ni and Zn are rather decoupled from the profiles of Mn and the negative correlation of Cr and Ni and the very weak positive correlation with Zn suggests that another mechanism must be responsible for the distribution of these elements.

7.2.2: Trace element associations with sulphidic phases:(As, Ni, Zn and Pb).

Metal sulphide formation under reducing conditions has been shown to result in enrichment of trace elements including As, Ni, Zn and Pb within sediments containing elevated levels of reduced Fe and S. Despite enrichment of S relative to Cl in the lower section of the core (Figure 6.3) the development of a strongly reduced zone appears uncertain. Comparison of the Fe and S depth/profiles with those of As, Ni, Zn and Pb reveal no corresponding elevated levels of Pb or Ni (Figure 6.1 & Figure 7.1). Slightly elevated levels of Zn are apparent with a minor increase in As concentration at the very base of the core. This may well be an artifact resulting from analysis of the coarser sands and gravels present at the base of the sediment prism. Cr shows some degree of enrichment in the base but the exact association here is not clear. The negative correlation coefficient of the

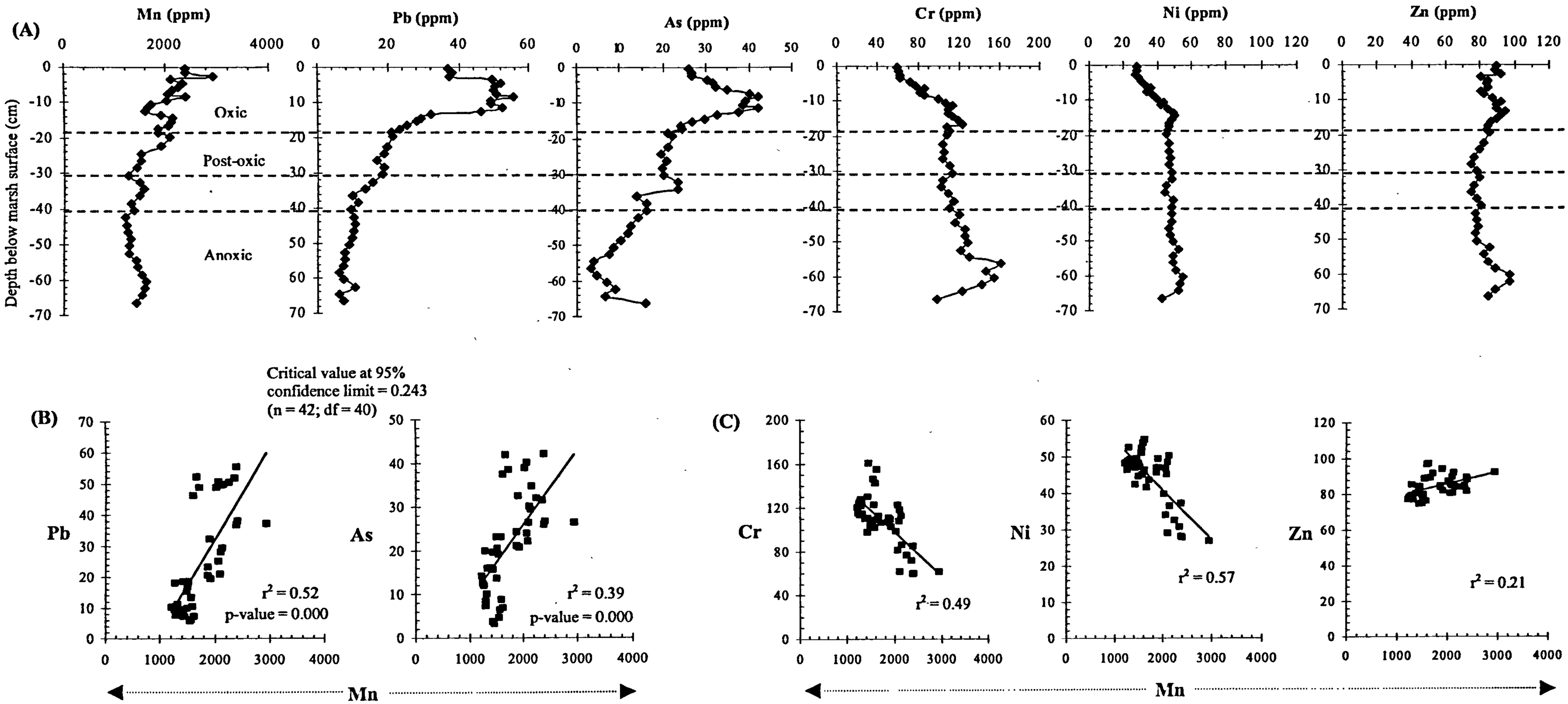

Figure 7.1: (A) Horizontal correlation between Mn (ppm) and Pb, As, Cr, Ni and Zn for the marsh core from Loch Scridain. (B) Linear correlation plot of Mn with Pb and As. (C) Correlation of Mn with Cr, Ni and Zn.

concentration data below 38 cm depth ($r^2 = 0.35$) suggest very little association of these elements and the formation of significant quantities of chromium sulphide (Cr_2S_3) is unlikely.

7.2.3: Trace element associations with organic material (As, Pb, Cu, Ni, and Zn)

Trace elements such as As and P are known to be intimately involved with a suite of biological processes and are similarly recycled within near-shore marine environments (Caetano and Vale, 2002). The process of organic matter decomposition is also believed to exert a significant influence upon the cycling of a range of sedimentary trace metals (Lord and Church, 1983, Cacador et al., 1996). The strong binding capacity of organic material for metal ions also strongly influences trace metal distributions (Rashid, 1974; Bendell-Young and Harvey, 1992; Luther *et al.*, 1992). Rashid (1985) highlights the important role of humic substances in controlling trace metal distribution. Their influence tends to be predominant within the sedimentary prism owing to the high surface activities (Rashid, 1985). Additionally, the reaction between sedimentary organic matter and dissolved sulphide species may enhance the manufacture of organic-thiol complexes. These have also been shown to be intrinsically involved in the post-burial redistribution of metal species in salt marsh environments (Ferdelman *et al.*, 1991). The root mass (rhizosphere) of marsh vegetation represents an important source of *in-situ* organic matter to the microbial populations within the sediment sub–surface (Gardener *et al.*, 1988). Decomposition of this fraction of marsh sediments also results in the formation of fulvic and humic complexes and contributes to the overall sedimentary content of these organic-based acid complexes (Pellanbarg and Church, 1979).

Three dominant mechanisms by which trace metals can become affiliated with sediment organic material have been proposed by Rashid (1985) and these are as follows:

- **Physical adsorption:** via electrostatic attraction between organic complexes and trace element cations.

- **Cation exchange:** whereby the hydrogen ions within the organic molecules are replaced by metallic cations. Exchange of metallic ions is greater with increased pH.

- **Chelation and complexing reactions:** occur through the process of electron transfer resulting in the solid bonding of metal species and formation of organo-metallic ring complexes.

The role of humic materials in sequestering trace metals in the solid phase is complex but studies have shown that the humic fraction of sedimentary material is often enriched in metals (Swanson *et al.*, 1966; Rashid and Leonard 1973). Direct association with organic particulate matter and the flocculation of dissolved and colloidal complexes are considered to be the principal association mechanisms in the solid phase (Bendell-Young and Harvey, 1992; Tessier *et al.*, 1996). In the dissolved (pore-water) phase, association of dissolved humic acids is thought to enhance metal dissolution leading to the formation of organo-metallic complexes (Rashid and Leonard, 1973). As a general rule levels of metal enrichment have been shown to coincide with sections of marsh sediments that are also enriched with organic matter (Rashid and Leonard, 1973; Rashid, 1985). A number of other studies investigating marsh geochemistry have highlighted the strong correlation between sediment organic matter and concentrations of As, Cu, Cd, Pb, Ni and Zn (Allen *et al.*, 1990; Caçador *et al.*, 1996).

Data for Cu and Cd are not available for the Loch Scridain core, however, comparison with the LOI depth profile with those of Pb and As reveals some degree of coupling (Figure 7.2). In the upper oxic zone Pb and As show enriched sub-surface concentrations which coincide with fluctuating levels of organic matter between 6.3 to 9.5 wt %. In the underlying post-oxic sediments levels of As and Pb broadly correlate to increasing abundance of organics.

Correlation of these elements with the LOI data gives r^2 values of 0.39 for Pb and 0.55 for As. Here the degrees of freedom (df = 40) gives a critical value of 0.243 revealing a significant association between these metals and organic matter throughout the core. Cr, Ni and Zn depth profiles are decoupled from the distribution of organic material in the core from Loch Scridain (Figure 7.2) again implying that another mechanism is responsible for their distribution within the sediment prism.

7.2.4: Normalization of geochemical data: problems and issues

In many studies of marsh geochemistry the procedure of normalization for geochemical constituents has been routinely undertaken (see also overview in Chapter

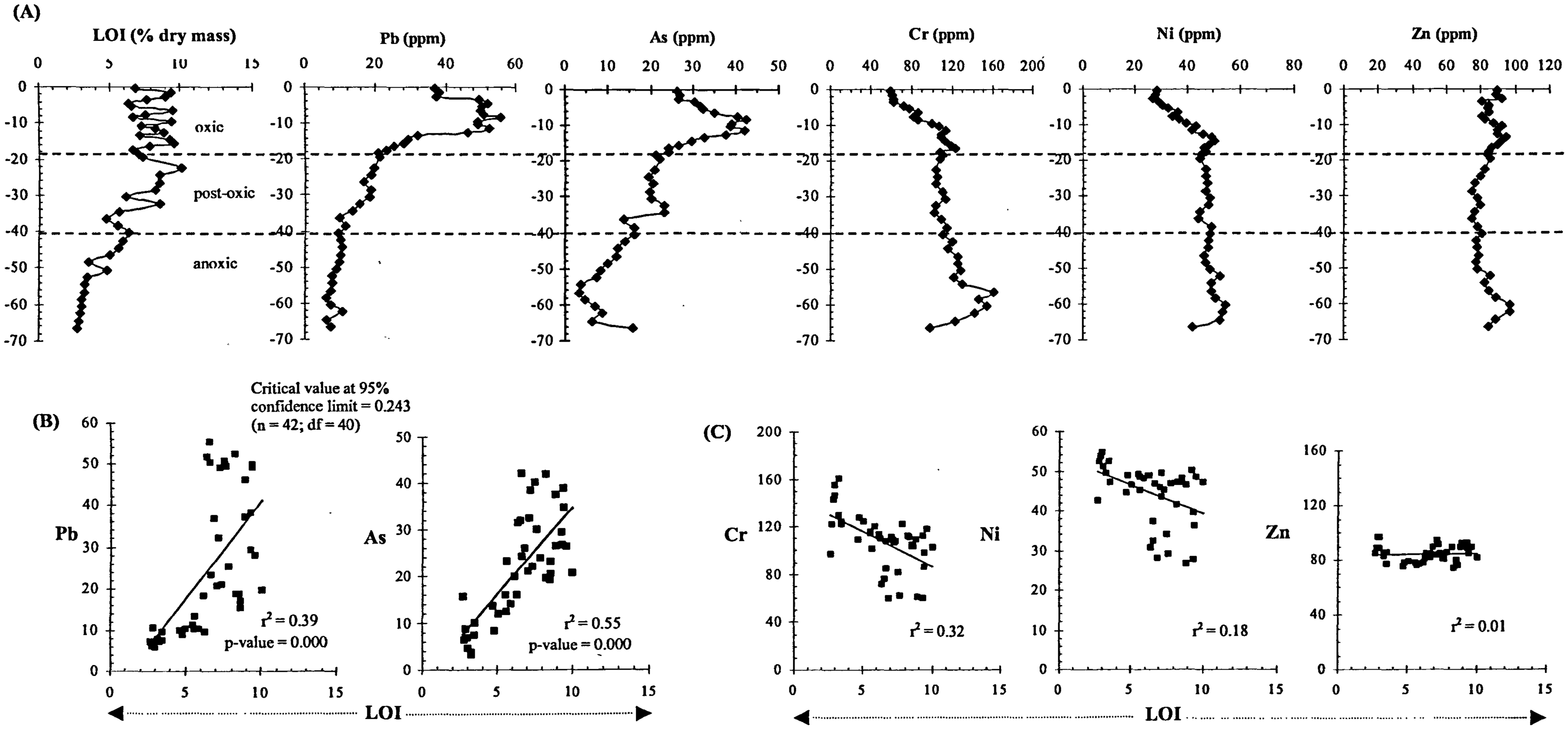

Figure 7.2: (A) Horizontal correlation between organic content (via LOI 550°C proxy % dry mass) and the trace metals Pb, As, Cr, Ni and Zn (ppm) for the marsh core from Loch Scridain. (B) Linear correlation plots of LOI with Pb and As. (C) Correlation of LOI with Cr, Ni and Zn

Three). The principal reason for this manipulation of data is to provide a correction factor to remove the effects of variation in sediment grain-size and mineralogical effects on natural heavy metal concentrations. This provides a geochemical mechanism for estimating anthropogenic (excess) heavy metal concentrations above background levels.

A comprehensive overview of the procedure for normalizing geochemical data from estuarine and coastal shelf sediments is provided by Ackermann (1980). Expansion on the methodological aspects can be found in Loring (1991) and these are further summarized in Rae (1997). In many studies the use of Al as a suitable normalizing constituent of estuarine sediments has been employed (e.g. Ackermann, 1980; Din, 1992; Cortesao and Vale, 1995; Cundy and Croudace, 1995; Dyer *et al.*, 2002) to name but a few. Rae (1997) highlights the fact that there is no one standard technique in operation for normalizing estuarine geochemical data. Furthermore, she highlights the routine determination of Rb in X-R-F spectrometry analysis and suggests that in combination with the geochemical characteristics and behaviour of Rb that this is a more convienient normalizing element.

In the papers by Loring (1990 and 1991) attention is drawn to the pitfalls of using Al in formerly glaciated terrains owing to the presence in estuarine sediments of detrital aluminosilicate minerals, in particular the feldspars. This author suggests that the presence of such feldspars results in the distinct likelyhood of trace metal concentrations not varying directly with sediment grain-size fluctuations (Loring 1990 and 1991). He suggests the use of rare earth elements such as lithium as more suitable for normalizing purposes in such settings. Loring (1991) also highlights and suggests the use of statistical correlation to ascertain the strength of the relationship between potential normalizing elements in particular trace metal constituents. A demonstration of the applicability of the use of lithium to normalize estuarine sediments derived from the Gulf of St Lawrence is provided by Loring (1990).

With regard to the present study the area of Argyll has been significantly modified by successive periods of glacial erosion during the Late Quaternary. The large fjord environments that characterize much of the western Scottish coast would formerly have been highly erosional terrains with ice transporting large volumes of terrestrial material seaward. Much of this eroded sediment will have undergone significant polycyclic re-dispersal and deposition as sea-levels rose during the Holocene. This raises the question as to how significant is the supply of dissolved aluminosilicate minerals derived from the continued sub-areal weathering of igneous rocks and re-distributed material on the concentration of Al

in contemporary saltmarshes? This presents certain problems in terms of deciding upon the most suitable normalizing element for the geochemical data obtained in this study.

In order to address this issue as comprehensively as possible and within the confines of the data, statistical correlation of various trace metal concentrations and potential normalizers such as Al and Rb have been undertaken (Table 7.1). Unfortunately, determination of Li as proposed by Loring (1991) is not possible using x-r-f spectrometry and owing to the financial constraints of the project determination of Li has not been undertaken. Table 7.1 highlights the problematic issue of selecting a suitable normalizing element from the distribution of elements analyzed from the four marsh sites. At Loch Scridain, Al would appear to be the better normalizing element for all trace elements excepting Zn. At Loch Don Rb is the superior normalizing element for all trace elements except Cu. Within the core from Loch Creran Rb correlates relatively poorly in comparison to Al which although not yielding high positive correlation values suggests that of the two alternatives available in this study Al is possibly more suitable. The head of Loch Etive is situated within the Caledonian igneous complex of the south-western Highlands (Figure 4.35). Here it is surprising to note that the correlation between most trace elements is higher for Al apart from Cr and V. In order to address the issue of normalization of trace element data for this study the correlation calculations provide a more detailed insight into which of these two elements is most suitable from the differing geological settings (Table 7.1). Interestingly, some variability is indicated within individual core sequences. The normalization of certain trace element data initially follows the indications given by the correlation data in Table 7.1. In forthcoming sections it will be shown that other potential normalizing elements are also worthy of consideration. Additional insight into background element concentrations within the study region is possible via inspection of the British Geological Survey (BGS) Regional Geochemical Atlas for the Argyll region (BGS, 1999).

Contained within this volume are a vast number of data pertaining to a wide range of major and trace element concentrations derived from the extensive sampling undertaken. This facilitates some estimation of natural concentrations of trace metals within the surrounding catchments of the four sites derived from the basal geology (Table 7.2). However, attention is drawn here to the use such data for determining accurate enrichment of trace elements which have been shown to be unsatisfactory for coastal sediments from the Virginia shelf (Rule, 1986). Of use for comparative purposes here are the data for trace element concentrations for various rock-types derived from the summarized data throughout the BGS atlas for the Argyll region. The following sections of this chapter contain data

Trace Element	**Loch Scridain** *n = 42*		**Loch Don** *n = 16*		**Loch Creran** *n = 21*		**Loch Etive** *n = 43*	
	Al	*Rb*	*Al*	*Rb*	*Al*	*Rb*	*Al*	*Rb*
As	-0.48	-0.14	-0.57	0.96	0.09	-0.69	0.50	-0.29
Cr	0.68	0.96	0.39	0.06	0.20	-0.60	0.33	0.47
Cu	na	na	-0.66	0.87	0.29	-0.48	na	na
Mo	na	na	-0.65	0.92	-0.57	-0.22	na	na
Ni	0.78	0.95	-0.45	0.92	0.18	-0.48	0.52	0.54
Pb	-0.81	-0.56	-0.48	0.93	0.17	-0.69	0.60	-0.18
Zn	0.24	0.15	-0.66	0.94	0.25	-0.49	0.62	0.48
V	0.67	0.94	0.08	0.53	0.15	-0.72	0.38	0.58
C_{org}	0.05	0.03	-0.28	0.68	0.14	-0.73	-0.09	-0.86
Rb	0.75		-0.64		0.08		0.18	

Table 7.1: Correlation coefficients (r) for the Metal/Al and Metal/Rb and Organic carbon (C_{org}) for the marsh cores from Argyll. (n = number of samples from each core and all calculations are performed at the 95% confidence level. na indicates samples not analysed for the particular element owing to constraints with respect to x-r-f spectrometer outside the control of the thesis author).

Trace Metal	**Loch Scridain**	**Loch Don**	**Loch Creran**	**Loch Etive**
As	< 16 ppm	< 10 ppm	max = 40 ppm generally < 24 ppm	max = 16 ppm generally < 12 ppm
Cr	320-360 ppm	320 ppm	160 ppm	160 ppm
Cu	< 88 ppm	< 72 ppm	< 64 ppm	< 96 ppm
Ni	< 144 ppm	< 144 ppm	max = 88 ppm generally < 42 ppm	max = 132 ppm generally < 28 ppm
Pb	max = 180-200 ppm	< 65 ppm	< 70 ppm	max = 110 ppm generally < 70 ppm
Zn	320-340 ppm	120-200 ppm	240-280 ppm	160-280 ppm

Table 7.2: Background trace metal concentrations (ppm) for the catchment areas surrounding the four estuary sites in Western Scotland. Loch Scridain & Loch Don, Isle of Mull and Loch Creran & Loch Etive, mainland Argyll. Source: BGS Geochemical Atlas of Argyll.

which have been normalized using the correlation data in Table 7.1 as a preliminary guide but also include alternative suggestions based upon extended linear correlation of the raw data.

7.2.5: Association of trace elements with the fine sediment fraction.

As and Pb have been implicated in both redox associated reactions and affiliation with the organic fraction of the sediment matrix (Figures 6.4, Figure 7.2). Thus far, the analysis of trace metal profiles and geochemical associations with redox sensitive elements and organic sediment constituents from the Loch Scridain core has not identified a dominant mechanism responsible for the distribution of trace metals.

Figure 7.3 shows correlation plots of the trace metals (Cr, Ni and Zn) with trace elements associated with the fine sediment fraction (e.g. Rb, TiO_2, Y and Nb). However due care must be taken when using TiO_2 for such inferences as this can also be found in association with sands as the heavy mineral ilmenite.

For Ni and Cr the correlation coefficients suggest that these trace metals are indeed associated with the fine fraction. This is most likely to result from adsorption of metals onto clay particles. The correlation of Zn is however not indicative of this element being adsorbed onto clay mineral surfaces (Figure 7.3). The exact mechanism controlling the distribution of Zn is unclear being only weakly associated with Mn ($r^2 = 0.21$). Following the procedure undertaken by Loring (1991) correlation with Al and Rb was undertaken to assess the capability of these elements as potential normalizers for trace metal geochemical data from this core (Table 7.1).

From the correlation data presented in Figure 7.3 it becomes clear that both Ni and Cr are strongly correlated with yttrium. The same is also true for both Pb and As (r^2 values of 0.77 and 0.65 respectively). Yttrium is a constituent of rare-earth elements also routinely analysed by X-R-F spectrometry. As such Y may represent a suitable element with which to normalize trace metal constituents within marsh sediments from the head of Loch Scridain which have undergone a complex depositional history as a result of Late Quaternary climatic fluctuations. Normalized depth profiles for Pb, As, Cr and Ni are shown in Figure 7.4. This results in little change to the overall profiles for Pb and As. For those of Cr and Ni the profiles are generally similar apart from the upper section of the core (surface down to 14 cm) where enrichment of both Cr and Ni is visible. This corresponds to the depth interval

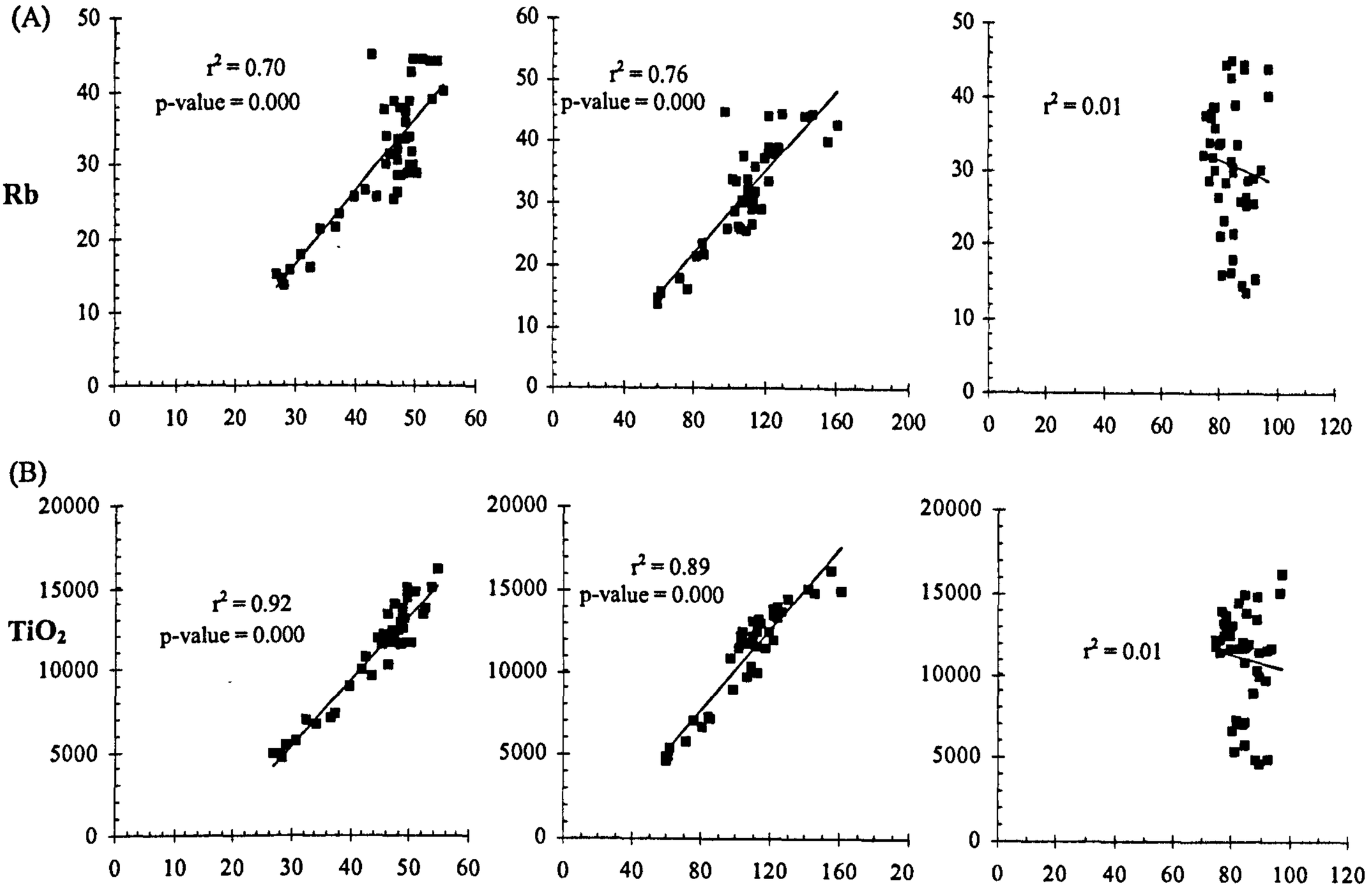

Figure 7.3: Correlation plots of Ni, Cr and Zn (ppm) with indicator elements of the fine sediment fraction within the Loch Scridain core. (A) Rubidium (ppm); (B) Titanium (ppm); (C) Yttrium (ppm); (D) Niobium (ppm), (see also Figure 6.3). (Critical value at the 95% confidence level = 0.243; n= 42; df=40).

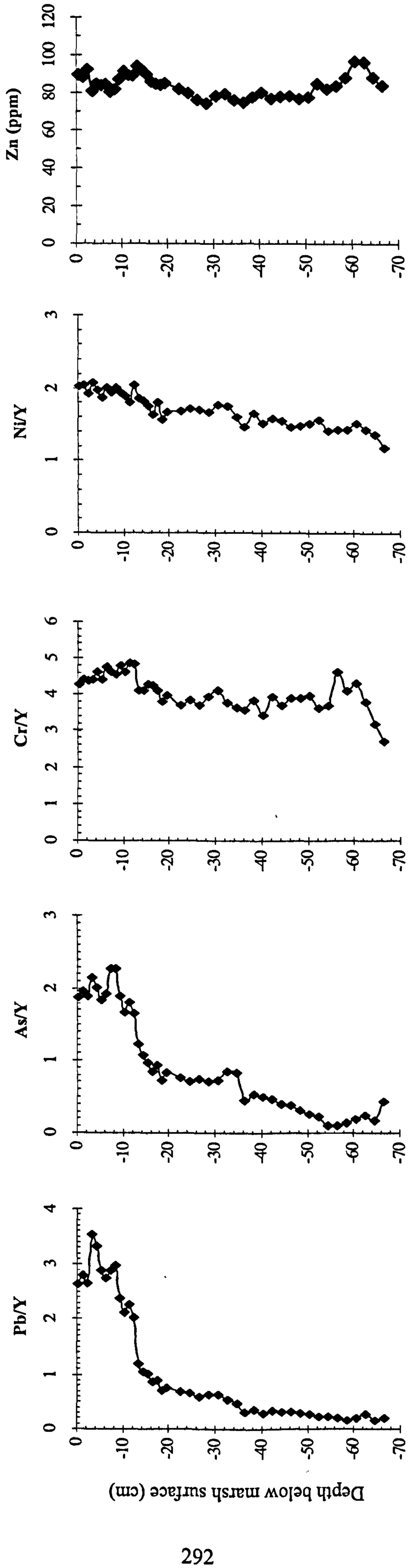

Figure 7.4: Normalized depth profiles of the trace metals and Pb, As, Cr and Ni with Y and the concentration profile of Zn ppm, not normalized) in accordance with the correlation data from Table 7.1 developed from the study by Loring (1990). Metal correlations performed in this study suggest that Y is a superior normaliser for this study site.

over which enrichment of Zn occurs (Figure 7.1) with corresponding slight increases in SiO_2 and K_2O element abundance and dry bulk density (Figure 4.7).

Concentrations of trace metals are quite variable in comparison to background crustal values from the surrounding catchments of the four sites. (Table 7.2). At Loch Scridain only As appears to be significantly enriched above background concentrations with Pb, Cr, Ni and Zn all being well below surrounding crustal values. This indicates that the marsh at Loch Scridain is not acting as a significant sink for weathered trace metal species.

7.2.6: Major and Trace element fluxes

Use of the ^{210}Pb derived chronology (CRS model, see Chapter Five) permits the reconstruction of depositional fluxes of certain trace elements to the marsh surface over time. Element fluxes are calculated from the following equation:

$$\textbf{El flux}_{(Z)} = \textbf{El}_{(CON)} \times \textbf{S}_{(R)} \times \rho_{(SED)}$$

where: El flux $_{(Z)}$ = the element flux at depth z ($\mu g\ cm^{-2}\ yr^{-1}$)

El $_{(CON)}$ = the element concentration ($\mu g\ g^{-1}$)

$S_{(R)}$ = the ^{210}Pb derived sedimentation rate ($cm\ yr^{-1}$)

and $\rho_{(SED)}$ = the sediment dry bulk density ($g\ cm^{-3}$)

Trace metal distributions have been shown to be not significantly influenced by post-depositional redox controlled reactions in the marsh core from Loch Scridain. This permits the identification of variations in the depositional history of differing trace metals owing to increased confidence that the record of sedimentation has been preserved. Solid-phase major detrital element flux profiles are shown in Figure 7.5a. and depth/flux profiles for a range of trace metals are shown in Figure 7.5b. These profiles indicate that no one particular element displays a distinct depositional history distinct from the other trace metals indicative of a single and ubiquitous source of these elements to the marsh surface over time.

Major element fluxes of Fe, MnO, TiO_2 and K reveal relatively unchanging inputs throughout much of the period of historical deposition dated with the ^{210}Pb method. Steady-state conditions are interrupted in the near-surface sediments above 3 cm depth where maximum values for all elements ($mg\ cm^2\ yr^{-1}$) are recorded. This section corresponds to a

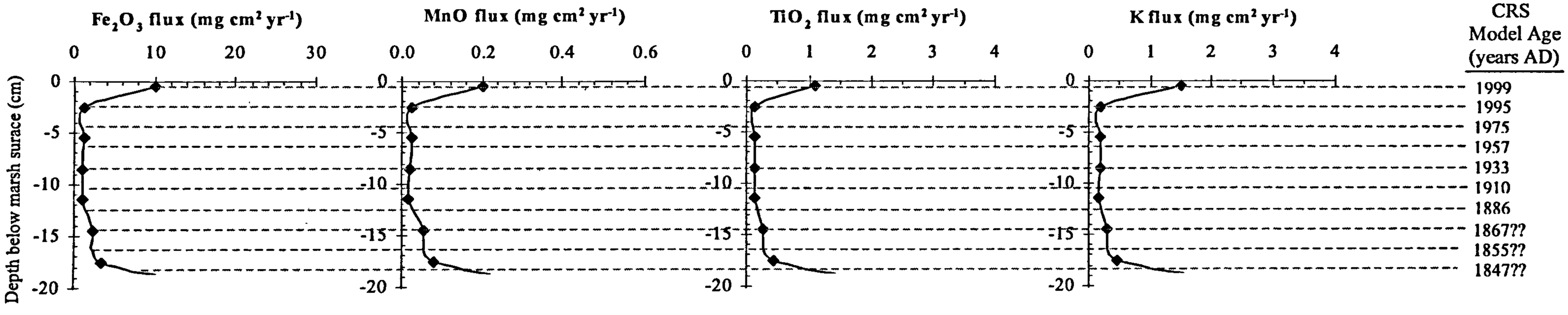

Figure 7.5a: Major element fluxes (mg cm^2 yr^{-1}) for the marsh core from Loch Scridain based upon ^{210}Pb (CRS model) derived rates of accretion. The lower horizontal dashed line indicates the maximum reliable limit of the radiometric dating. Flux calculations below this are estimation only based upon the lack of physical disturbance to this core which in some cases can reliably extend the capability of the ^{210}Pb method. Depositional flux (mg cm^2 yr^{-1}) = Sediment Dry Bulk Density (g cm^3) x Sedimentation Rate (cm a^{-1}) x Metal abundance (wt %). Sedimentation rates are those derived from the ^{210}Pb CRS modeled age.

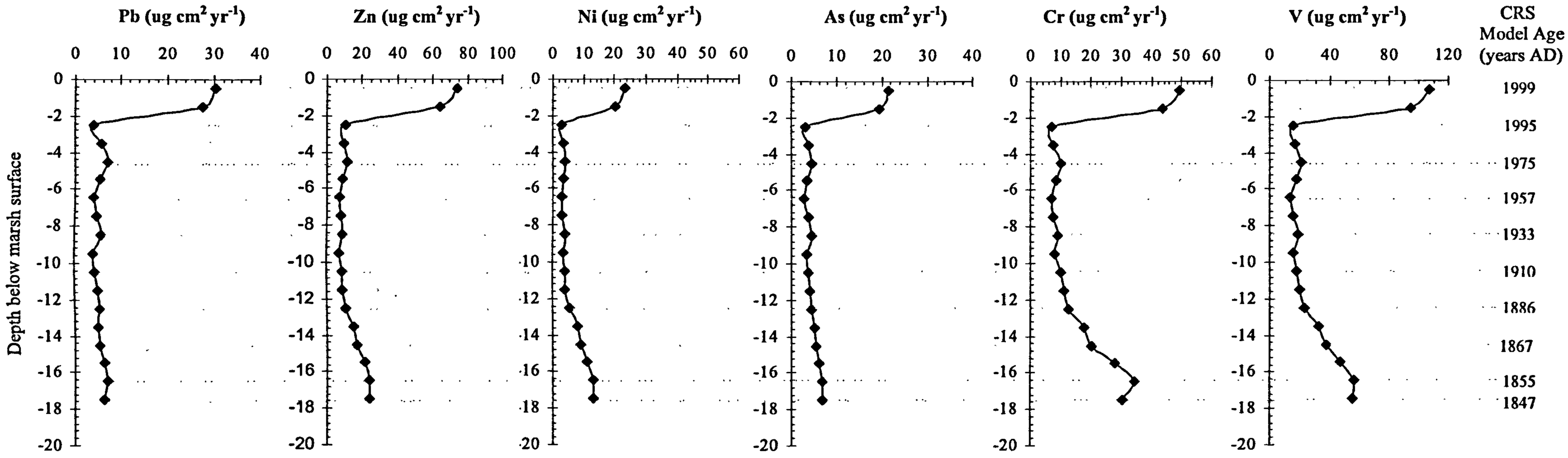

Figure 7.5b: Solid-phase derived flux/depth profiles of Pb, Zn, Ni, As, Cr and V for the marsh core from Loch Scridain with CRS model derived ^{210}Pb ages. Depositional flux (ug cm^2) = Sediment Dry Bulk Density (g cm^3) x Sedimentation Rate (cm a^{-1}) x Metal concentration (ppm). Sedimentation rates are those derived from the ^{210}Pb CRS modeled age.

similar section of the trace metal profiles shown in Figure 7.5b. All calculated trace element flux profiles show a significant increases in the flux of individual elements from c. 3 cm depth to the marsh surface over a c. 5 year period of marsh development to 1995AD strongly suggesting a significant recent increase in elemental concentrations deposited on the marsh surface.

7.2.7: Enrichment of Iodine and Bromine.

Br and I are both major anionic constituents of seawater (Br = ~70ppm; I= ~ 60ppm; Malcolm and Price, 1984). Water flooding marsh surfaces introduces large quantities of both these elements to the sediments and the pore waters contained within the sediment interstices. It is therefore likely that tidal flooding represents the largest single source of these halogens to western Scottish marshes (inferred from field observations of tidal flooding).

Malcolm and Price (1984) identified concentrations of I and Br of up to 721 ppm and 801 ppm respectively in surficial sediments taken from the lower anoxic basins within Loch Etive. Data recorded from other study sites for further comparison is presented in Table 2.2. with an overview of the geochemistry of these elements presented in Chapter Two. Within fluctuating redox conditions experienced by salt marsh sediments the relationship between iodine and organic carbon has the potential to become decoulpled (Malcolm and Price, 1984). This is particularly true within the upper oxic sediments where iodine concentration can be enhanced in the presence of free oxygen over the tidal cycle.

Bromine on the other hand is less redox sensitive and tends to behave in a less dynamic fashion. The concentration of Br has been shown to be intrinsically linked to the abundance of organic material with values of 278 ppm recorded in the Panama Basin where organic carbon values were a mere 2.5 wt % (Pedeson amd Price, 1980). Edmunds (1996) has highlighted the presence of the bromine-rich surface layer of the sea-surface which directly results from the enrichment of bromine in marine aerosols relative to chlorine and the increased concentration of organic carbon found in the upper ocean surface. As a consequence, the regular tidal flooding coupled with the presence of both marine and terrestrial organic matter in salt marsh environments can be expected to be highly enriched in Br.

Depth profiles of I and Br from the Loch Scridain marsh core are presented in Figure 7.6. These indicate that the upper oxic sediments are highly enriched with I and Br above the 40 cm depth increment whilst LOI values do not exceed 10 wt %. Average core concentrations for I and Br are 236 (ppm) and 84 (ppm) with maximum values for I (451 ppm) occurring at 34-35 cm depth corresponding to the redox controlled precipitation of iodate immediately above the redox-cline (Figure 6.3). Maximum concentration of Br (223 ppm) occurs within the near-surface sediments at a depth of 7-8 cm. The Br concentration profile closely resembles those of Pb and As and correlation plots reveal the strong positive association between Bromine and Pb and As (r^2 value of 0.94 and 0.86; Figure 7.7). This is a likely consequence of the interaction of the bromine-rich surface microlayer with vegetation and sediment material over the tidal cycle. Pellenbarg (1984) has shown that this process can exert a significant influence upon the deposition of brominated metals.

I/LOI and Br/LOI range from 22-80 and 5-32 and fall within the lower range of values reported for other geographical areas in the available literature listed in Table 2.2. These values are remarkably similar to the ratios reported from the Tamar estuary (south-west UK) by Upstill-Goddard and Elderfield (1988). Consequently these I/LOI and Br/LOI ratios are lower than those reported for surficial sediments from Loch Etive by Malcolm and Price (1984).

Correlation plots of I vs. LOI and Br vs. LOI reveal r^2 values of 0.67 and 0.47 respectively taken over the entire depth of the core (Figure 7.6). The concentrations of organic matter, I and Br below the inferred weak redox boundary of this core are all much reduced by comparison to the oxic sediments. Also shown in Figure 7.6 is the depth profile for ferric Fe and the correlation plot for Fe vs I. Ullman and Aller (1980) have suggested that an important sink for I exists at the sediment water interface and that this may be due to association of I with Mn oxides in the sediment surface. Correlation of the Loch Scridain data reveal a positive association of Mn with I distribution in this core ($r^2 = 0.57$) suggesting I is being scavenged to some extent by Mn oxyhydroxides (Figure 7.6). Similarly, the correlation of I with Fe ($r^2 = 0.50$) suggests that a comparable mechanism is responsible for the association with ferric oxyhydroxides evident in this core.

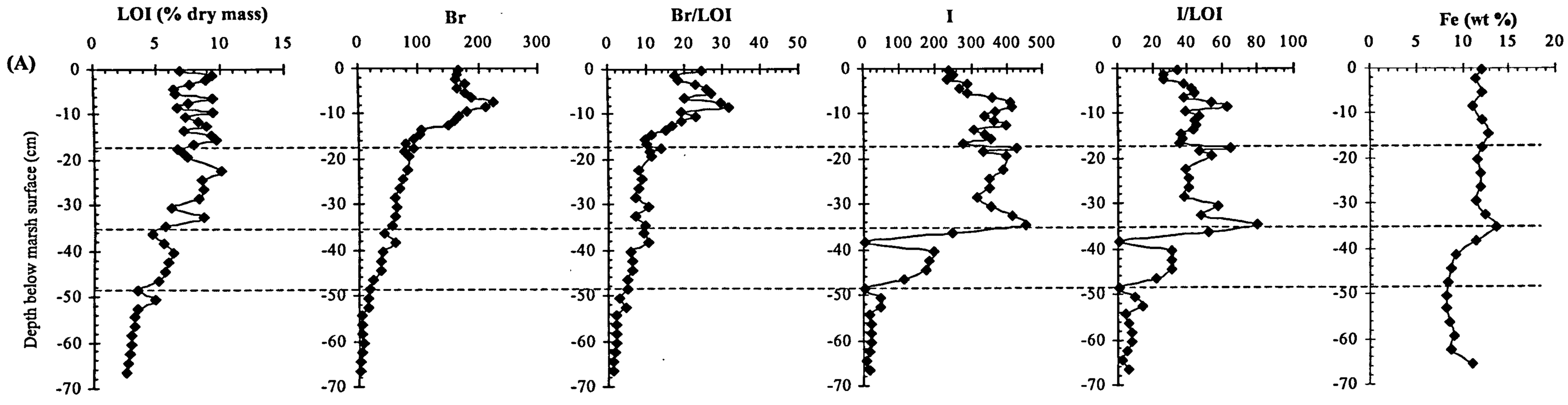

Figure 7.6: (A) Depth profiles of organic content (via LOI 550°C, % dry mass), Iodine & Bromine (ppm) and Ferric Iron (wt %), with ratios of I/LOI and Br/LOI for the Loch Scridain marsh core. (B) Correlation of LOI with I and Br. (C) Correlation of I with ferric Fe.

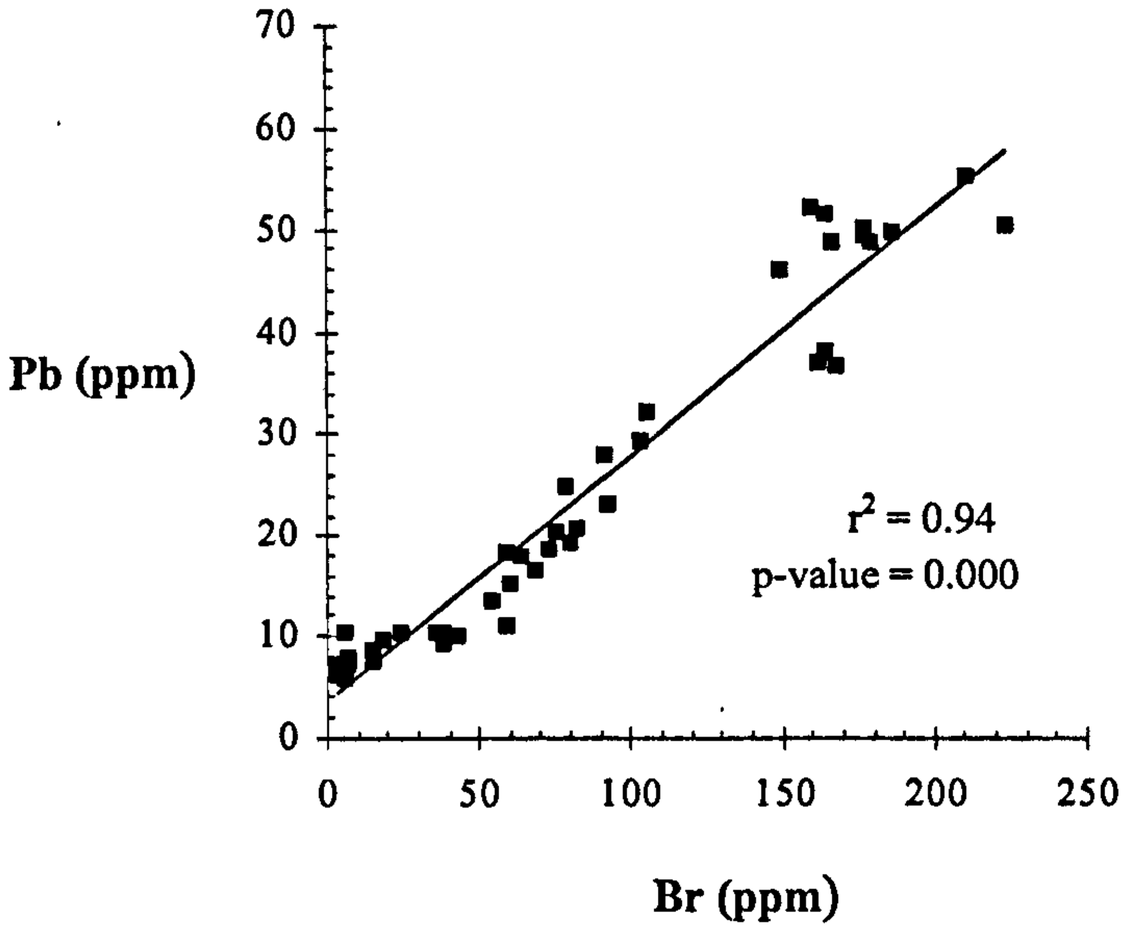

Critical value at the 95% confidence level = 0.304 (n = 42; df = 40)

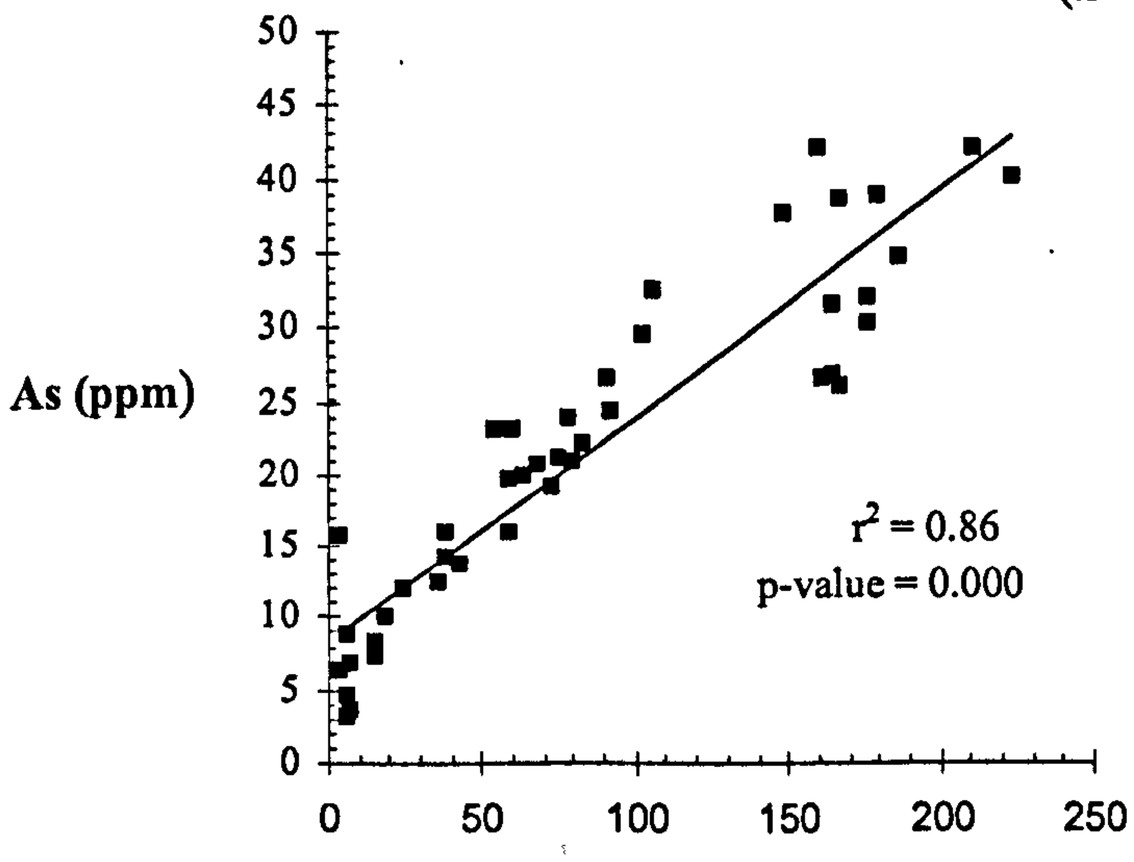

Figure 7.7: Graphical correlation plots to show the association of Bromine with the trace metals Pb and As in the marsh core from Loch Scridain.

7.3: Loch Don

7.3.1: Manganese association with trace metals

Fe and Mn profiles indicate that diagenetic recycling of these redox-sensitive elements has taken place within the marsh sediments from Loch Don. Manganese oxides have considerable capacity to act as substrates permitting adsorption of many divalent trace metals into the Mn-oxide lattice (Hem, 1978; Lewis, 1997). Concentration profiles of trace metals in natural waters have the potential to be significantly influenced by sorption processes onto Mn oxyhydroxide surfaces (Shaw *et al.*, 1990).

Horizontal correlation of Mn with trace metals reveals that despite a strong degree of similarity with regard to trace metal concentrations the profiles these elements are unlikely to be influenced by adsorption to Mn oxyhydroxide surfaces (Figure 7.8). Linear correlation reveals low values for Pb and As (r^2= 0.30 and 0.39 respectively). Similar to the association with Fe, As distribution does not appear to be controlled by early diagenetic redox-sensitive species and the distribution of Pb does not appear to be significantly altered via adsorption processes onto Mn oxyhydroxides. Linear regression of Mn with the remaining trace metals Cr, Cu, Ni and Zn reveals lower correlation coefficients with r^2 values of 0.05, 0.23, 0.39 and 0.37 respectively (Figure 7.8). This suggests that in comparison to the core from Loch Scridain, trace metal distributions are not being significantly modified by early diagenetic reactions in the Loch Don Core depite the obvious diagenetic signature of both Fe and Mn oxyhydrides within the oxic/post oxic zones.

7.3.2: Trace metal association with sulphidic phases.

In anoxic saltmarsh sediments calculations predict the formation of thermodynamically stable forms of trace metal sulphides (Luther *et al.*, 1980). Furthermore, the same authors have identified the presence of framboids of mixed zinc and iron sulphide minerals as well as revealing the incorporation of nickel into pyrite (Luther *at al*, 1980, Lewis, 1997). The concentration profiles of the trace metals Pb, As, Cr, Cu, Ni and Zn in the Loch Don core indicate that slight enrichment of all these elements has occurred within the sediments containing elevated levels of reduced sulphur (Figure 7.8). Slight enrichment within this section of the core (between 30-40 cm) are likely to result from the known

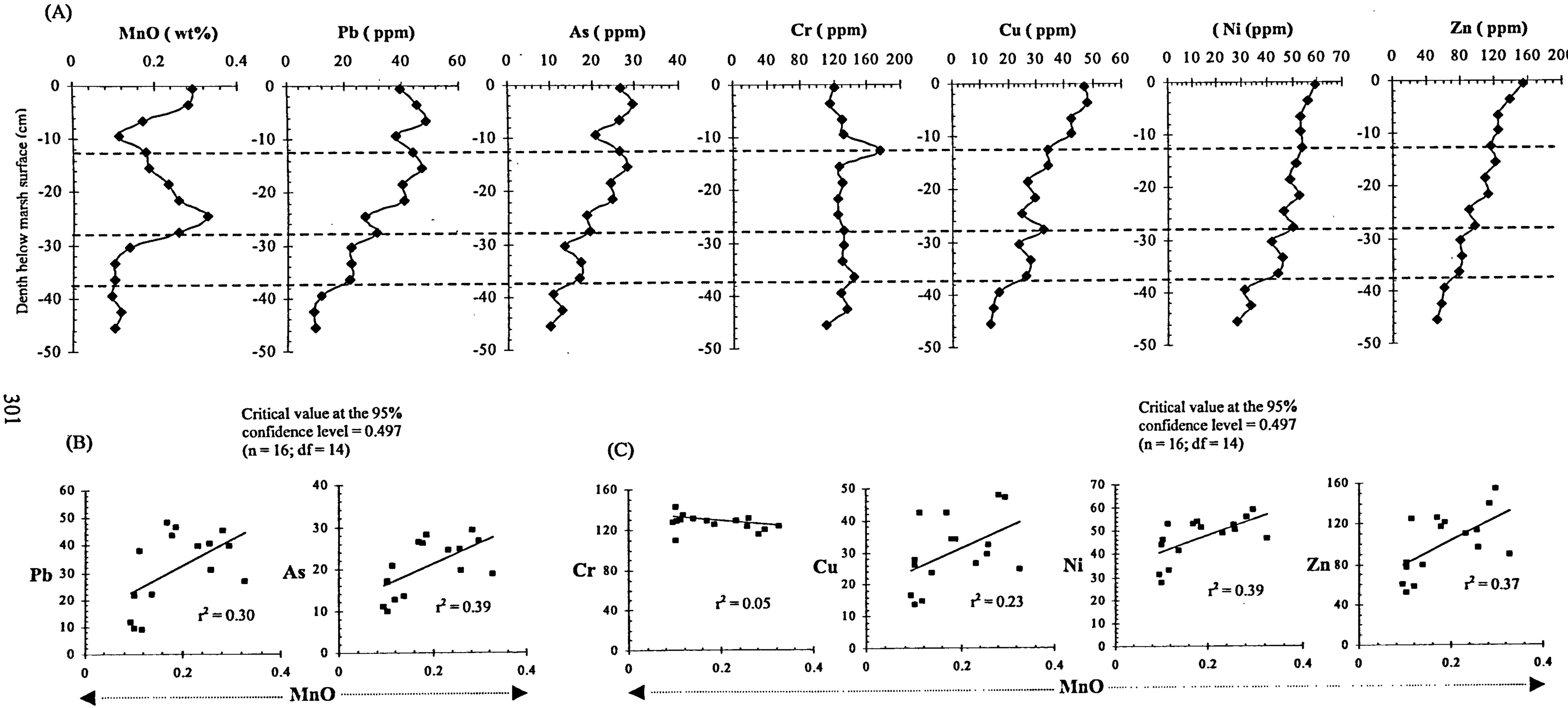

Figure 7.8: (A) Horizontal correlation between MnO (wt %) and Pb, As, Cr, Cu, Ni and Zn (ppm) for the marsh core from Loch Don. (B) Linear correlation plots of Mn with Pb and As. (C) Correlation of MnO with Cr, Cu, Ni and Zn.

association of trace metals with sulphide minerals via cation scavenging processes (Jean and Bancroft, 1986).

However, the diagenetic peaks within the reduced section of the core are not as substantial when compared to studies of reduced sediments from other geographical locations (e.g. Huerta-Diaz and Morse, 1992; Morse, 1994; Cundy and Croudace, 1996; Thompson *et al*, 2002). This suggests that the development of fully anoxic conditions has not occurred. (discussed in Chapter Eight).

7.3.3: Trace element associations with organic material

A detailed overview of the processes that influence the geochemical association of trace metals with organic material has been presented in section 7.2.3. Horizontal correlation of the loss on ignition depth profile from Loch Don (as a proxy for organic carbon content) reveals a strong similarity with the depth profiles for Pb and As (Figure 7.9). This is confirmed by the linear regression plots showing r^2 values of 0.72 and 0.93 for Pb and As respectively. Weaker associations are apparent for the trace metals Cu, Ni and Zn with correlation coefficients of 0.53, 0.57 and 0.43 respectively. The distribution of Cr within these sediments is decoupled from the distribution of organic carbon (r^2 = 0.01). The distribution of Pb, As, Cu, Ni and Zn would appear to coincide with the development of marsh vegetation in the marsh at Loch Don, inferred from the LOI profile (Figure 7.9). It is likely that one or all of the processes responsible for trace metal association with sedimentary organic material outlined in section 7.2.3 have influenced the down-core element distributions. LOI derived values for organic carbon content are lower within these western Scottish marshes in comparison to other UK coastal wetlands (e.g. McCaffrey and Thompson, 1980; Cundy *et al.*, 1994; Thompson *et al.*, 2002). It is therefore probable that metal enrichment may be taking place within the organic-rich silt-clay fractions of the sediment where high ion-exchange capacities exist (Williams *et al.*, 1996).

7.3.4: Association of trace elements with the fine fraction.

Previous analyses of trace element behaviour within the core from Loch Don indicate that metals are not being significantly scavenged by Mn oxyhyroxides (Figure 7.8) although stronger associations with organic material have been demonstrated (Figure 7.9).

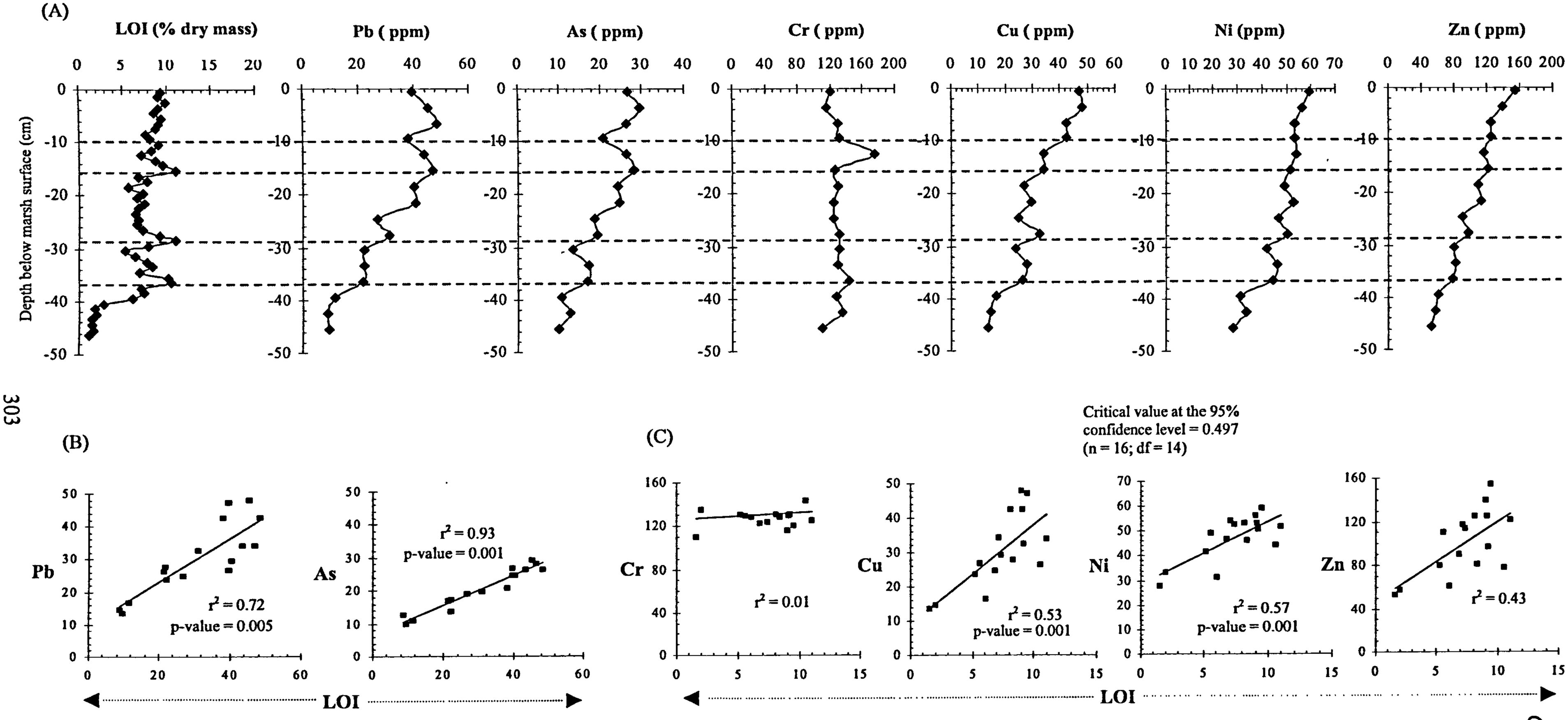

Figure 7.9: (A) Horizontal correlation between organic content (via LOI % dry mass) and Pb, As, Cr, Cu, Ni and Zn (ppm) for the marsh core from Loch Don. (B) Linear correlation plots of LOI with Pb and As. (C) Correlation of LOI with Cr, Cu, Ni and Zn.

Correlation plots of trace metal distributions with key indicator elements of the fine fraction of marsh sediments (Rb, Ti, Y and Nb) are presented in Figure 7.10. These highlight the positive association of trace metal distributions with fine particulate material presumably through adsorption onto clay mineral surfaces. The graphical plots also support the data presented in Table 7.1, which indicates the suitability of Rb as a normalizing agent for the marsh sediments from Loch Don. Normalized depth profiles for trace metals are presented in Figure 7.11. These profiles highlight the generally increasing concentrations of Pb, As, Cr, Cu Ni and Zn. The peak in Cr, Cu, Ni and Zn apparent at a depth of 10-11 cm corresponds to a slight decline in $^{210}Pb_{total}$ activity (Bq g^{-1}) at the same depth interval (Figure 5.7) and a distinct peak in dry bulk density (Figure 4.18). Slight enrichment of CaO abundance at the same depth increment suggests in-wash of marine derived older sediment. In the upper near-surface layers Cu, Ni and Zn all show enrichment relative to the lower sections of the core beneath 10-11 cm depth. Cr concentration declines in the near-surface layers possibly as a result of association with heavier mineral phases.

Similar to the core from the Loch Scridain site, trace metal concentrations are all below estimated background concentrations with the exception of As which shows slight enrichment in the upper 24 cm of the core. This indicates that the marsh sediments in the core from Loch Don are also not a significant sink for dissolved or detrital weathered metals.

7.3.5: Major and Trace element fluxes

Major element fluxes of Fe, Mn, Ti and K reveal a period of maximum element flux between 21-31 cm (Figure 7.12a). For the Fe and Mn profiles these peaks correspond to enrichment as a result of diagenetic precipitation of these elements (Figure 6.5). However, K and Ti are not redox-sensitive and a lower peak is also visible between 31-37 cm depth. The increased flux in K and Ti over this depth increment represents enhanced detrital input at the beginning of the last century with the overlying peak indicative of increased fine particulate material deposited on the marsh surface over the period 1911-1928 AD. This corresponds to an increase in organic matter content (Figure 7.9) and may therefore represent increased sediment accumulation in response to vegetative growth. These two periods of enhanced major element flux are also recorded in the calculated trace element flux profiles shown in Figure 7.12b. Over the depth extending from 4-22 cm (corresponding to a 60 year period from 1928-1988 AD) trace metal fluxes reveal a period of reduced quite constant flux. Within the uppermost section of the core all trace element fluxes are seen to increase up to

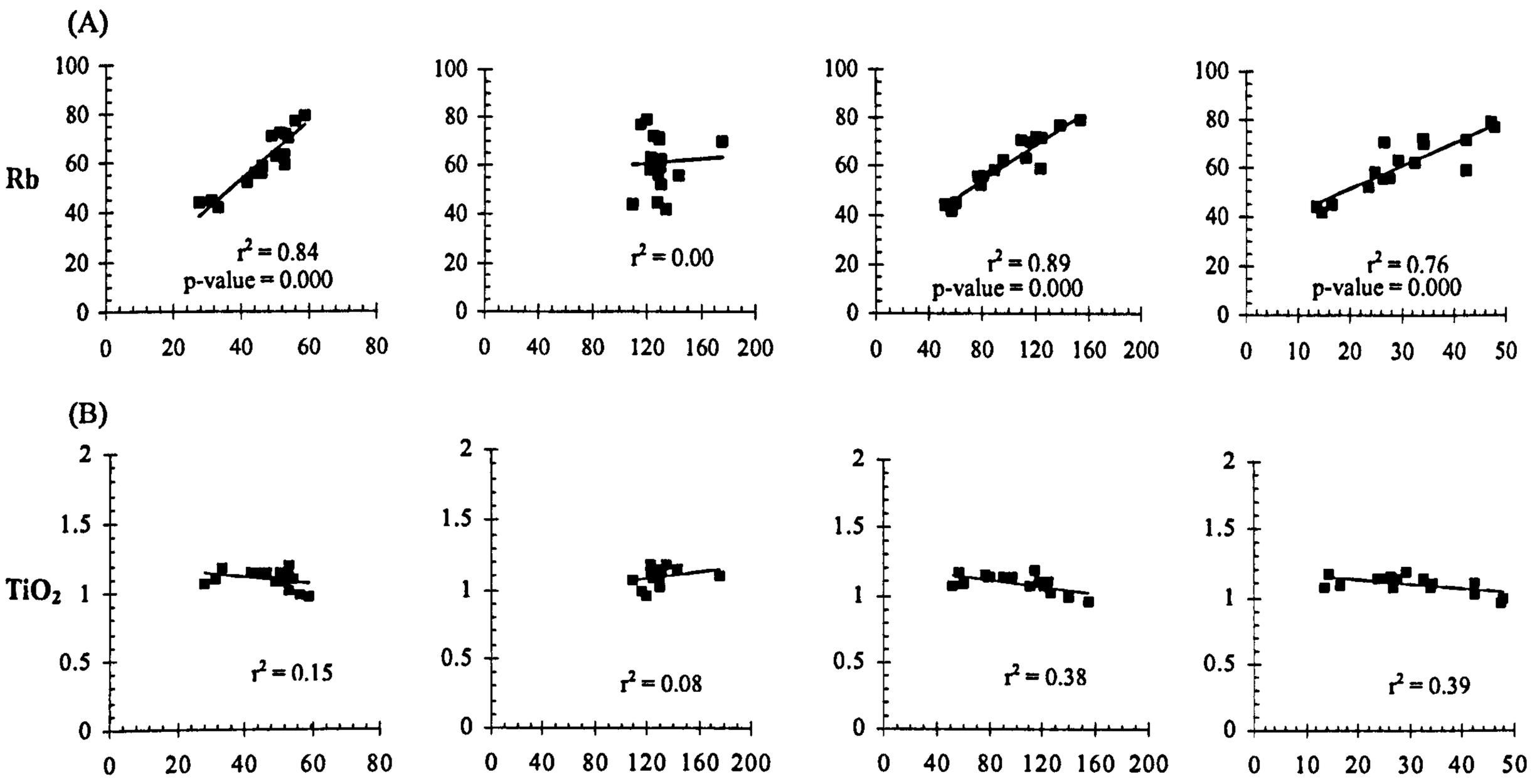

Figure 7.10: Correlation plots of Ni, Cr, Zn and Cu (ppm) with indicator elements of the fine sediment fraction within the Loch Don marsh core. (A) Rubidium (ppm); (B) Titanium (ppm); (C) Yttrium (ppm) and (D) Niobium (ppm). (Critical value at the 95% confidence level =0.497; n=16; df = 14).

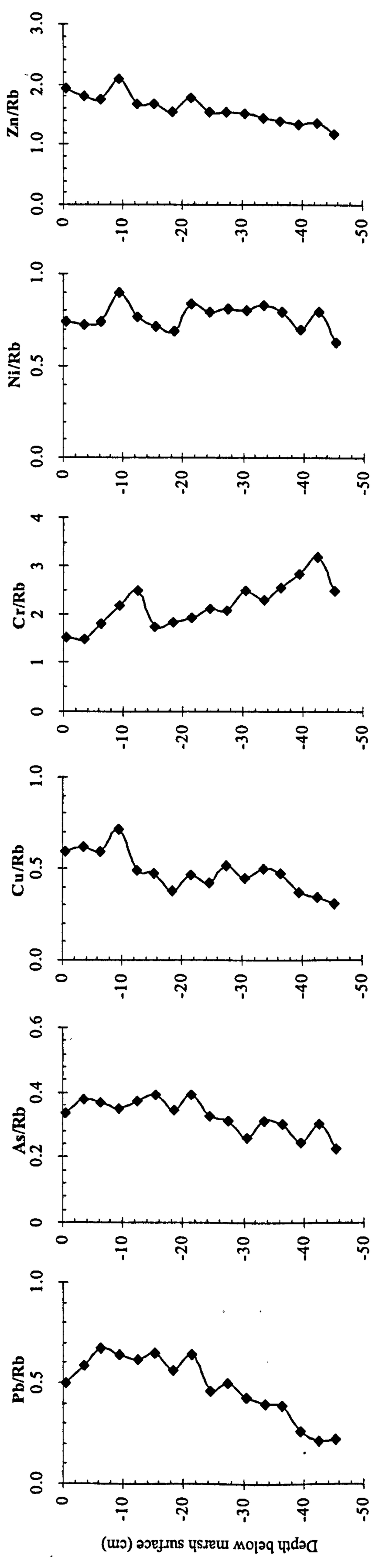

Figure 7.11: Down-core depth concentration profiles of heavy metals normalized to Rb for the marsh core from Loch Don in accordance with metal-normalizing agent data presented in Table 6.1 developed from the study of Loring (1990).

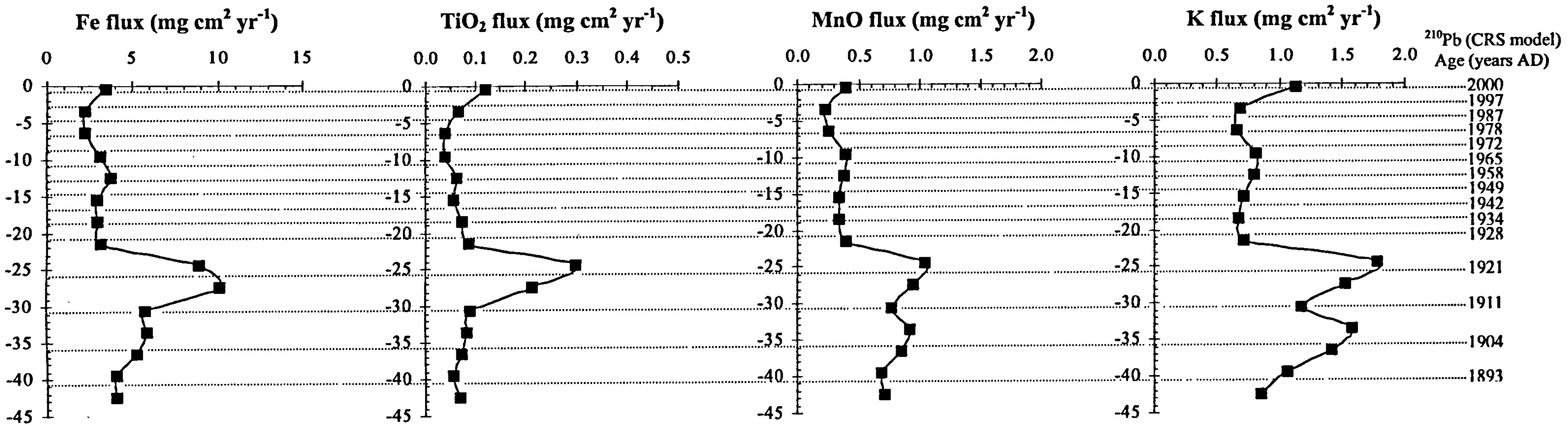

Figure 7.12a: Major element fluxes (mg cm^2 yr^{-1}) for the marsh core from Loch Don based upon ^{210}Pb (CRS model) derived rates of accretion. Depositional flux (mg cm^2) = Sediment Dry Bulk Density (g cm^3) x Sedimentation Rate (cm a^{-1}) x Metal concentration (wt %). Sedimentation rates are those derived from the ^{210}Pb CRS modeled age.

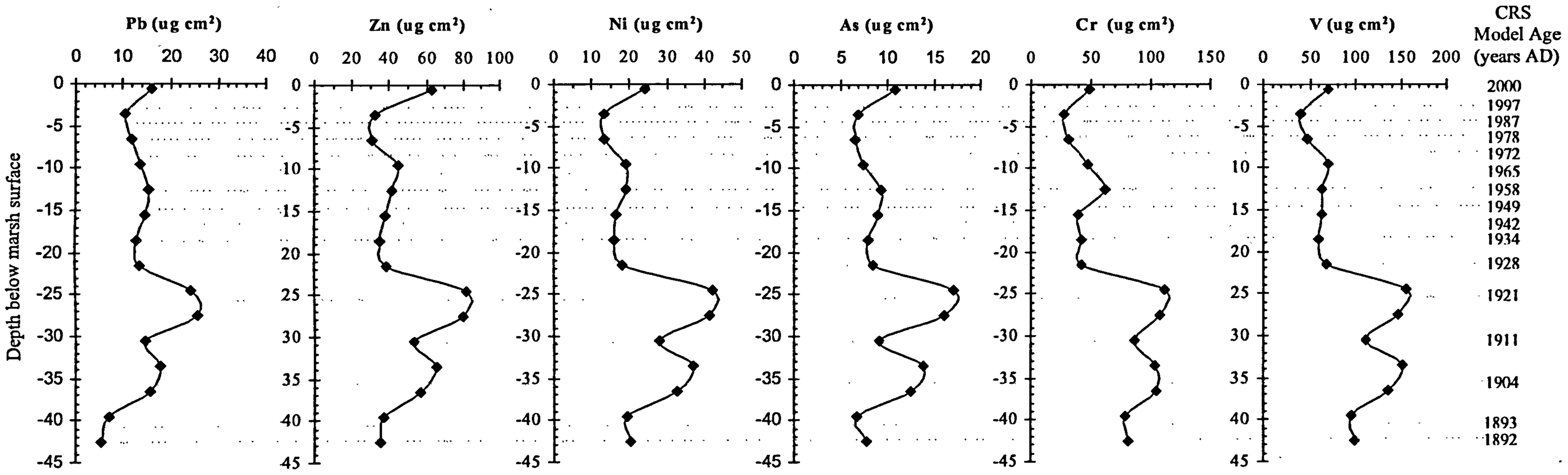

Figure 7.12b: Solid-phase derived flux/depth profiles of Pb, Zn, Ni, As, Cr and V for the marsh core from Loch Don with CRS model derived ^{210}Pb ages. Depositional flux (ug cm^2) = Sediment Dry Bulk Density (g cm^3) x Sedimentation Rate (cm a^{-1}) x Metal concentration (ppm). Sedimentation rates are those derived from the ^{210}Pb CRS modeled age.

the present day (time of sampling) of 1999 AD suggesting a significant recent increase in elemental concentrations in the near-surface sediments recently deposited on the marsh surface (Figure 7.12b).

7.3.6: Enrichment of Iodine and Bromine

Depth profiles of I and Br from the Loch Don marsh core are presented in Figure 7.13. These indicate that the upper oxic sediments are highly enriched with I and Br above the 40 cm depth increment whilst LOI values do not exceed 12 wt %. Maximum recorded concentrations for Br are up to 1190 (ppm) in the near surface sediments whilst for I the maximum value is 418 (ppm) at 15-16 cm depth. The concentrations of organic matter, I and Br below the inferred weak redox boundary of this core at 30-31 cm depth are much reduced in comparison to the oxic overlying sediments. Average concentration values for I and Br throughout the core are 237 (ppm) and 552 (ppm) respectively and are within the values obtained by Malcolm and Price (1984) for surficial sediments within Loch Etive. I/LOI and Br/LOI ratios range from between 17 –70 and 17-132 respectively and are somewhat lower than reported ratios of these elements to marine carbon described by Malcolm and Price (1984) for the Loch Etive sediments. However, these ratio values are broadly comparable to those reported in the literature derived from different geographical locations listed in Table 2.2.

Correlation plots of I vs. LOI and Br vs. LOI reveal r^2 values of 0.39 and 0.47 respectively taken over the entire depth of the core (Figure 7.13). This latter value demonstrates the similar level of Br association with organic material evident in the core from western Mull at the head of Loch Scridain. Ullman and Aller (1980) have suggested that an important sink for I exists at the sediment water interface and that this may be due to association of I with Mn oxides in the sediment surface. Correlation of the Loch Don solid phase data For I reveals a weak positive association of Mn with I distribution in this core (r^2 = 0.49) suggesting that some I is being scavenged by Mn oxyhydroxides. Similarly, the correlation of I with Fe ($r^2 = 0.58$) suggests that a comparable mechanism is responsible for the stronger association with Fe_2O_3 and that scavenging of I by Fe oxyhydroxides also influences the distribution of this halogen (Figure 7.13). The Br concentration profile closely resembles those of Pb and As and correlation plots reveal the strong positive association between Bromine and Pb and As (r^2 value of 0.84 and 0.86; Figure 6.23b). Similar positive correlations also exist between Br and Cu, Ni and Zn (r^2 values of 0.94, 0.86

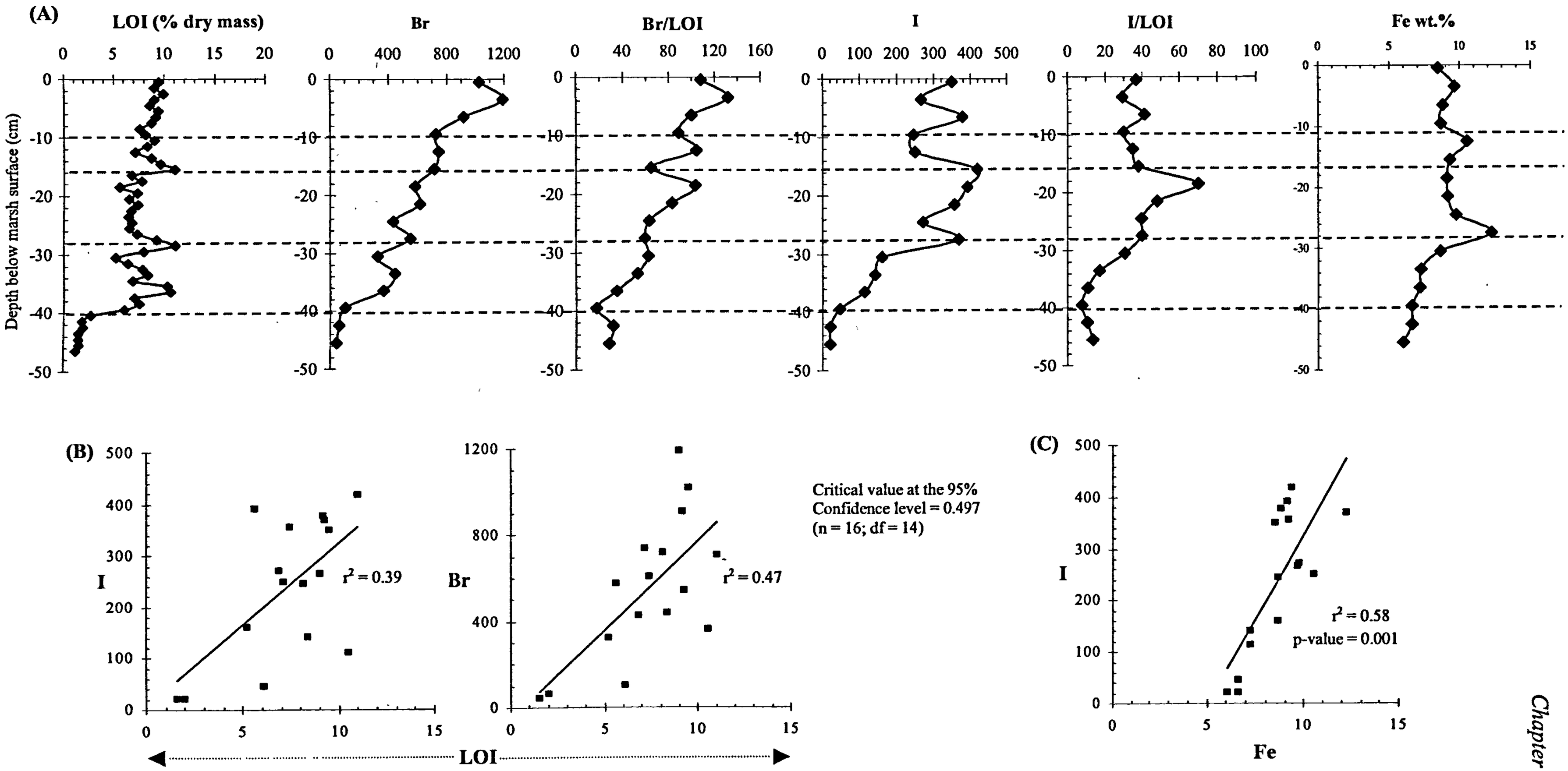

Figure 7.13: (A) Depth profiles of organic carbon (via LOI % dry mass), Iodine & Bromine (ppm) and Ferric Iron (wt %), with ratio profiles of I/LOI and Br/LOI for the Loch Don marsh core. (B) Correlation of LOI with I and Br. (C) Correlation of I with ferric Fe.

and 0.94 respectively). This is a likely consequence of the interaction of the bromine-rich surface microlayer with vegetation and sediment material over the tidal cycle. Pellenbarg (1984) has shown that this process can exert a significant influence upon the deposition of brominated metals (Figure 7.14). Comparison of the r^2 values suggests that bromination of these trace metals is an active process in this marsh as opposed to the more simple explanation of association of elements with organic matter (Figures 7.9 & 7.14).

7.4: Loch Creran

7.4.1: Association of trace metals (As, Pb, Cr, Cu, Ni and Zn) with Mn

Horizontal correlation between the depth profile for MnO and trace metal distributions reveals that adsorption of Pb and As onto Mn oxyhydroxides partially controls the distribution of these elements (Figure 7.15). Linear correlation supports this view with r^2 values of 0.59 and 0.57 for Pb and As respectively over the entire core depth. Less similarity exists between the profiles of Cr, Cu, Ni and Zn with the profile for MnO indicating that to a large extent the distribution of these elements are rather decoupled from that of Mn and are therefore being controlled by other mechanisms than diagenetic remobilisation (Figure 7.15).

7.4.2: Trace metal association with sulphidic phases.

Similar to the core from Loch Don, the iron and sulphur down-core profiles from Loch Creran do not exhibit significant enrichment of these redox-sensitive elements below the inferred redox-cline (situated at 48 cm depth) shown in Figures 6.9 & 6.11. This section of the core is characterised by significant enrichment of reduced sulphur. Inspection of the down-core profiles of the trace metals Pb, As, Cr, Cu, Ni and Zn all show that no significant enrichment indicative of strongly reducing conditions has taken place at a corresponding depth (Figure 7.15). As such the formation of authigenic metal sulphide minerals and trace metal scavenging by iron sulphides is considered to be rather insignificant in this core at depth. Fe does seem to be retained within the post-oxic and oxic layers and therefore low levels of reduced iron within the anoxic zone may also partially account for the lack of metal sulphide formation.

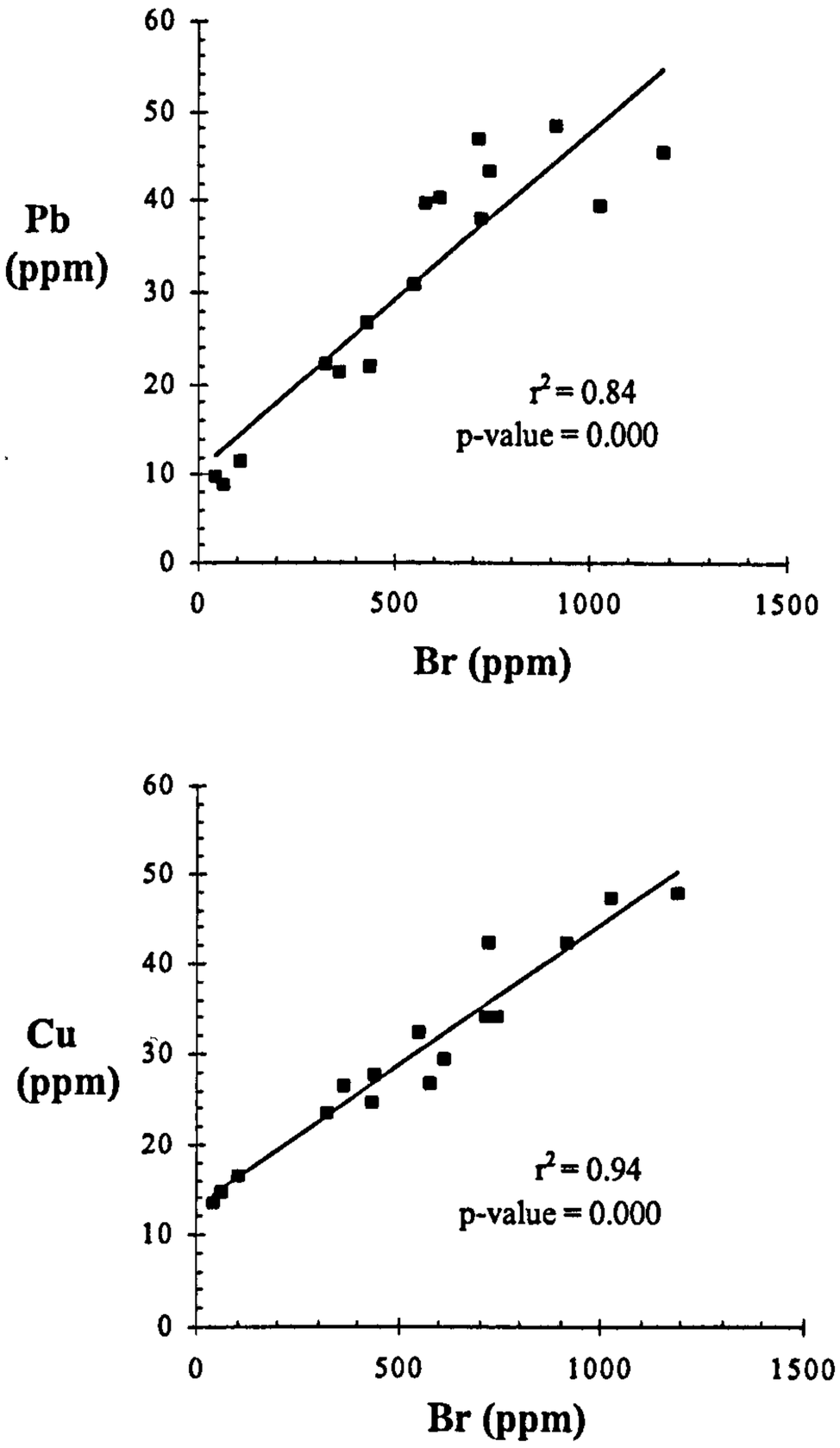

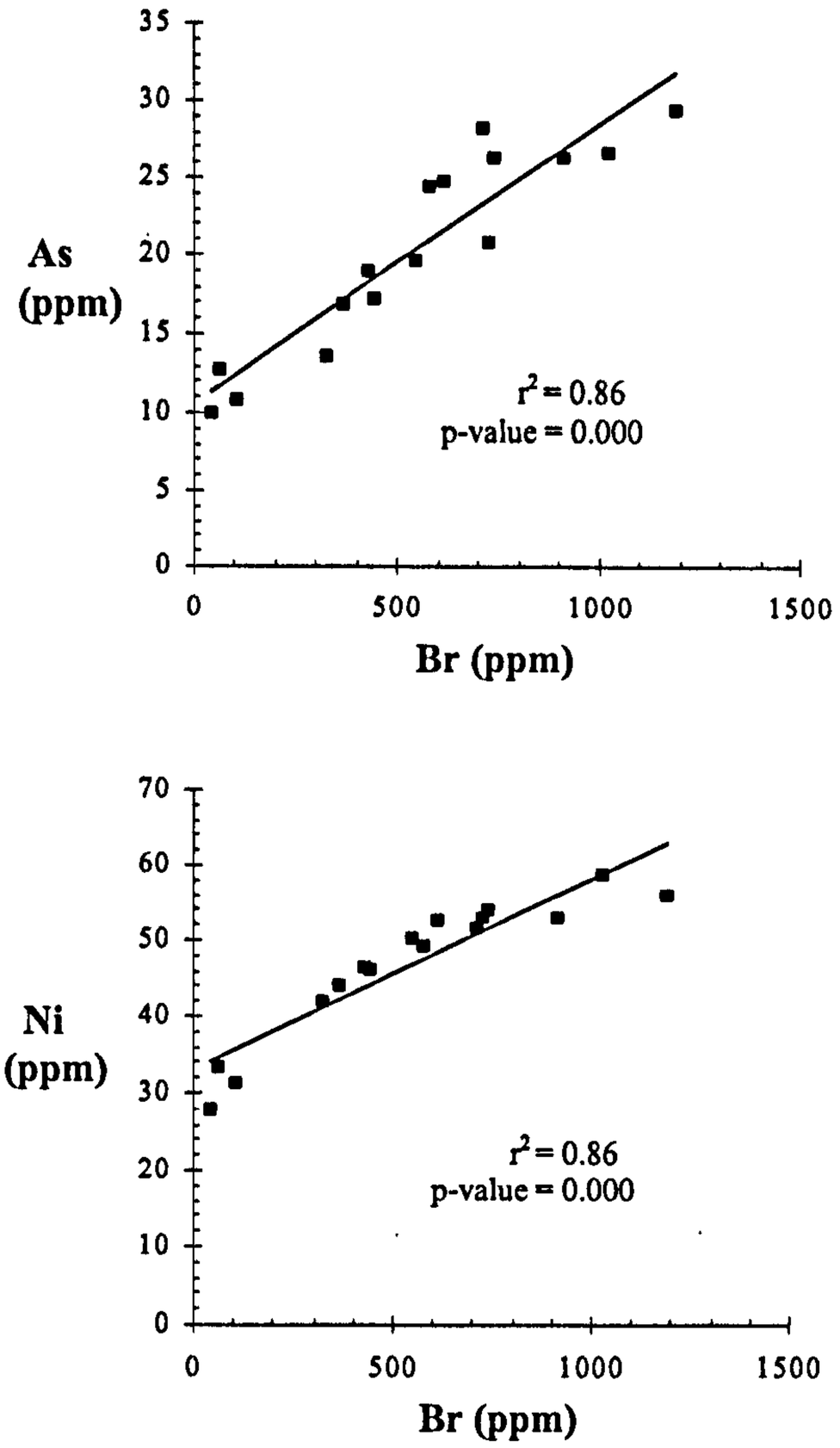

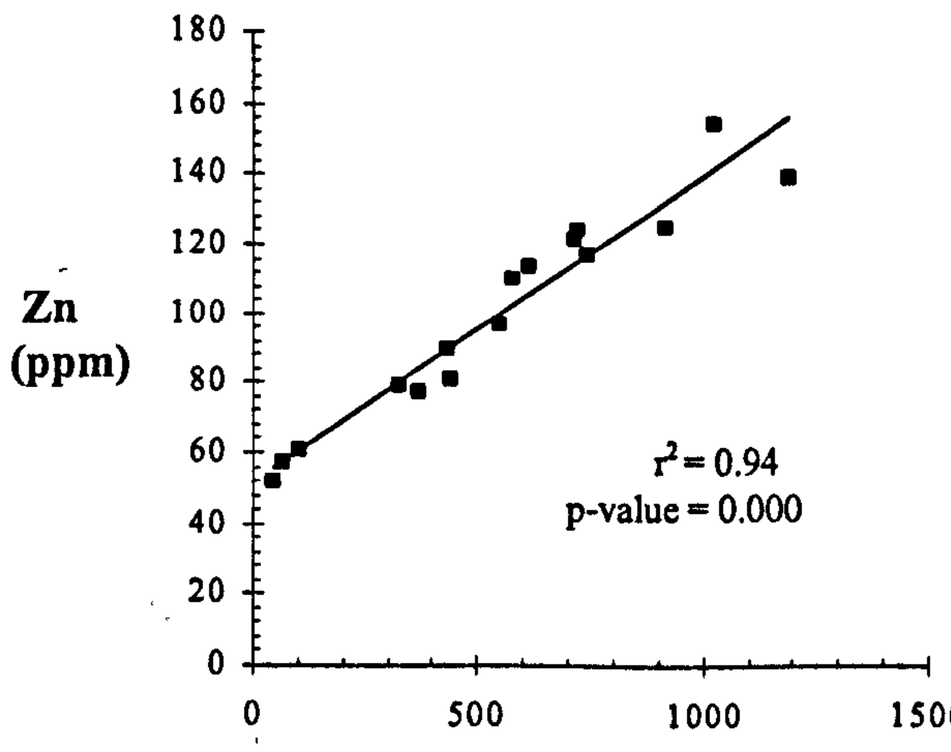

Critical value at the 95% confidence level = 0.497 (n = 16; df = 14)

Figure 7.14: Positive linear correlations to show bromination of trace metals in the marsh core from Loch Don.

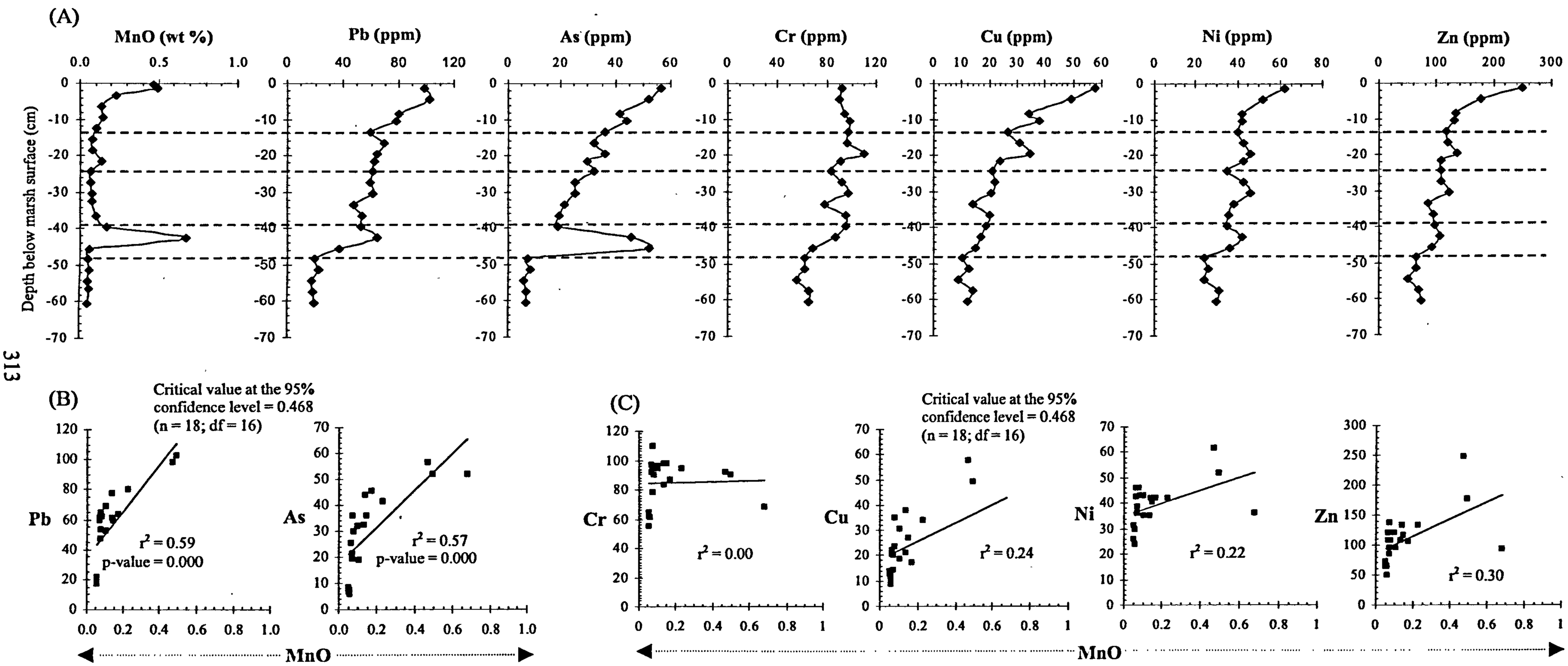

Figure 7.15: (A) Horizontal correlation between MnO (wt %) and the trace metals Pb, As, Cr, Cu, Ni and Zn (ppm) for the marsh core from Loch Creran. (B) Linear correlation of MnO with Pb and As. (C) Correlation of MnO with Cr, Cu, Ni and Zn.

7.4.3: Trace metal associations with organic material (As, Pb, Cr, Cu, Ni, and Zn)

The down-core profiles of trace metals within the Loch Creran marsh core show a strong horizontal correlation with the organic carbon distribution derived from loss on ignition (Figure 7.16). Profiles for Pb and As are strongly correlated with loss on ignition (r^2 values of 0.71 and 0.70 respectively) indicating that the distribution of these trace elements is significantly influenced by the distribution of organic material. Certainly, enrichment of Pb and As between the depth interval of 40-48 cm corresponds to gradually increasing values for loss on ignition over the same depth interval (Figure 7.16), although in the previous section adsorption to MnO oxyhydroxides also points to a diagenetic influence at this depth in the core. Unlike the core from Loch Don there is greater correlation between loss on ignition distribution and the trace metal profiles of Cr, Cu, Ni and Zn (Figure 7.16).

7.4.4: Association of trace elements with the fine fraction.

Some adsorption of Pb and As onto Mn oxyhyroxides is indicated within the sediments from Loch Creran (Figure 7.15). It is therefore probable that alteration of at least part of the distribution profiles of these elements is due to diagenetic chemical reactions particularly at the base of the post-oxic zone (Figure 7.15). Other trace metals (Cr, Cu, Ni and Zn) do not appear to be influenced by diagenetic processes to the same degree. These same trace metals, particularly Pb and As, do appear to be strongly associated with the level of organic material present in the marsh sediments (Figure 7.16).

Correlation of trace metal distributions with key indicator elements of the fine fraction (Rb, TiO_2, Y and Nb) are shown in Figure 7.17. These graphical plots clearly indicate that metal adsorption onto fine particulate material (clay particles) is taking place in this core. Furthermore these data also suggest that Yttrium is likely to be a superior normalizing agent when compared to the correlation of both Al and Rb shown in Table 7.1. Trace metal profiles normalized to yttrium are shown in Figure 7.18. The normalized down-core profiles clearly show the effect of early-diagenetic reactions to the lower sections of the Pb, As and Cr distributions. Normalized Cu, Ni and Zn profiles all exhibit comparable distributions with a strong horizontal similarity throughout. Cr is seen to fluctuate within the mid-depths of the core due to the likely association with other heavy minerals (e.g.TiO2, Figure 4.28). Importantly, all the normalized trace element profiles indicate significant

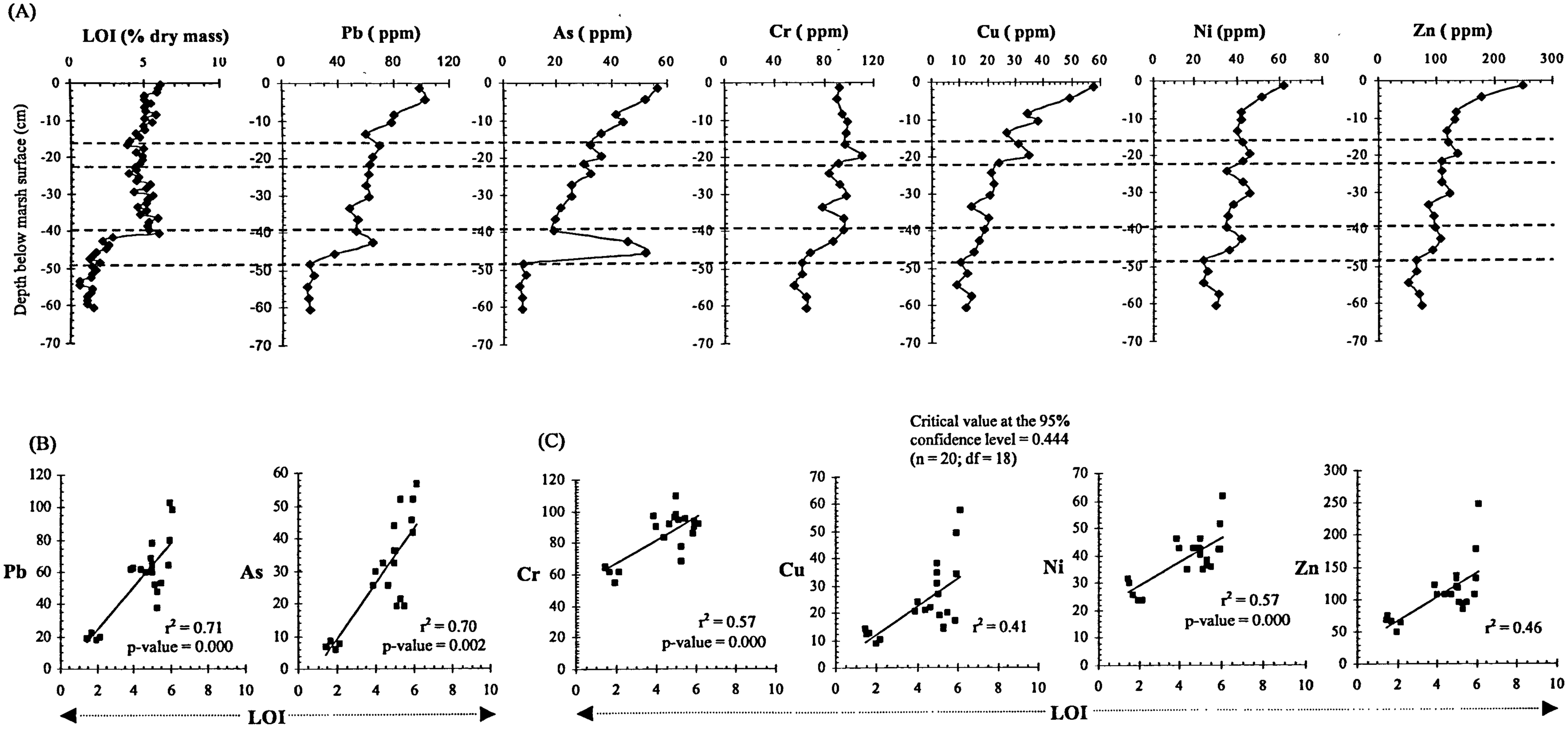

Figure 7.16: (A) Horizontal correlation between organic content (via LOI % dry mass) and Pb, As, Cr, Cu, Ni and Zn (ppm) for the marsh core from Loch Creran. (B) Linear correlation plots of LOI with Pb and As. (C) Correlation of LOI with Cr, Cu, Ni and Zn.

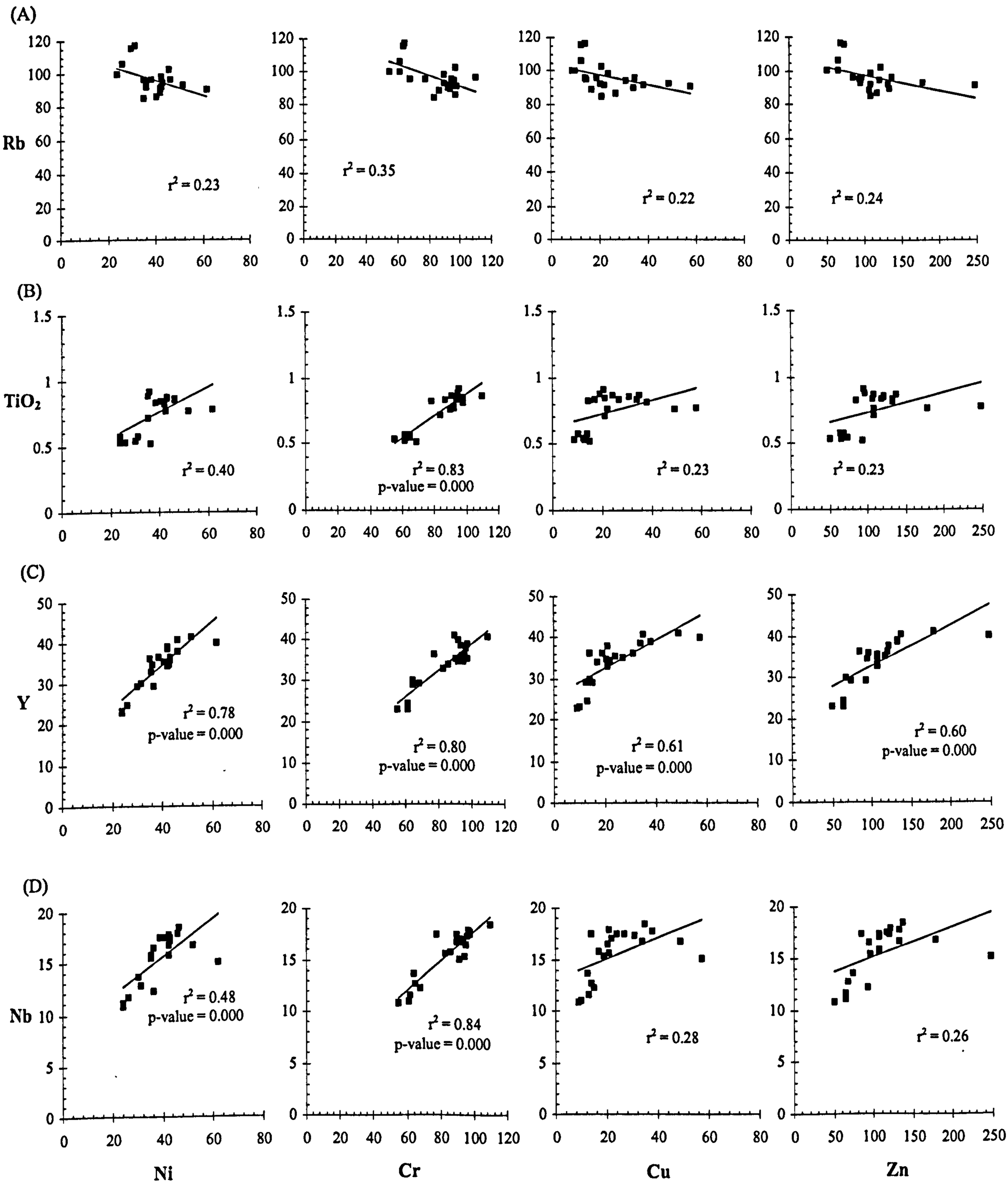

Figure 7.17: Correlation plots of Ni, Cr and Zn with indicator elements of the fine sediment fraction within the Loch Creran core. (A) Rubidium (ppm); (B) Titanium (ppm); (C) Yttrium (ppm) and (D) Niobium (ppm). (Crtical value at the 95% confidence level =0.433; n=21; df=19).

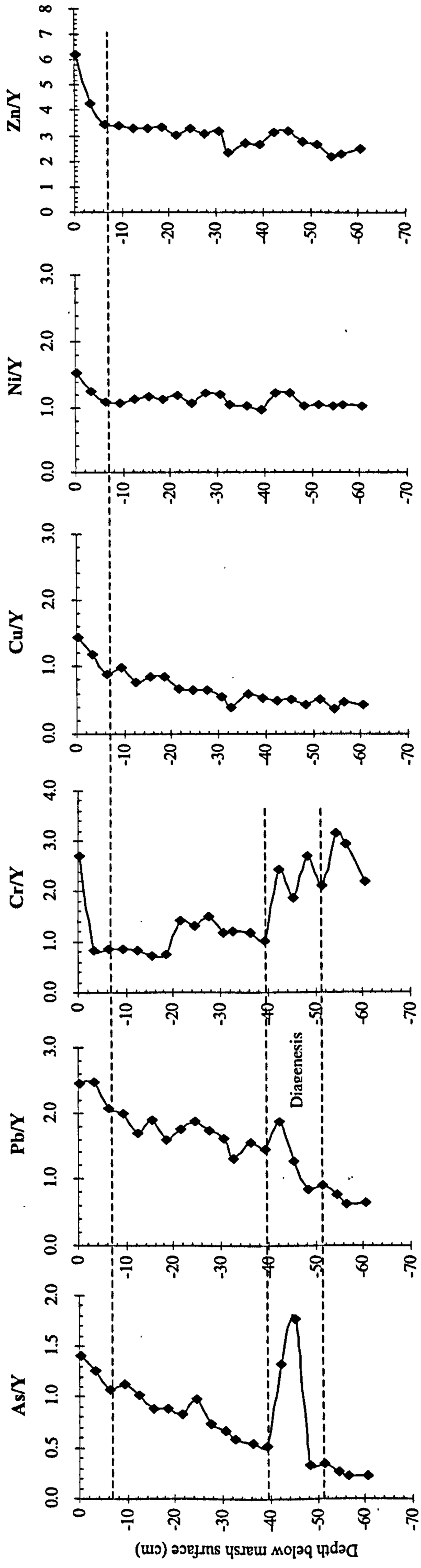

Figure 7.18: Down-core depth concentration profiles of heavy metals normalized to Y for the marsh core from Loch Creran in accordance with metal-normalizing agent data presented in Table 6.1 developed from the study of Loring (1990). Note the near-surface zone of metal enrichment evident within the Cr, Cu, Ni and Zn profiles and the zone of diagenetic controlled enrichment at depth in the As, Pb and Cr profiles (see text for discussion).

enrichment in the near-surface layers apart from Cr which may indicate the preferential association of this element with other heavy detrital mineral phases (Figure 7.18).

Despite this relative enrichment in the upper section of the core, the concentration of all trace metals are below estimated background values with the exception of As (Table 7.2). Similar to the sites on Mull As is enriched throughout the upper half of the core sequence. It is therefore clear that the Loch Creran Marsh sediments are also not acting as a significant sink for weathered metal species.

7.4.5: Detrital and trace metal fluxes

Calculated fluxes of major elements are shown in Figure 7.19a. The flux profiles for Fe and Mn show two distinct peaks situated between 20-24 cm and 10-16 cm related to diagenetic enrichment (Figure 6.9). K and Ti are not associated with specific redox-reactions and the flux profiles of these elements indicate two distinct lower phases of enhanced detrital input to the marsh. These are situated between 20-25 cm and 10-17 cm and correspond to two time periods of marsh development from ~1910-1924 AD and 1945-1964 AD. Above these peaks detrital inputs are more constant in contrast to the Fe and Mn profiles. In the near-surface layers fluxes of K and Ti increase significantly from 2-3 cm depth corresponding to 1995 AD. The major element detrital fluxes are mirrored by all the trace metal calculated flux profiles shown in Figure 7.19b. These also highlight the very recent increased annual flux of heavy metals being deposited on the marsh surface.

7.4.6: Enrichment of Iodine and Bromine

Concentration/depth profiles of I and Br from the Loch Creran marsh core are presented in Figure 7.20. These indicate that the upper oxic sediments are highly enriched with I and Br above the 40-44 cm depth increment whilst LOI values do not exceed 7 wt %. The maximum recorded concentration for Br occurs in the surface sediments with a value of are 1776 ppm in the near surface sediments whilst for I the maximum value is 634 ppm at 10-11 cm depth. The concentrations of LOI, I and Br below the inferred weak redox boundary of this core at 48 cm depth are much reduced in comparison to the oxic overlying sediments (Figure 7.20). Average concentration values for I and Br throughout the core are

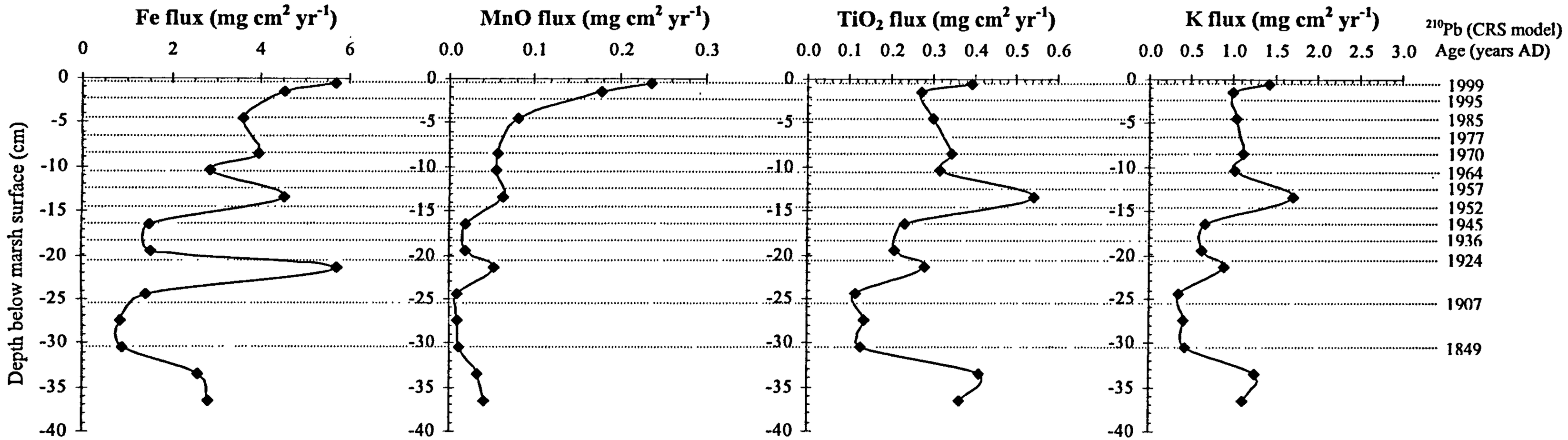

Figure 7.19a: Major element fluxes (mg cm^2 yr^{-1}) for the marsh core from Loch Creran based upon ^{210}Pb (CRS model) derived rates of accretion. Depositional flux (mg cm^2) = Sediment Dry Bulk Density (g cm^3) x Sedimentation Rate (cm a^{-1}) x Metal concentration (wt %).

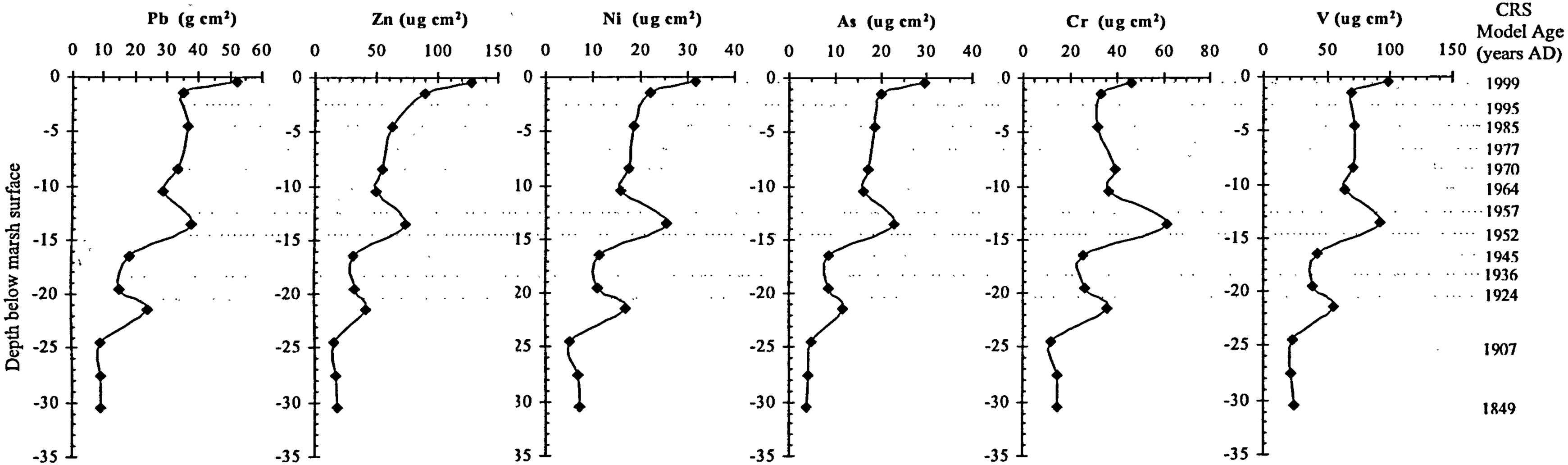

Figure 7.19b: Solid-phase derived flux/depth profiles of Pb, Zn, Ni, As, Cr and V for the marsh core from Loch Creran with CRS model derived ^{210}Pb ages. Depositional flux (ug cm^2) = Sediment Dry Bulk Density (g cm^3) x Sedimentation Rate (cm a^{-1}) x Metal concentration (ppm).

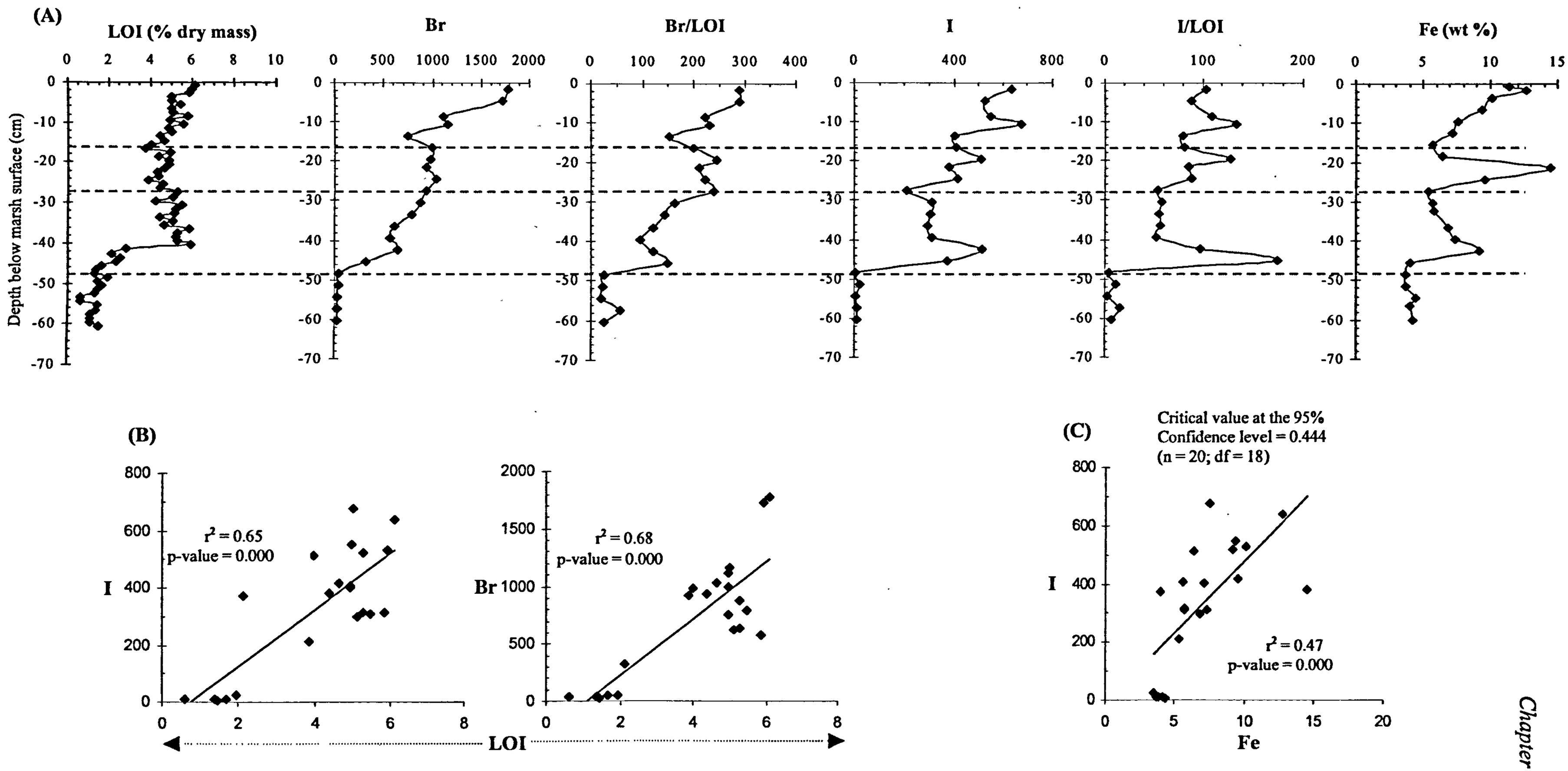

Figure 7.20: (A) Depth profiles of organic matter content (via LOI % dry mass), Iodine & Bromine (ppm) and Ferric Iron (wt %), with ratios of I/LOI and Br/LOI for the Loch Creran marsh core. (B) Correlation of LOI with I and Br. (C) Correlation of I with ferric Fe.

328 ppm and 732 ppm respectively and are within the values obtained by Malcolm and Price for surficial sediments within Loch Etive. I/LOI and Br/LOI ratios range from between 15 – 173 and 25-291 respectively and are somewhat lower than reported ratios of these elements to marine carbon described by Malcolm and Price (1984) for the Loch Etive sediments. However, these ratio values are broadly comparable to those reported in the literature derived from different geographical locations listed in Table 2.2.

Horizontal correlation of the concentration depth profiles for I, Br and organic material (via LOI) shows the broad similarity in the distribution of these elements. This is confirmed by the linear regression of I vs. LOI and Br vs. LOI yielding r^2 values of 0.65 and 0.68 respectively taken over the entire depth of the core (Figure 7.20). This latter value demonstrates the similar level of Br association with organic matter evident in the core from western Mull at the head of Loch Scridain. Ullman and Aller (1980) have suggested that an important sink for I exists at the sediment water interface and that this may be due to association of I with Mn oxides in the sediment surface. Correlation of the Loch Creran solid phase data for I reveals a weak positive association of Mn with I distribution in this core (r^2 = 0.23) suggesting that very little I is being scavenged by Mn oxyhydroxides. The correlation of I with Fe (r^2 = 0.47) suggests that a comparable mechanism is responsible for the stronger association with Fe_2O_3 and that scavenging of I by Fe oxyhydroxides does to some extent influences the distribution of this halogen (Figure 7.20). The Br concentration profile closely resembles those of Pb, Cu, Ni and Zn and to a lesser degree Cr and As. Graphical correlation plots reveal the strong positive association between Br and Pb, Cu, Ni, and Zn (r^2 values of 0.95, 0.82, 0.84 and 0.82 respectively; Figure 7.21). A weaker positive relationship exists between Br and the metals As and Cr (r^2 values of 0.62 and 0.52 respectively). These associations are likely to result from the interaction of the bromine-rich surface microlayer with vegetation and sediment material over the tidal cycle. Comparison of the r^2 values obtained for correlation of trace metals with LOI and Br suggests that bromination of metals is likely to be an active geochemical process in the Loch Creran marsh as opposed to only association of these elements with the organic fraction (Figures 7.16 & 7.21).

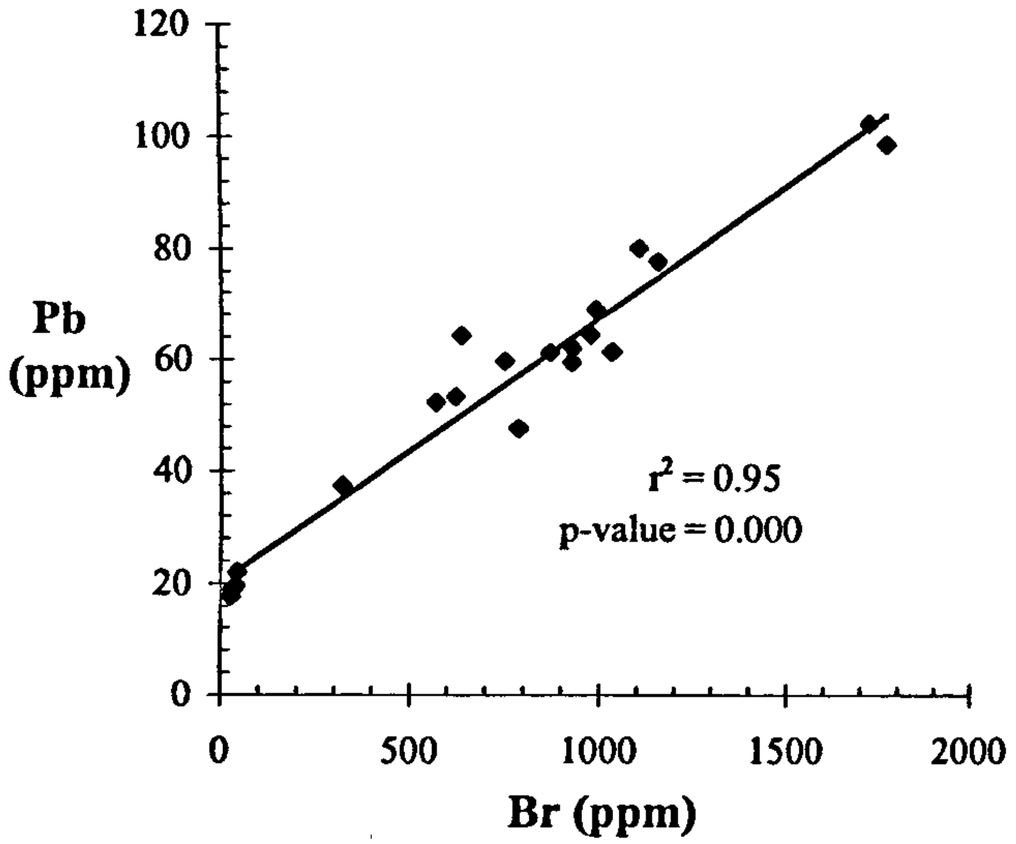

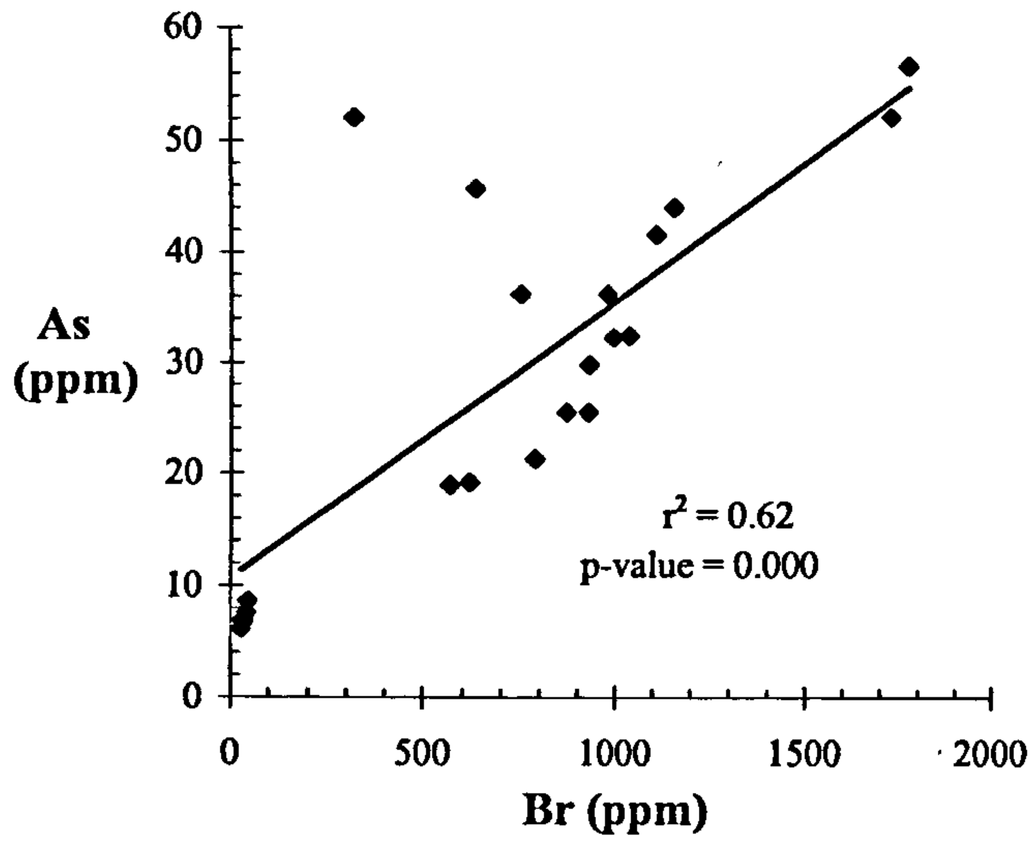

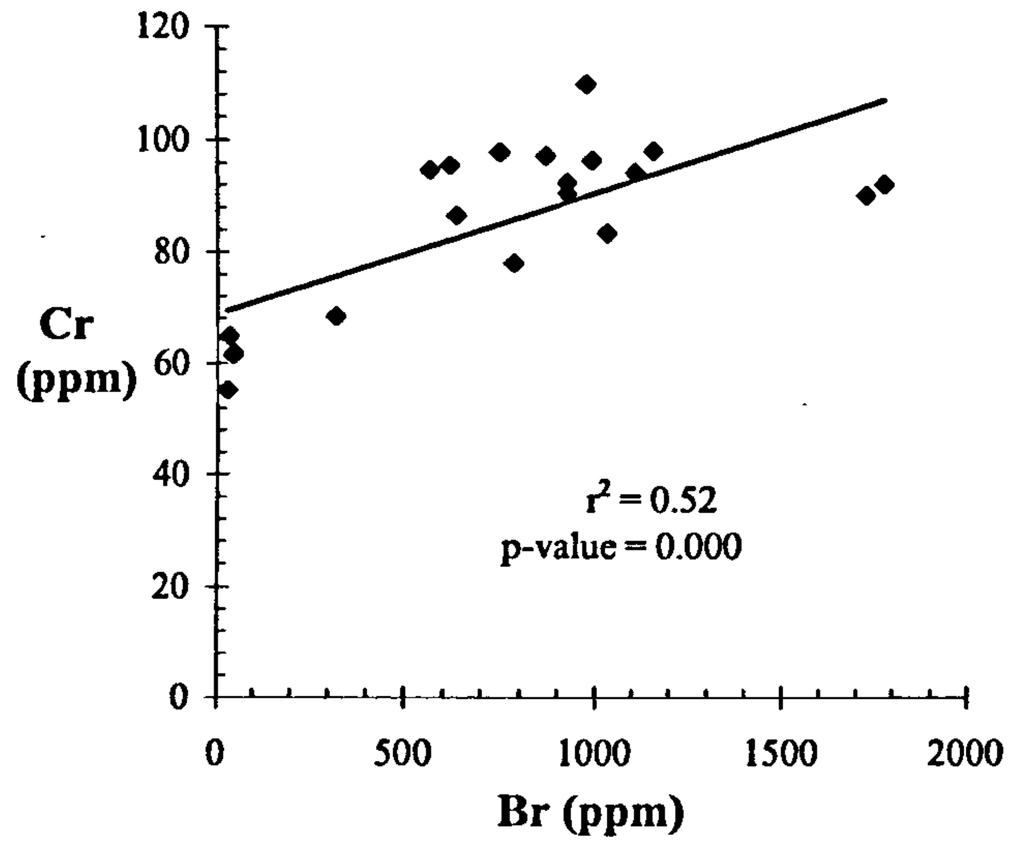

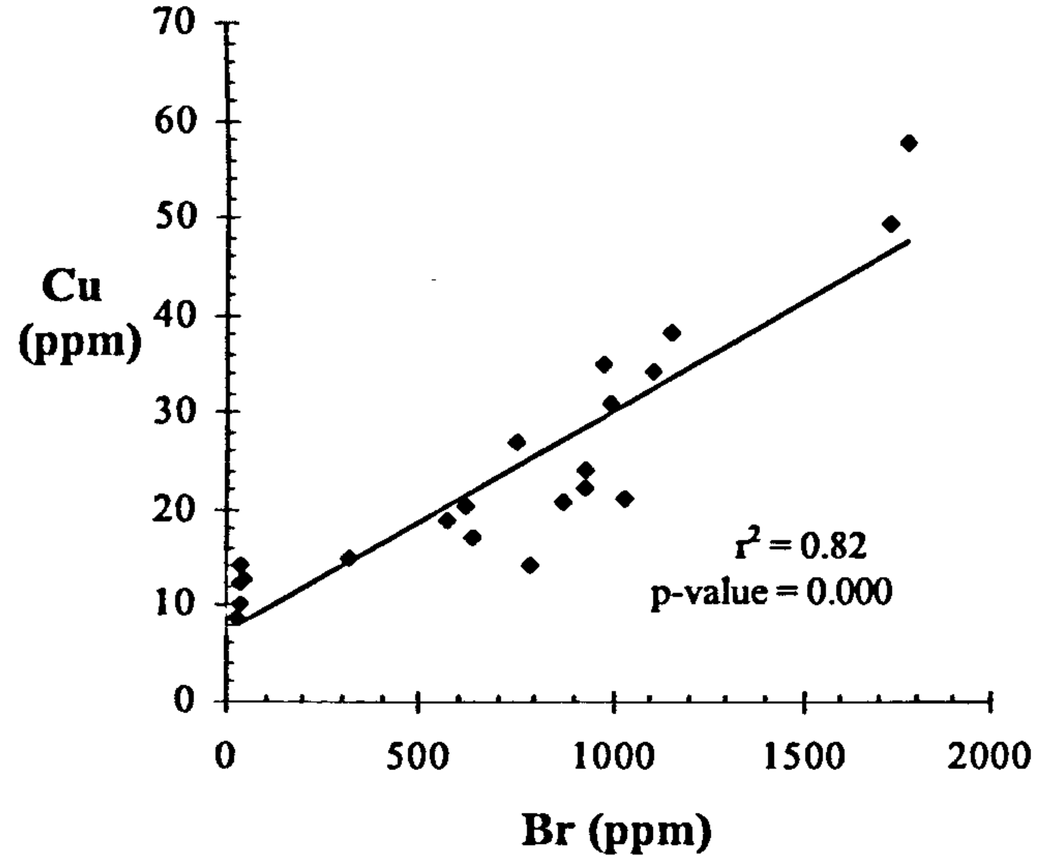

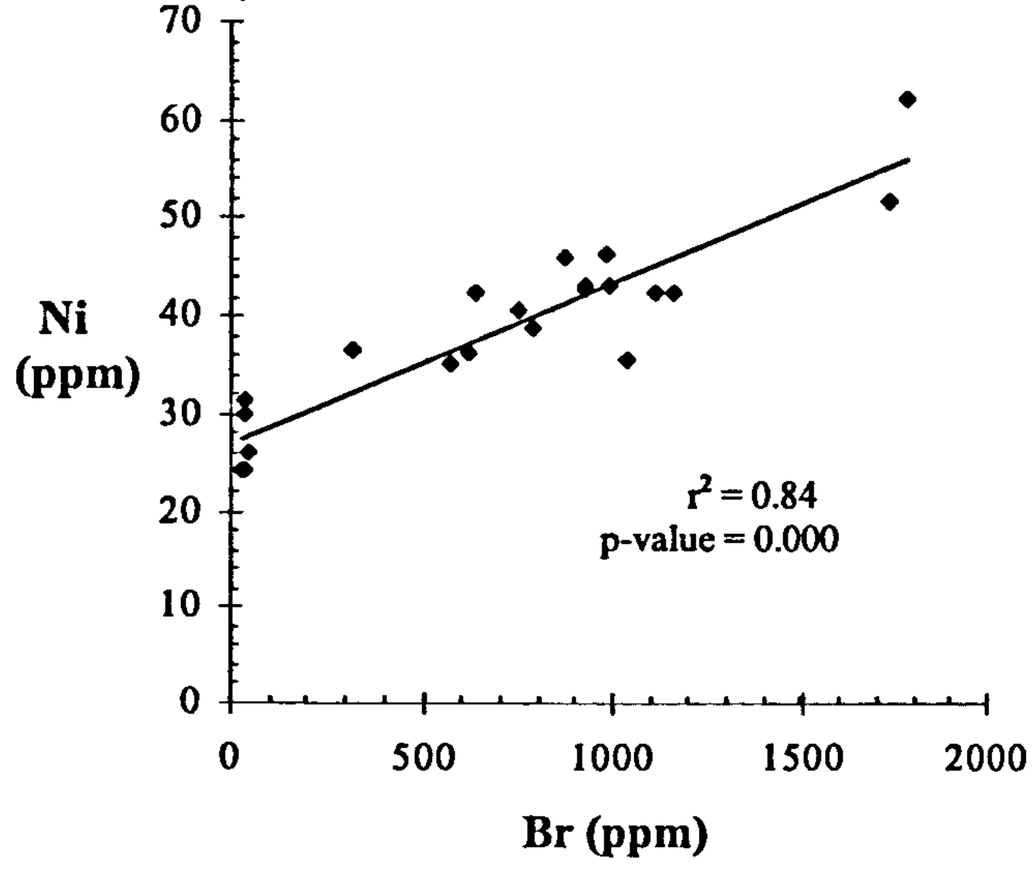

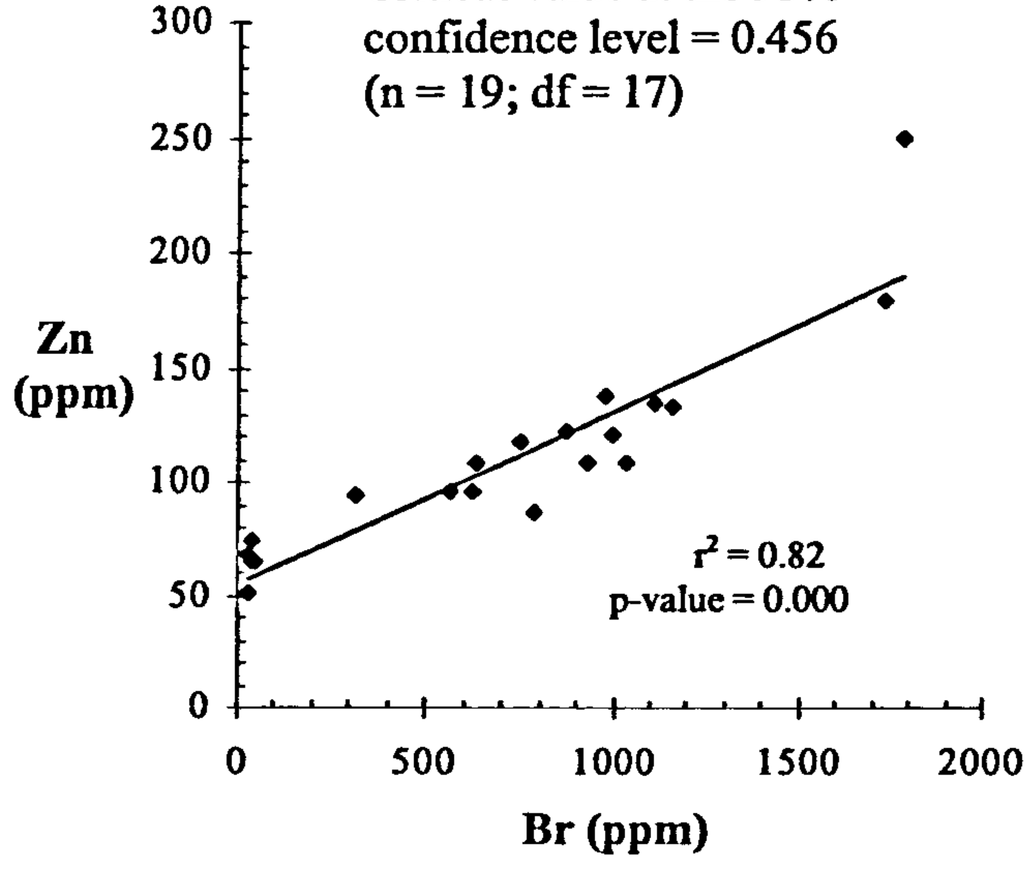

Critical value at the 95% confidence level = 0.456 (n = 19; df = 17)

Figure 7.21: Positive linear regression correlation plots to show bromination of trace metals in the marsh core from Loch Creran.

7.5: Loch Etive

7.5.1: Association of Mn with As, Pb, Cu, Cr and Zn

The potential for trace metals to become adsorbed onto Mn oxyhydroxide surfaces within marsh oxic sediments can seriously influence the down-core distribution of these and other associated elements. These processes have been highlighted in some of the preceding sections.

Mn recycling between the surficial sediments and the overlying, largely anoxic, water column of the fjord have been investigated by Overnell, (2002) and Overnell *et al.* (2002). Mixing processes in the upper highly anoxic basin of Loch Etive are controlled by the strong density discontinuity that isolates the bottom water here for lengthy periods of the year. Renewal events are infrequent and confined largely to summer months when the dilution of saline water from the River Etive is much reduced (Edwards and Edelsten, 1977). The study by Overnell *et al.* (2002) has revealed that significantly more Mn is recycled within the water column than undergoes burial in the surficial sediments. This suggests that detrital oxidized Mn within the water column (particularly in summer months) may represent a potential source of solid-phase Mn to the marsh which is then capable of post-depositional reactions with metal species.

Horizontal correlation of trace metal profiles with that of Mn for the entire core depth from the Loch Etive marsh sequence reveals a low positive correlation coefficient for Pb and As (r^2 = 0.29 and 0.25 respectively Figure 7.22). Similar low positive values are recorded for Cr and Ni (r^2 = 0.11 and 0.39 respectively). Interestingly in this core the distribution of Zn reveals a strong positive correlation (r^2 = 0.71) with Mn. Reducing the number of variables to correspond to the true depth of marsh sediments records similarly low positive correlation coefficients for Pb, As, Cr and Ni (r^2 values of 0.26, 0.25, 0.04 and 0.06 respectively). These trace metals are therefore not being significantly adsorbed onto Mn oxyhydroxide surfaces and their down-core distribution is largely unaffected by early diagenetic recycling of Mn. However, Zn distribution in the Loch Etive sediments does appear to be more positively associated with Mn in both the entire core and the upper 28 cm (r^2 = 0.61), suggesting that Zn distribution is being influenced by Mn oxyhydroxide recyling.

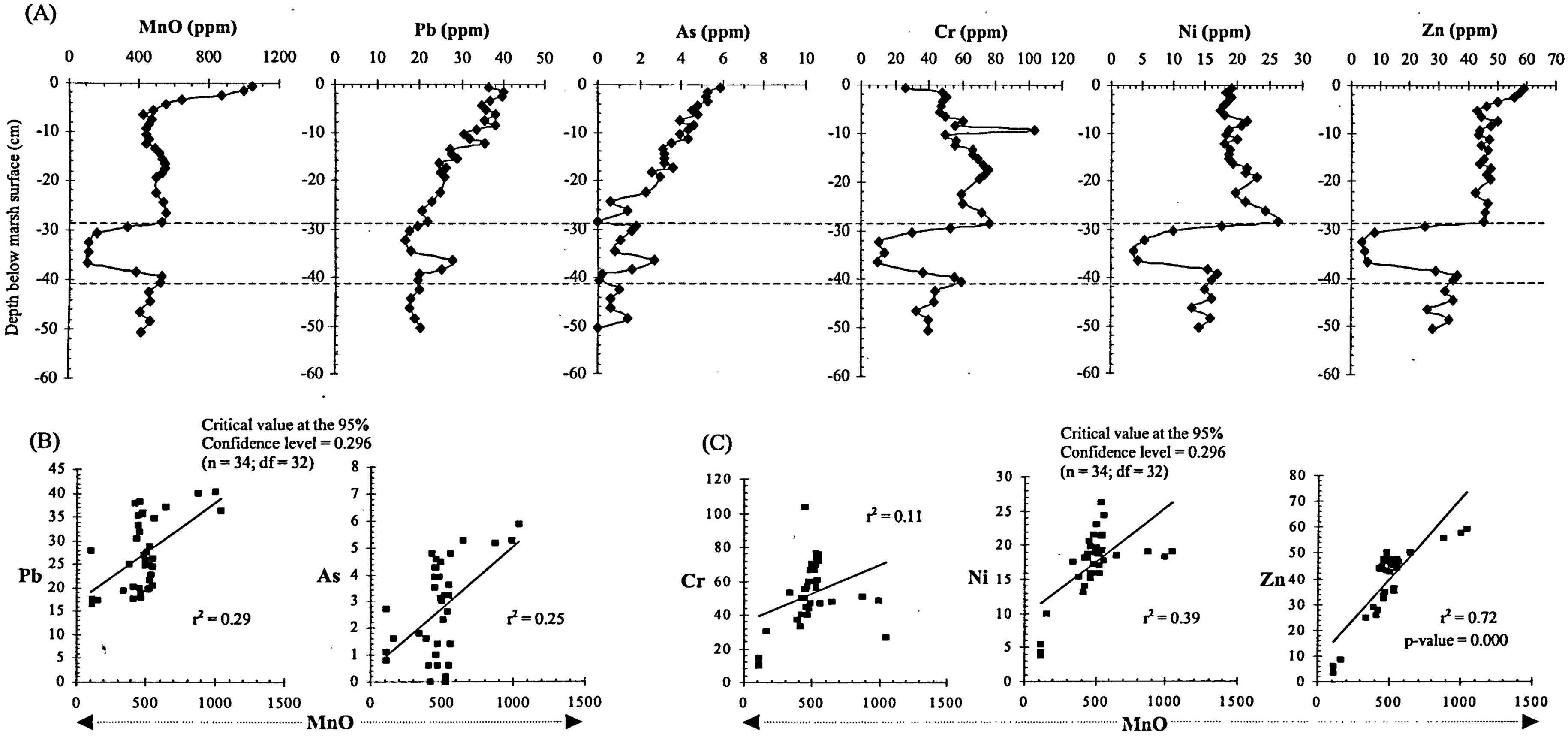

Figure 7.22: (A) Horizontal correlation between MnO (wt %) and the trace metals Pb, As, Cr, Cu, Ni and Zn (ppm) for the marsh core from Loch Etive. (B) Linear correlation of MnO with Pb and As. (C) Correlation of MnO with Cr, Cu, Ni and Zn.

7.5.2: Trace metal associations with organic material (As, Pb, Cr, Ni, and Zn)

In the Loch Etive marsh as with other aspects of the geochemistry of this core element associations are complicated by the highly variable stratigraphy (Figure 4.37). Over the entire core depth both horizontal and linear correlation indicate weakly positive values for Pb and As (r^2 = 0.07 and 0.10 respectively; Figure 7.23). Significant enrichment of organic material does correspond to the elevated concentrations of Pb and As within the black silty sand unit (discussed above). Weak negative relationships exist for the metals Cr, Ni and Zn which indicate that over the entire core depth very little complexation between these trace metals and organic material has taken place (Figure 7.23). However, the influence of the differing stratigraphic units within this core must be taken into account in making such assessments. If we therefore consider the uppermost 28 cm as being more representative of the true extent of marsh development at this site these relationships are somewhat altered. Pb and As distributions are seen to be slightly more strongly associated with the LOI profile although organic material only partially explains the distribution of these elements (see above). Linear correlation of Cr, Ni and Zn with LOI for the upper 28 cm of the core (Figure 7.24) indicate that the association between organic matter and these elements is somewhat poorer than for the entire core depth (r^2 values of 0.18, 0.19 and 0.00 respectively) suggesting that other marsh processes must be responsible for the distribution of these trace metals.

7.5.3: Association of trace elements with the fine fraction.

Adsorption of trace metals onto Mn oxyhydroxide minerals appears to be limited within the Loch Etive marsh core for all metals except Zn. (Figure 7.22). This may be the result of competition for adsorption sites by ferric oxides. Within the upper 28 cm of this core (i.e. the real extent of marsh development) the concentration profiles of Mn and Zn closely resemble one another particularly within the near-surface sediments indicating that the distribution of Zn is being infuenced by the diagenetic recycling of Mn. Alternatively this association may result as a consequence of the remobilization of dissolved Zn species following burial in the near-surface sediments and subsequent degradation of the carrier phase (Lewis, 1997). Correlation of trace metal distributions with key indicators of fine particulate sedimentary material (e.g. Rb, Ti, Y and Nb) indicate that Cr, Ni and Zn are all strongly associated with the fine fraction (Figure 7.25). Adsorption of metal species onto fine

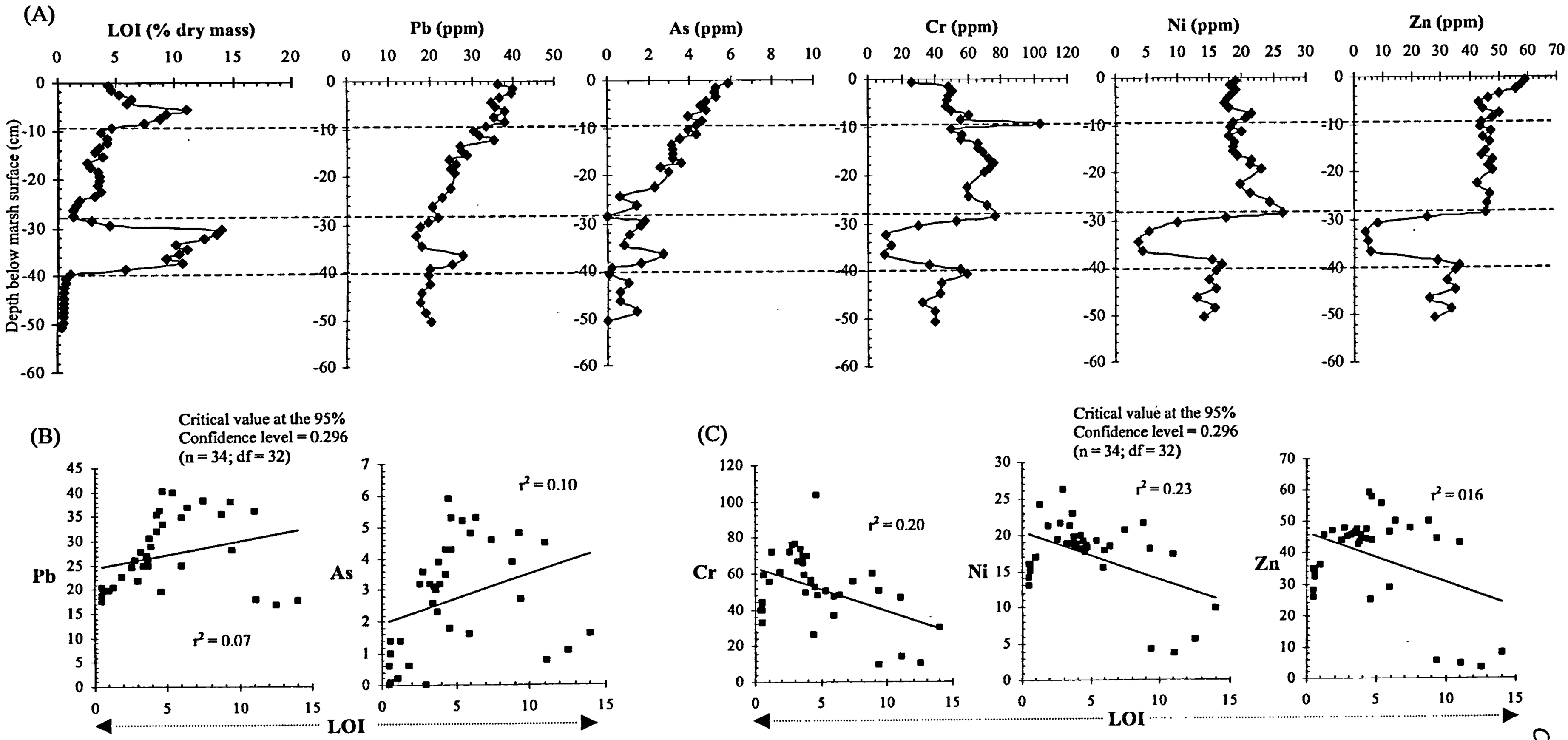

Figure 7.23: (A) Horizontal correlation between organic content (via LOI % dry mass) and the trace metals Pb, As, Cr, Ni and Zn (ppm) for the marsh core from Loch Etive. (B) Linear correlation of LOI with Pb and As. (C) Correlation of LOI with Cr, Ni and Zn.

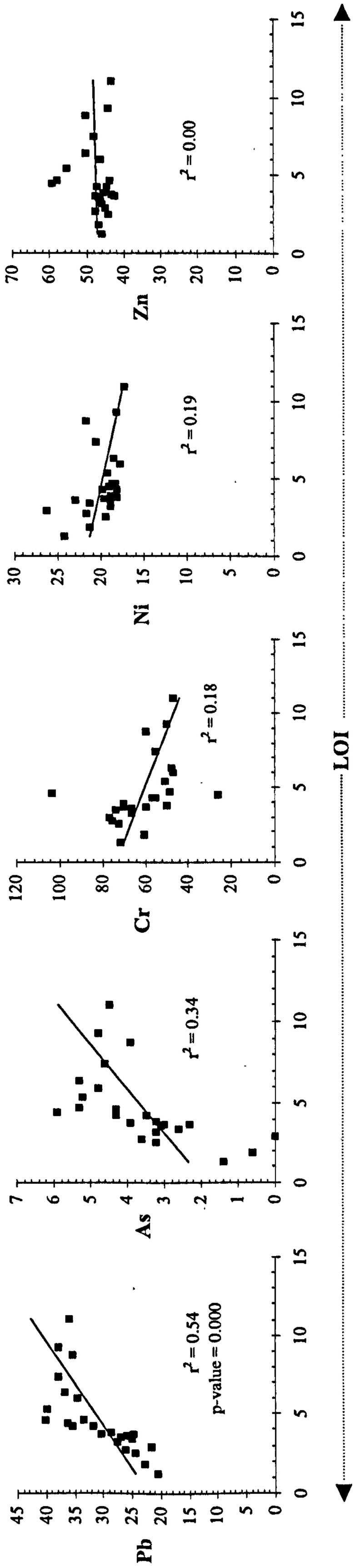

Figure 7.24: Correlation between organic content (via LOI % dry mass) and the trace metals Pb, As, Cr, Ni and Zn (ppm) for the uppermost 28 cm depth from the Loch Etive marsh core.

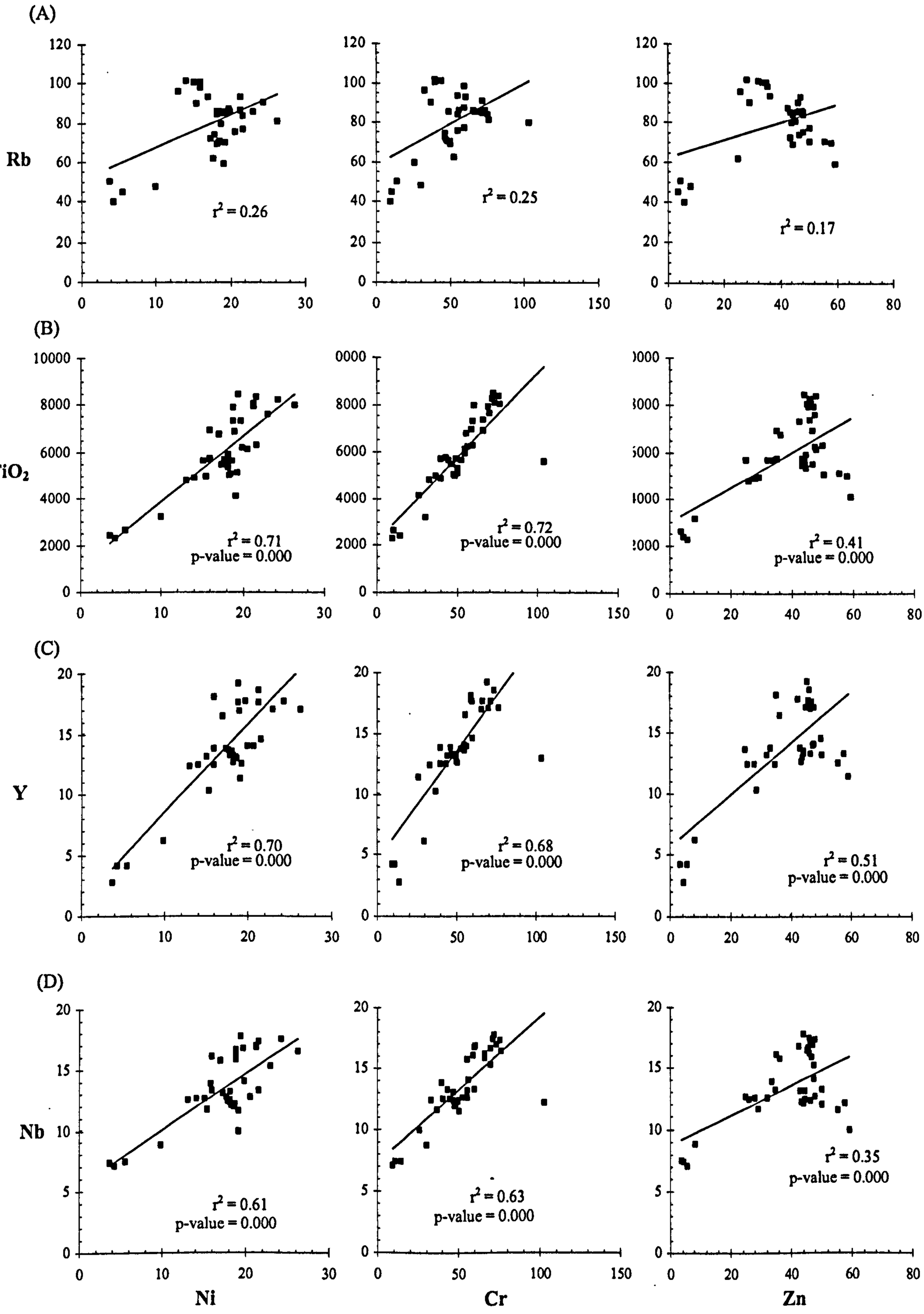

Figure 7.25: Correlation plots of Ni, Cr and Zn (ppm) with indicator elements of the fine sediment fraction within the Loch Etive marsh core. (A) Rubidium (ppm); (B) Titanium (ppm); (C) Yttrium (ppm) and (D) Niobium. (Critical value at the 95% confidence level = 0.325; n=34; df = 32)

clay particles and incorporated organic material is likely to be the principal mechanism governing this association. From the graphical regression plots yttrium would appear to be a superior normalizing agent when compared to the correlation data for Al and Rb shown in Table 7.1. Normalized trace metal distributions to yttrium are shown in Figure 7.26. These profiles highlight the differential distribution of elements within the black silty sand which shows significant enrichment of Pb and As, not immediately obvious from the cluster analysis plots shown in Figure 4.40. Cr and Ni show fluctuating concentration throughout this sub-unit whilst Zn is relatively depleted. Pb and As show a steady increase in element concentration above 29 cm. Cr, Ni and Zn normalized profiles show fluctuating concentrations which clearly show periods of enhanced and reduced metal input (Figure 7.26). Apart from Cr all normalized metal profiles show significant enrichment of heavy metals in the near-surface sediments, which corresponds to an increase in dry bulk density over the same depth increment (Figure 4.39).

Concentrations of all trace metals are much reduced in comparison to background crustal values (Table 7.2) indicating that in similarity to the other marsh environments these marsh sediments are not acting as sink for weathered metals. Overall the marshes from Argyll investigated in this study do not appear to have experienced any undue contamination from elevated trace metal inputs.

7.5.4: Detrital major and trace element fluxes

Detrital fluxes of major element oxides (Fe, Mn, Ti and K) for the upper 28cm from the Loch Etive marsh core are shown in Figure 7.27a. These profiles are plotted against depth and the CRS model ^{210}Pb derived ages for the sediment increments. All element flux profiles are characterized by the significant peak indicating the influx of mineralogenic material between 14 and 18 cm depth, corresponding to an 11 year period from ~1926-1937 AD. This does not correspond to the depths at which diagenetic enrichment of Fe and Mn oxides occurs in Figure 6.13 and suggests a detrital input to the marsh surface. This is further confirmed by the calculated flux profiles for trace metal elements shown in Figure 7.27b. A significant increase in elemental fluxes is evident at the same depth/age period further indicating enhanced detrital input to the marsh surface. In the upper near-surface sediments all profiles of major and trace element fluxes apart from that of Cr indicate an increase in detrital input to the marsh surface over the last ten years.

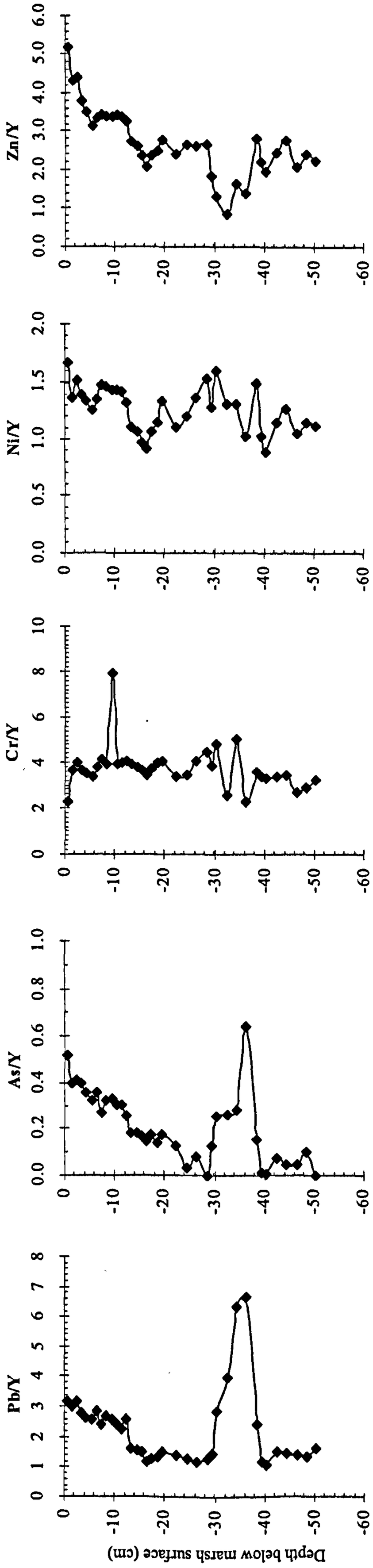

Figure 7.26: Trace metal concentration profiles for Pb, As, Cr, Ni and Zn normalized to Y the marsh core from Loch Etive. Note the relative enrichment of Pb, As, Cr and Ni within the peat soil unit (29-41 cm depth) with a corresponding depletion of Zn and enrichment of elements within the surface sediments (see text for discussion).

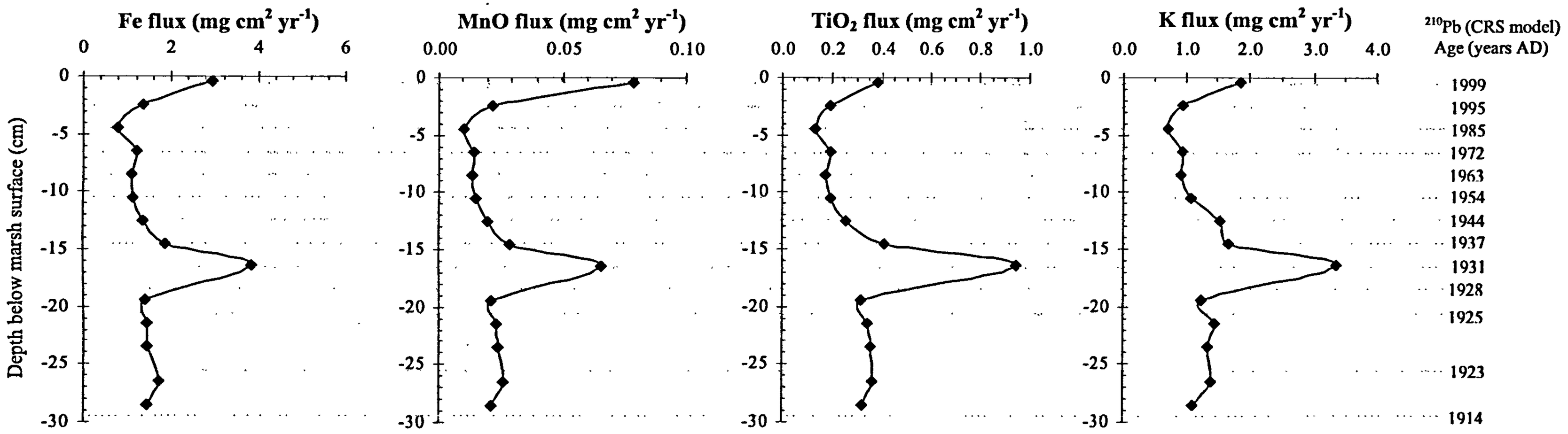

Figure 7.27a: Major element fluxes (mg cm^2 yr^{-1}) for the marsh core from Loch Etive based upon ^{210}Pb (CRS model) derived rates of accretion. Depositional flux (mg cm^2) = Sediment Dry Bulk Density (g cm^3) x Sedimentation Rate (cm a^{-1}) x Metal concentration (wt %).

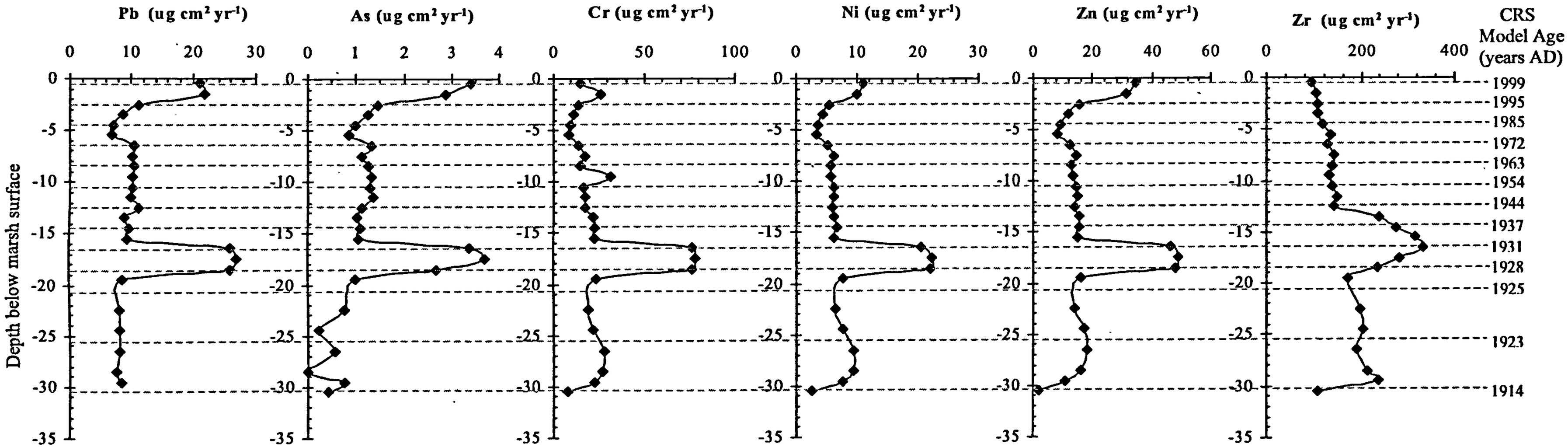

Figure 7.27b: Solid-phase derived flux/depth profiles of Pb, Zn, Ni, As, Cr and V for the marsh core from Loch Etive with CRS model derived ^{210}Pb ages. Depositional flux (ug cm^2 yr^{-1}) = Sediment Dry Bulk Density (g cm^3) x Sedimentation Rate (cm a^{-1}) x Metal concentration (ppm). Sedimentation rates are those derived from the ^{210}Pb CRS modelled age.

7.5.5: Enrichment of Iodine and Bromine

Concentration/depth profiles of I and Br from the Loch Etive marsh core are presented in Figure 7.28. These indicate that the upper oxic sediments above 29 cm depth are highly enriched with I and Br with concentrations of both elements increasing toward the surface of the marsh. In this section of the core LOI values attain a maximum value of 14 wt % at 5 cm depth. The maximum recorded concentration for Br occurs in the surface sediments with a value of are 587 ppm whilst for I the maximum value is 583 ppm at 2-3 cm depth. Average concentration values for I and Br throughout the entire core are 249 ppm and 236 ppm respectively and are within the range of values obtained by Malcolm and Price for surficial sediments within Loch Etive. I/LOI and Br/LOI ratios range from between 8-155 and 15-132 respectively and are somewhat lower than reported ratios of these elements to marine carbon described by Malcolm and Price (1984) for the Loch Etive sediments. However, these ratio values are broadly comparable to those reported in the literature derived from the different geographical locations listed in Table 2.2. Horizontal correlation of the concentration depth profiles for I, Br and organic material (LOI) for the entire core suggests a broad similarity in the distribution of these elements with decoupling of these profiles in the near surface sediments. This is confirmed by the linear regression correlation plots of I vs. LOI and Br vs. LOI yielding a low positive correlation for both elements (r^2 values of 0.07 and 0.29 respectively) taken over the entire core depth (Figure 7.28). Correlation of the Loch Etive solid phase data for I reveals a weak positive association of Mn with I distribution in this core ($r^2 = 0.38$) suggesting that very little I is being scavenged by Mn oxyhydroxides. The correlation of I with Fe ($r^2 = 0.45$) suggests that a comparable mechanism is responsible for the slightly stronger association with Fe and that scavenging of I by Fe oxyhydroxides does weakly influence the distribution of this halogen (Figure 7.28).

However, trace element distributions have been strongly influenced by the more varied stratigraphy recorded in the Loch Etive core (Figure 4.37). Visual inspection suggests that the uppermost 28 cm are more representative of the true extent of coastal peat development in this marsh setting. Recalculation of the linear regression parameters for I and Br yield only slightly stronger association between these elements and organic matter (r^2 values of 0.21 and 0.29 respectively). The result for the correlation with MnO is very slightly reduced ($r^2 = 0.36$) at this depth. In this upper section of the core the association with Fe is slightly increased supporting the interpretation of the partial role of Fe oxyhydroxides with respect to I distribution.

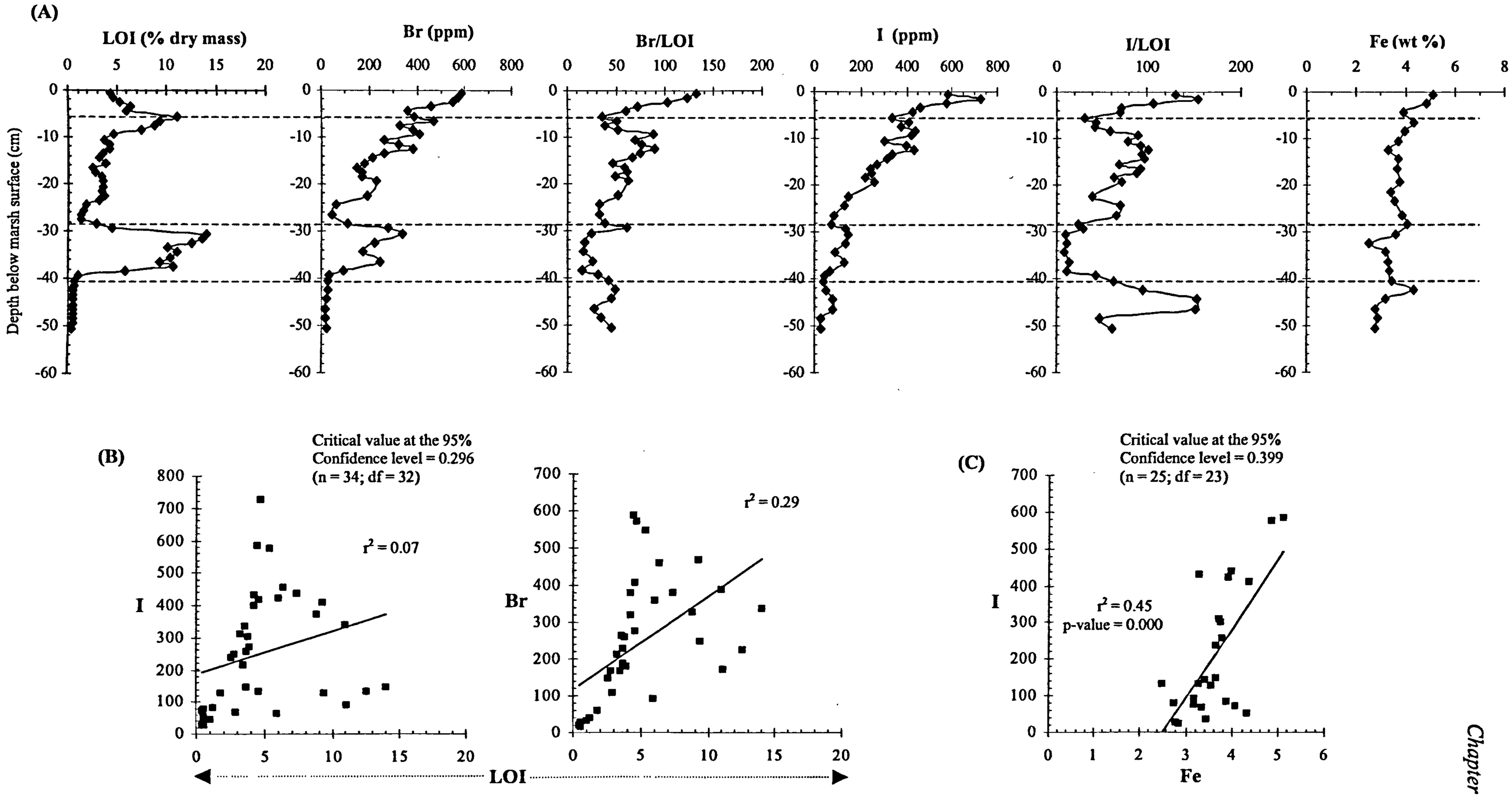

Figure 7.28: (A) Depth profiles of organic content (via LOI % dry mass), Iodine & Bromine (ppm) and Fe (wt %), with ratios of I/LOI and Br/LOI for the Loch Etive marsh core. (B) Correlation of LOI with I and Br. (C) Correlation of I with ferric Fe.

The Br concentration profile closely resembles those of Pb, As and Zn and to a lesser degree Cr and Ni. Correlation graphical plots reveal the strong positive association between Bromine and Pb, As and a somewhat weaker association with Zn (r^2 values of 0.89, 0.79 and 0.38 respectively; Figure 7.29). A weak negative relationship exists between Br and the metals Cr and Ni in this core (r^2 values of 0.32 and 0.36 respectively). These correlation coefficients indicate that bromination of Cr and Ni is not taking place within the Loch Etive sediments (Figure 7.29). Bromination of Pb, As and Zn is likely to arise from the interaction of the bromine-rich surface microlayer with vegetation and sediment material over the tidal cycle. Pellenbarg, (1984) has shown that this process can exert a significant influence upon the deposition of brominated metals and this is certainly the case for the metals within the marsh core from Loch Etive.

7.6: Uranium geochemistry in the Argyll marshes

The importance of saltmarsh and mangrove environments as an important coastal sink for oceanic dissolved U has been reported by Church *et al.* (1996). Various mechanisms are thought to be responsible for the enrichment of dissolved U within the near-surface sediments of saltmarshes (Church *et al.*, 1981). These include some or all of the following:

- Re-complexation of dissolved uranium carbonate complexes transported to the marsh surface by tidal currents into phosphate/humic forms (Sarin and Church, 1994)

- Mixing of these stronger uranium complexes with the dissolved products of chemical diagenesis including Fe and humic acids diffusing up through the sedimentary prism into the near-surface sediments.

- Scavenging of particulate colloids following estuarine flocculation processes over a tidal cycle (Eastman and Church, 1984).

- The resultant concentration and burial of uranium as an iron oxide form (Fe_2O_3) or humic acid complex.

The distribution of uranium within the marsh cores from Loch Don and Loch Creran has been obtained as a result of the enhanced capability of the Philips MAGIX Pro X-R-F

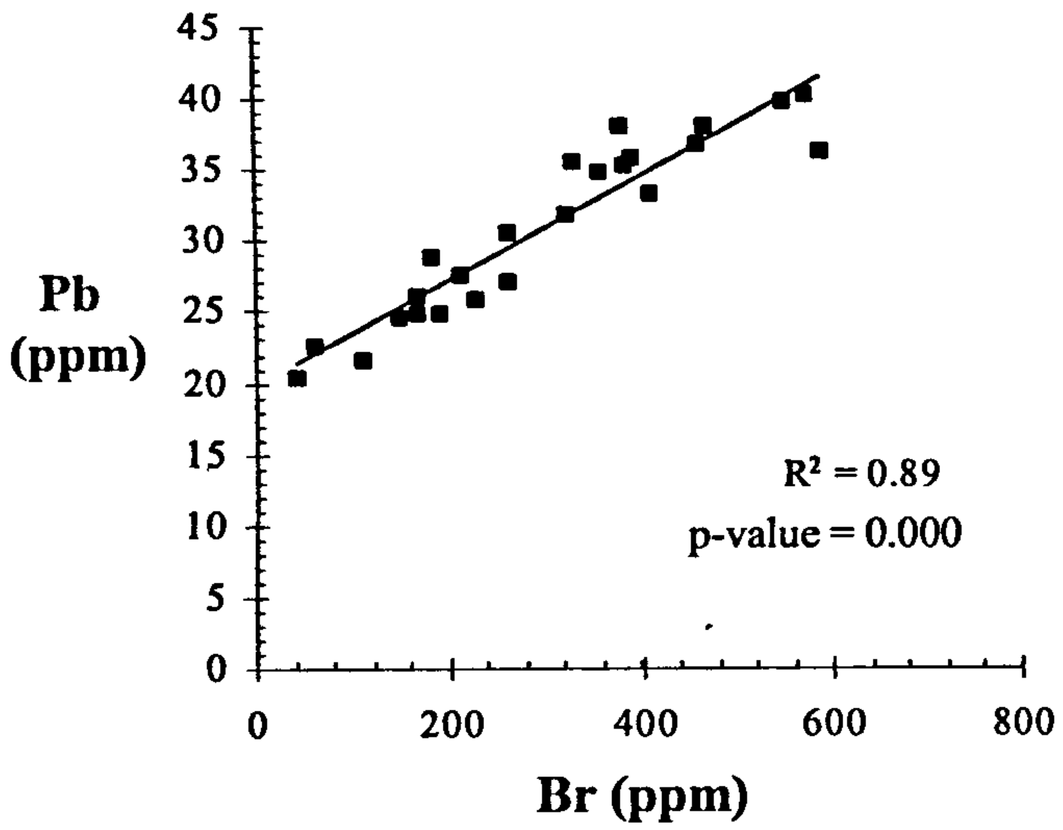

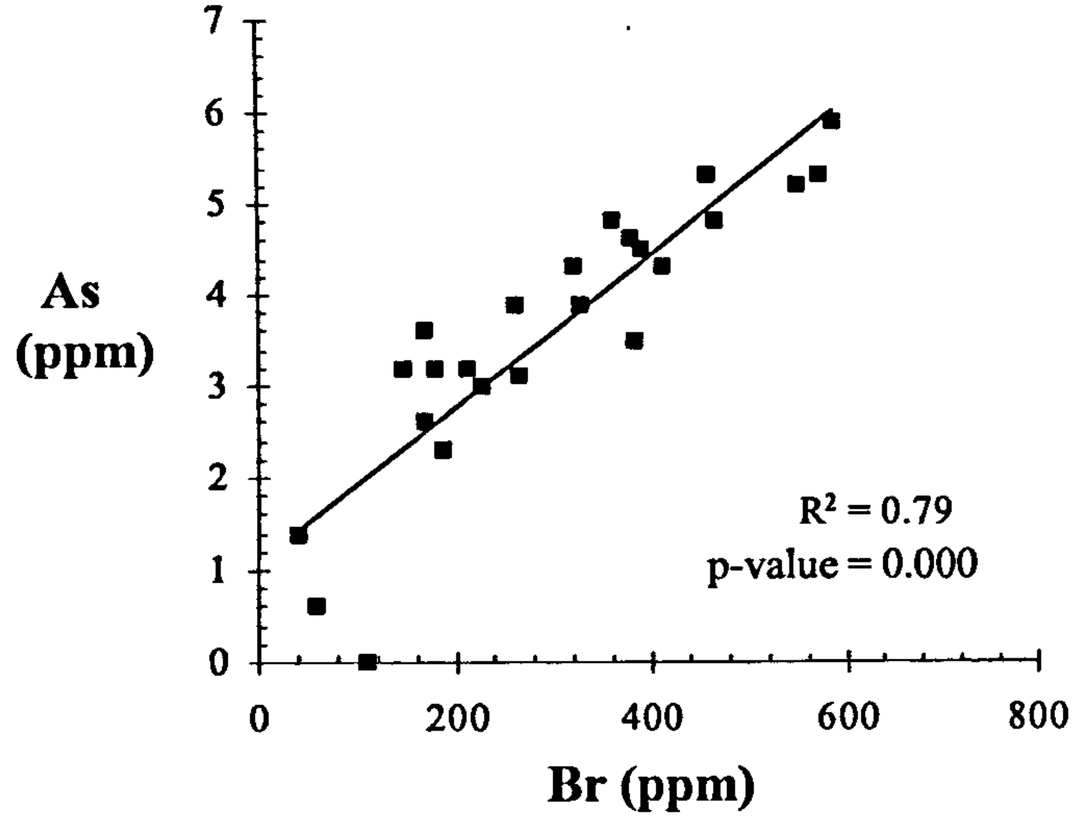

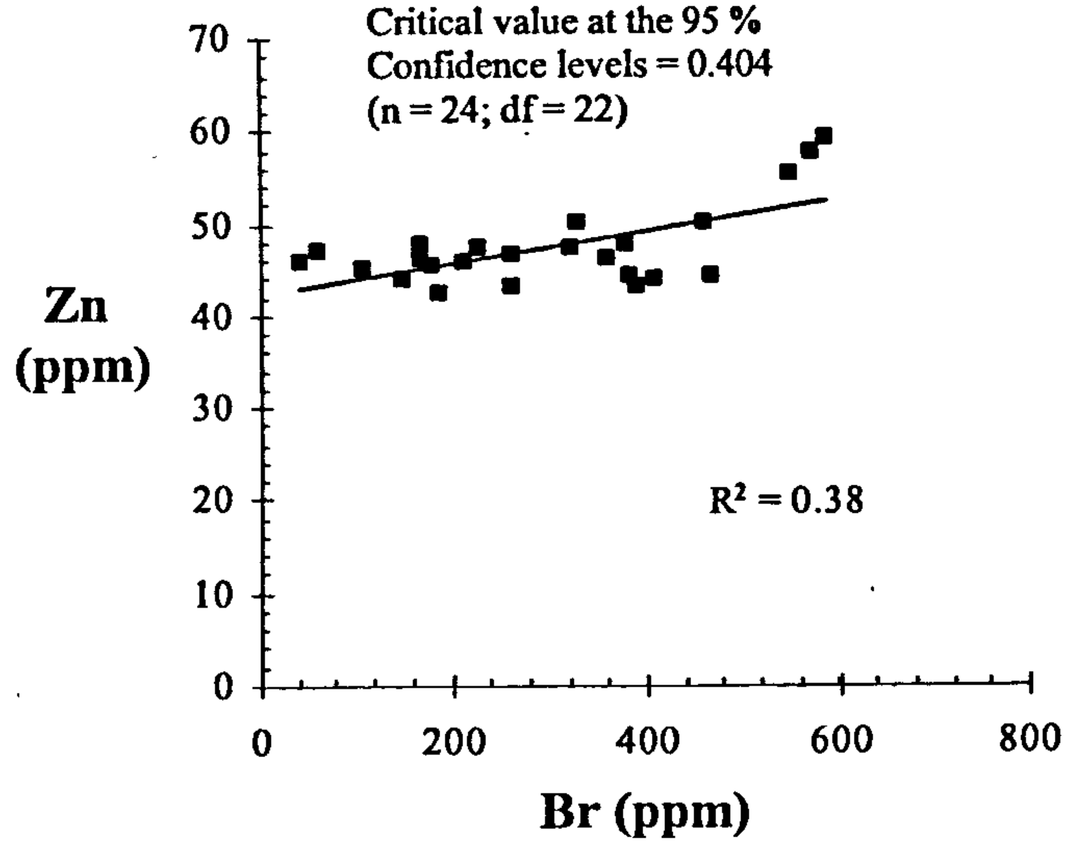

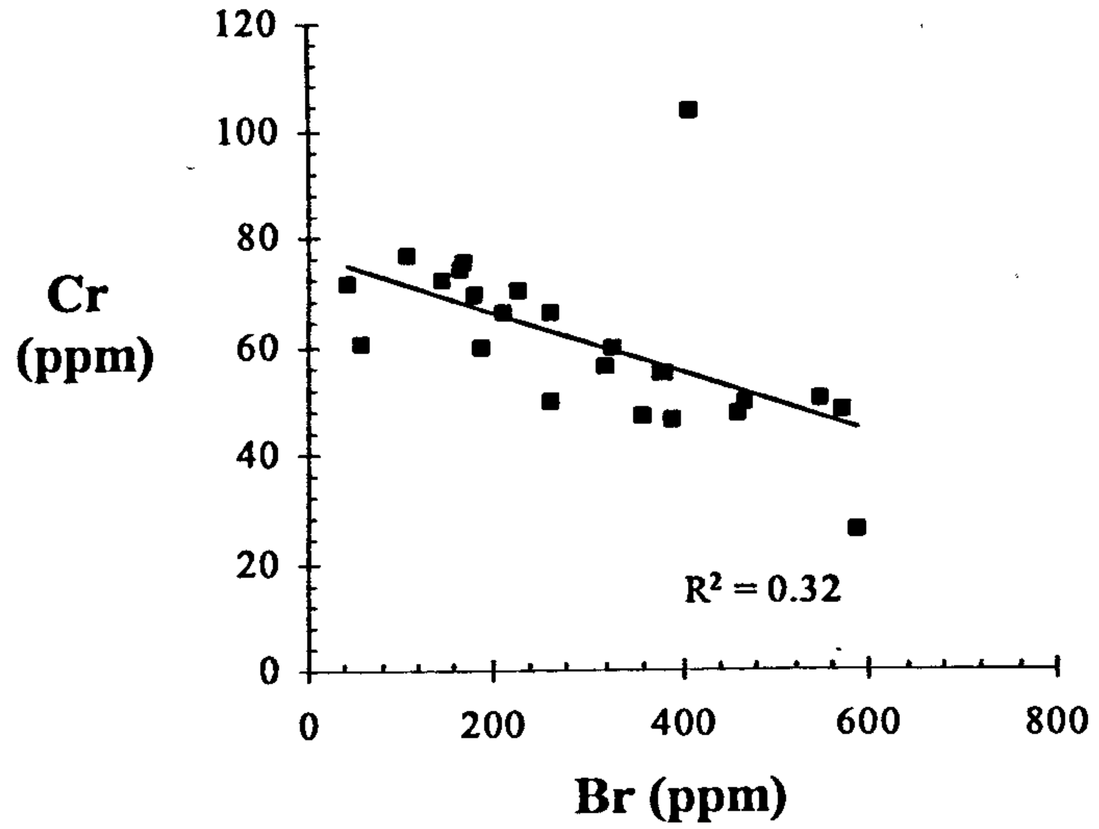

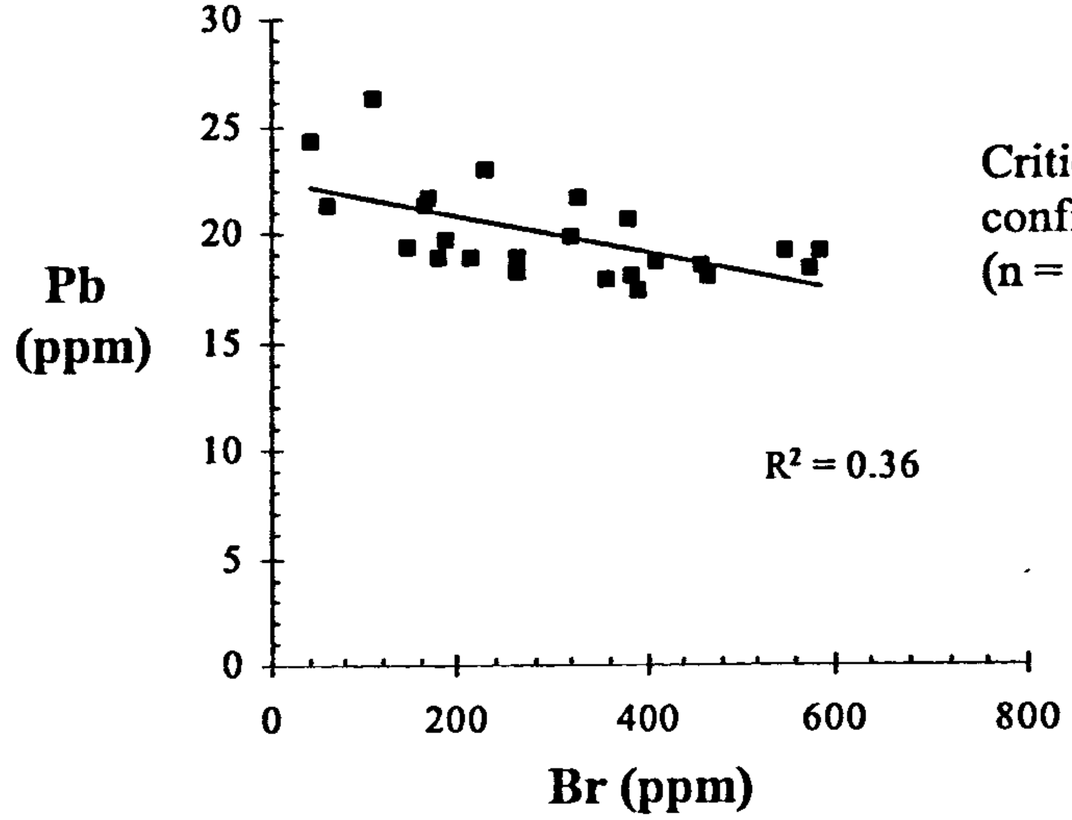

Figure 7.29: Linear regression correlations between Br and the trace metals Pb, As, Cr, Ni and Zn in the upper 28 cm of the marsh core from Loch Etive. Positive relationships for Pb, As indicate bromination of these metal within the marsh sediments. The critical value at the 95% confidence level reveals no significant bromination of Zn.

spectrometry system. This supercedes the PW1400 wavelength dispersive system which was replaced during the analysis of the Argyll marsh sediment sequences.

The down-core profile of U concentration in the Loch Don core is shown in Figure 7.30a. This clearly indicates that U is indeed enriched within the near-surface layers of the marsh sediments at this site. Concentration of U declines down to 30-31 cm depth below which the enriched layers in the reduced section of this core probably occur a result of diffusion of dissolved $[UO_2(CO_3)_3]^{4-}$ from the water column to the sediments following release from Fe and Mn oxyhydroxide as they too are reduced in anoxic conditions (Barnes and Cochran, 1993).

Figure 7.30b shows the graphical plots of linear correlation between uranium, major element oxides and LOI (as a proxy for organic content). These plots give some insight into the behaviour of U within the dominantly mineralogenic sediments of this marsh. The strongly negative correlation with CaO ($r^2 = 0.85$) suggests that decoupling of the dissolved uranyl complex is likely to have occurred. The strongly positive correlation with P ($r^2 = 0.74$) and to a lesser extent LOI ($r^2 = 0.55$) indicates that re-complexing of uranium with P and humic substances has indeed occurred as suggested by Sarin and Church (1994) in their study of U within the Delaware and Chesapeake estuaries, USA. Linear correlation with the redox-sensitive Fe and Mn oxides reveals low positive values (r^2=0.29 and 0.27 respectively) indicative of little association between these redox-sensitive elements. A strongly positive correlation does exist between U and K (as a proxy for fine detrital/flocculated material) suggesting that particulate scavenging is the dominant processs resulting in enrichment of U within the near-surface sediments (Figure 7.30 a & b). The study by Church *et al.* (1996) highlights that uranium particulate scavenging takes place predominately over the Spring tidal cycle (i.e. bi-monthly) and during the summer months when the marsh surface is most acidic. Although no pH data have been acquired for the Loch Don marsh surface sediments it is likely that acidic conditions were prevalent here owing to the summer period during which sampling took place. This would facilitate enhanced scavenging and concentration of U resulting in the surface enrichment visible in the concentration depth/profile (Figure 7.30a). Scavenging of uranium is suggested by Church *et al.* (1996) to predominate during Spring tides over the marsh surface. Hence, this process is linked to the altitude of the accumulated sediments and the depth of tidal inundation relative to the tidal prism. This may, therefore, be a geochemical process which is more specific to high (mature) marsh environments and may account for the enriched near-surface concentrations visible in the Loch Don core.

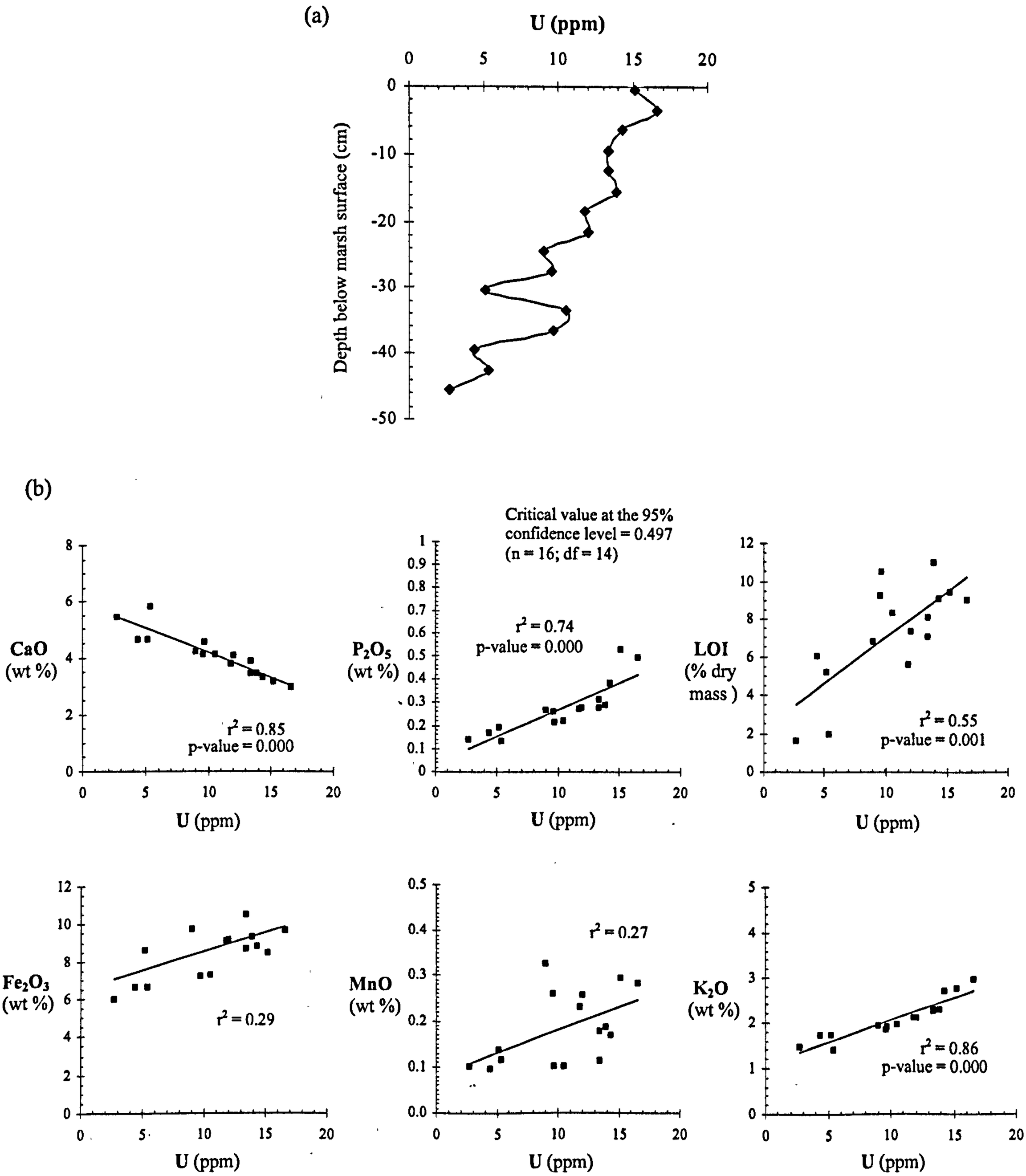

Figure 7.30: (a) Down-core profile of Uranium concentration (ppm) in the marsh core from Loch Don. (b) Linear correlation plots of U (ppm) with CaO (wt %), P_2O_5 (wt %), LOI (% dry mass), Fe_2O_3 (wt %), MnO (wt %) and K_2O (wt %).

The down-core distribution of uranium distribution in the Loch Creran marsh core is shown in Figure 7.31a) and demonstrates that U concentrations increase steadily up through the core profiles towards the surface. In the near-surface layers U is significantly enriched (maximum value of 33.6 ppm) relative to the underlying sediments. Graphical plots of linear regression correlation between uranium, major element oxides and LOI (as a proxy for organic content) are shown in Figure 7.31b. These plots give some insight into the behaviour of U within the dominantly mineralogenic sediments of this marsh. The strongly positive correlation with CaO ($r^2 = 0.62$) suggests that decoupling of dissolved uranyl complex is slower to occur within these sediments. The strongly positive correlation with P ($r^2 = 0.74$) and LOI ($r^2 = 0.65$) indicates that complexing of uranium with P and humic substances is occurring as suggested by Sarin and Church (1994) in their study of U within the Delaware and Chesapeake estuaries, USA. Linear correlation with the redox-sensitive Fe and Mn oxides reveals a stronger positive values for Fe ($r^2 = 0.52$) than for Mn ($r^2 = 0.16$) indicative of the predominance of Fe oxyhydroxides as receptor sites for U adsorption (Figure 7.31b). A strongly positive correlation does not exist between U and K (as a proxy for fine detrital/flocculated material) suggesting that particulate scavenging is less significant in terms of contributing to the enrichment of U within the near-surface sediments. However, correlation with other trace elements associated with the fine sediment fraction (e.g. Nb, Rb, V and Y) record positive correlation coefficients (0.60, 0.43, 0.79 and 0.83 respectively) indicating that a strong association with fine particulate material does indeed exist within these sediments.

The study by Church *et al.* (1996) highlights that uranium particulate scavenging takes place predominately over the Spring tidal cycle as previously mentioned (i.e. bi-monthly) and during the summer months when the marsh surface is most acidic. Although no pH data has been acquired for the Loch Etive marsh surface sediments it is likely that acidic conditions were prevalent as this core was extracted during a summer period of exceptionally hot weather during 2000. This would facilitate enhanced scavenging and concentration of uranium resulting in the surface enrichment visible in the concentration depth/profile (Figure 7.31a) and can be used to infer geochemical processes indicative of high marsh environments.

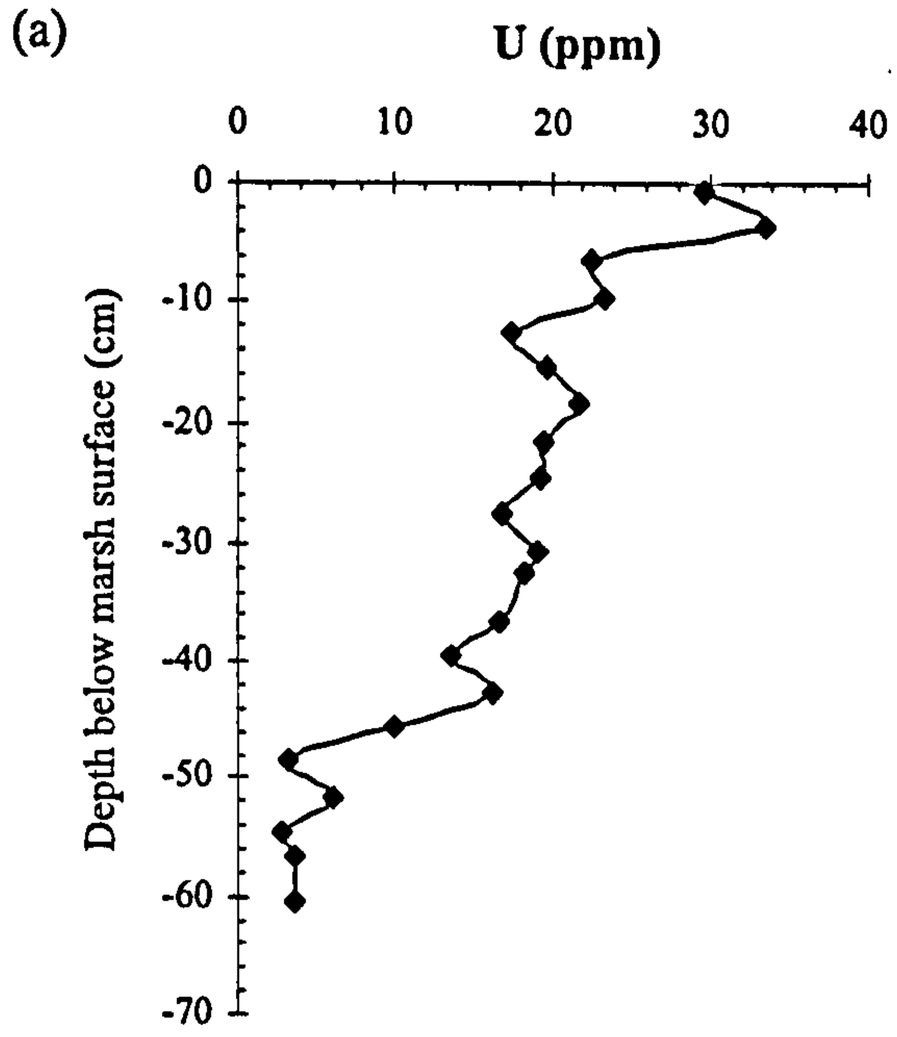

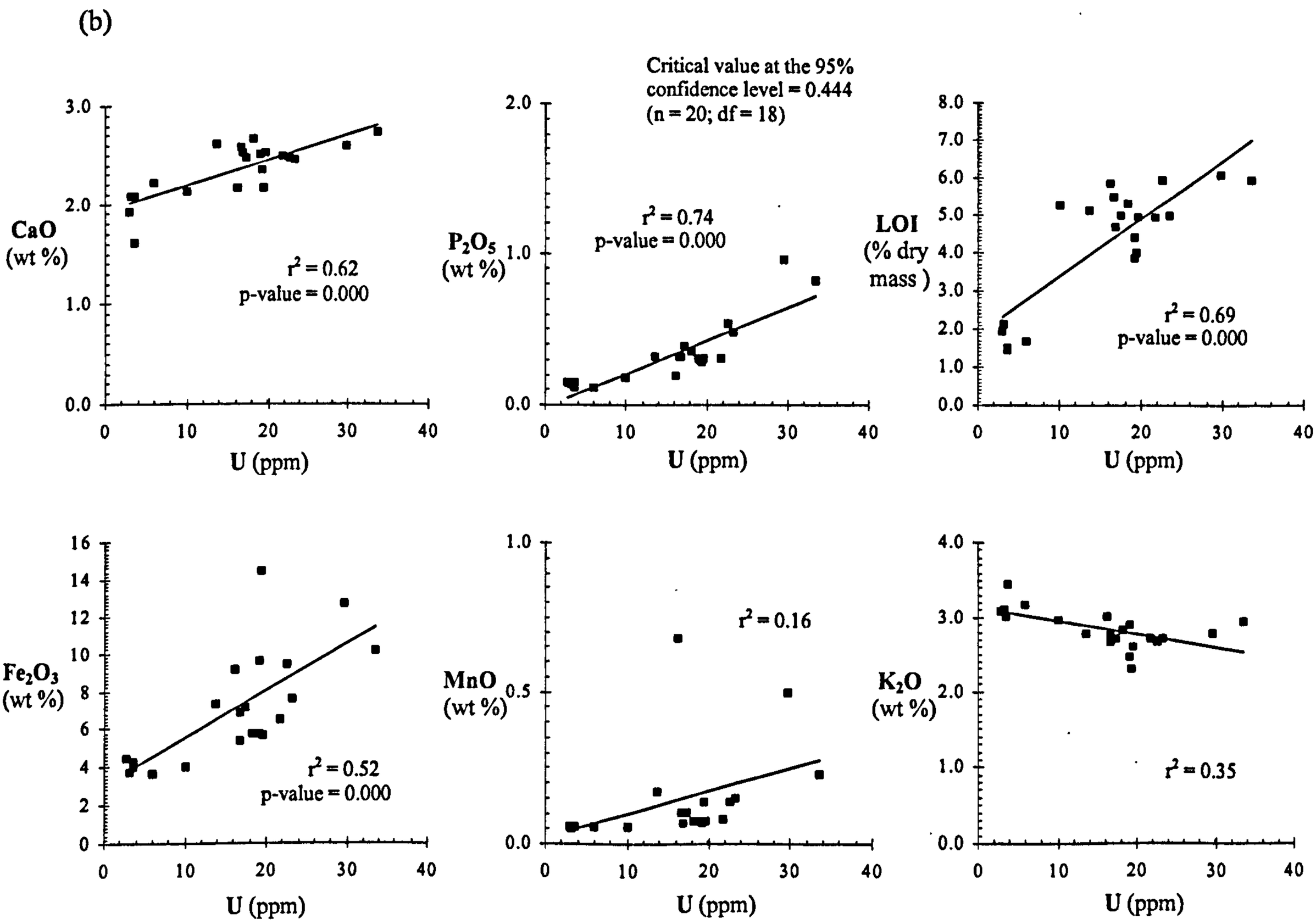

Figure 7.31: (a) Down-core profile of Uranium concentration (ppm) in the marsh core from Loch Creran. (b) Linear correlation plots of U (ppm) with CaO (wt %), P_2O_5 (wt %), LOI (% dry mass), Fe_2O_3 (wt %), MnO (wt %) and K_2O (wt %).

7.7: Principal Components Analysis of the Argyll marsh sequences

Principal components analysis (PCA) is one of several multivariate statistical techniques which facilitate the simultaneous manipulation of large data sets comprising any number of variables. PCA can generally be thought of in terms of an extension of fitting straight lines and planes by least-squares regression (Ter Braak, 1995). Essentially the PCA method reduces the number of variables of specific data being studied. A large number of variables are reduced to a small number of uncorrelated variables rendering enhanced ease of data interpretation (Rollinson, 1993).

PCA works by calculating the maximum amount of spread (variance) around the mean of all the data points. The analysis then projects this graphically as a line in p-dimensional space, referred to as the first eigenvector. Matrix algebra computation is then used to project the original data onto this first eigenvector and these form the 1st principal component coordinates. The calculated variance of these coordinates form the first set of eigenvalues and represent the spread of the data along the direction of the first eigenvector. Further eigenvectors are then calculated and the same matrix algebra produces the relevant eigenvalues specific to these additional lines of best fit. Importantly, each eigenvector and its associated eigenvalues is graphically projected at right angles to the preceeding eigenvector. The 2nd calculated eigenvalues represent the maximum amount of spread at right angles to the 1st eigenvalues in this p-dimensional space and so on. This transformation of the data into a set of eigenvectors continues in gradually decreasing order of explanation until the total variance of the data set is accounted for.

In ideal situations PCA has an advantage over other ordination methods in that the first few principal components may explain a high proportion of the variance. If this is the case, then the remaining eigenvalues representing other variables can often be discarded in terms of explaining and interpreting the data. Setting a standard percentage value for the acceptable levels of explained variance are not straight-forward. Clarke and Warwick (1994) have suggested that a PCA graphical plot that accounts for as much as 70-75% of the variance described by the 1st and 2nd eigenvalues is likely to provide a good overall description and structure of the original data.

In this study the variables under consideration are major element geochemistry oxides and trace elements from the four marsh core sequences. During the development of marsh sediments the down-core elemental profiles can be subject to various physical and chemical phenomena that may affect the recorded depositional record. Table 7.3 lists these

different phenomena and the key elements that are assumed to be indicative of processes and conditions within the sediment prism.

PCA was undertaken on the original data from Loch Scridain using the MINITAB statistical software computation package. Correlation of the calculated eigenvalues and the individual elements from the original data sets is shown in Table 7.3. This information can be used to reveal the extent to which certain differing processes/phenomena have influenced the geochemical signature within the marsh core.

Phenomenon	**Assumed indicator elements**
Coarse grained sedimentary material	Si, Zr
Fine grained sedimentary material	Al, K, Nb, Rb, Ti and Y
Early diagenesis	Fe, Mn, P, As, V and S
Heavy mineral content	Zr, Ti, Y, Ce, Th, U and Y
Pollution/contamination	As, Cr, Cu, Ni, Pb and Zn
Marine derived elements	Ca, Mg, Sr, Na, I, Br, Cl and S

Table 7.3: Assumed indicator elements for various phenomena that influence the down-core profiles of saltmarsh sediments. (Note that some cross over between elements can also occur with some being indicative of more than one process). Where this is seen to take place more detailed assessment of elemental distribution/behaviour may be necessary. (Modified from Dyer, 2001).

7.7.1: Loch Scridain

What is immediately obvious from the analysis of the Loch Scridain core are the low overall eigenvalues for all elements which only range from + 0.254 to – 0.267 (P_2O_5 and Sr respectively for the 1st principal component; see Appendix 6.1). The low positive values for Fe_2O_3 and MnO and those for Pb, As and S indicate that diagenetic processes account for a proportion of the 54% variance recorded in the 1st principal component loadings. The 2nd principal component loadings are of similar low overall values. Highest positive values suggest that heavy mineral input in part influences the marsh (e.g. Ce and La) with the additional influence of coarse material with a marine source suggested by the grouping of SiO2, CaO and MgO. The 15.3% variance recorded by the PC2 eigenvalues also indicates a contribution from Fe oxyhydroxide recycling.

These data are illustrated in the graphical plot of PCA 1 and PCA 2 components shown in Figure 7.32. Highlighted in this plot are the positions of the various key elements discussed above which relate to the variety of marsh depositional processes listed in Table 7.3. Further analysis of the component loadings for the 3rd principal component, reveals that heavy mineralogenic material (TiO_2 and Zn), along with diagenetic processes (indicated by MnO, Fe_2O_3 and V) account for a further 12.4 % of the variance in the data. The identification of a marsh phenomena/physical process from the 4th principal component loadings does not reveal any extra detail with these eigenvalues recording 8.4% of the total variance. Al remains positively weighted in all the calculated eigenvalues. This is possibly indicative of the constant relative abundance of this element derived from the weathering and subsequent input of dissolved aluminium-rich feldspars throughout the period of marsh development. The low total difference between positively and negatively weighted component loadings in all the eigenvalues suggests that despite the significance of diagenetic processes other phenomena also influence the depositional signature in this marsh core. This is likely to related to the complicated history of sedimentary material now present in the modern marsh system.

7.7.2: Loch Don

Calculated eigenvalues for the Loch Don geochemistry data reveal low values similar to those in the core from Loch Scridain (Appendix 6.2). SiO_2, TiO_2, Th and Zr are the only elements for which positive eigenvalues are recorded indicating that coarse–grained sediment and heavy mineral phases account for a proportion of the 60% of variance recorded by the the 1st principal component loadings. However the eigenvalues of opposite sign are not significantly large and could therefore be interpreted to not vary inversely with other phenomena. The diagenetic indicator elements Fe_2O_3 and MnO have similar negative values as do the component loadings for S and P_2O_5, and As. Indicator elements for fine-grained sedimentary material (Rb, Y, Nb, K_2O) also show similar low negative values. Additionally those elements used for indicating the influence of marine input to the marsh sediments (Na_2O, MgO, I, Br, Cl and S) also suggest that this process contributes in part to the total PC1 variance (Appendix 6.2). Inspection of the PC2 component loadings reveals that this eigenvector and associated values accounts for a further 11.7% of the variance in the sample data. The result of the PCA is that 71.5% of the variance is explained by the eigenvalues

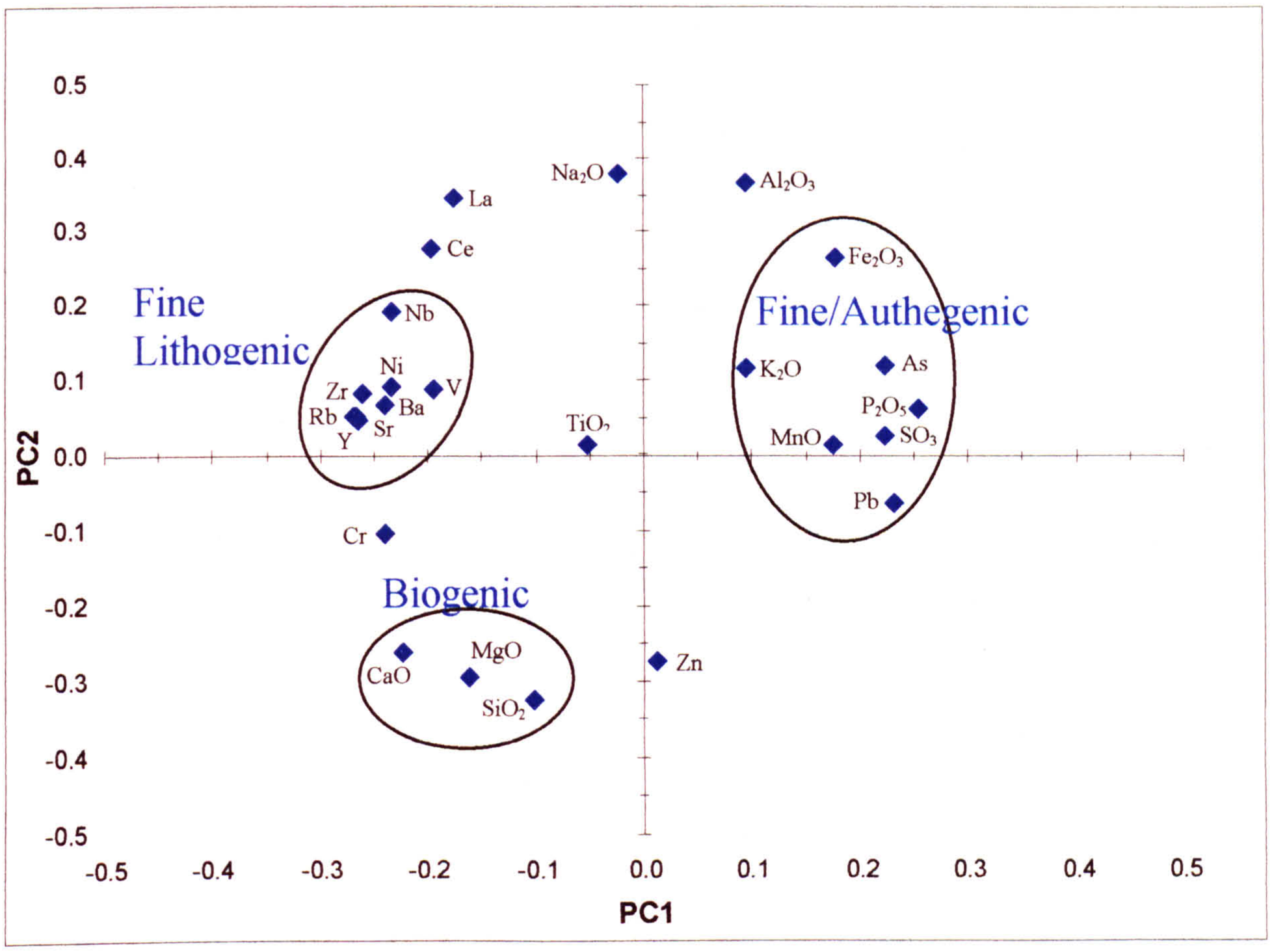

Figure 7.32: Principal component loadings plotted as PC1 versus PC2 for the marsh core geochemistry from Loch Scridain.

obtained for the first two principle components however it is not really possible to discern whether one of the proposed phenomena that influence the sedimentary record within marsh environments has been of greater significance than any of the others listed in Table Appendix 6.2.

A graphical plot of the PC1 vs PC2 eigenvalues is presented in Figure 7.33 In the diagram the positive loadings include the elements SiO_2, Zr, Th and Ba which occur with CaO and to a lesser extent Sr suggesting a marine source for the coarser-grained material and some heavier mineralogical components. The large number of negative PC1 eigenvalues are also somewhat delineated by the positive and negative values associated with the PC2 eigenvector. PC2 positive values result in the grouping of the redox sensitive elements SO_3, P_2O_5, MnO with fine-grained sediment indicators such as Rb, K_2O. The presence of MgO, Na_2O, Cl and Br suggests a common association with marine derived particulate matter. Similarly, the negative PC2 eigenvalues result in the grouping of other redox-sensitive elements (e.g. Fe_2O_3 and As) with U, Ce, Ni and Cr representing coarser grained material and other heavy minerals. Consequently, it must be assumed that the input of heavy minerals, coarse and fine-grained sediment material and marine inputs must all contribute through similar weighting to the record of deposition in this marsh core.

7.7.3: Loch Creran

Similar to the cores from the Isle of Mull PCA of the geochemistry data from Loch Creran reveals low eigenvalues for the four principal components (Appendix 6.3). Despite the calculated positive and negative eigenvalues these cannot be said to vary inversely thereby permitting the identification of any one particular sedimentary phenomena or process responsible for the 68.1% variance derived from the PC1 and PC2 component loadings. The graphical plot of PCA1 versus PCA2 loadings is presented in Figure 7.34. Positive values are recorded for SiO_2, K_2O, Ba, Bi, Rb, Sr, Th, Co and Zr suggesting a contributory influence from coarse-grained material and heavy minerals but also including fine material derived from a marine source. The diagenetic elements, Fe_2O_3 and MnO have similar negative component loadings as do the elements As, V and Mo. Positive PC2 values are recorded for TiO2, Y Sb, Cr and Nb. The inclusion within this group of MgO and CaO suggests the influence of fine sedimentary material derived from a marine source also. A large group of tightly bunched elements is also present with eigenvalues that exhibit a small

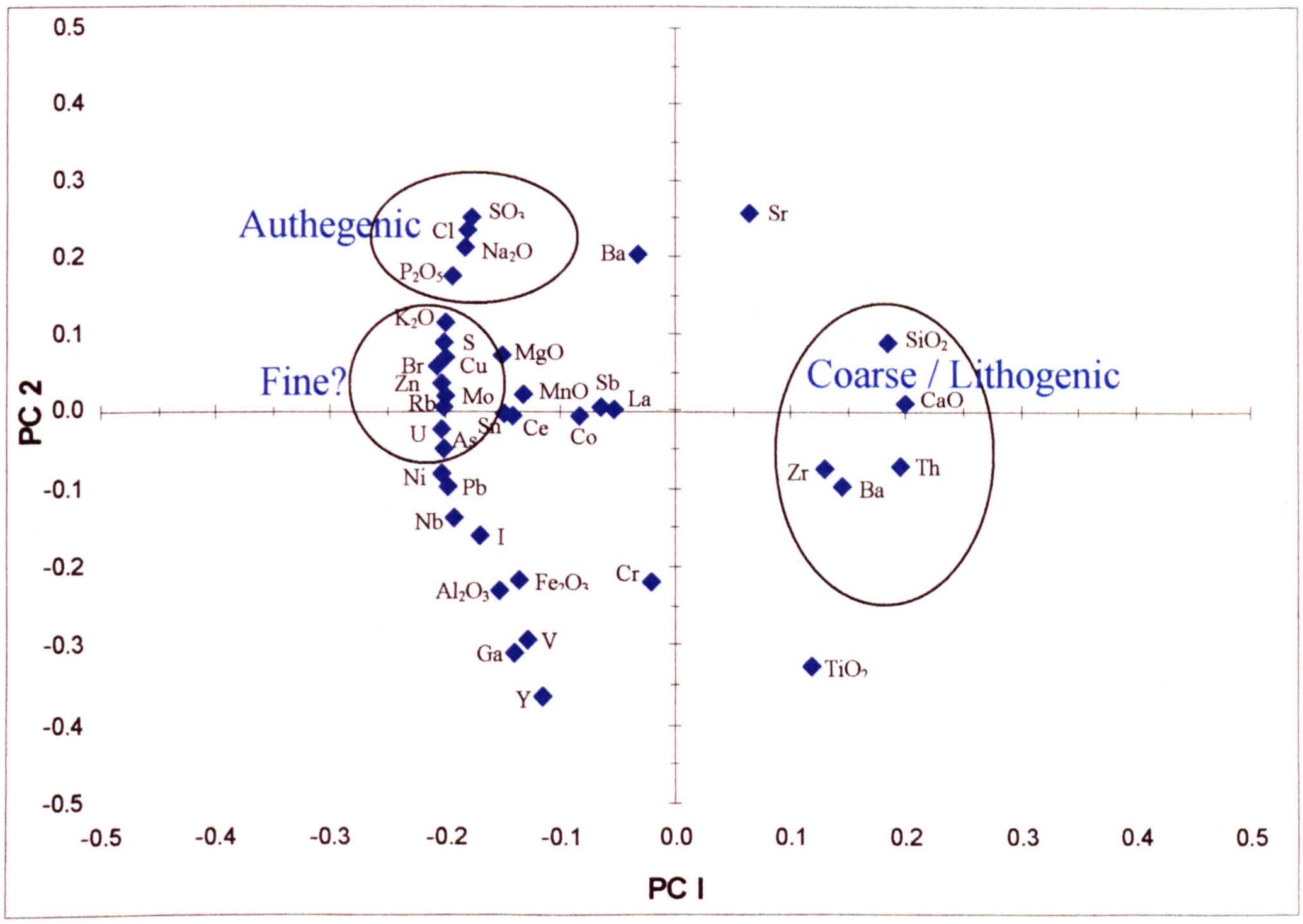

Figure 7.33: Principal component loadings plotted as PC1 versus PC2 for the marsh core geochemistry from Loch Don.

overall variance from the PC2 eigenvector. This group includes Pb, Ni, Zn, Cu, Ce and U indicative of influence of heavy minerals/metals. The presence of I, Cl, Na_2O implies the association of these elements from a marine source. Equally weighted in the component loadings here are also the redox-sensitive elements SO_3 and P_2O_5 (Figure 7.34).

PCA therefore suggests that many of the listed phenomena/processes in Table 7.3 act together to result in the geochemical record of marsh development at this site. No one particular process appears to influence the depositional record to a greater or lesser extent.

7.7.4: Loch Etive

As with the other cores investigated in this study, the calculated eigenvalues derived from PCA of geochemical data from Loch Etive does not reveal large opposing positive and negative values. It is therefore difficult to ascertain any significant inverse variation between indicator elements for the different processes listed in Table 7.3. Importantly the collective influence of several indicator elements for diagenetic reactions, coarse and fine-grained material, heavy minerals and derivation from marine sources account for 74.6% of the variance. This result is likely to have been affected by the different stratigraphic units evident in this core (Figure 4.37) and the lack of a well-defined redox zonation within the upper coastal peat section of the core (Figure 6.14).

Nevertheless, the graphical plot of PC1 vs PC2 component loadings, presented in Figure 7.35 does highlight certain groups of elements associated with different marsh processes. For example, SO_3, K_2O and Na_2O are clustered together possibly indicative of marine derived sulphate and fine particulate matter supplied to the marsh surface. Similarly, the redox sensitive elements Fe_2O_3, MnO, P_2O_5 and As are grouped together along with Pb and Al_2O_3. CaO and MgO are positioned in close proximity suggesting a common marine source for these elements. A larger cluster of eigenvalues is contolled by the 1st principal component eigenvector. This group contains both heavy minerals (Zr, TiO2, Ni, V, Ce and Cr) and elements indicative of fine sediment input including Rb and Y. The inclusion of Sr here suggests a marine source also.

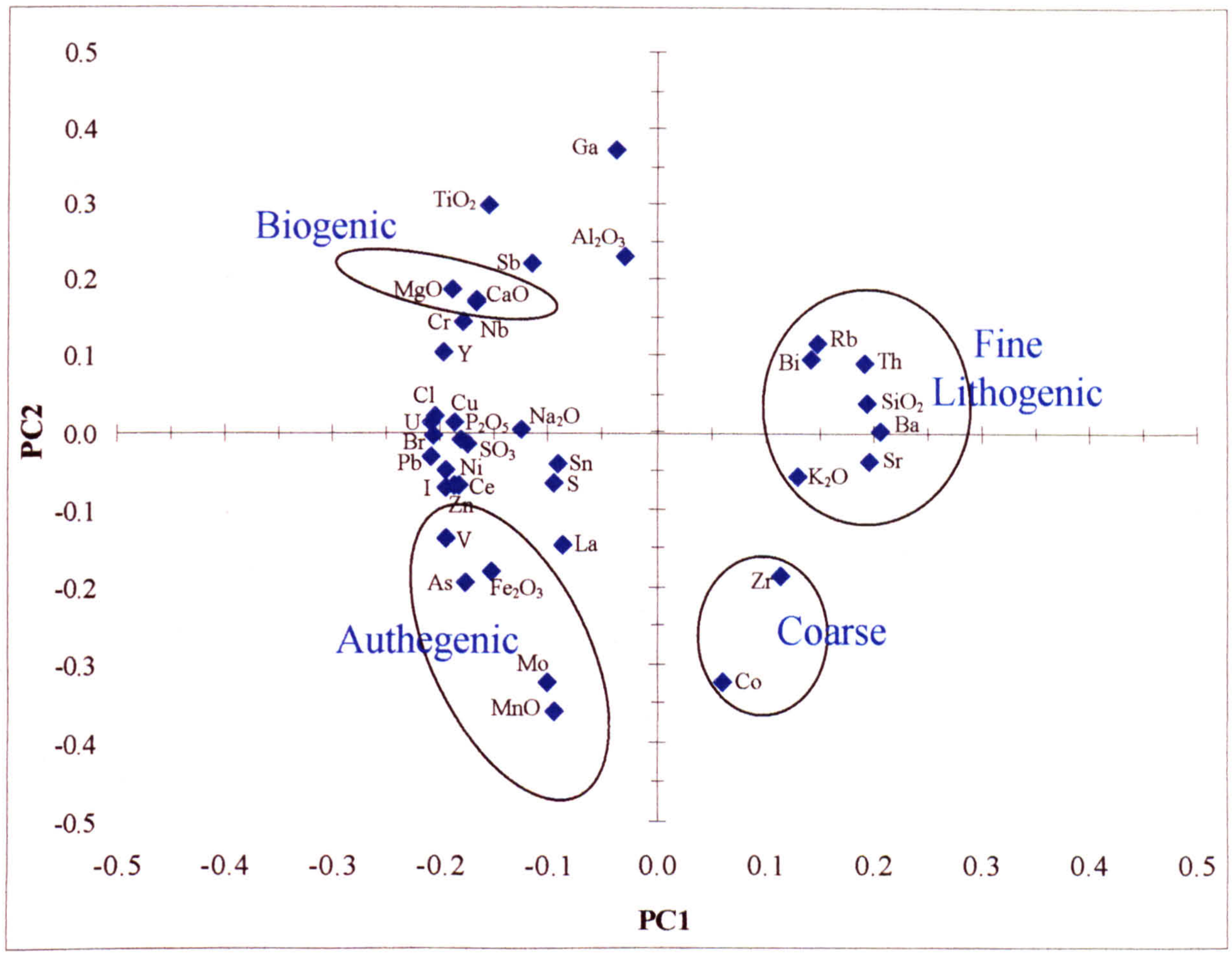

Figure 7.34: Principal component loadings plotted as PC1 versus PC2 for the marsh core geochemistry from Loch Creran.

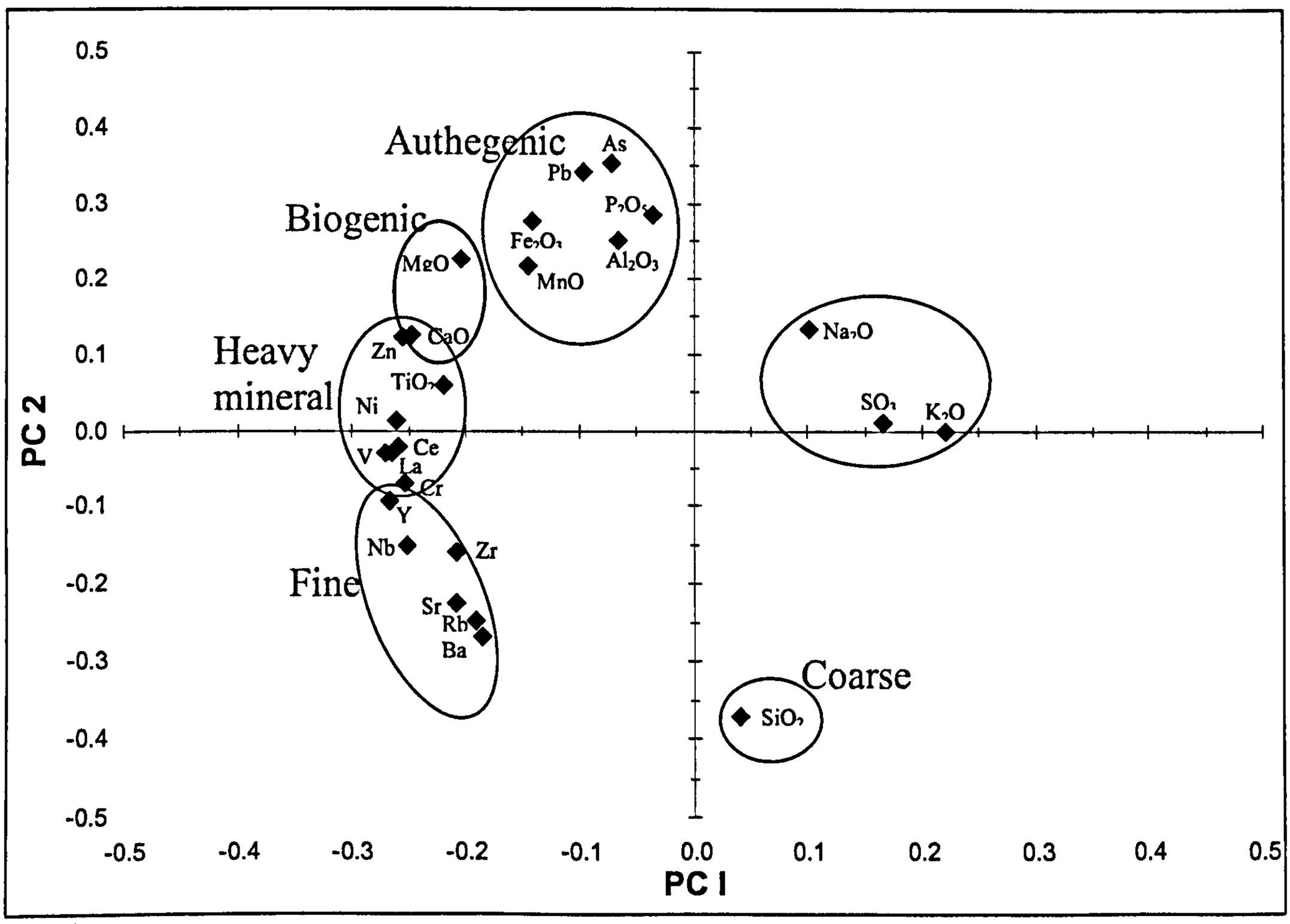

Figure 7.35: Principal component loadings plotted as PC1 versus PC2 for the marsh core geochemistry from Loch Etive.

7.8: Summary of Chapter Seven

Detailed geochemical analysis reveals the differential influence of a variety of marsh evolutionary processes within the four marsh cores from Argyll. Trace metal distributions are principally controlled by adsorption to the fine (clay) fraction but other processes including bromination of metal species, particularly within the near-surface sediments also influence the distribution of these elements. In general metal distributions do not appear to be significantly modified by the diagenetic recycling of Fe or Mn oxyhydroxides. Heavy metals are also associated to a lesser degree with organic complexation processes. The distribution of halides, in particular I and Br reveals that these elements are significantly enriched within the marsh surface layers of all cores and that ratios of Br/LOI and I/LOI are within the values obtained from other published literature.

Heavy metal concentrations in all marsh cores do not indicate any significant enrichment above background crustal values with the exception of As at three of the sites (on Mull & Loch Creran) where concentrations in the upper sections of the cores are slighty elevated. These elevated levels are not considered to represent significant or abnormal contamination.

The U distributions from two cores indicates that surface enrichment of this element is occurring from sites situated across the Firth of Lorne at Loch Don and Loch Creran. This geochemical process is inferred to be indicative of U sequestering within high (mature) marsh settings.

Principal components analysis of the four marsh sequences reveals that of the inferred marsh development phenomena investigated no one process acts alone to become the dominant mechanism influencing the evolution of these highly mineralogenic sediments.

The following Chapter now discusses the broader findings of this research by pulling together the various analytical data to provide an interpretation of the recent evolution of coastal wetlands in the Argyll region. The implications for current larger-scale processes that influence coastal environments are discussed.

Chapter Eight

ANALYSIS AND DISCUSSION

8.1: Introduction

The application of radiometric dating techniques has revealed distinct evolutionary differences between the four marsh sites investigated from the Argyll region of western Scotland. Rates of marsh sedimentation are seen to vary between the site at Loch Scridain and those sites situated on the south-east of Mull and on the mainland at Loch Creran and Loch Etive. Geochemical analysis supports the use of the depositional record of key radionuclides for dating purposes and is used to assess the reliability of such records for the establishment of geochronological models and other geochemical processes, which have influenced the evolution of these marshes. Comparison with available storm frequency data is used to further assess the use of the selected study sites in terms of their potential for preserving a record of deposition related to coastal forcing.

The following chapter now discusses the findings from this research within the context of regional influences upon the development of coastal wetlands from this part of northern Britain.

8.2: Field site characteristics and the marsh sediments

Some general observations made at each site during the course of this study support some of the ideas put forward by Adam (1978) with regard to the areal extent of marsh development and composition of the vegetation communities. Steep mountain topography surrounds the heads of Loch Creran and Loch Etive on the mainland. This results in a narrow coastal strip where saltmarshes are able to develop (Figures 4.25 & 4.35). At these two sites the contemporary marsh exists more as discrete pockets of inter-tidal sediments sheltered from the influence of the rivers Creran and Etive respectively by anticedent fluvial bars of material ranging from large boulders to coarse sand. These features suggest that channel migration at the head of these lochs has been an active process prior to the development of the present extent of marsh sediments at these two sites. This process does not appear to have influenced the marsh sediments within areas from which cores have been extracted.

Investigative coring and field observations indicate that the developed marsh sequences vary significantly in depth over quite short distances across the marsh surfaces as a function of the underlying fluvial substrate. This results in the transition from low to high (mature) marsh

environments also occurring over short lateral distances which are not specifically linked to distances from marsh morphological features such as tidal channels and salt pans. Hence, the underlying coarse material has exerted a significant influence upon the development of the Argyll marsh sediments relative to the tidal frame.

The upper marsh area at Loch Don on the south-east of Mull (Figures 4.13 & 4.15) is more extensive than within the two mainland estuarine settings owing to this site being more akin to a lowland estuary lacking the influence of major rivers. Small byrnes do discharge freshwater into the Loch Don estuary at a number of locations however, the presence of distinct underlying fluvial deposits is less significant at this site. The marsh here has developed upon a coarse polygenetic substrate consisting of antecedent material derived from Devensian glacial erosion which has been subsequently re-worked by marine processes during the Holocene (Gray, 1974). The depth of marsh sediment is more uniform than that seen at the other three sites as a result of the differing geographical setting and underlying morphology of the upper marsh area. However, the gradient from the marsh edge to the position of the high water mark (inferred from the most recent upper strandline field evidence) can be steep in some places (< 20 metres).

At Loch Scridain on the west coast of Mull, the inter-tidal saltmarsh occupies a large area owing to the wider expanse and more gently sloping nature of the lowland coastal strip than that observed at the other sites in this study (Figure 4.4). The marshes here have developed upon coarse underlying fluvial substrate. Certainly, air photographic evidence from this site clearly shows the development of small modern deltaic deposits within inner Loch Beg where the River Colladoir converges with the inter-tidal environment. Field observations reveal that these are quite extensive and have obviously migrated in the past in response to river discharge and sediment load delivered to the head of this estuary. Small contemporary alluvial fans are evident at the seaward end of the main river and more minor marsh channels. However, this fluvial sedimentation does not influence the modern marsh other than providing a potential minor source of coarser clastic material. This does not appear to be undergoing significant redistribution over successive tidal cycles. The older fluvial deposits form a suitable substrate on which pioneer (lower) marsh plant species have become established (Adam, 1978; Langlois *et al.*, 2003).

At all four sites plant communities are dominated by the saltmarsh grass *Puccinellia maritima* which has been shown to exert a pronounced effect upon sediment stabilization, micro-topography dynamics and the geomorpho-genesis of coarse sedimentary low inter-tidal

environments (Langlois *et al.*, 2003). This species has played an important part in the development of pioneer and low marsh habitats within the Argyll region. However, other physical hydrodynamic parameters including exposure to wave action, tidal currents and sediment supply will also have influenced the spatial distribution of low inter-tidal pioneer areas.

Across the study transect the two cores from sites on the Isle of Mull and that from Loch Creran are characterized by homogenous well-mixed sediments consisting of coarse to fine sand with silt and fine clay material. These marshes contain relatively low levels of organic material in comparison to some other UK locations (e.g. the Solent estuary system, Cundy and Croudace, 1995; Cundy *et al.*, 1997). This is in direct contrast to the observations of Adam (1978) for other marsh settings in western Scotland to the north and south of the present study area.

The lower levels of organic material present in the Argyll marshes investigated in this research are considered to result from two principal factors. Firstly, the marsh vegetation consists predominately of tall marsh grass species (e.g. *Puccinellia maritima* and others). These are characteristically less succulent and more hardy than herbaceous halophytic species such as *Halimonia portulacoides* found in more southerly marsh environments. Additionally, the below-ground rhizome development of these marsh grass species is possibly not as extensive as other halophytes and may also be more limited by seasonal variations in light and temperature.

Secondly, these marshes have a prolonged history of intermittent grazing use by local landowners as identified by Adam (1978) from other sites. Both cattle and sheep have been observed on the marshes during successive field visits indicating that this practice is still continuing at all the sites investigated in the present study, albeit on an irregular basis. The combination of these two factors results in the marshes being dominated by clastic material (silts and sands) and containing low quantities of organic material.

8.3: Evolution of the Argyll marshes

8.3.1: Loch Scridain (western Isle of Mull): core sedimentology

Major element geochemical data indicate very little variation in sediment source with time as shown by the profiles of Si (as an indicator of coarse material) and Al and K (indicative of fine sediment inputs, Figure 8.1). The dry bulk density profile indicates a striking reduction in

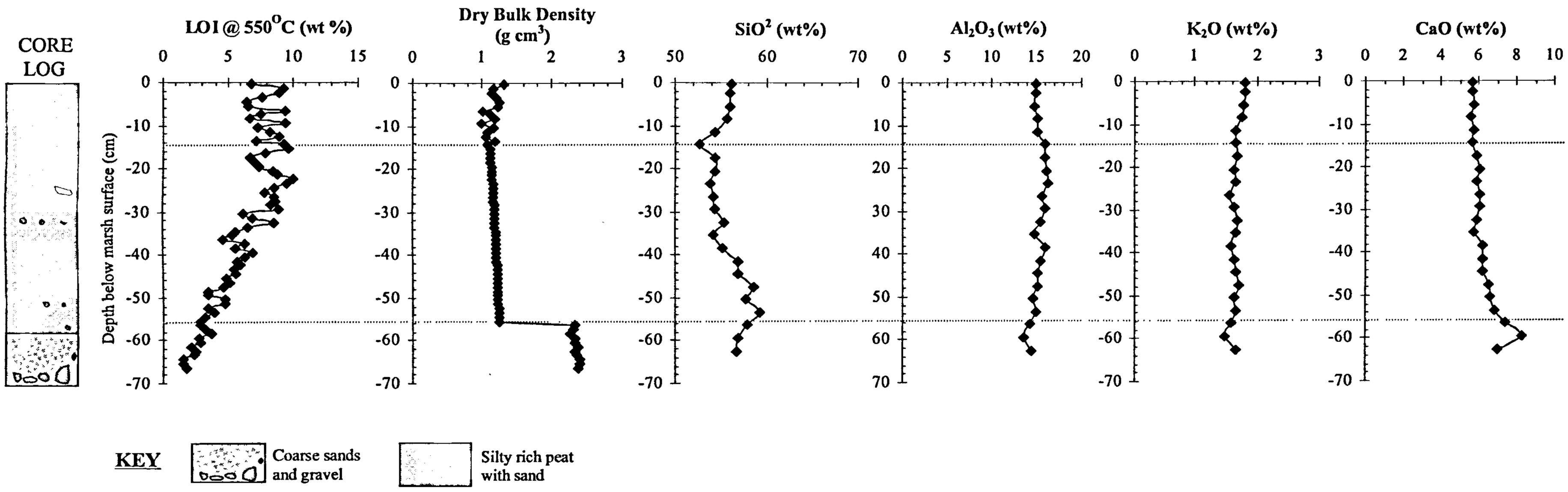

Figure 8.1: Summary diagram showing element oxide abundance (wt %, according to x-r-f convention) and concentration-depth profiles for organic carbon (via LOI proxy method), SiO_2, Al_2O_3, K_2O and CaO from the Loch Scridain marsh core.

values above 57-58 cm from which point values are remarkably constant upward through the core to a depth of 15cm. The lower section of the dry bulk density profile below 57-58 cm depth and elevated values for sediment density corresponds well with the visual stratigraphy and represents values associated with the underlying coarse deposits. The rapid decline in sediment dry bulk density above this depth increment is accompanied by gradually increasing values of organic matter (via LOI) and a decline in the relative abundance of Si. As such the 57-58 cm depth increment is taken to represent the onset of marsh conditions at this site and the development of halophytic vegetation (Figure 8.1). Continuing gradual decline of Si is accompanied by increasing values for organic carbon resulting from in-situ production of marsh vegetation and slight increases in Al and K indicating increasing concentration of fine material. The lower and middle sections of the core clearly show the development of marsh and the subsequent gradual fining of material with increasing organic input up to 15-16 cm depth. Above this depth dry bulk density can be seen to fluctuate above and below the lower more stable values. This is accompanied by fluctuating LOI input to the marsh surface with a concomitant increase in the abundance of Si indicating an increase of coarser material from 15-16 cm to the marsh surface (Figure 8.1). Trace elements including Pb, As, Zn and Br (Figure 4.12) also show increased concentrations within the near surface sediments which are derived from detrital inputs as opposed to diagenetic precipitation (discussed below).

Various positive correlations have been identified that indicate the association of organic matter with various major element components of the marsh soil (Figure 4.10a and b; summarized in Figure 4.11). These analyses show that organic matter is predominantly associated with the redox-sensitive elements Fe, Mn, SO_3 and P_2O_5 and hence post depositional diagenetic reactions in the Loch Scridain core. The weaker association with TiO_2 implies that some organic material is coupled to detrital inputs to the marsh. The actual strength of relationships between major element abundances and LOI values is highly dependent upon the accuracy and hence error associated with measurement via the X-R-F technique. Error is determined by summation of the values obtained for the twelve key major elements. These should comprise 100% in total and error can, therefore, be assessed from the deviation under or over the 100% figure. Measurement error associated with the major elements abundances for the Loch Scridain marsh core are shown in the table presented in Appendix 4.1 which includes the summation data. These clearly demonstrate that the range of error is small ranging from 0.02 – 1.38% providing a high quality data set from this core.

Problems associated with LOI determination have been highlighted in Chapter Three (section 3.5). Some discussion is directed towards the accuracy relating to values where organic carbon is low (i.e. below 10 % dry mass). Visual inspection of the core reveals that clay is indeed present as a minor component of the sediment matrix. However, the dominant fraction of these mineralogenic sediments is silt with fine to coarse sands increasing toward the base (from visual inspection of oven-dried sediment). The very dark colour and organic texture of the marsh peats in many other coastal locations within western Scotland perhaps led Adam (1978) to conclude that the marshes he studied consisted of highly organic-rich sediments. LOI measurements have revealed that this is not the case in the sequence extracted from Loch Scridain with relatively low values being recorded in this marsh (maximum 10% dry mass at 22-23 cm depth; Figure 8.1). Nevertheless, consideration of the data with the visual observations of dried material, coupled with the down-core profiles of K_2O lends support to the argument of overall low clay content and hence confidence in the LOI measurement obtained from these mineralogenic sediments. This further provides a high degree of confidence that the statistical relationships between organic carbon and major element abundances are real and robust.

Statistical analysis using the CONIS least sum of squares (Grimm, 1991) identifies two distinct zones from the major and trace element geochemistry and these are subdivided into further chemozones (Figures 4.9 & 4.12). The major division between LSrid A and LSrid B is the product of diagenetic procesess (discussed below). Further subdivisions of the geochemical zonation correspond well with the lower visual stratigraphy in the core and are related to the transition from coarse underlying substrate into more organic-rich finer marsh sediments above 56-57 cm depth. The uppermost chemozone LScridB2 results directly from the increased sediment accumulation within the near-surface layers of the core (discussed in section 8.3.2 below).

8.3.2: Redox geochemistry

Down-core profiles of Fe/Al and Mn/Al indicate the presence of peaks situated between 35-36 cm and 14-16 cm depth respectively (Figure 6.1). These peaks are attributed to redox controlled diagenetic remobilization of Fe and Mn and correspond well with the theoretically derived reaction profiles for these elements (Froelich *et al.*, 1979; Santschi *et al.*, 1990). Within accumulating sediments undergoing reduction reactions the occurrence of a significant peak in

dissolved Mn below a high near-surface concentration of solid-phase Mn strongly suggests that diagenetic remobilzation has taken place (McCaffrey and Thompson, 1980; Thompson *et al.*, 1995). These reactions involve the dissolution of Mn^{4+} and subsequent re-oxidation following redistribution of Mn in sediment pore-waters within oxidizing sediments. The diagenetic enrichment of Fe occurs at greater depths than the diagenetic enrichment of Mn owing to the greater stability of Fe oxyhydroxides within the upper more mildly reducing conditions where peaks indicative of Mn enrichment are generally located (Froelich *et al.*, 1979; Brumsack and Gieskes, 1983; Zwolsman *et al.*, 1993). The down-core profile of S indicates that significant enrichment has occurred within the upper 16-17 cm of the Loch Scridain core. This is attributed to active erosion of the fronting lower marsh environment resulting in the deposition and subsequent loss via oxidation of sulphide-rich suspended matter and sulphide minerals derived from eroded older material (Figure 8.2). Similar conclusions have been derived from studies within the Solent and Sheldt estuaries (Lewis 1997; Zwolsman *et al.*, 1993, Thompson *et al.*, 2002).

Other trace element profiles provide further constraint upon the position of key redox boundaries within this core. The S/Cl ratio plot clearly indicates enrichment of S relative to Cl below 50 cm depth although the maximum ratio of ~ 0.7 at 63-65 cm is not indicative of strongly anoxic conditions (Cundy and Croudace 1995; Figure 6.3). Preferential remobilization of iodine is known to take place relative to organic carbon during early diagenesis (Price and Calvert, 1977; Upstill-Goddard and Elderfield, 1988; Thompson *et al.*, 2002). Iodine has been shown to be released more rapidly than Br with peaks in iodine indicating enrichment occurring at active oxidation fronts resulting in solid-phase peaks above the redoxcline in low oxygen conditions (Thompson *et al.*, 1993). Similar diagenetic recycling of trace metals such as As and V can also be used to define the redox zonation of marsh sediments (Figure 6.3). Ratio plots of S/Cl, I/Br, As/Al and V/Al all show coincident peaks with that of Fe/Al at 35-36 cm depth Figures 6.1 & 6.3). The base of these peaks therefore marks the onset of reducing conditions at depths below 36-40cm with a zone of weakly anoxic/sulphidic conditions shown by the lower enrichment of Sl and V at depth. The peak in Mn at 14-15 cm marks the base of the transition between oxic and sub-oxic Eh conditions. A summary of the redox geochemistry of this core is presented in Figure 8.2.

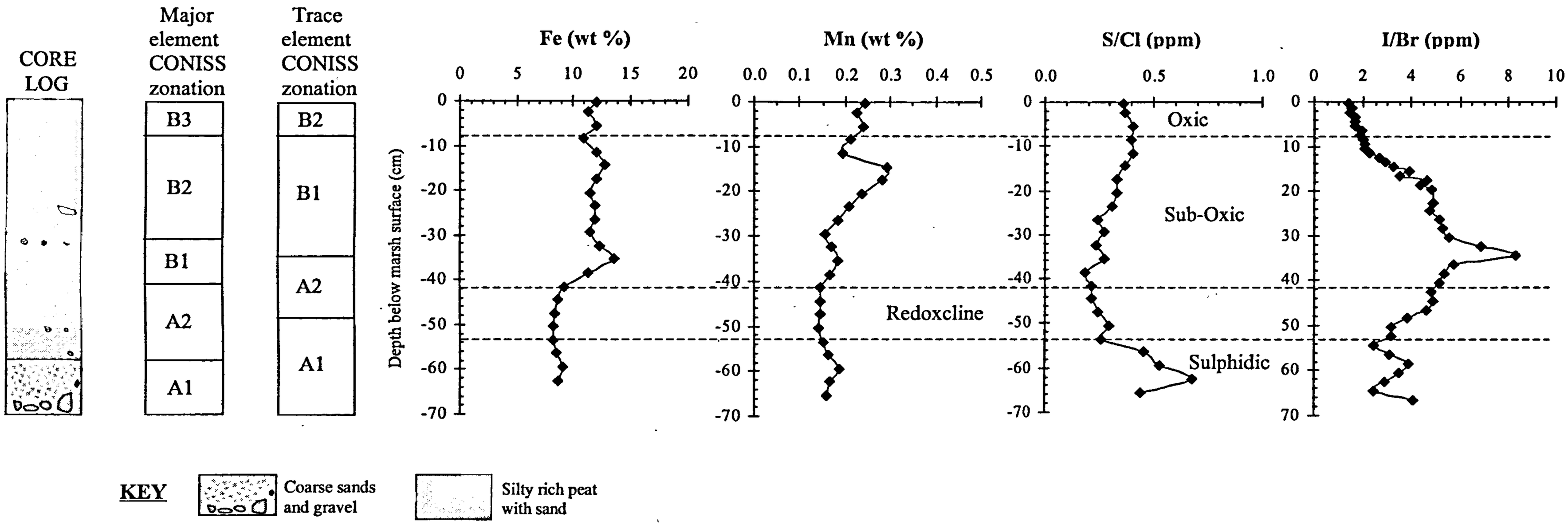

Figure 8.2: Summary diagram showing the CONISS least sum of squares major and trace element geochemical zonation within the marsh core from Loch Scridain. Also shown are the profiles of Fe and Mn (wt % abundance) and the down-core ratio plots of the redox-sensitve elements S/Cl and I/Br (ppm).

The distinct redox zonation evident in this core influences the CONISS derived major and trace element chemozones described from the cluster analysis performed using the Tilia software (Figures 4.9 & 4.12). Clearly the transition between zones A and B corresponds well with the inferred redoxcline (Figure 8.2).

8.3.3: Core geochronology (^{210}Pb and ^{137}Cs dating and ^{241}Am profiles)

Measured $^{210}Pb_{excess}$ activity, i.e. that in disequilibrium with the background ^{226}Ra activity reveals an approximate exponential decline in activity (Figure 8.3) closely resembling the theoretical exponential decline in activity proposed by Appleby and Oldfield (1992) for undisturbed sediments. This indicates that the marsh core from Loch Scridain has not undergone significant disturbance or changes in sediment supply over the period of time corresponding to the maximum capability of the ^{210}Pb method (circa 120 years). The $^{210}Pb_{excess}$ profile supports the major element geochemical data (discussed in section 8.2.2 above) and indicates very stable marsh historical deposition with no changes in the exponential activity slope likely to be caused by significant variation of sediment accumulation or source (Cundy and Croudace 1996). Additionally, there is little evidence from the sediment composition data for large-scale deposition, erosive events or standstills in marsh vertical accretion which would result in inflections in the $^{210}Pb_{excess}$ profile visible as decreases or increases in specific ^{210}Pb activity (Cundy and Croudace 1996). The entire inventory of $^{210}Pb_{excess}$ is concentrated above the redox-cline in the oxic and post-oxic sediments. There is no obvious change in the shape of the low activities recorded at depth in the $^{210}Pb_{excess}$ profile close to the vicinity of the redox boundary situated between 41-54 cm depth or the oxic/sub-oxic boundary inferred at 14-15 cm depth where enrichment of Mn is apparent (Figure 8.2). This would be expected if significant ^{210}Pb migration had taken place as a result of Fe and Mn recycling.

Under stable marsh conditions where no obvious variation in sediment source is apparent and bioturbation appears to be negligble it is possible to extend the time period of the ^{210}Pb methodology further back to ca.150 years (A.B.Cundy pers. comm.). Additionally, owing

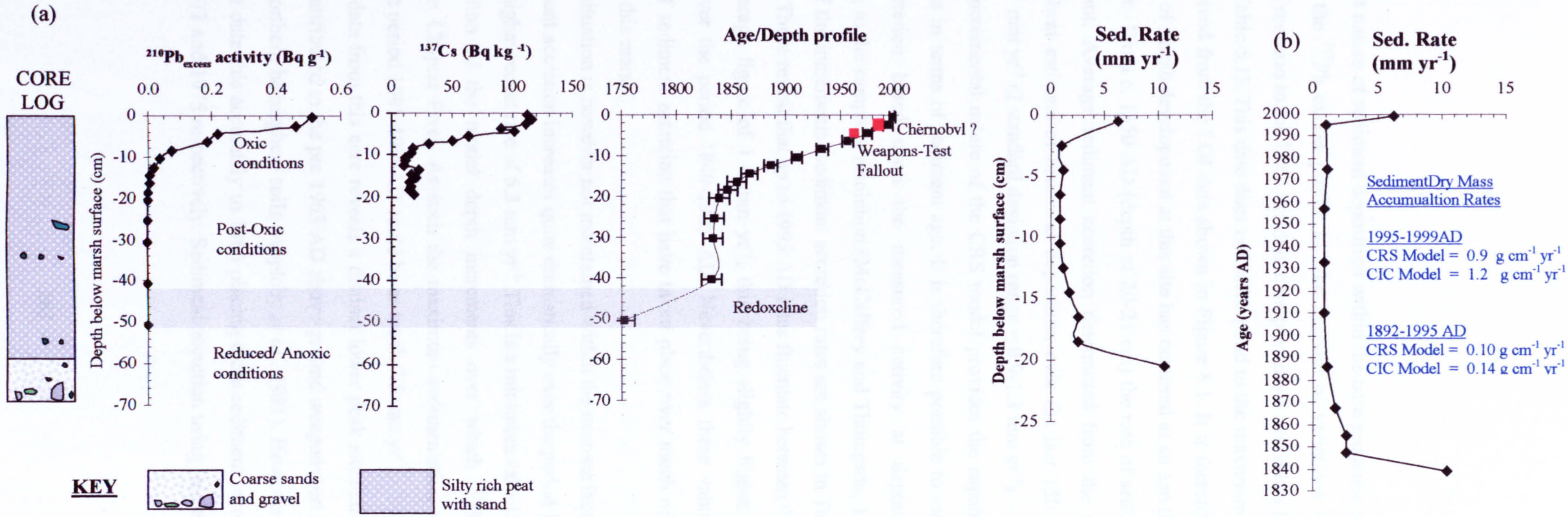

Figure 8.3: (a) Summary diagram showing the core log and radiometric activity profiles for ^{210}Pb and ^{137}Cs from the marsh core from Loch Scridain. Also shown are the age vs. depth model derived from the CRS model calculations and the profile of sedimentation rate versus depth. (b) Sedimentation rate versus CRS model calculated age (years AD).

to the constant nature of sediment deposition within the core sequence it has not been necessary to normalize the ^{210}Pb excess profile to take account of variations in sediment mineralogy. Applying this scenario to the Loch Scridain core provides a maximum lower date of c.1850 AD (± 13 years; Table 5.1). This date does not correspond to the maximum depth of inferred marsh sediments derived from the LOI data shown in Figure 8.1. It is therefore reasonable to assume that the onset of marsh development at this site has occurred at an age that pre-dates the reliable scope of ^{210}Pb. From c. 1850 AD (depth of 20-21 cm) the rate of sediment accretion has been almost constant. Average sediment accretion determined from the simple model therefore provides a robust estimate of historical deposition over the last 150 years with a calculated average of 1.1 mm yr^{-1} (2 standard deviation range = 0.9-1.3 mm yr^{-1}).

The incremental nature of the CRS model provides the capability to analyze discrete depth horizons in terms of sediment age. It is therefore possible to model differential rates of sediment accretion based upon the measured activity at depths throughout the core corresponding to the sampling resolution (McCaffrey and Thompson, 1980; Cundy *et al* 1998). Calculation of the incremental sediment accretion rates are shown in Table 5.1 and summarized in Figure 8.3. These reveal that up to 1995 AD rates fluctuate between 0.8 mm yr^{-1} to 2.5 mm yr^{-1} with an average figure of 1.4 mm yr^{-1}, this being slightly higher than the simple model estimations over the period 1849-1995 AD. Nevertheless these values highlight the general stable rates of sediment accretion that have taken place over much of the historical period of deposition on this marsh.

This situation is however not maintained within the near-surface layers of the core. CRS derived sediment accretion increases quite dramatically over the period 1995-1999 AD to yield a significantly higher recent rate of 6.3 mm yr^{-1}. This is a minimum calculated rate dependent upon the manipulation of the model depth increments over which ^{210}Pb activity is measured (highlighted in Chapter Five). As such the maximum sedimentation rate for the near-surface layers over the period 1995-1999AD could be as much 7.5 mm yr^{-1}.

^{137}Cs data from this core reveals a distinct lower peak situated at 4.5 cm depth (Figure 8.3) which is attributed to the pre 1963 AD above-ground weapons test signature found in many undisturbed northern hemisphere soils (Appleby *et al.*, 1991). However, both the CIC and CRS models do not date this accurately to 1963 placing these sediment increments some 9-12 years younger at 1972 and 1975 respectively. Sediment accretion using this marker horizon assuming

1963 AD yields a rate of 1.4 mm yr^{-1} being slightly higher than that derived from the ^{210}Pb models.

A definitive source for the upper broader peak situated between the surface and 3.5 cm depth also poses problems for accurate dating purposes. This peak is very likely to include activity derived from the 1986 Chernobyl accident. However, it is possible that the pathway of radiocaesium from the Kiev reactor explosion may have resulted in lesser quantities of atmospherically derived ^{137}Cs deposition on the western side of Mull (Cambray *et al.*, 1987). If this is the case then ^{137}Cs in the near-surface sediments will be a function of catchment derived activity being leached into the Colladoir River delivered to the marsh surface and superimposed upon that derived from earlier Sellafield discharges and other labelled material possibly resulting from marsh erosion. Due to the short half-life of ^{134}Cs ($t½$ = 2.06 years) the $^{134}Cs/^{137}Cs$ ratio cannot be used to corroborate the Chernobyl signature in the Argyll marshes as ^{134}Cs has decayed to activity levels below detection or may in fact now be absent .

Visual inspection of the CRS derived age/depth curve (Figure 8.3) clearly shows a distinct inflection in the profile at 20-21 cm depth below the reliable limit of the ^{210}Pb method. It is therefore not possible to determine whether the steeper section of this profile between 20-21 cm and 40-41 cm accurately represents a period of more rapid sediment accumulation associated with a lower (juvenile) marsh setting using ^{210}Pb dating. Such environments are known to develop at a faster rate owing to the increased periodicity of tidal flooding and sediment deposition (Stumpf, 1983; Reed, 1990; Pethick, 1992; Allen, 2000). If marsh initiation is considered to have developed above 56-57 cm which seems reasonable given the compositional and LOI data, then it would also be reasonable to assume that the steeper section of the profile does indeed relate to older low marsh conditions. All that can be said here, is that the marsh at this site began to develop at some point during the nineteenth century, prior to the reliable scope offerred by the ^{210}Pb method. Above the inflection on the age/depth profile the prolonged period of steady-state accretion and is likely to represent rates of sediment accumulation taking place on a mature marsh surface.

CIC and CRS model ages plotted against cumulative dry mass shown in Figure 5.5 indicate the overall good agreement between these ^{210}Pb model derived sediment accumulation rates and those derived from the ^{137}Cs activity profiles Dry sediment is used to obtain actual mass accumulation over time and facilitates the elimination of errors relating to the true position

of activity peaks and possible effects resulting from autocompaction of marsh sediment (Allen, 2000).

Both the CIC and CRS models show good agreement with regard to accumulated mass over the period c. 1850-1995 AD with values of 0.14 and 0.10 g cm yr^{-1}. For the most recent period of increased sediment accretion the ^{210}Pb models deviate from one another with values of 1.2 and 0.90 g cm yr^{-1} for the period 1995 – 1999AD. Importantly the increased sediment accumulation on the marsh surface has occurred since the two periods of known anthropogenically derived ^{137}Cs. This accounts for the higher cumulative mass value obtained if the upper peak is considered to contain a ^{137}Cs Chernobyl marker horizon (accumulated masses of 0.17 and 0.19 g cm yr^{-1} for 1963 AD and 1986 AD respectively). This is additionally important as the higher rate of sediment dry mass accumulation recorded from the ^{210}Pb CRS model calculations is supported by the increased mass accumulation determined from the upper ^{137}Cs marker horizon.

Sediment accretion over the period of inferred mature marsh conditions does appear to conform to Pethicks' (1981) model with reduced accumulation rates over the ca. 70 year period which is now being disrupted by elevated sediment accretion rates on the marsh surface.

8.3.4: Element fluxes and marsh evolution

Changes in sediment accumulation rates resulting from either rapid deposition or removal of material are known to produce inflections in the $^{210}Pb_{excess}$ activity profiles used for dating purposes (Cundy *et al.*, 2003). These can be identified using the CIC and/or CRS dating models (McCaffrey and Thompson, 1980; Appleby and Oldfield, 1992; Appleby, 2001; Cundy *et al.*, 2003). In environmental settings where sediment accumulation may be subject to changing energy conditions or changes in rates of sediment accretion complex element distributions can sometimes be revealed using radionuclide activity profiles alone. In sediments where significant changes are recorded the use of element flux calculations provides a mechanism for examining the accumulation of elements and their distributions whilst taking into account variations in rates of sediment accretion (Cundy *et al.*, 2003).

In the marsh core from Loch Scridain, the 150 year period of historical deposition (derived from the CRS model calculations) is quite uniform apart from that which has occurred

over the last decade or so. Calculated major element fluxes for Fe, Mn, Ti and K and the trace metals Pb, Zn, Ni, As, Cr and V (Figures 7.5a & 7.5b) reveal the steady input of sedimentary material to the marsh surface over the period of historical deposition. In the near-surface layers a significant increase of element flux is recorded in all profiles. For the redox-sensitive elements Fe, Mn, As, and V the increased surface flux does not correspond to peaks related to early diagenesis within this core (Figure 8.2)

The similarity of these profiles to those of Ti, K, and other trace metals indicates that the increased flux evident within the near-surface of the core is due to increased detrital sediment input. The correlation of trace metals (particularly Ni and Zn) with indicator elements of the fine sediment matrix (Figure 7.3) provides evidence of particle associated increases in metal fluxes over the most recent period of marsh evolution.

Overall concentrations of trace metals in the Loch Scridain core (Figure 7.1) reflect a complex pattern of both natural weathering processes and deposition of poly-genetic material on the marsh surface over time. Enrichment of Pb and As in the upper 15 cm broadly corresponds to a period of increasing marsh instability recorded in the dry bulk density profile. Horizontal correlation with the redox-sensitive elements Fe, Mn and S reveals generally weak associations indicating a lack of diagenetic influence on the profiles of these trace metals.

Inspection of the down-core profile of Br indicates a very close horizontal correlation with the distribution of Pb and As. The strong positive linear correlation indicates that bromination of these metals is the principal geochemical process influencing Pb and As distribution (Pellenbarg, 1984) resulting in the enriched section of the core above background concentrations (Figure 7.1 & Table 7.2).

Other trace metal distributions, i.e. those of Ni and Cr, are not influenced by physical and chemical association with organic carbon (via LOI) or diagenetic processes. Distribution of Ni and Cr is governed by the fine fraction of the sediment matrix and hence association with clay particulate matter. Concentrations of these elements are significantly lower than background crustal levels reflecting the observed low clay content of the core (Table 7.2). Zn on the other hand seems to be more independent and not directly influenced by physical or redox-driven processes. Concentrations are much lower than background crustal values (Table 7.2) indicating that supply to the marsh from catchment derived weathering is not a major source of Zn. Therefore, the source of Zn to the marsh surface is considered to be derived from on-going

marsh re-distribution processes over time with slight enrichment in the upper decimetre of the core (age =1910 ±4 years to present) linked to discrete fluctuations in mineralogenic input.

8.4.1: Loch Don (south-eastern Isle og Mull): core sedimentology

Geochemical data from the Loch Don core (Figure 8.4) also show that throughout the period of marsh development overall sediment input and sources over time have not altered significantly. LOI values correspond well with the visual stratigraphy at depth with increases in organic carbon content evident between 40-41 cm depth. This corresponds to decreases in Si and authigenic Ca formation with slightly increasing values for Al and K. This strongly suggests that initiation of saltmarsh conditions occurred at 40-41 cm depth with elevated LOI values attained at 37-38 cm depth representing the influence of pioneer marsh vegetation. Despite some minor fluctuation in Si abundance above 30 cm depth (Figure 8.4) the dry bulk density profile clearly indicates the stability of the accumulated material with a gradual up-core reduction indicative of a gradual fining of material upwards through the core. Depth profiles of Al and K (indicative of clay content) support this interpretation and a gradual increase in fine material is inferred from the increasing abundance of Al and K towards the marsh surface.

Positive correlation between LOI and the elements Fe, Mn and S point to associations driven by post-depositional diagenetic reactions with these redox-sensitive elements (Figures 4.20a and 4.20b; summarized in Figure 4.21; discussed in section 8.4.2 below). Positive correlations with Al, K, P and Na indicate associations linked to vegetative litter, organic complexes and marsh surface evapo-transpiration processes (Turner, 1999). Correlations with Ti (as a proxy for detrital input) support the regression analysis for LOI with only Si and Ca displaying significant positive associations indicating that these components are derived from detrital input. Average LOI values are slightly lower within the Loch Don core than those recorded from western Mull at Loch Scridain. Maximum values occur at three distinct depth horizons (Figure 8.4) which do not appear to be intrinsically linked to depositional process and may reflect the influence of diagenetic reactions.

Two distinct chemozones are identified in the core using the CONISS least sum of squares analysis (Figure 4.19 & Figure 4.22; summarized in Figure 8.5). For the major elements the main zonation between LDonA and LDonB results from the redox behaviour of Fe and Mn

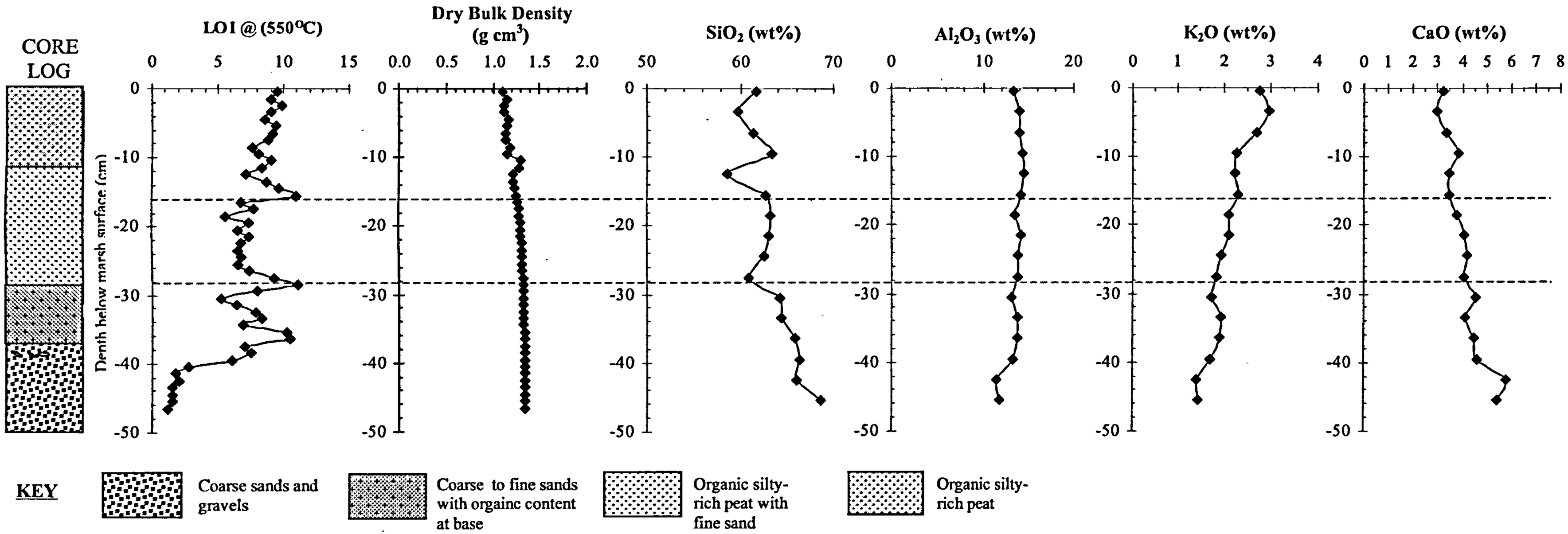

Figure 8.4: Summary diagram showing depth profiles of LOI (% dry mass) and Dry Bulk Density (g cm^3) with element oxide abundance (according to x-r-f convention) for SiO_2, Al_2O_3, K_2O and CaO for the Loch Don marsh core.

(discussed below). Other sub-zones present relate to compositional differences within the coarse sediment layer at the base of the core and in particular the upper near-surface layer characterized by increased sediment accumulation (discussed in section 8.4.3 below).

Chemozones identified from the trace element concentration data clearly show the influence of the compositional variations within the lower and near-surface sub-zones. The section of the core sequence extending from 40-41cm up to 5-6 cm depth reflects the more uniform concentration profiles of many trace elements over this depth interval (Figure 4.22)

8.4.2: Redox geochemistry

Early diagenetic reactions in the Loch Don core have resulted in a distinct profile displaying peaks in both Fe and Mn (Figure 8.5). The bulk of the core profile is exposed during Low Water on the neap tide (LWONT) and this situation is exacerbated during Spring tides (HWOST). As a result of this variable exposure the surface sediments down to 30 cm depth are highly oxidized. This has resulted in enrichment of both Fe and Mn at depth increments that are situated close together (between 22 and 32 cm depth). This is in direct contrast to the core from Loch Scrdain where the peak in Mn clearly defines the base of the sub-oxic boundary at a higher altitude in the sequence. Additionally, a somewhat smaller peak in Fe occurs at 12-13 cm depth which corresponds to a decline in Mn element abundance. The presence of the sub-surface peak in solid-phase Mn beneath the surface enrichment recorded in the core points to significant early diagenetic remobilzation having taken place within the sediment prism. The uppermost peak in Fe also strongly suggests that the oxidizing conditions resulting from exposure at low tides has resulted in the reduced stability of Fe oxyhydroxides within sub-oxic conditions causing precipitation of Fe. This peak also corresponds to a small increase in S and organic matter content which may be due in part to the oxidation of authegenic Fe sulphide minerals. These are present on the upper estuary marsh surface owing to the ongoing erosion of the fringing outer estuary marsh areas which are now providing a source of material to the upper estuary area (discussed in section 8.10 later in this chapter).

Redox-sensitive trace element ratio profiles highlight the true position of the redoxcline in this core (summarized in Figure 8.5). The S/Cl down-core profile clearly shows sustained enrichment below 38-40 cm depth. Comparatively, the I/Br profile displays multiple peaks

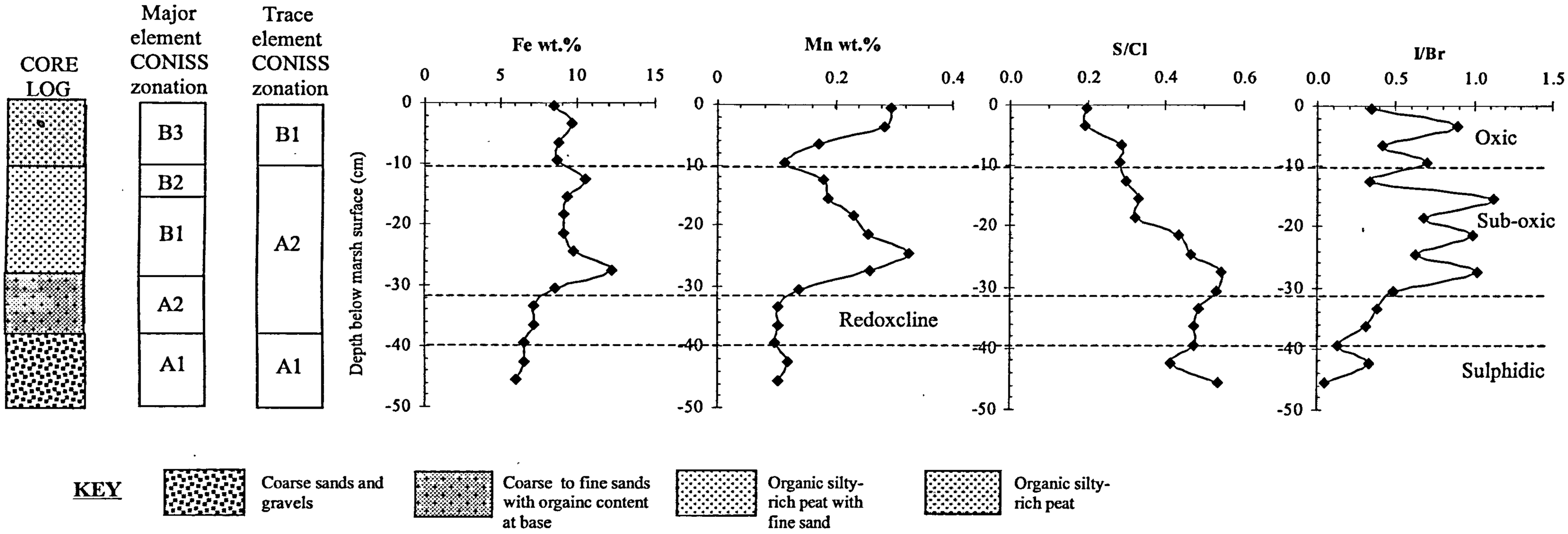

Figure 8.5: Summary diagram showing the CONISS least sum of squares major and trace element geochemical zonation within the marsh core from Loch Don. Also shown are the profiles of Fe and Mn (wt % abundance) and the down-core ratio plots of the redox-sensitve elements S/Cl and I/Br.

between 14-31 cm which clearly demonstrate the fluctuating precipitation of Iodate and a zone of sub-oxic to oxic conditions resulting from tidal exposure. As and V profiles are not so well defined although the small peak in both these elements at 22-23 cm depth indicates a sub-oxic environment. In the V/Al profile reducing conditions at depth are highlighted by the enrichment of V at 42-43 cm depth which corresponds to smaller peaks in reduced I and As within the lower more sulphidic section of the core (Figure 7.7).

The major element geochemical zonation is strongly influenced by the early diagenetic signature in this marsh. The boundary between the two distinct chemozones (LDon A and LDon B) clearly corresponds to the redox zonation resulting from the remobilization of Fe and Mn within the core (Figure 4.19). Similarly, the boundary obtained from the statistical analysis of the trace element data is also influenced by the diagenetic behaviour of I, As and V (Figures 4.22 & 7.7). Chemical sub-zones within the core correspond to the basal stratigraphy and the increased detrital input to the marsh in the near-surface layers, discussed in the next section.

8.4.3: Core geochronology (^{210}Pb and ^{137}Cs dating)

The $^{210}Pb_{excess}$ activity profile from Loch Don approximates an exponential decline in ^{210}Pb activity with increased depth (Figure 8.6). The decay with depth is only interrupted to a limited extent by a slight inflection between 11-12 cm depth suggesting deposition of material which has slightly increased the measured activity. The lack of significant inflections in this decay profile coupled with the compositional geochemistry data indicates that the sediments in this sequence are largely undisturbed and represent a constant record of the depositional history in this marsh (Cundy and Croudace, 1996). The redox zonation (discussed in the previous section) indicates that the entire $^{210}Pb_{excess}$ activity is present in the oxic and sub-oxic sediments. No obvious change to the shape of ^{210}Pb decay profile can be attributed to early diagenetic processes inferred from the comparison with down-core profiles of Fe, Mn, Sl/Cl and I/Br (Figure 8.5).

Marsh initiation is inferred from the various geochemical data to have commenced at 40-41 cm depth (Figure 8.4). This corresponds to a ^{210}Pb derived date of 1893 AD (± 5 years) which is well within the capability of the ^{210}Pb method. Over the circa 107 year period of marsh evolution the simple model reveals an average rate of sediment accretion of 3.4 mm yr^{-1}.

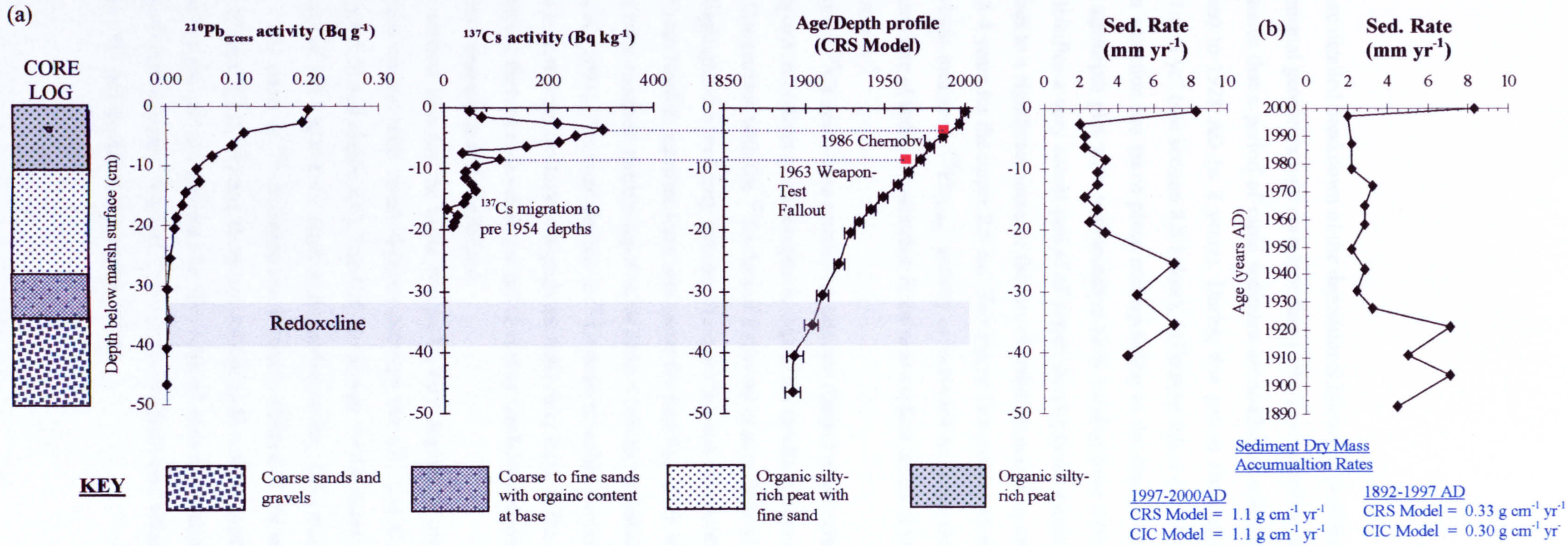

Figure 8.6: (a) Summary diagram showing the core log and radiometric activity profiles for ^{210}Pb and ^{137}Cs from the marsh core from Loch Don. Also shown are the Age/Depth model derived from the CRS model calculations and the profile of sedimentation rate versus depth. (b) Sedimentation rate versus CRS model calculated age (years AD). The inferred position of the redoxcline is also indicated.

A more detailed breakdown of the depositional history is possible using the CRS model derived incremental geochronology corresponding to the core sampling resolution. (Figure 8.6). This demonstrates that a period of rapid sediment accumulation occurred between circa. 1893 AD (± 5 years) to 1928 AD (± 2 years). During this period rates of accumulation fluctuate between 5-7.1 mm yr^{-1} (see section 8.8 below). Following this a *ca.* 70 year period of reduced more uniform accretion has taken place corresponding to the change in gradient at 20-21 cm depth on the age/depth plot with sedimentation rates varying from 2.0-3.3 mm yr^{-1}. The CRS model also identifies a very recent period of marsh development within the surface sediments that corresponds to a significant increase the rate of sediment accretion calculated at 8.3 mm yr^{-1} over the last 3-4 years for the upper 2.5 cm. This figure increases to 10 mm yr^{-1} if the sampling depth over which measured $^{210}Pb_{excess}$ activity is extended to cover the entire upper 3.0 cm. Hence the recent rate of sediment accretion in the near-surface layers of the core lies in the range of 8.3 – 10.0 mm yr^{-1}.

Measured ^{137}Cs down-core activity reveals two distinct peaks which are attributed to pre 1963 AD weapons test fallout and atmospheric deposition resulting from the Chernobyl accident (Figure 8.6). Comparison with the ^{137}Cs data of Callaway *et al.*, (1996b) from the north Norfolk marshes UK highlights the similarity between these profiles and those obtained from Loch Don.

The North Norfolk marshes were also under the pathway taken by the Chernobyl plume and will also have received marine input of Sellafield labeled material present in North Sea (Thompson *et al.*, 2001). The rapid decline in ^{137}Cs activity within the near-surface sediments of the Loch Don core reflects the lack of significant freshwater input to the upper estuary site with reduced catchment derived radio-caesium and declining discharges during the latter part of the twentieth century emanating from Sellafield.

^{210}Pb derived ages for the these two peaks vary depending upon the model used for geochronological control with some disparity between the CIC and CRS derived ages being apparent (Figure 5.10 and Figure 8.6). The CIC model age for the lower peak attributed to 1963 AD gives an age of 1964 AD (± < 1 year) with a corresponding CRS model derived age of 1972 (± < 1 year). The onset of ^{241}Am deposition is clearly defined at the same depth as the lower peak in ^{137}Cs (Figure 5.11). Plotting these two radionuclide activity profiles against cumulative dry mass removes any effects that may be the result of auto-compaction processes Hence the horizontal correlation between ^{137}Cs and ^{241}Am at this depth are real effects and it is not possible to assign a pre 1963 AD marker horizon using ^{241}Am.

Having identified the overall compositional stability of these sediments the reasons for this difference in calculated age are not fully understood but may be the result of either slight remobilization of ^{137}Cs (see below) or masking of the true peak owing to Sellafield derived inputs.

At depths below 14-15 cm, measured ^{137}Cs activity has been detected at depths which pre-date both Sellafield discharges and above-ground atmospheric weapons testing. The correlation between ^{137}Cs activity and K ($r^2 = 0.65$; $p = 0.63$, $n = 10$) indicates a significant association of Cs with the clay mineral fraction in these sediments (Comans *et al.*, 1989). Weaker positive correlations exist between the redox sensitive elements Mn and S ($r^2 = 0.05$ & 0.40) and with Cl ($r^2 = 0.41$). Although not statistically significant, these values suggest that partial remobilization of Cs has taken place, most probably within the sediment pore waters resulting in partial displacement of some ^{137}Cs to deeper and hence older sediment depths. Similar behaviour of ^{137}Cs and actinides has been documented elsewhere (e.g. Evans *et al.*, 1983; Davis *et al.*, 1984; Anderson *et al.*, 1987; Hunt and Kershaw, 1990; Short, 1995; Plater and Appleby, 2004). However, this does not appear to have been significant enough to compromise the position of the peaks in higher activity attributed to 1963 AD and the 1986 AD Chernobyl accident. Despite the obvious displacement of some Cs, comparison with the data of Callaway *et al.* (1996b) strongly suggests that the peaks in this core used for dating horizons are in fact reliable. Certainly the CRS model dates provide a robust chronology for the Chernobyl signature in the upper section of the core at this site. The lack of any horizontal correlation with the ^{241}Am profile lends further supports to this peak being associated with deposition derived from Chernobyl.

Sediment age plotted against cumulative dry mass (Figure 5.10) also highlights the discrete differences between the CIC and CRS models and the timescales obtained from the ^{137}Cs data. Further highlighted via the CRS model approach in this graph is the point at which the sedimentation rate changes and is reduced from an estimated 0.96 g cm yr^{-1} to 0.33 g cm yr^{-1}. This reduction in estimated sediment accumulation is inferred here to represent the transition from low to high marsh environments where sedimentation is intimately controlled by tidal flooding periodicity. This period of development corresponds well with the change in gradient on the age/depth profile (Figure 8.6). Also of importance are the slight differences in estimated sediment accumulation derived from the two ^{137}Cs dating horizons. Increased mass accumulation using the Chernobyl marker horizon compared to the value obtained from 1963 AD supports the

argument for the recent increase in marsh sedimentation. This is therefore a real effect and not merely an artifact of the ^{210}Pb model calculations.

8.4.4: Detrital and trace element distributions, fluxes and marsh evolution

Calculation of major and trace element fluxes to the marsh surface over time provide a useful mechanism for examining the accumulation of elements and their resultant distribution. This is particularly useful where radiometric dating methods reveal variation in the actual rates of vertical accretion over time (Cundy *et al.*, 2003).

Fluxes of both major and trace elements within the Loch Don marsh core are calculated using the CRS model derived ages and are shown in Figures 7.12a and Figure 7.12b. These profiles clearly show a period of fluctuating element fluxes between the period of initial marsh development circa 1893 AD which diminishes after circa 1921 AD. Although an early diagenetic influence is responsible for the major peaks in the Fe and Mn profiles (Figure 8.5), the flux calculations for the detrital major elements Ti and K also indicate enrichment over the same depth interval indicating that detrital inputs have also contributed to the peaks in Fe and Mn. All element flux profiles show a distinct decline in material above 20-21 cm depth. This corresponds to the reduction in sedimentation rates visible in the age/depth profiles at the same depth. The decline in flux does not recover within the period of depositional history extending from post 1921 AD to post 1987 AD. The interpretation here based upon geochemical flux calculations is that the marsh has undergone a transitional phase from low (immature) marsh with more rapid sedimentation rates to high (mature) marsh where all element fluxes are significantly reduced corresponding to lower rates of sediment accumulation.

Trace metal profiles indicate that the marshes here contain concentrations of heavy metals that reflect background crustal values (Figure 7.8; Table 7.2) apart from As which shows a slightly enriched distribution above 30 cm depth. Pb and As are strongly implicated in physical and chemical reactions with Cu, Ni, and Zn being more weakly associated with LOI values. Here the association between LOI and trace metals is most probably the result of a suite of mechanisms including physical adsorption, chelation reactions and cation exchange processes in the solid-phase (Bendell-Young and Harvey, 1992; Tessier *et al.*, 1996).

Trace metal distributions do not appear to be strongly influenced by the diagenetic recycling of Fe and Mn. The strong horizontal and linear correlation with Br indicates that bromination of metal species is a highly active geochemical process in the Loch Don marsh and exerts a major control on all metal profiles apart from Cr which is likely to be associated with other heavy mineral components.

8.5: Loch Creran (mainland Argyll)

8.5.1: Core sedimentology

In the core from Loch Creran the onset of increased LOI values at depth corresponds well with the visual stratigraphy indicating a transition from the underlying coarse sands and gravels to finer sediments consisting of silt and clay material with visible root fragments above 40-41 cm depth (Figure 8.7). Over the same depth interval a corresponding decrease in the abundance of Si is also mirrored in the profile of sediment dry bulk density. This lowermost section of the core indicates that fine material input/content is uniform within the basal stratigraphy (inferred from the Al and K profiles). The average organic carbon content of the Loch Creran core is lower than those recorded within the Isle of Mull cores within an overall value of 3.9 (% dry mass). This figure increases slightly to 5.1 (% dry mass) in the upper 40 cm. Comparison of the visual stratigraphy with the LOI profile indicates the transition from sand flat to marsh conditions above 40 cm depth. The middle section of the core between 40 and 16 cm depth is characterized by uniform dry bulk density and LOI values indicating general stable sedimentary conditions in terms of supply and source of organic and inorganic material. The only exception to this is the decline in both coarse and fine material evident at 20-21 cm depth inferred from the major element profiles shown in Figure 4.28 (summarized in Figure 8.8). This decline is not recorded by a corresponding inflection in the LOI or dry density profiles. However, at the same depth increment Fe abundance can be seen to increase significantly which strongly suggests the influence of diagenetic Fe precipitation (discussed in section 8.5.2 below).

Regression analysis of LOI with the major element compositional data reveals that organic matter is positively correlated with Mg, Ti and Ca indicative of a strong association with marine detrital input to this marsh (Figure 4.32). Organic material is also to a lesser degree

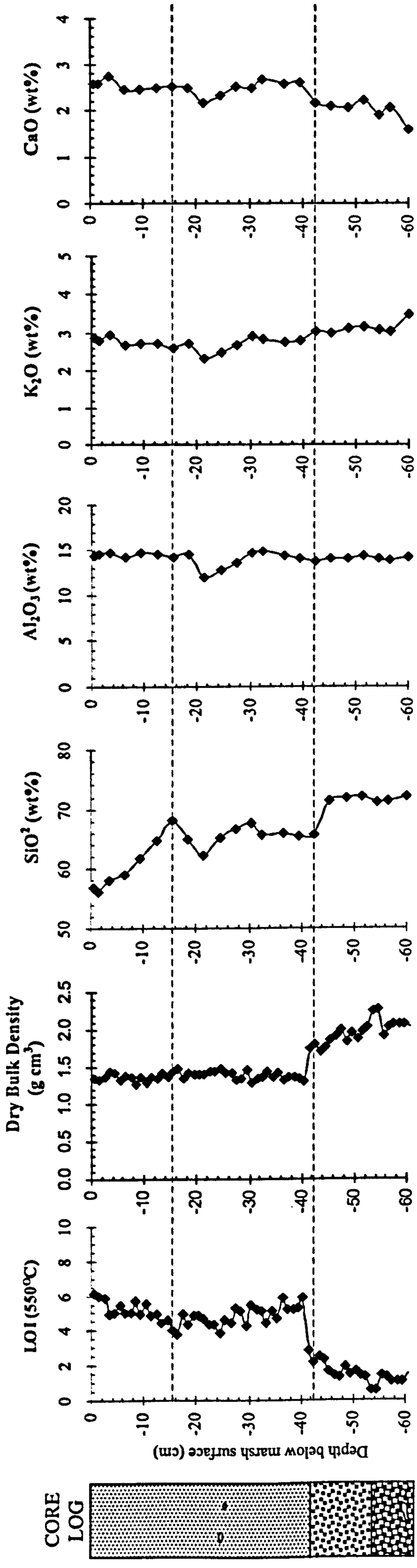

Figure 8.7: Summary diagram showing element oxide abundance (wt % according to x-r-f convention) and concentration-depth profiles for organic carbon (via LOI proxy method), SiO_2, Al_2O_3, K_2O and CaO from the Loch Creran marsh core.

positively correlated with the redox sensitive elements Fe, Mn, S and P (see section 8.5.2. below). A weaker association is inferred with marsh evapo-transpiration processes from the correlation with Na. Organic matter is not associated with either the coarse or fine fraction of the sediment matrix as inferred from the strongly negative correlation with K and Si. Similar regression analysis using Ti (as proxy for detrital material) reveals that Ti is strongly positively correlated with Mg, Ca, S, P and Na which are associated with the influence of sea-water and hence marine input. The association with Fe confirms that iron is partially transported to the marsh surface as a detrital component. Within the core from Loch Creran, Ti is negatively correlated with other indicators of detrital material including Si and K, showing that the coarse/fine sand component and fine clay material is not ultimately derived from marine inputs. It is therefore postulated that at this site ongoing erosion of established sand bars and beach material results in redistribution of these sediments onto the marsh surface which is not related to the elemental composition of seawater flooding the marsh.

CONISS analysis reveals a differing zonation derived from major and trace element geochemistry. Major element chemozones show two distinct zones (LCreA and LCreB Figure 4.30; summarized in Figure 8.8). LCreA can be sub-divided into three further zones. The lowermost zone is a product of the stratigraphic change at 40-41 cm depth from coarse sediment to finer more organic-rich marsh peat. Additionally, this zonation is also influenced by the redox controlled peaks in Fe and Mn which occur immediately above the same depth (discussed below). The boundary between chemozones LCreA2 and LCreA3 is principally a product of the large peak in Fe between 18 and 25 cm depth which is diagenetic in origin (see section 8.5.2). The upper chemozone (LCreB1) is defined by the statistical analysis owing to the greater abundance of Fe, Mn, P and S present in the near-surface sediments. CONISS analysis of the trace element concentration data again defines two distinct zones but the sub-divisions of these are broadly compatible with those from the major element data (Figure 4.33; summarized in Figure 8.8). For the trace element data the chemozones firstly reflect the obvious stratigraphical difference between the underlying coarse sediments and the compositional change into the marsh peat above 40-41 cm depth. The boundary between trace element derived chemozones LCreB1 and LCreB2 reflect the influence of peaks in the various redox sensitive elements (discussed in the following section). The uppermost zone is most certainly a product of enhanced sedimentation within the most recent near-surface layers and the influence of increased trace element detrital inputs to the upper marsh surface (see sections 8.5.3 and 8.5.4 below). This

includes significant enrichment of the metals including As, Co, Ni, Pb, U, Zn and the halide elements I, Br, S and Cl (Figure 4.33).

8.5.2: Redox geochemistry

Early diagenesis has resulted in the development of a distinct redox zonation in the core from Loch Creran (Figures 7.9 & 7.11). Similar to the sequence from Loch Don on Mull diagenetic enrichment of Fe and Mn occurs at the same depth increment for both elements between 39-45 cm. Over the same depth interval organic carbon also increases representing the transition into coastal peat sediments from the underlying coarse sands and gravel substrate. In this core the redox boundary inferred from Fe and Mn enrichment has developed at the base of the coastal peat and uppermost section of underlying medium to coarse sands. This may reflect the influence of soluble Fe and Mn transported in sediment pore waters into the basal coarse substrate under reducing conditions during tidal flooding.

A further peak indicative of significant Fe enrichment occurs at a shallower depth of between 18-25 cm with a corresponding minor peak in Mn. This upper peak does not correspond to significant enrichment of other mineralogenic elements suggesting that this is also the result of redox migration.

The down-core profile of S/Cl clearly shows significant enrichment of S relative to Cl below 48-49 cm (Figure 8.8). Conversely, the I/Br ratio displays a significant peak between 39-45 cm comparative to those of Fe and Mn indicating that the redoxcline is situated in the zone between these distinct enriched depth intervals. Further trace element ratio plots of As/Al, V/Al and Mo/Al all indicate that the redoxcline in this sediment prism lies immediately below these peaks (Figure 6.11)

The Loch Creran core is significantly darker in the basal section in comparison to the cores from Mull. This indicates that the underlying sands and gravels with very low organic content are somewhat more anoxic than the cores from sites on Mull. Above the redoxcline sub-oxic conditions are indicated by trace element ratio plots which show enrichment corresponding to the peaks in Fe and Mn at a depth of 18-25 cm. Fe, Mn, S, As and V all show significant enrichment in the near surface sediments (Figures 6.9 & 6.11). This results from the enhanced deposition of sulphide-rich minerals and the subsequent formation of authegenic ferric iron and

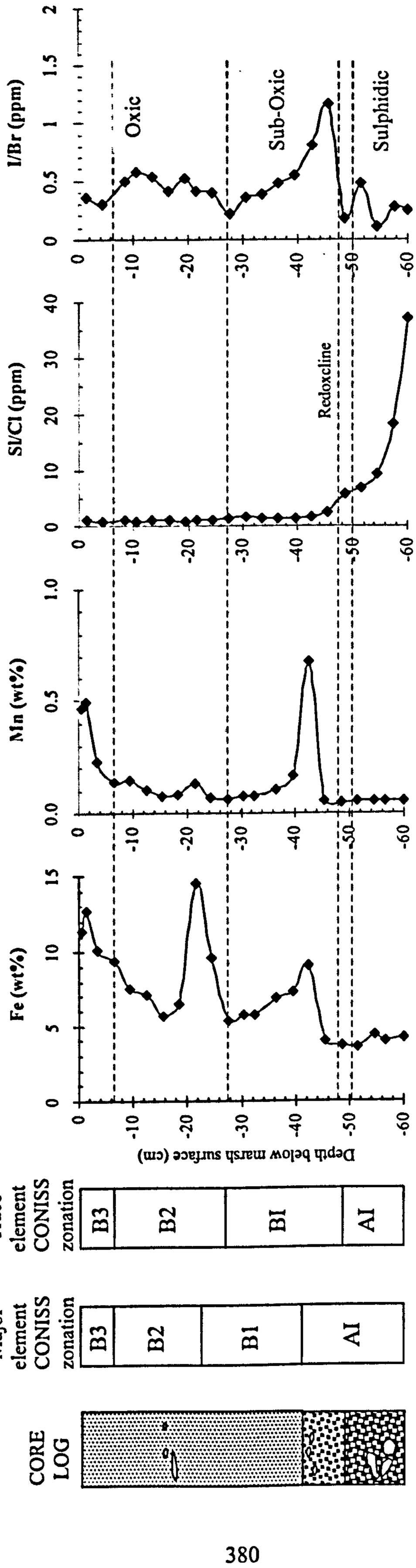

Figure 8.8: Summary diagram showing the CONISS least sum of squares major and trace element geochemical zonation within the marsh core from Loch Creran. Also shown are the profiles of Fe and Mn (wt % abundance) and the down-core ratio plots of the redox-sensitive elements S/Cl and I/Br (ppm).

Mn oxyhydroxides and the precipitation of migrating Fe^{2+} within the oxic/sub-oxic zones of the core.

8.5.3: Core geochronology (^{210}Pb and ^{137}Cs dating and ^{241}Am profiles)

The down-core $^{210}Pb_{excess}$ activity profile from Loch Creran approximates an exponential type decay curve with only a minor inflection indicative of either deposition or removal of material at a depth of 12-13 cm (Figure 8.9) The predominance of stable depositional conditions is re-enforced by the profiles of detrital elements such as Ti, Si, Al, and K and further indicates no significant changes in either the type or source of material supplied to the marsh surface over time.

Background levels of ^{210}Pb are reached at a depth of 30-31 cm with the inferred redoxcline and the transition to more anoxic conditions occurring over the depth interval 38-42 cm. Consequently, the entire inventory of measured $^{210}Pb_{excess}$ is contained within the oxic and sub-oxic sediments (Figure 8.9). No obvious changes in the $^{210}Pb_{excess}$ decay curve that coincide with peaks in the redox-sensitive element profiles of Fe or Mn (Figure 8.8), are evident providing an indication that little migration of ^{210}Pb has taken place linked to early diagenetic processes.

Simple model calculations reveal an average rate of sediment accretion of 3.7 mm yr^{-1} (2 standard deviation range = 3.2 - 4.5 mm yr^{-1}) for the whole sequence. Various geochemical data (major element profiles, LOI, and dry bulk density) show that the initiation of coastal marsh sediments has occurred at a depth of 40-41 cm (see above section). This is immediately above the coarser sands and gravels where LOI, dry bulk density and major element data fluctuate in accordance with the onset of finer organic sediments. Dating of this depth horizon yields an estimated age (1768 ± 8 years). This is far beyond the reliable scope of the ^{210}Pb methodology so the conclusion here is that coastal peat was forming at least before 1849 (± 5 years) which is the next youngest date estimation within the core. In sediments with an undisturbed depositional record such as exist in the Loch Creran core this may well be a reasonable estimate of the true age at this depth. It is therefore more appropriate in terms of marsh geochronology to assign a pre 1849 AD age for the initiation of coastal peat sediments within this core. The upper 25-26 cm contain the bulk of sediments that have accumulated over the last 95-99 years. The CRS model ages (Figure 8.9) reveal that the rate of sedimentation over this time period has fluctuated

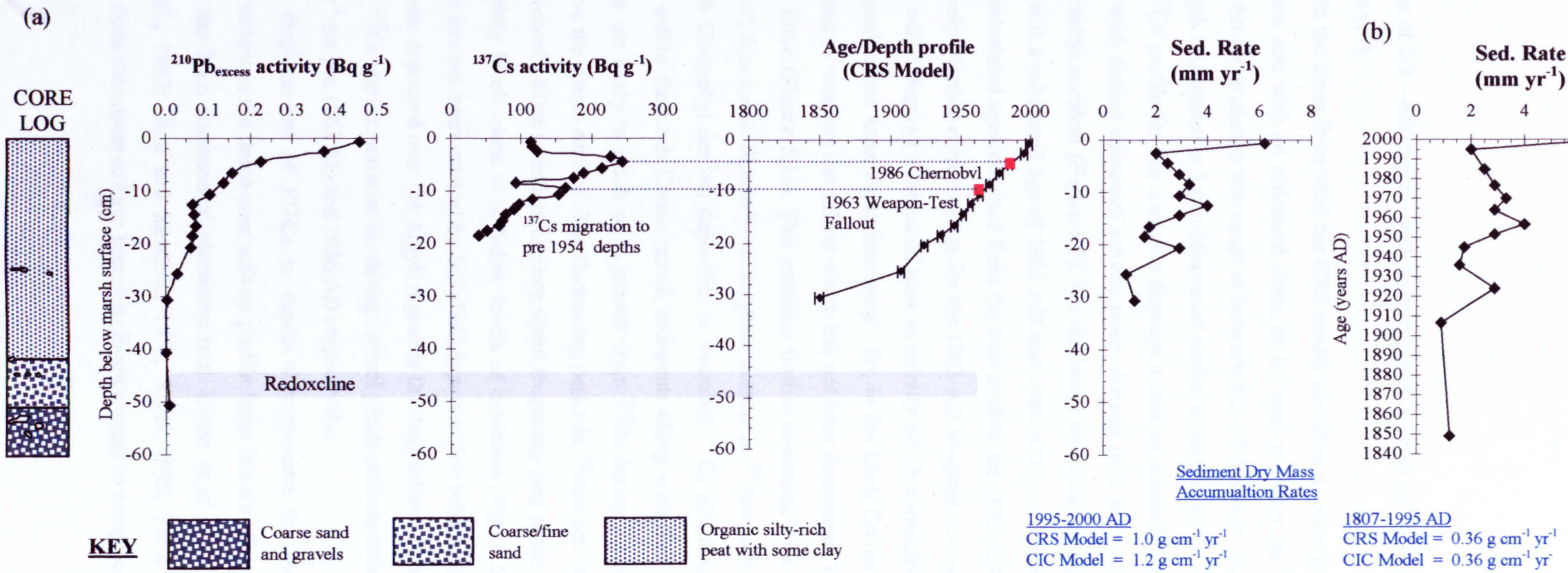

Figure 8.9: (a) Summary diagram showing the core log and radiometric activity profiles for ^{210}Pb and ^{137}Cs from the marsh core from Loch Scridain. Also shown are the Age/Depth model derived from the CRS model calculations and the profile of sedimentation rate versus depth. (b) Sedimentation rate versus CRS model calculated age (years AD).

between values of 0.9 – 4.0 mm yr^{-1} with an average of 3.3 mm yr^{-1} (2 standard deviation range = 2.7 - 4.3 mm yr^{-1}).

As with the cores from Mull the CRS model identifies a recent and significant increase in sedimentation rate with an estimated value of 6.2 mm yr^{-1} over the last four years marsh development. An accumulation rate range of between 6.2 – 7.5 mm yr^{-1} is obtained if the model calculation depth is extended to 3 mm (discussed further in section 8.10).

The ^{137}Cs profile for this core also displays a striking similarity to the data of Callaway *et al.* (1996b) with distinct measured activity peaks derived from pre 1963 weapons testing and the 1986 Chernobyl accident (Figure 8.9). For the lower weapons-test peak the ^{210}Pb CRS and CIC models yield a calculated age of 1964 AD and 1965 AD (± <1 year). For the Chernobyl signature the calculated ages obtained from the two models are 1985 AD and 1987 AD (± < 1 year) respectively. Further corroboration for the 1963 AD weapons test peak is provided by the ^{241}Am profile, which displays a measured peak in activity which correlates horizontally with the ^{137}Cs activity peak at the same depth increment. So, in the Loch Creran core there is a ^{241}Am signature relating to weapons test fallout which has not been determined in the other cores from Mull or Loch Etive (Figure 5.16). This provides further constraint with regard to the inferred ^{137}Cs peak in all four cores. Similarly, a complete decline in ^{241}Am activity corresponds to the depth at which Chernobyl derived deposition is recorded. ^{137}Cs discharges from Sellafield are also apparent within the Loch Creran marsh sediments along with fluctuating peaks in ^{241}Am activity. These are likely to result of in-growth from ^{241}Pu during transport to and following deposition upon the marsh surface. The fluctuating peaks in ^{241}Am activity do not appear to be related to the record of late twentieth century storm frequency (see section 8.8 below) and are a product of activty levels close to or below levels of detection (Figure 5.16). Importantly, the ^{137}Cs signature has not been masked by Sellafield inputs which reflects the high levels of ^{137}Cs activity that were deposited over the Argyll region in the days following the Chernobyl accident. Using the two ^{137}Cs marker horizons for dating control yields sedimentation rates of 2.7 mm yr^{-1} and 3.5 mm yr^{-1} for pre 1963 AD and 1986 AD respectively.

Some displacement of 137Cs to depths that pre-date the onset of anthropogenic discharges is evident in the down-core activity profile from this site. Similar behaviour of ^{137}Cs and actinides has been documented elsewhere (e.g. Evans *et al.*, 1983; Davis *et al.*, 1984; Anderson *et al.*, 1987; Hunt and Kershaw, 1990; Short, 1995; Plater and Appleby, 2004). However, this does not appear to have been significant enough to compromise the position of the

peaks in higher activity attributed to 1963 AD and the 1986 AD Chernobyl accident. Despite the obvious displacement of some Cs, comparison with the data of Callaway *et al.* (1996b) strongly suggests that the peaks in this core used for dating horizons are in fact reliable.

The graphical plot of cumulative sediment dry mass versus age (Figure 5.15) removes any possible effects on the true position of both ^{137}Cs dating horizons and the ^{210}Pb activity chronology that may derive from auto-compaction (Allen, 2000). In producing this plot actual sediment mass accumulation can also be assessed which corroborates the previous estimations of actual sediment (vertical) accretion derived from both the CIC and CRS ^{210}Pb models. Most importantly, the estimated dry mass accumulation derived from the ^{137}Cs dating clearly shows the increase in estimated sediment mass accumulation resulting from the two ^{137}Cs marker horizons (Figure 5.15). The 1963 AD peak yields a dry mass accumulation rate of 0.45 g cm yr^{-1} with an increased value of 0.53 g cm yr^{-1} obtained using the Chernobyl marker. This provides confidence that the recent increase in sedimentation rate recorded in the near-surface sediments measured by the ^{210}Pb CRS model calculations is in fact a real effect and not an artifact of the model.

8.5.4: Element fluxes and marsh evolution

The major peak in Fe and Mn corresponding to the redoxcline between 38-44 cm depth are not included in the flux profiles (Figure 7.19a). However, two distinct peaks are visible at shallower depths in the Fe and Mn flux plots at 20-24 cm and 10-15 cm. These correspond to peaks in both the Ti and K profiles demonstrating that the Fe and Mn peaks are in part due to detrial inputs.

Similar peaks are also observed in the trace metal flux profiles where the lowermost peak shown also corresponds to enrichment over the same depth interval in the I/Br, V/Al and Mo/Al distributions (Figure 7.19b). This enriched increment is therefore influenced in part by both detrital and diagenetic processes. The uppermost peak in the trace metal flux profiles is clearly not linked to early diagenetic reactions and demonstrates the influence on marsh development arising from increased sedimentation over the period 1945 AD to 1964 AD (CRS model derived dates). This also corresponds to an increase in the relative abundance of Si over the same depth interval which strongly suggests the influence of higher energy conditions. A similar period of enhanced sedimentation is not recorded at the other three sites over the same

calculated time-period. All detrital flux profiles highlight the recent influence of increased mineralogenic input within the surface sediment layers. Surface enrichment of Fe and Mn is due to the formation of authigenic Fe and Mn oxyhydroxides derived from the material being actively eroded from the frontal area of the marsh at this site (discussed further in section 8.10).

Trace metal concentration profiles show that Pb and As are strongly associated with organic carbon and are also influenced by the diagenetic cycling of Fe and Mn. A distinct zone of enrichment corresponds to the large peak in Mn between 38-48 cm depth inferred to represent the transition from sub-oxic to reduced conditions. The other metals (Cr, Cu, Ni and Zn) show little correlation with the redox-sensitive elements and a stronger association with organic carbon in these sediments. All metal profiles indicate that concentrations throughout the core are generally below the background levels found in the crustal material surrounding the Loch Creran catchment (Table 8.1). Correlation of the metal distributions within the core reveal that bromination of all trace metal species analysed is an active geochemical process taking place in the marsh at Loch Creran (Pellenbarg, 1984; Figure 7.21).

8.6: Loch Etive (mainland Argyll)

8.6.1: Core sedimentology

The core from the head of Loch Etive displays a distinctly different stratigraphy from the other three sites investigated (Figure 8.10). Both major and trace element geochemistry down-core profiles (Figures 4.40 and 4.33) highlight the significant difference in elemental composition of the black silty sand situated between 29 and 41 cm depth compared to the underlying and overlying sand sub-units. The major element profiles of Mg, Ca and Ti show depletion of these elements within this sub-unit corresponding to enrichment of S and P suggesting a terrestrial source for this deposit. The LOI profile (as a proxy for organic content) also shows that this unit is significantly enriched in organic matter adding further support for a terrestrial origin.

The enrichment of S within this sub-unit reflects the actual pre-depositional concentration and diagenetic chemical reactions involving organic carbon. Most trace elements including those indicative of detrital material (e.g. heavy metals and fine particulates) clearly

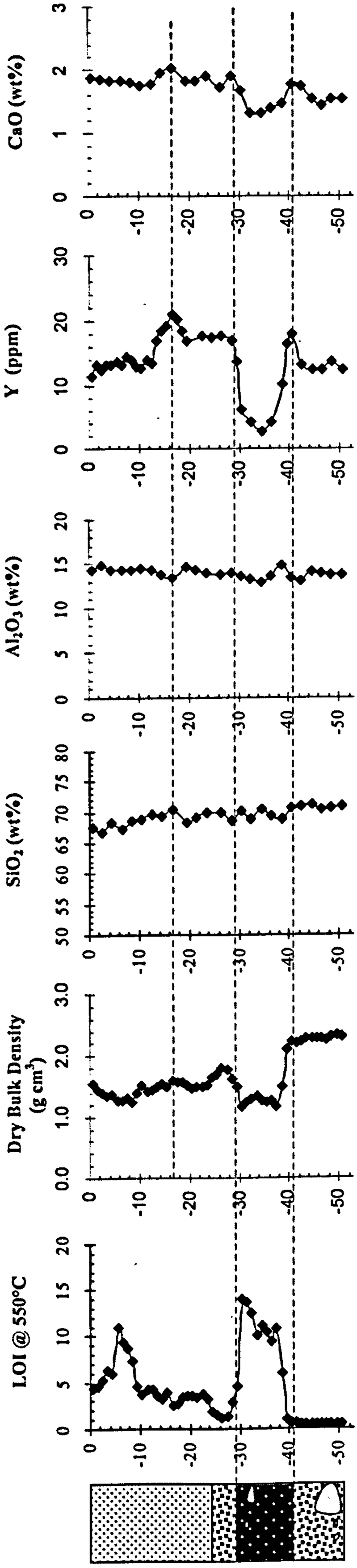

Figure 8.10: Summary diagram showing element oxide abundance (according to x-r-f convention) and concentration-depth profiles for organic carbon (via LOI proxy method), calcium carbonate SiO_2, Al_2O_3, Y and CaO from the Loch Etive marsh core.

indicate depleted concentrations within this deposit (Figure 4.33). Despite this other elemental profiles (e.g. Si, Al, K) indicate very little alteration to the element abundance/concentration throughout the sediment prism suggesting that the accumulated core sub-units have the same general provenance. The source of this material is likely to be derived from fluvial transport of weathered and eroded material from the Glen Etive catchment and the sandy pocket-type beach situated within the central area at the head of Loch Etive (Figure 4.36). This small morphological feature is developing from the active erosion of the material from which the Late Holocene shoreline identified by Gray (1974) and the underlying fluvial sands and gravels upon which this older peat deposit has formed.

LOI values are relatively depleted in the coarse-fine grained sand units below and above the silty black sand (Figure 8.10). These values decrease immediately above this layer. At a depth of 23-24 cm organic carbon content increases steadily upward through the core to reaching a maximum value of 11.0 % dry mass between 5-6 cm depth in the overlying uppermost sub-unit.

Isocon diagrams (Grant, 1986; Cundy *et al.*, 1997) successfully highlight the distinct geochemical compositional differences between the various sub units of this sequence (Figures 4.44a and 4.44b). These graphical plots (shown in Figures 4.44a & b) clearly show that the uppermost lithological unit is significantly enriched in all elements apart from SO_3 (also as Sulphur). Some elements plot on or very close to the line of equal concentration including Si which is the major component of the entire sediment sequence. This further supports the view that much detrital material is derived from catchment weathering and ongoing erosional activity around the head of the loch. The isocon plots also clearly demonstrate that the over and underlying sand units are chemically different to the black silty sand. However, the presence of organic lenses towards the base of the finer overlying sand indicates that the upper surface of the black silty sand unit may have experienced some erosion of material and incorporation of organic carbon into the basal section of this sub-unit.

Linear regression correlation between the measured LOI and the various major element components reveals that organic carbon is predominately associated with S, P and Na. This reflects the influence of increasing sulphate abundance in the near-surface sediments, vegetative conditions and evapo-transpiration processes occurring on the less frequently flooded mature marsh surface. Organic matter does not appear to be associated with the key redox-sensitive elements Fe and Mn. There is also very limited association between organic matter and trace

metal components. This leads to the conclusion that the increased concentration of metal species within the upper marsh peat is not significantly influenced by the rhizosphere and is not the product of complexation reactions with the organic coatings of Fe and Mn oxyhydroxides (Figure 7.23). There is no discernible association between organic material and the mineralogenic components of the marsh sediments inferred from the poor correlation obtained with Ti, Mg, Ca and Si down-core profiles (Figure 4.42). Correlation with Ti (as a proxy for mineralogenic input) reveals the close association with Ca and Mg which are major components of sea-water and here point to marine influence. Weaker associations are apparent with Fe and Mn which indicates that in part the distribution of Fe and Mn abundance is derived from detrital input as well as early diagenetic reactions.

CONISS analysis of the geochemical data identifies three distinct chemozones from major and trace element raw data (Figures 4.40 & 4.43; summarized in Figures 8.11 & 8.12). The uppermost zone (LEt C) is further subdivided into two sub-zones. The lowermost zones (LEt A and LEt B) for both major and trace elements strongly reflect the visual stratigraphy and are a product of the differing lithological units identified in this core. Chemozone LEt C1 represents the deposition of fine sand from 23-24 cm depth extending to the marsh surface and the transition from a sand flat environment into marsh peat. The near-surface chemozone (LEt C2) represents the increased deposition of Mn, Zn and in particular the halide elements I, Br, and Cl (see section 8.6.4 below).

8.6.2: Diatom analysis of the Loch Etive core

Diatom analysis of the Loch Etive core indicates that the black silty sand unit (corresponding to diatom zone LEt AD2) is predominately comprised of pennate oligohalobous taxa. These include *Eunotia fallax*, *Navicula radiosa*, *Pinnularia microstauron* and importantly the freshwater species *Tabellaria floculosa*. Significant breakage and fragmentation of many other large oligohalobous taxa has been observed within this deposit (identified from substantial fragments of *Nitszchia*, *Pinnularia* and *Synedra* species). Poor preservation of these taxa stongly suggests very rapid deposition of the black silty sand unit with large pennate taxa being subjected to extensive communition resulting in the severe level of breakage and fragmentation evident in the prepared slides (Figure 4.45; summarized in Figure 8.11).

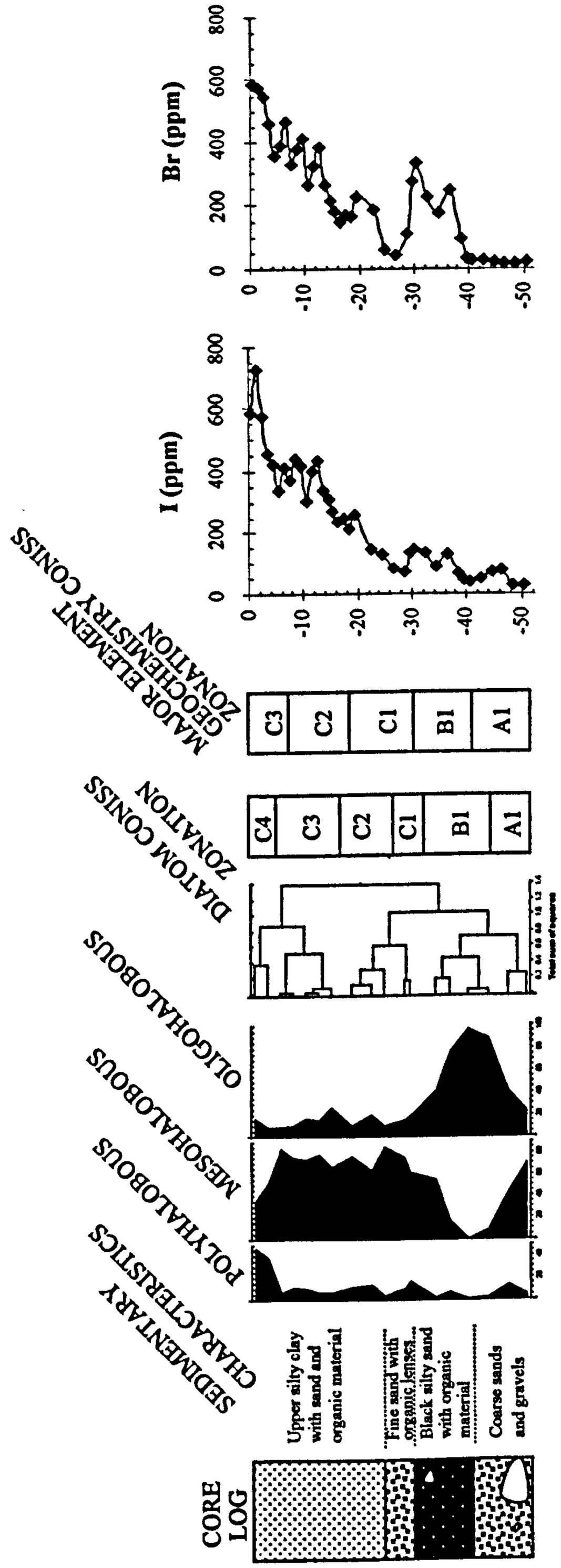

Figure 8.11: Summary diagram of Diatom analysis with CONISS zonation in relation to core stratigraphy, major element CONNIS zonation and down-core depth profiles of the seawater trace elements I and Br (ppm).

A key consideration in the study of coastal sedimentary environments employing diatom analysis is the extent to which the inter-tidal environment under investigation has been influenced by autochthonous and allochthonous diatom valves (Vos and de Wolf, 1988; 1993). In the case of the black silty/sand unit, the predominance of freshwater species including *Tabellaria flocculosa* and those of the *Cymbella, Eunotia, Navicula and Pinnularia* taxa certainly indicate that these are autochthonous on the basis of sedimentary/lithological structure as proposed by Vos and de Wolf (1993). However, these species are now incorporated into an inter-tidal sedimentary sequence therefore supporting the view that in terms of the evolution of the marsh stratigraphy these species are in fact allochthonous. The same logic can be applied to those marine/brackish epipsammic and epiphytic species (e.g. *Cocconeis scutellum*, *Navicula directa* and *Caloneis aemula*) that are incorporated into the black silty/sand. These represent the transition of autochthonous taxa to those of the allochthonous classification owing to their removal from the preferred ecological conditions of sandy inter-tidal settings.

Such conditions characterize the underlying coarse sands and gravels at the base of the core (diatom zone LEt AD1). However, this lower stratigraphical unit includes a complex signature of both mesohalobous species (e.g. *Acnanthes delicatula* and *Pinnularia lundii* var. *baltica*) with some marine/brackish epiphytes (e.g. *Cocconeis scutellum*, *Navicula directa*). Here these species are considered to be more representative of the autochthonous taxa. The presence of abundant oligohalobous species indicates the extent to which allochthonous taxa influence the inter-tidal sand-flat environment as a result of freshwater mixing at the head of this fjord.

At the base of the overlying finer sand (diatom zone LEt AD2) which grades into the upper coastal peat the decline in oligohalobous species is a function of elevational change relative to the tidal frame and the change in lithology. Allochthonous taxa persist due to continued supply of tidally-mixed brackish water, however, the bulk of autochthonous diatoms include many of the mesohalobous species relative to the abundance of polyhalobous and oligohalobous valves (Figure 4.45).

Within the upper coastal peat mesohalobous taxa predominate up through the core to the near-surface layers (Diatom zones C1–C3). These represent the bulk of the autochthonous species consisting of marine and brackish water epipsammic and epiphytic valves in the silty/sandy and relatively clay deficient marsh sediment. The upper surface (Diatom zone C4) represents the influx of allochthonous species of marine/brackish taxa relative to mesohalobous

valves derived from increased erosion of the lower inter-tidal environment. Comparison with the I and Br down-core geochemical profiles supports the relative species abundance change with more marine/brackish species corresponding to enrichment of these sea-water elements in recent years (Cundy *et al.*, 2002).

Within this marsh setting the epipsammic and epiphytic species fall into the tychoplanktonic classification of Vos and de Wolf (1993) being found in the both the sand/flat and upper coastal peat as a function of the generally silty/coarse substrate of these sediments. These species help to interpret the more complex depositional history of the Loch Etive marsh being a sedimentary sequence describing overall marine transgression through time. The presence of marine (allochthonous) valves in the near-surface layers supports the general interpretaion from the study area of recent marine transgression relating to RSL rise in western Scotland (see below).

8.6.3: Redox geochemistry

The more variable stratigraphy recorded in the core from Loch Etive has exerted a pronounced effect upon redox-zonation and the signature of early diagenetic reactions (Figure 6.13) The use of geochemical data and diatom analysis have illustrated that this core contains a more complex depositional history than has been recorded in cores from the other three sites.

Down-core profiles of Fe and Mn both display relative depletion in the black silty sand unit, however, the distribution of these elements shows no real discernable evidence of peaks in element abundance relating to early diagenetic enrichment within the coastal peat. Ratio plots of redox-sensitive trace elements further reveals a more complex diagenetic signature. The down-core profile of S/Cl shows a distinct zone of enrichment which corresponds to the black silty sand unit identified as being terrestrial in origin (section 8.63 above; Figure 8.12). The additional small peak in As/Al over the same depth interval indicates that enrichment within this stratigraphical unit is a product of actual element concentration rather than early diagenetic processes (Figure 6.16). The I/Br ratio shows two distinct peaks at depths below 40-41cm and immediately above 28-29 cm (Figure 8.12). Certainly the uppermost peak may reflect the base of the sub-oxic zone and with smaller peaks in As/Al and V/Al strongly supporting this argument (Figure 6.16). However, the basal peaks in I/Br and V/Al are not considered to be caused by

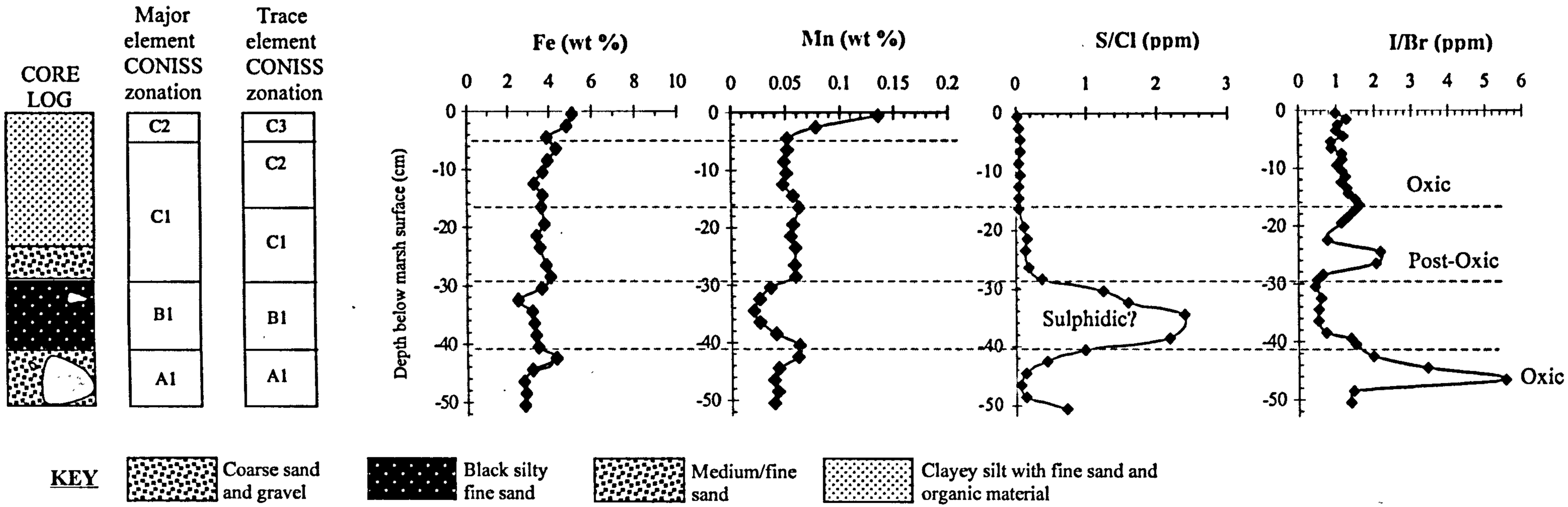

Figure 8.12: Summary diagram showing the CONISS least sum of squares major and trace element geochemical zonation within the marsh core from Loch Etive. Also shown are the profiles of Fe and Mn (wt % abundance) and the down-core ratio plots of the redox-sensitve elements S/Cl and I/Br (ppm).

reduction of I and V owing to the complete exposure of sediments at this depth to oxidizing conditions for lengthy periods. Additionally, the generally coarse nature of the sediments underlying the true extent of coastal peat will have enhanced the removal of I and V to deeper depths where concentration in the solid-phase has then taken place.

Sampling was undertaken over the spring tidal cycle and field observations clearly revealed that the surface was regularly flooded over this period. Further observations also revealed that during highest neap tides the marsh surface was also exposed. It therefore becomes clear this core sequence is exposed to oxidizing conditions for much of the diurnal tidal cycle. Temporary reducing conditions in the upper sediment layers are only experienced for a limited few days over the spring tidal period. The combination of the variable stratigraphy and predominant exposure to oxic conditions would seem to have resulted in an inverted redox-zone which can sometimes become apparent in marsh sediments containing organic-rich buried peat layers (A.B.Cundy pers. comm.). This geochemical phenomena provides a suitable explanation for the apparent redox zonation within this core.

8.6.4: Core geochronology (^{210}Pb and ^{137}Cs dating)

Measured $^{210}Pb_{excess}$ activity in the Loch Etive core closely approximates the theoretical decline in activity with increased depth (Wise, 1980; Appleby and Oldfield,1992; Appleby, 2002) despite the obvious visual and measured geochemical differences between the differing stratigraphical units (Figure 4.37 & Figure 8.13). Redox conditions within the core are also notably different (see previous section) with oxic and sub-oxic conditions predominating throughout the core profile. All the $^{210}Pb_{excess}$ activity above background levels used for dating is therefore concentrated within the oxic and sub-oxic sediments. The development of a distinct zone of reduced conditions in this sequence is highly problematic with no distinct peaks at depth indicative of metal sulphide formation and reduced conditions within the upper marsh sediments. Significant increased S content is however apparent in the black silty sand unit identified as a terrestrial (freshwater) deposit. Hence it is difficult to ascertain whether this peak is in fact the product of either diagentic post-depositional reactions or an artifact of deposition of S and organic-rich material from terrestrial sources. The latter scenario here may be the most probable explanation owing to a lack of S and anoxic conditions within the underlying coarse sand unit.

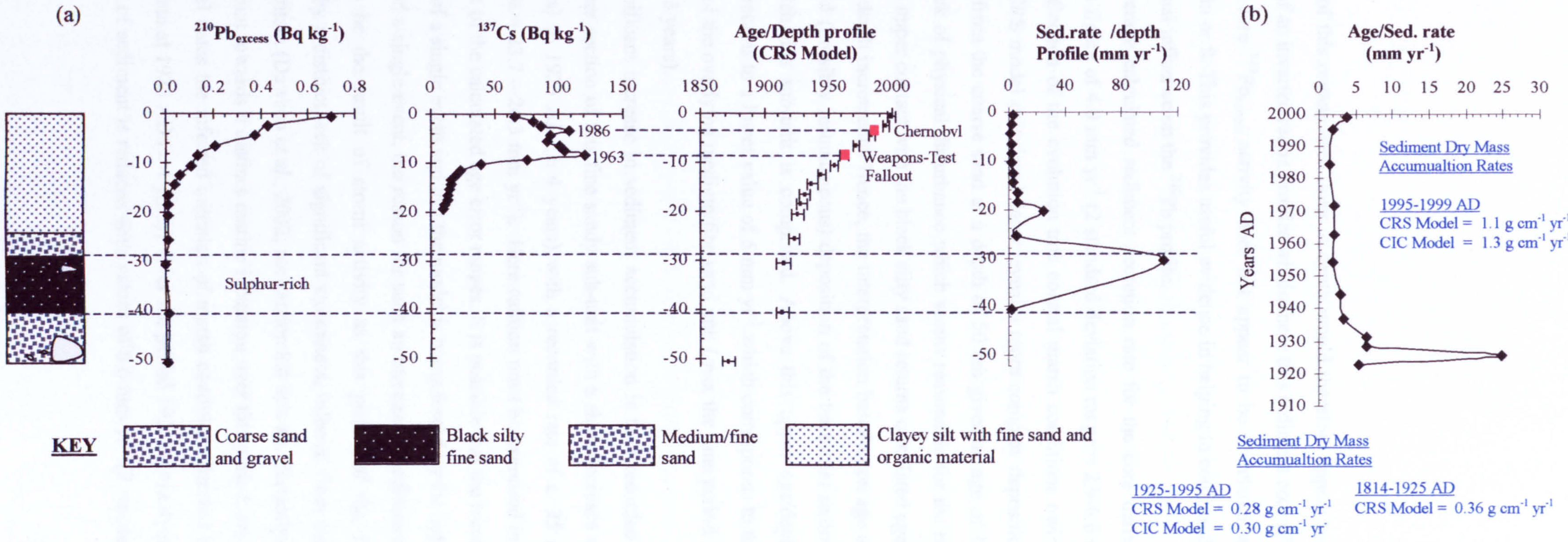

Figure 8.13: (a) Summary diagram showing the core log and radiometric dating profiles from $^{210}Pb_{excess}$ and ^{137}Cs activity for the Loch Etive marsh core. Also shown are the age/depth model profile obtained from the CRS model calculations and the profile of sedimentation rate versus depth. (b) Sedimentation rate versus calculated age.

The presence of this organic-rich layer at depth would therefore appear to have influenced the development of an inverted redox profiles within these this sediment core (Figure 8.12).

Down-core $^{210}Pb_{excess}$ activity does not appear to be correlated with minor diagentic peaks in Fe, Mn or S. This provides useful evidence in helping to confirm the lack of diagenetic post-depositional influence on the ^{210}Pb profile.

An average calculated sediment accretion rate for the core derived from the simple model yields a figure of 4.0 mm yr^{-1} (2 standard deviation range = 2.9-6.6 mm yr^{-1}). This is not an accurate reflection of the evolution true coastal marsh conditions owing to the differential stratigraphy. CRS model calculated dates reveal a more complex depositional history. A basal date obtained from the coarse sand at a depth of 50 cm gives an age of 1872 AD (± 6 years) assuming a lack of physical disturbance which seems reasonable for the base of the sequence. The lower and upper contact with the black silty sand returns calculated ages of 1914 AD (± 4-5 years) at both depth increments. Hence, the interpretation based upon age and depth of material is of very rapid (possibly instantaneous) deposition of the terrestrial sedimentary layer (11 cm depth) of which this sub-unit is comprised. Above this upper age/depth interval sediment accumulation returns to a lower value of 5 mm yr^{-1} which corresponds to the lower section (25-30 cm depth) of the overlying medium/fine sand unit (over the time period 1914 AD (± 4 years) – 1923 AD (± 3 years).

A significant increase in sediment accumulation is then recorded by the ^{210}Pb model within the upper section of this fine sandy sub-unit with a sharp increase over the period 1923 AD (± 3 years) to 1925 AD (± 4 years) with a recorded rate of c. 25 mm yr^{-1} (2 standard deviation range = 23.7 – 26.3 mm yr^{-1}). Here caution must be exercised in the interpretation of ages as a result of the calculated age error ranges. It is possible that the increase in sedimentation is the product of a single event and that the model is being forced by the apparent age difference. If this is indeed a single event, the reason for such an increase in sedimentation is unclear. This is unlikely to be the result of storm activity as this period of the Twentieth century is characterized by a distinct lack of significant storminess, inferred from the gale day frequency for northern Britain (Dawson *et al.*, 2002; see section 8.8 below). Certainly the geochemical and diatom data point towards a distinct marine incursion over this period. At a depth of 20-21 cm the CRS model dates the inferred initiation of marsh conditions derived from the multi-proxy geochemical data at 1925 AD (± 4 years). Over the period 1925 AD (± 4years) to 1931 AD (± 3 years) the rate of sediment is reduced with values of 6.6 mm yr^{-1} (2 standard deviation range =

6.3-6.9 mm yr^{-1}). This corresponds to a depth interval between 20-21 cm and 16-17 cm where the visual stratigraphy, LOI, dry density profiles and diatom data indicate the development of low marsh sediments.

Sediment accumulation over the next *circa* 70 year period to 1995 AD (± < 1 year) is estimated by the CRS calculations to fluctuate between 1.5 mm yr^{-1} to 3.3 mm yr^{-1}. As with the other three cores investigated in this study a very recent and significant increase in sedimentation rate estimated at between 6.2-7.5 mm yr^{-1} has been recorded over the last circa 4 years (see further discussion below).

Measured ^{137}Cs activity reveals two distinct peaks at depths corresponding to pre 1963 AD weapons testing and the Chernobyl accident in this core. Here the CRS model calculations provide robust corroboration that these peaks can be attributed to these know marker horizons with ages of 1963 AD (± 2 years) and 1985 AD (± < 1 year) for the base of the upper activity peak. These dated horizons help to constrain further the inferred activity peaks evident in the other cores from the Argyll region. These marker horizons yield sedimentation rates of 2.4 mm yr^{-1} and 2.9 mm yr^{-1} for the lowermost and upper peaks respectively. These values are in good overall agreement with the estimated rates of accretion derived from ^{210}Pb dating of the upper marsh section of the core. CIC model ages are less reliable and this is demonstrated in the graphical plots of cumulative dry mass versus age for the different models employed. Far better agreement is attained between the CRS model accumulated mass and the ^{137}Cs dating horizons (Figure 5.20 & Figure 8.14). Discrepancy between the CIC model accumulated mass may be due to the lack of ^{210}Pb material entering the marsh depositional system which, if the case, provides increased confidence in the predominance of atmospherically derived $^{210}Pb_{excess}$ for much of the marsh depositional history.

Importantly, in similarity to the upper near-surface sediments of the other cores studied from the Argyll region, a distinct difference in accumulated sediment dry mass is revealed by the ^{137}Cs dating activity marker horizons. Calculated dry mass accumulation here yields a value of 0.34 g cm yr^{-1} for the lower 1963 AD peak and an increased figure of 0.45 g cm yr^{-1} for the 1986 Chernobyl peak. This provides clear evidence that the Chernobyl dating marker is identifying the increased recent sedimentation now taking place on the marsh surface and that the ^{210}Pb estimations are real effects and not merely an artifact of the ^{210}Pb calculation method.

In direct contrast to the other sites, no ^{241}Am has been detected in the marsh sediments from Loch Etive. This is due to activity levels within these sediments being below levels of

detection via gamma spectrometry. Some displacement of ^{137}Cs is evident in the down-core activity profile from this marsh. Similar behaviour of ^{137}Cs has been documented elsewhere (e.g. Evans *et al.*, 1983; Davis *et al.*, 1984; Anderson *et al.*, 1987; Hunt and Kershaw, 1990; Short, 1995; Plater and Appleby, 2004). However, this does not appear to have been significant enough to compromise the position of the peaks in higher activity attributed to 1963 AD and the 1986 AD Chernobyl accident. Despite the obvious displacement of some Cs, comparison with the data of Callaway *et al.* (1996b) strongly suggests that the peaks in this core used for dating horizons are in fact reliable.

8.6.5: Element fluxes and marsh evolution

The more complex stratigraphy of the Loch Etive core coupled with the differential rates of accretion resulting from the distinct stratigraphical variation renders comparison with the other three cores somewhat problematic if the entire core depth is considered. With this particular core more meaningful comparison with regard to marsh sedimentation processes is possible from in-depth analysis of the upper section above the black silty terrestrial unit i.e. the true extent of coastal peat development.

Major and trace element flux calculations provide a more comprehensive overview of the depositional history when rates of sediment accretion have varied over time (Cundy *et al.*, 2003). Down-core profiles of calculated major and trace metal fluxes for the uppermost 30 cm of the core are shown in Figures 7.27a and Figure 7.27b. Major element flux profiles reveal a distinct zone of enrichment for all elements between 15-20 cm. This is only accompanied by a very slight peak in the Mn profile with no evidence of a concomitant zone of enrichment for that of Fe. The fact that the detrital elements Ti and K also show a distinct peak at the same depth provides clear evidence of the influence of mineralogenic input and indicates that the peaks in Fe and Mn are not soley due to diagenetic processes. Further evidence of increased deposition is recorded in the trace element flux profiles (Figure 7.27b), which display a similar large increase in deposition over the time-period circa 1927 AD – 1933 AD (CRS model derived ages). The influence of storm activity here cannot be discounted (see section 8.8 below). However, reference to the major element down-core profiles shows that, over this depth interval, Si abundance only increases slightly relative to Al and K. On the other hand Ti, Ca, P and Na values all increase which points to an increase in marine derived sedimentation and the influence

of marsh vegetation. Therefore, this period of rapid sediment accumulation is likely to represent the early development of coastal peat and colonization of the inter-tidal fine sand substrate by vegetation (e.g. *Puccinellia maritima*) and the formation of low saltmarsh conditions. This may also provide further evidence of the capability of *Puccinellia maritima* as a species which promotes rapid sedimentation and marsh development via the trapping of both coarse and fine material (Langlois *et al.*, 2003). The effect of this can be seen in the profiles of Y (Figure 8.10) and profiles of V and Nb (indicative of fine material) and Ce, La and Zr indicative of coarser-grained (heavier) clastic input (Figures 4.40 & Figure 4.43). This adequately explains the visible presence of lenses of fine to medium sand also present within the depth interval with which these elements are intimately associated. Element fluxes are quite uniform over the period 1944 AD – 1995 AD after which the flux calculations provide clear evidence of the rapid increase in sedimentation rate in the near-surface sediments (Figures 7.27a & 7.27b).

Trace metal concentrations vary considerably within the Loch Etive core. Pb and As are relatively enriched within the black silty sand unit whilst Cr, Ni and Zn are significantly depleted. All metal concentrations are enriched within the marsh soil relative to this underlying unit however these values are all well below natural background values recorded from the surrounding catchment geology (Table 7.2). This indicates that the marshes here are not acting as significant sinks for material derived from natural weathering or marine detrital inputs. The only exception to this is the increased concentration of Mn resulting from ongoing marine erosion of the seaward edge of the marsh and formation of authigenic Mn oxyhydroxides in the near-surface sediments.

Correlation with the distribution of Zn indicates that adsorption to Mn oxyhydoxides coatings is taking place which has not been seen in the other cores studied. The other trace metals are not influenced by the diagenetic recycling of Mn in the marsh sediments if this core.

Pb and As are less strongly associated with organic matter and there appears to be little association between LOI and the other trace metals Cr, Ni and Zn. A very similar situation exists with regard to the behaviour of the halide elements I and Br. Neither of these trace elements seems to be influenced by physical or chemical association with organic matter although some weak scavenging of I by Fe oxyhydroxides has occurred. Bromination of Pb and As appears to be an active geochemical process but this is not influencing the distribution of Cr, Ni or Zn in the Loch Etive core. Adsorption of metals by the fine fraction appears to be the dominant process governing the distribution of these elements in the Loch Etive marshes. Therefore, the

fact that these sediments do not appear to be acting as a significant sink for metal species given the poor association with other sediment constituents reflects the low clay content of these marshes.

8.7: Site interpretations

Radiometric dating of marsh sediment sequences from the Argyll region coupled with detailed solid-phase geochemical analyses has revealed distinct differences regarding the evolution of the most recent phase of saltmarsh development at selected sites. The radionuclide (^{210}Pb and ^{137}Cs) activity-decay curves coupled with solid phase major and trace element distributions show that physical disturbance has been minimal. Therefore, these sites are considered to represent robust sites with respect to the study of marsh sedimentation processes and relationship with historical and present-day sea-level movements. The strong correlation with indicators of the fine sediment fraction show that both radionuclides are significantly adsorbed to the clay mineral fraction and fine particulate material. Furthermore the generally oxic nature of the marsh sediments results in a lack of significant association with redox-sensitive major and trace elements and indicates that remobilzation owing to reduced conditions has been minimal. In the case of ^{137}Cs some remobilization has occurred but this has not been significant enough to compromise the overall depositional record within the cores.

The marsh at Loch Scridain on the western side of Mull is older than the other three sites. Marsh sedimentary conditions characterized by the various geochemical analyses have initially developed at a date beyond the most reliable extent to which the ^{210}Pb method can be extended back in historical time. Solid-phase geochemical data clearly shows that the marsh sediments have not experienced significant erosional or depositional events that compromise the depositional record of $^{210}Pb_{excess}$. Despite the geographical location and orientation of Loch Scidain the influence of major storms upon the sedimentary history appears to be minimal (see section 8.8 below). This results entirely from the protection afforded by the surrounding mountainous topographic and constricted entrance to the inter-tidal marsh area due to the volcanic dyke intrusions that make up the Aird of Kinloch (Figure 4.4). This has formed a protective wall-like structure laterally traversing the head of Loch Scridain, delineating it from the inner area of Loch Beg and has provided a significant natural defence from storm activity.

Measured rates of sediment accretion indicate that the marsh has been accreting at between 0.9-1.3 mm yr^{-1} for most of the period for which ^{210}Pb is reliable as a dating tool (i.e. the past 120-150 years). This model estimation is in very good agreement with the estimations of twentieth century sea-level rise (1.0 ± 0.15 mm yr^{-1}) as proposed by Shennan and Woodworth (1992). This figure also compares favourably with the more recent estimations of Nakada and Inoue (in press) who derive an estimated figure of ca. 1.5 mm yr^{-1} for twentieth century global sea-level rise (GSLR) from five stations around the Baltic sea and sites from Brest and San Francisco. As such, the high marsh environment at the head of Loch Scridain would appear to have attained the type of asymptotic relationship with twentieth century sea-level rise as proposed by the empirical work of Pethick (1981) for the marshes of North Norfolk, UK.

This apparent steady-state is likely to be severely compromised by the recent increase in sediment accretion now taking place on the marsh surface which is more than five times the estimated rate over the past century since ca. 1995 AD (see section 8.9 below).

The marsh at Loch Don is extremely well protected from the influence of storm induced wave activity by nature of its topographical setting and orientation (Figure 4.13). It is difficult to envisage how storm activity could seriously affect marsh sedimentation processes at any time at this site other than by contributing to extreme high water or increasing tidal surge energy in conjunction with periods of low atmospheric pressure.

^{210}Pb dating suggests that marsh inception here has taken place at some point prior to 1893 AD (± 5 years). Marsh accretion has proceeded with more rapid rates (average rate of 5.9 mm yr^{-1}) characteristic of the low marsh environment inferred from the age/depth curve (Figure 8.9) between 1893 AD (± 5 years) and 1928 AD (± 2 years). This figure corresponds with a period of enhanced sediment accretion recorded in the Loch Etive core over a similar age/depth interval and in all probability represents the morphodynamic response to colonizing vegetation in a developing low marsh coupled with the influence of short-term marine incursion (French, 1993).

The apparent decline in sedimentation rate after 1928 AD (Figure 8.6) is interpreted as the transition from low to high (mature) marsh conditions with a reduced average to 1997 AD of 2.6 mm yr^{-1}. This figure is significantly higher than the estimated rate of twentieth century sea-level rise of 1.0 (± 0.15 mm yr^{-1}, Shennan and Woodworth, 1992; and 1.5 mm yr^{-1}, Nakada and Inoue, in press) and is in better agreement with the earlier estimation provided by Peltier and Tushingham (1989) of 2.4 ± 0.9 mm yr^{-1}. Very recent rates of sediment accumulation have

increased dramatically at this site with current rates estimated from the ^{210}Pb model to be now in excess of 8 mm yr^{-1} with an estimated maximum of 10 mm yr^{-1} (see section 8.9 below). This estimated increase is supported by the ^{137}Cs results.

In the core from Loch Creran marsh inception estimated from sediment age and geochemical analysis commenced at a time that pre-dates the capability of the ^{210}Pb model with an age sometime prior to 1849 AD at a depth above 40 cm (Figure 8.9). The age/depth curve here identifies an inflection indicating an apparent increase in sediment accretion corresponding to 1907 AD at a depth of 25-26 cm. The reason for an increased rate of accumulation in the section of the modeled profile that relates to the mature marsh is not clear. A possible explanation may be due to the height of the underlying coarse substrate relative to the tidal frame which has affected the rate of sedimentation during the development of low (immature marsh) at the coring location. Alternatively, pre-existent elevation of underlying substrate relative to the tidal frame may have promoted the later development of mature marsh conditions.

From the period 1907 AD (± 2 years) to 1995 (± < 1 year) the average rate of marsh accretion was 2.6 mm yr^{-1}. This figure is in very close agreement with rates over a similar time period recorded in the Loch Don core, being in closer agreement with the global sea-level rise estimations of Peltier and Tushingham (1989). Very recent sedimentation on the marsh surface at Loch Creran has significantly increased above the rates of estimated 20th century sea-level rise (Shennan and Woodworth, 1992; Nakada and Inoue, in press).

The sedimentary evolution of the Loch Etive core has been altogether more complex over the historical time-period. The basal coarse-grained sand represents an estuarine sand/flat environment inferred from geochemical evidence and the recorded presence of predominately benthic marine/brackish epipsammic diatom taxa. The overlying black silty sand then represents the rapid deposition of a terrestrial deposit of differing source from the underlying and overlying units. This interpretation is inferred from the distinct geochemical composition (major and trace element data), the predominance of freshwater diatom taxa and the geochronology from samples at the base and top of the unit. Field observation at low tide revealed that this unit is quite extensive within the surrounding marsh and forms a distinct sedimentary deposit unlikely to have originated from direct human activity. The interpretation therefore is that this material has originated as either a landslide or a sudden flash flood deposit resulting in rapid (instantaneous) deposition over a substantial area of sand/flat environment prior to any development of coastal

peat. The exact cause of this movement of material is unknown but may be linked to deforestation activity prior to the planting of the nearby lower slopes within Glen Etive.

Fine to medium sand has continued to be deposited post 1914 AD (± 4 years) with colonization by vegetation (*Puccinellia maritima*) initiating the development of marsh sediments by ca. 1923 AD (± 3 years). A very rapid period of marsh development then ensues with sedimentation rates ranging from 5.0 mm yr^{-1} to as much as 25 mm yr^{-1} up to ca. 1931 AD (± 3 years). The very high rate within this time-period is not recorded in the other cores studied. This may therefore be related to the influence of storm activity however, a coarsening of material is not recorded by the geochemistry and in particular the dry-bulk density over this time-period. Diatom analysis does indicate the predominance of marine/brackish taxa lending support for the influence of marine incursion over the interpreted low marsh environment (see section 8.6.4).

From 1931 AD (± 3 years) sedimentation rates decline to an average value of 2.3 mm yr^{-1} for the ca. 64 year period interpreted here as a significant period of high (mature marsh) conditions. This rate is still significantly above the estimations of 20th century relative sea-level rise provided by Shennan and Woodworth (1992) and Nakada and Inoue (in press) but does correspond well with the earlier estimations of Peltier and Tushingham (1989).

^{210}Pb dating model estimations also reveal that the very recent rates of sediment accumulation over the last ca. 5 years or so have accelerated with a rate of between 6.2-7.5 mm yr^{-1} recorded in the near-surface sediments. This corresponds well with the age/depth interval in the other three cores across the study transect where a similar acceleration has also been recorded and is well in excess of the 20th century global sea-level rise estimations of Shennan and Woodworth (1989) and Nakada and Inoue (in press).

In all cores the historical rates of marsh accretion show distinct inflections in the age/depth curves. These may highlight a transition from low marsh with more rapidly accumulating sedimentary environments to mature (high marsh) settings with reduced sedimentation rates. Hence, the evolution of these marshes may therefore conform to the empirical work of Pethick (1981) with a declining rate of sediment accumulation as a function of increasing marsh elevation relative to the tidal frame (Allen, 1997).

The Argyll marshes all exhibit characteristic transgressive morphological behaviour as a direct response to rising sea-level throughout most of the 20th century. Temporary increases in sedimentation rates identified by the CRS model dating may reflect inter-decadal variation in the rate of sea-level rise (French, 1993). Unfortunately, owing to the lack of longer-term tide-gauge

data direct comparison between the ^{210}Pb incremental dates and decadal variation in relative sea-level has not proved possible for the purposes of this study.

The distinct fluctuations in sedimentation rates over the last c. 70 years in the cores from Loch Don, Loch Creran and Loch Etive represent episodes of marsh 'catch-up' in response to periods of lower suspended sediment deposition. What does appear to be apparent is a general smoothing of sedimentation rates over the 50-70 year period of mature marsh development at these three sites. This kind of morphodynamic response has been previously recorded in the more organic marshes of Connecticut, USA, by McCaffrey and Thompson (1980).

Very recent sediment accumulation now appears to be driven by a regional acceleration of mean sea-level as significant increases have been detected at all four sites which traverse known isobases for Holocene shoreline surfaces (Smith *et al.*, 2002; Figure 4.2). The increased sedimentation does not appear to be influenced by the low rates of estimated current differential uplift across the study region (Firth and Stewart, 2000; Shennan and Horton, 2002).

^{210}Pb excess activity profiles, solid-phase geochemical evidence and elemental flux calculations all indicate that the source of increased material is derived from the active erosion of fronting low marsh areas at each site (see section 8.10 below). Recent acceleration in surface deposition therefore represents a de-coupling of the relationship between uplifting depositional surfaces and relative sea-level rise, which appears to have been in a state of quasi-equilibrium throughout much of the mid to late twentieth century. This is most likely due to the composition of the marsh sediment material. The low organic carbon and clay content of the marsh cores which contain larger quantities of silt and sand material may result in these sediments being highly sensitive to minor fluctuations in mean sea-level that occur as noise within the overall average trend.

Marsh sedimentary status as a function of the difference between rates of net vertical accretion and overall relative sea-level rise has been examined in a number of geographically contrasting areas (Stevenson *et al.*, 1986, 1988; French, 1993). This approach considers the sedimentary status (either accretion deficit or surplus) by plotting the calculated figure against tidal range (Stevenson *et al.*, 1986). In so doing, the differences in marsh compositional variability in relation to tidal energy become more distinct (French, 1993; Figure 2.7).

Using this approach sediment accretion data for the Argyll marshes are examined for the ca. 70 year period to ca. 1995 AD and for the recent period to 2000 AD over which time significant acceleration in sediment accumulation is recorded (Figure 8.14a). In this diagram the

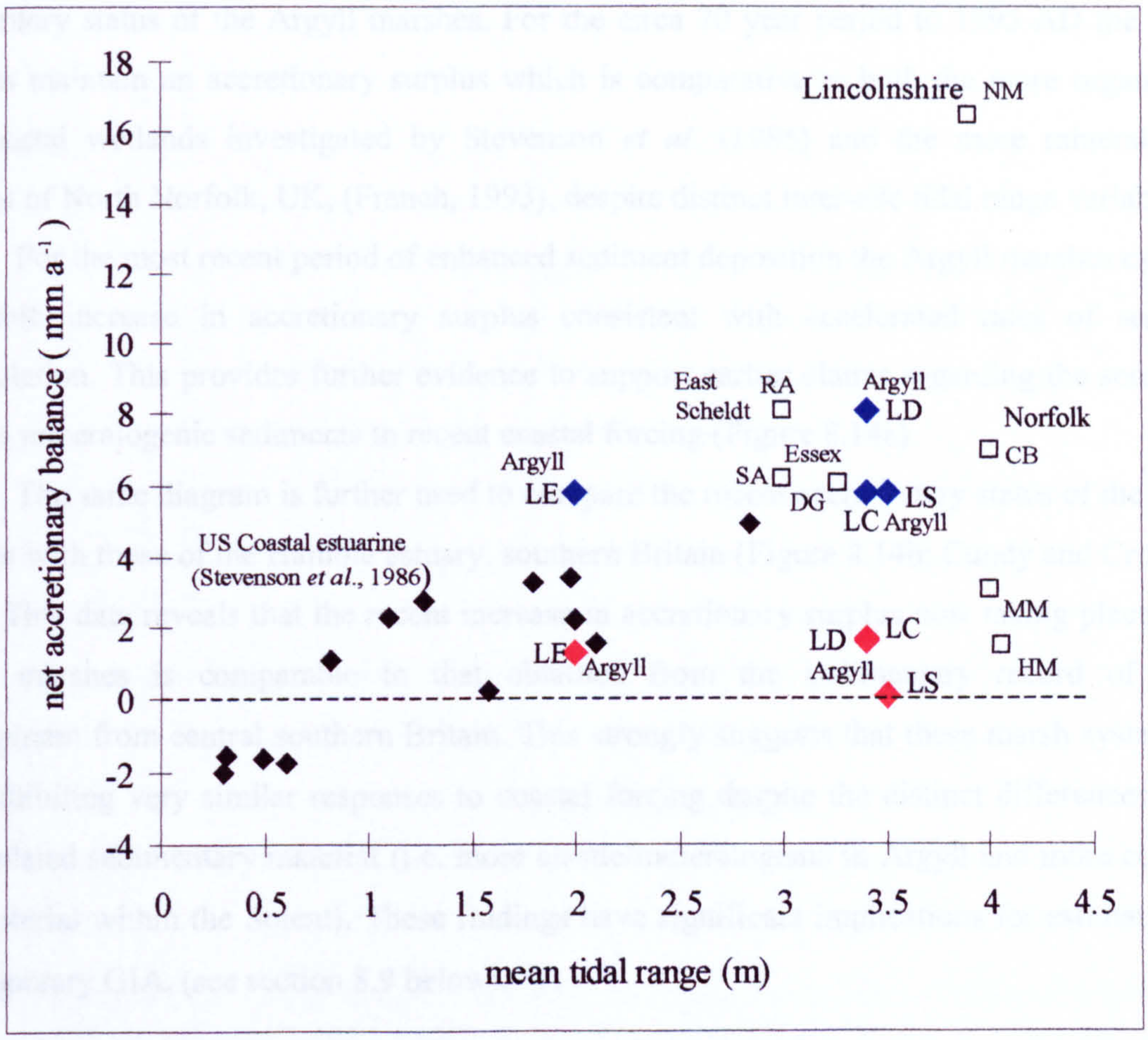

Figure 8.14a: Plot of accretionary balance (mean annual accretion-local sea-level rise) versus mean tidal range (after French, 1993). Included are data for the Argyll marshes for the ca.70 year period to 1995 AD (red diamonds). The recent change in accretionay balance for the same marshes over the period 1995 AD to 2000 AD (blue diamonds) based upon estimated relative sea-level rise for the region from Dawson *et al.* (2001).

LS = Loch Scridain LD = Loch Don LC = Loch Creran LE = Loch Etive

CB = Cockle Bight, Scolt Head Island. MM = Missel Marsh, Scolt Head Island

HM = Hut Marsh, Scolt Head Island. DG = Dengie Marsh, Essex

NM = New Marsh, Gilbratar Point. RA = Rattekaai, East Sheldt, The Netherlands

SA = St. Annaland, East Sheldt, The Netherlands

data are presented as a function of marsh accretion minus the estimated rate of sea-level rise for the region during the twentieth century (derived from Shennan and Woodworth, 1992). Comparison with data from other geographical regions provides a useful indication of the sedimentary status of the Argyll marshes. For the circa 70 year period to 1995 AD the Argyll marshes maintain an accretionary surplus which is comparative to both the more organic-rich U.S coastal wetlands investigated by Stevenson *et al.* (1986) and the more mineralogenic marshes of North Norfolk, UK, (French, 1993), despite distinct inter-site tidal range variability.

For the most recent period of enhanced sediment deposition the Argyll marshes exhibit a noticeable increase in accretionary surplus consistent with accelerated rates of sediment accumulation. This provides further evidence to support earlier claims regarding the sensitivity of these mineralogenic sediments to recent coastal forcing (Figure 8.14a).

The same diagram is further used to compare the recent accretionary status of the Argyll marshes with those of the Hamble estuary, southern Britain (Figure 8.14b; Cundy and Croudace, 1996). This data reveals that the recent increase in accretionary surplus now taking place in the Argyll marshes is comparable to that obtained from the sedimentary record of marsh development from central southern Britain. This strongly suggests that these marsh systems are now exhibiting very similar responses to coastal forcing despite the distinct differences in the accumulated sedimentary material (i.e. more clastic/mineralogenic in Argyll and more cohesive fine material within the Solent). These findings have significant implications for estimations of contemporary GIA, (see section 8.9 below).

8.8: Influence of storms and the North Atlantic Oscillation (NOA) on marsh development.

The influence of storms upon saltmarsh development is well documented in the literature (Andersen *et al.*, 1992; French and Spencer, 1993; Guntenspergen, *et al.*, 1995; Risi *et al.*, 1995; Devoy, 1996; Wheeler *et al.*, 1999; Smith, 2000). Following storm activity, increased quantities of coarse and suspended sediment can become deposited on the marsh surface leading to significant enhancement of sediment accretion rates over short periods of time. This is particularly true for high marsh environments (French and Spencer, 1993).

In recent years speculation surrounding the frequency of North Atlantic storminess and linkages to the NAO index (either positive or negative) over historical time has led to an increase in the number of published investigations regarding the variability of the NAO index and

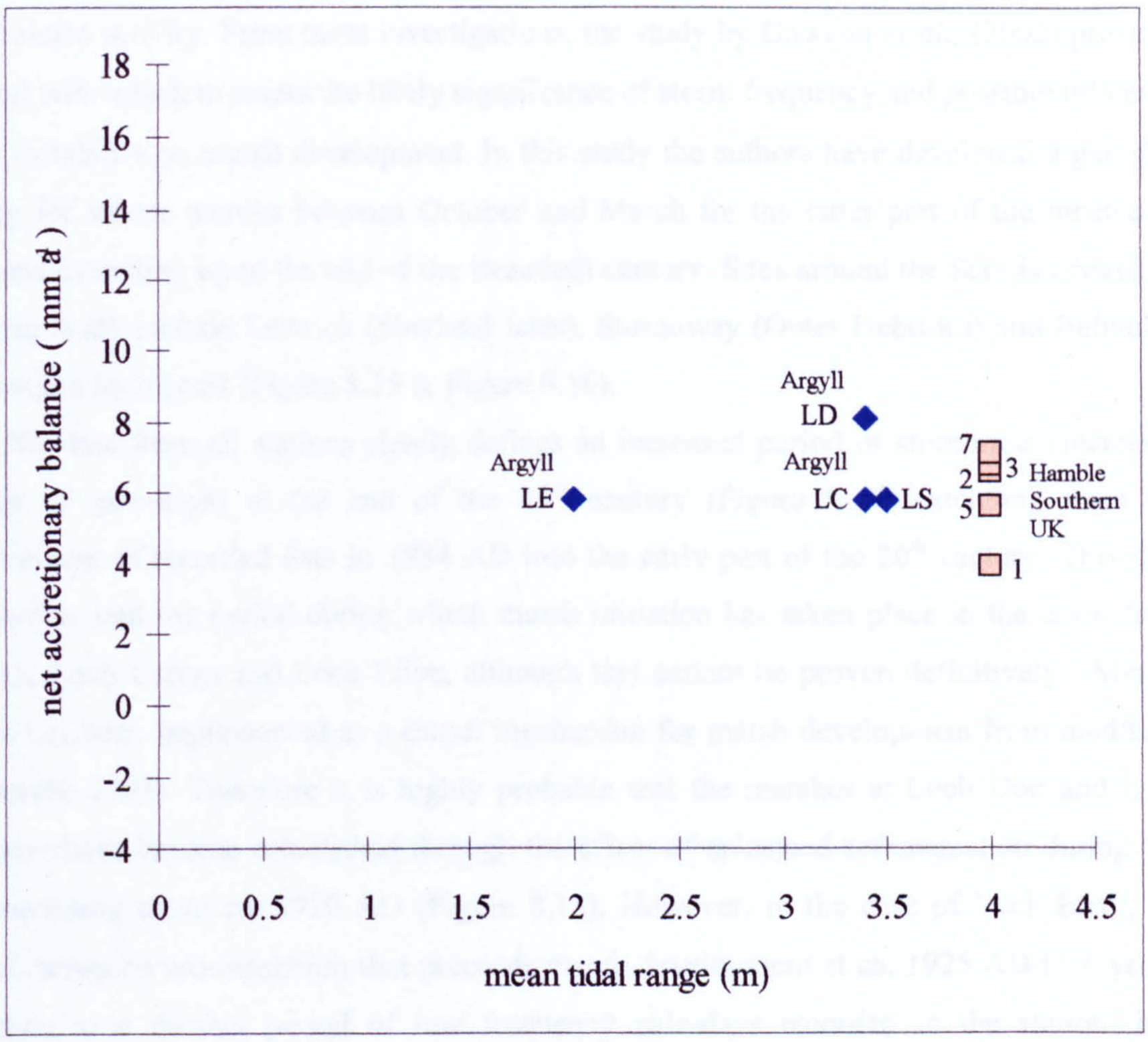

Figure 8.14b: Plot of accretionary balance (mean annual accretion-local sea-level rise) versus mean tidal range, (after French, 1993), for the current status of marshes from Argyll western Scotland in comparison to that derived from a transect or cores across marshes from the Hamble estuary, (Solent), Southern UK (Cundy & Croudace, 1995).

Western Scotland: (blue diamonds)

LS = Loch Scridain LD = Loch Don LC = Loch Creran LE = Loch Etive
(Dominated by *Puccinellia maritima*)

Hamble estuary (Solent), southern UK: marsh core transect: (light brown squares)

1 = Rear, landward edge of salt marsh, *Spartina.*

2 = Mid-marsh area, *Halimone portulacoides.*

3 = Seaward edge of marsh mound, *Halimone portulacoides.*

5 = Mid-marsh mound, *Halimone portulacoides.*

7 = Centre of Spartina/ *Halimone portulacoides* mound.

recorded storm activity. From these investigations, the study by Dawson *et al.*, (2002) proves a useful tool with which to assess the likely significance of storm frequency and possible influence of NAO variability on marsh development. In this study the authors have developed a gale-day frequency for winter months between October and March for the latter part of the nineteenth century and extending up to the end of the twentieth century. Sites around the Scottish coastline used in the study include Lerwick (Shetland Isles), Stornoway (Outer Hebrides) and Belmullet on the western Irish coast (Figure 8.15 & Figure 8.16).

The data from all stations clearly defines an increased period of storminess (increased frequency of gale-days) at the end of the 19th century (Figure 8.15) extending from the commencement of recorded data in 1884 AD into the early part of the 20th century. This may well coincide with the period during which marsh initiation has taken place in the cores from Loch Don, Loch Creran and Loch Etive, although this cannot be proven definitively. Marine incursion has been implemented as a causal mechanism for marsh development from mud/sand flats (French, 1993). Therefore it is highly probable that the marshes at Loch Don and Loch Creran may have become established through the effect of enhanced sedimentation during this period extending up to ca. 1920 AD (Figure 8.15). However, in the case of Loch Etive, the period of increased sedimentation that preceeds marsh development at ca. 1925 AD (± 4 years) corresponds to a distinct period of low frequency gale-days recorded in the station data, particularly that from Stornoway (Figure 8.17). This suggests that an alternative marine mechanism to storm activity may be responsible for the marine incursion evident at this time at the head of the fjord. At Loch Scridain saltmarsh sediments were already well established with relatively higher rates of sediment accumulation (inferred from the ^{210}Pb dating models) occurring prior to 1884 AD which may be the result of similar gale-frequency days during the mid nineteenth century for which there is little reliable data.

As previously mentioned the likelihood of storms directly influencing the upper inter-tidal area at Loch Don is less certain. However, the effect upon tidal current velocities as a result of increased wave height due to storm activity and tidal surges corresponding to storm periods may have resulted in enhanced levels of suspended sediment being transported into the upper estuary area. Therefore it is highly probable that increased suspended sediment concentrations transported to upper inter-tidal areas have been responsible for marsh development at Loch Don and Loch Creran.

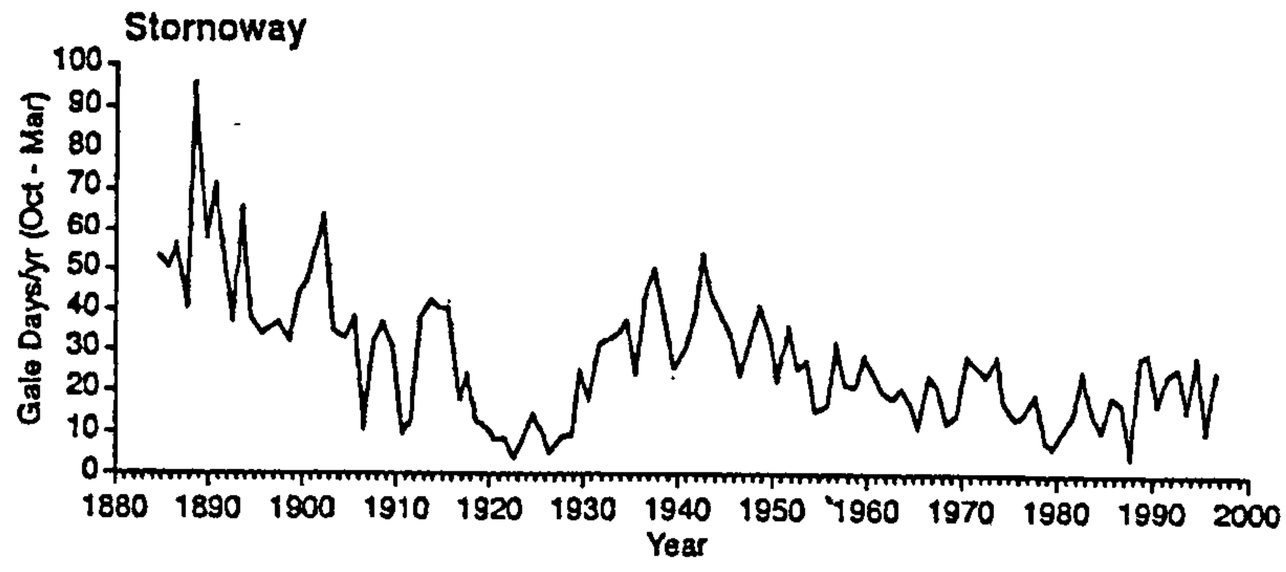

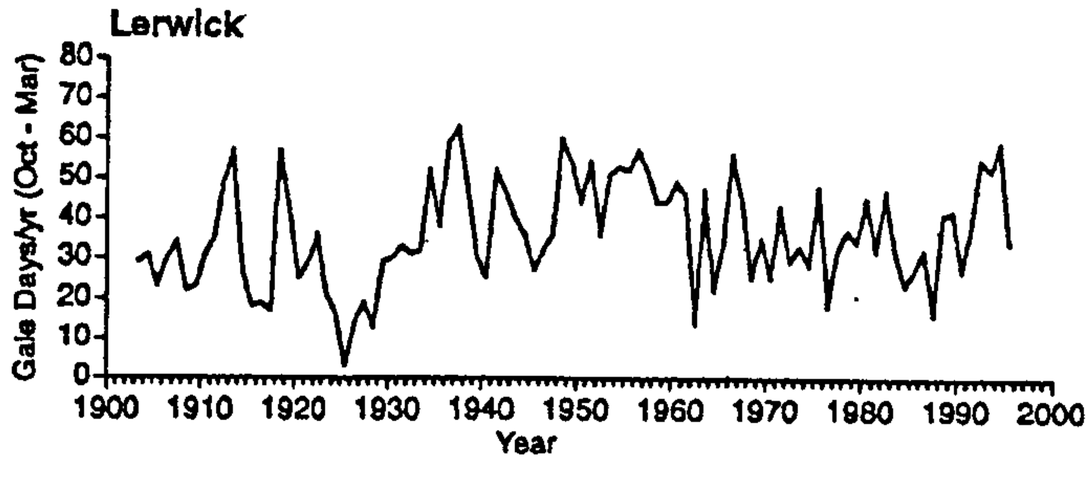

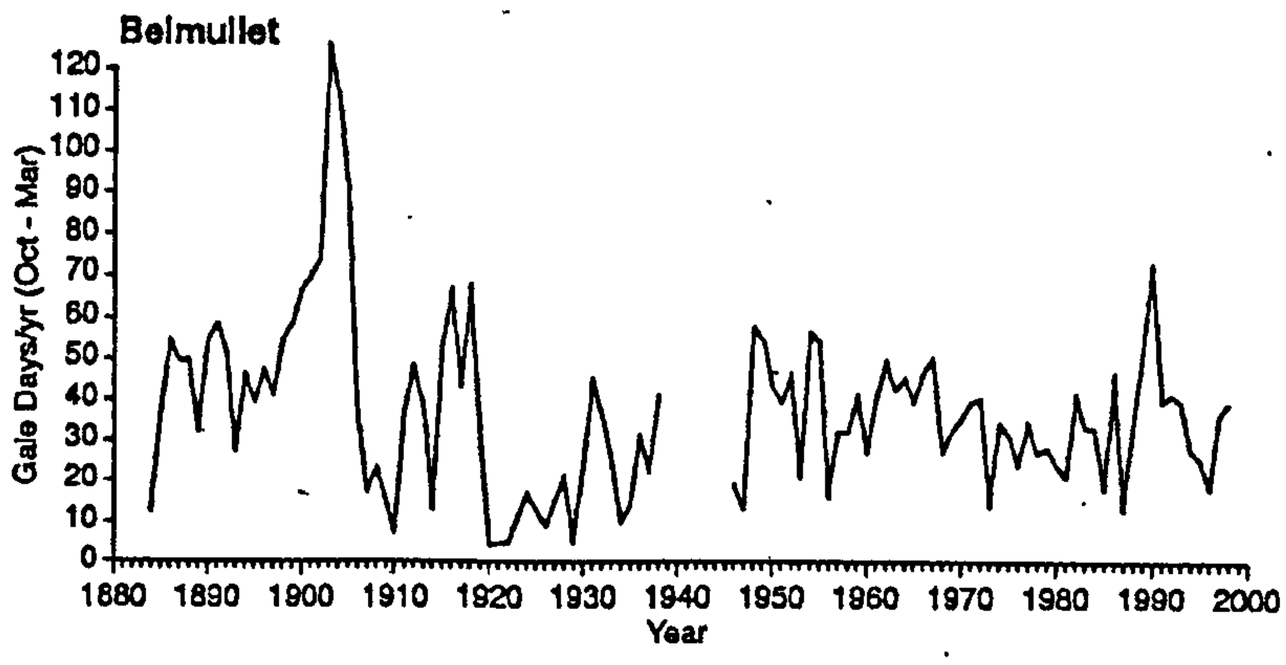

Figure 8.15: Gale–day frequency for the north-east Atlantic from recording stations at Stornoway (Outer Hebrides), Lerwick (Shetland Islands) and Belmullet (western Ireland). Values are calculated as winter period months October to March inclusive (source: Dawson et al., 2002).

(A)

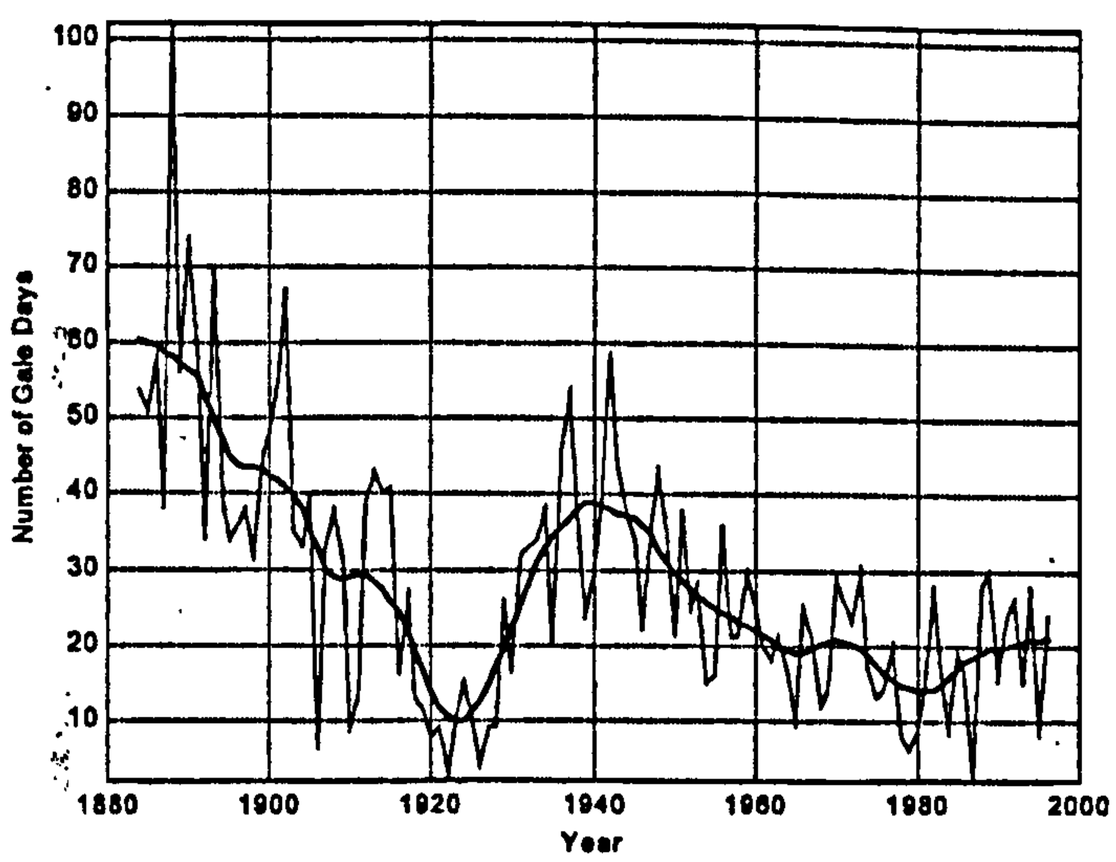

(B)

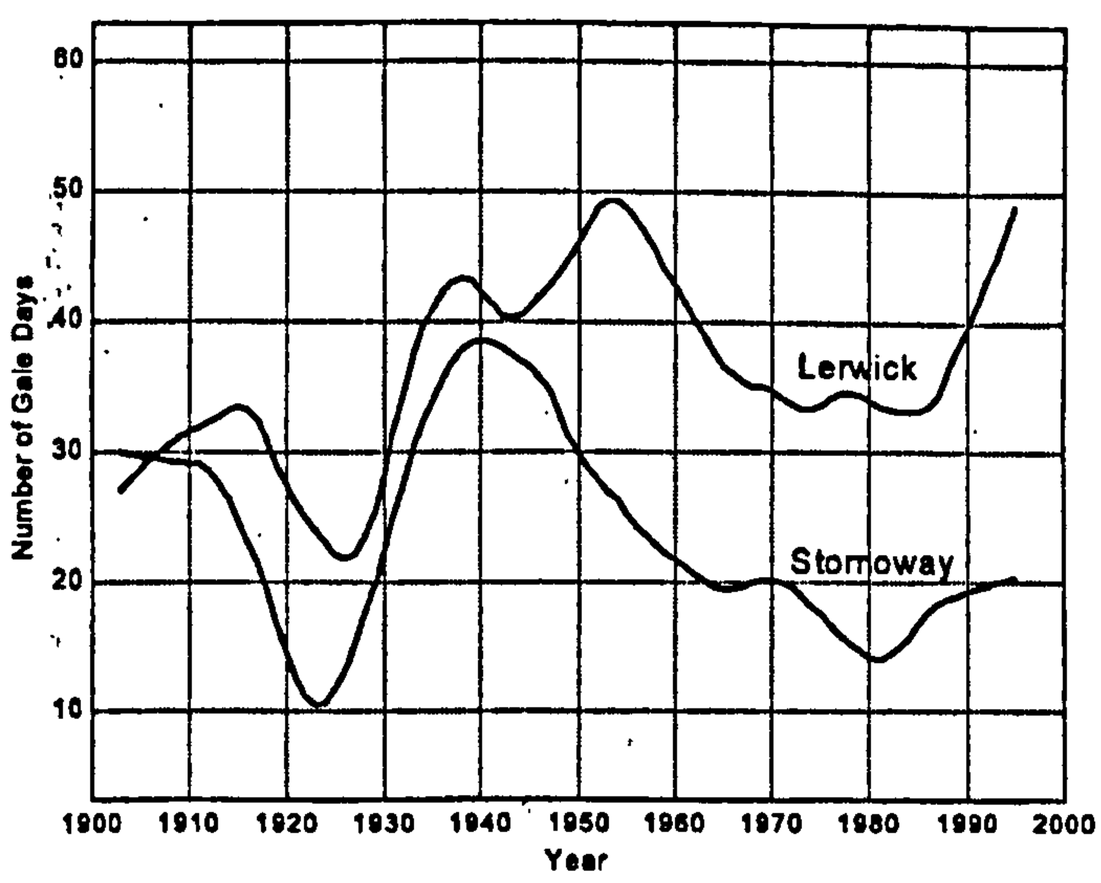

Figure 8.16: A) Gale-day frequencies for Stornoway (winter 1884 AD to 1996 AD) with LOWESS smoothed curve and B) Comparison of Stornoway and Lerwick gale-day frequencies (LOWESS smoothed), from winter 1903 AD to 1995 AD.

The gale-day frequency data from Stornoway can further be used as a proxy for storm activity in western Scotland for the period extending from the late 1920s to the end of the last century. Following the exceptionally low period of storm activity that characterises the period from ca. 1910 AD to 1929 AD, the Stornoway record of gale-days is one of low frequency and greater inter-annual variability throughout (Dawson *et al.*, 2002) with a moderately higher frequency of gale-days occurring in the period ca.1931 AD to 1952 AD (Figure 8.16). In the cores from sites on Mull there is no evidence to suggest that this mid-20th century increase in gale-day frequencies has influenced a concomitant increase in marsh sedimentation rates over this period. The higher rates of sediment accumulation over this period in the Loch Creran core may well be influenced by enhanced suspended sediment concentrations. Solid-phase geochemical profiles of major and trace elements do not record significant increased inputs of coarser material over this time period. However, support for this argument is gleaned from the major and trace metal flux profiles from Loch Creran which shows enhanced flux to the marsh surface over the period ca. 1945 AD to ca. 1957 AD suggesting that storm activity may have increased suspended sediment fluxes over this time assuming accommodation space was provided by continuing Twentieth century sea-level rise. No further evidence exists in any of the four cores for enhanced sediment accumulation during this mid-twentieth century period of relatively higher gale-day frequencies (Figure 8.16).

During the latter half of the last century the gale-day frequency from the Stornoway record shows a significant and continuous decrease to the early 1980s with only a moderate rise in frequency corresponding to increased North Atlantic storminess recorded in the data from Belmullet and Lerwick (Figure 8.15). There is no evidence to suggest that any of the four marsh cores have experienced higher rates of sedimentation during this period. Such findings are a direct consequence of individual marsh settings and surrounding topography coupled with the fact that at this stage in their evolution all cores surfaces had already attained maturity relative to the tidal frame. Dawson *et al.* (2002) further highlight that there appears to be little in the way of correlation between NAO index and storm frequencies for the North Atlantic. This is further emphasized in the graphical plots of gale-day frequency with NAO index for the Stornoway and Belmullet stations over the period 1983 AD to 1996 AD (Figure 8.17). Hence there appears to be no discernible link between NAO index and rates of marsh sedimentation within the four sites studied in the Argyll region.

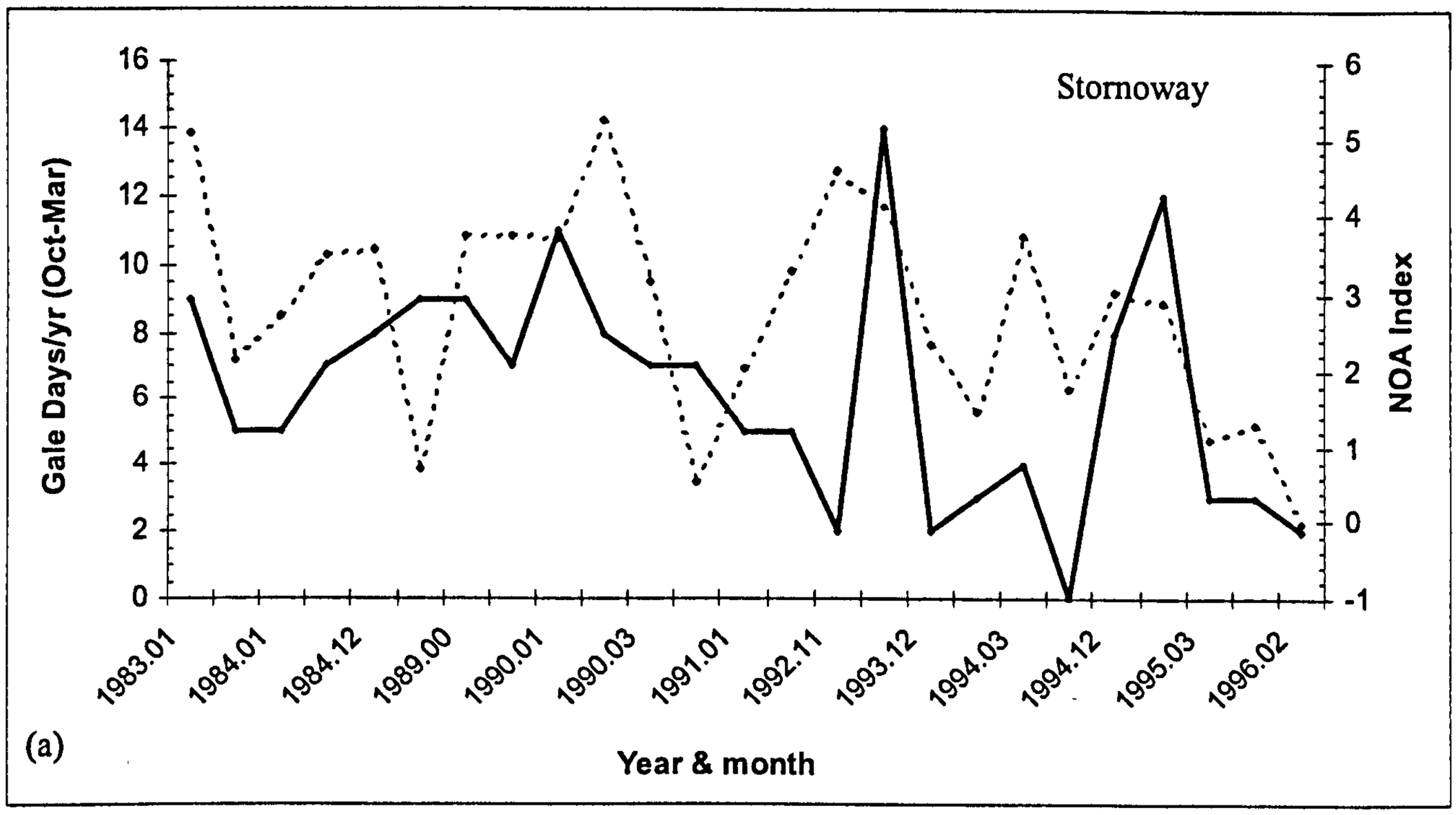

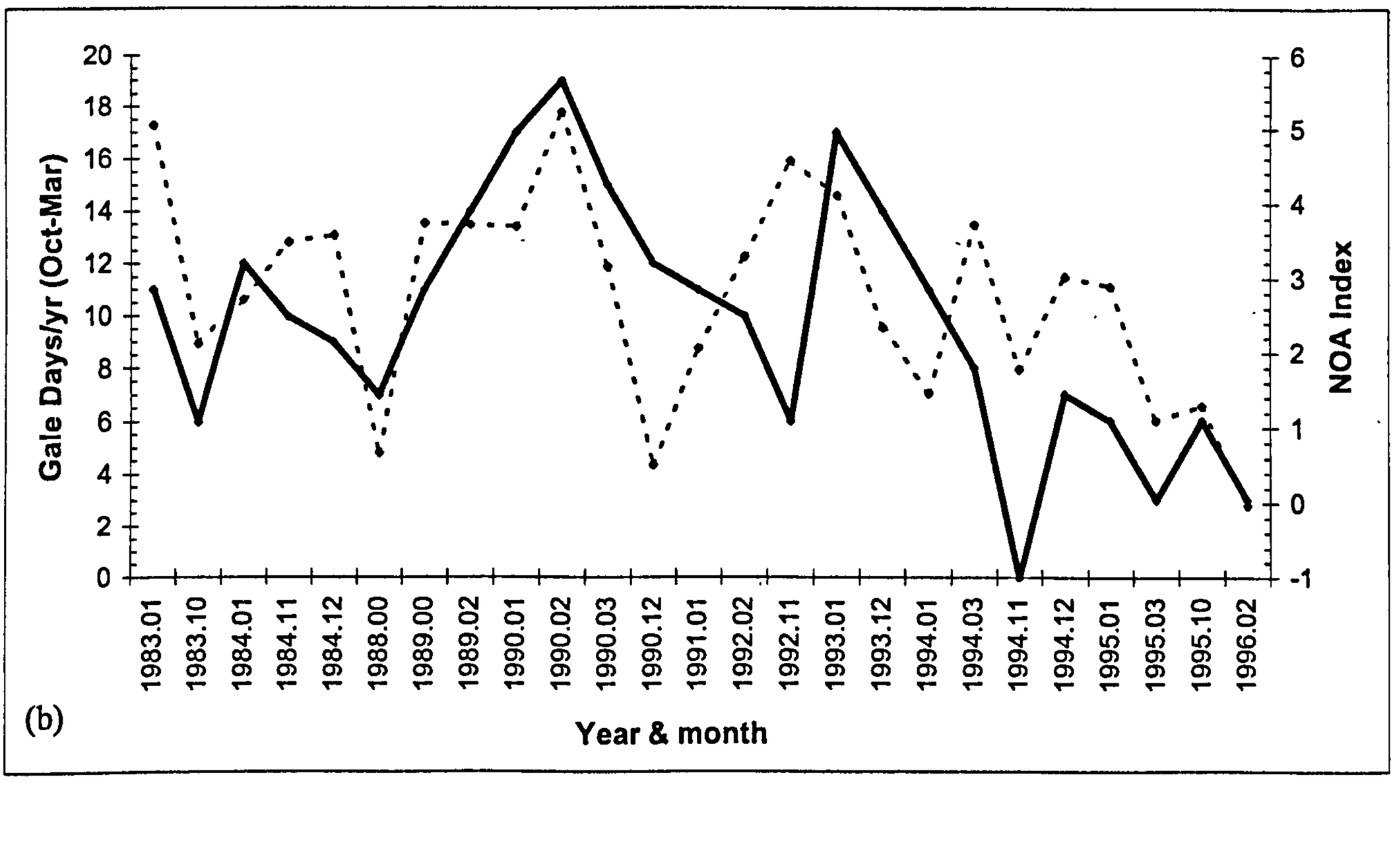

Figure 8.17: Comparison of gale-day frequency with NOA Index for the latter part of the last century (1993-1996 October to March) from a) Stornoway, Outer Hebrides and b) Belmullet, Western Ireland. (Blue line represents gale-day frequency/year; black dashed line represents NOA Index).

8.9: Implications for glacio-isostatic modelling

Significant effort has been focused upon evaluation of Holocene land- and sea-level changes resulting from the glacio-isostatic adjustment (GIA) of the UK landmass following the retreat of Devensian ice (e.g. Shennan 1989; Smith, 2002: Shennan and Horton 2002 and references therein). The wealth of different approaches employed by the vast number of authors involved with such investigations (see review in Chapter One of this thesis) has resulted in a comprehensive high quality data set covering much of Great Britain. This has proved attractive to workers focussing effort on modeling Late Devensian and Holocene GIA processes (e.g. Lambeck, 1995; Peltier, 1998; Peltier *et al.*, 2002). Shennan and Horton (2002) highlight the general improvements of the modeling approach in recent years. However, despite significant advances in predicting present relative sea-level (RSL) changes around Great Britain the modelling approach still suffers from disagreements with observed (RSL) data. This is particularly true for Scotland where refinement of estimated rates of crustal uplift has resulted from the analyses of RSL data in Shennan, (1989) and by Shennan and Horton (2002) with that of Firth and Stewart (2000). The most recent estimations from Shennan and Horton (2002) are shown in Figure 8.18.

Importantly, all these rheological-based models indicate that crustal uplift is ongoing (e.g. Shennan, 1989; Shennan and Woodworth, 1992; Lambeck, 1995; Peltier, 1998; Shennan and Horton, 2000; Peltier *et al.*, 2002). A key point with regard to these estimations is that the geophysical models are largely based upon extrapolations derived from the youngest Holocene date from any particular site. Such analyses therefore really represent a first estimate with regard to present day/recent geodynamics within western Scotland (see critiques in Firth and Stewart, 2000; Stewart *et al.*, 2000) and are maximum possible values as highlighted in the earlier analysis by Shennan (1989).

There are virtually no data in the published literature pertaining to RSL movements derived from empirical studies of contemporary/historical lowland coastal depositional settings (e.g. saltmarshes) from either the east or the west coast of Scotland. Some observational data do exist in the form of morphological studies relating to other types of coastal landforms (e.g. sand beaches, and spits), (e.g. Firth *et al.*, 1995; Comber, 1995; Hansom, 2001). These are now considered to be actively responding to the influence of rising sea-levels. Studies from lowland coastal marsh settings are noticeably absent in the literature.

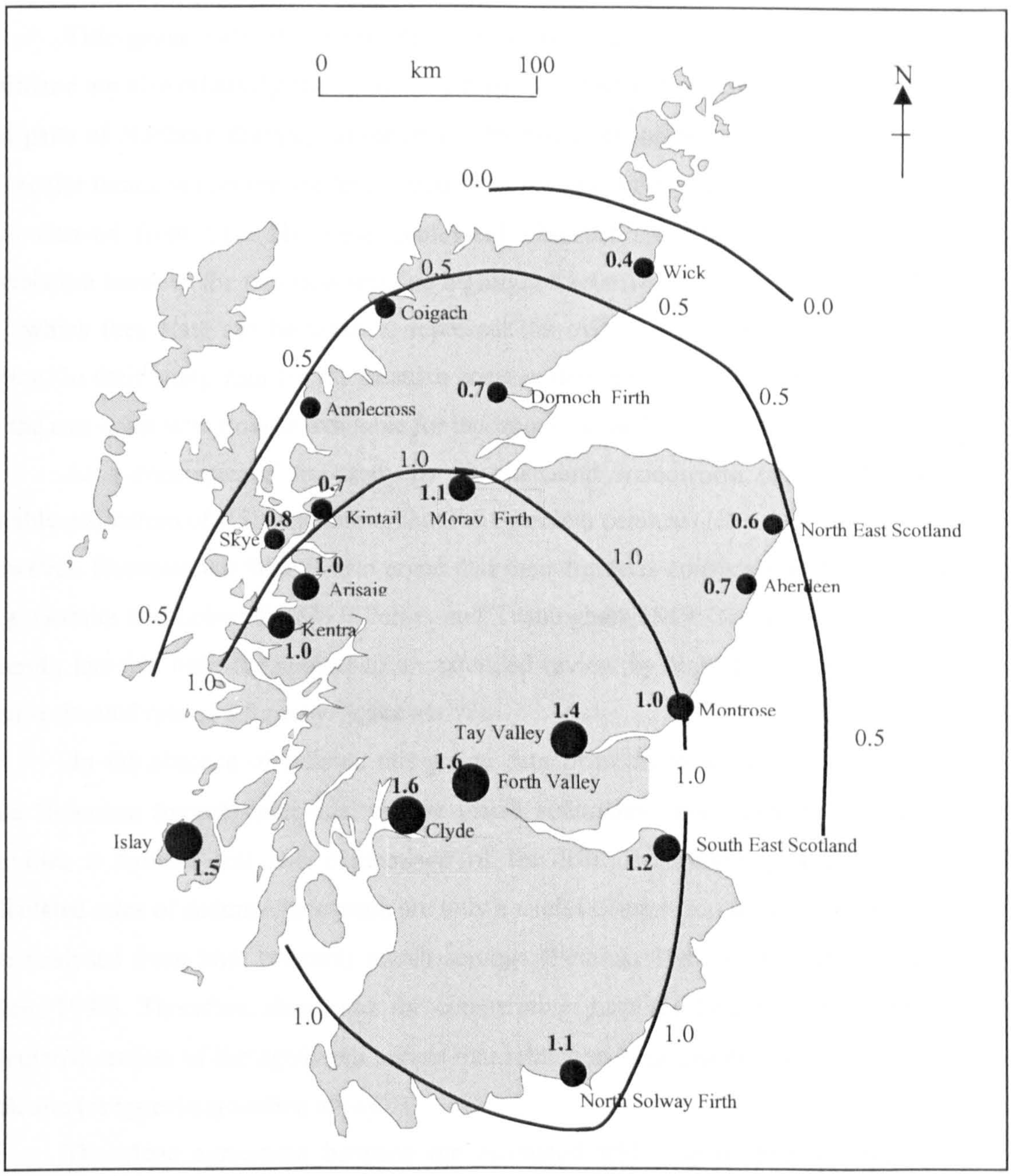

Figure 8.18: Most recent estimations of Late Holocene relative land-/ sea-level changes (mm yr^{-1}) in Scotland where all values (bold print) represent relative land uplift and hence estimated sea-level fall. Sites shown are locations in Scotland from which individual sea-level points have been grouped and analysed. Inferred contour lines are hand-drawn in line with the original authors interpretation and rates are indicated with standard text (redrawn from Shennan *et al.*, 2002).

Tide-gauge data of suitable duration to ascertain reliable trends around the Scottish mainland are also relatively sparse in comparison to other parts of Britain (e.g. the English coast and parts of Northern Europe). In the review by Shennan and Woodworth (1992) a comparison of secular trends in relative sea-level throughout the twentieth century has been undertaken with data derived from Late Holocene geological observations. These authors identify a good correlation between the two data sets and highlight a relative sea-level rise of ca. 1.0 ± 0.15 mm yr^{-1} which they state can be taken to represent the overall twentieth century RSL rise for the region. In their study data for the Scottish coast is derived from Aberdeen and Dunbar situated on the east coast with no data available for incorporation in the analysis from the west coast.

As a consequence, the study by Shennan and Woodworth (1992) provides the most reliable estimation of RSL rise throughout the twentieth century (1.0 ± 0.15 mm yr^{-1}; see above). However, Shennan and Woodworth argue that their figure is consistent with earlier estimations (e.g. Gornitz and Lebedeff, 1987; Peltier and Tushingham,1989; Trupin & Wahr, 1990). Only recently has this been the subject of an extended review by Nakada and Inoue (in press) with their estimated rate of 1.5 mm yr^{-1}, see above).

In the absence of reliable tide-gauge data from the west coast, radiometric dating of Late Holocene (recent) inter-tidal mature marsh sediments undertaken in this study therefore provides a modern test and comparison of the RSL rise model predictions. Importantly, calculated rates of sediment accretion are only a useful comparison with historical trends in RSL rise analysed from high (mature) marsh settings (Pethick, 1981; Cundy and Croudace, 1995; Allen, 1997). Therefore, data used for comparative purposes here is that obtained from the calculated section of the age/depth curves that relates to high marsh inter-tidal conditions from each site (see previous section above).

The close agreement between the estimated RSL rise of Shennan and Woodworth (1992), (1.0 ± 0.15 mm yr^{-1}) and the average rate of sediment accretion measured in the Loch Scridain marsh core (1.1 mm yr^{-1}) indicates a steady state equilibrium throughout the 20th century to 1995 AD between marsh accretion and regional RSL rise.

On the south-east of Mull at Loch Don sediment accumulation has proceeded at an average rate of 2.6 mm yr^{-1} for the ca. 70 year period to 1997 AD. At Loch Creran the same rate of accumulation is recorded over an almost identical ca. 70 year period. These rates are significantly above the regional RSL rise suggested by Shennan and Woodworth (1992) and Nakada and Inoue (in press) and are more closely related to the earlier estimations of Peltier and

Tushingham (1989). Similarly, sedimentation in the core from Loch Etive corresponding to mature marsh conditions is in closer agreement with the higher estimations of Peltier and Tushingham (1989) with a rate of 2.3 mm yr^{-1} over the last ca. 60 years.

Apart from the Loch Scridain core, the other three cores all show comparatively elevated rates of sediment accumulation (above the regional RSL rise estimations) over the ca. 60-70 year period corresponding to inferred mature marsh settings. An exact explanation for this is not straightforward. This may indicate that the marshes here are yet to achieve equilibrium with relative sea-level movements. Alternatively, increased suspended sediment concentrations may be higher within the Loch Don estuary and the Loch Creran and Loch Etive inter-tidal areas. This would then provide a mechanism for the deposition of elevated levels of sediment on the marsh surface over the spring tidal cycle. French (1993), identifies a local relative accumulation rate in the marshes of North Norfolk UK of 2 mm yr^{-1} under a scenario of eustatic sea-level rise of between 0.9-1.1 mm yr^{-1}, with these estimations taken from earlier studies (e.g. Mörner, 1973; Pirazzoli, 1998). This includes an ongoing crustal subsidence of ca. 1 mm yr^{-1} for the east coast of England (Shennan, 1989). Here, the comparison between the more clastic marshes of Argyll and those of the Norfolk coast is striking when consideration is given to the current estimated differential crustal response of these geographical regions of Britian.

An alternative, and at this stage speculative, mechanism that could enhance sediment accretion at these sites may result if extrapolated Late Holocene estimations of current crustal uplift for western Scotland are far less than the current maximum estimations of Shennan and Horton, 2000). These rates are depicted in Figure 8.18. Firth and Stewart (2000) highlight the more likely ongoing rates derived from reassessment of the post-glacial exponential decline in GIA undertaken by Smith *et al.*,(1993) and Firth *et al.*, (1997). These authors propose a minimum calculated rate of between 0.2–1.0 ± 0.1 mm ^{14}C yr^{-1} which may better explain the increase in marsh accretion identified across the Firth of Lorne and at the Loch Etive site.

The idea that crustal uplift could have now ceased has not received much scientific credence other than the conceptual models which describe the decline in altitude of the peripheral fore-bulge and movement towards the centre of former maximum ice thickness during GIA (Gray, 1974; Nikonov, 1980). The concept of crustal down-warping and/or down faulting around the western margin of highland Britain as a mechanism to explain Tertiary and Quaternary relief has previously been suggested (e.g. Linton, 1951). In the third part of a trilogy addressing the relief of the British Isles, Clayton and Shamoon (1999) highlight evidence from

their newly developed mapping methodology (see Clayton and Shamoon, 1998a & 1998b). This study strongly suggests that this concept should be taken seriously. However, this work does focus upon the longer-term evolution of relief within the British Isles and largely ignores the effect of Late Quaternary glaciations and GIA processes. Nevertheless, in the absence of significant Late Quaternary neotectonic activity (Johnston *et al.*, 1999) such a mechanism may contribute to the more complex geodynamic setting around the western Scottish mainland as suggested by the combination of these various lines of enquiry coupled with existing uplift scenarios and the results from coastal wetland sedimentary dynamics obtained from this study.

An important point to emphasize here is that there does appear to be a state of equilibrium between marsh evolution and estimated sea-level rise recorded in the Loch Scridain core sediments on western Mull which strongly implies crustal stability with no down-warping. Throughout the twentieth century record of deposition in the core there appears to be no discernable increase in sedimentation over the high (mature) marsh age/depth that might be associated with crustal subsidence on the west of Mull. The situation across the Firth of Lorne is more complicated and whether the increased rate of sedimentation is actually linked to a hitherto unconsidered phenomena or results simply as a response to increased suspended sediment concentrations at these sites remains to be answered.

An important finding here is the distinct similarity between the accretionary status of the Argyll marshes and those from the Hamble estuary, central southern Britain. This suggests that both systems are responding to coastal forcing in terms of net accretionary surplus. However, mass accumulation rates may differ owing to the differential densities of the material being deposited at each site (see section 8.7). The inference made here is that current rates of crustal uplift in western Scotland may now be extremely low or may in fact have ceased.

A definitive resolution to this question may only be possible with the deployment of global positioning systems linked to tidal gauge stations (e.g. Ashkenazi *et al.*, 1997). Initial data from this work is now beginning to be introduced and although of short duration does seem to support recent estimations (e.g. Shennan and Woodworth, 1992; Shennan and Horton, 2002 and Nakada and Inoue, in press) for the data derived from GPS monitoring at Aberdeen (Terfele *et al.*, in press).

8.10: Recent marsh accretion implications for future coastal management

In the study by Pethick (1999), statistical analysis of Holocene RSL changes from north-west Scotland is combined with 1993 Intergovernmental Pannel on Climate Change (IPCC) predictions for future global sea-level rise to 2050AD (Figure 8.19). This analysis predicts that a significant change in RSL tendency will be experienced around the western Scottish coast at the end of the Twentieth/beginning of the Twenty-first century with estimations of near-future average sea-level rise of ~ 4 mm yr^{-1} over the next half century (Figure 8.19 d). More recent predictions derived from improved models of predicted global sea-level rise now give average estimations of 4.3 mm yr^{-1} to 2100 AD (IPCC, 2001). The predicted change in relative sea-level direction outlined in Pethick (1999) is complimented by the study of Dawson *et al.* (2001). These authors highlight the fact that most tide-gauge stations around the Scottish coast including some more modern stations not used for 20th century relative sea-level predictions are now recording a relative sea-level rise. Although not utilized in the longer-term tidal data analyses of Shennan and Woodworth (1992) and Shennan and Horton (2002), two stations on the west coast provide data that is intriguing. Firstly, the station at Ullapool in the north-west provides data covering a 16 year period of reduced local reference estimations (Figure 8.19). This indicates a local relative sea-level rise of 3.16 ± 2.36 mm yr^{-1} (data from Permanent Service for Mean SeaLevel (PMSL), Proudman Oceanographic Laboratories). Secondly, and more controversial is the data obtained from the recent implementation of a tide-gauge at Port Ellen on the Isle of Islay. Here a very short duration data set (< 10 years) suggests a RSL rise of 3.54 ± 2.36 mm yr^{-1} (data from PSMSL, Proudman Oceanographic Laboratories). Obviously, these data are to be treated with caution in light of the short time series and large error estimations resulting from noise associated with short-term measurements. Dawson *et al.* (2001) have defined four distinct zones around the Scottish coast that have been experiencing variable trends in relative sea –level as a result of the twentieth century estimations and differential crustal uplift of the Scottish mainland (Figure 8.20). These averaged estimations are seen to alter significantly in the estimated scenario to 2050 AD by these authors. Of major importance here is the relative position of the marsh sites investigated in this study relative to the zones defined by Dawson *et al.* (2001) (Figure 8.20). The marsh at the head of Loch Scridain is situated approximately on the border of zones I and II where relative sea-level is predicted to have been falling or where present RSL change is uncertain (Figure 8.20). Rates of sediment accretion over much of the

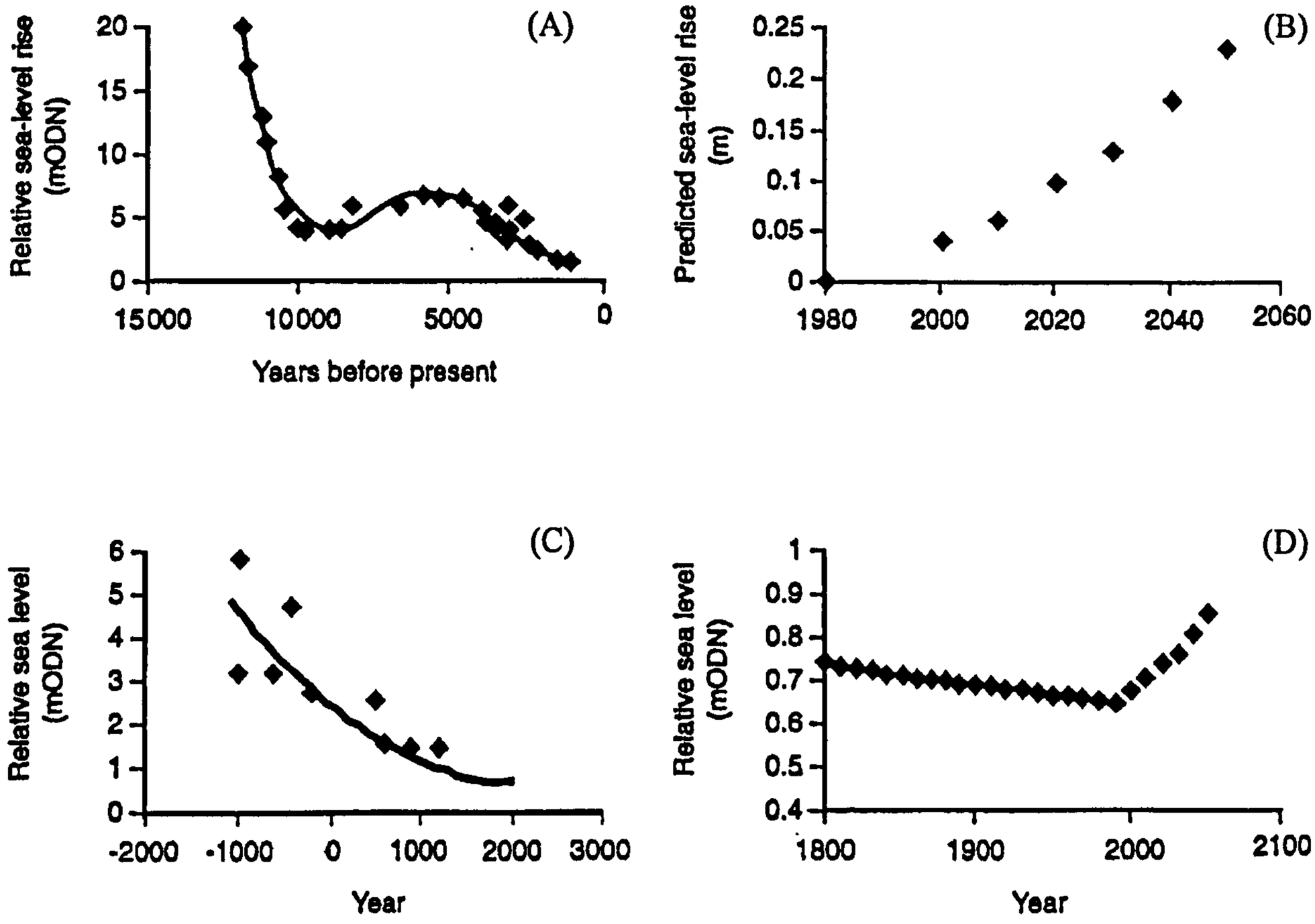

Figure 8.19: Analysis of past relative sea-level changes with IPCC projected increases for the region of western Scotland (source: Pethick, 1999). Graphical plots are as follows: A) Best-fit regression of Holocene RSL change for north-west Scotland (Shennan et al., 1995). B) IPCC predicted sea-level rise to 2050 AD (Warrick, 1993). C) Best-fit regression to the data in (A) for the period 2000 BC to 1000 AD extrapolated to 2050 AD. D) Addition of curves from (B) and (C) to give predicted change in RSL to 2048 AD (After Pethick, 1999; see discussion in text relating to recent findings of the present study).

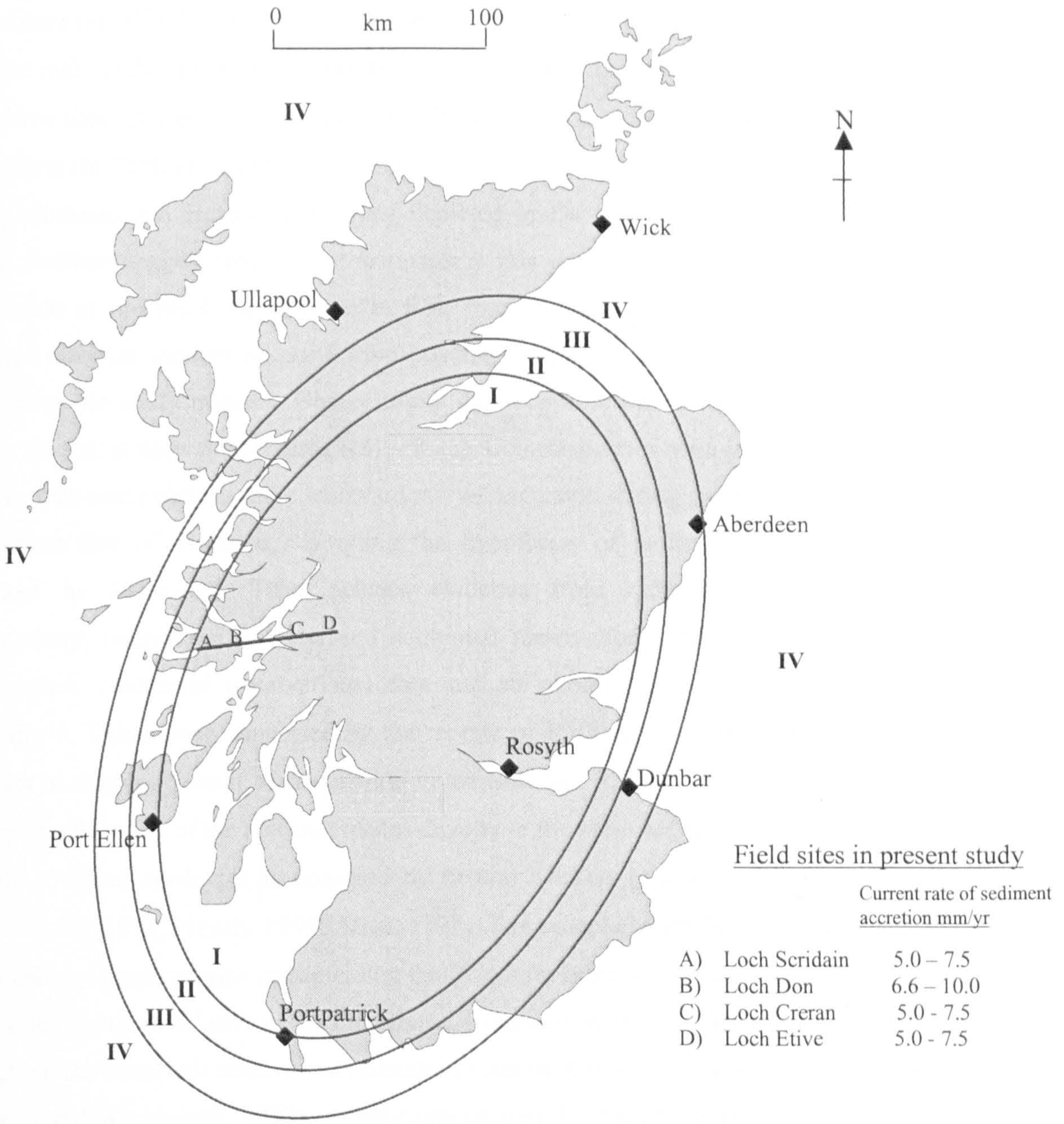

Figure 8.20: Present estimated rates of relative sea-level change around Scotland and best estimates of sea-level rise for 2050 AD with tide gauge stations used for data acquisition. Note the position of the marsh study sites relative to these zones (redrawn from Dawson *et al.*, (2001).

past century (to 1995 AD) from this core indicate that the marsh has been able to keep pace with RSL rise making this site more compatible with zone III of Dawson *et al.* (2001). Data from the other three sites for the last ca.70 years to 1995 AD suggest a RSL rise of greater magnitude for sites within the Firth of Lorne and Loch Etive than that proposed by Shennan and Woodworth (1992), Shennan and Horton (2002) and depicted in Dawson *et al.* (2001), in their zone I. Recent findings suggest that the entire region is now experiencing sedimentation rates more comparable to the predicted increase in RSL rise proposed by Pethick (1999) and that the predicted rates for western Scotland from Dawson *et al.* (2001) are now being exceeded at all sites across the study transect. Observational data supports this notion with extensive marsh erosion evident at each site (Figures 8.21 – 8.23). Communication with local landowners around the site areas also points to more landward marine incursion during recent years. A summary of the various line of evidence supporting the hypothesis of recent relative sea-level rise is presented in Table 8.1. This includes evidence from radiometric dating, soild-phase geochemistry, microfossil analysis and additional observational data derived from field site investigation. Additional observational data and air photographic evidence are presented in Appendix 7. This is also supported by the reports of Firth *et al.* (2000 & 2002), where field evidence of ongoing frontal marsh erosion in the Solway Firth and Firth of Clyde is presented. An important finding of the research relates directly to the proposed morphodynamic response of marshes to rising sea-levels as proposed by several workers (e.g. Pethick, 1981; Reed, 1990, 1995; Pethick, 1992; French, 1993; Allen, 1997). The accepted view derived from such studies, is that under a steady marine transgression the long-term morphological response of the marsh is to migrate landwards relative to the tidal frame. Comparison of the determined rates of accretion throughout the twentieth century with estimated rates of RSL rise obtained from tide-gauge data (Shennan and Woodworth, 1992) strongly suggest that the Argyll marshes have responded in a comparative way throughout much of the time-period governing the evolution of these sedimentary sequences.

Currently, the Argyll marshes do not appear to be conforming to this projected response. Evidence has been presented which highlights the significant increase in marsh sediment accretion in all four sites and the widespread active erosion of the lower marsh environment at all the sites studied. This would appear to currently involve the rapid removal of material from the frontal low marsh environment in response to a regional acceleration of relative sea level

(a)

(b)

Figure: 8.21: Views looking a) south-west and b) south-eastward showing active marsh erosion within the low-marsh area at Loch Scridain, western Isle of Mull.

(a)

(b)

Figure 8.22: Active marsh erosion at a) Outer Loch Don close to the Gorten Farm peninsula and b) the seaward edge of fronting marsh at Loch Creran

(a)

(b)

Figure 8.23: a) overview of frontal (seaward edge) of marsh at Loch Etive and b) view from frontal edge toward high marsh taken from point indicated in a showing extent of active erosion.

Method of enquiry/analysis		Key findings
Radiometric dating	^{210}Pb	Recent significant increase in the rate of sediment accretion (between 5-10 mm/yr) on the surface the Argyll marshes recorded at all four sites derived from the CRS model dating. This is well above the estimated rate of relative sea-level rise for the Twentieth century implying a regional coastal forcing influence.
	^{137}Cs	Supports the ^{210}Pb results for longer-term average rates of accretion. Importantly, estimated rates of accretion are higher using the 1986 AD Chernobyl marker horizon in comparison to that from the 1963 AD Weapons Test signature indicating a sedimentation increase after 1986 AD. Dry mass accumulation rates also indicate significant recent increases indicative that this is a real process and not an artefact of the ^{210}Pb derived geochronological models.
	^{241}Am	Not used extensively for dating purposes owing to generally low levels of detection. Where this is not the case, higher activity levels prove useful in corroborating the 1963AD ^{137}Cs marker horizon. The presence of ^{241}Am within the near-surface sediments of the marshes does indicate the continuing influence of marine derived activity from Sellafield or re-worked material.
Geochemistry		Elevated major (detrital) element abundances and trace element concentrations within the near-surface sediments of all four marsh cores coupled with increased fluxes of detrital and trace metals over the same age vs. depth time period.
Microfossil (diatom analysis)		A very recent increase in the relative abundance of epipsammic polyhalobous benthic taxa within the near-surface sediments of the Loch Etive marsh core, likely to be derived from the ongoing marsh erosion at the seaward edge of this site.
Geomorphology (field observations)		Significant active erosion of the frontal sections of marshes at all four sites (see field photographs contained in chapter 8 & Appendix 7. Marshes in many areas show evidence for severe tidal scour, with in some cases, complete removal of material revealing the underlying coarser fluvial substrate. At Loch Creran, tidal flooding has resulted in the landward migration of *Puccinellia maritima* which is now colonizing the lower section of former lawn within the garden at Druimavuic House. At Loch Etive, evidence of established Oak and Beech trees now dying due to increased salinity, now influencing a freshwater filght-pond.
Aerial photography		At Loch Don a 1946 AD photograph clearly indicates that former, abandoned Runrigs (coastal allotments) situated at the head of inner Loch Don were being incised by encroaching marsh channels.
Local knowledge		At all sites local landowners, farmers and estate workers have stated that they now consider the sea to be encroaching and flooding the most seaward areas of livestock pasture more regularly compared to the decades preceding the 1990s. This supports some of the observational data.

Table 8.1: Summary of evidence derived from the various methods of enquiry to support the hypothesis of recent relative sea-level rise in western Scotland.

rise. The morphological adjustment currently taking place (highlighted in Figures 8.22, 8.23 and 8.24) may be enhanced by the less cohesive nature of these sediments in comparison to more southerly coastal wetlands. Adaptation of these marshes in response to changing hydrologic conditions is currently resulting in significant morphological alteration to the low marsh environment, which appears to be reverting to sand/mudflat with widespread remnant marsh tussocks evident at all site. These show evidence of active tidal-scouring signifying the predominance of tidal energy as opposed to incident wave energy in this process. Between the remnant tussock marsh morphology there is little evidence to suggest that new pioneer (low marsh) environments are forming.

As such, the marshes of Argyll display a morphological response to accelerated regional sea-level rise that deviates somewhat from the standard models of marsh migration documented in previous studies (Pethick, 1981; Stevenson *et al.*, 1986; Reed, 1990, 1995; Pethick, 1992; French, 1993; Cahoon and Reed, 1995; Allen, 1997).

Active erosion of the Argyll marshes may not have yet received the full attention of coastal managers within western Scotland as suggested by Pethick (1999). The current acceleration of regional RSL rise presents serious challenges for future coastal management strategies regarding the potential adjustment of lowland coastal habitats and archaeological preservation.

Chapter Nine

CONCLUSIONS

9.1: Conclusions of the study

Radiometric dating using ^{210}Pb provides a robust method for establishing models of marsh sedimentary evolution within the coastal wetlands of Argyll, western Scotland. The determination of activity peaks in ^{137}Cs resulting from known periods of anthropogenic environmental discharges (e.g. pre-1963 AD above-ground weapons testing and the 1986 AD Chernobyl accident) provides an independent dating method with which to compare ^{210}Pb derived sediment accumulation rates. Despite the detection of measurable ^{137}Cs and ^{241}Am activity at depths within the four cores that pre-date the onset of anthropogenic discharges, peaks in ^{137}Cs are well preserved. Remobilization of ^{137}Cs and ^{241}Am has occurred in these sediments (see Chapter Five). However, this has not displaced the position of activity peaks of these radionuclides used for dating purposes

In the core from Loch Scridain the peak in ^{241}Am activity attributed to 1963 AD provides a better marker horizon with which to identify the likely position of the ^{137}Cs activity peak associated with weapons fallout. This is not immediately obvious in the ^{137}Cs activity profile from this site due masking of the weapons fallout signature by input from Sellafield discharges.

In the cores from Loch Don, Loch Creran and Loch Etive, good general agreement is obtained between the CIC and CRS models which clearly identify the presence of ^{137}Cs and ^{241}Am at age/depths that pre-date the onset of anthropogenic inputs. In the cores from mainland Argyll the CRS age model clearly provides more accurate constraints upon artificial activity marker horizons. In the case of the core from Loch Don, the activity peak associated with pre-1963 AD weapons-test fallout is better constrained by the CIC model with the 1986 Chernobyl peak being more accurately determined via the CRS model.

^{210}Pb flux calculations give improved insight regarding the robustness of the dating models. In all cores the ^{210}Pb decay-corrected flux is in good general agreement with studies undertaken elsewhere (see Table 5.8) for much of the core depth analysed. This supports the use of the CRS model as the more appropriate dating model with atmospheric derived ^{210}Pb being the dominant source to the marsh surfaces. The apparent increase in ^{210}Pb flux recorded in the near-surface layer of the cores may now be compromising the dominance of atmospheric inputs with a current component of detrital delivery to the marsh surfaces.

The highly oxidized conditions throughout most of the core depths enhances the preservation of the depositional record as these sediments are flooded less frequently by tidal inundation thereby promoting the dominance of oxic conditions (see below).

Analysis of the solid-phase geochemical constituents of the four cores reveals that these marshes consist of highly mineralogenic material that has a complex poly-genetic origin at each site owing to the surrounding geology and Quaternary climatic history of the region. Organic carbon content (via LOI 550°C) is generally low (< 12 wt % at all sites). This is due in part to the prevailing climatic conditions, the nature of marsh sedimentary material and relatively poor diversity of the marsh vegetation at the four sites which are dominated by *Puccinellia maritima* in mature marsh settings. Little association between radionuclides and organic matter is evident in any of the marsh sequences.

Redox zonation in the cores reveals that oxic conditions prevail throughout much of the total depth of these sequences and that the formation of sulphidic conditions with associated formation of metal sulphides in highly anoxic sediments is not well established in all cores. As a result the entire inventory of $^{210}Pb_{excess}$ and ^{137}Cs activity is present within the oxidized sediments thereby minimizing the extent to which reducing conditions are effective in remobilization of the depositional record of these radionuclides.

Modeled rates of sediment accretion in the lower marsh settings suggest that marsh initiation may in part be due to short-term marine incursions during latter part of the nineteenth century. Over this time-period storm activity (derived from the proxy measurement of gale-day frequencies) was significantly enhanced relative to the record from the twentieth century. The significant marine incursion recorded in the cores from Loch Don and Loch Etive as an increase in sedimentation rates and geochemical fluxes of elements over a short time-scale during the mid to late 1920s is not fully understood. This period corresponds to an unprecedented period of low storm activity over the last ca. 120 years. In light of this a hitherto unconsidered mechanism must be sought to provide an explanation.

Distinct inflections in the modelled age/depth curves represent a transitional period in marsh evolution from low (immature) to high (mature) conditions as predicted in the published literature. These latter periods are characterized by overall marsh stability at all sites with reduced average sediment accumulation over the ca. 70 year period corresponding to this gradient change relative to that recorded in the lower sections of all cores. Fluctuations in mature marsh sedimentation rates may represent periods of marsh 'catch-up' following a period during which suspended sediment concentrations were reduced.

Rates of recorded sedimentation across the study transect vary considerably with a state of quasi-equilibrium (asymptotic) conditions evident in the marsh at Loch Scridain on the west of Mull. Within the Firth of Lorne differential marsh sites at Loch Don and Loch

Creran record a near-identical record of sediment accretion that is greater than twice the estimated rate of regional RSL rise for the region. A similar but slightly reduced rate of sediment accretion is also recorded from the marsh sediments at the head of Loch Etive. These increased rates of accretion may reflect enhanced suspended sediment concentrations at these sites over a sustained period during the twentieth century and therefore the response of these particular inter-tidal environments to coastal forcing.

However, all the marsh cores record a period of sedimentary evolution during which the marshes have been able to keep pace with the estimated rates of twentieth century sea-level rise. Detailed examination of the Loch Etive core using diatom analysis to support the radiometric dating and geochemical techniques confirms the interpretation of these sequences as being representative of a near steady-state marine transgressive phase through out much of the twentieth century.

Very recent increases in the rates of sediment accretion strongly suggest the influence of a regional coastal forcing mechanism, which corresponds to a previously predicted reversal and increase in the rate of RSL rise for the coastline of western Scotland at the end of the twentieth century. This is now manifest in a transition from relatively stable marsh depositional conditions to what appears to be a rapid marine transgression across the study region.

Much of this material is being derived from active erosion of the fronting low marsh environments at each site. The predominantly silty/sandy substrate of the sediments with low organic carbon content renders these marshes highly susceptible to coastal forcing as material is more easily removed by tidal currents and incident wave activity. This has implications for contaminant remobilisation within lowland coastal settings around the western coast. Comparison of the solid-phase geochemical data and background catchment concentrations reveal low (often below background) levels of metal concentrations. This supports the general viewpoint that these coastal inter-tidal settings represent near-pristine environments with no evidence of anthropogenically derived metal concentrations.

However, these marshes do contain significant quantities of the artificial radionuclide ^{137}Cs derived from a combination of pre-1963 AD above-ground weapons testing, Sellafield discharges and the 1986 AD Chernobyl accident. Erosion of marsh sediments therefore has the potential to re-introduce ^{137}Cs into the tidal prism thereby facilitating redistribution within western Scottish lowland coastal environments.

The recent response of marsh environments within western Scotland will require continued monitoring to assess the future morphodynamic response of valuable lowland coastal habitats under a scenario of continued rapid regional RSL rise. Management

strategies may be required that address the likely future reduction of valuable and ecologically important lowland coastal habitats within western Scotland.

9.2 Unanswered questions

The marshes investigated in this study are all situated within topographic settings which provide extremely sheltered conditions for marsh development. This research has not focused attention towards more exposed sites which are plentiful around the west coast of Scotland. Marshes that have developed in such settings may have responded to historical sea-level movements in a different manner and are likely to be even more susceptible to coastal forcing and storm activity.

The higher rates of sedimentation recorded from the marshes within the Firth of Lorne and at Loch Etive greatly exceed those from Loch Scridain which is in good agreement with the published estimations of twentieth century RSL rise for N W Europe. This raises further questions with regard to present-day rates of crustal uplift at sites in closer proximity to the inferred centre of maximum GIA. If the increased rates of sedimentation on these marshes are in fact the product of greater suspended sediment concentrations reaching the evolving marsh surfaces then extension of the research undertaken in this thesis is required to ascertain whether or not this is the case. If this proves to be unsubstantiated then a definitive answer may only be realized through the deployment of Global Positioning Systems situated in close proximity to the existing (thus far short-term) tide gauge stations around the western Scottish coastline. The stations at Ullapool and Port Ellen may therefore be good candidates for such work and this may be enhanced by the study of marshes also situated in close proximity to these tide gauge stations.

In light of the findings of this research continued monitoring of coastal wetlands with regard to the apparent rapid response to increased relative sea-level rise, now causing significant erosion and redistribution of material, is an urgent requirement.

References

Ackerman, F. (1980). Aprocedure for correcting grain-size effects in heavy metal analysis of estuarine and coastal sediments. *Environmental Technology Letters*, **1**, 518-527.

Adam, P. (1978). Geographical variation in British saltmarsh vegetation. *Journal of Ecology*, **66**, 339-366.

Adam, P. (1990). *Saltmarsh ecology*. Cambridge University Press. pp. 461.

Allard, B., Olofsson, U. and Torstenfelt, B. (1984). Environmental actinide chemistry. *Inorganica Chimica Acta*, **94**, 205-221.

Allen. JRL. and Rae, J.E. (1988). Vertical salt-marsh accretion since the roman period in the Severn Estuary, southwest Britain. *Marine Geology*, **83**, 225-235.

Allen. JRL. (1989). Evolution of salt-marsh cliffs in muddy and sandy systems: a qualitative comparison of British west-coast estuaries. *Earth Surface Processes and Landforms*, 14, 85-92.

Allen. J.R.L. (1990). Salt marsh growth and stratification: A numerical model with special reference to the Severn Estuary, southwest Britain. *Marine Geology*, 95, 77-96.

Allen. J.R.L. (1990). Constraints on measurement of sea-level movements from salt-marsh accretion rates. *Journal of the Geological Society, London,* (short paper), Vol. **147**, 5-7.

Allen. J.R.L., (1991). Salt-marsh accretion and sea-level movement in the inner Severn Estuary, southwest Britain: the archaeological and historical contribution. *Journal of the Geological Society, London,* Vol. **148**, 485-494.

Allen, J.R.L. (1997). Simulation models of salt-marsh morphodynamics: some implications for high-intertidal sediment couplets related to sea-level change: *Sedimentary Geology*, 113, 211-223.

Allen, J.R.L. (2000). Holocene coastal lowlands in NW Europe: autocompaction and the uncertain ground. *In*: Pye, K. and Allen, J.R.L (eds). 2000. *Coastal and Estuarine Environments: sedimentology, geomorphology and geoarchaeology*. Geological Society, London, Special Publications, **175**, 239-252.

Allen, J.R.L. (2000). Morphodynamics of Holocene salt marshes: a review sketch from the Atlantic and Southern North Sea coasts of Europe. *Quaternary Science Reviews*, **19**, 1155 – 1231.

Allen, J.R.L. and Pye, K. (1992). (Eds). Saltmarshes: Morphodynamics, Conservation and Engineering Significance. Cambridge University Press. pp. 184.

Allen. J.R.L., Rae, J.E. and Zanin, P.E. (1990). Metal speciation (Cu, Zn, Pb) and organic matter in an oxic salt marsh, Severn Estuary, South-west Britain. *Marine Pollution Bulletin,* **21**, 574-580.

Allen, J.R.L. and Duffy, M.J. (1998). Medium-term sedimentation on high intertidal mudflats and salt marshes in the Severn Estuary, SW Britain: the role of wind and tide. *Marine Geology*, **150**, 1-27.

Allen, J.R.L. and Duffy, M.J. (1998). Temporal and spatial depositional patterns in the Severn Estuary, southwestern Britain: intertidal studies at spring-neap and seasonal scales, 1991-1993. *Marine Geology*, **146**, 147-171.

Allen, J. R. L., Rae, J.R., Longworth, G., Hasler., S.E. and Ivanovich, M. (1993). A comparison of the 210-Pb dating technique with three other independent dating methods in an oxic salt-marsh sequence. *Estuaries*, **16**, 670 - 677.

Alexander, C.R., Smith, R.G., Calder, F.D., Schropp, S.J. and Windom, H.L. (1993). The historical record of metal enrichment in two Florida estuaries. *Estuaries,* **16**, 627-9-637.

Alvisi, F. and Frignani, M. (1996). ^{210}Pb-derived sediment accumulation rates for the central Adriatic Sea and crater lakes Albano and Nemi (central Italy). *Memoirs Institute of Italian Idrobiology*, **55**, 241-246

Anderson, J.G.C. (1937). The Etive granite complex. *Quaterly Journal of the Geological Society of London,* **93**, 487-532.

Anderson, T. J., Mikkelsen, O.A., Møller A.L. and Pejrup, M. (2000.). Deposition and mixing depths on some European inter-tidal mudflats based on ^{210}Pb and ^{137}Cs activities. *Continental Shelf Research*, **20**, 1569-1591.

Anderson, R.F., Schiff, S.L. and Hesslein, R.H. (1987). Determining sediment accumulation and mixing rates using ^{210}Pb, ^{137}Cs and other tracers: problems due to post-depositional mobility or coring artifacts. *Canadian Journal of Fisheries and Aquatic Science*, **44**. 231-5-250.

Andrews, J.T. (1968). Postglacial Rebound in Artic Canada: similarity and prediction of uplift curves. *Canadian Journal of Science*, **5**, 39.

Anspaugh, L.R., Catlin, R.J. and Goldman, M. (1988). The global impact of the Chernobyl reactor accident. *Science*, **242**, 1513-1519.

Appleby, P.G. and Oldfield, F. (1978). The calculation of Pb-210 dates assuming a constant rate of supply of unsupported Pb-210 to the sediment. *Catena,* **5**, 1-8.

Appleby, P. G., Richardson, N. and Nolan, P.J. (1991). ^{241}Am dating of lake sediments. *Hydrobiologi,* **214**, 35 - 42.

Appleby, P.G. and Oldfield, F. (1992). Application of 210-Lead to sedimentation studies. *In*: Ivanovich, M. and Harmon, R.S. (eds). *Uranium series disequilibrium: appplications to earth, marine and environmental sciences*. Oxford Science, 2nd Edition, Oxford, 731-783.

Appleby, P.G. (2001). Chronological techniques in recent sediments. *In*: W.M. Last and J. P. Smol, (eds). *Tracking Enviromental Change Using Lake Sediments. Volume 1: Basin Analysis, Coring and Chronological Techniques*. Kluwer Academic Publishers, Dordrecht, The Netherlands. pp 171-203.

Armentano, T.V. and Woodwell, G.M. (1975). Sedimentation rates in a Long Island marsh determined by ^{210}Pb dating. *Limnology and Oceanography* , **20**, 452-456.

Aston, S.R. and Duursma, E.K. (1973). Concentration effects on ^{137}Cs, ^{65}Zn, ^{60}Co and ^{106}Ru sorption by marine sediments, with geochemical implications. *Netherlands Journal of Sea Research*, **6**, 225-240.

Barnes, C.E. and Cochran, J.K. (1993). Uranium geochemistry in estuarine sediments: Controls on removal and release processes. *Geochimica et Cosmochimica Acta,* Vol. **57**, p. 555-569.

Bartolody, J., Chritiansen, H. and Kunzendorf, H. (2004). Long term variations in backbarrier salt marsh deposition on the Skallingen peninsula – the Danish Wadden Sea. *Marine Geology*, **203**, 1-21.

Batchelor, R.A. (1987). Geochemical and petrochemical characteristics of the Etive granitoid complex, Argyll. *Scottish Journal of Geology*, **23**, 227-249.

Battarbee, R.W. (1986). Diatom Analysis. *In*: Berglund, B.E. (ed.), *Handbook of Holocene Palaeoecology and Palaeohydrology*. John Wiley and Sons Ltd, Chichester. pp. 896 p. 527 – 570.

Battiston, G.A., Degetto, S., Gerbasi, R., Sbrignadello, G. and Tositti.L. (1988). The use of Pb-210 and Cs-137 in the study of sediment pollution in the Lagoon of Venice. *Science of the Total Environment,* **77**, 15-23.

Beaudion, A. (2003). A comparison of two methods for estimating the organic matter content of sediments. *Journal of Palaeolimnology*, **29**, 387-390.

Beeftink, W.G. (1966). Vegetation and habitat of the salt marshes and plains of in the south-western part of the Netherlands. *Wentia*, **15**, 83-108.

Beeftink, W.G. (1979). The structure of salt marshes in relation to environmental disturbances. *In*: Jeffries, R.L. and Davy, A.J. (eds). *Ecological processes in coastal environments*. Blackwell Scientific Publications, Oxford, 77-94.

Beeftink, W.G. and Rozema. (1988). The nature and functioning of salt marshes. In: Salomans, W., Bayne, B.L., Duursma, E.K. and Förstner, U. (eds.), *Pollution of the North Sea: An assessment.* Springer, Berlin, pp. 59-87.

Belzile, N. and Tessier, A. (1990). Interactions between arsenic and iron oxyhydroxides in natural sediments. *Geochimica et Cosmochimica Acta*, **54**, 103 109.

Bendell-Young, L. and Harvey, H.H. (1992). The relative importance of manganese and iron oxides and organic matter in the sorption of trace metals by surficial lake sediments. *Geochimica et Cosmochimica Acta,* **56**, 1175-1186.

Benninger, L.K., Aller, R.C., Cochran, J.K. and Turekian, K.K. (1979). Effects of biological mixing on the ^{210}Pb chronology and trace metal distribution in a Long Island Sound sediment core. *Earth and Planetary Science Letters*, **43**, 241-259.

Benoit, G. and Hemmond, H.F. (1990). ^{210}Pb and ^{210}Pb remobilization from lake sediments in relation to manganese cycling. *Environmental Science and Technology*, **24**, 1224-1234.

Benoit, G. and Hemmond, H.F. (1991). Evidence for diffusive redistribution of ^{210}Pb in lake sediments. *Geochimica et Cosmochimica Acta*, **55**, 1963-1975.

Berner, R.A. (1980). *Early Diagenesis: a theoretical approach.* Princeton University Press, Princton, New Jersey. 241 pp.

Berner, R.A. (1981). A new geochemical classification of sedimentary environments. *Journal of Sedimentary Petrology*, **51**, 359-365.

Berner, R.A. (1985). Sulphate reduction, organic matter decomposition and pyrite formation. *Philosophical Transactions of the Royal Society of London*, Series A. **315**, 25-38.

Bertine, K.K. and Turekian, K.K. (1973). Molybdenum in marine deposits, *Geochimica et Cosmochimica. Acta*, **37**, 1415-1434

Beyens, L and Denys, L, (1982). Problems in diatom analysis of deposits: Allochthonous valves and fragmentation. *Geologie en Mijnbouw*, **61**, 159-162.

BGS. (1995). *The Grampian Highlands.* British Regional Geology. British Geological Survey, Keyworth, UK. pp. 214.

BGS (1990). *Regional geochemical atlas: Argyll.* (Keyworth, Nottingham, British Geological Survey.

Bierman, P., Lini, A., Zehfuss, P., Church, A., Davis, P.T., Southon, J. and Baldwin, L. (1997). Post-glacial ponds and alluvial fans: Recorders of Holocene landscape history. *GSA Today*, Vol 7 No. 10, 1-8.

Binford, M. W. (1990). Calculation and uncertainty analysis of ^{210}Pb dates for PIRLA project lake sediment cores. *Journal of Paleolimnology*, **3**. 253 - 267.

Bloom, A.L. (1964). Peat accumulation and compaction in a Connecticut coastal marsh. *Journal of Sedimentary Petrology,* **34**, 599 - 603.

Bloom, A.L. and Stuvier, M. (1963). Submergemce of the Connecticut coast. *Science*, **139**, 332-334.

BNFL. (1998). Annual report on discharges and monitoring of the environment, 1998. British Nuclear Fuels plc.

Bonnet, P.J.P., Appleby, P.G. and Oldfield, F. (1988). Radionuclides in coastal and estuarine sediments from Wirral and Lancashire. *Science of the Total Environment*, **70**, 215-236.

Bradley, P.E., Economides, B.E., Baxter, M.S. and Ellet, D.J.(1988). Sellafield radiocaesium as a tracer of water movement in the Scottish coastal zone. *In*: Guary, J.C., Guegueniat, P. and Pentreath, R.J. (eds). *Radionuclides: a tool for oceanography*. Elsevier Publishing Ltd, 281 - 293.

Brezonik, P.L. and Engstom, D.R. (1998). Modern and historic accumulation rates of phospherous in Lake Okeachobee, Florida. *Journal of Palaeolimnology*, **20**, 31-46.

Bricker, S.B. (1993). The history of Cu, Pb and Zn inputs to Narragansett Bay, Rhode Island as recorded by salt marsh sediments. *Estuarie.* **16**, 589-607.

Brick-Urso, S., Nixon, S.W., Cochran, J.K., Hirschberg, D.J. and Hunt, C. (1989). Accretion rates and sediment accumulation in Rhode Island salt marshes. *Estuaries,* **12**, 300-317.

Brown, S.L. (1998). Sedimentation on a Humber saltmarsh. *In*: Black, K.S., Paterson, D.M. and Cramp, A. (eds). *Sedimentary Processes in the Intertidal Zone*. Geological Society, Lonodon, Special Publications, **139**, 69-83.

Boulegue, J., Lord, C.J. and Church, T.M. (1982). Sulphur speciation and associated trace metals in the pore waters of Great Marsh, Delaware. *Geochimica et Cosmochimica Acta*, **46,** 453-464.

Boumans, R.M.J. and Day, J.W. (1993). High precision measurements of sediment elevation in shallow coastal areas using a sedimentation-erosion table. *Estuaries*, **16**, 375-380.

Bourma, A.H. (1963). A graphic presentation of the facies model of salt marsh deposits. *Sedimentology*, **2**, 122 -129.

Boyle, J. (2001). Inorganic geochemical methods in palaeolimnology. *In*: Last, W.M. and Smol, J.P. (eds.), *Tracking Environmental Change Using Lake Sediments. Volume 2: Physical and Geochemical Methods*. Kluwer, Dordrecht, pp. 504. p. 83-141.

Boyle, J. (2004). A comparison of two methods for estimating the organic matter content of sediments. *Journal of Palaeolimnology*, **31**, 125-127.

Brumsack, H.L. and Gieskes, J.M. (1983). Interstitial water trace metal chemistry of laminated sediments from the Gulf of California, Mexico. *Marine Chemistry*, **14**, 89-106.

Burckle, L.H., 1978. Marine Diatoms. *In:* Haq, B.U. and Boursma, A. (Eds). *Introduction to Marine Micropalaeontology*. Elsevier Publishers Ltd, 245–266, pp. 376.

Burdige, D.J. (1993). The biogeochemistry of Mn and Fe reduction in marine sediments. *Earth Science Reviews*, **35**, 249-284.

Carter, R.W.G. (1992). Sea-level changes: past, present and future. *Quaternary Proceedings*, No. **2**, 111-132.

Cacador, I., Vale, C. and Catarino, F. (1996). Accumulation of Zn, Pb, Cu, Cr and Ni in sediments between roots of the Tagus Estuary salt marshes, Portugal. *Estuarine, Coastal and Shelf Science.* **42**, 393 - 403.

Caetano, M. and Vale, C. (2002). Retention of arsenic and phospherous in iron-rich concretions of Tagus salt marshes. *Marine Chemistry*, **79**, 261-271.

Calvert, S.E. and Pedersen, T.F. (1993). Geochemistry of recent oxic and anoxic sediments: Implications for the marine record. *Marine Geology*, **113**, 67-88.

Cahoon, D.R. and Reed, D.J. (1995). Relationships among marsh surface topography, hydroperiod and soil accretion in a deteriorating Louisiana salt marsh. *Journal of Coastal Research*, **11**, 357-369.

Cahoon, D.R., Lynch, J.C. and Powell, A.N. (1996). Marsh vertical accretion in a southern California estuary, USA. *Estuarine, Coastal and Shelf Science,* **43**, 19-32.

Cahoon, D.R. and Lynch, J.C. (1997). Vertical accretion and shallow subsidence in a mangrove forest of southwestern Florida, USA. *Mangroves and Salt Marshes*, **1**, 173-186.

Cahoon, D.R., French, J.R., Spencer, T., Reed, D.J. and Möller, I. (2000). Vertical accretion versus elevational adjustment in UK saltmarshes: an evaluation of alternative methodologies. *In*: Pye, K. and Allen, J.R.L (eds). 2000. *Coastal and Estuarine Environments: sedimentology, geomorphology and geoarchaeology*. Geological Society, London, Special Publications, **175**, 223-238.

Callaway, J.C., Nyman, J.A. and DeLaune, R.D. (1996a). Sediment accretion in coastal wetlands: a review and simulation of model processes. *Current Topics in Wetland Bio-geochemistry*, **2**, 2-23.

Callaway, J.C., DeLaune, R.D. and Patrick, W.H. Jnr. (1996b). Chernobyl ^{137}Cs used to determine sediment accretion rates at selected northern European coastal wetlands. *Limnology and Oceanography,* **4**, 444-450.

Callaway, J.C., DeLaune, R.D. and Patrick, W.H. (1998). Heavy metal chronologies in selected coastal wetlands from Northern Europe. *Marine Pollution Bulletin*. **Vol. 36**, No. 1. 82-96.

Cambray, R.S., Cawse, P.A., Garland, J.A., Gibson, J.A.B., Johnson, P., Lewis, G.N.J., Newton, D., Salmon, L. and Wade, B.O. (1987). Observations on radioactivity from Chernobyl accident. *Nuclear Energy*, 26, 77-101.

Canfield, D.E., Thamdrup, B. and Hansen, J,W. (1993). The anaerobic degradation of organic matter in Danish coastal sediments: iron reduction, manganese reduction and sulphate reduction. *Geochimica et Cosmochimica Acta*, **57**, 3867-3883.

Cartaxana, P. and Lloyd, D. (1999). N_2, N_2O and O_2 profiles in a Tagus estuary salt marsh. *Estuarine, Coastal and Shelf Science*, **48**, 751-756.

Carter, M.W. and Moghissi, A.A. (1977). Three decades of nuclear testing. *Health Physics*, **33**, 55-71.

Carruesco, C. and Lapaquellerie, Y. (1985). Heavy metal pollution in the Arcachon Basin (France): bonding states. *Marine Pollution Bulletin*, **16** , 493-497.

Carter, R.W.G., Orford, J.D., Jennings, S.C., Shaw, J. and Smith, J.P. (1992). Recent evolution of a paraglacial estuary under conditions of rapid sea-level rise: Chezzetcook Inlet, Nova Scotia. *Proceedings of the Geologists Association*, **103**, 167-185.

Casey, W.H. and Lasaga, A.C. (1987). Modelling solute transport and sulphate reduction in marsh sediments. *Geochimica et Cosmochimica Acta*, **51**, 1109-1120.

Cearreta, A., Irabien, M.J., Leorri, E., Yusta, I., Croudace, I.W. and Cundy, A.B. (2000). Recent anthropogenic impacts on the Bilbao Estuary, Northern Spain: geochemical and microfaunal evidence. *Estuarine, Coastal and Shelf Science*, **50**, 571-592

Chanton, J. P., Martens, C.S and Kipphut, G.W. (1983). Lead-210 sediment geochronology in a changing coastal environment. *Geochimica et Cosmochimica Acta*, **47**, 1791 - 1804.

Chapman, V.J. (1942). Studies in salt marsh ecology. Section VIII. *Journal of Ecology*, **29**, 69-82.

Chapman, V.J. (1960). *Saltmarshes and Salt Deserts of the World*. Leonard Hill, London.

Chester, R. (2003). *Marine Geochemistry*. 2nd Edition. Blackwell Science Ltd, pp 506.

Chibowski, S. and Zygmunt, J. (2002). The influence of the sorptive properties of organic soils on the migration rate of 137Cs. *Journal of Environmental Radioactivity*, **61**, 213-223.

Christensen, E. R. (1982). A model for the radionuclides in sediments influenced by mixing and compaction. *Journal of Geophysical Research*, **87**. (No. C1), 566-572.

Church, T.M., Lord, C.J. and Somayajulu, B.L.K. (1981). Uranium, Thorium and Lead nuclides in a Delaware salt marsh sediment. *Estuarine, Coastal and Shelf Science*, **13**, 267-275.

Church, T.M., Sarin, M.M., Fleisher, M.Q. and Ferdelman, T.G. (1996). Salt marshes: an important coastal sink for dissolved Uranium. *Geochimica et Cosmochimica Acta.* **60**, 3879-3887.

Clark, J.S. and Patterson, W.A. (1985). The development of a tidal marsh: upland and oceanic influences. *Ecological Monographs,* **55**, 189-217.

Clark, M.J. and Smith, F.B. (1988) Wet and dry deposition of Chernobyl releases. *Nature*, **332**, 245-249.

Clayton, K. and Shamoon, N. (1998a). A new approach to the relief of Great Britain: I. The machine-readable database. *Geomorphology*, **25**, 31-42.

Clayton, K. and Shamoon, N. (1998b). A new approach to the relief of Great Britain: II. A classification of rocks based on relative resistance to denudation. *Geomorphology*, **25**, 155-171.

Clayton, K. and Shamoon, N. (1999). A new approach to the relief of Great Britain III. Derivation of the contribution of neotectonic movements and exceptional denudation to the present relief. *Geomorphology*, **27**, 173-189.

Clifton, R.J. and Hamilton, E.I. (1982). The application of radioisotopes in the study of estuarine sedimentary processes. *Estuarine, Coastal and Shelf Science,* **14**, 433-446.

Clifton, R.J., Watson, P.G., Davey, J.T. and Frickers, P.E. (1995). A study of processes affecting the uptake of contaminants by intertidal sediments using the radioactive tracers ^{7}Be, ^{137}Cs and unsupported ^{210}Pb. *Estuarine, Coastal and Shelf Science*, 41, 459-474.

Cochran, J.K., Carey, A.E., Sholkovitz, E. and Suprenant, L.D. (1986). The geochemistry of uranium and thorium in coastal marine sediments and sediment porewaters. *Geochimica et Cosmochimica Acta,* **50**, 663-680.

Coleman, M.L., Hedrick, D.B., Lovley, D.R., White, D.C. and Pye. K. (1993). Reduction of Fe (III) in sediments by sulphate-reducing bacteria. *Nature,* **361**, 436-438.

Comans, R.N.J. and Hockley, D.E. (1992). Kinectics of cesium sorption on illite. *Geochimica et Cosmochimica Acta,* **56**, 1157-1194.

Comans, R.N.J., Middelberg, J.J., Zonderhuis, J., Woittiez, J.R.W., de Lange, G.J., Das, H.A. and van der Weijden, C.H. (1989). Mobilization of radiocaesium in pore waters of lake sediments. *Nature,* **339**, 367-369.

Comans, R.N.J., Haller, M. and De Preter, P. (1991). Sorption of cesium on illite: non-equilibrium behaviour and reversibility. *Geochimica et Cosmochimica Acta*, **55**. 433-440.

Comans, R.N.J., Hilton, J., Voitsekhovitch, G., Laptev, G., Popov, V., Madruga, M.J., Bulgakov, A., Smith, J.T., Movchan, N. and Konoplev. (1998). Acomparative study of radiocaesium mobility measurements in soils and sediments from the catchment of a small upland oligotrophic lake (Devoke Water, U.K.). *Water Resources*, **32**, No.9, 2846-2855.

Comber, D.P.M. (1995). Culbin Sands and the Bar. *Scottish Geographical Magazine*, **111**, (1), 54-57.

Connor, R. and Chmura G. (2000). Seasonal below-ground growth dynamics of Spartina alterniflora, Spartina patens and Plantago maritima in a Bay of Fundy Salt Marsh. *Marine Ecology Progress Series,* **Vol. 204**, 101-110.

Craft, C.B., Seneca, E.D. and Broome, S.W. (1993). Vertical accretion in microtidal regularly and irregularly flooded estuarine marshes. *Estuarine, Coastal and Shelf Science*, **37**, 371-386.

Cremers, A., Elsen, A., De Preter, P. and Maes, A. (1988). Quantitative analysis of radiocaesium retention in soils. *Nature*, **335**, 247-249.

Crooks, S, and Pye, K. (2000). Sedimentological controls on the erosion and morphology of saltmarshes: implications for flood defence and habitat recreation. *In*: Pye, K. and Allen, J.R.L (eds). 2000. *Coastal and Estuarine Environments: sedimentology, geomorphology and geoarchaeology.* Geological Society, London, Special Publications, **175**, 208-222.

Croudace, I.W. and Williams-Thorpe, O. (1988). A low dilution, wavelength-dispersive X-ray procedure for the analysis of archaeological rock artifacts. *Archaeometry*, **30**, 227-236.

Croudace I.W. and Gilligan, J. (1990). Versatile and accurate trace element determinations of in iron-rich and other geological samples using X-ray fluorescence analysis. *X-ray Spectrometry*, **19**, 117-123.

Croudace, I.W. (1991). A reliable and accurate procedure for preparing low activity efficiency calibration standards for germanium gamma-ray spectrometers. *Journal of Radioanalytical, Nuclear and Chemistry Letters,* **153, (2),** 151-162.

Croudace, I.W. and Cundy, A.B. (1995). Heavy metal and hydrocarbon pollution in recent sediments from Southamton Water, Southern England: A geochemical and isotopic study. *Environmental Science and Technology*, **29**, 1288–1296.

Crozaz, G., Picciotto, E. and De Breuck. (1964). Antarctic snow chronology with ^{210}Pb. *Journal of Geophysical Research*, **69**, 2597-2604.

Crozaz, G. and Langway, C.C. (1966). Dating Greenland firn-ice cores with ^{210}Pb. *Earth and Planetary Science Letters*, **1**, 194-196.

Crusius, J., Calvert, S., Pederson, T. and Sage, D. (1996). Rhenium and molybdenum enrichments in sediments as indicators of oxic, sub-oxic and sulphidic conditions of deposition. *Earth and Planetary Science Letters*, 145, Issue 1-4, 65-78.

Cundy, A.B. (1994). Radionuclide and geochemical studies of recent sediments from the Solent estuarine system. PhD Thesis, University of Southampton.

Cundy, A.B. and Croudace, I.W. (1995a). Sedimentary and geochemical variations in a salt marsh/mud flat environment from the mesotidal Hamble estuary, southern England. *Marine Chemistry*, **51**, 115-132.

Cundy, A.B. and Croudace, I.W. (1995b). Physical and chemical associations of radionuclides and trace metals in estuarine sediments: an example from Poole Harbour, southern England. *Journal of Environmental Radioactivity*, **29**, 191-212.

Cundy, A.B. and Croudace, I.W. (1996). Sediment accretion and recent sea level rise in the Solent, Southern England: Inferences from radiometric and geochemical studies. *Estuarine, Coastal and Shelf Science*, **43**, 449-467.

Cundy, A.B., Croudace, I.W., Thompson, J. and Lewis, J.T. (1997). Reliability of salt marshes as "Geochemical Recorders" of pollution input: A case study from contrasting estuaries in Southern England. *Environmental Science and Technology,* **31**. 1093-1101.

Cundy, A.B., Collins, P.E.F., Turner, S.D., Croudace, I.W. and Horne, D. (1998). 100 years of environmental change in a coastal wetland, Augusta Bay, southeast Sicily: evidence from geochemical and palaeoecological studies. *In*: Black, K.S., Paterson, D.M. and Cramp, A. (eds). *Sedimentary Processes in the Intertidal Zone*. Geological Society of London Special Publication, **139**, 243-254.

Cundy, A.B., Kortekaas, S., Dewez, T., Stewart, I.S., Collins, PEF., Croudace, I.W., Maroukian, H., Papanastassiou, G., Gaki-Papanastassiou, P., Pavloupous, K. and Dwason, A.G. (2000). Coastal wetlands as recorders of earthquake subsidence in the Aegean: a case study of the 1984 Gulf of Atalanti earthquakes, Central Greece. *Marine Geology*, 170, Issues 1-2, 3-26.

Cundy, A.B., Long, A.J., Hill, C.T., Spencer, C. and Croudace, I.W. (2002). Sedimentary response of Pagham Harbour, southern England to back-barrier breaching in AD 1910. *Geomorphology,* **46**, 163-176.

Cundy, A.B., Croudace, I.W., Cearreta, A. and Irabien, M.J. (2003). Reconstructing historical trends in metal input in heavily-disturbed, contaminated estuaries: studies from Bilbao, Southampton Water and Sicily. *Applied Geochemistry*, **18**, 311-325.

Cutter, G.A. and Velinsky, D.J. (1988). Temporal variations of sedimentary sulphur in a Delaware salt marsh. *Marine Chemistry*, **23**, 311-327.

Daoust, R.J., Moore, T.R., Chmura, G.L. and Magenheimer, J.F. (1996). Chemical evidence of environmental changes and anthropogenic influences in a Bay of Fundy saltmarsh. *Journal of Coastal Research*, **12.** (2), 520-533.

Davis, C.A. (1910). Salt marsh formation near Boston and its geological significance. *Economic Geology*, **5**, 623-639.

Davis, R.B., Hess, C.T., Norton, S.A., Hanson, D.W., Hoagland, K.D. and Anderson, D.S. (1984). ^{137}Cs and ^{210}Pb dating of sediments from soft-water lakes in New England (USA) and Scandanavia, a failure of ^{137}Cs dating. *Chemical Geology*, **44**, 151-185.

Davidson-Arnott, R.G.D., van Proosdij, D., Ollerhead, J. and Schostak, L. (2002). Hydrodynamics and sedimentation in salt marshes: examples from a macrotidal marsh, Bay of Fundy. *Geomorphology*, **48**, 209-231.

Dawson, A.G. (1980b). The Low Rock Platform in Western Scotland. *Proceedings of the Geologists' Association*, **91**, 339-344.

Dawson, A.G. (1982). Lateglacial sea-level changes and ice limits in Islay, Jura and Scarba, Scottish Inner Hebrides. *Scottish Journal of Geology*, **18**, 253-265.

Dawson, A.G. (1984). Quaternary sea-level changes in western Scotland. *Quaternary Science Reviews*, **3**, 345-368.

Dawson, S. and Smith, D.E. (1997). Holocene relative sea-level changes on the margin of a glacio-isostatically uplifted area: an example from Caithness, Scotland. *The Holocene*, **7.** (1), 59-77.

Dawson, S., Dawson., A.G. and Edwards, K.F. (1998). Rapid Holocene relative sea-level changes in Gruinart, Isle of Islay, Scottish Inner Hebrides. *The Holocene*, **8.** (2), 183-195.

Dawson, A.G., Smith, D.E. and Dawson, S. (2001). *The Potential Impacts of Climate Change on the Sea Levels around Scotland.* Scottish Natural Heritage, Research Survey and Monitoring Report No. **178**. Perth: Scottish Natural Heritage.

Dawson, A.G., Hickley, K., Holt, T., Elliot, L., Dawson, S., Foster, I.D.L., Wadhams, P., Jonsdottir, I., Wilkinson, I., McKenna, J., Davis, N.R. and Smith, D.E. (2002). Complex North Atlantic Oscillation (NAO) Index signal of historic North Atlantic storm-track changes. *The Holocene,* 12, (3), 363-369.

Day, J.P and Cross, J.E. (1981). ^{241}Am from the decay of ^{241}Pu in the Iris Sea. *Nature*, **292**, 43-45

Day, J.W., Rybczyk, J., Scarton, F., Rismondo, A., Are, D. and Cecconi, G. (1999). Soil accretionary dynamics, sea-level rise and the survival of wetlands in Venice Lagoon: A field and modelling approach. *Estuarine, Coastal and Shelf Science*, **49**, 607-628.

Degens, E.T. and Mopper, K. (1976). Factors Controlling the Distribution and Early Diagenesis of Organic Material in Marine Sediments. *In*: Riley, J.P. and Chester, R. (Eds.). *Chemical Oceanography*, London. Academic Press. pp. 414, p. 59-113.

de Jonge, V.N. (1985). The occurrence of 'epipsammic' diatom populations: a result of interaction between physical sorting of sediment and certain properties of diatom species. *Estuarine, Coastal and Shelf Science,* **21**, 607-622.

DeLaune, R.D., Patrick, W.H. and Buresh, R.K. (1978). Sedimentation rates determined by ^{137}Cs dating in a rapidly accreting salt marsh. *Nature,* **275.** 532-533.

DeLaune., R.D., Baumann, R.H. and Gosselink, J.G. (1983). Relationships among vertical accretion, coastal submergence, and erosion in a Louisiana Gulf coast marsh. Journal of *Sedimentary Petrology*, **53.** (1), 147-157.

DeLaune., R.D., Nyman, J.A. and Patrick, W.H. (1994). Peat collapse, ponding and wetland loss in a rapidly submerging coastal marsh. *Journal of Coastal Research*, **10.** (4), 1021-1030.

Denys, L. (1984). Diatom analysis of coastal deposits: methodological aspects. *Bulletin van de Begische Vereniging voor Geologie*, **93**, 291-295.

Denys, L. and Batemann, C. (1995). Holocene evolution of relative sea-level and local mean water spring tides in Belgium – a first assessment. *Marine Geology*, **124**, 1-19.

Denys, L. and DeWolf, H. (1999). Diatoms as indicators of coastal palaeo-environments and relative sea-level change. *In:* Stoermer, E.F. and Smol, J.P. (eds). *The Diatoms: Applications for the Environmental and Earth Sciences*. Cambridge University Press. 277-297, pp.469.

Dijkema, K.S. (1984). Development and classification of main salt marshes biotypes in Europe. *In*: Dijkema, K.S., Beeftink, W.G., Doody, J.P., Gehu, J.M, Heydemann, B. and Rivas- Martinez, S. (eds). *Salt Marshes in Europe*. Strasbourg Council of Europe, 8-15.

Dijkema, K.S. (1987). The Geography of salt marshes in Europe. *Zeitschrift für Geomorphologie*, **31**, 489-199.

Din, Z.B. (1992). Use of aluminium to normalise heavy-metal data from estuarine ans coastal sediments of Straits of Melaka. *Marine Pollution Bulletin*, **24**, No. 10, 484-491.

Doody, J.P. (1992). The conservation of British saltmarshes. In: Allen, J.R.L.and Pye, K. (eds). Saltmarshes: Morphodynamics, Conservation and Engineering Significance. Cambridge University Press. pp. 184.

Douglas, B.C. (1991). Global sea-level rise. *Journal of Geophysical Research*, **96**, 6981-6992.

Dyer, F.M. (2001). The effect of rising sea-levels on the process of marsh sediment accretion: a radiochemical and geochemical study. PhD University of Southampton, Unpublished, pp. 297.

Dyer, F.M., Thompson, J., Croudace, I.W., Cox, R. and Wadsworth, R.A. (2002). Records of change in salt marshes: A radiochronological study of three Westerschelde (SW Netherlands) marshes. *Environmental Science and Technology*, **36**, 854-861.

Eades, L.J., Farmer, J.G., MacKenzie, A.B., Kirika, A. and Bailey-Watts. (1998). High-resolution profile of radiocaesium deposition in Loch Lomond sediments. *Journal of Environmental Radioactivity*, **39**, 107-115.

Eastman, K.W. and Church, T.M. (1984). Behaviour of iron, manganese, phosphate and humic acid during mixing in a Delaware salt marsh creek. *Estuarine, Coastal and Shelf Science*, **18**, (4), 447-458.

Eckman, J.E. and Nowell, A.R.M. (1984). Boundary skin friction and sediment transport about an animal-tube mimic. *Sedimentology*, **31**, 851-862.

Edwards, A. and Edelsten, D.J. (1977). Deep water renewal of Loch Etive: A three basin Scottish fjord. *Estuarine and Coastal Marine Science*, **5**, 575-595.

Elderfield, H., and Truesdale, V.W. (1980). On the biophilic nature of iodine in seawater. *Earth and Planetary Science Letters*, **50**, 105-114.

Elderfield, H., McCaffrey, R.J., Luedtke, N., Bender, M. and Truesdale,V.W. (1981).Chemical Diagenesis in Narragansett Bay sediments. *American Journal of Science*, **281**, 1021-1055.

Emery, K.O. and Aubrey, D.G. (1985). Glacial rebound and relative sea-levels in Europe from tide-gauge records. *Tectonophysics,* **120**, 239-255.

Eronen M., Kankainen, T and Tsukada, M. (1987). Late Holocene sea-level record in a core from the Puget lowland, Washington. *Quaternary Research,* **27**, 147-159.

Evans, D.W., Alberts, J.J. and Clark, R.A. III. (1983). Reversible ion-exchange fixation of caesium-137 leading to remobilization from resevoir sediments. *Geochimica et Cosmochimica Acta,* **47**, 1041-1049.

Fabbi, B.P. (1978). Geology. *In*: Herglotz, H.K and Birks, L.S. (eds.), *X-ray spectrometry.* Practical Spectrometry Series Vol 2. Marcel Dekker, Inc. pp. 518.

Farmer, J.G. and Lovell, M.A.(1986). Natural enrichment of arsenic in Loch Lomond sediments. *Geochimica et Cosmochimica Acta,* **50**, 2059-2067.

Ferdelman, T.G. Church, T.M. and Luther III, G.W. (1991). Sulphur enrichment of humic substances in a Delaware salt marsh sediment core. *Geochimica et Cosmochimica Acta,* **55**, (4), 979-988.

Firth, C. R. (1993). Late Devensian and Holocene Glacio-isostatic Uplift Patterns in Scotland. *Quaternary Proceedings*, **No. 3**, 1-14.

Firth, C.R. and Stewart, I.S. (2000). Postglacial tectonics of the Scottish glacio-isostaic uplift centre. *Quaternary Science Reviews*, **19**, 1-22.

Firth, C.R., Collins, P.E.F. and Smith, D.E. (1997). Scottish Natural Heritage focus on Firths coastal landforms, processes and management options IV. The Firth of Forth. Scottish Natural Heritage, Edinburgh, pp 106.

Firth, C.R., Collins, P.E.F. and Smith, D.E. (2000). *Focus on Firths:* coastal landforms, processes and management options. V. The Solway Firth. Report No. 128, Sottish Natural Heritage. pp. 120.

Firth, C.R., Collins, P.E.F. and Smith, D.E. (2002). *Coastal processes and management of Scottish estuaries.* VI. The Firth of Clyde. Review No. 108, Sottish Natural Heritage. pp. 106.

Fitton, G. (1998). X-ray flourescence spectrometry. *In*: Gill, R. (ed.), *Modern Analytical Geochemistry: An introduction to quantitative analysis for earth, environmental and material scientists.* Longman, pp. 329.

Flather, R. A., J. A. Williams and D. L. Blackman (2001). STOWASUS-2100: regional storm, wave and surge scenarios for the 2100 century. EU, EU ENV4-CT97-498, 31pp.

Flower, R.J. (1993). Diatom preservation: experiments and observations on dissolution and breakage in modern and fossil material. *Hydrobiologica,* **269/270**, 437-484.

Flynn, W.W. (1968). Determination of low levels of polonium-210 in environmental metrials. *Analytica Chimica Acta*, **43**, 221-227.

French, J.R. and Burningham, H. (2003). Tidal marsh sedimentation versus sea-level rise: a southeast England estuarine perspective. *Proceedings Coastal Sediments '03*, Sheraton Sand Key, Clearwater, Florida. pp. 14.

French, J.R (1993). Numerical simulation of vertical marsh growth and adjustment to accelerated sea-level rise, North Norflok, UK. *Earth Surface Processes and Landforms*, **18**, 63-81.

French, J.R. and Spencer, T. (1993). Dynamics of sedimentation in a tide dominated backbarrier salt marsh, Norfolk, United Kingdom. *Marine Geology*, **110**, 315-331.

French, J.R. and Stoddart, D.R. (1992). Hydrodynamics of salt marsh creek systems: implications for marsh morphodynamic development and matter exchange. *Earth Surface Processes and Landforms*, **17**, 235-252.

French, J.R., Spencer, T. and Stoddart, D.R. (1990). Backbarrier marshes of the North Norfolk coast: geomorphic development and response to rising sea levels. *University College London, Discussion Papers in Conservation*, **54**, 28 pp.

French, P.W. (1996). Implications of a saltmarsh chronology for the Severn Estuary based on independent lines of dating evidence. *Marine Geology*, **135**, 115-125.

Frey, R.W. and Basan, P.B. (1978). Coastal Salt Marshes. *In*: Davis, R.J. (Ed). Coastal Sedimentary Environments. New York. Springer-Verlag. 716 pages pp. 225-301.

Froelich, P.N., Klinkhammer, G.P., Bender, M.L., Luedtke, N.A., Heath, G.R., Cullen, D., Dauphin, P., Hammond, D., Hartman,B. and Maynard, V. (1979). Early oxidation of organic matter in pelagic sediments of the eastern equatorial Atlantic: Sub-oxic diagenesis. *Geochimica et Cosmochimica Act,* **43**, 1075-1090.

Gaillard, J.F., Pauwels, H. and Michard. G. (1989). Chemical diagenesis in coastal marine sediments. *Oceanologica Acta,* **12**, 175 –187.

Gallagher, K.A., Wheeler, A.J. and Orford, J.D. (1996). An assessment of the heavy metal pollution of two tidal marshes on the north-west coast of Ireland. *Proceedings of the Royal Irish Academy*,**Vol. 96 B**, 177-188.

Gardener, L.R., Sharma, P. and Moore, W.S. (1988). A regeneration model for the effect of bioturbation by fiddler crabs on ^{210}Pb profiles in salt marsh sediments. *Journal of Environmental Radioactivity*, **5**. 25-36.

Gale, S.J. and Hoare, P.G. (1991). Quaternary sediments: Petrographic methods for the study of unlithified rocks: New York, Belhaven Press, pp. 201-229.

Gehrels, W.R., (1994). Determining relative sea-level change from salt-marsh foraminifera and palnt zones on the coast of Maine, USA. *Journal of Coastal Research*, **10**, 990-1009.

Gehrels, W.R., Roe, H.M. and Charman, D.J. (2001). Foraminifera, testate amoebae and diatoms as sea-level indicators in UK saltmarshes: a quantitative multiproxy approach. *Journal of Quaternary Science*, **16**, (3), 201-220.

Gehrels, W.R. and Leatherman, S.P. (1989). Sea-Level Rise: Animator and Terminator of Coastal Marshes, Vance Bibliographies, Monticello, IL, 39 pp.

Gehrels, W.R., Kirby, J.R., Prokoph, A., Newnham, R.M., Achterberg, E.P., Evans, E.H., Black, S., Scott, D.B., in press. Onset of recent rapid sea-level rise in the western Atlantic Ocean. *Quaternary Science Reviews.*

Gill, R.C.O. (1997). Modern Analytical Geochemistry: An introduction to qualitative chemical analysis techniques for Earth, Environment and Marerials Scientists. Longman Publishers, pp. 329.

Gillham, M.E. (1957c). Coastal vegetation of Mull and Iona in relation to salinity and soil reaction. *Journal of Ecology*, **46**, 757-778.

Gilmore, G.R. and Hemmingway, J.D.(1995*). Practical gamma spectrometry*. John Wiley and Sons, pp. 322.

Glooschenko, W.A. and Capobianco, J.A. (1980). Geochemistry of a subarctic salt marsh environment. *Marine Geology*, **37**, Issue 3-4, 231-240.

Goff, J.R. (1997). A chronology of natural and anthropogenic influcences on coastal sedimentation, New Zealand. *Marine Geology*, **138**, 105-117

Goldberg, E.D., (1963). *Geochronology with ^{210}Pb in radioactive dating*. IAEA, Vienna, 121-131.

Gornitz, V. and Lebedeff, S. (1987). Global sea-level changes during the last century. *In*: Nummedal, D., Pilkey, O.H. and Howard, J.D. (eds). Sea Level Change and Coastal Evolution, SEPM Special Publication No. 41, pp. 3-16.

Graff, J. (1981). An investigation of the frequency distributions of annual sea-level maxima at ports around Great Britain. *Estuarine, Coastal and Shelf Science*, **12**, 389-449.

Grant, J.A. (1986). The isocon diagram: a simple solution to Gresens' equation for metasomatic alteration. *Economic Geology*, **81**, 1976-1982.

Gray, J., Jones, S.R. and Smith, A.D. (1995). Discharges to the environment from the Sellafield site 1951-1992. *Journal of Radiological Protection*, **15**, 99-131.

Gray, J. M. (1974). Lateglacial and postglacial shorelines in western Scotland. *Boreas*, **3**, 129-138.

Gray, J. M. (1978). Low-level shore platforms in the south-west Scotish Highlands: altitude age and correlation. *Transactions of the Institute of British Geographers*, NS, **3**, 151-164.

Gray, J. M. (1983). The measurement of shoreline altitudes in areas affected by glacioisostasy, with particular reference to Scotland. *In*: Smith, D.E and Dawson, A.G. (eds). *Shorelines and Isostasy*. Academic Press, London, 97-128.

Gray, J. M. (1985). Glacio-isostatic shoreline development in Scotland: An Overview. London. Department of Geography and Earth Science, Queen Mary College, University of London. 61. pp.

Green, C. (1984). Saltings and sea defences on the Gwent levels. Conference of River Engineers, Cranfield.

Grimm, E. (1991). TILIA and TILIA.GRAPH. Illinois State Museum, Illinois.

Grimshaw, H.M. (1989). Loss on ignition. *In*: Allen, S.E. (Ed). *Chemical Analysis of Ecological Materials*. Blackwell Scientific Publications, Oxford, 15-16.

Guary, J.C., Guigueuiat, P. and Pentreath, P.J. (1988). *Radionuclides: A tool for Oceanography*. Elsevier Applied Science, pp. 461.

Guntenspergen, G.R., Cahoon, D.R., Grace, J., Steyer, G.D., Fournet, S., Towsen, S.J. and Foote, A.L. (1995). Disturbance and recovery of the Louisiana coastal marsh landscape from the impact of Hurricane Andrew. *Journal of Coastal Research*, **21**, 324-339.

Hamilton, E.I. and Clarke, K.R. (1984). The recent sedimentary history of the Esk estuary, Cumbria, UK: The application of radiochronology. *Science of the Total Environment*, **35**, 741-747.

Hansom, J.D. (2001). Coastal sensitivity: A view from the beach. *Catena*, **42**, 291-305.

Hardaway, C., Sheu, W., Meriwether, J.R., Sneddon, J. and Beck, J. (1998). The effect of diagenetic processes on the radiochronology of soft sediments using ^{210}Pb and ^{137}Cs. *Microchemical Journal.* **58**, 127-134.

Harris, A.L. and Pitcher, W.S. (1975). The Dalradian Supergroup. 52-75 *In*: Harris, A.L., and others (eds.), *A Correlation of Pre-Cambrian rocks in the British Isles*. Special Report of the Geological Society of London, No. **6**.

Harrison, E.Z. and Bloom. A.L. (1977). Sedimentation Rates on tidal salt marshes in Connecticut. *Journal of Sedimentary Petrology,* **47**, 1484 - 1490.

Hartley, B. (1986). A Check-List of the Freshwater, Brackish and Marine Diatoms of the British Isles and Adjoining Coastal Waters. *Journal of the Marine Biological Association*, **66**, 611 - 640.

Hartley, B., Barber, H.G. and Carter, J.R. (1996). *An Atlas of British Diatoms*. P.A. Sims, (ed.). Biopress Ltd., Bristol. pp. 601.

Harvey, G.R. (1980). A study of the chemistry of iodine and bromine in marine sediments. *Marine Chemistry*, **8**, 327-332.

Haslett, S.K., Cundy, A.B., Davis, C.F.C., Powell, E.S. and Croudace, I.W. (2003). Salt marsh sedimentation over the past c. 120 years along the west Cotentin coast of Normandy (France): Relationship to sea-level rise and sediment supply. *Journal of Coastal Research*, **19**, (3), 609-620.

Hatton, R.S., DeLaune, R.D. and Patrick, W.H. (1983). Sedimentation, accretion and subsidence in marshes of Barataria Basin, Louisiana. *Limnology and Oceanography*, **28**, 494-502.

Haynes , J. and Dobson, M. (1969). Physiography, foraminifera and sedimentation in the Dovey Estuary (Wales). *Geological Journal*, **6**, 217-256.

He, Q. and Walling, D.E. (1996). Use of fallout 210Pb measurements to investigate longer-term rates and patterns of overbank sediment deposition on the floodpalins of lowland rivers. *Earth Surface Processes and Landforms,* **21**, 141-154.

Helz, G.R., Setlock, G.H., Cantillo, A.Y. and Moore, W.S. (1985). Processes controlling the regional distribution of ^{210}Pb, ^{226}Ra and anthropogenic zinc in estuarine sediments. *Earth and Planetary Science Letters,* **76**. 23-34.

Helz, G.R., Miller, C.V., Charnock, J.M., Mosselmans, J.F.W., Pattrick, R.A.D., Garner, C.D. and Vaughan, D.J. (1996). Mechanism of molybdenum removal from the sea and its concentration in black shales: EXAFS evidence. *Geochimica et Cosmochimica Acta*, 60, (19), 3631-3642.

Hem, J.D. (1978). Redox processes at surfaces of manganese oxides and their effects on aqueous metal ions. *Chemical Geology,* **21**, 199-218.

Hemphill-Haley, E. (1995a). Intertidal diatoms from Willapa Bay, Washington: Application to studies of small-scale sea-level changes. *Northwest Science*, **69**, 29-45.

Hendey, N.I.(1964). An introductory account of the smaller algae of British coastal waters. *Fish. Invest. Ser. 4, Part 5, Bacillariophyceae (Diatoms)*, pp 1-317. (London).

Huerta-Diaz, M.A. and Morse, J.W. (1990). A quantitative method for the determination of trace metal concentrations in sedimentary pyrite. *Marine Chemistry*, **29**. 119-144.

Hines, M.E., Knollmeyer, S.L. and Tugel, J.B. (1989). Sulphate reduction and other sedimentary biogeochemistry in a northern New England salt marsh. *Limnology and Oceanography*, **34**, 578-590.

Houghton, J.T., Ding, Y., Griggs, D.J. Nouger, M., van der Linden, P.J., Dai, X., Maskell, K. and Johnson, C.A. (2001). Climate Change 2001: The Scientific basis. Intergovernmental Panel on Climate Change: Contribution of working group I to the Third Assessment Report. Cambridge University Press, pp. 94.

Howarth, R.W. and Teal, J.M. (1979). Sulphate reduction in a New England salt marsh. *Limnology and Oceanography*, **24**, 999-1013.

Huerta-Diaz, M.A. and Morse, J.W. (1992). Pyritization of trace metals in anoxic marine sediments. *Geochimica et Cosmochimica Acta,* **56**, (7), 2681-2702.

Hunt, G.J. and Kershaw, P.J. (1990). Remobilisation of artificial radionuclides from the sediment of the Irish Sea. *Journal of Radiological Protection*, **10**, 147-151.

Hutchinson, S.E. and Prandle, D. (1994). Short-term sediment dynamics in a South-eastern U.S.A. *Spartina* marsh. *Journal of Coastal Research*, **11**, 370-380.

Hydraulics Research Ltd. (1987). The effectiveness of saltings. Report SR 109, Hydraulics Research Ltd., Wallingford.

Jardine, W.G. (1975). Chronology of Holocene marine transgression and regression in south-western Scotland. *Boreas*, **4**, 173-196.

Janssen-Stelder, B. (2000). A system analysis of salt marsh development along the mainland coast of the Dutch Wadden sea. Netherlands Geographical Studies 275. PhD Thesis, University of Utrecht.

Jean, G.E. and Bancroft, G.M. (1986). Heavy metal adsorption by sulphide mineral surfaces. *Geochimica et Cosmochimica Acta,* **50**, 1455-1463.

Jenkins, R. (1974). *An Introduction to X-ray Spectrometry*. Heyden, pp. 163.

Jennings, S.C., Carter, R.W.G. and Orford, J.D. (1993). Late Holocene salt marsh development under a regime of rapid relative-sea-level rise: Chezzetcook Inlet, Nova Scotia: Implications for the interpretation of palaeo-marsh sequences. *Canadian Journal of Earth Sciences*, **30**, 1374 - 1384.

Jennings, S.C., Carter, R.W.G. and Orford, J.D. (1995). Implications for sea-level research of salt marsh and mudflat accretionary processes along paraglacial barrier coasts. *Marine Geology,* **124,** 129 - 136.

Johnson, D.W. (1967). *'The New England-Acadian Shoreline.'* Hafner, New York.

Johnston, P., Wu, P. and Lambeck, K. (1998). Dependence of horizontal stress magnitude on load dimensions in glacial rebound models. *Geophysical Journal International*, **132**, 41-60.

Jones, R. (1997). *Mull in the Making*. Published by Rosalind Jones, Craigmore, Aros, Isle of Mull, pp 41.

Juggins, S. (1992). Diatoms in the Thames estuary, England: ecology, palaeoecology and salinity transfer function. *Bibliography Diatomology*, **25** 1-216.

Kaye, C.A. and Barghoorn, E.S. (1964). Late Quaternary sea-level change and crustal rise at Boston, Massachusetts, with notes on the auto-compaction of peat. *Geological Society of America Bulletins*, **75**, 63-80.

Kearney, M.S. and Stevenson, J.C. (1991). Island land loss and marsh vertical accretion rate: evidence for historical sea-level changes in Chesapeake Bay. *Journal of Coastal Research*, **7**, 403-415.

Kearney, M.S., Stevenson, J.C. and Ward, L.G. (1994). Spatial and temporal changes in marsh vertical accretion rates at Moine Bay: implications for sea-level rise. *Journal of Coastal Research*, **10**, 1010 - 1020.

Kershaw, P.J., Woodhead, D.S., Malcolm, S.J., Allington, D.J. and Lovett, M.B. (1990). A sediment history of Sellafield discharges. *Journal of Environmental Radioactivity*, **12**, 201-241.

Kershaw, P.J. and Woodhead, D.S. (1991). *Radionuclides in the study of Marine Processes.* Elsevier Applied Science, pp.393.

Kim, G., Hussain, N., Church, T.M. and Carey, W.L. (1997). The fallout isotope ^{207}Bi in a Delaware salt marsh: a comparison with ^{210}Pb and ^{137}Cs as a geochronological tool. *The Science of the Total Environment*, **196**, 31-41.

Kim, G., Alleman, L.Y. and Church, T.M. (2004). Accumulation records of radionuclides and trace metals in two contrasting Delaware salt marshes. *Marine Chemistry,* **87**, 87-96.

Kirchner, G. and Elhers, H. (1998.). Sediment geochronology in changing coastal environments: potentials and limitations of the ^{137}Cs and ^{210}Pb methods. *Journal of Coastal Research*, **14**, (2), 483 - 492.

Knoll G. F. (1989). *Radiation Detection and Measurement*, John Wiley & Sons, 2nd edition. pp.529

Koide, M. Soutar, A. and Goldberg, E.D. (1972.). Marine geochronology with ^{210}Pb. *Earth and Planetary Science Letters*, **14**, 442 - 446.

Kostka., Joel. E. and Luther, G.W. (1994). Partitioning and speciation of solid phase iron in saltmarsh sediments. *Geochimica et Cosmochimica Acta*, Vol. **58**, No. 7, 1701-1710

Krammer, K. and Horst-Lange Bertalot, H.C. (1986). Bacillariophyceae. I. Teil. Naviculaceae. *In: Süsswassserflora von Mitteleuropa*, Band 2/1, pp 876.

Krammer, K. and Horst-Lange Bertalot, H.C. (1988). Bacillariophyceae. 2. Teil. Bacillariaceae, Epithemiaceae, Surirellaceaea.. *In: Süsswassserflora von Mitteleuropa*, Band 2/2.

Krammer, K. and Horst-Lange Bertalot, H.C. (1991). Bacillariophyceae. 3. Teil. Zentrische Diatomeen, Diatoma, Meridion, Asterionella, Tabbellaria, Fragilaria, Eunotia und Verwandte, Peronia und Actinella. *In: Süsswassserflora von Mitteleuropa*, Band 2/4, pp. 230.

Krammer, K. and Horst-Lange Bertalot, H.C. (1991). Bacillariophyceae. 4. Teil. Acnanthes, Navicula, Gomphonema, Kritische Nachtraege, Literature. *In: Süsswassserflora von Mitteleuropa.*

Krishnaswarmy, S., Lal, D., Zhang, H. and Davison, W. (1994). Geochronology of lake sediments. *Earth and Planetary Science Letters*, **11**, 407-414.

Lambeck, K., Johnston, P. and Nakada, M. (1990). Holocene glacial rebound and sea-level change in NW Europe. *Geophysical Journal International*, **103**, 451 - 468.

Lambeck, K. (1991). A model for Devensian and Flandrian glacial rebound and se-level changes in Scotland. *In*: Sabadini, R., Lambeck, K. and Boschi, E. (eds). *Glacial Isostasy, Sea-Level and Mantle Rheology*: Kluwer Academic Publishers, Dordrecht, 33-61.

Lambeck, K. (1993a). Glacial rebound of the British Isles I: Preliminary model results. *Geophysical Journal International*, **115**, 941-959.

Lambeck, K. (1993a). Glacial rebound of the British Isles II: a high resolution, high precision model. *Geophysical Journal International,* **115**, 960-990.

Lambeck, K. (1995). Late Devensian and Holocene shorelines of the British Isles and North Sea from models of glacio-hydro-isostatic rebound. *Journal of the Geological Society, London.* **152**, 437-448.

Lambeck, K. and Johnston, P. (1995). Land subsidence and sea-level change: contributions from the melting of the last great ice sheets and the isostatic adjustment of the Earth. *In*: Barends, F.B.J., Brouwer, F.J.J. and Schröder, F.H. (eds). *Land Subsidence.* Balkema, Rotterdam, 3-18.

Langlois, E., Bonis, A. and Bouzillé, J.B. (2003). Sediment and plant dynamics in saltmarshes pioneer zone: Puccinellia maritima as a key species. *Estuarine, Coastal and Marine Science*, **56**, 239-249.

Lee. S.V. and Cundy, A.B. (2001). Heavy metal contamination and mixing processes in sediments from the Humber Estuary, Eastern England. *Estuarine, Coastal and Shelf Science*, **53**, No. 5, 619-636.

Letzsch, W.S.and Frey, R.W. (1980). Deposition and erosion in a Holocene salt marsh, Sapelo Island, Georgia. *Journal of Sedimentary Petrology*, **50**, 529 - 542.

Leonard, L. A., Hine, A. C., Luther, M. E., Stumpf, R. P., and Wright, E. E., (1995). Sediment transport processes in a west-central Florida open marine marsh tidal creek; the role of tides and extra-tropical storms. *Estuarine, Coastal and Shelf Science*, **41**, 225-248.

Lewis, J.T. (1997). The record of deposition and the migration of elements in saltmarshes. PhD Thesis, University of Southampton, (unpublished). pp. 225.

Linton, D.L. (1951). Problems of Scottish scenery. *Scottish Geographical Magazine*, **67**, 65-85.

Livingston, H.D., Bowen, V.T. and Kupferman, S.L. (1982). Radionuclides from Windscale discharges I: nonequilibrium tracer experiments in high-latitude oceanography. *Journal of Marine Research,* **40**, (1), 253 - 272.

Livingston, H.D., Bowen, V.T. and Kupferman, S.L. (1982). Radionuclides from Windscale discharges II: their dispersal in Scottish and Norwegian coastal circulation. *Journal of Marine Research,* **40** (4), 1227 - 1258.

Litherland, M. (1980). The stratigraphy of the Dalradian rocks around Loch Creran, Argyll. *Scottish Journal of Geology*, **16**, 105-123.

Long, A. (1992). Coastal responses to changes in sea-level in the East Kent Fens and southeast England U.K.over the last 7500 years. *Proceedings of the Geologists' Association*, **103**, 187-199.

Longmore, M.E., Torgersen, T., O'Leary, B.M. and Luly, J.G. (1986). Caesium-137 redistribution in the sediments of the playa, Lake Tyrrell, northwestrn Victoria. I. Stratigraphy and caesium-137 mobility in the upper sediments. *Palaeogeography, Palaeoclimatology and Palaeoecology,***54**, 181-195.

Longworth, G., Carpenter, B., Bull, R., Toole, J. and Nicholls, A. (1998). *The Radiochemical Manual.* AEA Technology Plc, Oxford, UK, pp. 321.

Lord, C.J. and Church, T.M. (1983). The geochemistry of salt marshes: sedimentary ion diffusion, sulphate reduction and pyritisation. *Geochimica et Cosmochimica Acta*, **47**. 1381-139.

Loring, D.H. (1984). Trace-metal geochemistry of sediments from Baffin Bay. *Canadian Journal of Earth Sciences*, **21**, 1368-1378.

Loring, D.H. (1991). Normalization of heavy-metal data from estuarine and coastal sediments. *ICES Journal of Marine Science*, **48**. 101-115.

Lord, III, C.L. and Church, T.M. (1983). The geochemistry of salt marshes: Sedimentary ion diffusion, sulphate reduction and pyritization. *Geochimica et Cosmochimica Acta,* Vol. **47**. 1381-1391.

Lomenick, T.F. and Tamura, T. (1965). Naturally occuring fixation of 137Cs on sediments of lacustrine origin. *Soil Science Society of America Proceedings*, **29**, 383-386.

Lopez, F. and Garcia, M. (1998). Open channel flow through simulated vegetation: suspended sediment transport modeling. *Water Resources Research*, **34**, (9), 2341-2352.

Luoma, S.N. (1990). Processes affecting metal concentrations in estuarine and coastal marine sediments. *In:* Furness, R.W. and Rainbow, P.S. (eds.). *Heavy metals in the Marine Environment.* CRC Press Ltd. 256 pp.

Luther, G.W. III. and Church, T.M. (1988). Seasonal cycling of sulphur and iron in pore waters of a Delaware salt marsh. *Marine Chemistry*, **23**, 295-309.

Luther, G.W., III, Giblin, A., Howarth, R.W. and Ryans, R.A. (1982). Pyrite and oxidized iron mineral phases formed from pyrite oxidation in salt marsh and estuarine sediments. *Geochimica et Cosmochimica Acta*, **46**, 2665-2669.

Luther, G.W. III, Kostka, J.E., Church, T.M., Sulzberger, B. and Stumm, W. (1992). Seasonal iron cycling in a salt marsh sedimentary environment: the importance of ligand complexes with Fe(II) and Fe(III) in the dissolution of Fe(III) minerals and pyrite, respectively. *Marine Chemistry*, **40**, 81-103.

Luther, G.W. III, Shellenbarger, P.A. and Brendell, P.J. (1996). Dissolved organic Fe(III) and Fe(II) complexes in salt marsh pore waters. *Geochimica et Cosmochimica Acta*, **60**, 951-960.

Lyle, M. (1983). The brown-green colour transition in marine sediments: a marker of the Fe(II) and Fe(III) redox boundary. *Limnology and Oceanography*, **28**, 1026-1033.

Mackenzie, A. B., Scott, R.D. and Williams, T.M. (1987). Mechanisms for northwards dispersal of Sellafield waste. *Nature,* **329**, 42 - 45.

MacKenzie, A.B., Farmer, J.G. and Sugden, C.L. (1997). Isotopic evidence of the relative retention and mobility of lead and radiocaesium in Scottish ombrotrophic peats. *The Science of the Total Environment,* **203**, (2), 115-127.

MacKenzie, A.B., Logan, E.M., Cook, G.T. and Pulford, I.D. (1998). Distributions, inventories and isotopic composition of lead in ^{210}Pb dated peat cores from contrasting biogeochemical environments: Implications for lead mobility. *The Science of the Total Environment*, **223**, 25-35.

Malcolm, S.J. and Price, N.B. (1984). The behaviour of iodine and bromine in estuarine sediments. *Marine Chemistry*, **15**, 263-271.

Mantoura, R.F.C., Dickson, A. and Riley, J.P. (1978). The complexation of metals with humic materials in natural waters. *Estuarine, Coastal and Marine Science*. **6**, 387-408.

McCann, S.B. (1968). Raised shore platforms in the western Isles of Scotland. *In*: Bowen, E.G., Carter, H. and Taylor, J.A. (eds), *Geography at Aberystwyth*. University of Wales Press, Cardiff, 22-34.

McHenry, J.R., Ritchie, J.C. and Gill, A.C. (1973). Accumulation of fallout caesium-137 in soils and sediments in selected water sheds. *Water Resource Reserves*, **9**, 676-686.

McCaffrey, R.J. and Thompson. J. (1980). A record of the accumulation of sediment and trace metals in a Connecticut salt marsh. *Advances in Geophysics,* **22**, 195-236.

McIntire, C.D. and Moore, W.W. (1977). Marine littoral diatoms: ecological considerations. *In*: Werner, D. (ed.). *The Biology of Diatoms*. Botanical Monographs, Vol. 13. Balckwell Scientific Publications, pp. 333-371.

McKay, W. A. and Baxter, M.S. (1985). Water transport from the North-East Irish Sea to Western Scottish coastal waters: Further observations from time-trend matching of Sellafield radiocaesium. *Estuarine, Coastal and Shelf Science.* **20**, (4), 471 - 480.

McKinley, I.G., Baxter, M.S., Ellet, D.J. and Jack, W. (1981). Tracer Applications of Radiocaesium in the Sea of the Hebrides. *Estuarine, Coastal and Shelf Science*, **13**, 69 - 82.

Mercone, D., Thompson, J., Abu-Zied, R.H., Croudace, I.W. and Rohling, E.J. (2001). High-resolution geochemical and micropalaeontological profiling of the most recent eastern Mediterranean sapropel. *Marine Geology*, **177**, 25-44.

Middelberg, J.J., de Lange, G.J. and van Weijden, C.H. (1987). Manganese solubility control in marine pore waters. *Geochimica et Cosmochimica Acta,* **51**, 759-763.

Milan, C.S., Swenson, E.M., Turner, R.E. and Lee, J.M. (1995). Assessment of the 137Cs method for estimating sediment accumulation rates: Louisiana salt marshes. *Journal of Coastal Research,* **11**, 296-307.

Miller, K.M. and Heit, M. (1986). A time resolution methodology for assessing cores that are dated by 137Cs. *Limnology and Oceanography*, **31**, 1292-1300.

Morford, J.L and Emerson, S. (1999). The geochemistry of redox sensitive trace metals in sediments. *Geochimica et Cosmochimica Acta,* Vol. **63**, No. 11/12. 1735-1750.

Moorhead, K.K. and Brinson, M.M. (1995). Response of wetlands to rising sea-level in the lower coastal plain of North Carolina. *Ecological Applications*, **5**, 261-271.

Mörner, N.A. (1971). The Holocene eustatic sea-level problem. *Geologie en Mijnbouw*, **50**, 699-702.

Mörner, N.A. (1980). Late Quaternary sea-level changes in north-western Europe: a synthesis. *Geologiska Föreningens i Stockholm Förhandlingar*, Vol **100**, part 4, 381-400. Stockholm.

Morse, J.W. (1994). Interactions of trace metals with authegenic sulphide minerals: Implications for their bioavailability. *Marine Chemistry,* **46**, 1-6.

Murray, J.W., Alve, E. and Cundy, A.B. (2003). The origin of modern agglutinated foraminiferal assemblages: evidence from a stratified fjord. *Estuarine, Coastal and Shelf Science*, **58**, 677-697.

Nakada, M. and Inoue, H. (in press). Rates and causes of recent global sea-level rise inferred from long tide gauge records. *Quaternary Science Reviews*.

Nedwell., D.B., and Abraham, J.W. (1978). Bacterial sulphate reduction in relation to sulphur geochemistry in two contrasting areas of salt marsh sediments. *Estuarine, Coastal and Shelf Science*, **6**, 341-351.

Nelson, A.R. and Kashima, K. (1993). Diatom zonation in southern Oregon tidal marshes relative to vascular plants, Foraminifera and sea-level. *Journal of Coastal Research*, **9**. (3), 673-697.

Nikonov, A.A. (1980) Manifestations of gacio-isostatic processes in Northern Countries during the Holocene and at present. *In*: N.A.Mörner (ed). *Earth Rheology, Isostasy and Eustacy*. John Wiley and Sons p.599 pp. 341-354.

Nikitina, D.L., Pizzuto, J.E., Schwimmer, R.A., Ramsey, K.W. (2000). An updated Holocene sea-level curve for the Delaware coast. *Marine Geology*, **171**, 7-10.

Nittrouer, C.A., Sternberg, R.W., Carpenter, R. and Bennet, J.T. (1979) The use of Pb-210 geochronology as a sedimentological tool: application to the Washington continental shelf. *Marine Geology*, **31**, 297 - 316.

Norton, S.A., Bienert, Jr. R.W, Binford, M.W and J.S. Kahl. (1992). Stratigraphy of total metals in PIRLA sediment cores. *Journal of Paleolimnology*, **7**, 191-214.

Norton-Smith, J. (2001). Why should we believe ^{210}Pb geochronologies? *Journal of Environmental Radioactivity*, **55**, 121-123.

Nozaki, Y., DeMaster, D.J., Lewis, D.M. and Turekian, K.K. (1978). Atmospheric ^{210}Pb fluxes determined from soil profiles. *Journal of Geophysical Research*, **83**, 4047-4051.

Nyman, J.A., Carloss, M., DeLaune, R.D. and Patrick, Jnr, W.H. (1994). Erosion rather than plant die-back as the mechanism of marsh loss in an estuarine marsh. *Earth Surface Processes and Landforms*, **19**, 69-84.

Nyman, J.A., Crozier, C.R. and DeLaune, R.D. (1995). Roles and patterns of hurricane sedimentation in an estuarine marsh lanscape. *Estuarine, Coastal and Shelf Sciemce*, **40**, 665-679.

Oenema, O. and DeLaune, R.D. (1988). Accretion rates in salt marshes in the Eastern Scheldt, south-west Netherlands. *Estuarine, Coastal and Shelf Science,* **26**, 379-394.

Oremland, R.S. and Taylor, B.F. (1978). Sulphate reduction and methanogenesis in marine sediments. *Geochimica et Cosmochimica Acta*, **42**, 209-214.

Orson, R., Panageotou, W. and Leaterman, S.P. (1985). Response of tidal salt marshes of the U.S. Atlantic and Gulf coasts to rising sea levels. *Journal of Coastal Research*, **1**. (1), 29-37.

Orson, R.A., Warren, R.S. and Niering, W.A. (1998). Interpreting sea-level rise and rates of vertical marsh acretion in Southern New England tidal salt marsh. *Estuarine, Coastal and Shelf Science,* **47**, 419-429.

Overnell, J. (2002). Manganese and iron profiles during early diagenesis in Loch Etive, Scotland. Application of two diagenetic models. *Estuarine, Coastal and Shelf Science,* **54**, 33-44.

Overnell, J., Brand, T. Bourgeois, W. and Statham, P.J. (2002). Manganese dynamics in the water column of the upper basin of Loch Etive, a Scotish Fjord. *Estuarine, Coastal and Shelf Science.* **55**, 481-492.

Parkinson, R.W. (1994). Sea-level rise and the fate of tidal wetlands. *Journal of Coastal Research.* **10**, 987 - 989.

Palmer, A.J.M. and Abbot, A. (1986). Diatoms as indicators of sea-level change. *In*: O. van de Plassche. (Ed*). Sea-Level Research: a manual for the collection and evaluation of data.* Geo books, Norwich. p.457-487, pp.618.

Paterson, D.M. (1997). Biological mediation of sediment erodibility: ecology and physical dynamics. *In*: Burt, N., Parker, R. and Watts, J. (eds). *Cohesive Sediments*, 215-230.

Patrick, R. and Reimer, C.W. (1966-1975). *The Diatoms of the United States*. Monographs of the Academy of Natural Sciences of Philadelphia, Vol **1**, (1966). Vol **2**, (1975). pp. 213.

Peacock, J.D. (1971). Terminal features of the Creran Glacier of Loch Lomond Readvance age in western Benderloch, Argyll, and their significance in the late-glacial history of the Loch Linnhe area. *Scottish Journal of Geology*, **7**, (4), 349 - 356.

Pederson, T.F., and Price, N.B. (1980). The geochemistry of iodine and bromine in sediments of thePanama Basin. *Journal of Marine Research*, **38**, 397-411.

Pellenbarg, R.E. (1984). On *Spartina alterniflora* litter and trace metal biogeochemistry of a salt marsh. *Estuarine, Coastal and Shelf Science,* **18**, 331-346.

Pellenbarg, R.E. and Church, T.M. (1979). The estuarine surface microlayer and trace metal cycling in a salt marsh. *Science,* **203**, 1010-1012.

Peltier, W.R. (1999). Global sea-level rise and glacial isostatic adjustment. *Global and Planetary Change*, **20**, 93-123.

Peltier, W.R. (2002). On eustatic sea-level history: Late glacial maximum to Holocene. *Quaternary Science Reviews,* **21**, 377-396

Peltier, W.R. and Andrews, J.T. (1976). Glacial isostatic adjustment I: The forward problem. *International Reviews of the Astronomical Society*, **46**, 605-646.

Peltier, W.R. and Tushingham, A.M. (1989). Global sea level rise and the greenhouse effect: might they be connected? *Scienc,*. **244**, 806-810.

Peltier, W.R., Shennan, I., Drummond, R. and Horton, B.P. (2000). On the post-glacial isostatic adjustment of the British Isles and the shallow visco-elastic structure of the Earth. *Geophysical Journal International*, **178**, 443-475.

Peirson, D. H., Cambray, R.S. and Spicer, G.S. (1966). Lead-210 and polonium-210 in the atmosphere. *Tellus*, **18**, (2). 427-433.

Pennington, W., Cambray, R.S., Eakins, J.D. and Harkness, D.D. (1976). Radionuclide dating of the recent sediments of Blelham Tarn. *Freshwater Biology*, **6**, 317-331.

Pethick, J. (1980). Salt marsh initiation during the Holocene transgression: the example of the North Norfolk marshes, England. *Journal of Biogeography*, **7**, 1-9.

Pethick, J. (1981). Long-term accretion rates on tidal salt marshes. *Journal of Sedimentary Petrology,* **51**, 571 - 577.

Pethick., J.S. (1992). Saltmarsh Geomorphology. In: Allen, J.R.L.and Pye, K. (eds). Saltmarshes: Morphodynamics, Conservation and Engineering Significance. Cambridge University Press. pp. 184.

Pethick., J.S. (1999). Future sea-level changes in Scotland: Options for coastal management. *In*: Baxter, J.M., Duncan, K., Atkins, S.M. and Lees, G. (eds). *Scotlands Living Coastline*. Published by the Stationary Office, London. pp. 209.

Plater, A.J. and Appleby, P.G. (2004). Tidal sedimentation in the Tees estuary during the 20th century: radionuclide and magnetic evidence of pollution and sedimentary response. *Estuarine, Coastal and Shelf Science,* **60**. 179-192.

Plater, A.J. and Shennan, I. (1992). Evidence of Holocene sea-level change from the Northumberland coast, eastern England. *Proceedings of the Geologists' Association*, **103**. 201-216.

Playford, K., Lewis, G.N.J. and Carpenter, R.C. (1992). *Radioactive fallout in air and rain: results to the end of 1990.* AEA-EE-0362, HMSO.

Postma, H. (1967). Sediment transport and sedimentation in the estuarine environment. *In*: Lauff, G. H. (ed.) *Estuaries*. A.A.A.S. Publ. **83**, 158-79.

Postma, H. (1980). Sediment transport and sedimentation. *In*: Olausson, E. and Cato, I. (eds.) *Chemistry and Biochemistry of Estuaries,* Wiley, New York, pp. 153-85.

Prandle, D. and Beechley, J. (1991). Marine dispersion of caesium-137 released from Sellafied and Chernobyl. *Geophysical Research Letters*, **18**, 1723-1726.

Price, N.B. (1976). Chemical diagenesis in sediments. *In*: Riley, J.P. and Chester, R. (eds). *Chemical Oceanography*. Vol. 6, p 1-58. Academic Press, pp 414.

Price, N.B. and Calvert, S.E. (1977). The contrasting geochemical behaviours of iodine and bromine in recent sediments from the Namibian shelf. *Geochimica et Cosmochimica Acta,* **41**, 1769-1775.

Price, N.B. , Calvert, S.E. and Jones, P.G.W. (1970). The distribution of iodine and bromine in the sediments of the south west Barents Sea. *Journal of Marine Research*, **28**, 22-34.

Pye, K., Coleman, M.L., and Duan, W.M. (1997). Microbial activity and diagenesis in saltmarsh sediments, North Norfolk, England. *In*: Jickells, T.D. and Rae, J.E. (eds.). *Biogeochemistry of intertidal sediments*. Cambridge environmental chemistry series / 9. Cambridge University Press. pp. 193.

Rae, J.E. (1997). Trace metals in deposited intertidal sediments. *In*: Jickells, T.D. and Rae, J.E. (eds.). *Biogeochemistry of intertidal sediments*. Cambridge environmental chemistry series / 9. Cambridge University Press. pp. 193.

Radakovitch, O., Charmasson, S., Arnaud, M. and Bouisset, P. (1999). 210Pb and caesium accumulation in the Rhône Delta sediments. *Estuarine, Coastal and Shelf Science*, **48**, 77-92.

Rashid, M.A. (1985). Geochemistry of marine humic compounds. Spinger-Verlag, New York, pp. 300.

Rashid, M. A. (1974). Humic compounds of the sedimentary environment: their chemical nature and geochemical significance. In: Offshore geology of eastern Canada. *Geological. Survey of Canada, paper 74-30,* **1**, 123-132.

Rashid, M. A. and Leonard, J. D. (1973). Modification in the solubility and precipitation behavior of various metals as a result of their interaction with sedimentary humic acid. *Chemical. Geology,* **11**, 89-97.

Redfield, A.C. (1972). Development of a New England salt marsh. *Ecological Monographs*, **2**, 201-237.

Redfield, A.C. and Rubin, M. (1962). The age of salt marsh peat and its relation to recent changes in sea level at Barnstable, Massachusetts. *Proceedings of the Natural Academy of Sciences, U.S.A.* **48,** 1728-1735.

Reddy, K.R. and D'Angelo, E.M. (1997). Biogeochemical indicators to evaluate pollutant removal efficiency in constructed wetlands. *Water Science and Technology*, **35**, (5), 1-10.

Reed, D.J. (1988). Sediment dynamiics and deposition in a retreating coastal salt marsh. *Estuarine, Coastal and Shelf Scienc,* **26,** 67-79.

Reed, D.J. (1989). Patterns of sediment deposition in subsiding coastal marshes, Tereborne Bay, Louisiana: the role of winter storms. *Estuaries,* **12,** 222-227.

Reed, D.J. (1990). The impact of sea-level rise on coastal marshes. *Progress in Physical Geography*, **14,** 465 - 481.

Reed, D.J. (1995). The response of coastal marshes to sea-level Rise: Survival or Submergence? *Earth Surface Processes and Landforms*, **20,** 39-48.

Reed, D.J. (2002). Sea-level rise and coastal marsh sustainability: geological and ecological factors in the Mississipi delta plain. *Geomorphology,* **48,** 233-243.

Ridgeway, I.M. and Price, N.B. (1987). Geochemical associations and post-depositional mobility of heavy metals in coastal sediments: Loch Etive, Scotland. *Marine Chemistry*, **21,** 229-248.

Riley, J.P. and Chester, R. (1976). *Chemical Oceanography*. Academic Press, London. pp 414.

Ritchie, J.C. and McHenry, J.R. (1990). Application of radioactive fallout caesium-137 for measuring soil erosion and sediment accumulation rates and patterns: a review. *Journal of Environmental Quality,* **19,** 215-233.

Ritchie, W. (1985). Inter-tidal and sub-tidal organic deposits and sea level changes in the Uists, Outer Hebrides. *Scottish Journal of Geology*, **21,** (2), 161 - 176.

Robbins, J.A. (1978). Geochemical and geophysical applications of radioactive lead. *In*: Nriagu, J.O. (ed.), *Biogeochemistry of lead in the environment.* Elsevier Scientific, Amsterdam, pp. 285-393.

Robbins, J.A. and Edington, R.R. (1975). Determination of recent sedimentation rates in Lake Michigan using Pb-210 and Cs-137. *Geochimica et Cosmochimica Acta*, **39**, 285-304.

Robbins, J.A., Edington, R.R. and Kemp, A.L.W. (1978). Comparitaive 210-Pb, 137-Cs and pollen geochronologies of sediments from Lakes Ontario and Erie. *Quaternary Research,* **10**, 256-278.

Robinson, M. (1982). Diatom analysis of Early Flandrain lagoon sediments from East Lothian, Scotland. *Journal of Biogeography*, **9**, 207-221.

Robinson, M. (1993). Microfossil analyses and radiocarbon dating of depositional sequences related to Holocene sea-level change in the Forth Valley, Scotland. *Transactions of the Royal Society of Edinburgh*, **84**, 1-60.

Rogowski, A.S. and Tamura, T. (1970). Environmental mobility of caesium-137. *Radiation Botany*, **10**, 35-45.

Rollinson, H.R. (1993). Another look at the constant sum problem in geochemistry. *Mineralogical Magazine*, **56**, 469-475.

Roman, C.T., Peck, J.A., Allen, J.R.L, King, J.W. and Appleby, P.G. (1997). Accretion of a New England (U.S.A.) salt marsh in response to inlet migration, storms and sea-level rise. *Estuarine, Coastal and Shelf Science*, **45**, 717-727.

Romeyn, L., and Bouwman, L.A. (1983). Food selection and consumption by estuarine nematodes. *Hydrobiological Bulletin*, **17**, 103-109.

Round. F.E. (1971). Benthic Marine Diatoms. *Oceanography and Marine Biology Annual Reveiws*, **9**, 83-139.

Ryves, D.B., Juggins, S., Fritz, S.C. and Battarbee, R.W. (2001). Experimental diatom dissolution and the quantification of microfossil preservation in sediments. *Palaeogeography, Palaeoclimatology and Palaeoecology*, **172**, 99-113.

Ruz, M.H., Allard, M., Michaud, Y. and Héquette, A. (1998). Sedimentology and evolution of sub-artic tidal flats along a rapidly emerging coast, eastern Hudson Bay, Canada. *Journal of Coastal Research*, **14**, 1242 - 1254.

Salomans, J.C. and Mook, W.G. (1977). Trace metal concentrations in estuarine sediments: mobilization, mixing or precipitation? *Netherlands Journal of Sea Research*, **11**, 19-129.

Santschi, P., Hohner., P., Benoit, G. and Buchholtz-Ten-Brink, M. (1990). Chemical processes at the sediment-water interface. *Marine Chemistry*, **30**, 269-315.

Sarin, M.M. and Church, T.M. (1994). Behaviour of uranium during mixing in the Delaware and Chesapeake estuaries. *Estuarine, Coastal and Shelf Science*. **39**, (6), 619-631.

Scott-Anderson, R., Borns, Jnr, H.W., Smith, D.C and Race, C. (1992). Implications of rapid sediment accumulation in a small New England salt marsh. *Canadian Journal of Earth Sciences*, **29**, 2013-2017.

Scott, D.B. and Medioli, F.S. (1978). Vertical zonation of marsh foraminifera as accurate indicators of former sea-levels. *Nature*, **272**, 528-531.

Selby, K.A., Smith, D.E., Dawson, A.G. and Mighall, T.M. (2000). Late Devensian and Holocene relative sea-level and environmental changes from an isolation basin in southern Skye. Scottish *Journal of Geology*, **36**, 73-86.

Shaler, N.S. (1885). Sea-coast swamps of the Eastern United States. United States Geological Survey, Annual Report, 6th, pp. 359-368.

Shaw, T.J., Gieskes, J.M. and Jahnke, R.A. (1990). Early diagenesis in differing depositional enviroments: the response of transition metals in pore water. *Geochimica et Cosmochimica Acta*, **54**, 1233-1246.

Shennan, I. (1983). Holocene crustal movements and sea level changes in Great Britain. Journal of *Quaternary Science*, **4**, 77-89.

Shennan, I. And Horton, B.P. (2002). Holocene land- and sea-level changes in Great Britain. *Journal of Quaternary Science*, **17**, (5-6), 511-526.

Shennan, I. and Woodworth, P.L. (1992). A comparison of late Holocene and twentieth century sea-level trends from the UK and North Sea region. *Geophysical Journal International*, **109**, 96-105.

Shennan, I., Innes, J.B., Long, A. and Zong, Y. (1993). Late Devensian and Holocene relative sea-level changes at Rumach, near Arisaig, northwest Scotland. *Norsk Geologisk Tidsskrift,* **73**, 161-174.

Shennan, I., Innes, J.B., Long, A. and Zong, Y. (1994). Late Devensian and Holocene relative sea-level changes at Loch nan Eala, near Arisaig, northwest Scotland. *Journal of Quaternary Science,* **9**, 261 - 283.

Shennan, I., Innes, J.B., Long, A. and Zong, Y. (1995a). Late Devensian and Holocene relative sea-level changes in Northwestern Scotland: new data to test existing models. *Quaternary International,* **26**, 97 - 123.

Shennan, I., Innes, J.B., Long, A. and Zong, Y. (1995b). Holocene relative sea-level changes and coastal vegetation history at Kentra Moss, Argyll, northwest Scotland. *Marine Geology*, **124**, 43 - 59.

Shennan, I., Lambeck, K., Horton, B.P., Innes, J.B., Lloyd, J.M., McArthur, J.J., Purcell, T. and Rutherford, M.M. (2000a). Late Devensian and Holocene records of relative sea-level changes in northwest Scotland and their implications for glacio-hydroisostatic modelling. *Quaternary Science Reviews*, **19**, 1103-1136.

Shennan., I., Peltier, W.R., Drummond, R. and Horton, B.P. (2002a). Global to local scale parameters determining relative sea-level changes and the post-glacial adjustment of Great Britain. *Quaternary Science Reviews*, **21**, 397-408.

Shi, Z. (1993). Recent saltmarsh accretion and sea-level fluctuations in the Dyfi Estuary, central Cardigan Bay, Wales, UK. *Geo-Marine Letters*, **13**, 182-188.

Shi, Z., Lamb, H.F. and Collins, R.L. (1995). Geomorphic change of saltmarsh tidal creek networks in the Dyfi Estuary, Wales. *Marine Geology,* **128**, 73-83.

Shimmield, G.B. and Pederson, T.F. (1990). Geochemistry of reactive trace metals and halogens in hemipelagic continental margin sediments. *Reviews of Aquatic Science*, **3**, 255-279.

Short, D. (1995). Radionuclides as Tracers of Pollutant Trace Metals in Lakes. PhD Thesis, University of Liverpool, Unpublished.

Shotyk, W., Nesbitt, H.W. and Fyfe, W.S. (1990). The behaviour of major and trace elements in complete vertical peat profiles from three Sphagnum bogs. *International Journal of Coal Geology*, **15**, (3), 163-190.

Simonsen, R. (1969). Diatoms as indicators in estuarine environments. *Veröffentlichungen Instituts für Meeresforschung Bremerhaven*, **11** 287-291.

Sissons, J.B. (1972). Dislocation and non-uniform uplift of raised shorelines in the western part of the Forth Valley. *Transactions of the Institute of British Geographers*, **55**, 145-159.

Sissons, J.B. (1974a). The Quaternary in Scotland: a review. *Scottish Journal of Geology*, **10**, 34-37.

Sissons, J.B. (1982). The so-called high 'interglacial' rock shoreline of western Scotland. *Transactions of the Institute of British Geographers,* NS, **7**, 205-216.

Sissons, J.B. (1983). Shorelines and isostasy in Scotland. *In*: Smith, D.E. and Dawson, A,G. (eds). *Shorelines and Isostasy*. Academic Press, London, 209-225.

Smith, D. E. (1997). Sea-Level Change in Scotland During the Devensian and Holocene. *In*: Gordon, J.E. (Ed.) *Reflections on the Ice Age in Scotland*. Glasgow, Scottish Natural Heritage: 136-151.

Smith, D.E. and Cullingford, R.A. (1985). Flandrian relative sea-level changes in the Montrose Basin area. *Scottish Geographical Magazine*, **101**, 92-104.

Smith, D. E., Firth, C.R., Turbayne, S.C. and Brooks, C.L. (1992). Holocene relative sea-level changes and shoreline displacement in the Dornoch Firth area, Scotland. *Proceedings of the Geologists' Association,* **103**, 237-257.

Smith, D.E., Dawson, A.G., Hickey, K.R. Firth, C.R., Brooks, C.L., Dawson, S. and Shi, S. (1993). *Climate Change, Sea Level Rise and Associated Impacts in Europe*: Final Report on Work undertaken by Coventry University. Coventry University, Coventry.

Smith,D.E., Dawson, A.G., Dawson, S., Firth., C.R., Collins, P.E.F., Cullingford, R.A., de la Vega, A.C., Brooks, C.L., Charlesworth, S., Duggan, S., Horne, D., Hickey, K., Mighall, T., Pearson, S., Stewart, I.S., Selby, K. and Wells, J.M. (1995). *Relative Sea-Level Changes and Extreme Flooding Events Around European Coasts.* EU Third Framework, Contract Number: EV5V CT93 0266, Final Report, Coventry University, pp 1-15.

Smith, D.E., Firth, C.R., Brooks, C.L., Robinson, M. and Collins, P.E.F. (1999). Relative sea-level rise during the Main Postglacial Transgression in NE Scotland U.K. *Transactions of the Royal Society of Edinburgh: Earth Sciences,* **90**, 1-27.

Smith, D. E., Cullingford, R.A., Firth, C.R. (2000). Patterns of isostatic land uplift during the Holocene: evidence from mainland Scotland. *The Holocene,* **10**, (4), 489-501.

Smith, J.T., Appleby, P.G., Hilton, J. and Richardson, N. (1997). Inventories and fluxes of ^{210}Pb, ^{137}Cs and ^{241}Am determined from the soils of three small catchments in Cumbria, UK. *Journal of Environmental Radioactivity*, **37**, 127-142.

Spears, D.A. and Kanaris-Sotiriou, R. (1976). Titanium in some Carboniferous sediments from Great Britain. *Geochimica et Cosmochimica Acta*, **40**, 345-351.

Spencer, K.L., Cundy, A.B. and Croudace, I.W. (2003). Heavy metal distribution and early-diagenesis in salt marsh sediments from the Medway Estuary, Kent, UK. *Estuarine, Coastal and Shelf Science,* **57**, 43-54.

Stanners, D.A. and Aston, S.R. (1979). The determination of estuarine sedimentation rates by $^{134}Cs/^{137}Cs$ ratios and other artificial radionuclide profiles. *Estuarine, Coastal and Shelf Science*, **9**, 529-541.

Stanners, D.A. and Aston, S.R. (1981a). ^{134}Cs: ^{137}Cs and ^{106}Ru: ^{137}Cs ratios in intertidal sediments from the Cumbria and Lancashire coasts, England. *Estuarine, Coastal and Shelf Science*, **13**, 409-417.

Stanners, D.A. and Aston, S.R. (1981b). An improved method for determining sedimentation rates by the use of artificial radionuclides. *Estuarine, Coastal and Shelf Science,* **13**, 101-106.

Stephenson, D. and Gould, D. (1995). British Regional Geology: *The Grampian Highlands*. British Geological Survey, 4th Edition. HMSO, London, pp 261.

Stevenson, J.C., Kearney, M.S. and Pendleton, E.C. (1985). Sedimentation and erosion in a Chesapeake Bay brackish marsh system. *Marine Geology*, **67**, 213 - 235.

Stevenson, J.C., Ward, L.G. and Kearney, M.S. (1986). Vertical accretion in marshes with varying rates of sea-level rise. In: Wolfe, D.A. (Ed). Estuarine Variability. Academic Press, Orlando, Florida. pp. 241-259.

Stevenson, J.C., Ward, L.G. and Kearney, M.S. (1988). Sediment transport and trapping in marsh systems: Implications of tidal flux studies. *Marine Geology,* **80**, 37-59.

Stoddart, D.R., Reed, D.J. and French, J.R. (1989). Understanding salt-marsh accretion, Scolt Head island, Norfolk, England. *Estuaries*, **12**, 228-236.

Stoermer, E.F. and Smol, J.P. (1999). (eds.), *The Diatoms: Applications for the Environmental and Earth Sciences*. Cambridge University Press. pp. 496.

Stratton Noller, J. (2000). Lead-210 geochronology. *In*: Stratton Noller, J., Sowers, J.M. and Lettis, W.R. (eds). *Quaternary Geochronology: Methods and Applications*. American Geophysical Union, pp 582.

Stumpf, R.P. (1983). The Process of Sedimentation on the Surface of a Salt Marsh. *Estuarine, Coastal and Shelf Research*, **17**, 495-508.

Sundby, B., Vale, C., Cacador, I., Catarino, F. Madureira, M.J. and Caetano, M. (1998). Metal-rich concretions on the roots of salt marsh plants: Mechanism and rate of formation. *Limnology and Oceanography*, **43**, 245-252.

Synge, F.M. and Stephens, N. (1966). Late and post-glacial shorelines and ice limits in Argyll and north-east Ulster. *Transactions of the Institute of British Geographers*, 39, 101-125.

Syvitski, J.P.M. and Shaw, J. (1995). Sedimentology and Geomorphology of Fjords. *In*: Perillo, G.M.E. (ed.). *Geomorphology and Sedimentology of Estuaries*. Volume 53. Developments in Sedimentology. Elsevier Science. pp. 113-178.

Ter Braak, C.J.F. (1995). Multivariate methods. *In*: Jongman, R.H.G. (ed.), Data Analysis in Community and Landscape Ecology. Cambridge University Press. pp. 299.

Temmerman, S., Govers, G., Meire, P. and Wartel, S. (2003). Modelling long-term tidal marsh growth under changing tidal conditions and suspended sediment concentrations, Scheldt estuary, Belgium. *Marine Geology*, **193**, 151-169.

Terferle, F.N., Bingley, R.M., Williams, S.D.P., Baker, T.F. and Dodson, A.H. (submitted). Using continuous GPS and absolute gravity to separate vertical land movements and changes in sea-level at tide gauges in the UK. *Article submitted to the Royal Society*. pp. 13.

Tessier, A., Fortin, D., Belzile, N., DeVitre, R.R. and Leppard, G.G. (1996). Metal sorption todiagenetic iron and manganese oxyhydoxides and associated organic matter: narrowing the gap between field and laboratory measurements. *Geochimica et Cosmochimica Acta*, **60**, 387-404.

Thampdrup, B., Finster, K., Fossing,H., Wurgler Hanson, J. and Barker Jorgensen., B. (1994). Thiosulphate and sulphite distributions in pore water of marine sediments related to manganese, iron and sulphur geochemistry. *Geochimica et Cosmochimical Acta*, **57**, 579-595.

Thompson, J., Higgs, N.C., Croudace, I.W., Colley, S., and Hydes, D.J. (1993). Redox zonation of elements at an oxic / suboxic boundary in deep sea sediments. *Geochimica et Cosmochimica Acta,* **58**. 67-73.

Thompson, J., Higgs, N.C., and Colley, S. (1996). Diagenetic redistributions of redox-sensitive elements in northeast Atlantic glacial / interglacial transition sediments. *Earth and Planetary Science Letters,* **139**, 365-377.

Thompson, J., Dyer, F.M. and Croudace, I.W. (2001). Records of radionuclide deposition in two U.K. salt marshes in the United Kingdom with contrasting redox and accumulation conditions. *Geochimica et Cosmochimica Acta*, **66**, 1011-1023.

Tooley, M.J. (1982). Sea-level changes in northern England. *Proceedings of the Geologists' Association*, **93**, 43-51.

Tooley, M.J. (1992). Recent Sea-Level Changes. In: Allen, J.R.L. and Pye, K. (eds.), *Saltmarshes: Morphodynamics, Conseravtion and Engineering Significance*. Cambridge University Press, pp.184, p 19-41.

Tooley, M.J. and Jelgesma, S. (1992). The future of European coastal lowlands. In: Tooley, M.J. and Jelgersma, S. (eds.), *Impacts of Sea Level Rise on European Coastal Lowlands*. Blackwell, Oxford, 219-250.

Tröften, P.E. (1997). Neotectonics and paleoseismicity in southern Sweden. PhD Thesis, Stockolm University, Akademitryck, Edsbruck, pp. 124.

Turekian, K.K., Nozaki, Y. and Benninger, L.K. (1977). Geochemistry of atmospheric radon and radon products. *Annual Reviews of Earth and Planetary Sciences*, **5**, 227-255.

Turner. S.D. (1999). High resolution palaeoenvironmental analyses of coastal wetland sediments from south east Sicily. PhD Thesis, Brunel University. (Unpublished).

Ullman, W.J. and Aller, R.C. (1980). Dissolved iodine flux from estuarine sediments and implications for the enrichement of iodine at the sediment water interface. *Geochimica et Cosmochimica Acta*, **44**, 1177-1184.

Upstill-Goddard, R.C. and Elderfield, H. (1988). The role of diagenesis in the estuarine budgets of iodine and bromine. *Continental Shelf Research*, **8**, 405-430.

Urban, N.R., Eisenreich, S.J., Grigal, D.F. and Schurr, K.T. (1990.). Mobility and diagenesis of Pb and ^{210}Pb in peat. *Geochimica et Cosmochimica Acta,* **54**, 3329 - 3346.

Valette-Silver, N.J. (1993). The use of sediment cores to reconstruct historical trends in contamination of estuarine and coastal sediments. *Estuaries,***16**. 577-588.

van der Molen, J. (1997). Tidal distortion and spatial differences in surface flooding characteristics in a salt marsh: implications for sea-level reconstruction. *Estuarine, Coastal and Shelf Science*, **45**, 221-233.

van der Weijden, C.H. (2002). Pitfalls of normalization of marine geochemical data using a common devisor. *Marine Geology*, **184**, 167-187.

Van Eerdt, M.M. (1985). Salt marsh cliff instability in the Oosterschelde. *Earth Surface Processes and Landforms*, 10. 95-106.

van de Plassche, O. (1982). Sea-level change and water-level movements in the Netherlands during the Holocene. *Mededelingen Rijks Geologische Dienst*, **36**, 1-93.

van de Plassche, O. (1986). *Sea Level Research: a Manual for the collection and Evaluation of Data.* A contribution to IGCP Projects 61 and 200, Geo Books, Norwich, pp.

van de Plassche, O. (1991). Late Holocene sea-level fluctuations on the shore of Connecticut inferred from transgressive and regressive overlap boundaries in salt marsh deposits. *In*: Gayes, P.T., Lewis, R.S. and Bokuniewicz, H.G. (eds.). *Quaternary coastal evolution of southern New England. Journal of Coastal Research, Special Issue* No. 11, 159-179.

van de Plassche, O. (2000). North Atlantic climate-ocean variations and sea-level in Long Island Sound, Connecticut, since 500 cal yr A.D. *Quaternary Research*, *53*, 89-97.

van Wijnen, H.J. and Bakker, J.P. (2001). Long-term surface elevation change in salt marshes: a prediction of marsh response to future sea-level rise. *Estuarine, Coastal and Shelf Science*, **52**, 381-390.

Velde, B., Church, T. and Bauer, A. (2003). Contrasting trace element geochemistry in two American and French salt marshes. *Marine Chemistry*, **83**, 131-144.

Vernberg, F.J. (1993). Salt-marsh processes: A review. *Environmental Toxicology and Chemistry.* **12**, 2167-2195.

Viles, H. and Spencer, T. (1995). *Coastal Problems: geomorphology, ecology and society at the coast.* Edward Arnold, London.

Vos, P.C. and de Wolf, H. (1998a). Methodological aspects of palaeo-ecological diatom research in coastal areas of the Netherlands. *Geologie en Mijnbouw*, **67**, 31-40.

Vos, P.C. and de Wolf, H. (1993a). Diatoms as a tool for reconstructing sedimentary environments in coastal wetlands: methodological aspects. *Hydrobiologica*, **269/270**, 285-296.

Vos, P.C. and de Wolf, H. (1993b). Reconstructon of sedimentary environments in Holocene coastal deposits of the southwest Netherlands; the Poortvliet boring; a case study of palaeoenvironmental research. *Hydrobioliga*, **269/270**, 297 - 306.

Ward, L.G. (1981). Suspended-material transport in marsh tidal channels, Kiawah Island, South Carolina. *Marine Geology*, **40**, 139-154.

Ward, L.G., Kearney, M.S. and Court Stevenson, J. (1998). Variations in sedimentary environments and accretionary patterns in estuarine marshes undergoing rapid submergence, Chesapeake Bay. *Marine Geology*, **151**, 111-134.

Warren, R.S. and Neiring, W. (1993). Vegetation change on a Northeast tidal marsh: Interaction of sea-level rise and marsh accretion. *Ecology*, **74**, 96-103.

Wehrli, B., and W. Stumm. (1989). Vanadyl in natural waters: Adsorption and hydrolysis promote oxygenation. *Geochimica et Cosmochimica Acta*, **53**, 69–77.

Werner, D. (1977). *The Biology of Diatoms*. Blackwell Scientific Publications, pp 498.

Wheeler, A.J., Orford, J.D. and Dardis, O. (1999). Saltmarsh deposition and its relationship to coastal forcing over the last century on the north-west coast of Ireland. *Geologie en Mijnbouw*, **Vol. 77.** Issue 3-4, 295-310.

Widdows, J., Brown, S., Brinsley, M.D., Salkeld, P.N. and Elliot, M. (2000). Temporal changes in intertidal sediment erodability: influence of biological and climatic factors. *Continental Shelf Research*, **20**, 1275-1289.

Williams, T.P., Bubb, J.M. and Lester, J.N. (1994). Metal accumulation within saltmarsh environments: A Review. *Marine Pollution Bulletin*. **28**. (No. 5): 277 - 290.

Williams, T.M., MacKenzie, A.B., Scott, R.D., Piece, N.B. and Ridgeway, I.M. (1988). Radionuclide distributions in the surface sediments of Loch Etive. *In*: Guary, J.C., Guegueniat, P. and Pentreath, R.Y. (Eds.), International Symposium on Radioactivity and Oceanography: *Radionuclides-a Tool for Oceanography*. Cherbourg France, pp. 341-350.

Windom, H.L., Schropp, S.J., Calder, F., Ryan, J.D., Smith Jr., R.G., Burney, L.C., Lewin, F.G. and Rawlinson, C.H. (1989). Natural trace metal concentrations in estuarine and coastal marine sediments of the Southeastern United States. *Environmental Science and Technology*, **23**, 314-320.

Witkowski, A., Horst-Lange-Bertalot, H. C., and Metzeltin, D. (2000). *Diatom Flora of Marine Coasts I. Iconographia Diatomologica.* Annotated Diatom Micrographs, Volume 7. A.R.G. Gantner Verlag K.G, pp. 925.

Wise, S. M. (1980). Caesium-137 and Lead-210: A review of the techniques and some applications in geomorphology. *In:* Cullingford, R.A., Davidson, D.A. and Lewin, J. (eds.), *Timescales in Geomorphology.* John Wiley and Sons Ltd. 109 - 127, pp. 360.

Wood, M.E., Kelley, J.T. and Belknap, D.F. (1989). Patterns of sediment accumulation in the tidal marshes of Maine. *Estuaries*, **12**, 237-246.

Woodworth, P.L. (1987). Trends in UK mean sea level. *Marine Geodesy*. **11**, 57-87.

Woolnough, S.J., Allen, J.R.L. and Wood, W.L. (1995). An exploratory numerical model of sediment deposition over tidal salt marshes. *Estuarine, Coastal and Shelf Science*, **41**, 515-543.

Wright, W.B. (1911). On a pre-glacial shoreline in the western Isles of Scotland. *Geological Magazine*, **48**, 97-109.

Yapp, R.H., Johns, D. and Jones, O.T. (1916). The salt marshes of the Dovey Estuary. Part I. Introductory. *Journal of Ecology*, **4**, 27-42.

Yapp, R.H., Johns, D. and Jones, O.T. (1917). The salt marshes of the Dovey Estuary. Part II. The salt marshes. *Journal of Ecology*, **5**, 65-103.

Yapp, R.H. (1922). The Dovey marshes in 1921. *Journal of Ecology*, **10**, 18-23.

Zong, Y. and Tooley, M.J. (1996). Holocene sea-level changes and crustal movements in Morecambe Bay, northwest England. *Journal of Quaternary Science*, **11**, 43-58.

Zong, Y. and Horton., B.P. (1998). Diatom zones across intertidal flats and coastal saltmarshes in Britain. *Diatom Research*, **13**, (2), 375-394.

Zue, Z. (1992). Dynamic behaviour of ^{210}Pb, ^{210}Pb and ^{137}Cs in coastal and shelf environments. Thesis Rijksuniversiteit Utrecht, Geologica Ultraiectina No. **87.**

Zwolsman, J.J.G., Berger, G.W. and Van Eck, .G.T.M. (1993). Sediment accumulatuion rates, historical input, post-depostional mobility and retention of major elements and trace metals in salt marsh sediments of the Scheldt estuary, SW Netherlands. *Marine Chemistry*, **44**, 73 - 94.

Zwolsman, J.J.G., Van Eck, B.T.M. and Berger, G.W. (1996). Spatial and temporal distribution of trace metals in sediments from the Scheldt Estuary, South-west Netherlands. *Estuarine, Coastal and Shelf Science*, **49**, 55-79.

Zwolsman, J.J.G., Van Eck, B.T.M. and Van Der Weijden, H. (1997). Geochemistry of dissolved metals (cadmium, copper, zinc) in the Scheldt estuary, southwestern Netherlands: Impact of seasonal variability. *Geochimica et Cosmochimica Acta,* **61**, No. 8, 1935-1652.

APPENDICES

APPENDIX ONE

APPENDIX 1.1: Detail of ^{210}Pb dating method using the proxy method of ^{210}Po determination following acid leaching and auto-deposition on Ag discs (After: Flynn, 1966).

Method:

1. Weigh 1-3 g of dry powdered sediment accurately, into a 250ml glass beaker. Tare scales to zero.
2. Add approx. 0.5 ml of ^{209}Po yield tracer by pipette and record weight immediately. (Tracer is diluted in $HN0_3$ and fizzing will be observed when tracer is added to sediment sample).
3. Slowly add 30 ml of freshly prepared aqua regia and leave sample to digest for 3-5 hours.
4. Add a further 20 ml of aqua regia, cover with a watch glass and gently reflux on a hotplate for a further 4 hours (or overnight).
5. Allow to cool, and then filter the supernatant. Wash the residue 3 times with distilled water, after which the sediment residue can be safely disposed of.
6. Collect the supernatant in a 250ml conical flask and gently evaporate to dryness. (Take care not to over-heat to minimize loss of solution through 'bumping').
7. Redisolve in a small volume of 6M HCl and carefully evaporate to dryness, (this ensures conversion of the extract into the chloride form).
8. Redissolve in 5.5 ml of 6M HCl. Transfer the solution to a Po plating cell (100ml beaker). Wash the conical flask several times with distilled water and add washings to the Po plating cell. Using distilled water make up the volume of liquid in the cell to 40ml. At this point the molarity of the solution should be approxomately 0.8M.
9. Add approximatetly 1.5g of Ascorbic Acid (reducing agent) to the cell and stir until the solution changes to a pale green/yellow colour.
10. Add a pre-prepared polished silver disc in the disc holder to the Po cell using prewashed stainless steel tongs.
11. Leave to plate for 36 hours or more, on a warm hotplate away from draught.
12. Inspect the cell regularly during the early stages of plating to ensure that the discs are not discolouring (i.e. turning black) and the volume of plating solution is maitained. If discs do become tainted replace with newly polished clean disc.
13. At the end of the plating procedure remove the disc, wash down with distilled water followed by a rinse in acetone. Label the sample on the back and leave covered for a minimum of 24 hours before counting on the alpha spectrometer.

Reagents:

Aqua Regia (3:1 $HCl:HN0_3$)

6M HCl

209Po yield tracer (approximately 4.28 dpm/ml)

Ascorbic acid.

APPENDIX 1.2

Preparation method for determination of major and trace elements by XRF Spectrometry.

Major and trace elements concentrations were determined using X-ray fluorescence on both the Philips PW 1400 and Philips Magix Pro sequential X-ray spectrometers at the Southampton Oceanography Centre under the supervision of Dr. I.W. Croudace. The procedure follows that outlined in Croudace and Williams-Thorpe (1988).

Preparation of samples for major elements (fused glass beads)

1. Oven-dried samples were ground for two minutes in a motorised tungsten-carbide (5-sample) giratory Tema mill.
2. Sediment samples were then ignited at 850°C to remove carbonates.
3. A sub-sample of 0.8g of powdered sediment was then accurately weighed (error range ±0.0002 g) and 4 g of lithium metaborate/lithium tetraborate "eutectic" flux (ratio = 4:1) then added. This mixture was then carefully homogenized.
4. Individual samples were then melted at 1150°C in platinum crucibles over a dual oxygen/propane burner and then carefully decanted into pre-heated platinum moulds and allowed to cool. In the early stages of cooling the sample is gently oscillated to ensure homogenization of the fused bead sample.
5. Samples were then carefully labelled and run on the XRF spectrometer with standard reference materials (e.g. BCR-1).

Major element abundances are determined as oxides according to XRF convention and given as % abundance of ashed sample. Precision in measurement is routinely less than 1 % r.s.d (relative standard deviation).

Preparation of samples for trace elements (pressed powder pellets)

1. Approximately 8-10 grams of oven-dried sample were powdered for up to 3 minutes in a motorised tungsten-carbide (5-sample) giratory Tema mill to produce a homogenized sample with a distinct rock-flour consistency. (Samples are dried at a maximum of 45°C to avoid loss of volatile elements).
2. Prior to pelleting, between 10-15 drops of 8% PVA glue (to act as a binder) was added to the powdered samples and carefully homogenized.
3. Samples were them pressed in an automatic 'pelletizer' set at 12 tons per square inch prssure for approximately 15 seconds.

4. The pressed pellet was then carefully removed and labelled and allowed to dry prior to XRF analysis.
5. Powder pellets are run of the XRF with international standards (e.g. MAG-1 Marine Shale).

Element concentrations of pressed powder pellets are given in parts per million (ppm) and the precision is routinely < 5%. In this study trace element data accuracy was generally < 3%.

APPENDIX 1.3

Microscopic identification of diatoms is only possible following rigorous cleaning of sediment sub-samples. This entails the removal of organic matter and unwanted mineral material. The method outlined here follows the procedure given in Batterbee (1986).

Preparation of samples for Diatom analysis.

1. Approximately 1 g (wet weight) sub-sample of sediment is taken from selected core depth increments and placed in glass beaker.
2. Approximately 20 ml of Hydrogen peroxide (H_2O_2) is then added and the sample is then heated on a hotplate set at 90°C in a fume cupboard to remove unwanted organic matter. After half an hour coarse plant material can also be removed.
3. The sample beaker is then removed from the heat source and 1-2 drops of HCl (50%) are added to remove any remaining H_2O_2 and carbonates. The beaker sides should then washed down with distilled water to ensure sample integrity.
4. The samples should then be allowed to cool in a fume cupboard (as chlorine is generated from the HCl). Once cool the samples are decanted into centrifuge tubes leaving coarse material in the beaker.
5. Samples are then centrifuged at 1200 rpm for 4 minutes.
6. The supernatant is decanted off and the pellet re-suspended by gently tapping the base of the tube. This is then topped up with distilled water and re-centrifuged as before.
7. The washing process is repeated at least three times. In clay-rich samples the fine clay particulate material can be removed by addition of a few drops of very weal ammonia solution. The clay is then decanted off with the supernatant.

Preparation of Diatom slides

1. The cleaned diatom suspension is then cleaned to a suitable concentration (neither totally clear or milky). Fine particles should be just visible when the suspension is held up to the light.
2. Place cover slips to be used on settling out trays in a position where they will be undisturbed away from dust and air currents.
3. Using a 1 ml pipette, place up to 0.5 ml of well mixed diatom suspensiononto each labelled cover slip, cover and leave to dry for at least two days.
4. Heat a hotplate in a fume cupboard to 130°C.

5. Place 1 drop of Naphrax mounting fluid onto the centre of the glass slide and then invert the dried cover slip for the sample and place onto the slide over the drop of mounting fluid.
6. Heat the slide for 15 minutes to drive of the toluene in the Naphrax taking care to avoid fumes (toluene is a know carcinogen).
7. Take due acre to eliminate any trapped bubbles arising from the heating procedure and then remove the slide and allow to cool.
8. Once cool check the cover slip to ensure that it is firmly fixed to the slide by gently pushing with a fingernail. If any movement occurs the slide must be re-heated.

The slides are now ready to be counted using a light microscope (100 x magnification) and suitable immersion oil with a refractive index comparable to the lens configuration.

APPENDIX 1.4

Determination of organic content via the Loss on Ignition (LOI) proxy method

1. Sub-samples at consecutive 1 cm depth intervals were extracted from the all the cores using a clean scalpel. No shell or coarse clastic material was removed prior to combustion.
2. The sediment samples were oven dried at 50°C for a minimum of 24 hours and powdered using a pestle and mortar.
3. Powdered sediment was then added to a pre-weighed ceramic crucible and re-weighed following taring of the balance.
4. The samples were then combusted at an ignition temperature of 550°C for 2 hours in a vented furnace, allowed to cool in a dry atmosphere and re-weighed.
5. The samples were then combusted for a second time at an ignition temperature of 850°C for 12 hours and then re-weighed.
6. Loss on ignition was calculated as a percentage of the dry sample mass lost (e.g. Grimshaw, 1989) from the following equation:

$$\text{Loss on ignition (\% dry mass)} = \left(\frac{\text{Post combustion loss (g)}}{\text{Pre-combustion mass (g)}} \right) \times 100$$

APPENDIX TWO

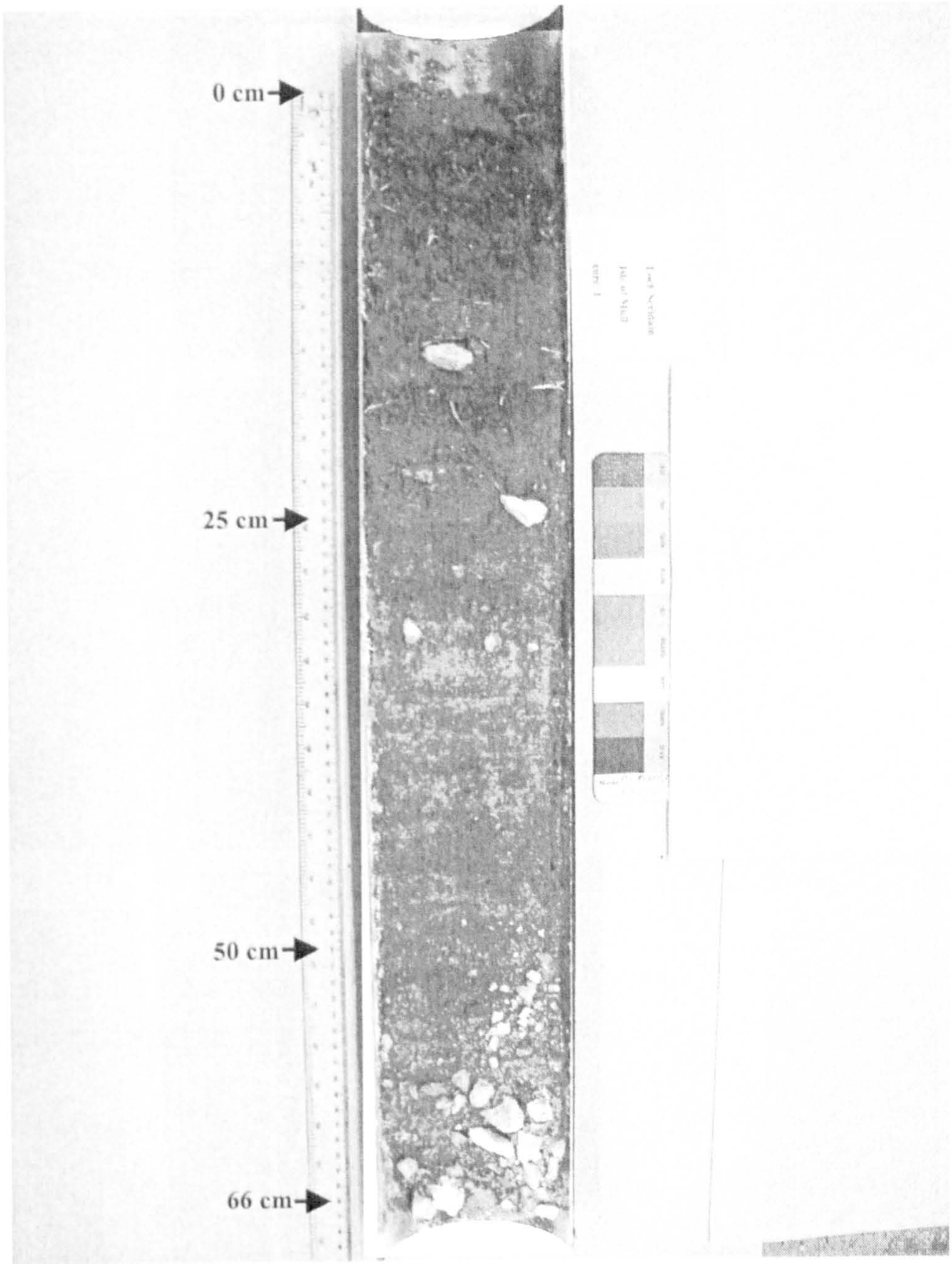

Appendix 2.1: Digital photographic image of the sediment sequence (core 1) acquired from the Head of Loch Scridain, Western Isle of Mull, Argyll showing the general sediment colour and organic content.

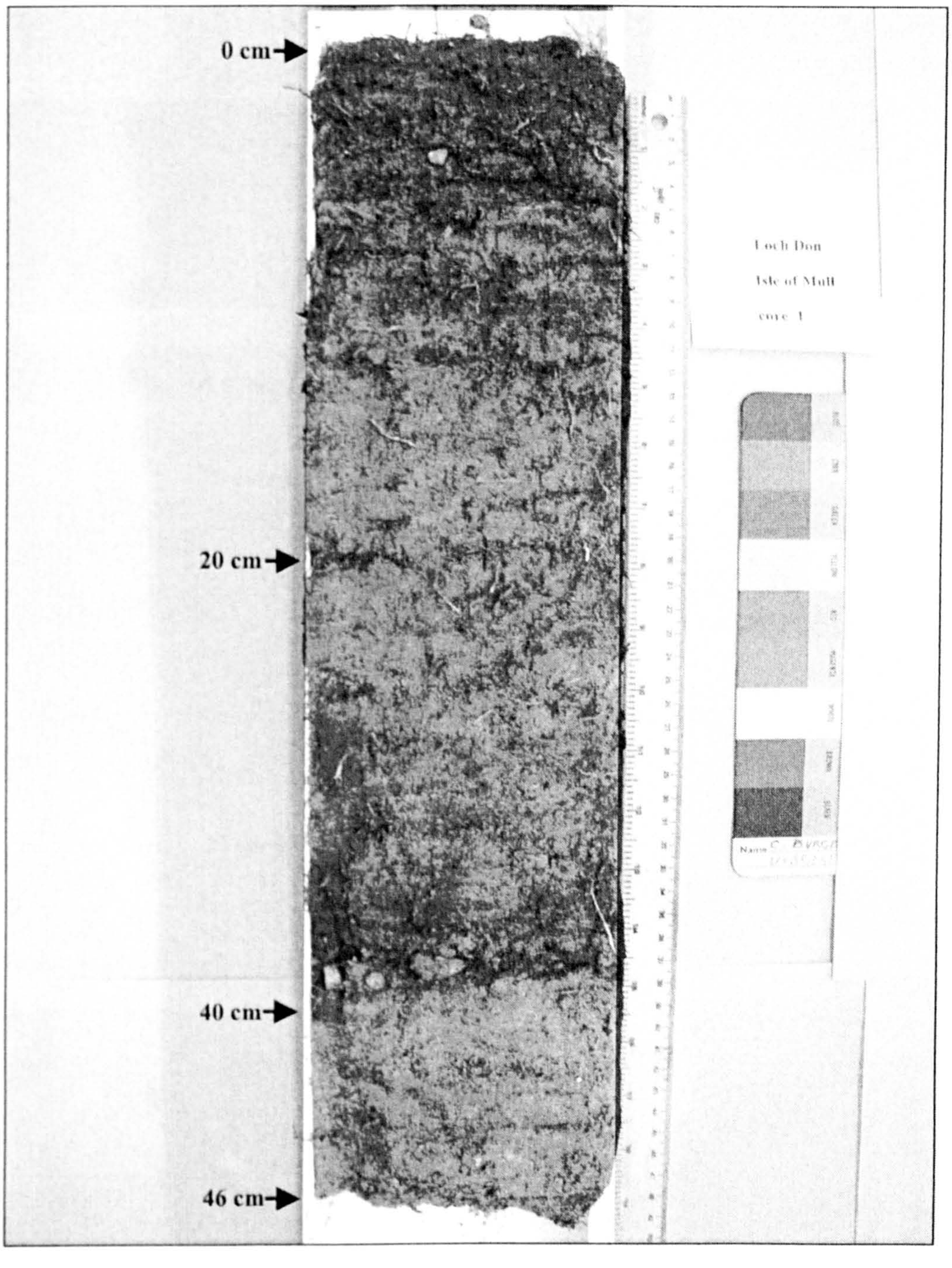

Appendix 2.2: Digital photograph of the acquired sedimentary sequence from Loch Don (core 4) Isle of Mull, Argyll taken under laboratory conditions to show the general characteristics of the sediment colour and characteristics.

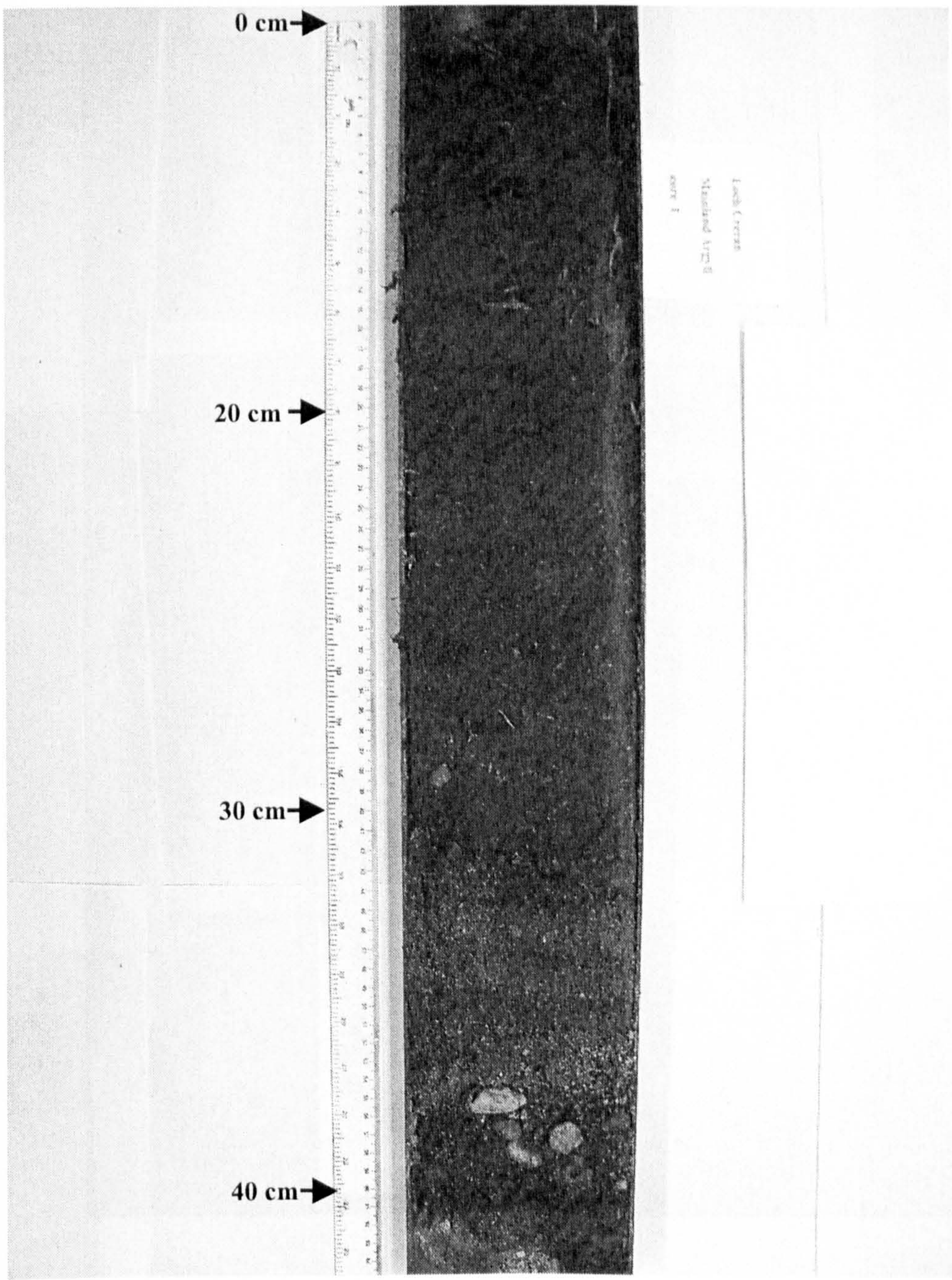

Appendix 2.3: Digital photographic image of the sedimentary sequence acquired from Loch Creran, mainland Argyll to show general sediment characteristics and organic material.

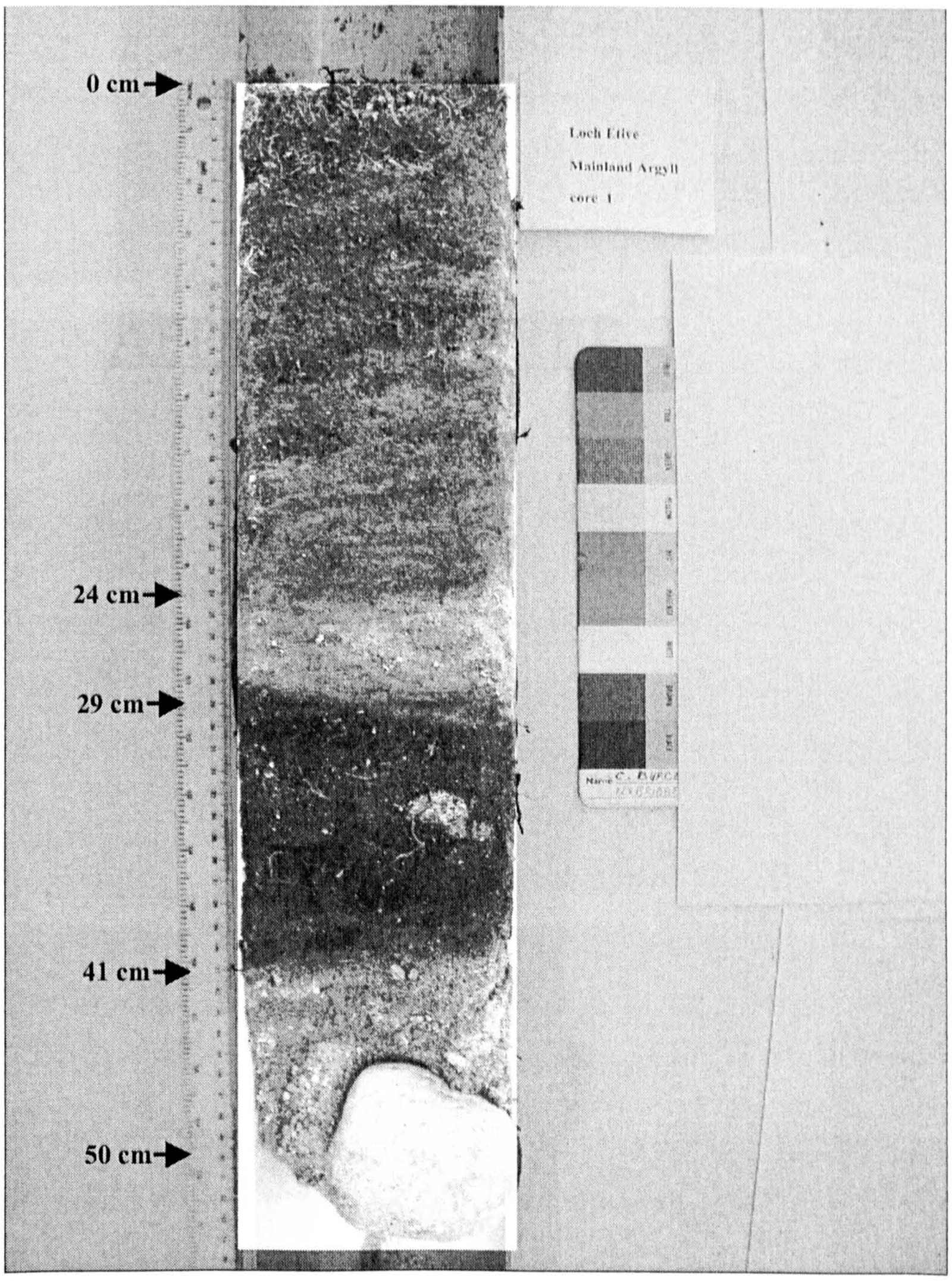

Appendix 2.4: Digital photographic image of the sedimentary sequence acquired from the Head of Loch Etive, mainland Argyll, taken under laboratory conditions showing distinct sedimentary units, sediment colour and organic material with marine redistributed sands and gravels. (Note the presence of the large granite cobble at the base).

APPENDIX THREE

Appendix 3.1: Aerial photograph (1988) of the area surrounding the Head of Loch Scridain, Western Isle of Mull, Argyll. (Source: Royal Commision for Historical and Archaeological Monuments of Scotland, (RCHAMS), Edingburgh).

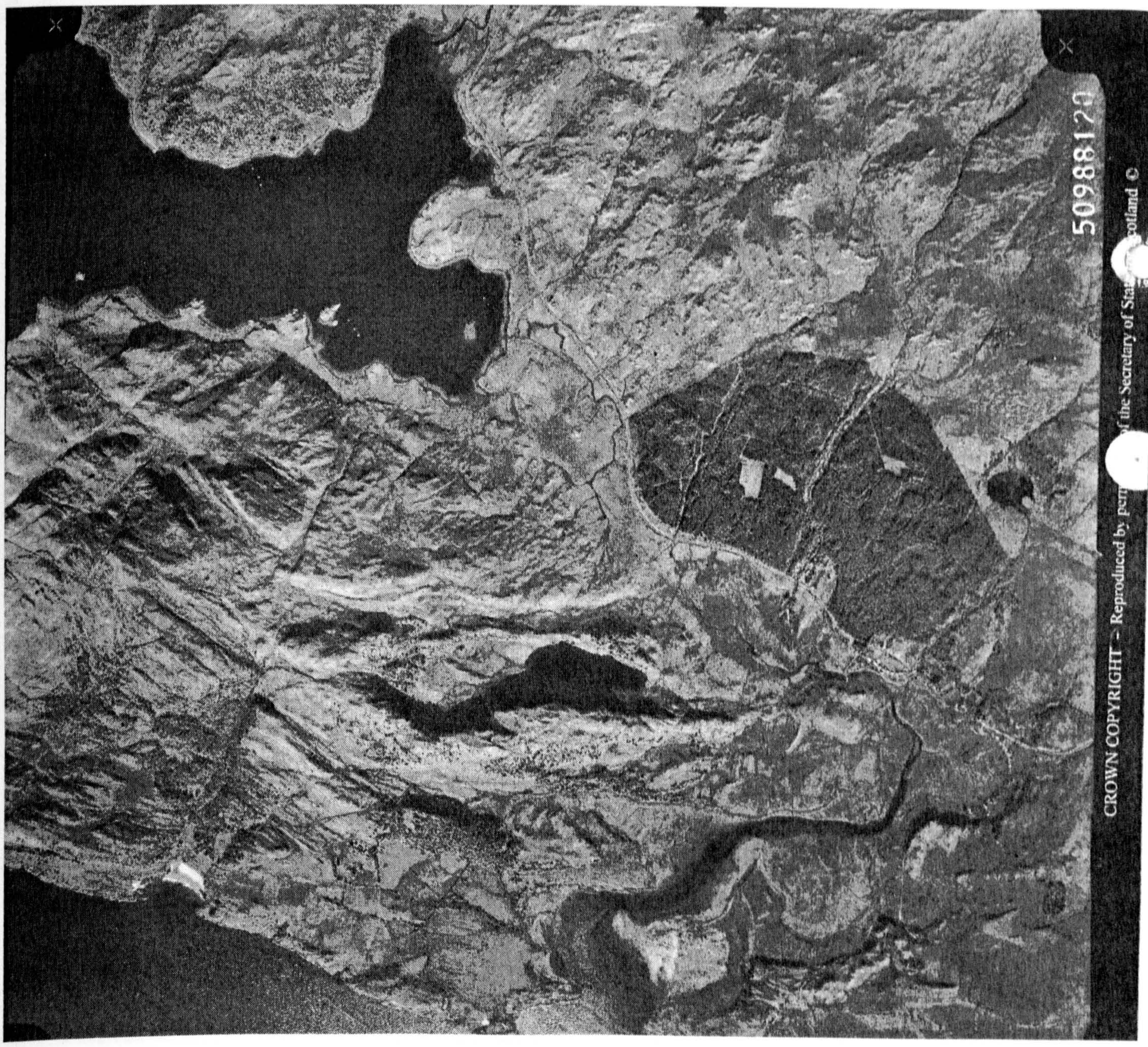

Appendix 3.2: Aerial photograph (1988) of the area surrounding Loch Don, South-East Isle of Mull. (Source: Royal Commision for Historical and Archaeological Monuments of Scotland, (RCHAMS), Edingburgh).

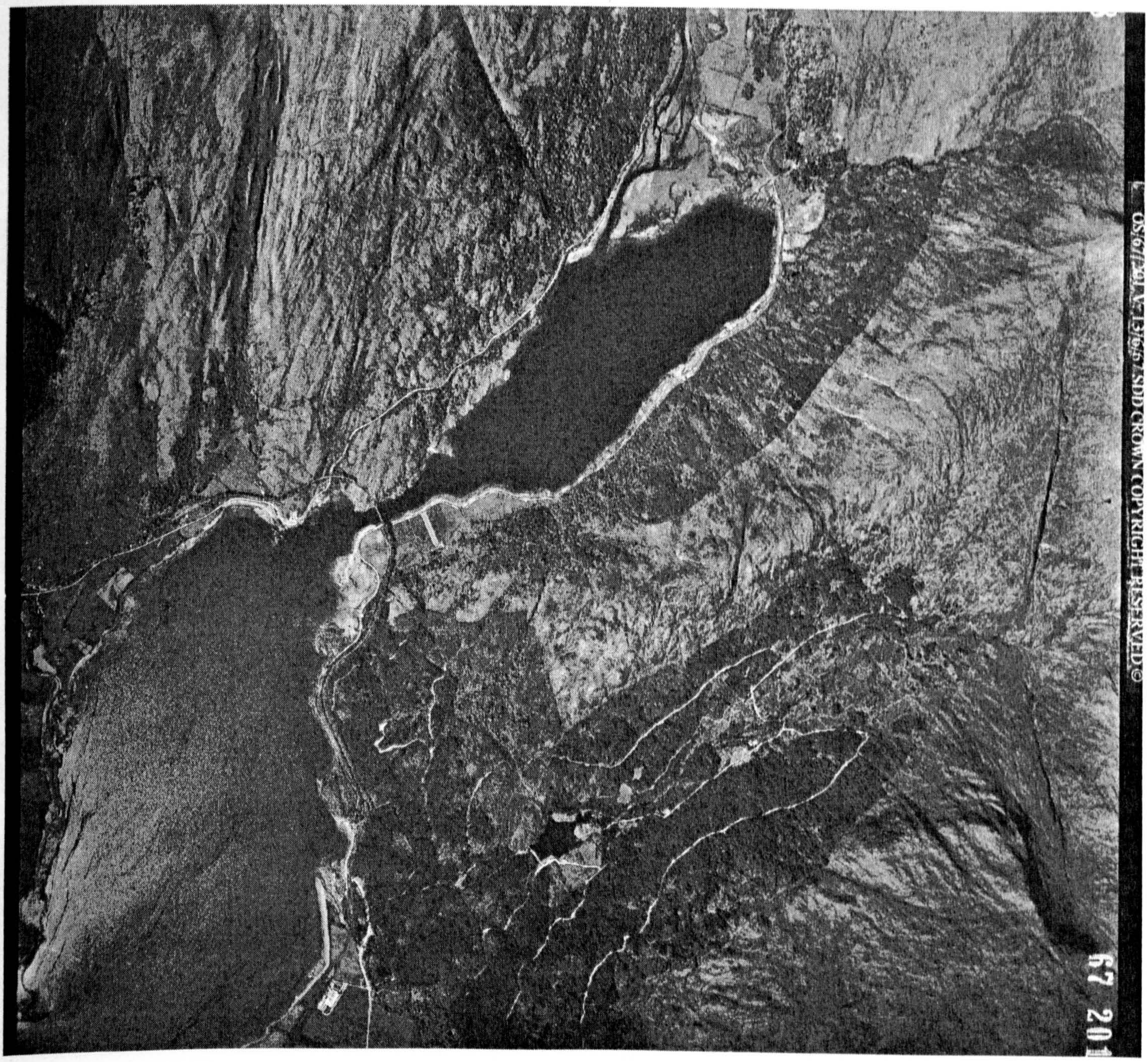

Appendix 3.3: Aerial photograph (1988) of the area surrounding the head of Loch Creran and lower Glen Creran, mainland Argyll.
(Source: Royal Commision for Historical and Archaeological Monuments of Scotland, (RCHAMS), Edingburgh).

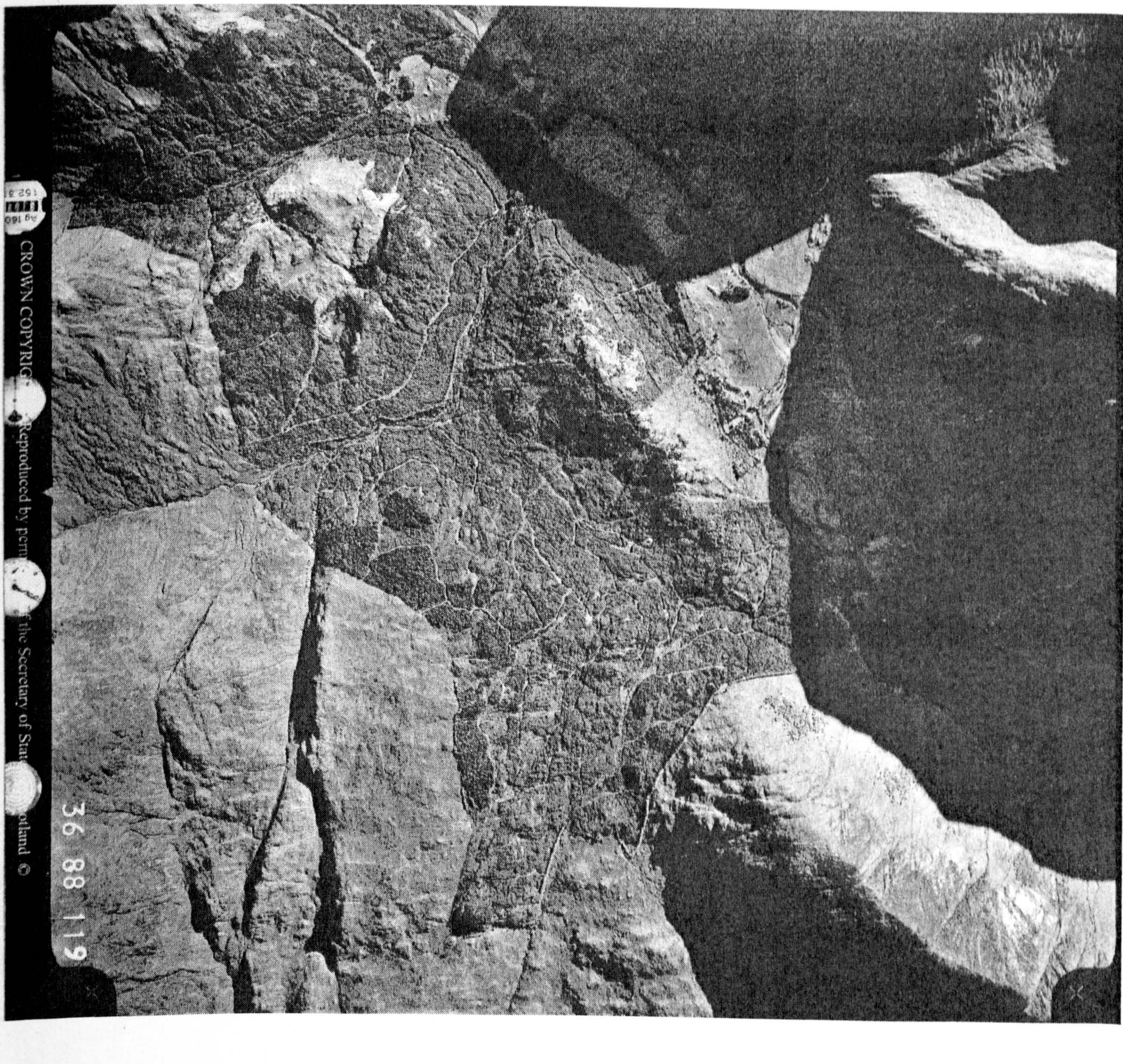

Appendix 3.4: Aerial photograph (1988) of the area surrounding the head of Loch Etive and lower Glen Etive, mainland Argyll. (Source: Royal Commision for Historical and Archaeological Monuments of Scotland, (RCHAMS), Edingburgh).

APPENDIX FOUR

Depth below marsh surface (cm)	SiO2	TiO2	Al2O3	Fe2O3	MnO	MgO	CaO	Na2O	K2O	P2O5	SO3	LOI
-0.5	56.12	1.33	15.03	12.11	0.24	4.16	5.69	3.35	1.81	0.44	0.40	6.84
-2.5	56.03	1.31	14.98	11.45	0.23	4.32	5.68	3.40	1.80	0.43	0.39	7.64
-5.5	56.05	1.34	14.83	12.18	0.24	4.25	5.73	3.34	1.78	0.45	0.41	6.56
-8.5	55.61	1.40	15.15	11.03	0.21	4.41	5.63	3.38	1.76	0.43	0.31	6.61
-11.5	54.36	1.45	15.19	12.04	0.19	4.44	5.74	3.45	1.67	0.42	0.32	8.25
-14.5	52.63	1.50	16.08	12.77	0.29	4.57	5.64	3.46	1.67	0.44	0.39	9.30
-17.5	54.32	1.50	15.94	12.10	0.28	4.45	5.94	3.48	1.69	0.40	0.27	6.64
-20.5	54.37	1.47	16.14	11.61	0.24	4.34	6.09	3.61	1.64	0.31	0.31	8.40
-23.5	53.86	1.51	16.30	11.96	0.21	4.31	5.90	3.52	1.67	0.34	0.30	9.50
-26.5	54.24	1.48	15.59	11.97	0.18	4.40	6.04	3.48	1.57	0.32	0.31	8.95
-29.5	54.33	1.46	15.96	11.49	0.16	4.27	6.05	3.55	1.63	0.31	0.34	9.91
-32.5	55.31	1.39	15.47	12.45	0.17	4.14	5.89	3.93	1.70	0.29	0.36	10.13
-35.5	54.25	1.33	14.92	13.70	0.18	4.02	5.73	3.47	1.67	0.30	0.31	9.20
-38.5	55.14	1.45	16.08	11.40	0.17	4.39	6.25	3.59	1.58	0.27	0.30	9.30
-41.5	56.86	1.40	15.44	9.25	0.14	4.42	6.25	3.53	1.63	0.25	0.29	9.87
-44.5	56.78	1.34	15.25	8.76	0.14	4.35	6.21	3.61	1.66	0.24	0.34	11.36
-47.5	58.57	1.36	15.16	8.46	0.14	4.34	6.60	3.57	1.71	0.21	0.31	10.55
-50.5	57.60	1.30	14.69	8.31	0.14	4.37	6.60	3.46	1.63	0.20	0.32	11.25
-53.5	59.11	1.37	14.93	8.29	0.15	4.54	6.90	3.80	1.66	0.19	0.26	11.78
-56.5	57.83	1.38	14.38	8.58	0.16	4.89	7.45	3.27	1.58	0.18	0.24	11.90
-59.5	56.91	1.60	13.59	9.10	0.19	5.59	8.33	2.91	1.48	0.17	0.22	12.43
-62.5	56.65	1.40	14.43	8.70	0.16	4.87	7.03	3.37	1.67	0.21	0.26	11.61
-65.5	54.56	1.31	14.65	11.15	0.16	4.60	6.81	3.88	2.04	0.22	0.22	11.47
Core Average	55.72	1.41	15.22	10.82	0.19	4.45	6.27	3.50	1.68	0.31	0.31	9.54
2 Stand. Dev	3.22	0.16	1.31	3.32	0.09	0.62	1.32	0.41	0.21	0.19	0.11	3.62

Appendix 4.1: Major element abundance (% ashed mass of oxides) from the Loch Scridain core, western Isle of Mull, Argyll.

Depth below marsh surface (cm)	As	Ba	Br	Ce	Cr	I	La	MnO	Nb	Ni	Pb	Rb	Sr	TiO2	V	Y	Depth below marsh surface (cm)	Cl	S
-0.5	26.1	117.8	167.55	18.7	59.6	237.71	8.8	2387.4	6.4	28.2	36.7	13.9	112.5	4624	130.2	13.9	-0.5	36322.439	13066.39
-1.5	26.8	121.4	164.39	19	60	247.98	9.1	2405.3	6.9	27.9	38	14.7	112.1	4874.5	130.7	13.6	-2.5	34492.848	12791.43
-2.5	26.6	115.3	161.62	25.8	61.6	234.69	11.2	2941.3	7.4	26.9	37.1	15.4	116.4	4965.4	134.4	14	-5.5	26705.782	10855.96
-3.5	30.2	132.1	176.56	20.7	62	287.65	12	2109.7	7.2	29.1	49.5	16	124	5402.6	141.3	14	-8.5	23007.227	9133.53
-4.5	31.6	142.4	164.89	28.8	72.1	268.74	14.1	2351.2	8.2	30.8	51.8	18	128.8	5742.6	149.6	15.6	-11.5	16199.969	6609.97
-5.5	32.1	165.7	176.51	29.2	76.8	290.52	14.8	2248.3	7.7	32.6	50.4	16.3	132.8	6984.8	164.7	17.4	-14.5	14105.853	5231.22
-6.5	34.8	177.9	186.82	29.7	86.2	356.53	15.2	2152.6	8.2	36.5	49.8	21.6	139.2	7141	169.8	18.1	-17.5	15407.904	5096.08
-7.5	40.2	159.1	223.12	30.2	81.6	408.62	15	2061.9	8	34.1	50.7	21.3	130.4	6717.5	168.2	17.6	-20.5	14380.589	4807.96
-8.5	42.2	182.5	210.66	29	85.1	413.72	15.3	2389.3	9.1	37.3	55.4	23.3	134.3	7350.1	177.5	18.6	-23.5	16241.133	5038.44
-9.5	39	210.3	179.35	34.5	98.7	367.91	16.1	2023.9	9.6	39.8	48.9	25.8	149	8955.2	184.9	20.5	-26.5	19758.159	4924.30
-10.5	38.6	235.7	166.63	33	106.7	337.24	15.7	1716.6	9.5	43.7	48.9	25.7	155.7	9666.7	193.6	23.1	-29.5	17493.298	4801.72
-11.5	42	252.5	159.60	36	112.7	363.63	17.4	1663.9	10.6	41.7	52.3	26.5	154.5	9985.2	207.2	23.1	-32.5	18560.165	4415.31
-12.5	37.6	261.3	149.11	33	109.4	398.70	16.4	1610.3	10.3	46.4	46.2	25.4	154	10303.6	203.2	22.6	-35.5	14288.542	3963.49
-13.5	32.6	311.6	105.54	42.2	109.5	306.45	19.9	1902.3	11.5	49.5	32.2	30.2	164.3	11655.5	203.1	26.7	-38.5	23083.154	4329.63
-14.5	29.5	277.5	103.04	39.6	112.7	336.51	20	2132.1	11.8	50.3	29.3	28.9	163.9	11634.4	205.2	27.5	-41.5	17883.734	3851.07
-15.5	26.5	288.7	91.22	42.1	118.2	355.44	20.3	2100.9	11.4	48.5	28	28.8	162.9	11468.9	200.3	27.5	-44.5	19797.851	4372.96
-16.5	24	335.5	78.53	39.5	122.4	276.40	21.2	2063	11.4	46.9	25.1	33.5	173.1	11891.5	202.1	28.7	-47.5	19630.547	4901.61
-17.5	24.3	263.5	92.55	48.9	107.8	426.34	19.3	1870	11.6	47	23.3	30.5	163.7	11688.8	198.7	26.1	-50.5	17063.551	5126.53
-18.5	21.2	310.9	75.40	50.5	111	330.45	21.4	1872	11.2	45.8	20.6	31.4	173.4	12135	197.4	29.1	-53.5	15640.402	4076.90
-19.5	22.2	280	82.60	46.4	107.8	397.02	22.4	2085.5	11.1	45.3	20.9	30	164.6	11876.6	203	27.1	-56.5	12692.147	5778.88
-22.5	20.9	292.2	80.05	51.4	103	389.92	22.3	1921.4	11.2	47.1	19.4	28.5	165.5	11675.3	197.8	27.8	-59.5	10237.387	5388.92
-24.5	19.3	287	73.03	49.5	105.1	350.01	20.3	1525.1	11.3	47.2	18.6	26.3	166	12398	205.3	27.3	-62.5	8352.4587	5703.63
-26.5	20.6	290.9	68.08	47.3	103.6	350.06	20.5	1508.5	11.6	47.6	16.8	28.7	170.8	12191.9	206.2	27.9	-66.5	10328.172	4534.42
-28.5	19.7	325.2	58.98	49.6	111	313.95	19.8	1431.6	11.6	47.1	18.5	32.2	171.4	12153.4	204.3	28.1			
-30.5	20	313	63.61	39.8	113.5	354.01	18	1279.1	11.9	48.8	18.1	30.2	166.6	12485.3	210.6	27.6	Core Average	18333.622	6007.2135
-32.5	23.2	315.3	60.14	50.5	103.9	413.16	19.6	1492.1	11.6	48.3	15.4	33.6	169.4	11689.8	204.2	27.6			
-34.5	23.2	356.5	53.84	45.4	102.1	450.92	22.6	1574.7	12.3	45.2	13.4	33.8	168.9	11476.2	202	28.1			
-36.5	13.7	413.7	42.56	41.1	108.8	243.98	19.6	1501.8	11.6	44.7	9.9	37.6	180.9	11843.1	185.8	30.4			
-38.5	16	334.7	59.05	44.3	114.7	4.39	20.8	1321.7	11.2	49.3	11.2	31.8	176.8	13155.8	206.6	29.9			
-40.5	16.1	423	37.89	47.7	110.4	195.62	22.2	1375.2	12.9	48.8	9.5	33.9	199.7	13144	211.1	32.1			
-42.5	14.2	374.4	37.62	42.3	120.3	182.33	19.8	1216.6	11.8	48.3	10.3	37.4	179.1	12457.4	204.2	30.6			
-44.5	12.5	375.2	35.63	44.9	115.4	173.50	18.9	1239.6	11.1	48.4	10.4	35.9	182.9	12913.6	207.1	31.3			
-46.5	12	380.6	24.42	54.6	125.1	112.76	19	1261.9	11.5	46.5	10.3	38.7	188.3	13385.7	192.5	31.9			
-48.5	10.1	362.5	17.99	42.7	125	3.52	19	1314.7	11.6	47.3	9.6	37.9	190.8	14019.9	205.7	32			
-50.5	8.4	406	15.02	35.7	127.6	47.95	21.7	1294.4	11.7	49	8.8	38.8	192.7	13741.1	205.8	32.2			
-52.5	7.5	405.2	15.12	39.8	121.9	48.49	20.3	1293.1	12.1	52.6	7.7	39.1	189.5	13805.3	207.2	33.7			
-54.5	3.8	442.3	6.49	39.6	130.1	15.70	17	1429.5	11.6	49.5	7.8	44.4	199.4	14414.1	192.4	35.2			
-56.5	3.3	406.3	6.29	39.4	160.9	19.63	16	1458.5	11.4	49.4	7.4	42.7	193.3	15018.5	207.5	34.7			
-58.5	4.7	505	5.92	38.3	146.4	23.30	15.5	1548.9	13.9	51.1	5.9	44.6	192.1	14823.2	218.6	35.5			
-60.5	7	483.9	6.58	45.7	155	22.97	17.8	1623.2	12.8	54.7	7.4	40.1	196.2	16202.5	221.8	35.9			
-62.5	8.8	566.8	5.32	56.1	142.7	15.44	20	1593.7	14.5	53.8	10.5	44.1	219.8	15115.3	214.8	37.4			
-64.5	6.5	538.8	3.22	55.6	122.7	7.97	19.7	1562.4	13.3	52.4	6.2	44.1	208.8	13477.2	197.2	38.5			
-66.5	15.7	737.8	3.82	63.6	97.7	15.70	27.5	1427.8	16.3	42.5	7.3	45	204.7	10817.9	162.8	36			
Core Average Conc.	30.85	167.05	26.90	163.45	10.93	24.55	84.19	44.37	21.75	107.65	191.55	318.09	18.22	40.50	1750.77	1750.77			

Appendix 4.2: Trace element concentration data (ppm) for the Loch Scridain marsh core determined from pressed poweder pellets. Data for chlorine and sulphur have been determined using the same depth increments as for major element geochemistry

Depth below marsh surface (cm)	SiO2	TiO2	Al2O3	Fe2O3	MnO	MgO	CaO	K2O	Na2O	P2O5	SO3	LOI
-0.5	61.76	0.96	13.44	8.46	0.30	3.36	3.20	2.78	4.96	0.53	5.27	9.49
-3.5	59.70	0.99	14.03	9.64	0.28	3.29	2.97	2.96	5.41	0.50	5.36	9.02
-6.5	61.40	1.02	13.99	8.81	0.17	3.19	3.34	2.70	4.62	0.38	3.47	9.14
-9.5	63.36	1.11	14.37	8.68	0.11	3.24	3.87	2.28	3.94	0.28	2.19	8.14
-12.5	58.64	1.10	14.57	10.51	0.18	3.24	3.47	2.26	3.99	0.32	2.41	7.12
-15.5	62.71	1.08	14.17	9.32	0.19	3.14	3.45	2.31	3.59	0.29	1.68	11.00
-18.5	63.23	1.08	13.63	9.11	0.23	3.02	3.78	2.12	3.52	0.27	1.61	5.60
-21.5	62.99	1.19	14.21	9.16	0.26	3.27	4.09	2.12	3.51	0.28	1.59	7.40
-24.5	62.53	1.14	13.91	9.75	0.33	3.15	4.22	1.95	3.25	0.27	1.31	6.84
-27.5	60.87	1.15	13.96	12.27	0.26	3.07	4.10	1.86	3.19	0.26	1.20	9.24
-30.5	64.15	1.14	13.15	8.64	0.14	3.08	4.62	1.75	3.10	0.19	1.03	5.23
-33.5	64.41	1.14	13.91	7.26	0.10	3.05	4.13	1.96	3.32	0.22	1.10	8.35
-36.5	65.83	1.15	13.89	7.20	0.10	3.13	4.52	1.92	3.41	0.22	1.14	10.53
-39.5	66.40	1.10	13.32	6.62	0.10	2.95	4.66	1.72	3.09	0.17	0.81	6.05
-42.5	66.06	1.18	11.61	6.63	0.12	3.23	5.82	1.41	2.77	0.13	0.54	1.99
-45.5	68.76	1.07	11.90	6.03	0.10	2.92	5.44	1.47	2.98	0.14	0.62	1.58
Core Average	63.30	1.10	13.63	8.63	0.19	3.14	4.10	2.10	3.67	0.28	1.96	7.30
2 Stand. Dev.	5.07	0.13	1.59	3.12	0.15	0.24	1.51	0.86	1.45	0.22	2.91	5.26

Appendix 4.3: Major element abundance (% ashed mass of oxides) from the Loch Don core south-eastern, Isle of Mull, Argyll.

Depth below marsh surface (cm)	As	Ba	Bi	Br	Ce	Cl	Co	Cr	Cu	Ga	I	La	Mo	Nb	Ni
-0.5	26.80	357.07	1.40	1026.40	46.90	107412.30	43.90	120.40	47.30	15.30	349.20	25.20	6.50	12.30	59.00
-3.5	29.40	298.01	0.10	1190.30	105.00	107782.00	45.60	115.90	48.00	15.10	265.70	28.10	10.60	12.10	56.20
-6.5	26.40	350.30	-0.10	915.10	76.40	54371.90	33.10	129.20	42.40	16.00	377.20	43.10	8.20	13.00	53.20
-9.5	20.80	351.78	-0.20	722.60	55.70	53534.30	36.50	130.60	42.40	17.10	245.20	46.00	5.80	11.40	53.00
-12.5	26.30	354.68	0.40	742.40	42.10	49473.70	51.90	176.00	34.20	16.80	248.90	41.40	5.90	12.40	54.10
-15.5	28.30	370.71	0.40	712.70	57.50	34754.20	32.80	125.20	34.10	17.40	418.70	28.60	7.20	12.40	51.60
-18.5	24.50	363.92	0.20	579.30	61.70	32919.80	34.00	129.50	26.70	16.80	391.80	29.80	6.40	12.20	49.20
-21.5	24.80	357.62	-0.60	614.20	54.40	25978.40	39.70	123.40	29.40	17.20	356.00	10.50	5.80	12.00	52.80
-24.5	18.90	359.12	0.30	431.90	71.00	21615.50	50.10	123.10	24.80	14.80	271.20	7.00	4.40	11.30	46.50
-27.5	19.60	361.35	0.50	549.00	60.50	19944.50	42.00	130.90	32.50	16.00	368.40	20.40	3.80	11.40	50.50
-30.5	13.60	371.56	0.40	326.20	34.80	15458.70	34.40	130.90	23.60	15.20	160.30	12.40	2.20	10.70	41.90
-33.5	17.30	366.12	-0.40	441.70	70.90	22627.40	40.60	128.70	27.70	15.80	141.50	20.70	2.70	11.50	46.30
-36.5	16.90	382.80	0.10	364.20	39.60	18878.90	29.00	143.40	26.40	16.40	113.00	51.20	2.80	10.90	44.30
-39.5	10.90	356.59	0.10	104.10	26.80	9058.70	24.10	128.10	16.60	13.20	46.90	16.30	0.90	9.20	31.40
-42.5	12.70	362.10	0.40	63.00	54.20	6558.60	47.50	134.50	14.60	13.30	21.20	26.30	1.10	9.00	33.40
-45.5	10.00	406.27	0.10	44.50	15.00	5500.00	30.10	109.90	13.60	12.40	21.10	28.50	0.90	8.50	27.90
Average core conc.	20.45	360.63	0.19	551.73	54.53	36616.81	38.46	129.98	30.27	15.55	237.27	27.22	4.70	11.27	46.96

Appendix 4.4a: Trace element concentrations (ppm) determined from pressed dry powder pellets for the marsh core from Loch Don Isle of Mull, Argyll.

Depth below marsh surface (cm)	Pb	Rb	S	Sb	Sn	Sr	Th	U	V	Y	Zn	Zr
-0.5	39.6	79.20	21037.50	78.60	2.40	239.10	-3.20	15.20	173.80	27.90	154.50	268.60
-3.5	45.3	77.10	20641.70	76.80	4.60	215.10	-5.70	16.60	174.40	27.30	139.40	248.20
-6.5	48.4	71.80	15557.90	76.90	1.50	215.50	-3.80	14.30	188.30	28.80	125.60	258.00
-9.5	38.1	59.20	15176.60	77.70	3.00	223.00	-3.50	13.40	197.20	30.00	124.60	272.00
-12.5	43.5	70.00	14705.20	78.10	7.90	215.30	-2.80	13.40	180.00	30.40	117.20	293.30
-15.5	46.8	72.30	11407.80	76.80	1.60	214.60	-1.90	13.90	200.50	31.00	121.40	280.20
-18.5	39.8	70.70	10590.60	77.60	-0.20	209.20	0.10	11.80	182.50	29.70	110.30	289.40
-21.5	40.5	63.30	11322.10	78.00	3.40	215.20	-0.80	12.00	203.70	30.30	113.70	268.20
-24.5	26.8	58.30	10106.40	77.80	-3.00	219.80	0.00	9.00	171.50	28.20	90.20	274.90
-27.5	31.0	62.40	10844.60	77.20	-2.20	209.50	-0.70	9.60	179.20	31.40	96.90	283.40
-30.5	22.2	52.20	8194.20	77.00	-1.50	224.30	1.40	5.20	169.30	27.90	79.70	287.00
-33.5	22.0	55.80	11068.90	76.90	-5.30	233.20	0.00	10.50	189.60	30.20	81.40	255.10
-36.5	21.5	55.60	8934.20	77.40	-1.40	231.00	0.70	9.70	184.40	29.00	77.50	270.60
-39.5	11.6	44.80	4286.70	76.60	-1.90	225.20	1.70	4.40	155.00	25.80	60.50	295.50
-42.5	8.9	42.00	2727.10	77.30	-1.60	225.00	1.50	5.40	165.40	26.00	57.60	310.20
-45.5	9.7	44.10	2955.90	77.30	-2.90	226.50	2.20	2.70	143.90	24.60	52.40	286.30
Average core conc.	30.98	61.18	11222.34	77.38	0.28	221.34	-0.93	10.44	178.67	28.66	100.18	277.56

Appendix 4.4b: Trace element concentrations (ppm) determined from pressed dry powder pellets for the marsh core from Loch Don Isle of Mull, Argyll.

Depth below marsh surface (cm)	SiO2	TiO2	Al2O3	Fe2O3	MnO	MgO	CaO	K2O	Na2O	P2O5	SO3	LOI
-0.5	56.84	0.78	14.37	11.37	0.47	3.98	2.58	2.86	4.04	0.89	4.18	6.11
-1.5	56.12	0.76	14.62	12.69	0.50	4.03	2.60	2.80	4.10	0.97	4.21	5.95
-3.5	58.01	0.84	14.78	10.11	0.23	4.28	2.74	2.94	4.59	0.83	5.91	4.98
-6.5	59.21	0.82	14.27	9.39	0.14	3.67	2.48	2.67	3.87	0.54	3.01	5.02
-9.5	61.89	0.85	14.69	7.59	0.15	3.67	2.47	2.72	3.78	0.48	2.37	4.96
-12.5	64.82	0.86	14.52	7.17	0.10	3.52	2.48	2.73	3.61	0.38	1.99	4.98
-15.5	68.10	0.87	14.33	5.68	0.07	3.34	2.53	2.60	3.48	0.31	1.27	4.00
-18.5	65.11	0.87	14.53	6.49	0.08	3.41	2.50	2.72	3.39	0.31	1.68	4.39
-21.5	62.21	0.72	12.12	14.49	0.13	2.52	2.17	2.31	3.21	0.28	2.21	4.67
-24.5	65.30	0.77	12.84	9.57	0.07	2.74	2.35	2.47	3.50	0.30	2.20	3.88
-27.5	66.78	0.85	13.70	5.41	0.07	3.19	2.52	2.67	3.74	0.32	2.47	5.30
-30.5	67.73	0.83	14.71	5.74	0.07	3.13	2.51	2.90	3.78	0.31	1.84	5.49
-32.5	65.85	0.92	14.85	5.80	0.07	3.53	2.67	2.83	3.79	0.36	2.45	5.13
-36.5	66.02	0.89	14.43	6.88	0.10	3.40	2.58	2.76	3.67	0.32	1.84	5.86
-39.5	65.47	0.84	14.20	7.36	0.17	3.31	2.61	2.78	3.84	0.33	1.99	5.29
-42.5	65.77	0.52	13.77	9.15	0.68	2.25	2.17	3.02	3.55	0.19	1.29	2.15
-45.5	71.50	0.57	14.10	4.05	0.06	2.19	2.13	2.98	3.61	0.18	1.07	1.68
-48.5	71.79	0.53	14.17	3.75	0.05	2.18	2.08	3.11	3.54	0.14	0.73	1.95
-51.5	72.03	0.53	14.37	3.65	0.06	2.01	2.22	3.17	3.70	0.11	0.66	1.45
-54.5	71.12	0.57	14.10	4.48	0.05	1.91	1.93	3.08	3.53	0.14	0.81	0.60
-56.5	71.38	0.54	14.04	4.02	0.06	2.26	2.09	3.02	3.44	0.14	0.84	1.37
-60.5	72.18	0.57	14.32	4.27	0.05	1.98	1.61	3.45	3.06	0.12	0.83	1.50
Core Average	65.69	0.74	14.17	7.23	0.16	3.02	2.36	2.84	3.67	0.36	2.08	3.94
2 Stand. Dev.	9.77	0.28	1.24	5.94	0.33	1.45	0.55	0.48	0.62	0.48	2.56	3.49

Appendix 4.5: Major element abundance (% ashed mass of oxides) from the Loch Creran core mainland Argyll.

Depth below marsh surface (cm)	As	Ba	Br	Ce	Cl	Co	Cr	Cu	Ga	I	La	Mo	Nb	Ni
-0.5	56.6	442.93	1775.9	138.3	29039	108.6	92.1	57.7	17.2	635	44.3	8.8	15.1	61.9
-3.5	52.1	446.66	1729.2	128.5	34676.9	33.9	90.1	49.2	17.7	528.8	52.9	11.5	16.8	51.7
-6.5	41.5	515.97	1109.7	111.1	24791	33.6	94.1	34.1	18.8	547.7	49.4	7.8	16.7	42.2
-9.5	43.9	515.46	1157.2	118.5	24648.9	34	97.9	38.2	18.3	673.6	39.8	8.2	17.7	42.1
-12.5	36.1	487.67	750.6	135	21129.5	29.3	97.7	26.9	17.9	402.4	49.5	8.2	17.5	40.4
-15.5	32.2	550.96	992.7	113.7	25185.3	26.7	96.3	30.8	18	407.2	54.4	6.5	17.3	43
-18.5	36.1	530.88	978.2	128	24789.3	30.7	109.9	34.9	20	511	52.2	7.9	18.4	46.2
-21.5	29.8	563.54	928.4	105.3	23750.1	50.9	90.4	23.9	18.2	379.1	65.1	4.8	17.4	42.9
-24.5	32.4	521.37	1035.4	108.5	25641.1	43.7	83.4	21.2	16.1	416.3	55	7.6	15.7	35.2
-27.5	25.5	564.24	927.8	108.5	22921	51.9	92.3	22.2	17.2	210	34.7	6.7	17.1	42.7
-30.5	25.5	586.64	869.7	119.5	22255.2	45	97.1	20.8	18.9	314.1	28.2	5.8	17.9	46
-32.5	21.4	554.80	786.6	118.4	22467.4	43.6	78	14.2	18.4	309.2	34.2	6.1	17.4	38.5
-36.5	19.3	530.91	619.4	116.4	22872.5	41.2	95.4	20.3	17.7	296.9	41.7	6.2	16.5	36.1
-39.5	19	554.55	568.9	69.5	19997.7	36.4	94.6	18.9	19.1	313.3	66.2	6.4	15.4	35.1
-42.5	45.6	555.02	636	152.5	20445.7	83.6	86.5	17.1	16.5	519.1	58.7	20	15.8	42.2
-45.5	52	642.02	319.9	83.5	11394.5	55.6	68.3	14.9	16.5	372.9	54.6	18.5	12.2	36.3
-48.5	7.6	753.96	42	55.4	2647.6	62.6	61.4	10.2	16.7	7.5	23.1	2	11	24
-51.5	8.6	789.97	44.8	52.1	3102.6	51.8	61.8	12.8	17.3	21.8	35.2	2.6	11.6	26
-54.5	6.1	772.92	27.6	43.2	1230.2	72.8	55.1	8.8	16.8	3.2	17.4	1.9	10.8	24
-56.5	6.9	738.81	33.1	61.2	1366.5	88.7	64.8	14	18.7	9.1	44.4	1.7	12.7	31.4
-60.5	6.8	738.56	35.6	60.3	901.8	64	64.4	12.4	18.7	9	52.7	2.4	13.6	30
Average core conc.	28.81	588.47	731.84	101.30	18345.42	51.84	84.36	23.98	17.84	327.96	45.41	7.22	15.46	38.95

Appendix 4.6a: Trace element concentrations (ppm) determined from pressed dry powder pellets for the marsh core from Loch Creran Isle of Mull, Argyll.

Depth below marsh surface (cm)	Pb	Rb	S	Sb	Sn	Sr	Th	U	V	Y	Zn	Zr
-0.5	98.8	90.7	28637.3	78.2	0.7	271.7	-6.2	29.7	194	40.1	248.6	194.9
-3.5	102.5	93	33289	77.7	-3.2	275.9	-5.9	33.6	201.1	41.3	178.1	183.5
-6.5	80.1	89.7	24281.3	77.9	2.3	285.7	-0.3	22.6	168.9	38.7	133.1	198.8
-9.5	77.7	91.5	23834.3	78.6	-0.2	285.6	-0.7	23.3	171.7	39	132.4	173.6
-12.5	59.8	86.5	20894.8	77.8	-1.5	306.3	3.3	17.4	146.8	35.3	116.9	181.6
-15.5	69	94.7	26659.8	78.5	2.5	323.9	0.3	19.6	156.6	36.3	120.3	187.1
-18.5	64.5	96.3	23745.8	77.6	-0.2	305.3	2	21.8	158	40.7	137.2	166
-21.5	62.2	98.5	27062.1	77.4	0.5	322	0.5	19.4	138.3	35.6	107.8	306.7
-24.5	61.5	85	30771.6	77.4	0	304	-1	19.2	154.3	33	107.9	328.8
-27.5	59.6	91.9	30890.4	77.4	4	332.3	1	16.8	138.9	34.6	107.5	320
-30.5	61.4	102.5	34092.1	77.9	-4.3	317.9	2.5	19.1	155.8	37.9	121.7	285.7
-32.5	47.7	96.1	32648.3	77.4	-1.5	313.6	2.8	18.2	107.1	36.4	85.7	331.4
-36.5	53.5	92.6	30173.8	77	-1.1	309.3	3.4	16.7	140.7	34.7	95.2	330.7
-39.5	52.5	96.1	29485.5	77.4	-0.9	314	2.6	13.7	134.1	36.1	96.1	290.3
-42.5	64.3	88.8	31834.2	76.8	-0.9	311.6	1.7	16.2	205.9	34.2	107	313.8
-45.5	37.5	95.4	26930.1	77.1	-0.6	384.6	4.4	10	143.6	29.4	93.3	339.4
-48.5	19.6	100.1	15764	77.7	-1.8	413	5.2	3.2	57.5	23.1	64.2	313.1
-51.5	22	106.2	21588.5	77.2	-2.1	420.5	5.9	6	71.5	24.5	65.2	317.1
-54.5	17.6	100.3	11703.8	77.3	-4.5	421.3	6.5	2.9	57.1	23	50.5	288.7
-56.5	18.9	117	25080.7	77.3	-6.6	356	10	3.6	72.4	30	68.3	276.2
-60.5	19.1	115.9	33565.2	76.8	-0.1	366.5	8.6	3.7	74.3	29.2	73.7	238.6
Average core conc.	54.75	96.61	26806.31	77.54	-0.93	330.52	2.22	16.03	135.65	33.96	110.03	265.05

Appendix 4.6b: Trace element concentrations (ppm) determined from pressed dry powder pellets for the marsh core from Loch Creran Isle of Mull, Argyll.

Depth below marsh surface (cm)	SiO2	TiO2	Al2O3	Fe2O3	MnO	MgO	CaO	Na2O	K2O	Na2O	K2O	P2O5	SO3	LOI
-0.5	67.51	0.66	14.40	5.10	0.14	1.88	1.87	3.92	3.25	3.92	3.25	0.24	0.12	4.45
-2.5	66.77	0.71	14.90	4.84	0.08	1.97	1.85	4.04	3.48	4.04	3.48	0.24	0.25	5.37
-4.5	68.32	0.65	14.32	3.91	0.05	1.73	1.82	4.24	3.51	4.24	3.51	0.18	0.25	5.99
-6.5	67.31	0.71	14.33	4.34	0.05	1.89	1.84	3.92	3.43	3.92	3.43	0.19	0.22	9.32
-8.5	68.67	0.63	14.39	3.96	0.05	1.71	1.80	4.89	3.41	4.89	3.41	0.16	0.16	7.41
-10.5	69.01	0.65	14.56	3.72	0.05	1.71	1.75	4.02	3.58	4.02	3.58	0.14	0.16	4.26
-12.5	69.60	0.61	14.40	3.29	0.05	1.70	1.77	4.90	3.65	4.90	3.65	0.14	0.22	4.25
-14.5	69.29	0.80	13.79	3.70	0.06	1.57	1.97	3.77	3.31	3.77	3.31	0.16	0.13	3.22
-16.5	70.55	0.90	13.43	3.64	0.06	1.62	2.04	3.75	3.18	3.75	3.18	0.19	0.13	2.56
-19.5	68.39	0.83	14.76	3.78	0.06	1.91	1.82	3.92	3.32	3.92	3.32	0.17	0.12	3.63
-21.5	69.08	0.79	14.37	3.40	0.06	1.96	1.83	4.00	3.40	4.00	3.40	0.16	0.14	3.63
-23.5	69.79	0.87	14.01	3.55	0.06	1.66	1.91	3.67	3.28	3.67	3.28	0.16	0.15	3.41
-26.5	69.82	0.82	13.87	3.86	0.06	1.82	1.73	3.52	3.14	3.52	3.14	0.13	0.12	3.23
-28.5	68.72	0.89	14.06	4.06	0.06	2.00	1.92	3.94	3.14	3.94	3.14	0.17	0.18	1.28
-30.5	70.19	0.62	13.72	3.62	0.04	1.07	1.67	4.29	3.19	4.29	3.19	0.26	0.66	2.94
-32.5	68.92	0.45	13.39	2.49	0.03	0.76	1.31	3.98	3.74	3.98	3.74	0.16	0.48	13.99
-34.5	70.56	0.43	12.92	3.18	0.02	0.72	1.33	4.14	3.57	4.14	3.57	0.18	0.70	12.55
-36.5	69.45	0.48	13.65	3.28	0.03	0.79	1.40	4.22	3.67	4.22	3.67	0.17	0.46	11.10
-38.5	68.84	0.59	14.99	3.36	0.04	1.52	1.48	4.73	3.86	4.73	3.86	0.16	0.25	11.10
-40.5	70.63	0.79	13.45	3.45	0.06	1.21	1.78	3.79	3.46	3.79	3.46	0.10	0.11	9.39
-42.5	70.85	0.79	13.18	4.32	0.06	1.25	1.76	3.69	3.33	3.69	3.33	0.09	0.10	5.92
-44.5	71.18	0.49	14.19	3.17	0.04	1.19	1.56	4.06	3.66	4.06	3.66	0.09	0.10	0.60
-46.5	70.33	0.45	14.07	2.76	0.04	1.17	1.46	4.13	3.62	4.13	3.62	0.09	0.15	0.55
-48.5	70.74	0.50	13.88	2.86	0.04	1.20	1.55	4.03	3.69	4.03	3.69	0.09	0.16	0.54
-50.5	70.91	0.46	13.87	2.79	0.04	1.13	1.54	3.97	3.53	3.97	3.53	0.09	0.17	0.45
Core average	69.42	0.66	14.04	3.62	0.05	1.48	1.71	4.06	3.45	4.06	3.45	0.16	0.23	5.25
2 Stand. Dev	2.34	0.30	1.03	1.22	0.04	0.79	0.39	0.68	0.39	0.68	0.39	0.09	0.33	7.74

Appendix 4.7: Major element abundance (% ashed mass of oxides) from the Loch Etive core mainland Argyll.

Depth below marsh surface (cm)	As	Ba	Br	Ce	Cl	Cr	I	La	MnO	Nb	Ni	Pb	Rb	Sl	Sr	TiO2	Va	Y	Zn	Zr
-0.5	5.9	522.6	587.30	44.5	705.98	26.3	583.25	25.3	1045.8	10	19.1	36.3	59.5	34113.57	327.4	4149.2	54.8	11.4	59.3	162.9
-1.5	5.3	608.6	573.56	49.4	687.44	48.3	726.99	28.5	995.2	12.1	18.3	40.2	70.3	1856.46	369.9	5019.9	66.6	13.3	57.8	180.3
-2.5	5.2	595.4	549.02	54.1	596.10	50.5	574.34	27.9	873.3	11.6	19.2	39.9	70.5	14399.67	353.1	5124.1	64.6	12.6	55.6	187.1
-3.5	5.3	618.6	458.06	51.5	602.72	47.9	456.87	28.4	645.3	12	18.5	36.9	70.9	12448.84	362.3	5069	62.9	13.2	50.3	184.1
-4.5	4.8	678.5	358.14	53.9	644.02	47.1	423.43	29.6	559.1	12.4	17.8	34.7	74.4	10629.56	363.2	5506.2	64.9	13.3	46.5	204.8
-5.5	4.5	663.1	388.77	49.3	711.82	46.6	338.31	27.4	482.7	13.1	17.3	35.9	72.5	1054.48	388.2	5497.5	62.5	13.8	43.2	232.3
-6.5	4.8	636.2	467.16	46.4	835.32	50.1	410.18	26.8	426.1	12.5	18.1	38	69.4	10245.82	366.4	5346.2	65	13.3	44.4	219.5
-7.5	3.9	733.6	328.09	50	612.36	60	374.35	28.6	478.2	13.3	21.6	35.5	77.2	8574.76	406.5	6317.6	68.9	14.6	50.2	242
-8.5	4.6	714.2	379.17	56	577.26	55.3	438.41	31.8	456.4	12.7	20.6	38.1	75.6	11061.94	394.3	6140.2	66.9	14.1	47.9	240.7
-9.5	4.3	707.9	409.18	49.6	512.32	103.4	417.57	27	445.5	12.2	18.7	33.4	79.9	8765.42	408.8	5624.2	61.2	13	44	227.8
-10.5	3.9	786.9	261.69	48.7	487.01	49.7	301.83	29.2	442.5	12.3	18.2	30.5	85.6	7604.65	432.4	5730	60	12.7	43.5	237.9
-11.5	4.3	778.1	320.93	51.2	521.30	56.3	397.81	29	460.9	14.1	19.9	31.9	86.2	9856.64	447	6230.4	64.1	14	47.4	258.3
-12.5	3.5	751.8	381.75	55.2	624.06	55.2	431.25	26.6	446.6	13.2	18.1	35.3	84.4	10911.29	431	5934.4	65.1	13.6	44.5	245.6
-13.5	3.1	782.5	262.78	56.7	588.74	66.3	336.35	31.3	490.3	15.9	18.9	27	85.9	9254.79	449.9	6920.1	73.4	17	46.8	416.5
-14.5	3.2	801.6	212.73	59.4	468.49	66.5	310.95	32.6	513.4	16.2	18.8	27.6	85.4	8443.27	451.2	7358.6	75	17.6	45.9	436.8
-15.5	3.2	808	180.32	64.4	372.12	69.7	270.99	33	527.8	16.7	18.8	28.8	85.6	7988.62	453.2	7908.7	77.8	19.2	45.6	545.3
-16.5	3.2	826.9	148.04	56.9	290.70	72.3	237.77	31.8	548.3	17.8	19.4	24.5	84.9	6008.50	452.5	8460.6	75.7	21.1	44.2	578.1
-17.5	3.6	808.7	168.34	71.5	321.22	75.6	246.46	36.3	548.5	17.3	21.6	26.1	84	5988.97	444.5	8359.1	82.5	20.2	47.8	492.3
-18.5	2.6	822.4	167.07	55.7	486.16	73.8	216.06	29.2	532.3	17	21.3	24.9	86.3	6354.35	444.2	8088.8	75.7	18.6	46.4	409
-19.5	3	829.4	227.31	54.1	740.12	70.1	258.62	32.9	500.7	15.3	23	25.9	85.7	6506.52	434.7	7621.2	76.2	17.1	47.7	297.1
-22.5	2.3	834.3	187.77	60.4	627.62	59.6	144.83	31.6	502.9	16.8	19.7	24.8	87.4	3647.34	438	7328.4	70	17.8	42.6	345.8
-24.5	0.6	859.9	59.66	61.9	423.12	60.4	129.20	28	543.2	16.9	21.3	22.7	93.1	3256.38	452.1	7951.1	71	17.6	47	356.8
-26.5	1.4	895.1	41.14	58	423.34	71.7	84.69	32.5	553.7	17.5	24.3	20.5	90.6	2135.57	435.8	8250.9	76.7	17.7	46	330.6
-28.5	0	867.5	109.47	67	657.10	76.5	70.57	35.9	529.9	16.5	26.3	21.7	81.2	1775.87	430.2	8032.5	80.8	17.1	45.2	374.8
-29.5	1.8	629.1	276.12	48.5	1259.26	52.8	134.41	21.6	339.9	12.7	17.7	19.5	62.1	2284.64	343	5698.3	62.5	13.7	25	414.6
-30.5	1.6	447.6	335.80	26.8	4665.55	30	147.44	14.5	159	8.8	9.9	17.5	47.8	3721.13	238.3	3201.8	30.9	6.2	8.2	188.7
-32.5	1.1	390.2	223.23	20.9	5253.75	10.6	132.89	11	110.3	7.5	5.5	16.6	44.9	3286.28	221.9	2634.7	19.3	4.2	3.6	115.3
-34.5	0.8	423	173.05	21	5537.82	14.1	92.29	9.6	109.4	7.4	3.7	17.8	50.5	2310.33	217.2	2418.6	18	2.8	4.6	125.6
-36.5	2.7	328.4	247.21	18.1	6247.32	9.6	130.94	10	107.9	7.1	4.3	27.9	40.1	2826.43	200.3	2310.2	17.9	4.2	5.8	96.9
-38.5	1.6	817.1	91.05	40	6946.24	37	66.66	23.5	384.4	11.7	15.4	25	90.2	3197.04	424.7	4983.8	45.7	10.3	29	149.5
-39.5	0.2	922.2	32.06	50.7	1643.93	55.5	44.08	26.9	528.4	15.8	17	19.9	93.5	1672.67	486.1	6778.2	65.3	16.5	36.3	323.2
-40.5	0.1	908.5	25.20	47.4	429.99	59.4	38.00	29.1	525.8	16.1	16	19.6	98.5	962.35	483.1	6953.4	72.6	18.1	35.2	446.2
-42.5	1	1009.6	26.58	43.6	200.83	44.4	52.98	22.9	457.6	12.6	15.1	19.8	101.2	1340.02	517.7	5676.8	64.6	13.2	32.2	278.9
-44.5	0.6	931.5	21.79	57.1	122.97	43.4	75.57	28.6	470.1	13.3	16	18	100.7	1914.41	486.1	5760.2	58.7	12.5	34.9	237.3
-46.5	0.6	975.4	14.19	37.9	267.62	33	79.04	23.3	411.9	12.5	13.1	17.6	96	1987.61	491.9	4815.6	42.3	12.4	25.9	230.6
-48.5	1.4	988	17.99	38.8	469.77	40	26.06	25.8	463.8	13.9	15.9	18.8	100.3	656.76	493	5721.1	52.9	13.8	33.4	238.7
-50.5	0	953.4	20.00	43.4	226.30	40.1	27.58	22.6	419.3	12.6	14.1	20.3	101.6	695.42	505.1	4914.8	44.3	12.5	27.9	192
Average core conc	2.70	747.45	235.99	49.19	1264.53	52.14	249.43	26.77	487.47	13.44	17.36	27.01	79.84	6209.15	406.63	5941.52	61.01	13.90	38.97	282.27

Appendix 4.8: Trace element concentrations (ppm) determined from pressed powder pellets for the marsh core from Loch Etive mainland Argyll

	SiO2	TiO2	Al2O3	Fe2O3	MnO	MgO	CaO	Na2O	K2O	P2O5	SO3	LOI
SiO2	1.00											
TiO2	-0.40	1.00										
Al2O3	-0.60	0.28	1.00									
Fe2O3	-0.86	0.15	0.50	1.00								
MnO	-0.57	0.31	0.34	0.63	1.00							
MgO	0.27	0.49	-0.59	-0.50	-0.09	1.00						
CaO	0.56	0.22	-0.67	-0.72	-0.47	0.86	1.00					
Na2O	-0.09	-0.36	0.45	0.11	-0.27	-0.55	-0.32	1.00				
K2O	-0.13	-0.61	-0.05	0.25	0.17	-0.35	-0.34	0.41	1.00			
P2O5	-0.59	0.04	0.43	0.75	0.79	-0.47	-0.82	-0.12	0.32	1.00		
SO3	-0.25	-0.28	0.36	0.48	0.43	-0.64	-0.75	0.03	0.18	0.71	1.00	
LOI	-0.62	0.26	0.75	0.66	0.50	-0.57	-0.78	0.13	-0.07	0.72	0.70	1.00

Appendix 4.9: Correlation matrix for major element raw data from the Loch Scridain marsh core

	Rb	Sr	Y	Zr	Nb	Pb	Zn	Ni	As	Cr	V	Ba	La	Ce	MnO	TiO2	Al (ppm)
Rb	1.0000																
Sr	0.9645	1.0000															
Y	0.9710	0.9851	1.0000														
Zr	0.9698	0.9763	0.9795	1.0000													
Nb	0.8901	0.9147	0.9186	0.9549	1.0000												
Pb	-0.8341	-0.8388	-0.8742	-0.8372	-0.7637	1.0000											
Zn	-0.1096	-0.1013	-0.0888	-0.0476	-0.0463	0.2853	1.0000										
Ni	0.8281	0.8754	0.9006	0.8407	0.8389	-0.7195	-0.0370	1.0000									
As	-0.7872	-0.7735	-0.8002	-0.7544	-0.6130	0.9313	0.1910	-0.5874	1.0000								
Cr	0.8634	0.8588	0.8802	0.8226	0.7512	-0.6736	0.0620	0.8966	-0.6510	1.0000							
V	0.6923	0.7493	0.7663	0.6943	0.7282	-0.5559	-0.0990	0.9389	-0.4032	0.8618	1.0000						
Ba	0.9332	0.9282	0.9226	0.9738	0.9296	-0.7959	-0.0166	0.7235	-0.7339	0.7200	0.5501	1.0000					
La	0.6453	0.7181	0.7134	0.7309	0.8197	-0.5942	-0.2854	0.7098	-0.3495	0.5050	0.6562	0.6763	1.0000				
Ce	0.7304	0.7969	0.7974	0.8193	0.8624	-0.6990	-0.1738	0.7381	-0.5039	0.5808	0.6361	0.7606	0.8592	1.0000			
MnO	-0.7600	-0.7905	-0.7742	-0.7387	-0.6915	0.7101	0.4696	-0.7435	0.6160	-0.6845	-0.7042	-0.6909	-0.5784	-0.6094	1.0000		
TiO2	0.8979	0.9296	0.9496	0.8889	0.8431	-0.8246	-0.1090	0.9583	-0.7419	0.9419	0.8935	0.7824	0.6677	0.7352	-0.7882	1.0000	
Al (ppm)	-0.2653	-0.1629	-0.1329	-0.1928	-0.0357	0.0433	-0.3426	0.0981	0.2800	-0.1998	0.1817	-0.3050	0.3306	0.2201	0.0070	-0.0234	1.0000

CORRELATION COEFFICENTS (r) for the metal: Rb and the metal: Al
with trace metal elements in the Loch Sridain marsh core

	Rb	Al	r2
As	-0.79	0.28	
Cr	0.86	-0.20	>0.65
Ni	0.83	0.10	
Pb	-0.83	0.04	0.45-0.65
Zn	-0.11	-0.34	
Zr	0.97	-0.19	<-0.65
V	0.69	0.18	

Apendix 4.10: Correlation matrix of trace element raw data from the Loch Scridain core. Also shown are the correlation coefficients r for the normalizing elements Al and Rb with various trace metals (After: Loring, 1990)

	SiO2	TiO2	Al2O3	Fe2O3	MnO	MgO	CaO	K2O	Na2O	P2O5	SO3	LOI
SiO2	1											
TiO2	0.33	1.00										
Al2O3	-0.72	-0.08	1.00									
Fe2O3	-0.85	-0.04	0.65	1.00								
MnO	-0.65	-0.31	0.35	0.68	1.00							
MgO	-0.62	-0.26	0.34	0.34	0.48	1.00						
CaO	0.83	0.61	-0.80	-0.61	-0.55	-0.51	1.00					
K2O	-0.74	-0.74	0.62	0.42	0.52	0.66	-0.93	1.00				
Na2O	-0.66	-0.81	0.45	0.30	0.46	0.67	-0.83	0.96	1.00			
P2O5	-0.75	-0.77	0.50	0.46	0.66	0.71	-0.88	0.95	0.95	1.00		
SO3	-0.65	-0.83	0.36	0.30	0.53	0.70	-0.79	0.93	0.98	0.97	1.00	
LOI	-0.57	-0.27	0.81	0.48	0.31	0.39	-0.77	0.68	0.54	0.60	0.48	1.00

Appendix 4.11: Correlation matrix for major element raw data from the Loch Don marsh core

	As	Ba	Bi	Br	Ce	Cl	Co	Cr	Cu	Ga	I	La	Mo	Nb	Ni	Pb	Rb	S	Sb	Sn	Sr	Th	U	V	Y	Zn	Zr	Al (ppm)
As	1.000																											
Ba	-0.586	1.000																										
Bi	0.116	0.033	1.000																									
Br	0.927	-0.699	0.167	1.000																								
Ce	0.632	-0.782	-0.176	0.667	1.000																							
Cl	0.755	-0.696	0.357	0.908	0.531	1.000																						
Co	0.356	-0.429	0.259	0.343	0.460	0.348	1.000																					
Cr	0.117	0.005	0.059	0.013	-0.161	-0.091	0.297	1.000																				
Cu	0.842	-0.652	0.180	0.970	0.606	0.897	0.287	0.013	1.000																			
Ga	0.712	-0.201	-0.183	0.585	0.349	0.275	0.106	0.367	0.577	1.000																		
I	0.853	-0.343	0.136	0.748	0.505	0.483	0.204	-0.026	0.684	0.745	1.000																	
La	0.240	0.017	-0.035	0.266	-0.004	0.252	-0.179	0.428	0.347	0.313	0.008	1.000																
Mo	0.950	-0.703	0.030	0.947	0.728	0.808	0.287	-0.039	0.870	0.590	0.781	0.257	1.000															
Nb	0.918	-0.473	0.035	0.866	0.607	0.620	0.295	0.215	0.811	0.828	0.879	0.210	0.847	1.000														
Ni	0.917	-0.569	0.136	0.928	0.613	0.754	0.423	0.171	0.911	0.788	0.837	0.209	0.855	0.943	1.000													
Pb	0.966	-0.533	0.030	0.909	0.570	0.688	0.248	0.138	0.848	0.776	0.891	0.271	0.937	0.939	0.915	1.000												
Rb	0.963	-0.539	0.273	0.944	0.574	0.814	0.303	0.063	0.870	0.646	0.856	0.218	0.919	0.915	0.917	0.933	1.000											
S	0.852	-0.669	0.219	0.975	0.606	0.931	0.385	0.039	0.974	0.545	0.665	0.255	0.864	0.826	0.923	0.831	0.898	1.000										
Sb	0.289	0.084	0.359	0.248	-0.157	0.311	0.492	0.240	0.244	0.258	0.273	0.051	0.143	0.263	0.405	0.247	0.310	0.345	1.000									
Sn	0.725	-0.525	0.096	0.689	0.205	0.642	0.333	0.415	0.637	0.483	0.446	0.383	0.697	0.556	0.636	0.730	0.643	0.642	0.401	1.000								
Sr	-0.412	0.306	0.245	-0.235	-0.374	0.056	-0.116	-0.137	-0.116	-0.384	-0.551	0.034	-0.443	-0.363	-0.260	-0.490	-0.317	-0.066	0.180	-0.332	1.000							
Th	-0.857	0.750	-0.078	-0.954	-0.670	-0.883	-0.370	-0.066	-0.954	-0.503	-0.617	-0.377	-0.912	-0.760	-0.847	-0.851	-0.832	-0.927	-0.174	-0.737	0.239	1.000						
U	0.955	-0.634	0.063	0.953	0.679	0.816	0.346	0.125	0.924	0.723	0.764	0.360	0.925	0.906	0.946	0.922	0.926	0.922	0.285	0.679	-0.243	-0.917	1.000					
V	0.655	-0.240	-0.350	0.531	0.455	0.225	0.104	0.198	0.540	0.926	0.670	0.232	0.549	0.753	0.721	0.698	0.534	0.480	0.151	0.372	-0.291	-0.490	0.699	1.000				
Y	0.586	-0.126	-0.152	0.455	0.345	0.113	0.205	0.389	0.461	0.921	0.714	0.154	0.426	0.748	0.707	0.645	0.534	0.426	0.181	0.279	-0.419	-0.379	0.595	0.859	1.000			
Zn	0.932	-0.601	0.238	0.967	0.549	0.877	0.325	0.018	0.945	0.642	0.811	0.233	0.912	0.869	0.942	0.925	0.945	0.948	0.397	0.719	-0.216	-0.905	0.943	0.580	0.497	1.000		
Zr	-0.511	0.440	0.301	-0.666	-0.626	-0.578	-0.039	0.335	-0.678	-0.355	-0.376	-0.117	-0.604	-0.574	-0.590	-0.504	-0.538	-0.688	0.058	-0.132	-0.099	0.621	-0.632	-0.447	-0.275	-0.550	1.000	
Al (ppm)	-0.569	0.541	-0.466	-0.698	-0.369	-0.844	-0.179	0.386	-0.661	0.056	-0.360	-0.072	-0.651	-0.315	-0.450	-0.477	-0.637	-0.662	-0.099	-0.479	0.007	0.675	-0.542	0.078	0.174	-0.659	0.393	1.000

Correlation coefficients for the metal Rb, and the metal Al in Loch Don sediment core

	Rb	Al	r2
As	0.963	-0.569	
Cr	0.063	0.386	> 0.65
Cu	0.870	-0.661	
Ni	0.917	-0.450	0.45 - 0.65
Pb	0.933	-0.477	
Zn	0.945	-0.659	> -0.65
Zr	-0.538	0.393	

Apendix 4.12: Correlation matrix of trace element raw data from the Loch Don core. Also shown are the correlation coefficients r^2 for the normalizing elements Al and Rb with various trace metals (After: Loring, 1990)

	SiO2	TiO2	Al2O3	Fe2O3	MnO	MgO	CaO	K2O	Na2O	P2O5	SO3	LOI
SiO2	1.00											
TiO2	-0.57	1.00										
Al2O3	-0.06	0.26	1.00									
Fe2O3	-0.86	0.32	-0.38	1.00								
MnO	-0.58	-0.09	0.03	0.60	1.00							
MgO	-0.84	0.85	0.42	0.52	0.28	1.00						
CaO	-0.67	0.84	0.34	0.39	0.20	0.89	1.00					
K2O	0.51	-0.65	0.46	-0.60	0.02	-0.47	-0.56	1.00				
Na2O	-0.64	0.39	0.48	0.32	0.37	0.71	0.72	-0.05	1.00			
P2O5	-0.92	0.50	0.30	0.69	0.54	0.85	0.66	-0.28	0.78	1.00		
SO3	-0.89	0.54	0.19	0.69	0.44	0.83	0.67	-0.32	0.82	0.93	1.00	
LOI	-0.77	0.88	0.16	0.59	0.23	0.89	0.85	-0.64	0.52	0.70	0.70	1.00

Appendix 4.13: Correlation matrix for major element raw data from the Loch Creran marsh core

	As	Ba	Bi	Br	Ce	Cl	Co	Cr	Cu	Ga	I	La	Mo	Nb	Ni	Pb	Rb	S	Sb	Sn	Sr	Th	U	V	Y	Zn	Al (ppm)
As	1.00																										
	-0.80	1.00																									
	-0.70	0.68	1.00																								
Br	0.80	-0.91	-0.61	1.00																							
Ce	0.79	-0.89	-0.62	0.80	1.00																						
Cl	0.77	-0.97	-0.63	0.94	0.86	1.00																					
Co	-0.09	0.33	0.28	-0.21	-0.18	-0.40	1.00																				
Cr	0.58	-0.87	-0.47	0.75	0.82	0.88	-0.51	1.00																			
Cu	0.76	-0.80	-0.54	0.93	0.68	0.79	-0.09	0.64	1.00																		
Ga	-0.11	-0.14	0.08	0.10	0.06	0.13	-0.37	0.47	0.21	1.00																	
I	0.92	-0.90	-0.61	0.86	0.85	0.88	-0.26	0.78	0.80	0.11	1.00																
La	0.44	-0.48	-0.42	0.31	0.37	0.43	-0.22	0.41	0.25	0.23	0.47	1.00															
Mo	0.80	-0.50	-0.58	0.36	0.61	0.45	0.01	0.31	0.27	-0.31	0.64	0.46	1.00														
Nb	0.52	-0.83	-0.44	0.73	0.82	0.85	-0.54	0.95	0.58	0.46	0.72	0.42	0.25	1.00													
Ni	0.81	-0.85	-0.55	0.91	0.84	0.85	-0.01	0.75	0.89	0.20	0.82	0.35	0.45	0.71	1.00												
Pb	0.84	-0.94	-0.65	0.98	0.85	0.96	-0.24	0.79	0.90	0.12	0.91	0.37	0.47	0.76	0.91	1.00											
Rb	-0.69	0.77	0.65	-0.65	-0.70	-0.75	0.33	-0.60	-0.48	0.34	-0.74	-0.22	-0.57	-0.51	-0.48	-0.69	1.00										
S	0.35	-0.47	-0.28	0.43	0.47	0.49	-0.05	0.42	0.26	0.14	0.34	0.52	0.38	0.50	0.51	0.44	-0.07	1.00									
Sb	0.39	-0.45	-0.22	0.59	0.34	0.48	-0.29	0.48	0.65	0.23	0.52	-0.13	-0.10	0.43	0.49	0.56	-0.33	-0.16	1.00								
Sn	0.38	-0.44	-0.49	0.41	0.36	0.46	-0.28	0.45	0.31	-0.05	0.42	0.34	0.23	0.43	0.35	0.41	-0.51	0.23	0.23	1.00							
Sr	-0.70	0.94	0.57	-0.87	-0.84	-0.90	0.26	-0.86	-0.79	-0.32	-0.86	-0.51	-0.38	-0.85	-0.83	-0.90	0.58	-0.56	-0.43	-0.34	1.00						
Th	-0.80	0.85	0.58	-0.96	-0.72	-0.89	0.16	-0.63	-0.87	0.11	-0.83	-0.28	-0.42	-0.58	-0.83	-0.94	0.72	-0.35	-0.54	-0.44	0.75	1.00					
U	0.82	-0.93	-0.61	0.98	0.84	0.96	-0.30	0.80	0.91	0.16	0.89	0.36	0.42	0.78	0.91	0.99	-0.66	0.45	0.54	0.37	-0.89	-0.93	1.00				
V	0.90	-0.92	-0.68	0.86	0.92	0.91	-0.20	0.78	0.74	0.04	0.94	0.50	0.73	0.75	0.86	0.93	-0.72	0.56	0.36	0.39	-0.87	-0.83	0.90	1.00			
Y	0.71	-0.91	-0.54	0.88	0.82	0.90	-0.34	0.91	0.82	0.48	0.85	0.48	0.37	0.89	0.89	0.90	-0.49	0.55	0.49	0.35	-0.95	-0.74	0.91	0.86	1.00		
Zn	0.80	-0.81	-0.55	0.92	0.73	0.78	0.07	0.62	0.96	0.11	0.80	0.26	0.37	0.54	0.94	0.89	-0.49	0.38	0.55	0.32	-0.78	-0.87	0.89	0.79	0.80	1.00	
Al (ppm)	0.09	-0.13	-0.12	0.11	0.16	0.07	-0.07	0.20	0.29	0.28	0.14	-0.34	0.06	0.07	0.18	0.17	-0.01	-0.05	0.28	-0.26	-0.16	-0.05	0.16	0.15	0.22	0.25	1.00

Correlation coefficients (r) for the metal Rb and the metal Al and Y

	Rb	Al	Y
As	-0.69	0.09	0.71
Cr	-0.60	0.20	0.91
Cu	-0.48	0.29	0.82
Ni	-0.48	0.18	0.89
Pb	-0.69	0.17	0.90
Zn	-0.49	0.25	0.80
V	-0.72	0.15	0.86

r values

> 0.65

0.45 - 0.65

< -0.65

Apendix 4.14: Correlation matrix of trace element raw data from the Loch Creran core. Also shown are the correlation coefficients r^2 for the normalizing elements Al and Rb with various trace metals (After: Loring, 1990)

	SiO2	TiO2	Al2O3	Fe2O3	MnO	MgO	CaO	Na2O	K2O	P2O5	SO3	LOI
SiO2	1.00											
TiO2	-0.22	1.00										
Al2O3	-0.65	0.12	1.00									
Fe2O3	-0.64	0.56	0.34	1.00								
MnO	-0.46	0.50	0.33	0.78	1.00							
MgO	-0.63	0.71	0.69	0.67	0.63	1.00						
CaO	-0.34	0.88	0.28	0.67	0.65	0.81	1.00					
Na2O	-0.15	-0.45	0.39	-0.16	-0.28	-0.05	-0.27	1.00				
K2O	0.09	-0.77	0.15	-0.56	-0.50	-0.48	-0.72	0.51	1.00			
P2O5	-0.65	0.21	0.22	0.56	0.34	0.30	0.30	0.12	-0.37	1.00		
LOI	-0.35	-0.32	-0.11	0.00	-0.32	-0.30	-0.32	0.36	0.12	0.67	0.86	1.00

Appendix 4.15: Correlation matrix for major element raw data from the Loch Etive marsh core

	Rb	Sr	Y	Zr	Nb	Pb	Zn	Ni	As	Cr	V	Ba	La	Ce	MnO	TiO2	Al (ppm)
Rb	1.0000																
Sr	0.9800	1.0000															
Y	0.6704	0.7506	1.0000														
Zr	0.4244	0.5123	0.8415	1.0000													
Nb	0.7012	0.7559	0.9722	0.8425	1.0000												
Pb	-0.1791	-0.1063	0.1147	-0.1796	-0.0455	1.0000											
Zn	0.4808	0.5530	0.7647	0.3947	0.6713	0.6430	1.0000										
Ni	0.5390	0.6133	0.8519	0.5518	0.8134	0.3476	0.8874	1.0000									
As	-0.2887	-0.2064	0.0885	-0.1124	-0.0770	0.9209	0.5596	0.2762	1.0000								
Cr	0.4746	0.5540	0.8229	0.6696	0.7827	0.2478	0.7428	0.8458	0.2317	1.0000							
V	0.5760	0.6626	0.9392	0.7220	0.8841	0.3157	0.8820	0.9366	0.2664	0.8577	1.0000						
Ba	0.9777	0.9732	0.6906	0.4816	0.7304	-0.2768	0.4271	0.5576	-0.3714	0.4790	0.5834	1.0000					
La	0.6247	0.6949	0.9041	0.6273	0.8560	0.3420	0.8964	0.9335	0.2921	0.8181	0.9474	0.6221	1.0000				
Ce	0.5661	0.6381	0.8907	0.6805	0.8561	0.2948	0.8513	0.9092	0.2322	0.8187	0.9393	0.5625	0.9443	1.0000			
MnO	0.4336	0.4812	0.6245	0.2813	0.5285	0.5143	0.8623	0.6847	0.4220	0.5211	0.7152	0.3762	0.7195	0.6800	1.0000		
TiO2	0.6472	0.7094	0.9692	0.8363	0.9801	0.0295	0.7166	0.8710	0.0038	0.8372	0.9220	0.6802	0.8871	0.8932	0.5297	1.0000	
Al (ppm)	0.1757	0.2166	0.2579	-0.1619	0.1797	0.5989	0.6234	0.5191	0.5015	0.3332	0.3802	0.1175	0.4632	0.4068	0.5511	0.2124	1.0000

Correlation coefficients (r) for the metals Rb, Al & Y

	Rb	Al	Y	r values
As	-0.29	0.50	0.09	
Cr	0.47	0.33	0.82	> 0.65
Ni	0.54	0.52	0.85	
Pb	-0.18	0.60	0.11	0.45 - 0.65
Zn	0.48	0.62	0.76	
V	0.58	0.38	0.93	0.30 - 0.45

Apendix 4.16: Correlation matrix of trace element raw data from the Loch Etive marsh core. Also shown are the correlation coefficients r^2 for the normalizing elements Al and Rb with various trace metals (After: Loring, 1990)

APPENDIX FIVE

Calculation of 210Pb activity: Loch Scridain core 1

Activity of 209Po spike = 4.28 dpm/g

Sample name	sample mass (g)	Po-209 mass (g)	Po-209 total peak	Po-210 total peak	Po-210 activity (Bq/g)	Activity dpm/g	Error %
-0.5	2.0358	0.6401	1161	26803	0.518	31.07	3.00
-2.5	2.0235	0.5245	511	12914	0.467	28.04	4.51
-4.5	2.0671	0.5094	583	7424	0.224	13.43	4.30
-6.5	2.0093	0.4965	384	4126	0.189	11.36	5.34
-8.5	2.0151	0.5166	436	1901	0.080	4.78	5.31
-10.5	2.0286	0.5611	573	1258	0.043	2.60	5.04
-12.5	2.0272	0.5206	477	562	0.022	1.29	6.23
-14.5	2.0301	0.5657	488	265	0.011	0.65	7.63
-16.5	2.0034	0.5136	408	186	0.008	0.50	8.85
-18.5	2.0123	0.5138	467	178	0.007	0.42	8.81
-20.5	2.0039	0.6144	513	146	0.006	0.37	9.38
-25.5	2.0115	0.4909	523	151	0.005	0.30	9.24
-30.5	2.0119	0.5175	559	148	0.005	0.29	9.24
-40.5	2.0019	0.5272	454	157	0.006	0.39	9.26
-50.5	2.0172	0.5641	574	145	0.005	0.30	9.29

Appendix 5.1: Calculation of ^{210}Pb activity (via ^{210}Po activity) from the Loch Scridain marsh core

Loch Scridain 210Pb Dating Calcs (uses inventories) **CRS Model**

Eqn. Age at Depth = (1/decay const. 210Pb)*LN(unssupported inventory below depth x / unsupported inventory of entire core)

Depth cms	Po-210 Total Activity (Bq/g)	Value of Cons 210Pb at Depth	210Pb unsupp.	Dry Bulk Density	Sample hickness cn	Total Inventory	Inventory Below Depth x	Age of Sediment at Depth x (yrs)	Age 0	Error +/-	Age yrs BP
-0.5	0.5180	0.0049	0.51310	1.323	0.5	0.33941565	2.66498825	0	0	0.15	1999
-2.5	0.4670	0.0049	0.46210	1.138	2	1.0517396	2.3255726	-4.374867062	4.37	0.20	1995
-4.5	0.2240	0.0049	0.21910	1.262	2	0.5530084	1.273833	-23.70485495	23.70	1.02	1975
-6.5	0.1890	0.0049	0.18410	1.018	2	0.3748276	0.7208246	-41.98969471	41.99	2.24	1957
-8.5	0.0800	0.0049	0.07510	1.181	2	0.1773862	0.345997	-65.559564	65.56	3.48	1933
-10.5	0.0430	0.0049	0.03810	1.171	2	0.0892302	0.1686108	-88.64360395	88.64	4.47	1910
-12.5	0.0220	0.0049	0.01710	1.058	2	0.0361836	0.0793806	-112.8356108	112.84	7.02	1886
-14.5	0.0110	0.0049	0.00610	1.073	2	0.0130906	0.043197	-132.3758471	132.38	10.10	1867
-16.5	0.0080	0.0049	0.00310	1.124	2	0.0069688	0.0301064	-143.9697223	143.97	12.74	1855
-18.5	0.0070	0.0049	0.00210	1.136	2	0.0047712	0.0231376	-152.4244036	152.42	13.43	1847
-20.5	0.0060	0.0049	0.00110	1.147	2	0.0025234	0.0183664	-159.840463	159.84	14.99	1839
-25.5	0.0050	0.0049	0.00010	1.170	5	0.000585	0.015843	-164.5866142	164.59	15.20	1834
-30.5	0.0050	0.0049	0.00010	1.190	5	0.000595	0.015258	-165.7948289	165.79	15.33	1833
-40.5	0.0060	0.0049	0.00110	1.220	10	0.01342	0.014663	-167.0721777	167.07	15.47	1832
-50.5	0.0050	0.0049	0.00010	1.243	10	0.001243	0.001243	-246.3207166	246.32	22.89	1753
						2.66498825					
						Total Inven = 2.664988					

Appendix 5.2: CRS model calculations of marsh sediment age for the Loch Sridain marsh core

					Sed. Rate
Loch Scridain entire core depth	Lambda/Grad			0.313	**3.1 mm yr**
		1 Stand Dev.		0.259	**2.6 mm yr**
				0.359	**3.6 mm yr**
		2 Stand Dev.		0.216	**2.2 mm yr**
				0.567	**5.6 mm yr**

SUMMARY OUTPUT

Regression Statistics	
Multiple R	0.800388235
R Square	0.640621326
Adjusted R Squar	0.612976813
Standard Error	1.099265384
Observations	15

ANOVA

	df	*SS*	*MS*	*F*	*Significance F*
Regression	1	28.00254781	28.00254781	23.17354325	0.000338314
Residual	13	15.70899701	1.208384385		
Total	14	43.71154482			

	Coefficients	*Standard Error*	*t Stat*	*P-value*	*Lower 95%*	*Upper 95%*	*Lower 95.0%*	*Upper 95.0%*
Intercept	-1.892373322	0.459700921	-4.116531498	0.001214941	-2.885496593	-0.89925005	-2.885496593	-0.899250052
X Variable 1	0.099473078	0.020663759	4.813890656	0.000338314	0.054831749	0.14411441	0.054831749	0.144114407

Appendix 5.3: Summary output of analysis of variance for the ln $^{210}Pb_{excess}$ activity vs depth for the entire core depth of marsh sediment from Loch Scidain. Average sediment accretion (lambda/grad) = 0.03114 (^{210}Pb decay constant/ x-variable coefficient).

SUMMARY OUTPUT

Loch Scridain from 14.5 cms depth

Regression Statistics	
Multiple R	0.988709651
R Square	0.977546774
Adjusted R Squar	0.973804569
Standard Error	0.229378271
Observations	8

		Sed. Rate
Lambda/ Grad		0.1089 **1.1 mm yr**
1 Stand Dev.		0.1025 **1.0 mm yr**
		0.116 **1.2 mm yr**
2 Stand Dev.		0.094 **0.9 mm yr**
		0.128 **1.3 mm yr**

ANOVA

	df	*SS*	*MS*	*F*	*Significance F*
Regression	1	13.74404584	13.74404584	261.2221776	3.56761E-06
Residual	6	0.315686347	0.052614391		
Total	7	14.05973219			

	Coefficients	*Standard Error*	*t Stat*	*P-value*	*Lower 95%*	*Upper 95%*	*Lower 95.0%*	*Upper 95.0%*
Intercept	-0.177341631	0.155541713	-1.1401548	0.297681245	-0.55793877	0.203255509	-0.55793877	0.203255509
X Variable 1	0.286024119	0.017696918	16.16236918	3.56761E-06	0.242721289	0.329326949	0.242721289	0.329326949

Appendix 5.4: Summary output of analysis of variance for the ln $^{210}Pb_{excess}$ activity vs depth for the upper core depth 14-15 cm of marsh sediment from Loch Scidain. Average sediment accretion (lambda/grad) = 0.03114 (^{210}Pb decay constant/ x-variable coefficient).

Sample Depth (cm)	Height of Sed. in Vial (mm)	Sample Mass (g)	137Cs measured (Bq/kg)	137Cs corrected (Bq/kg)	Error %	241Am measured (Bq/kg)	241Am corrected (Bq/kg)	Error %
-0.5	9.5	3.18	155.32	112.61	6.13	4.39	3.18	1.64
-1.5	8.5	3.04	161.94	115.79	5.89	5.66	4.04	2.74
-2.5	8.25	3.021	157.15	110.79	6.37	5.82	4.10	2.69
-3.5	30.5	6.11	102.97	90.09	7.48	7.34	6.42	2.46
-4.5	21.5	5.22	125.81	101.27	6.18	8.73	7.03	2.19
-5.5	14.5	6.964	84.70	63.95	6.61	7.91	5.97	1.83
-6.5	23.5	6.13	61.61	50.21	6.94	7.74	6.31	1.97
-7.5	39.5	10.18	32.24	30.79	7.82	4.00	3.82	2.61
-8.5	15.5	8.302	21.71	16.61	10.70	1.92	1.47	0.89
-9.5	37	9.84	16.71	15.54	11.22	0	0.00	0.00
-10.5	28	7.88	12.24	10.40	12.20	0	0.00	0.00
-11.5	14	7.52	14.49	10.87	13.14	0	0.00	0.00
-12.5	29.5	9.37	11.21	10.03	13.11	0	0.00	0.00
-13.5	37.5	11.37	23.52	21.99	14.91	0	0.00	0.00
-14.5	18	9.15	20.09	15.67	13.33	0	0.00	0.00
-15.5	35.5	10.17	20.70	18.94	8.70	0	0.00	0.00
-16.5	38.5	8.7	14.84	14.03	10.65	0	0.00	0.00
-17.5	19.25	9.42	20.43	16.14	8.77	0	0.00	0.00
-18.5	28	8.53	16.68	14.18	10.92	0	0.00	0.00
-19.5	44	10.36	18.02	18.02	8.37	0	0.00	0.00

Appendix 5.5: ^{137}Cs and ^{241}Am measured and height corrected data derived from gamma spectrometry analysis of the Loch Scridain sediments from the marsh surface to 20 cm depth

Calculation of 210Pb Activity Loch Don core 4

Activity of spike = 4.28dpm/g

Sample Depth	Sample mass (g)	Po-209 mass (g)	Po-209 total peak	Po-210 total peak	Po-210 activity (Bq/g)	Activity dpm/g	Error %
-0.5	2.0099	0.6117	2349	22071	0.2040	12.2390	2.17
-2.5	2.0277	0.6484	2719	23352	0.1959	11.7543	2.03
-4.5	2.0056	0.6481	2732	13429	0.1133	6.7984	2.10
-6.5	2.0667	0.6046	2331	10731	0.0961	5.7641	2.29
-8.5	2.0235	0.6118	2472	7821	0.0682	4.0942	2.31
-10.5	2.0157	0.58	2735	6093	0.0457	2.7436	2.30
-12.5	2.0257	0.5154	2313	6520	0.0512	3.0696	2.42
-14.5	2.0418	0.5287	2373	4151	0.0326	1.9560	2.57
-16.5	2.2464	0.5657	1783	2667	0.0269	1.6122	3.06
-18.5	2.0402	0.4964	2011	2114	0.0182	1.0947	3.11
-20.5	2.0108	0.5333	2256	2029	0.0170	1.0209	3.06
-25.5	2.0177	0.5354	2180	1149	0.0100	0.5986	3.65
-30.5	2.0157	0.4963	2350	914	0.0068	0.4099	3.90
-35.5	2.0114	0.4477	1847	831	0.0071	0.4286	4.18
-40.5	2.1054	0.5110	2108	433	0.0037	0.2220	5.28
-46.5	2.0007	0.5035	2519	512	0.0036	0.2189	4.85

Appendix 5.6: Calculation of ^{210}Pb activity (via ^{210}Po activity) from the Loch Don marsh core

Loch Don 210Pb Dating Calculations: core 4 **(uses inventories), CRS Model**

Eqn. Age at Depth =(1 / Decay constant210Pb)*LN(unsupported inventory below depth x / unsupported inventory of entire core.

Sample Depth (cm)	Po-210 Activity (Bq/g)	Value of 210Pb Conc. At Depth	Unsupp. 210-Pb	Dry Bulk Density (g/cm3)	Sample Thickness (cm)	Total Inventory	Unsupp. Inventory Below Depth x	Age	Age +ve	LN 210Pb Activity	Age yrs (BP)	Error %	Age Error + / -
-0.5	0.2040	0.0036	0.2003837	1.102	0.5	0.110411439	1.68671	0	0	-1.58971501	2000	2.170	
-2.5	0.1959	0.0036	0.1923055	1.125	2	0.432687445	1.576298561	-2.1689	2.1689	-1.63012272	1997	2.026	0.0439
-4.5	0.1133	0.0036	0.1097061	1.178	2	0.258467514	1.143611116	-12.4736	12.4736	-2.17766249	1987	2.099	0.2618
-6.5	0.0961	0.0036	0.0924685	1.131	2	0.209163814	0.885143602	-20.7008	20.7008	-2.34269349	1978	2.285	0.4730
-8.5	0.0682	0.0036	0.0646358	1.179	2	0.152411333	0.732732269	-26.7692	26.7692	-2.6847852	1972	2.307	0.6177
-10.5	0.0457	0.0036	0.0421266	1.308	2	0.110203063	0.580320936	-34.2579	34.2579	-3.08507612	1965	2.302	0.7885
-12.5	0.0512	0.0036	0.0475604	1.218	2	0.115857087	0.470117873	-41.0209	41.0209	-2.97278986	1958	2.420	0.9928
-14.5	0.0326	0.0036	0.0290000	1.243	2	0.072094	0.354260786	-50.1073	50.1073	-3.42344299	1949	2.570	1.2878
-16.5	0.0269	0.0036	0.0232697	1.27	2	0.059105111	0.282166786	-57.4141	57.4141	-3.61675496	1942	3.059	1.7564
-18.5	0.0182	0.0036	0.0146450	1.287	2	0.037696294	0.223061675	-64.9623	64.9623	-4.00386284	1934	3.115	2.0236
-20.5	0.0170	0.0036	0.0134152	1.302	2	0.034933295	0.185365381	-70.9070	70.9070	-4.07364564	1928	3.060	2.1695
-25.5	0.0100	0.0036	0.0063765	1.322	5	0.042148607	0.150432086	-77.6128	77.6128	-4.60752383	1921	3.646	2.8294
-30.5	0.0068	0.0036	0.0032311	1.334	5	0.021551289	0.108283479	-88.1702	88.1702	-4.98627281	1911	3.898	3.4371
-35.5	0.0071	0.0036	0.0035436	1.3416	5	0.023770267	0.08673219	-95.2970	95.2970	-4.94154265	1904	4.177	3.9806
-40.5	0.0040	0.0036	0.0004000	1.347	5	0.002694	0.062961924	-105.5826	105.5826	-5.52146092	1893	5.280	5.5748
-46.5	0.0040	0.0036	0.0004000	1.351	6	0.0032424	0.060267924	-106.9869	106.9869	-5.52146092	1892	4.848	5.1865
						1.686436957							

Appendix 5.7: CRS model calculations of marsh sediment age for the Loch Don marsh core

Loch Don sediment accretion rates from entire core depth

SUMMARY OUTPUT

Regression Statistics	
Multiple R	0.970438357
R Square	0.941750605
Adjusted R Squ	0.937589934
Standard Error	0.326045411
Observations	16

Lambda/Grad		0.341495321	0.341 cm yr	**3.4 mm yr**
Stand. Dev.	(lower)	0.320211451	0.320 cm yr	**3.2mm yr**
	(upp	0.365810046	0.366 cm yr	**3.7 mm yr**
2 Stand. Dev.	(lower)	0.29888607	0.299 cm yr	**3.0 mm yr**
	(upp	0.398273223	0.398 cm yr	**4.0 mm yr**

ANOVA

	df	*SS*	*MS*	*F*	*Significance F*
Regression	1	24.06183306	24.06183306	226.3458437	4.89254E-10
Residual	14	1.488278545	0.10630561		
Total	15	25.55011161			

	Coefficients	*Standard Error*	*t Stat*	*P-value*	*Lower 95%*	*Upper 95%*	*Lower 95.0%*	*Upper 95.0%*
Intercept	-1.898111094	0.138013627	-13.75307016	1.59539E-09	-2.194121147	-1.602101041	-2.194121147	-1.602101041
X Variable 1	0.091187194	0.006061046	15.04479457	4.89254E-10	0.078187531	0.104186856	0.078187531	0.104186856

Appendix 5.8: Summary output of analysis of variance for the ln $^{210}Pb_{excess}$ activity vs depth for the entire core depth of marsh sediment from Loch Don. Average sediment accretion (lambda/grad) = 0.03114 (^{210}Pb decay constant/ x-variable coefficient).

Loch Don Sediment accretion from 20.5 cm depth

SUMMARY OUTPUT

Regression Statistics	
Multiple R	0.990456067
R Square	0.981003221
Adjusted R Squ	0.978892468
Standard Error	0.126849114
Observations	11

Lambda/Grad		0.238858677	0.238 2.4 mm/ yr
Stand. Dev.	(lower)	0.228270218	0.228 2.3 mm yr
	(upp	0.250477222	0.25 2.5 mm yr
2 Stand. Dev.	(lower)	0.216175065	0.216 2.2 mm yr
	(upp	0.266860832	2.668 2.7 mm yr

ANOVA

	df	*SS*	*MS*	*F*	*Significance F*
Regression	1	7.478385474	7.478385474	464.7645233	4.67996E-09
Residual	9	0.14481628	0.016090698		
Total	10	7.623201754			

	Coefficients	*Standard Error*	*t Stat*	*P-value*	*Lower 95%*	*Upper 95%*	*Lower 95.0%*	*Upper 95.0%*
Intercept	-1.503892646	0.07412562	-20.28843252	8.00204E-09	-1.671576577	-1.336208715	-1.671576577	-1.336208715
X Variable 1	0.130369976	0.006047294	21.55839798	4.67996E-09	0.116690036	0.144049916	0.116690036	0.144049916

Appendix 5.9: Summary output of analysis of variance for the ln $^{210}Pb_{excess}$ activity vs depth for the upper 20-21 cm core depth of marsh sediment from Loch Don. Average sediment accretion (lambda/grad) = 0.03114 (^{210}Pb decay constant/ x-variable coefficient).

Depth (cm)	Height of sed in vial (mm)	137Cs measured	137Cs corrected	Error %	241Am measured	241Am corrected	Error %
-0.5	18.5	61.4	48.20	5.83	6.00	4.71	3.00
-1.5	31	80.5	70.76	7.08	8.80	7.73	2.20
-2.5	20.5	275.0	218.63	17.90	14.60	11.61	4.82
-3.5	28	359.0	305.87	23.30	7.40	6.30	3.33
-4.5	32	286.0	253.16	17.70	8.60	7.61	2.67
-5.5	20	281.0	222.72	16.90	6.50	5.15	2.14
-6.5	45	156.0	158.10	9.52	3.60	3.65	1.22
-7.5	34	3.8	34.20	1.80	3.74	3.38	1.12
-8.5	17.25	139.3	107.61	8.22	3.71	2.87	1.00
-9.5	41	60.6	59.08	4.67	0.00	0.00	0.00
-10.5	36	42.6	39.24	2.94	0.00	0.00	0.00
-11.5	18.25	52.5	41.08	4.88	0.00	0.00	0.00
-12.5	44	51.8	52.21	4.51	0.00	0.00	0.00
-13.5	38	63.8	60.23	6.00	0.00	0.00	0.00
-14.5	28	49.7	42.34	4.37	0.00	0.00	0.00
-15.5	37.5	41.4	38.71	3.89	0.00	0.00	0.00
-16.5	41.5	6.2	6.05	2.50	0.00	0.00	0.00
-17.5	21.25	30.9	24.80	2.47	0.00	0.00	0.00
-18.5	43	20.8	20.73	2.50	0.00	0.00	0.00
-19.5	35.5	19.1	17.48	1.85	0.00	0.00	0.00

Appendix 5.10: ^{137}Cs and ^{241}Am measured and height corrected data derived from gamma spectrometry analysis of the Loch Don sediments from the marsh surface to 20 cm depth.

Calculation of ^{210}Pb Activity for Loch Creran Higher Marsh core 1

Sample Depth	Sample mass (g)	Po-209 mass (g)	Po-209 Total peak (g)	Po-210 Total peak (g)	Po-210 Activity (Bq/g)	Activity (dpm/g)	Error %
-0.5	1.8484	0.5362	2442	55381	0.4692870	28.16	2.07
-2.5	2.0004	0.5901	2899	52968	0.3844737	23.07	1.91
-4.5	2.0046	0.5328	2833	35078	0.2347563	14.09	1.95
-6.5	2.0028	0.5683	2603	21337	0.1659173	9.96	2.08
-8.5	2.0001	0.5412	2655	19886	0.1445711	8.67	2.07
-10.5	2.0132	0.5611	3308	19117	0.1148947	6.89	1.88
-12.5	2.0076	0.4864	2706	11266	0.0719533	4.32	2.14
-14.5	2.0001	0.5512	2959	11518	0.0765213	4.59	2.06
-16.5	2.0247	0.5055	1704	7741	0.0809060	4.85	2.68
-18.5	2.0164	0.5683	2733	9964	0.0732972	4.40	2.16
-20.5	1.9998	0.4922	2671	10827	0.0711675	4.27	2.16
-25.5	2.0235	0.5163	2496	5272	0.0384434	2.31	2.43
-30.5	2.0927	0.4879	2745	2409	0.0145952	0.88	2.79
-40.5	2.0025	0.5215	2719	1281	0.0087521	0.53	3.39
-50.5	2.0002	0.5306	2993	2847	0.0179998	1.08	2.62

Appendix 5.11: Calculation of ^{210}Pb activity (via ^{210}Po activity) from the Loch Creran marsh core

Loch Creran 210Pb Dating Calcs (uses inventories) **CRS Model**

Eqn. Age at Depth = (1/decay const. 210Pb)*LN(unssupported inventory below depth x / unsupported inventory of entire core)

Sample Depth (cm)	Po-210 Activity (Bq/g)	Value of 210 Pb Conc. At Depth	Unsupp. 210-Pb	Dry Bulk Density (g/cm3)	Sample Thickness (cm)	Inventory	Unsupported Inventory Below Depth x	Age	Age +ive	LN 210Pb Activity	Error %	Age (years AD)
-0.5	0.46929	0.0087	0.4606	1.354	0.5	0.31181738	4.2225895	0.0000	0.000	-0.756541	2.0677455	1999
-2.5	0.38447	0.0087	0.3758	1.366	2	1.02661377	3.910772117	-3.7479	3.748	-0.95588	1.907422	1995
-4.5	0.23476	0.0087	0.2261	1.429	2	0.64606891	2.884158345	-13.5263	13.526	-1.449207	1.9531784	1985
-6.5	0.16592	0.0087	0.1572	1.385	2	0.43549204	2.238089436	-21.6705	21.671	-1.796266	2.076148	1977
-8.5	0.14457	0.0087	0.1359	1.269	2	0.34484087	1.8025974	-28.6196	28.620	-1.933984	2.0662393	1970
-10.5	0.11489	0.0087	0.1062	1.297	2	0.27546913	1.45775653	-35.4382	35.438	-2.163739	1.883101	1964
-12.5	0.07195	0.0087	0.0633	1.352	2	0.17103698	1.182287403	-42.1642	42.164	-2.631738	2.1408218	1957
-14.5	0.07652	0.0087	0.0678	1.369	2	0.18569462	1.011250419	-47.1823	47.182	-2.570187	2.0610013	1952
-16.5	0.08091	0.0087	0.0722	1.481	2	0.21387403	0.825555802	-53.6975	53.698	-2.514468	2.6758863	1945
-18.5	0.07330	0.0087	0.0646	1.417	2	0.18306855	0.611681772	-63.3265	63.326	-2.613232	2.1593045	1936
-20.5	0.07117	0.0087	0.0625	1.405	2	0.17553372	0.428613218	-74.7477	74.748	-2.642719	2.1604474	1924
-25.5	0.03844	0.0087	0.0297	1.424	5	0.2117733	0.253079495	-91.6665	91.666	-3.258567	2.429655	1907
-30.5	0.01460	0.0087	0.0059	1.289	5	0.03799473	0.041306194	-149.8775	149.878	-4.227061	2.7917893	1849
-40.5	0.00875	0.0087	0.0001	1.315	10	0.00068563	0.003311465	-230.9186798	230.919	-4.73846	3.3888381	1768
-50.5	0.01800	0.0087	0.0093	1.881	10	0.17492878	0.002625831	-238.3686861	238.369	-4.01740	2.6179378	1761

Total Inventory = 4.2225895

Appendix 5.12: CRS model calculations of marsh sediment age for the Loch Creran marsh core

SUMMARY OUTPUT

Loch Creran
Sediment Accretion from entire core

Regression Statistics	
Multiple R	0.965845171
R Square	0.932856895
Adjusted R Square	0.927692041
Standard Error	0.328538951
Observations	15

ANOVA

	df	*SS*	*MS*	*F*	*Significance F*
Regression	1	19.49533443	19.49533443	180.6163067	5.31085E-09
Residual	13	1.40319195	0.107937842		
Total	14	20.89852638			

	Coefficients	*Standard Error*	*t Stat*	*P-value*	*Lower 95%*	*Upper 95%*	*Lower 95.0%*	*Upper 95.0%*
Intercept	-1.146132208	0.137391444	-8.342093035	1.40971E-06	-1.44294832	-0.849316096	-1.44294832	-0.849316096
X Variable 1	0.08299886	0.006175806	13.43935663	5.31085E-09	0.069656845	0.096340875	0.069656845	0.096340875

	cm yr^{-1}	mm yr^{-1}
Lambda/Grad	0.3752	**3.7**
Stand. Dev.	0.3492	**3.5**
	0.4053	**4.1**
2 Stand.Dev	0.3232	**3.2**
	0.4470	**4.5**

Appendix 5.13: Summary output of analysis of variance for the ln $^{210}Pb_{excess}$ activity vs depth for the entire core depth of marsh sediments from Loch Creran. Average sediment accretion (lambda/grad) = 0.03114 (^{210}Pb decay constant/ x-variable coefficient).

SUMMARY OUTPUT

Loch Creran
Sediment Accretion from 25.5 cm depth

	cm yr^{-1}	mm yr^{-1}
Lambda/Grad	0.3338	**3.30**
Stand. Dev.	0.3022	**3.00**
	0.3728	**3.70**
2 Stand Dev.	0.2707	**2.70**
	0.4351	**4.30**

Regression Statistics	
Multiple R	0.949475991
R Square	0.901504658
Adjusted R Square	0.891655124
Standard Error	0.247887743
Observations	12

ANOVA

	df	*SS*	*MS*	*F*	*Significance F*
Regression	1	5.624221171	5.624221171	91.52764384	2.38129E-06
Residual	10	0.614483334	0.061448333		
Total	11	6.238704505			

	Coefficients	*Standard Error*	*t Stat*	*P-value*	*Lower 95%*	*Upper 95%*	*Lower 95.0%*	*Upper 95.0%*
Intercept	-1.011056622	0.135086243	-7.484526937	2.09981E-05	-1.312047579	-0.710065664	-1.312047579	-0.710065664
X Variable 1	0.093289103	0.009751126	9.567008092	2.38129E-06	0.071562236	0.11501597	0.071562236	0.11501597

Appendix 5.14:Summary output of analysis of variance for the ln $^{210}Pb_{excess}$ activity vs depth for the upper 26 cm of marsh sediments from Loch Creran. Average sediment accretion (lambda/grad) = 0.03114 (^{210}Pb decay constant/ x-variable coefficient).

Sample Depth(cm)	Height of Sed in vial (mm).	137Cs measured	137Cs corrected	Error %	241Am measured	241Am corrected	Error %
-0.5	8	158.00	113.76	12.30	0.00	0.00	0.00
-1.5	8.5	162.00	116.64	12.30	0.00	0.00	0.00
-2.5	8.25	169.00	121.68	13.40	0.00	0.00	0.00
-3.5	30.5	256.00	226.56	15.60	6.10	5.40	2.50
-4.5	21.5	301.00	242.305	20.20	0.00	0.00	0.00
-5.5	14.5	285.00	215.175	18.50	7.80	5.89	3.43
-6.5	23.5	231.00	188.265	14.10	5.60	4.56	2.41
-7.5	39.5	183.00	174.765	11.00	4.80	4.78	1.54
-8.5	15.5	119.60	91.494	1.18	0.55	0.42	0.17
-9.5	37	175.00	162.75	11.50	6.50	6.05	2.73
-10.5	28	180.00	153	10.60	7.00	5.95	1.40
-11.5	14	153.00	114.75	10.30	4.30	3.66	2.19
-12.5	29.5	112.40	97.226	0.72	0.41	0.35	0.16
-13.5	37.5	96.70	90.4145	6.19	3.70	3.46	1.44
-14.5	18	99.40	77.532	5.96	3.90	3.04	1.13
-15.5	35.5	80.90	74.0235	5.34	3.20	2.93	1.41
-16.5	38.5	71.40	67.473	4.93	0.00	0.00	0.00
-17.5	19.25	64.30	50.797	4.69	0.00	0.00	0.00
-18.5	28	47.80	40.63	3.78	0.00	0.00	0.00
-19.5	44	40.30	40.703	3.22	0.00	0.00	0.00

Appendix 5.15: ^{137}Cs and ^{241}Am measured and height corrected data derived from gamma spectrometry analysis of the Loch Creran sediments from the marsh surface to 20 cm depth.

Calculation of 210Pb activity Loch Etive core 1

Activity of 209Po spike = 4.28 dpm/g

Sample name	sample mass (g)	Po-209 mass (g)	Po-209 total peak	Po-210 total peak	Po-210 activity (Bq/g)	Activity dpm/g	Error %
-0.5	2.0328	0.5353	1253	47328	0.7095	42.57	2.86
-2.5	2.0297	0.5412	1387	32281	0.4427	26.56	2.74
-4.5	1.9997	0.5608	1536	29634	0.3860	23.16	2.62
-6.5	2.0401	0.5559	1419	16134	0.2210	13.26	2.77
-8.5	2.0105	0.5718	828	5916	0.1450	8.70	3.71
-10.5	2.0556	0.5281	1295	8603	0.1217	7.30	2.98
-12.5	2.0651	0.5248	1361	5243	0.0698	4.19	3.04
-14.5	2.0158	0.5529	820	2067	0.0493	2.96	4.13
-16.5	2.0351	0.5558	837	1222	0.0284	1.71	4.49
-18.5	2.0161	0.533	858	1208	0.0266	1.59	4.46
-20.5	2.0081	0.5089	664	954	0.0260	1.56	5.05
-25.5	2.0839	0.5541	917	1138	0.0235	1.41	4.44
-30.5	1.9996	0.5698	809	526	0.0132	0.79	5.60
-40.5	2.0397	0.5139	790	993	0.0226	1.36	4.77
-50.5	2.2475	0.5192	860	821	0.0157	0.94	4.88

Appendix 5.16: Calculation of ^{210}Pb activity (via ^{210}Po activvity) from the Loch Etive marsh core

Loch Eive 210Pb Dating Calcs (uses inventories) **CRS Model**

Eqn. Age at Depth = (1/decay const. 210Pb)*LN(unssupported inventory below depth x / unsupported inventory of entire core)

Depth cms	Po- 210Pb Total Activity (Bq/g)	Value of Bkgrd. 210Pb at Depth	210Pb unsupp.	Dry Bulk Density	Sample Thickness (cms)	Total Inventory	Inventoty Below Depth x	Age of Sedment at Depth x (yrs)	convert to + Age	Age yrs BP
-0.5	0.7100	0.012	0.6980	1.559	0.5	0.544091	4.831382	0	0	1999
-2.5	0.4430	0.012	0.4310	1.399	2	1.205938	4.287291	-3.836785169	3.836785169	1995
-4.5	0.3860	0.012	0.3740	1.361	2	1.018028	3.081353	-14.44328095	14.44328095	1985
-6.5	0.2210	0.012	0.2090	1.262	2	0.527516	2.063325	-27.32221567	27.32221567	1972
-8.5	0.1450	0.012	0.1330	1.251	2	0.332766	1.535809	-36.45277599	36.45277599	1963
-10.5	0.1220	0.012	0.1100	1.515	2	0.3333	1.203043	-44.64606213	44.64606213	1954
-12.5	0.0700	0.012	0.0580	1.456	2	0.168896	0.869743	-54.53848818	54.53848818	1944
-14.5	0.0490	0.012	0.0370	1.545	2	0.11433	0.700847	-61.99737413	61.99737413	1937
-16.5	0.0280	0.012	0.0160	1.601	2	0.051232	0.586517	-67.71631923	67.71631923	1931
-18.5	0.0270	0.012	0.0150	1.569	2	0.04707	0.535285	-70.65152597	70.65152597	1928
-20.5	0.0260	0.012	0.0140	1.465	2	0.04102	0.488215	-73.60732021	73.60732021	1925
-25.5	0.0240	0.012	0.0120	1.696	5	0.10176	0.447195	-76.42559708	76.42559708	1923
-30.5	0.0130	0.012	0.0010	1.177	5	0.005885	0.345435	-84.71687032	84.71687032	1914
-40.5	0.0230	0.012	0.0110	2.245	10	0.24695	0.33955	-85.26867767	85.26867767	1914
-50.5	0.0160	0.012	0.0040	2.315	10	0.0926	0.0926	-126.9941777	126.9941777	1872
						4.831382				
						Tot. Inv. =4.8314				

Appendix 5.17: CRS model calculations of marsh sediment age for the Loch Etive marsh core

SUMMARY OUTPUT

Loch Etive
entire core depth

Regression Statistics	
Multiple R	0.838795056
R Square	0.703577146
Adjusted R Squar	0.680775388
Standard Error	0.741229033
Observations	15

ANOVA

	df	*SS*	*MS*	*F*	*Significance F*
Regression	1	16.95306529	16.95307	30.85626751	9.308E-05
Residual	13	7.142466235	0.54942		
Total	14	24.09553153			

	Coefficients	*Standard Error*	*t Stat*	*P-value*	*Lower 95%*	*Upper 95%*	*Lower 95.0%*	*Upper 95.0%*
Intercept	-1.321878046	0.309973983	-4.264481	0.000922061	-1.991536	-0.65222	-1.99153599	-0.652220098
X Variable 1	0.077398207	0.013933467	5.554842	9.30815E-05	0.0472968	0.1074996	0.047296787	0.107499627

Lambda/ Grad	0.402334902	**4.0 mm yr**
Stand. Dev.	0.340955099	**3.4 mm yr**
	0.490666159	**4.9 mm yr**
2 Stand Dev.	0.289675423	**2.9 mm yr**
	0.65839568	**6.6 mm yr**

Appendix 5.18: Summary output of analysis of variance for the ln $^{210}Pb_{excess}$ activity vs depth for the entire core depth of marsh sediments from Loch Etive. Average sediment accretion (lambda/grad) = 0.03114 (^{210}Pb decay constant/ x-variable coefficient).

SUMMARY OUTPUT

Sediment accretion from 30-31 cm depth

Lambda/Grad	0.2244809	2.2 mm yr^{-1}
Stand. Dev	0.2063661	2.1 mm yr^{-1}
	0.2460031	2.5 mm yr^{-1}
2 Stand. Dev	0.2460031	1.9 mm yr^{-1}
	0.2780756	2.8 mm yr^{-1}

Regression Statistics	
Multiple R	0.96027343
R Square	0.92212506
Adjusted R	0.91504552
Standard E	0.37876363
Observatio	13

ANOVA

	df	*SS*	*MS*	*F*	*Significance F*
Regressior	1	18.68621559	18.686216	130.25212	1.945E-07
Residual	11	1.578080772	0.1434619		
Total	12	20.26429636			

	Coefficients	*Standard Error*	*t Stat*	*P-value*	*Lower 95%*	*Upper 95%*	*Lower 95.0%*	*Upper 95.0%*
Intercept	-0.6495237	0.191715946	-3.3879483	0.0060568	-1.0714879	-0.2275596	-1.07148789	-0.227559554
X Variable	0.13874032	0.012156548	11.412805	1.945E-07	0.1119839	0.1654967	0.11198392	0.16549671

Appendix 5.19: Summary output of analysis of variance for the ln $^{210}Pb_{excess}$ activity vs depth for the upper depth of marsh sediments (30-31 cm to marsh surcae) from Loch Etive. Average sediment accretion (lambda/grad) = 0.03114 (^{210}Pb decay constant/ x-variable coefficient).

Sample Depth (cm)	Height of Sed. in Vial (mm)	Sample Mass (g)	137Cs measured (Bq/kg)	137Cs corrected (Bq/kg)	Error %
-0.5	21	6.778	82.01	65.61	6.36
-1.5	20	7.79	102.33	80.84	6.38
-2.5	22	6.62	106.58	86.33	7.42
-3.5	26	10.67	129.12	108.46	8.89
-4.5	19	8.052	118.78	93.84	7.60
-5.5	15.5	6.91	119.70	91.57	6.68
-6.5	27	11.28	120.50	101.22	6.88
-7.5	25.5	11.02	125.41	104.72	6.81
-8.5	19.5	8.555	152.54	120.51	7.83
-9.5	21	10.132	95.33	76.26	5.69
-10.5	27	12.124	45.92	38.58	3.00
-11.5	21	10.66	28.25	23.73	3.90
-12.5	27	11.991	23.72	19.93	2.00
-13.5	40	19.395	16.99	16.31	1.90
-14.5	29	15.07	18.51	15.92	3.40
-15.5	35	15.48	16.25	14.79	1.60
-16.5	27	12.435	15.78	13.25	1.80
-17.5	40	20.751	13.43	12.89	1.90
-18.5	23	12.513	13.69	11.09	1.50
-19.5	32	17.393	10.39	9.24	1.20

Appendix 5.20: ^{137}Cs measured and height corrected data derived from gamma spectrometry analysis of the Loch Etive sediments from the marsh surface to 20 cm depth. (NB. No 241Am activity recorded in this core)

Height [mm]	Detector1 Silica Coeff.	Detector2 Silica Coeff.
10	0.73	0.73
11	0.73	0.73
12	0.74	0.74
13	0.75	0.75
14	0.75	0.75
15	0.76	0.76
16	0.77	0.77
17	0.77	0.77
18	0.78	0.78
19	0.79	0.79
20	0.79	0.79
21	0.80	0.80
22	0.81	0.81
23	0.81	0.81
24	0.82	0.82
25	0.83	0.83
26	0.84	0.84
27	0.85	0.84
28	0.85	0.85
29	0.86	0.86
30	0.87	0.87
31	0.88	0.88
32	0.89	0.89
33	0.90	0.89
34	0.91	0.90
35	0.91	0.91
36	0.92	0.92
37	0.93	0.93
38	0.94	0.94
39	0.95	0.95
40	0.96	0.96
41	0.97	0.97
42	0.99	0.98
43	1.00	0.99
44	1.01	1.00
45	1.02	1.01

Appendix 5.21: Height correction coefficients for the two high purity Germanium coaxial well-type detectors used for gamma spectrometry, determined from measured diluted Amersham QCYK 8163 mixed gamma standard in silica-based matrix. Calculated coefficients have been applied to the measured activity in the Argyll marsh sediments.

(a)

Sample Depth (cm)	Mass of Sed Sample (g)	Ht of Sed Col from base of Scint. Vial (mm)
-0.5	3.18	9.5
-1.5	3.04	8.5
-2.5	3.021	8.25
-3.5	6.11	30.5
-4.5	5.22	21.5
-5.5	6.964	14.5
-6.5	6.13	23.5
-7.5	10.18	39.5
-8.5	8.302	15.5
-9.5	9.84	37
-10.5	7.88	28
-11.5	7.52	14
-12.5	9.37	29.5
-13.5	11.37	37.5
-14.5	9.15	18
-15.5	10.17	35.5
-16.5	8.7	38.5
-17.5	9.42	19.25
-18.5	8.53	28
-19.5	10.36	44

(b)

Sample Depth (cm)	Mass of Sed Sample (g)	Ht of Sed Col from base of Scint.Vial (mm)
-0.5	8.026	18.5
-1.5	9.17	31
-2.5	8.71	20.5
-3.5	7.23	28
-4.5	9.62	32
-5.5	9.076	20
-6.5	14.8	45
-7.5	10.49	34
-8.5	8.603	17.25
-9.5	13.92	41
-10.5	13.39	36
-11.5	9.995	18.25
-12.5	15.36	44
-13.5	14.68	38
-14.5	14.547	28
-15.5	13.93	37.5
-16.5	16.02	41.5
-17.5	11.218	21.25
-18.5	17.37	43
-19.5	11.42	35.5

Appendix 5.22a: Details of sample mass and height of sediment column in scintillation vial from a) Loch Scridain, western Mull and b) Loch Don, south-eastern Mull.

(a)

Sample Depth (cm)	Mass of Sed Sample (g)	Ht of Sed Col from base of Scint. Vial (mm)
-0.5	5.498	8
-1.5	8.187	16.25
-2.5	7.622	15.5
-3.5	7.511	15.25
-4.5	8.961	16.25
-5.5	6.930	14
-6.5	8.942	16.5
-7.5	11.033	20
-8.5	9.821	18
-9.5	10.139	18.5
-10.5	13.600	40
-11.5	12.390	31
-12.5	13.360	34
-13.5	22.290	45
-14.5	12.770	26
-15.5	16.879	36
-16.5	21.950	45
-17.5	18.309	36
-18.5	20.470	44
-19.5	19.480	36

(b)

Sample Depth (cm)	Mass of Sed Sample (g)	Ht of Sed Col from base of Scint. Vial (mm)
-0.5	6.778	21
-1.5	7.790	20
-2.5	6.620	22
-3.5	10.670	26
-4.5	8.052	19
-5.5	6.910	15.5
-6.5	11.280	27
-7.5	11.020	25.5
-8.5	8.555	19.5
-9.5	10.132	21
-10.5	12.124	27
-11.5	10.660	21
-12.5	11.991	27
-13.5	19.395	40
-14.5	15.070	29
-15.5	15.480	35
-16.5	12.435	27
-17.5	20.751	40
-18.5	12.513	23
-19.5	17.393	32

Appendix 5.22b: Details of sample mass and height of sediment column in scintillation vial from a) Loch Creran and b) Loch Etive, mainland Argyll.

APPENDIX SIX

Component	PC1	PC2	PC3	PC4
SiO2	-0.101	-0.325	-0.308	0.187
TiO2	-0.051	0.013	0.526	0.050
Al2O3	0.094	0.366	0.151	0.240
Fe2O3	0.177	0.265	0.184	-0.145
MnO	0.175	0.014	0.300	-0.213
MgO	-0.161	-0.293	0.238	-0.221
CaO	-0.223	-0.260	0.027	-0.094
Na2O	-0.024	0.380	-0.276	0.019
K2O	0.096	0.117	-0.320	-0.468
P2O5	0.254	0.062	0.147	-0.097
SO3	0.222	0.027	-0.057	0.171
Rb	-0.265	0.046	-0.052	-0.039
Sr	-0.267	0.052	-0.012	-0.027
Y	-0.269	0.054	0.017	-0.005
Zr	-0.260	0.083	-0.027	-0.156
Nb	-0.234	0.192	0.038	-0.205
Pb	0.232	-0.065	0.097	-0.110
Zn	0.013	-0.274	0.220	-0.413
Ni	-0.234	0.092	0.192	0.179
As	0.223	0.119	0.138	-0.120
Cr	-0.239	-0.104	0.159	0.138
V	-0.194	0.089	0.249	0.296
Ba	-0.241	0.067	-0.096	-0.268
La	-0.176	0.347	0.018	-0.098
Ce	-0.197	0.278	0.076	-0.192
% Variance	53.9	15.3	12.4	8.4

Key

heavy minerals

diagenesis

carbonate/marine

grain size(fine)

neutral

Pb & As association

Appendix 6.1: Principle component loadings resulting from PCA of the marsh core geochemistry from Loch Scridain.

	PC1	PC2	PC3	PC4
SiO2	0.184	0.090	-0.174	-0.061
TiO2	0.118	-0.328	0.084	0.028
Al2O3	-0.153	-0.231	-0.112	-0.039
Fe2O3	-0.135	-0.216	0.224	0.190
MnO	-0.132	0.022	0.289	0.338
MgO	-0.150	0.072	0.194	-0.133
CaO	0.199	0.010	0.075	-0.008
K2O	-0.199	0.115	-0.105	-0.020
Na2O	-0.183	0.212	-0.078	-0.051
P2O5	-0.193	0.173	0.035	0.016
SO3	-0.177	0.251	0.003	-0.023
As	-0.201	-0.051	0.006	0.002
Ba	0.144	-0.097	0.015	-0.201
Bi	-0.031	0.204	0.386	-0.091
Br	-0.207	0.059	-0.038	0.000
Ce	-0.141	-0.007	-0.110	0.320
Cl	-0.180	0.232	0.016	-0.055
Co	-0.082	-0.008	0.420	0.095
Cr	-0.020	-0.220	0.203	-0.392
Cu	-0.199	0.068	-0.068	-0.063
Ga	-0.140	-0.311	-0.079	-0.141
I	-0.169	-0.160	0.039	0.140
La	-0.052	0.000	-0.198	-0.484
Mo	-0.199	0.018	-0.079	0.074
Nb	-0.192	-0.138	-0.036	-0.006
Ni	-0.202	-0.081	0.039	-0.031
Pb	-0.198	-0.099	-0.040	-0.013
Rb	-0.201	0.006	0.021	0.006
S	-0.201	0.089	-0.008	-0.047
Sb	-0.064	0.004	0.391	-0.240
Sn	-0.149	-0.005	0.120	-0.242
Sr	0.064	0.256	-0.033	-0.269
Th	0.196	-0.073	0.065	0.043
U	-0.204	-0.024	-0.063	-0.065
V	-0.127	-0.293	-0.161	-0.077
Y	-0.116	-0.365	-0.015	-0.041
Zn	-0.204	0.034	0.022	-0.046
Zr	0.130	-0.075	0.329	-0.119
% Variance	59.8	11.7	7	6.2

Key

heavy minerals

grain size

diagenesis

neutral

carbonate/marine

Pb & As association

Appendix 6.2: Principle component loadings resulting from PCA of the marsh core geochemistry from Loch Don.

Component	PC1	PC2	PC3	PC4
SiO2	0.195	0.037	0.075	-0.035
TiO2	-0.155	0.297	0.122	0.070
Al2O3	-0.029	0.229	-0.361	-0.169
Fe2O3	-0.153	-0.180	0.081	0.023
MnO	-0.095	-0.359	-0.112	-0.186
MgO	-0.190	0.186	-0.097	0.022
CaO	-0.167	0.170	-0.024	0.120
K2O	0.131	-0.060	-0.308	-0.279
Na2O	-0.126	0.004	-0.331	0.115
P2O5	-0.181	-0.010	-0.257	0.034
SO3	-0.175	-0.017	-0.184	0.028
As	-0.177	-0.195	-0.030	0.015
Ba	0.206	0.002	-0.081	-0.008
Bi	0.142	0.096	-0.035	-0.071
Br	-0.206	-0.005	-0.056	0.055
Ce	-0.183	-0.070	0.088	-0.088
Cl	-0.205	0.021	0.098	0.051
Co	0.061	-0.323	-0.250	-0.149
Cr	-0.178	0.144	0.180	-0.077
Cu	-0.186	0.012	-0.192	-0.005
Ga	-0.037	0.372	0.057	-0.406
I	-0.195	-0.074	0.043	0.000
La	-0.087	-0.147	0.293	-0.268
Mo	-0.100	-0.324	0.073	-0.088
Nb	-0.168	0.173	0.227	-0.123
Ni	-0.194	-0.049	-0.072	-0.141
Pb	-0.209	-0.032	-0.035	0.021
Rb	0.150	0.117	-0.118	-0.367
S	-0.094	-0.067	0.141	-0.400
Sb	-0.115	0.221	-0.156	0.233
Sn	-0.092	-0.040	0.243	0.185
Sr	0.197	-0.037	-0.068	0.150
Th	0.193	0.089	0.076	-0.173
U	-0.208	0.012	-0.028	0.013
V	-0.194	-0.139	0.056	-0.075
Y	-0.197	0.103	0.056	-0.197
Zn	-0.186	-0.070	-0.186	-0.051
Zr	0.114	-0.187	0.179	0.113
% Variance	58.5	9.6	8.2	5.1

	heavy minerals		fine grained sediment
	diagenesis		coarse grained sediment
	carbonate/marine		neutral
	Pb & As association		

Appendix 6.3: Principle component loadings resulting from PCA of the marsh core geochemistry from Loch Creran

Component	PC1	PC2	PC3	PC4
SiO2	0.040	-0.372	0.010	0.043
TiO2	-0.219	0.059	-0.180	0.228
Al2O3	-0.066	0.252	0.387	-0.152
Fe2O3	-0.142	0.275	-0.133	0.211
MnO	-0.146	0.217	0.009	0.400
MgO	-0.204	0.225	0.144	0.060
CaO	-0.247	0.125	-0.043	0.119
Na2O	0.101	0.133	0.254	-0.513
K2O	0.221	-0.001	0.358	-0.092
P2O5	-0.035	0.285	-0.393	-0.239
SO3	0.165	0.011	-0.398	-0.400
Rb	-0.190	-0.249	0.245	0.040
Sr	-0.207	-0.224	0.233	0.006
Y	-0.268	-0.094	-0.043	-0.037
Zr	-0.209	-0.160	-0.203	-0.013
Nb	-0.251	-0.152	-0.090	-0.062
Pb	-0.096	0.343	0.173	-0.087
Zn	-0.256	0.121	0.074	-0.051
Ni	-0.261	0.013	-0.033	-0.195
As	-0.070	0.355	0.140	0.020
Cr	-0.254	-0.070	-0.095	-0.226
Va	-0.270	-0.031	-0.011	-0.151
Ba	-0.186	-0.268	0.202	-0.023
La	-0.265	-0.030	0.015	-0.178
Ce	-0.258	-0.020	-0.014	-0.226
% variance	50.9	23.7	8.8	6.2

Key

heavy minerals

grain size

diagenesis

neutral

carbonate

Pb & As association

Appendix 6.4: Principle component loadings resulting from PCA of the marsh core geochemistry from Loch Etive.

APPENDIX SEVEN

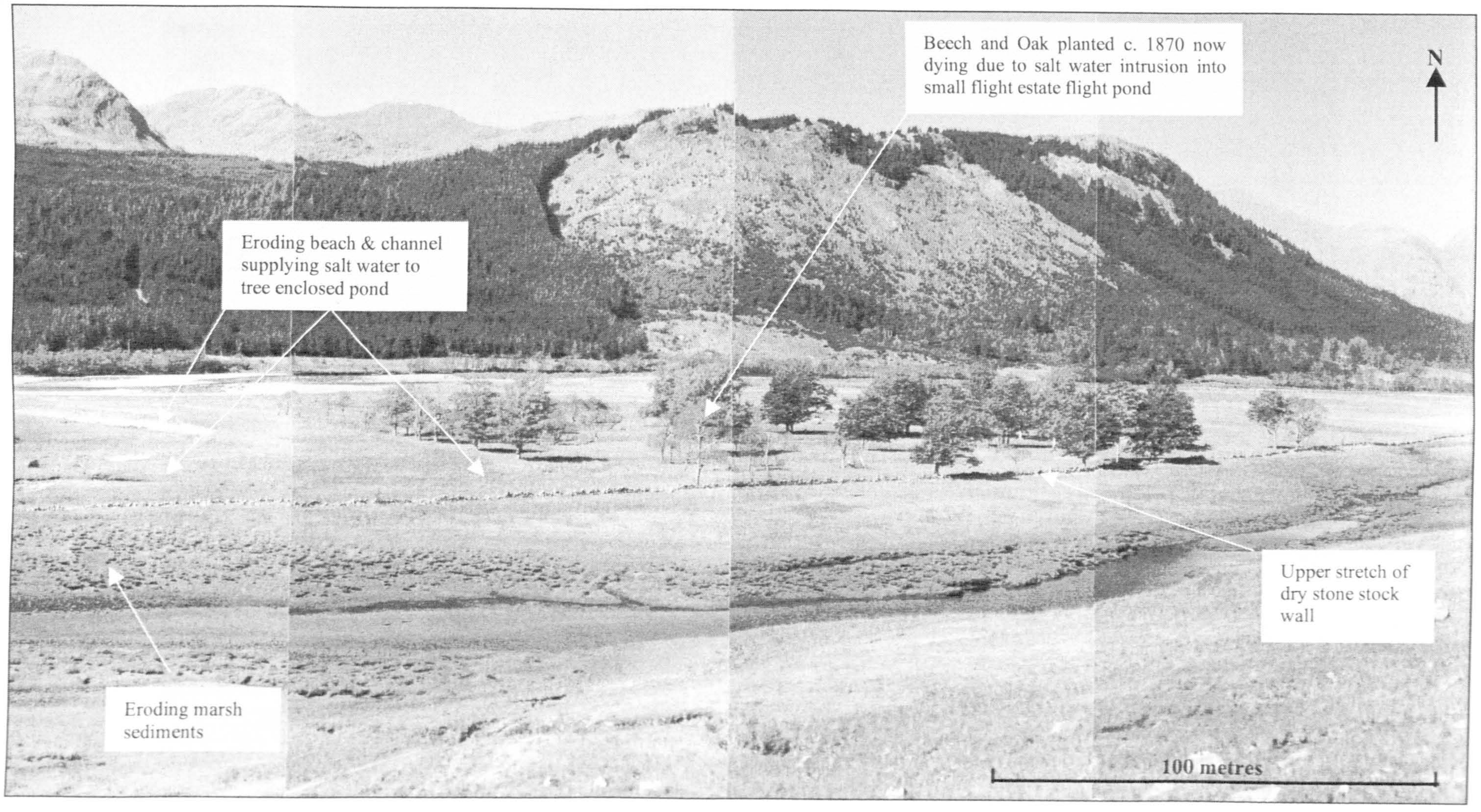

Appendix 7.1: 135mm photographic montage of the upper intertidal area at the head of Loch Etive, mainland Argyll to show general observational information relating to recent increased marine inundation.

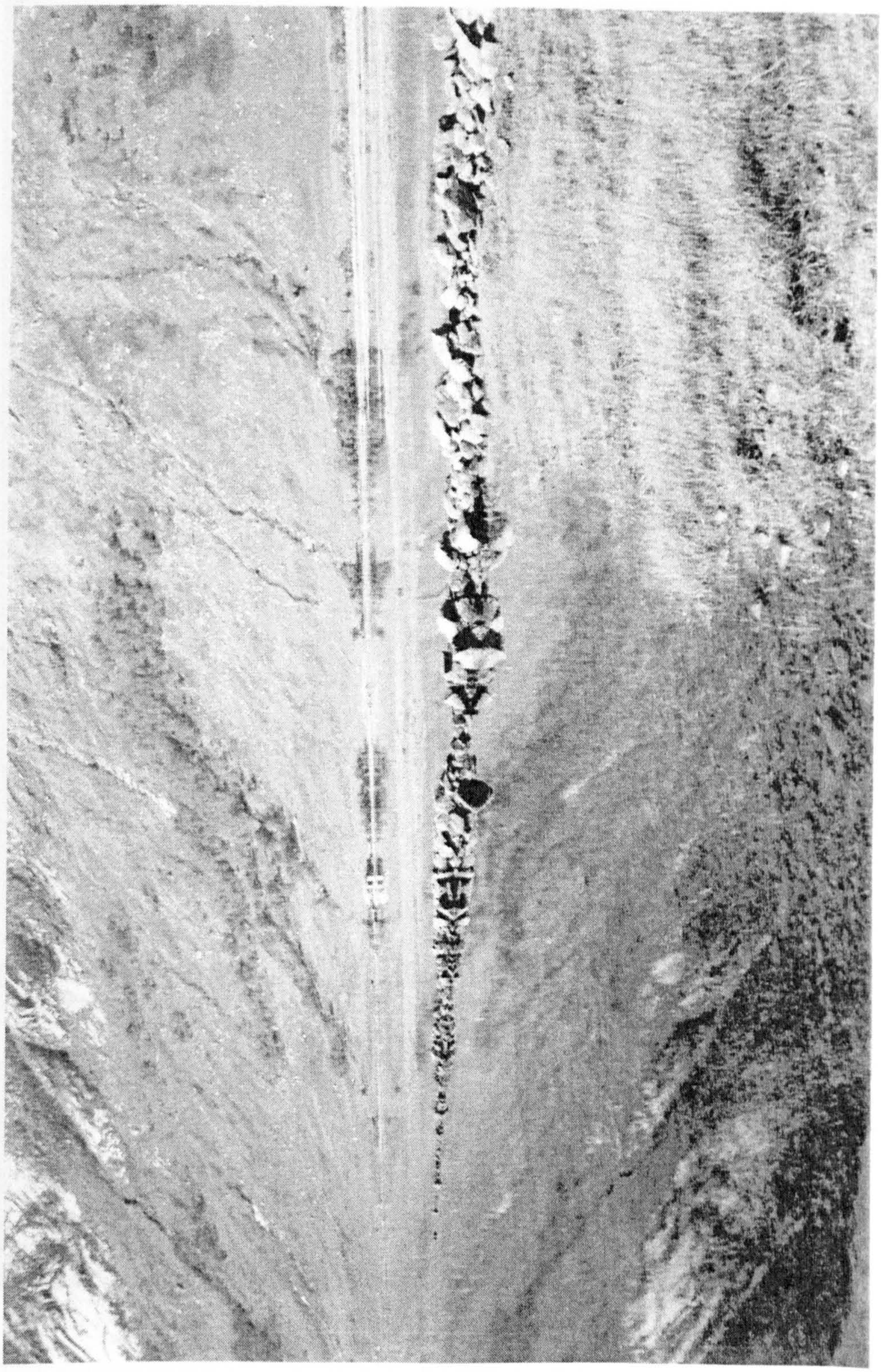

Appendix 7.2: Seaward end of the dry stone stock wall at the head of Loch Etive constructed c. 1800 AD, now being submerged at just below HWOST in October 2002

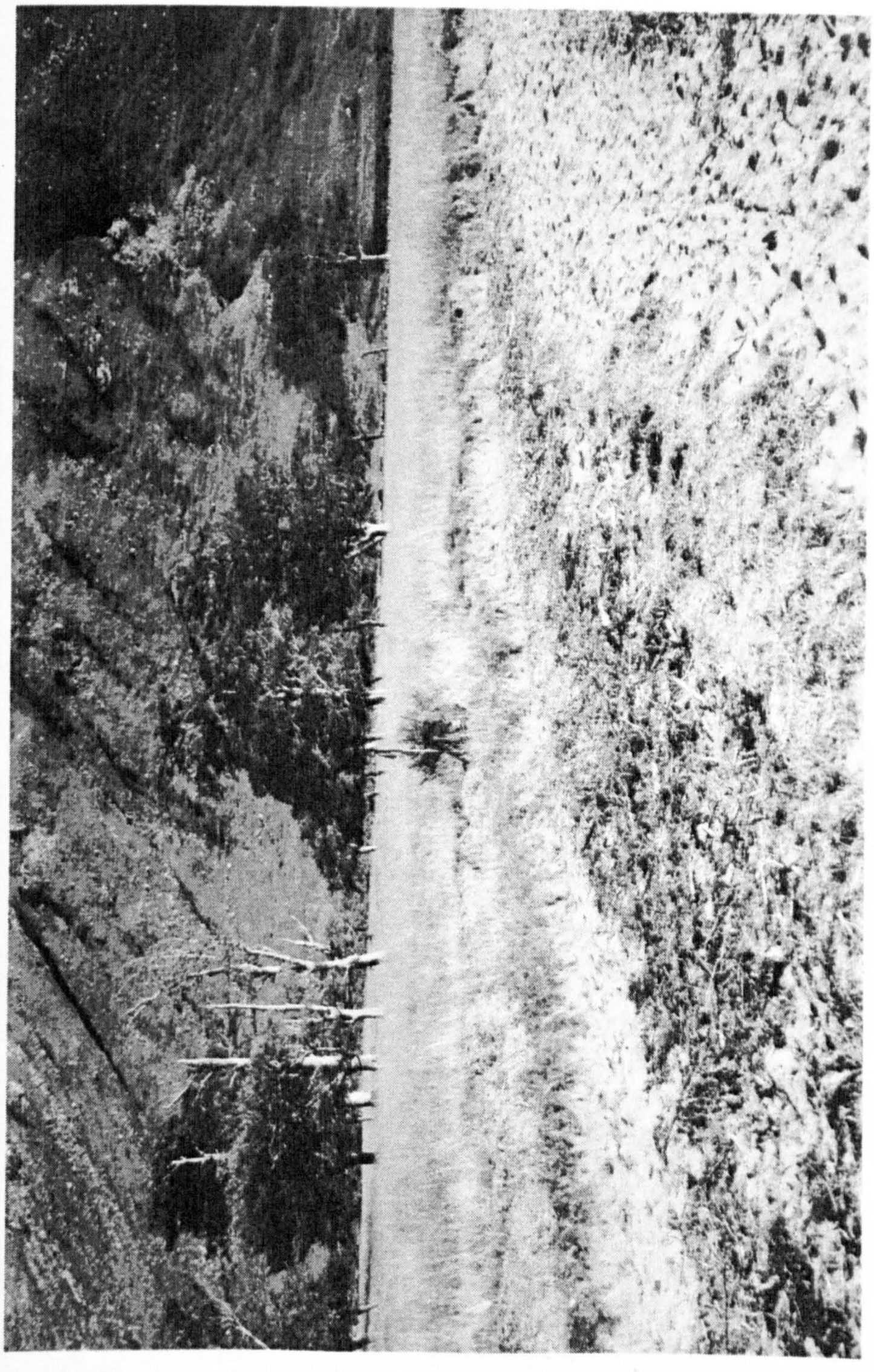

Appendix 7.3: Photograph to show central section of pocket beach formed at the head of Loch Etive (see appendix 7.1). Note the deposited flotsam from recent incursion of HWOST and dying beech trees encircling the estate flight-pond. (35 litre rucksack and walking pole (1.06 m) shown for scale).

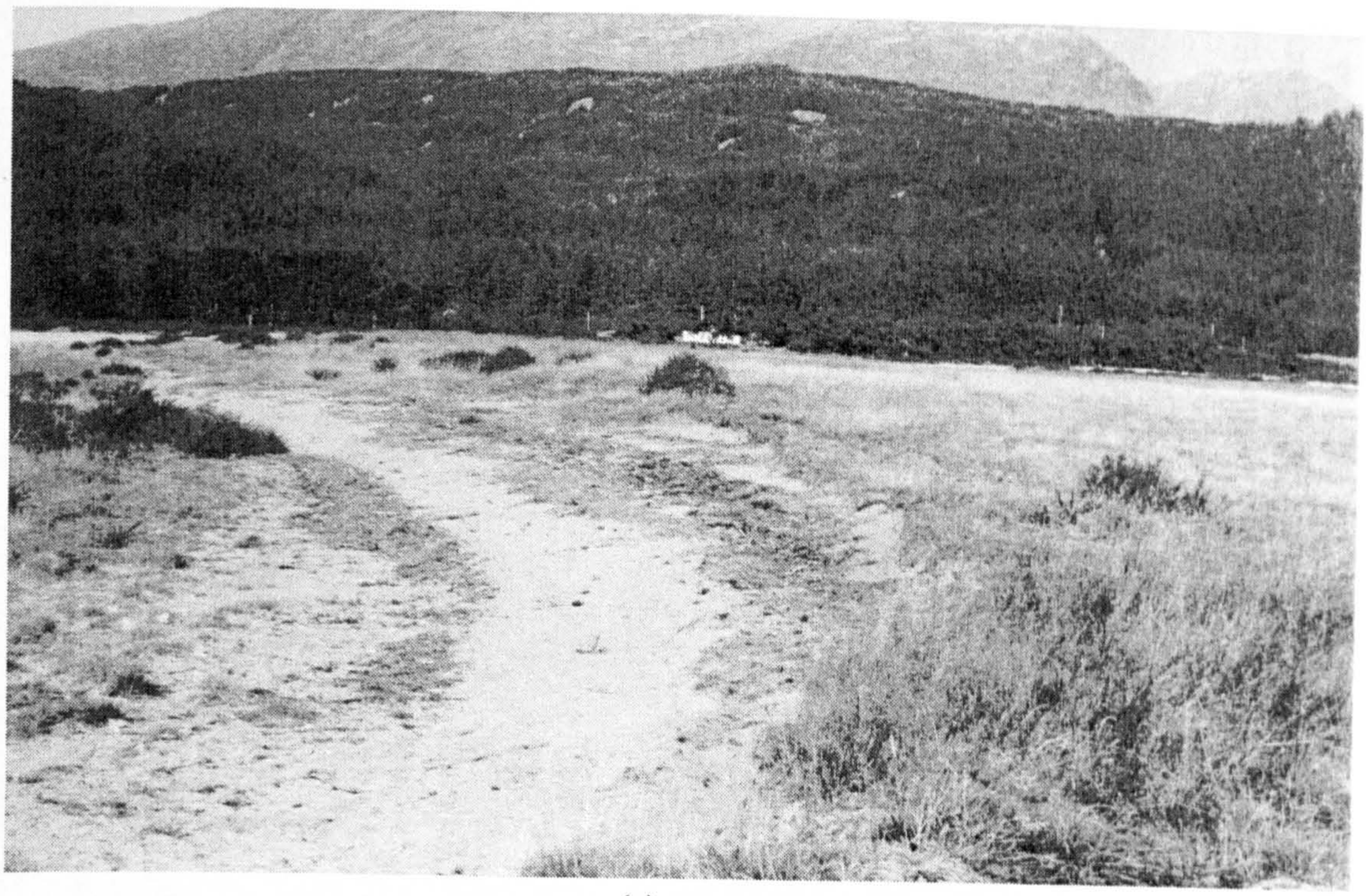

(a)

(b)

Appendix 7.4: Further photographs to show erosion of c. Mid-Late Holocene palaeo shoreline surface at the head of Loch Etive, immediately following spring tides. Note the presence of Goarse in relation to the beech cliff.

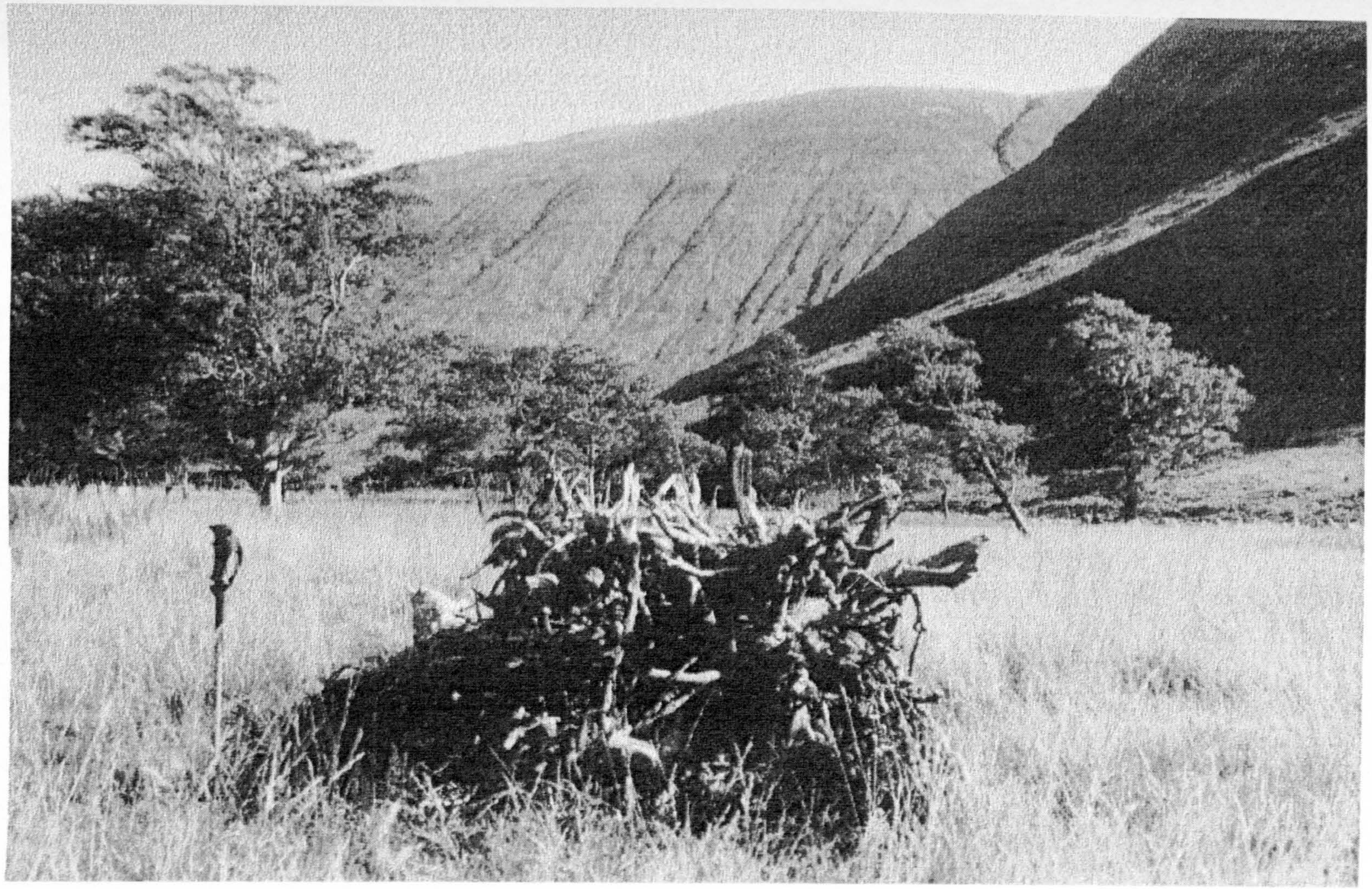

Appendix 7.5: Stump of beech tree (in situ) now regularly innundated by marine water on the spring tidal cycle at the head of Loch Etive. Around the stump and extending along the flood channel towards the trees the remains of large numbers of small fish were also observed. Note the height at of flotsam entrapped in the roots relative to the trees in the background. (Walking pole 1.06 m shown for scale.

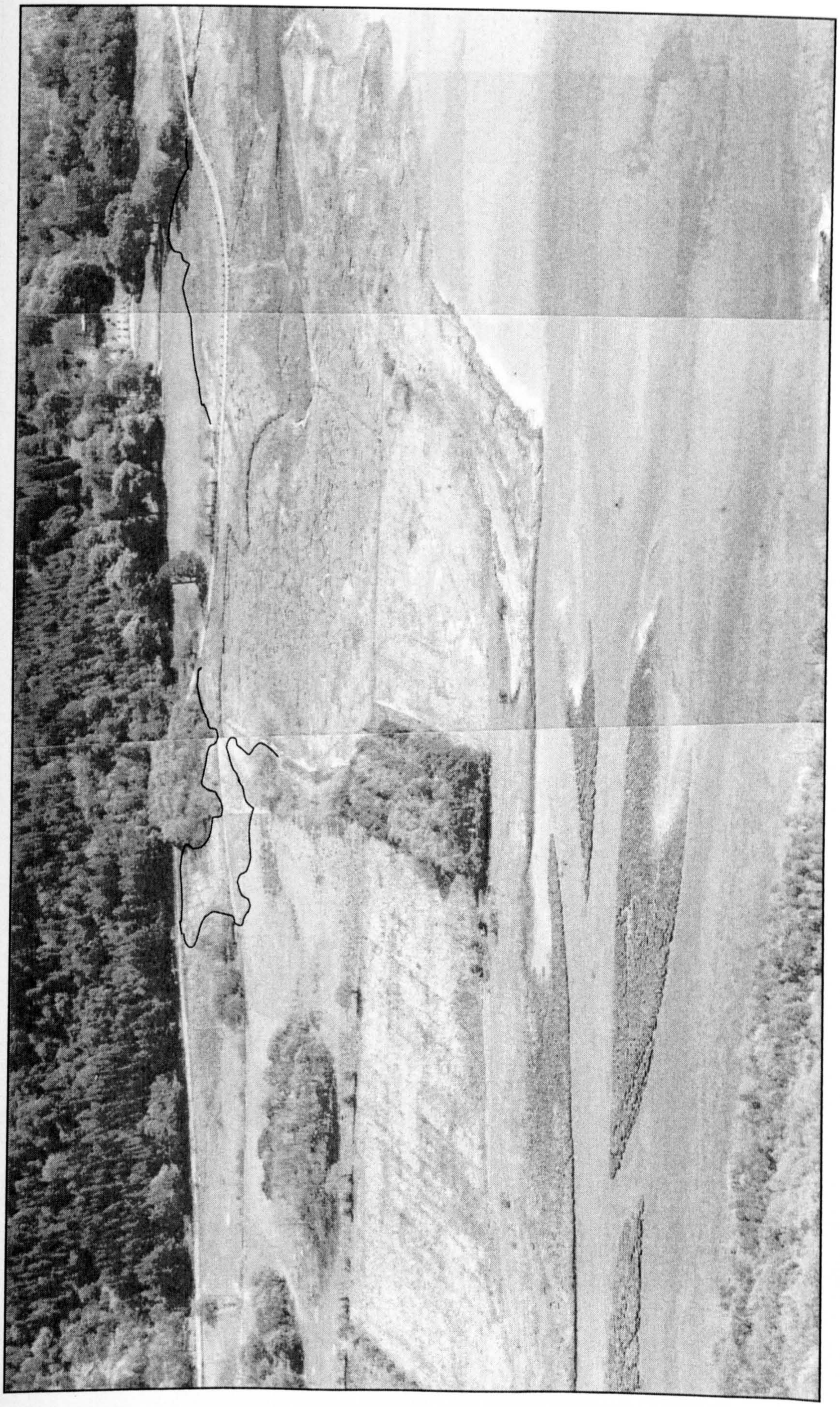

Appendix 7.6: Field 35 mm photograph of the marsh area at the head of Loch Creran. Note the area of grazing pasture above the main section of marsh and the delineated area at the seaward egde of the house garden lawn which is now being flooded and has reverted to high marsh vegetation (marked by the black lines).

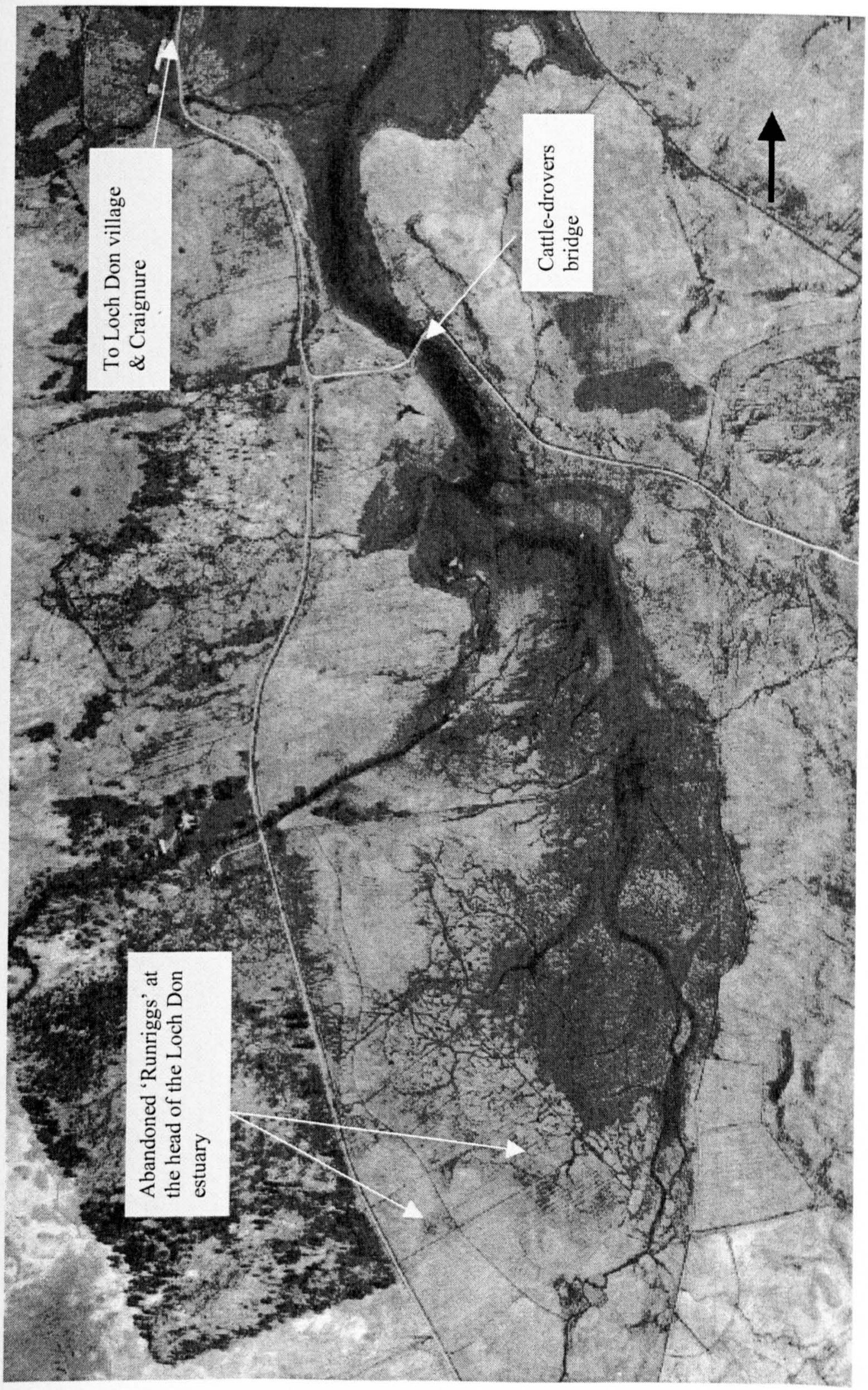

Appendix 7.7. Expanded section of 1946 air photograph of the head of the Loch Don estuary, Isle of Mull, showing abandoned 'Runriggs' (coastal allotments) being incised by marsh channels and colonized by marsh vegetation